

BN-600 Hybrid Core Benchmark Analyses

*Results from a Coordinated Research Project on Updated Codes and
Methods to Reduce the Calculational Uncertainties of the LMFR
Reactivity Effects*



IAEA

International Atomic Energy Agency

IAEA-TECDOC-1623

BN-600 Hybrid Core Benchmark Analyses

*Results from a Coordinated Research Project on Updated Codes and
Methods to Reduce the Calculational Uncertainties of the LMFR
Reactivity Effects*



IAEA
International Atomic Energy Agency

February 2010

The originating Section of this publication in the IAEA was:

Nuclear Power Technology Development Section
International Atomic Energy Agency
Wagramer Strasse 5
P.O. Box 100
A-1400 Vienna, Austria

BN-600 HYBRID CORE BENCHMARK ANALYSES

IAEA, VIENNA, 2009

ISBN 978-92-0-109409-4

ISSN 1011-4289

© IAEA, 2009

Printed by the IAEA in Austria

February 2010

FOREWORD

To those Member States who have or have had significant fast reactor development programmes, it is of the utmost importance to have validated up-to-date codes and methods for fast reactor core physics analysis in support of R&D activities in the area of actinide utilization and incineration. They have recently focused on fast reactor systems for minor actinide transmutation and on cores optimized for consuming rather than breeding plutonium; the physics of the breeder reactor cycle having already been widely investigated. Plutonium burning systems may have an important role in managing plutonium stocks until the time when major programmes of self-sufficient fast breeder reactors are established. For assessing the safety of these systems it is important to determine the prediction accuracy of transient simulations and their associated reactivity coefficients.

In response to Member States' expressed interest, the IAEA sponsored a Coordinated Research Project (CRP) on Updated Codes and Methods to Reduce the Calculational Uncertainties of the LMFR Reactivity Effects. This CRP was started in November 1999 and at the first meeting the members of the CRP endorsed a benchmark on the BN-600 hybrid core for consideration in its first studies. Benchmark analyses of the BN-600 hybrid core were performed during the first three phases of the CRP investigating different nuclear data and levels of approximations in the calculation of, safety related reactivity effects and their influence on uncertainties in transient analysis predictions. In an additional phase of the benchmark studies experimental data was used for the validation and verification of nuclear data libraries and methods in support of the previous three phases.

This report presents the results of the benchmark analyses of the hybrid UOX/MOX fuelled BN-600 reactor core. The aim of this report is to contribute to the reduction in uncertainties associated with reactivity coefficients and their influence on LMFR transient analyses.

The IAEA expresses its appreciation to all participants in the CRP for their dedicated efforts leading to this report. The IAEA officer responsible for this publication was Y.I. Kim of the Division of Nuclear Power.

EDITORIAL NOTE

The papers in these proceedings are reproduced as submitted by the authors and have not undergone rigorous editorial review by the IAEA.

The views expressed do not necessarily reflect those of the IAEA, the governments of the nominating Member States or the nominating organizations.

The use of particular designations of countries or territories does not imply any judgement by the publisher, the IAEA, as to the legal status of such countries or territories, of their authorities and institutions or of the delimitation of their boundaries.

The mention of names of specific companies or products (whether or not indicated as registered) does not imply any intention to infringe proprietary rights, nor should it be construed as an endorsement or recommendation on the part of the IAEA.

The authors are responsible for having obtained the necessary permission for the IAEA to reproduce, translate or use material from sources already protected by copyrights.

CONTENTS

1.	INTRODUCTION	1
2.	BASIC DATA AND ANALYTICAL METHODS	3
2.1.	Basic data.....	3
2.1.1.	Nuclear and delayed neutron data	3
2.1.2.	Energy release per fission and capture.....	3
2.2.	Analytical methods	3
2.2.1.	ANL.....	3
2.2.2.	CEA/SA.....	11
2.2.3.	CIAE	12
2.2.4.	FZK/IKET	13
2.2.5.	IGCAR	14
2.2.6.	IPPE.....	15
2.2.7.	JNC.....	16
2.2.8.	KAERI.....	18
2.2.9.	OKBM.....	19
3.	DESCRIPTIONS AND ANALYSES OF BENCHMARK PROBLEMS	20
3.1.	RZ homogeneous benchmark (Phase 1).....	20
3.1.1.	RZ benchmark model.....	20
3.1.2.	Description of the parameters calculated	29
3.1.3.	Comparison of results	31
3.2.	Hex-Z homogeneous benchmark (Phase 2).....	69
3.2.1.	Hex-Z benchmark model.....	69
3.2.2.	Description of the parameters calculated	69
3.2.3.	Comparison of results	69
3.2.4.	Summary of homogeneous benchmarks (Phase 1 and 2).....	109
3.2.5.	Influence of mesh size and number of energy groups.....	111
3.3.	Hex-Z heterogeneous and burnup benchmark (Phase 3).....	112
3.3.1.	Hex-Z heterogenous and burnup model.....	112
3.3.2.	Comparison of results	115
3.4.	BFS-62-3A experimental data analysis benchmark (Phase 5)	129
3.4.1.	Benchmark model	129
3.4.2.	Comparison of results	139
3.5.	Influence of basic nuclear data	141
4.	ULOF TRANSIENT ANALYSES	150
5.	RELATIONSHIP OF BFS-62-3A AND BN-600 HYBRID CORES	153
5.1.	Sodium void reactivity effect in BFS-62-3A and BN-600 hybrid cores	153
5.2.	Similarity and relevance of BFS-62-3A and BN-600 hybrid cores	154
6.	CONCLUSIONS.....	155
Appendix I:	The influence of an energy groups number and mesh size on results of reactivity coefficients calculations for BN-600 benchmark core.....	159
	<i>M.Farakshin, B.Vasilyev</i>	
Appendix II:	Sensitivity Analysis of JEF and JENDL	170
	<i>M. Ishikawa</i>	

Appendix III:	Effect of JFS set changes	181
	<i>M. Ishikawa</i>	
Appendix IV:	Simplified approach to dynamic process modelling	202
	<i>A. Danilytchev, D. Elistratov, V. Stogov</i>	
Appendix V:	Effect of JFS set changes (JNC's response to Action 4.3 in the 4th CRP meeting).....	215
	<i>M. Ishikawa</i>	
Appendix VI:	Description of benchmark model for Phase 5	218
	<i>G. Manturov, M. Semenov, A. Seregin, L. Lykova</i>	
Appendix VII:	Sensitivity analysis of JENDL-3.2, JEDL-3.3 and JEF-2.2 for BFS-62-3A critical experiments	241
	<i>M. Ishikawa</i>	
Appendix VIII:	Possible remaining reasons of the differences on SVRW between BFS-62-3A and BN-600 hybrid core	272
	<i>T. Hazama</i>	
Appendix IX:	Comparison of non-leakage and leakage terms of SVRW in BFS-62-3A and BN-600 hybrid core.....	277
	<i>A. Shono</i>	
Appendix X:	More information on the differences of SVRW between BFS-62-3A and BN-600 hybrid core.....	279
Appendix XI:	Representativity factors.....	284
	<i>G. Rimpault</i>	
REFERENCES		287
ABBREVIATIONS.....		291
LIST OF PARTICIPANTS		293
CONTRIBUTORS TO DRAFTING AND REVIEW.....		297

1. INTRODUCTION

This report presents the results of a series of four benchmark analyses for a hybrid UOX/MOX fuelled core of the BN-600 reactor. The benchmark was proposed during the first Research Coordination Meeting (RCM) of the Coordinated Research Project (CRP) on Updated Codes and Methods to Reduce the Calculational Uncertainties of the LMFR Reactivity Effects, which took place in Vienna from 24-26 November 1999 [1]. The general objective of the CRP is to validate, verify and improve methodologies and computer codes used for the calculation of reactivity coefficients in fast reactors aiming at enhancing the utilization of plutonium and minor actinides.

There has been no change in the view that energy production with breeding of fissile materials is the main goal of fast reactor development to ensure long-term fuel supply. However, before the breeding role of fast reactors is recognized economically, due to the increasingly available low-cost uranium from the 1980s onwards, the emphasis of fast reactor development shifted to incineration of stock-piled plutonium and partitioning and transmutation (P&T) of nuclear wastes to meet contemporary demands.

Following a proposal of the Russian Federation, at the 32nd Annual Meeting of the International Working Group on Fast Reactors (IWG-FR), held in May 1999, a hybrid UOX/MOX (mixed oxide) fuelled BN-600 reactor core that has a combination of highly enriched uranium (HEU) and mixed oxide (MOX) assemblies in the core region, was chosen as a calculational model [1].

The benchmark analyses were performed during four phases in the CRP. Phases 1, 2 and 3 of the benchmark analysis, which were completed during the period 1999-2001, consisted of RZ homogeneous benchmark (Phase 1), Hex-Z homogeneous benchmark (Phase 2), and Hex-Z heterogeneous and burnup benchmark (Phase 3). Phase 4 of the benchmark analysis, undertaken during the period 2002-2003, studied a BN-600 core fully loaded with MOX fuel. The Phase 4 results are to be addressed in another report. Phases 1, 2 and 3 are devoted to calculational benchmark analyses focusing on safety related reactivity effects and the influence of their calculational uncertainties on modelling transient analysis. Phase 5 of the benchmark analysis completed in 2005, verified uncertainties on reactivity coefficients and especially on the sodium void reactivity effect with BFS-62-3A experiments in support of the first three phases. The series of benchmarks clearly address the issues arising from the use of weapons-grade plutonium for energy production in the BN-600 reactor.

The specifications and input data for benchmark neutronics calculations, prepared by IPPE, have been defined in each phase against its specific purpose. The organizations participating in the CRP are: ANL from the USA, CEA and SERCO Assurance (SA) (its previous name was AEAT) from EU (France and the UK, respectively), CIAE from China, FZK/IKET from Germany (participated since Phase 4), IGCAR from India, JNC from Japan, KAERI from the Republic of Korea, IPPE and OKBM (participated till Phase 3) from the Russian Federation.

This report presents the results from the series of benchmark analyses of a hybrid UOX/MOX fuelled core of the BN-600 reactor performed during the period 1999-2005. The results for several reactivity parameters, obtained by the participants with their own state-of-the-art basic data and codes, were compared in terms of calculational uncertainty, and their effects on the ULOF transient behaviour of the hybrid BN-600 core. These were evaluated during the first three phases. In addition, the capability of predicting criticality and specifically the sodium void reactivity effect was checked by comparison with experimental measurements in the BFS-62-3A critical assembly, a full scale model of the BN-600 reactor hybrid core. Table 1.1 shows the contributions of the participants in the benchmark analyses.

This report first addresses the benchmark definitions and specifications used in each phase and briefly introduces the basic data, computer codes, and methodologies applied by the various participants. Then, the results of Phases 1, 2 and 3 obtained by the participants in terms of the calculated uncertainties and their effect on the core transient behaviour are inter-compared. The Phase 5 results obtained from the experimental data analysis are validated in terms of their calculated uncertainty. Finally the report addresses some conclusions drawn from the benchmarks.

TABLE 1.1. TASK PARTICIPATIONS IN BN-600 HYBRID CORE BENCHMARK ANALYSES

Participant	ANL			CEA/SA			CIAE			FZK/KET			IGCAR			IPPE			JNC			KAERI					
Phase	1	2	3	5	1	2	3	5	1	2	3	5	1	2	3	5	1	2	3	5	1	2	3	5	1	2	3
K_{eff}	D	D	D	D	D	D	D	D	M	M	M	M	D	D	D	D	D	D	T	T	T	T	D	D	D		
Fuel Doppler coefficient	D	D	D	D	D	D	D	D					D	D	D	D	D	D	T	T	T	T	D	D	D		
Steel Doppler coefficient	D	D	D	D	D	D	D	D					D	D	D	D	D	D	T	T	T	T	D	D	D		
Sodium density coefficient	D	D	D	D	D	D	D	D					D	D	D	D	D	D	T	T	T	T	D	D	D		
Sodium void worth									D	T			D	T			D			T				D	T		
Steel density coefficient	D	D	D	D	D	D	D	D					D	D	D	D	D	D	T	T	T	T	D	D	D		
Fuel density coefficient	D	D	D	D	D	D	D	D					D	D	D	D	D	D	T	T	T	T	D	D	D		
Absorber worth	D	D	D	D	D	D	D	D					D	D	D	D	D	D	T	T	T	T	D	D	D		
Control rod worth									D	T			D	T			D			T				D		D	
Expansion coefficients	D	D	D	D	D	D	D	D					D	D	D	D	D	D	T	T	T	T	T	D	D		
Power distribution	D	D	D	D	D	D	D	D					D	D	D	D	D	D	T	T	T	T	T	D	D		
β_{eff}	D	D	D	D	D	D	D	D					D	D	D	D	D	D	T	T	T	T	D	D	D		
Reaction rate distributions	D	D	D	D	D	D	D	D	T	T	T	T	D	T	D	D	D	D	T	T	T	T	T	D	D		

Note: D: Diffusion theory calculation T: Transport theory calculation M: Monte Carlo calculation

2. BASIC DATA AND ANALYTICAL METHODS

2.1. Basic data

2.1.1. Nuclear and delayed neutron data

Basic nuclear and delayed neutron data used for the benchmark analyses by the participants are given in Table 2.1. The standard multi-group cross-sections were generated based on the participants own evaluated nuclear data library, using their own current state-of-the-art data processing system. However, common delayed neutron data sets for fission yield fraction, decay constants, and neutron spectrum were used for the calculation of system kinetics parameters.

2.1.2. Energy release per fission and capture

The reactor flux is normalised by the following equation to the user-specified reactor power of 1470 MW_t:

$$P = \sum_r V_r c \sum_g \left(\sum_n N_{n,r} \sum_i w_i \sigma_g^{n,i,r} \right) \phi_{g,r},$$

where

P; reactor thermal power,

V_r; volume for region r,

c; conversion factor transforming MeV to MW,

N_{n,r}; number density for nuclide n and region r,

w_i; energy release per reaction i (fission and capture) (MeV/reaction),

σ_g^{n,i,r}; microscopic cross-section for energy group g, nuclide n, reaction i and region r,

φ_{g,r}; neutron flux for group g and region r.

Energy release (w_i) data per fission and capture used by the participants are given in Table 2.2.

In Phase 3, an energy release of 200 MeV per fission was assumed at the point of fission with zero energy per capture.

2.2. Analytical methods

Table 2.3 summarizes the individual computer codes used for the benchmark analyses by the participants, which are further described below. The effective cross-sections, condensed into a broader energy group structure, were generated individually by participants using their own cell codes which include different self-shielding treatments for the homogeneous and heterogeneous cell models. The number of condensed energy groups used ranges from 230 (fine groups) to 9 (coarse groups) with an upper energy boundary of ~ 10 MeV. Various specific heterogeneous cell modelling methods and specific code processing schemes were employed for the treatment of control rod heterogeneity.

2.2.1. ANL

Benchmark calculations were performed with the ANL suite of fast reactor physics codes. These tools have been extensively demonstrated in previous US physics experiments and fast spectrum test reactor (EBR-2 and FFTF) applications. Basic nuclear data is taken from the ENDF/B-V.2 multi-group cross-section data that is generated using the MC²-2 codes [2]. For structural materials, a resonance ‘screening’ procedure was utilised to pre-process broad resonances into the MC²-2 ‘smooth data’ library at the 2082 group level. Self-shielding effects of the remaining resonances are explicitly evaluated in MC²-2 assuming the narrow resonance approximation, allowing for Doppler broadening, scattering interference, and overlap with neighboring resonances.

TABLE 2.1. BASIC NUCLEAR AND DELAYED NEUTRON DATA

Participant	ANL	CEA/SA	CIAE	FZK/IKEF	IGCAR	IPPE	JNC	KAERI	OKBM
Nuclear Data									
• Nuclear data library	• (ENDFB-V.2)	• (JEF-2.2)	• LIB-IV-M	• (JEFF-3.0)	• CV2M (for Phase 1,2)/ XSET98 (for Phase 3,5)	• ABBN-93 (for Phase 1) ABBN-93.1 (for Phase 2)	• JENDL-3.2 (for Phase 1)	• KAFAX /F22	• ABBN-93 (for R-Z) ABBN-78 (for Hex-Z)
• Standard group constant set	• 2082	• 1968	• 46	• 30	• 25/26	• 26 (ABBN-93)	• 70 (JFS-3-J3.2R in Phase 5)	• 80	• 26
(No. of groups)						299 groups for main 16 isotopes			
						26 groups for the rest (ABBN-93.1)/ (ABBN-93.01a for Phase 5)			
Delayed Neutron Data									
• Delayed neutron yield	• ENDF/B-V	• R. J. Tuttle ¹⁾	• R. J. Tuttle	• ENDF/B-VI.7	• R. J. Tuttle	• R. J. Tuttle (79)	• R. J. Tuttle (79)	• ENDf/ B-VI	• ENDf/ (M.C. Brady ²⁾)
• Yield fraction and decay constant	• ENDF/B-V	• JEF-2.2 (Pu ²⁴² from ENDf/B-VI)	• G. R. Keepin ³⁾	• ENDF/B-VI.7 Keepin	• G. R. Keepin	• G. R. Keepin	• ENDf/ B-VI	• ENDf/ B-VI	• ABBN- 78, R. J. Tuttle for Pu ²⁴¹ and Pu ²⁴²
• Delayed neutron spectrum	• ENDF/B-V (U ²³⁸ and Pu ²⁴²)	• JEF-2.2 D. Saphier ⁴⁾	• D. Saphier	• ENDF/B-VI.7 D. Saphier	• D. Saphier	• D. Saphier	• ENDf/ B-VI	• D. Saphier	• D. Saphier

Notes: 1) R. J. Tuttle, 'Delayed-Neutron Data for Reactor-Physics Analysis,' Nucl. Sci. and Eng., 56, pp. 37 - 71 (1975).

2) M. C. Brady and T. R. England, 'Delayed Neutron Data Group Parameters for 43 Fissioning Systems,' Nucl. Sci. and Eng., 103, pp. 129-149 (1989).

3) G. R. Keepin, 'Physics of Nuclear Kinetics' (1965).

4) D. Saphier, et al., 'Evaluated Delayed Neutron Spectra and Their Importance in Reactor Calculation,' Nucl. Sci. and Eng., 62, pp. 660-694 (1977).

TABLE 2.2. ENERGY RELEASE DATA

(Unit : MeV/event)

Nuclide	ANL		CEA/SA		CIAE		Fission	Capture	IGCAR
	Fission	Capture	Fission	Capture	Fission	Capture			
^{235}U	193.74	6.88	196.29	6.55			190.00		6.37
^{236}U	194.49	5.49	194.14	5.12			0.00		7.00
^{238}U	198.06	5.68	201.03	5.48			190.70		6.86
^{239}Pu	199.92	6.51	200.91	6.53			196.20		6.38
^{240}Pu	199.47	5.23	204.18	5.24			196.20		5.33
^{241}Pu	201.99	6.30	204.56	6.31			196.20		6.20
^{242}Pu	201.58	5.23	206.41	5.03			196.20		6.00
FP	0.00	8.00	0.00	8.00			0.00		7.00
O	0.00	3.37	0.00	4.14					
Na	0.00	6.94	0.00	6.96			0.00		4.12
Fe	0.00	7.78	0.00	7.65			0.00		7.78
Cr	0.00	9.27	0.00	7.94			0.00		8.64
Ni	0.00	8.51	0.00	7.82			0.00		8.12
Mo	0.00	8.77	0.00	8.00			0.00		6.97
B^{10}	0.00	2.78	0.00	2.79			0.00		2.79
B^{11}	0.00	3.41	0.00	3.37			0.00		2.79
C	0.00	4.94	0.00	4.14					
Nuclide	IPPE		JNC		KAERI		OKBM		Average
	Fission	Capture	Fission	Capture	Fission	Capture	Fission	Capture	
^{235}U	193.10	6.80	193.71	6.55	198.80	6.89	193.10	6.80	194.11
^{236}U	191.60	6.80	191.61	5.13	191.21	5.49	191.60	6.80	192.44
^{238}U	193.80	6.80	194.79	4.81	193.71	5.68	193.80	6.80	195.13
^{239}Pu	0.00	0.00	199.92	6.53	198.30	6.52	199.60	6.80	199.14
^{240}Pu	0.00	0.00	197.79	5.24	194.71	5.23	197.40	6.80	198.29
^{241}Pu	0.00	0.00	201.97	6.31	200.10	6.30	201.30	6.80	201.02
^{242}Pu	0.00	0.00	200.87	5.03	194.71	5.23	200.30	6.80	200.01
FP							6.80	0.00	5.70
O							6.80	0.00	4.77
Na					0.00	6.95	0.00	6.80	6.36
Fe					0.00	7.79	0.00	6.80	7.56
Cr					0.00	8.52	0.00	6.80	8.23
Ni					0.00	9.28	0.00	6.80	8.11
Mo					0.00	8.78	0.00	6.80	7.86
B^{10}					0.00	2.79	0.00	2.80	2.79
B^{11}					0.00	3.42	0.00	6.80	3.96
C					0.00	4.95	0.00	6.80	5.21

TABLE 2.3. BASIC COMPUTER CODES USED FOR BENCHMARK ANALYSIS

(1/4)		Participant	ANL	CEA/SA	CIAE	FZK/IKET	IGCAR	IPPE	JNC	KAERI	OKBM
Cell calculation											
Effective cross- section Calculation	• MC ² -2 -ultra-fine B _g ² method	• ECCO - subgroup method	• 1DX-EXP - ABBN f-factor method	• ZMIX - ABBN f-factor method	• EFFCROSS - B ² method	• CONSYST - B ² method	• SLAROM - ABBN f-factor method	• TRANSX/ TWODANT - ABBN f-factor method	• COINSY/ MIM (for Hex-Z)	• TRANSX/ (for R-Z) MIM (for Hex-Z)	
Fuel SA heterogeneity	•	ECCO	• 1DX-EXP - Bell method	• ZMIX - Bell method	• NCELL - interface current method	• CASUP - Tone's method	• COHINT - collision probability method	• CASUP - reaction rate preservation method	• COHINT - reaction rate preservation method		
SHR heterogeneity	•	ECCO/ - BISTRO	reaction rate	preservation method							

TABLE 2.3. BASIC COMPUTER CODES USED FOR BENCHMARK ANALYSIS (CONTINUED)
(2/4)

Participant	ANL	CEA/SA	CIAE	IGCAR	IPPE	JNC	KAERI	OKBM
Core calculation								
<i>Phase 1 (R-Z Model)</i>								
• Condensed group (No. of groups)	• 230	• 33	• 12/29 -diffusion/ transport	• 25	• 18	• 18	• 9	• 26
• Diffusion theory calculation	• DIF3D - nodal diffusion method	• BISTRO - finite difference	• 2DB - finite difference	• ALCALMI - finite difference	• RHEIN - finite difference	• CITATION - finite difference	• SYNTES	
• Transport theory calculation	• VARI3D - nodal transport method	• BISTRO module - P_0S_4 , discrete ordinates method	• DOT3.5 - discrete ordinates method	• DOT	• TWODANT - discrete ordinates method	• TWOIRAN - P_3S_8 , discrete ordinates method	• TWODANT - discrete ordinates method	• TWOIRAN - P_3S_8 , discrete ordinates method
• Perturbation theory calculation (based on diffusion theory)	• VARI3D	• BISTRO module (for diff. and transport theory)	• PERT-V	• NEWPERT	• RHEIN	• PERKY		
• Monte Carlo theory calculation	• MCNP		• MCNP					

TABLE 2.3. BASIC COMPUTER CODES USED FOR BENCHMARK ANALYSIS (CONTINUED)
(3/4)

Participant	ANL	CEA/SA	CIAE	IGCAR	IPPE	JNC	KAERI	OKBM
<i>Phase 2&3 (Hex-Z Model)</i>								
• Condensed group constant Set (No. of groups)	• 230	• 33	• 12	• 25/26	• 18	• 18	• 9	• 26
• Diffusion theory flux/burnup calculation	• DIF3D/ REBUS-3 -nodal diffusion method	• H3D module	• HND/ CITATION -nodal diffusion method/ diffusion method for burnup	• 3DB/ FARCOBAB - for Tri-Z model	• TRIGEX	• CITATION	• DIF3D/ REBUS-3 - nodal diffusion method	• JARFR
• Transport theory calculation	• VARI3D - nodal transport method	• TGV/ VARIANT module - nodal transport method	• DOT (with transport correction)*	• TRIGEX	• NSHEX	• SOLTRAN - SP ₂ nodal transport method	• PERT-K	• JARFR
• Perturbation theory calculation	• VARI3D for Tri-Z model	• H3D module for diffusion theory	• HND for diffusion theory	• 3DPERT module	• PERKY	• PERT-K	• KENO/ MCNP	• MMK-
• Monte Carlo theory calculation	• MCNP	• MCNP						

* Transport correction given by (3D transport) = (3D diffusion) × (2D transport / 2D diffusion)

TABLE 2.3. BASIC COMPUTER CODES USED FOR BENCHMARK ANALYSIS (CONTINUED)

(4/4)	Participant	CEA/SA	CIAE	FZK/IKET	IGCAR	IPPE	JNC	KAERI
<i>Phase 5 (Hex-Z Model)</i>								
• Condensed group constant Set (No. of groups)	• 33	• 12	• 11/21	• 26	• 26	• 18	• 25	
• Diffusion theory flux calculation	• H3D module	• HND -nodal diffusion method	• KIN3D	• TREDFR for Tri-Z model	• TRIGEX	• CITATION with isotropic diffusion coeff. and Benoist's anisotropic diffusion coeff.	• DIF3D - nodal diffusion method	
• Transport theory calculation	• TGV/ VARIANT module - variational - nodal transport method	• DOT for R-Z model - S_8P_3 transport method	• VARIANT R-Z -nodal transport (P_3 and SP_3) method	• DOT	• DOT	• TWODANT for R-Z model - S_8 transport method	• MINHEX - S_4P_0 transport method	• TWODANT - for R-Z model
• Monte Carlo theory Calculation	• MCNP		• MMKENO					
• Other methods	• Mesh size correction using IPPE data	• Corrections for ultra-fine group ($\sim 100,000g$ below 50 keV) and mesh-size						

For eight benchmark material compositions (inner core, middle core, mixed oxide core, outer core, axial blanket, axial reflector, radial steel shield, and radial reflector), homogeneous ultra-fine-group flux calculations were performed using MC²-2. For regions that contained enriched fuel, the consistent P1 method was used with group-independent bucking search for the fundamental mode spectrum calculations performed with 2082 groups. In regions that do not contain enriched fuel, an infinite-medium fixed source MC²-2 calculation was done to determine the collapsing spectrum. In these fixed source calculations, the fixed source was an estimated 2082 group leakage spectrum (DB² ϕ) from an adjacent zone.

Two-hundred and thirty energy group cross-sections were generated for eight zones of the BN-600 reactor configuration at normal and elevated temperatures. For each of the enriched-fuel regions, the fundamental mode weighting spectrum was determined using the compositions specified in the benchmark. The group constant set used in all axial blanket zones was collapsed using an estimated leakage spectrum from the middle core zone as the fixed source in the MC²-2 calculation. Furthermore, the group constant set used in all axial reflector zones was collapsed using an estimated leakage spectrum from the axial blanket zone as the fixed source in the MC²-2 calculation. The group constant sets for the steel shield and reflector zones were obtained in a similar manner. The group constant set for the steel shield used an estimated leakage spectrum from the outer core zone as the MC²-2 fixed source and the estimated fixed source for the reflector zone calculation was an estimated leakage spectrum from the steel shield zone. Lumped fission product cross-sections were generated at the fuel operating temperatures. The lumped fission product model is based on isotopic data for 180 individual isotopes. Each lump is created from fission yields based on ²³⁵U, ²³⁸U, ²³⁹Pu, ²⁴⁰Pu and ²⁴¹Pu fission and subsequent transmutation in a typical fast reactor spectrum.

The core eigenvalue and flux distributions were computed using the DIF3D diffusion theory code [3] for both the Phase 1 (RZ) and Phase 2 (Hex-Z) geometries. In addition, the impact of higher order methods: nodal diffusion (DIF3D), nodal transport (VARI3D) [4], discrete ordinates transport (TWODANT) [5], continuous energy Monte Carlo (MCNP) [6] methods, was investigated in a preliminary manner. Regional reactivity coefficients were evaluated with the VARI3D first-order perturbation theory treatment based on the diffusion theory flux distributions. The flux calculations within the VARI3D code were performed by DIF3D using the finite difference triangle-Z (Tri-Z) option. Radial and axial expansion reactivity coefficients were determined using, diffusion-calculated, eigenvalue differences using the nodal Hex-Z option of DIF3D.

All calculations were normalized to 1470 MWt. Power was calculated with isotopic MeV/fission and MeV/capture factors which include gamma heating (i.e. local energy deposition model).

For the Phase 3 benchmark calculations the system eigenvalue, powers, and fluxes for the benchmark partial-MOX BOC core loading were determined using the nodal Hex-Z option of the DIF3D diffusion theory code and a 230 energy group structure. Given the BOC fuel loading, the REBUS-3 fuel cycle analysis code [7] was utilized to compute EOC compositions for each specified depletion region with the DIF3D flux solution module for the prediction of space and energy dependent flux. Region-dependent broad group cross-sections based on ENDF/B-V.2 were generated using the MC²-2 code for eight distinct material compositions of the BN-600 reactor configuration at normal and elevated temperatures. Lumped fission product cross-sections were generated at the fuel operating temperature. A similar methodology was employed for fuel management calculation of the EBR-II experimental reactor; and excellent agreement was observed between the calculational predictions and experimental data.

Control rod worths and reactivity feedback coefficients were calculated using both homogeneous and heterogeneous models. Burnup effects on fuel Doppler coefficient and sodium density coefficient were also determined. When heterogeneous models are used, the system eigenvalues were determined using the MCNP-4B Monte Carlo code. When homogeneous models are used, system eigenvalues were determined with either DIF3D or MCNP. These values were calculated with either first-order perturbation theory methods (Tri-Z geometry), nodal eigenvalue differences (Hex-Z geometry) or Monte Carlo eigenvalue differences. Both spatially-dependent and region-integrated values are provided.

2.2.2. CEA/SA

The calculations have been performed using the ERANOS code [8] and data system using the JEF 2.2 nuclear data cross-section libraries. This data set is different from the one issued by the NEA Databank due to the ^{239}Pu evaluation which differs in the transition energy range between the resolved and unresolved resonance energy ranges. Broad group cross-section data, in 33 neutron energy groups, have been prepared for a homogeneous representation of each material in the benchmark using the ECCO cell code [9]. This cell code performs a solution of the slowing down equation in 1968 energy groups, using a subgroup method within each fine group, and subsequently condenses the cross-section to the 33 group energy structure.

For the Phase 1 analysis with the RZ model, both diffusion and transport theory calculations have been performed. The transport theory results have been calculated using the BISTRO module that employs Sn theory with the S_4 approximation and the P_0 scattering approximation. Perturbation options are available for both diffusion and transport methods in the BISTRO module. Spatial distributions have been obtained with both solution methods.

For the Phase 2 analysis with the Hex-Z model, diffusion theory calculations have been carried out using the H3D module. The H3D module consists of a finite difference code capable of providing a 3-dimensional diffusion theory solution and perturbation options. Transport theory calculations were performed using the TGV/VARIANT module, however, no perturbation theory options are available. The TGV/VARIANT module employs the variational nodal method, with an order P_3 angular expansion of the flux and a P_0 anisotropic scattering approximation, to provide a 3 dimensional transport theory solution. Global reactor integrated transport theory results were therefore obtained based on the direct k_{eff} difference. Spatial transport distributions are restricted to the reactor power only. No transport theory perturbation spatial distributions have been submitted for this benchmark.

In answer to questions raised on the CEA/SA Phase 1 and 2 calculations, the following clarifications were given:

- Infinite dilution reaction rates given for nuclides which are not present in specific model regions have been assumed to have a number density of $1.0\text{E-}11 (\times 10^{24}) \text{ atoms/cm}^3$.
- For the Phase 2 benchmark all transport theory results have been derived from direct reactivity differences, no perturbation code being available for Hex-Z transport at the time of these calculations.

The European calculations for Phases 1, 2 and 5 of the benchmark were performed by SERCO Assurance. The European participation in Phase 3 of the benchmark analyses consists of a joint contribution from France (CEA Cadarache) and the UK (SERCO Assurance sponsored by BNFL, Winfrith).

As required by the Phase 3 benchmark specifications either a simple homogeneous representation, or an exact detailed heterogeneous description for the fuel and absorber sub-assemblies, has been used to produce 33 group resonance self shielded cross-sections and matrices for each material in the whole core model. The heterogeneity of the absorber rods has been represented by a specific set of procedures within the ERANOS code scheme that enable homogeneous equivalent cross-sections to be prepared for control rod absorbers. These procedures employ the reactivity equivalence method for the treatment of heterogeneous geometries which uses the Sn transport theory option of the BISTRO finite difference module.

For the Phase 3 whole core calculations Hex-Z diffusion theory calculations were performed using the H3D module for which perturbation options are available, and a set of spatial distributions are given. The transport theory calculations were again performed using the TGV/VARIANT variational nodal method with an order P_3 angular expansion of the flux and a P_0 scattering approximation. Global reactor integrated transport theory results are based on direct k -effective difference. Where appropriate, an extrapolation has been made to an infinitely fine mesh so as to remove any mesh dependent effects during the prediction of absolute core reactivity.

The fuel Doppler coefficient, sodium density coefficient, steel Doppler coefficient, and the steel density coefficient at both the start and end of cycle were calculated for both homogeneous and heterogeneous core models. In addition, the control rod worth at the start of cycle, and the reactivity loss with burnup, was calculated for both homogeneous and heterogeneous core geometries.

The ERANOS modelling for Phase 5 employed a homogeneous three-dimensional Hex-Z representation of the full BFS-62-3A core. No symmetry approximations were applied. Resonance-shielded cross-sections (in 33 energy groups) for each spatial region in the Hex-Z core model have again been prepared using the ECCO cell code. Based on these methods, appropriate modules have been used within the ERANOS code scheme to provide results for each of the parameters. The distribution of the SVRE coefficients was derived by first performing direct and adjoint flux solutions in diffusion theory with the H3D module, and then using the appropriate perturbation calculation modules within ERANOS. Resonance-shielded cross-sections (in 33 energy groups) for each spatial region in the Hex-Z core model have again been prepared using the ECCO cell code.

Based on these methods, appropriate modules have been used within the ERANOS code scheme to provide results for each of the parameters. The distribution of the SVRE coefficients was derived by first performing direct and adjoint flux solutions in diffusion theory with the H3D module, and then using the appropriate perturbation calculation modules within ERANOS.

2.2.3. CIAE

The one-dimensional diffusion code, 1DX [10] has been used to collapse few-group cross-sections from LIB-IV-M fine-group constants library, which is a modified version of LIB-IV [11]. The LIB-IV-M library has a 46 neutron energy group structure. The few-group cross-section set adopts a 12 neutron energy group structure. This 12-group cross-section library was used by diffusion codes. For transport calculations, a 171 neutron group, 36 gamma ray group AMPX format library NVITAMIN-C has been prepared based on ENDF/B-VI, CENDL-2, JENDL-3, JEF-2, etc. The NVITAMIN-C contains 101 materials, and 2 pseudo-fission products for ^{235}U and ^{239}Pu , respectively. The Petten AMPX/SCALE Code System PASC-1 has been used to prepare 29 neutron energy group ANISN formatted group cross-sections for each spatial region in the R-Z model, which were used by a transport code. A simple homogeneous representation has been used for all regions when calculating resonance self-shielded cross-sections.

The analyses of the proposed benchmark core in R-Z and Hex-Z representations have been carried out using the two-dimensional diffusion theory code 2DB [12] and three-dimensional hexagonal nodal diffusion theory code HND [13], respectively. The two-dimensional transport code DOT3.5 has been used for transport calculations in the R-Z representation. Kinetic parameters have been calculated by the perturbation theory code PERT-V [14] and perturbation module of the three-dimensional hexagonal nodal code for R-Z and Hex-Z representations, respectively.

The Monte Carlo theory calculation code MCNP [15] has been used to calculate the effective multiplication factor k_{eff} in both models.

For Phase 3 benchmark calculations, the heterogeneity effects of BN-600 benchmark core have been analyzed only at BOC. The 1DX code computes total cross-section for each fuel isotope applying the Bell modification to the rational approximation for heterogeneous geometry. Heterogeneous treatments have been given for the core fuel and axial blanket regions (LEZ, MEZ, MOX and HEZ). A three-dimensional hexagonal code has been used to calculate neutronic parameters for steady state. Dynamic characteristics have been analyzed by the perturbation theory module in the code.

The burnup calculation has been partly finished up to now and the burnup reactivity loss was calculated using the CITATION code.

In the Phase 5 benchmark calculations, the one-dimensional diffusion code 1DX-EXP which is a modified version of 1DX, was used to collapse few-group cross-sections from fine-group constants library LIB-IV-M which is a modified version of LIB-IV. The LIB-IV-M library has a 46-neutron

energy group structure and contains ABBN-type self-shielding factors. The few-group cross sections adopt 12 neutron groups.

The analysis of the proposed Phase 5 benchmark core in Hex-Z representation was carried out with the use of the three-dimensional hexagonal nodal diffusion theory code HND. The HND code calculates not only neutronics parameters for steady state but also dynamic characteristics by the perturbation model. The convergence criterion for pointwise flux was 0.00001.

A general-purpose Monte Carlo transport code MCNP was used to calculate k_{eff} for critical systems. The MCNP code treats an arbitrary three-dimensional configuration of materials in geometric cells. Pointwise cross-section data are used in the MCNP calculation.

The transport correction was evaluated by the difference between calculation results with the transport theory code DOT and the diffusion theory code CITATION using a RZ geometry model. The P_3 scattering matrices and S_8 calculations were used in the DOT calculations. The convergence criterion for pointwise flux was 0.0001.

2.2.4. FZK/IKET

FZK employed an 11-group nuclear data library in the CCCC (ISOTXS and BRKOXS) format [16] during the Phase 4 of the CRP. The library [17], which includes ABBN-type f-factors and is based on the KFKINR 26-group cross-section set, has been extended by some more recent data in particular for Minor Actinides (MAs). The 11-group library generated with a weighting function representing the neutron spectrum in a MOX-fuelled sodium cooled core, has been used at FZK for more than 10 years for SIMMER (an accident analysis code [18]) related applications, mainly for cores with Pu/MA fuel. Up to now it has not been used at FZK for cores containing a significant amount of ^{235}U .

A new code and data system, C4P [19], which includes fine-group cross-section libraries in an extended (for taking properly into account temperature-dependent neutron thermal-scattering matrices) CCCC format and related processing tools (in particular for condensation of fine-group data), have been developed at FZK recently. The main applications of these fine-group cross-section libraries are safety (with SIMMER) and scenario studies. The fine group libraries include data for 560 energy groups. Among alternative libraries corresponding to alternative data evaluations (ENDF, JEFF, JENDL) available, the JEFF 3.0 data is preferred (after performing a set of benchmark calculations) at present in general. For routine fast reactor calculations with the new data, a 30-group cross-section set (including f-factors) was derived from the 560-group library based mainly on JEFF 3.0 by using a weighting function that consists of a fission spectrum at fast energies (above about 2.5 MeV), a Maxwellian spectrum at thermal energies and a Fermi (1/E) spectrum between the fast and thermal energies. The 30-group set boundaries are similar to those of the 26-group set, except the region above 0.4 MeV. The calculation studies of the BFS-62 model were performed with the mentioned 11-group and 30-group libraries.

During all phases of the CRP, the ZMIX code [20] was employed for calculating the composition-dependent cross-sections on the basis of the CCCC data libraries. The code takes into account cross-section self-shielding/temperature effects by employing an f-factor method. A neutron spectrum for a particular composition, computed based on a homogeneous representation, is used for condensing composition-dependent cross-sections. The composition-dependent cross-sections can be produced in different formats, in particular those employed in the DANTSYS [21] and VARIANT [22] codes. ZMIX generates cross-section sets for cell components (fuel, structure, coolant). These sets can be used by DANTSYS for computing cell fluxes in cells of regular (e.g. cylindrical) geometry. For taking into account heterogeneity effects, ZMIX is then applied again: to employ these cell fluxes for performing cross-section homogenization and condensation. ZMIX can also be used (as well as DANTSYS and VARIANT) in a calculation route defined in the input of an extended version of the reactor code system RHEIN [23].

In the Phase 5 benchmark calculations after the ZMIX processing, (a) 11-group composition-dependent cross-sections were obtained from the 11-group library and (b) 21-group composition-dependent cross-sections were obtained from the 30-group library by using the

composition-dependent homogeneous spectra computed and used for averaging in ZMIX. The results of preliminary calculations have shown a large deviation of the absolute core reactivity (more than 1%) from the experimental value in the 11-group case. The main reason of this deviation was traced back to using of rather old evaluated data for ^{235}U . Then ^{235}U data in the 11-group library were replaced by the JEFF 3.0 based ^{235}U data.

Three-dimensional calculations with the 11- and 21-group composition dependent cross-sections were performed with the isotropic options of the VARIANT nodal transport code in Hex-Z geometry. Different angular discretization options were tried: diffusion and simplified P_3 (SP_3) in the 11-group case; diffusion, SP_3 , and P_3 in the 21 group case. Both SP_3 and P_3 are neutron transport options, but in the SP_3 case a reduced (compared to P_3) set of spherical harmonics is applied. Higher angular flux discretization (P_5) and anisotropic scattering (up to P_3) options of VARIANT were tried for a few cases. However, the results do not differ appreciably from the P_3/P_0 (flux/scattering order) ones.

2.2.5. IGCAR

The neutron cross-section library used during Phases 1 and 2 is the modified version of Cadarache version II 25 group library, CV2M. Cross-sections of some isotopes like ^{241}Pu , Cr, Ni have been replaced by newly processed cross-sections from JENDL-2 library. This library was found to give better results than a fully JENDL-2 based library for FBR cores in the 500 MW(e) size.

The computer codes, ALCIALMI, NEWPERT (perturbation theory) and ALEX (power distribution and reaction rates) were used for two dimensional calculations in Phase 1 analysis. The computer codes, 3DB, 3DPERT (perturbation theory) and 3DBAL (power distribution and reaction rates) were utilized for three dimensional calculations in Phase 2 analysis. All the computations were made based on diffusion theory methods in 25 neutron energy groups. The Doppler coefficient of steel was not estimated, because temperature dependant resonance cross-section tables for Fe, Cr and Ni were not available in CV2M. Transport theory effects were not included in the computations. Powers have been obtained from isotopewise fission and capture powers at the points of fission and capture, respectively in the calculation of power distribution.

The neutron cross-section library used in the Phase 3 and Phase 5 benchmark calculations is XSET98 commissioned recently in IGCAR. XSET98 data set gives group constants for 26 energy groups - from thermal to 14 MeV. It uses ABBN type self-shielding factor table. Two dimensional diffusion theory code NEWALCI, which is a modified version of ALCIALMI with a routine for obtaining region dependent spectra, is used to obtain region dependent spectrum shapes. These region dependent spectra were used by the 3D code FARCOBAB to obtain condensed microscopic and macroscopic cross-sections for k_{eff} and burnup calculations. Ten groups were selected for 3D core calculations. Burnup calculation has been done by dividing the core into different burnup zones in both axial and radial directions. A total of 30 burnup zones and 10692 burnable meshes were considered.

For the heterogeneous model, the data supplied by IPPE on fuel and absorber rod SHR were used. Fuel and blanket cell calculations were performed using 1D transport code NCELL which uses interface current method of solution of neutron transport. For SHR heterogeneity treatment, computer code COHINT was used. COHINT solves 2D neutron transport equation in cluster geometry by first flight collision probability method.

The Phase-5 benchmark models were analysed by diffusion theory. Three-dimensional calculations were done by TREDFR code [24] in 26 groups with 6 triangular meshes per fuel assembly. The number of triangles was 24,414. Total axial meshes were 54. It is estimated that further increase in axial meshes will not change results significantly. The convergence criteria were 0.000001 for k_{eff} and for point wise fission source, 0.001. The computations took 10-12 hours per case on 300 Mflops SGI computers.

2.2.6. IPPE

The analysis of the benchmark core in R-Z geometry presentation for Phase 1 has been performed by using the diffusion theory code, RHEIN, and the transport theory code, TWODANT [25], with the Russian standard version of ABBN-93 cross-section library [26] in 26 neutron energy groups. The ABBN-93 cross-section library data were processed into composition-dependent cross-sections by the group constant preparation system, CONSYST [27] and used for the analysis of reactor neutronics and the evaluation of delayed neutron parameters. The same spatial discretization and convergence criteria were used for diffusion and transport theory calculations. The TWODANT code analysis was made in P_3S_8 approximation. Both codes, RHEIN and TWODANT, employed first order perturbation theory relationships for determining space distribution of reactivity coefficients.

In the Phase 2 benchmark analysis, the calculations were mainly carried out with the new version, ABBN-93.1 cross-section library. This library includes 299-group data for 16 ‘main’ reactor isotopes and 28-group data for other isotopes. The 26-group composition-dependent cross-sections were obtained from this library, 299-group weighting spectrum being computed in CONSYST by employing the B2-approximation, the current-weighting option being used for all transport cross-sections. However, for reactivity evaluation an improved approach to be applied in the future will be to use flux weighted transport cross-sections for the steel reflector. This effect is estimated to increase in the absolute reactivity of the BFS-62-3A core by about 260 pcm. Basic core calculations for the Hex-Z model were performed with the use of the diffusion theory code, TRIGEX [28] and an 18-group cross-section set including diffusion coefficients. The 18 group cross-section set was obtained for each homogeneous composition by collapsing 26 group effective cross-sections with the weight of 26 group region dependent spectrum of neutron flux calculated by special module of TRIGEX code on the stage of preliminary iterations. Transport theory calculation results are obtained by introducing the transport correction to the TRIGEX diffusion theory calculation results. That is, transport values for

$$\text{reactivity coefficient (RC)} \text{ were given by } RC_{\text{HEX},Z}^* = RC_{\text{HEX},Z}^{\text{Diff}} \frac{RC_{R,Z}^{\text{Transp}}}{RC_{R,Z}^{\text{Diff}}}.$$

The TRIGEX code package was also used for perturbation theory calculations, based on diffusion first-order and exact perturbation theories to determine material worth and reactivity coefficients caused by the core expansion. Expansion reactivity coefficients were obtained based on the diffusion first order perturbation theory using similarity theory relationships (Shikhov’s formula), instead of the direct calculation approach used by the other participants.

IPPE performed simplified transient analyses of the ULOF accident in the hybrid BN-600 benchmark core using the results prepared by the CRP participants in Phases 1 and 2. In these simplified transient analyses, the contribution of individual reactivity coefficients to the transient is defined relative to the magnitudes of other reactivity effects in the balance as well as by the scheme using the coefficients, e.g. radial expansion. The progression of the ULOF transient is characterised by a reactivity balance between the fuel Doppler effect and radial core expansion. No principal differences in the progression of the ULOF transient was found in cases using the reactivity coefficients supplied by the different participants. The advanced methods used for obtaining reactivity coefficients give the following changes to the results from the ULOF transient: ~14 MW in maximum power; ~8% in total reactivity; ~7°C in sodium temperature and less than 10°C in fuel temperature. For the hybrid BN-600 core the influence of reactivity changes due to sodium density change on the accident process appears to be negligible.

In the Phase 5 benchmark calculations, the main series of calculations were performed using three-dimensional Hex-Z diffusion code TRIGEX with the ABBN-93 26 groups cross-section set [26]. For the purpose of the Phase 5 benchmark analysis, precise calculations were also carried out to provide equivalent experimental data and associated corrections for the criticality and sodium void reactivity effect (SVRE) values of the BFS-62-3A core using the Monte Carlo code MMKKENO [29] and the discrete ordinates code TWODANT. The MMKKENO and TWODANT calculations were based on the common system of group constants prepared by CONSYST [10] using the ABBN93.01a group data library. The MMKKENO calculations for the criticality used 299-group ABBN-93

cross-section set and P5 scattering approximation. The MMKKENO calculations were performed with 10 million active histories, and the statistical error was in the range $\pm 0.015\text{--}0.017\%$. The subgroup approximation was used for the ^{238}U isotope with the total number of about 450 groups.

To start calculations a ‘reference’ or ‘as built’ heterogeneous model was specified for the BFS-62-3A core. The heterogeneous model fully represents the real structure of the critical assembly without any simplification. In particular, it precisely represents specific compositions made of each single pellet and its can as well as the BFS tubes and the inter-tube sticks. An ‘exact’ homogeneous model was then constructed, based on the geometry of the ‘as built’ heterogeneous model by averaging the pellet compositions with their volumes so that the net material balance was preserved. Finally a ‘simplified’ homogeneous model was constructed so that all axial sizes of the fuel and control rods were adjusted to one consistent value, and the bottom part of the core support, grid plate and upper (empty) part of the tubes were removed. Using these homogeneous models the total heterogeneity and modelling effects were determined. Monte Carlo calculations were used to evaluate the correction for the whole core reactivity while the one-dimensional collision probability code FFCP was used to evaluate heterogeneity corrections for the SVRE values.

The uncertainty for the equivalent measured data for the criticality and SVRE values was evaluated to be a quadrature sum of the experimental uncertainty and the uncertainty associated with the bias estimated as one fourth of the applied correction factor.

Sodium void worths were calculated using the diffusion code TRIGEX with ABBN-93 26 group constants. The code TWODANT with S_8 transport approximation was used for evaluation of the transport effect based on the RZ model with homogeneously prepared constants. Since the BFS-62-3A core has no radial symmetry, models were constructed both for ‘key region’ and for ‘green region’ separately. Meshes with ~ 2 cm and ~ 1 cm were used. The transport effect was determined as the difference of extrapolated k_{eff} values obtained in diffusion and S_8 transport approximation for the aforementioned fine mesh. The TWODANT results for the transport effect were divided by six taking into account 60° sector of sodium void regions.

2.2.7. JNC

JNC has applied the following methodology to the Phase 1 and 2 benchmark analyses:

- Nuclear data library: JENDL-3.2 [30]
- Group constants: 70-group, ABBN-type self-shielding factor table
- Delayed neutron yield: R. J. Tuttle (1979)
- Delayed neutron yield fractions and decay constants: G.R. Keepin (1965)
- Delayed neutron spectra: D. Saphier (1977)
- Effective cross-sections: homogeneous, current-weighted transport cross-section (SLAROM code)
- Basic core calculation: 18-group, two-dimensional RZ model and three-dimensional Hex-Z model (CITATION code), in which the region-dependent fission spectra were applied.
- Transport theory and mesh size correction: 18-group, two-dimensional RZ model (TWOTRAN code) and three-dimensional Hex-Z model (NSHEX code based on the S_n -transport nodal method developed by JNC)
- Perturbation calculation: diffusion, first-order perturbation, reactivity mapping method (PERKY code).

Apart from the requested parameters, the following analyses were performed aiming at clarifying the transport effect: Doppler coefficients of fuel and steel by uniform temperature changes in all regions, density reactivity coefficients of sodium, steel, fuel and absorber due to 1% density change in all regions (diffusion and transport, direct calculation).

JNC has applied the following methodology to the Phase 3 benchmark analyses:

- Nuclear data library: JENDL-3.2
- Group constant: 70-group, ABBN-type self-shielding factor table
- Effective cross-section: current-weighted transport cross-section
- Heterogeneous cell model for fuel SA: one-dimensional cylindrical model with Tone's background cross-section method (CASUP code)
- Heterogeneous cell model for control rod: one-dimensional cylindrical super-cell model with the reaction rate distribution preservation method (CASUP code)
- Basic diffusion calculation: 18-group, Benoist's anisotropic D and three-dimensional Hex-Z model (CITATION code), in which the region-dependent fission spectra were applied.
- Transport theory and mesh size correction: 18-group, three-dimensional Hex-Z model (NSHEX code based on the S_n transport nodal method, which was developed by JNC.)

Diffusion and transport theory results are provided for k_{eff} , fuel Doppler coefficient, sodium density coefficient at both the start and end of cycle, and for both homogeneous and heterogeneous core models. In addition, the control rod worth at the start of cycle, and the reactivity loss with burnup, are provided for both homogeneous and heterogeneous geometries.

In the core benchmark analyses, JNC used the JFS-3-J3.2 set for Phase 1, 2 and 3, and the JFS-3-J3.2R after Phase 4, both of which are based on the Japanese evaluated nuclear data library, JENDL-3.2. The JFS-3-J3.2R set is a newly generated and revised version of the JFS set. The effect of the JFS set change in Phase 1, 2 and 3 was estimated during the Phase 4 study [31] and its results are addressed in Appendix VI in the report. The following methodology was applied to the Phase 5 benchmark analyses:

- Nuclear Data Library: JENDL-3.2,
- Group Constant Set JFS-3-J3.2R: 70-group, ABBN-type self-shielding factor table based on JENDL-3.2,
- Effective Cross-section: Current-weighted multi-group transport cross-section,
- Cell model for the BFS as-built tube and pellets:
 - 1.(Case 1) Homogeneous Model based on IPPE definition,
 - 2.(Case 2) Homogeneous atomic density equivalent to JNC's heterogeneous calculation only to cross-check the adjusted correction factors,
 - 3.(Case 3) Heterogeneous model based on JNC's evaluation: One-dimensional plate-stretch model (see Fig. 2.1) with Tone's background cross-section method (CASUP code),
- Basic diffusion Calculation: 18-group and three-dimensional Hex-Z model (by the CITATION code),
 - 1.(Case 1 and 2) Isotropic diffusion coefficients,
 - 2.(Case 3) Benoist's anisotropic diffusion coefficients,
- For sodium void reactivity, the exact perturbation theory was applied both to basic calculation and correction calculations,
- Ultra-fine energy group correction - approx. 100,000 group constants below 50 keV, and ABBN-type 175 group constants with shielding factors above 50 keV,
- Transport theory and mesh size correction: 18-group, three-dimensional Hex-Z model (the MINIHEX code based on the S_4-P_0 transport method, which was developed by JNC).

The effective delayed neutron fraction as the reactivity scale was fixed at 0.00623 by the IPPE evaluation. This value is 0.6% greater than when calculated by the JNC standard method, i.e. Tuttle (1979). The yield fraction and decay constant were from Keepin (1965) and the delayed neutron spectrum from Saphier (1977) was used.

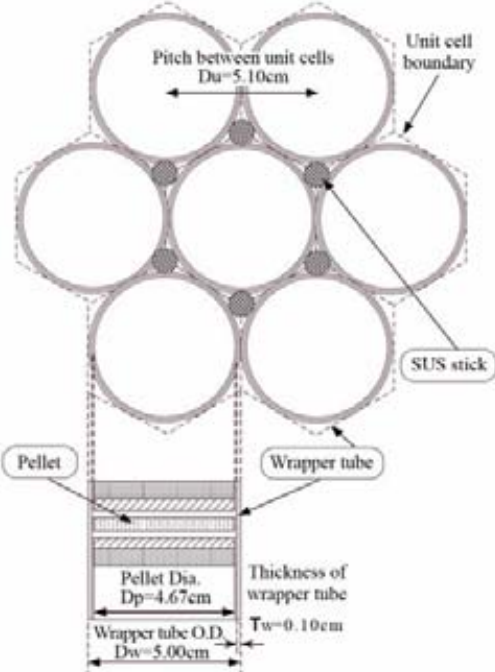


FIG. 2.1. Conceptual description of the BFS-2 fuels.

2.2.8. KAERI

The cross-sections were generated especially for the benchmark model based on the self-shielding f-factor approach. An 80-group neutron cross-section library version, KAFAKX (KAERI FAst XS)/F22 [32] was prepared in the MATXS library format based on the NEA issued version of the JEF-2.2 nuclear data. This version contains infinite dilute cross-sections for various temperatures and Bondarenko self-shielding f-factors. The composition-dependent, 9-group microscopic cross-section sets for all reactor constituent materials were generated from KAFAKX/F22 at the specified temperatures (1500 K for fuel isotopes including fission products and oxygen, 600 K for structural and coolant isotopes) by utilizing the effective cross-section generation module composed of TRANSX [33] and TWODANT [5] codes. The data processing in this module includes resonance and spatial self-shielding corrections, reactor and cell flux solutions and cross-section group collapsing. Neutron spectra necessary for group collapsing were obtained from the P_3S_8 transport theory calculations for the two dimensional, coarse meshed RZ model for the reference configuration with the TWODANT code. The 9-group structure has 1.2 and 1.5 lethargy widths for the first two energy groups, and a 1.0 lethargy width for the remaining 7 energy groups, with the highest energy boundary of 20.0 MeV. The 9-group cross-section set was used for all neutronics calculations.

The neutron multiplication factor k_{eff} and basic neutronics parameters such as neutron flux distribution, reaction rates were calculated by using three kinds of codes such as TWODANT, DIF3D [3] and SOLTRAN [34], associated with the 9-group cross-section set. The TWODANT code employing discrete ordinates approximation was used for two-dimensional (RZ) model calculations. The DIF3D and SOLTRAN codes were utilized for three-dimensional (Hex-Z) model calculations. The DIF3D code employs the coarse-mesh nodal diffusion approximation to the hexagonal-z geometry model. The SOLTRAN code that has been newly developed to improve the accuracy of the neutronics solver of the K-CORE System, solves a nodal simplified P_2 (SP_2) transport equation in hexagonal geometry.

Various reactivity parameters were calculated from either direct flux computations for the unperturbed and perturbed systems or the first order perturbation method based on diffusion theory using the PERT-K code [35]. The PERT-K code solves first order perturbation theory equations using the forward and adjoint flux solutions obtained from DIF3D calculations. The effective delayed neutron fraction, β_{eff} , was calculated by using the BETA-K code [36] that generates kinetic parameters

utilizing the DIF3D forward and adjoint flux solutions. For this calculation, the delayed neutron data such as yield values for 6 delayed neutron groups were prepared from the ENDF/B-VI file.

In the Phase 3 benchmark calculations, the effective multiplication factor k_{eff} and basic neutronics parameters were calculated by the DIF3D code through three-dimensional Hex-Z model calculations. The 3-dimensional burnup calculations were carried out using REBUS-3 [7]. Various reactivity parameters were calculated from either direct flux computations for the unperturbed and perturbed systems, or the first order perturbation theory calculations using the forward and adjoint flux solutions obtained from DIF3D calculations.

Burnup calculation was performed as a single stage calculation. The control rods were taken to be at the fixed insertion of the Phase 2 calculations. The core power was normalized assuming all power is deposited at the point of fission using an energy per fission of 200 MeV for all nuclides and 0 MeV per capture for all nuclides.

In the Phase 5 benchmark calculations, all calculation procedures and evaluations were performed by using the K-CORE System of KAERI. The 25-group effective cross section set has been generated from an 80-group neutron cross-section library, so called KAFAK/F22 and used for all core calculations. Three codes in K-CORE system were used in this benchmark analysis, TRANSX code for the effective cross-section generation, TWODANT transport code for the weighting spectra generation based on the RZ geometry, DIF3D diffusion code for the reactivity calculation in RZ and Hex-Z models. In this analysis, based on the RZ and Hex-Z homogeneous full core models, the sodium void reactivity effects were calculated for the voided regions. Also, several effects were checked such as effect of axial mesh size change, effect of different region spectrum weighting in cross-section collapsing, difference by using JEF-2.2 and ENDF-B/VI libraries.

2.2.9. OKBM

Benchmark analyses for Phases 1, 2 and 3 have been performed based on the specified RZ and Hex-Z models. The calculations were performed for the twelve required items comprehensively for the Hex-Z model using the JARFR code and with a somewhat limited scope for the RZ model using the SYNTES code. Due to the absence of a first-order perturbation theory routine in the SYNTES code, RZ spatial distributions of the reactivity coefficients were computed only for the most significant regions by direct k_{eff} calculations. All calculations have been performed using the diffusion approximation. OKBM activity was focused on the following points:

- Development of the basic Hex-Z benchmark model;
- Heterogeneous model development to complete the Phase 3 definition;
- Calculations relevant to the Phase 3 benchmark;
- Recalculation of the reactivity coefficients distributions with the use of fine mesh instead of coarse mesh method;
- Transient analysis based on reactivity coefficients obtained for Phase 2.

The additional version of a benchmark with the compositions and detailed geometry description for heterogeneous representation of FSAs and SHR was prepared.

The OKBM participation in Phase 3 of the benchmark analyses consists of rod worth, burnup, fuel Doppler and sodium density coefficients evaluations, based on Hex-Z homogeneous model only. The calculations have been performed applying the diffusion JARFR code with ABBN-78 cross-sections library as for Phase 2 studies. The results have been obtained with the use of coarse mesh method and improved algorithm equivalent to fine mesh method (6 triangular meshes per hexagon).

The calculations for revised analysis of the detailed reactivity coefficients distribution were carried out with the use of the fine mesh size and increased energy groups number in few-group calculation. Additionally the influence on results of the axial and planar mesh size, the number and principle of the boundaries choice for the few group energy division were investigated separately. OKBM also

proposed the principle of an optimum choice of energy group boundaries for the few group schemes for sodium density coefficient and its results were presented.

For transient studies ULOF transient calculations were performed with the SAS4A code and the simplified model, using the 8 (according to the number of CRP participants) sets of input data prepared in Phase 2. The existing spread in the reactivity coefficients was investigated in terms of the impact given to consequent spread in the basic integral parameters of the initial ULOF accident stage. A correlation of the spread in each reactivity coefficient with the values of corresponding full current reactivity components was also analyzed to understand the transient behaviors.

3. DESCRIPTIONS AND ANALYSES OF BENCHMARK PROBLEMS

3.1. RZ homogeneous benchmark (Phase 1)

3.1.1. RZ benchmark model

The RZ benchmark is a two dimensional representation of the Hex-Z benchmark. The two dimensional RZ benchmark has been performed prior to the three dimensional Hex-Z benchmark, as addition to the basic three dimensional benchmark (Phase 2).

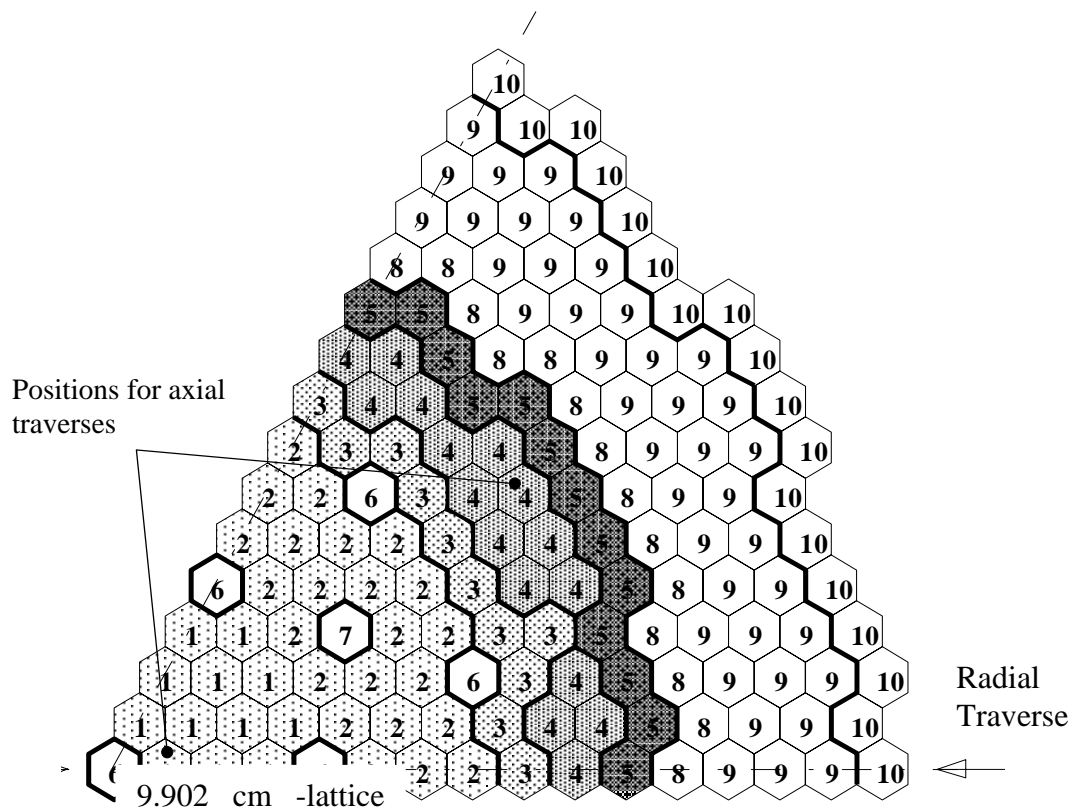
The calculational model corresponds to the 1470 MW•th total power BN-600 reactor at the beginning of an equilibrium cycle, when the impact of the control rods is the strongest. The core consists of a low enrichment inner zone (LEZ), a middle enrichment zone (MEZ) and a high enrichment outer zone (HEZ). Between MEZ and HEZ a mixed oxide zone (MOX) is located. Three control rod zones (SHRs) and one scram rod zone (SCR), consisting of 19 shim control rods and 6 scram control rods respectively, are interspersed radially in LEZ. The outer core zone is bounded by two steel shielding zones (SSAs), followed by one row of radial reflector subassembly (SA). The boundary condition $\varphi = 0$ is set.

A 60° sector of the layout of the benchmark core calculational model is shown in Fig. 3.1. This core layout will also be used as the Hex-Z calculational model in the Phase 2 and 3 analyses.

Differentiation of the compositions with respect to refuelling batches has not been considered: batch-averaged compositions are used, and the heterogeneous structure of the core subassemblies (SAs) has also been ignored. Differentiation of fissile fuel compositions as a function of core height is also not taken into account. However, differentiation of the axial blanket compositions as a function of height has been retained.

The compositions specified for each cell from top to bottom are indicated in Fig. 3.2. The general description of the compositions for various SA types is presented in Table 3.1, while the arrangement of the compositions and cell heights are given in Table 3.2. From the composition specifications, each enriched fuel zone with axially uniform atomic fractions has a burnup of 2-3%. The LEZ, MEZ and HEZ have uranium enrichments of 17, 21 and 26 wt% for feed fuel, respectively. The MOX contains plutonium of enrichment 21.3 wt% with 93.8 wt% ^{239}Pu content for feed fuel. In these specifications, it has been assumed that one fission produces one fission product (FP), corresponding to the definition of FP cross-section in nuclear calculations. All fuel isotopes have been modelled at a uniform temperature of 1500 K and all structural and coolant isotopes are at a uniform temperature of 600 K.

The RZ calculational model indicating the axial positions of the control rods is given in Fig. 3.3. In the SHR zone the bottom of the absorber is parked at the core midplane, whereas in the SCR zone the absorber is parked above the enriched fuel region. Axially, starting from the bottom, each driver fuel zone contains a lower reflector zone (20 cm), lower axial blanket (LB) zone (35.2 cm) and reflector zone (20.0 cm).



Subassembly Types

1, 2 - LEZ SA

3 - MEZ SA

4 - MOX SA

5 - HEZ SA

6 - SHR

7 - SCR

8 - SSA (1st row)

9 - SSA (2nd-4th rows)

10 - Radial reflectors

FIG. 3.1. Benchmark model layout (60° sector, rational symmetry).

Layer thickness (cm)	1 LEZ1 (inner)	2 LEZ2, 3 (outer)	3 MEZ	4 MOX	5 HEZ	6 SHR	7 SCR	8 SSA1 (1 st row)	9 SSA2 (2 nd -4 th rows)	10 RR
20.0	34	34	34	34	34	34	34	34	34	33
24.7	21	22	23	24	25	26	28	31	32	33
5.5	16	17	18	19	20	26	29	31	32	33
52.2	1	2	3	4	5	26	29	31	32	33
52.2	1	2	3	4	5	27	30	31	32	33
5.5	11	12	13	14	15	27	30	31	32	33
29.7	6	7	8	9	10	27	30	31	32	33
20.0	34	34	34	34	34	34	34	34	34	33

FIG. 3.2. Arrangement of the compositions and cell heights.

TABLE 3.1. GENERAL DESCRIPTION OF VARIOUS SUBASSEMBLY TYPE COMPOSITIONS

SA type No.	SA type	Composition No.	Description of composition
1	LEZ SA (inner): LEZ1	1 6 11 16 21 34	Fissile part Lower part of lower axial blanket Upper part of lower axial blanket Lower part of upper axial blanket Upper part of upper axial blanket Axial reflector
2	LEZ SA (outer): LEZ2, LEZ3	2 7 12 17 22 34	Fissile part Lower part of lower axial blanket Upper part of lower axial blanket Lower part of upper axial blanket Upper part of upper axial blanket Axial reflector
3	MEZ SA	3 8 13 18 23 34	Fissile part Lower part of lower axial blanket Upper part of lower axial blanket Lower part of upper axial blanket Upper part of upper axial blanket Axial reflector
4	MOX SA	4 9 14 19 24 34	Fissile part Lower part of lower axial blanket Upper part of lower axial blanket Lower part of upper axial blanket Upper part of upper axial blanket Axial reflector
5	HEZ SA	5 10 15 20 25 34	Fissile part Lower part of lower axial blanket Upper part of lower axial blanket Lower part of upper axial blanket Upper part of upper axial blanket Axial reflector
6	SHR	26 27 34	Absorbing part Follower + rod tail Axial reflector
7	SCR	28 29 30 34	Absorbing part in upper axial blanket Follower + rod tail Follower Axial reflector
8	SSA (1 st row): SSA1	31 34	Steel shielding Axial reflector
9	SSA(2 nd –4 th rows): SSA2	32 34	Steel shielding Axial reflector
10	RR	33	Radial reflector

TABLE 3.2. ISOTOPIC DENSITY

(Unit: 10^{24} nuclei / cm 3)

Isotope	Composition No.				
	1	2	3	4	5
^{235}U	.1169E-02*	.1180E-02	.1485E-02	.1686E-04	.1932E-02
^{236}U	.5324E-04	.5094E-04	.5613E-04	.5803E-06	.5157E-04
^{238}U	.6676E-02	.6686E-02	.6379E-02	.6377E-02	.6013E-02
^{239}Pu	.1392E-03	.1329E-03	.1136E-03	.1504E-02	.7589E-04
^{240}Pu	.4378E-05	.3911E-05	.2878E-05	.1343E-03	.1371E-05
^{241}Pu	.1151E-06	.8041E-07	.5895E-07	.8572E-05	.3803E-07
^{242}Pu	.0000E+00	.0000E+00	.0000E+00	.6862E-06	.0000E+00
FP**	.2427E-03	.2315E-03	.2530E-03	.2229E-03	.2125E-03
O	.1658E-01	.1658E-01	.1658E-01	.1653E-01	.1658E-01
Na	.7549E-02	.7549E-02	.7549E-02	.7549E-02	.7549E-02
Fe	.1287E-01	.1287E-01	.1287E-01	.1287E-01	.1287E-01
Cr	.2848E-02	.2848E-02	.2848E-02	.2848E-02	.2848E-02
Ni	.1627E-02	.1627E-02	.1627E-02	.1627E-02	.1627E-02
Mo	.2176E-03	.2176E-03	.2176E-03	.2176E-03	.2176E-03
^{10}B	-	-	-	-	-
^{11}B	-	-	-	-	-
C	-	-	-	-	-
Isotope	6	7	8	9	10
^{235}U	.2490E-04	.2490E-04	.2520E-04	.2560E-04	.2560E-04
^{236}U	.6000E-06	.6000E-06	.5000E-06	.4000E-06	.4000E-06
^{238}U	.8901E-02	.8901E-02	.8915E-02	.8931E-02	.8931E-02
^{239}Pu	.7680E-04	.7680E-04	.6470E-04	.5110E-04	.5110E-04
^{240}Pu	.1500E-05	.1500E-05	.1000E-05	.7000E-06	.7000E-06
^{241}Pu	.3000E-07	.3000E-07	.2000E-07	.2000E-07	.2000E-07
^{242}Pu	.0000E+00	.0000E+00	.0000E+00	.0000E+00	.0000E+00
FP	.8200E-05	.8200E-05	.6600E-05	.4600E-05	.4600E-05
O	.1803E-01	.1803E-01	.1803E-01	.1803E-01	.1803E-01
Na	.7549E-02	.7549E-02	.7549E-02	.7549E-02	.7549E-02
Fe	.1287E-01	.1287E-01	.1287E-01	.1287E-01	.1287E-01
Cr	.2848E-02	.2848E-02	.2848E-02	.2848E-02	.2848E-02
Ni	.1627E-02	.1627E-02	.1627E-02	.1627E-02	.1627E-02
Mo	.2176E-03	.2176E-03	.2176E-03	.2176E-03	.2176E-03
^{10}B	-	-	-	-	-
^{11}B	-	-	-	-	-
C	-	-	-	-	-

TABLE 3.2. ISOTOPIC DENSITY (CONTINUED)

(Unit: 10^{24} nuclei / cm 3)

Isotope	Composition No.				
	11	12	13	14	15
^{235}U	.2340E-04	.2360E-04	.2400E-04	.2440E-04	.2480E-04
^{236}U	.9000E-06	.8000E-06	.7000E-06	.6000E-06	.6000E-06
^{238}U	.8825E-02	.8835E-02	.8854E-02	.8873E-02	.8896E-02
^{239}Pu	.1337E-03	.1264E-03	.1107E-03	.9570E-04	.7750E-04
^{240}Pu	.3800E-05	.3300E-05	.2500E-05	.1800E-05	.1400E-05
^{241}Pu	.9000E-07	.7000E-07	.5000E-07	.4000E-07	.6000E-07
^{242}Pu	.0000E+00	.0000E+00	.0000E+00	.0000E+00	.0000E+00
FP	.2580E-04	.2400E-04	.2110E-04	.1770E-04	.1260E-04
O	.1803E-01	.1803E-01	.1803E-01	.1803E-01	.1803E-01
Na	.7549E-02	.7549E-02	.7549E-02	.7549E-02	.7549E-02
Fe	.1287E-01	.1287E-01	.1287E-01	.1287E-01	.1287E-01
Cr	.2848E-02	.2848E-02	.2848E-02	.2848E-02	.2848E-02
Ni	.1627E-02	.1627E-02	.1627E-02	.1627E-02	.1627E-02
O	.2176E-03	.2176E-03	.2176E-03	.2176E-03	.2176E-03
^{10}B	-	-	-	-	-
^{11}B	-	-	-	-	-
C	-	-	-	-	-
Isotope	16	17	18	19	20
^{235}U	.2440E-04	.2460E-04	.2470E-04	.2490E-04	.2510E-04
^{236}U	.6000E-06	.6000E-06	.5000E-06	.5000E-06	.5000E-06
^{238}U	.8870E-02	.8877E-02	.8885E-02	.8893E-02	.8909E-02
^{239}Pu	.9900E-04	.9340E-04	.8570E-04	.7950E-04	.6700E-04
^{240}Pu	.1900E-05	.1600E-05	.1300E-05	.1200E-05	.1000E-05
^{241}Pu	.3000E-07	.2000E-07	.2000E-07	.2000E-07	.4000E-07
^{242}Pu	.0000E+00	.0000E+00	.0000E+00	.0000E+00	.0000E+00
FP	.1710E-04	.1610E-04	.1540E-04	.1420E-04	.1060E-04
O	.1803E-01	.1803E-01	.1803E-01	.1803E-01	.1803E-01
Na	.7549E-02	.7549E-02	.7549E-02	.7549E-02	.7549E-02
Fe	.1287E-01	.1287E-01	.1287E-01	.1287E-01	.1287E-01
Cr	.2848E-02	.2848E-02	.2848E-02	.2848E-02	.2848E-02
Ni	.1627E-02	.1627E-02	.1627E-02	.1627E-02	.1627E-02
Mo	.2176E-03	.2176E-03	.2176E-03	.2176E-03	.2176E-03
^{10}B	-	-	-	-	-
^{11}B	-	-	-	-	-
C	-	-	-	-	-

TABLE 3.2. ISOTOPIC DENSITY (CONTINUED)

(Unit: 10^{24} nuclei / cm 3)

Isotope	Composition No.				
	21	22	23	24	25
^{235}U	.2560E-04	.2560E-04	.2570E-04	.2580E-04	.2580E-04
^{236}U	.4000E-06	.4000E-06	.3000E-06	.3000E-06	.3000E-06
^{238}U	.8929E-02	.8929E-02	.8933E-02	.8936E-02	.8942E-02
^{239}Pu	.5250E-04	.5250E-04	.4870E-04	.4630E-04	.4130E-04
^{240}Pu	.6000E-06	.6000E-06	.5000E-06	.5000E-06	.5000E-06
^{241}Pu	.0000E+00	.0000E+00	.0000E+00	.0000E+00	.2000E-07
^{242}Pu	.0000E+00	.0000E+00	.0000E+00	.0000E+00	.0000E+00
FP	.4900E-05	.4900E-05	.4500E-05	.4200E-05	.3400E-05
O	.1803E-01	.1803E-01	.1803E-01	.1803E-01	.1803E-01
Na	.7549E-02	.7549E-02	.7549E-02	.7549E-02	.7549E-02
Fe	.1287E-01	.1287E-01	.1287E-01	.1287E-01	.1287E-01
Cr	.2848E-02	.2848E-02	.2848E-02	.2848E-02	.2848E-02
Ni	.1627E-02	.1627E-02	.1627E-02	.1627E-02	.1627E-02
Mo	.2176E-03	.2176E-03	.2176E-03	.2176E-03	.2176E-03
$^{10}\text{B}^{10}$	-	-	-	-	-
^{11}B	-	-	-	-	-
C	-	-	-	-	-
Isotope	26	27	28	29	30
^{235}U	-	-	-	-	-
^{236}U	-	-	-	-	-
^{238}U	-	-	-	-	-
^{239}Pu	-	-	-	-	-
^{240}Pu	-	-	-	-	-
^{241}Pu	-	-	-	-	-
^{242}Pu	-	-	-	-	-
FP	-	-	-	-	-
O	-	-	-	-	-
Na	.9653E-02	.1958E-01	.1126E-01	.1958E-01	.2027E-01
Fe	.1310E-01	.7111E-02	.1092E-01	.7111E-02	.5060E-02
Cr	.2799E-02	.1216E-02	.2250E-02	.1216E-02	.8655E-03
Ni	.1322E-02	.1212E-03	.9109E-03	.1212E-03	.1438E-04
Mo	.3140E-03	.7655E-04	.2360E-03	.7655E-04	.8620E-04
^{10}B	.5113E-02	-	.1780E-01	-	-
^{11}B	.2045E-01	-	.4450E-02	-	-
C	.6392E-02	-	.5560E-02	-	-

TABLE 3.2. ISOTOPIC DENSITY (CONTINUED)

(Unit: 10^{24} nuclei / cm 3)

Isotope	Composition No.			
	31	32	33	34
^{235}U	-	-	-	-
^{236}U	-	-	-	-
^{238}U	-	-	-	-
^{239}Pu	-	-	-	-
^{240}Pu	-	-	-	-
^{241}Pu	-	-	-	-
^{242}Pu	-	-	-	-
FP	-	-	-	-
O	-	-	-	-
Na	.5638E-02	.5875E-02	.4860E-02	.1729E-01
Fe	.5252E-01	.5179E-01	.4630E-01	.1368E-01
Cr	.7636E-02	.7530E-02	.1340E-01	.2344E-02
Ni	.7447E-03	.7332E-03	.6280E-02	.4948E-04
Mo	.3589E-03	.3550E-03	-	.1487E-03
^{10}B	-	-	-	-
^{11}B	-	-	-	-
C	-	-	-	-

* Read as $.1169\text{E}-02 = .1169 \times 10^{-2}$.** For all compositions, ^{235}U fission products will be used.

FIG. 3.3. Calculational scheme of the RZ model indicating the axial position of the control rods.

3.1.2. Description of the parameters calculated

In Phase 1, the effective multiplication factor (k_{eff}), and the integral value and/or its spatial distribution of reactivity coefficients including kinetic parameters were calculated for the RZ calculational model by diffusion and transport theory methods, using homogeneous representations of the material regions. Spatial distributions of reactivity coefficients were obtained by first order perturbation theory method. Detailed description for each calculational Section is given in the followings.

3.1.2.1. Effective multiplication factor (k_{eff})

The effective multiplication factor is calculated for the reference conditions defined in Section 3.1.1.

3.1.2.2. Fuel Doppler coefficient (K_D^{fuel})

The fuel Doppler coefficient is calculated for a change in fuel temperature from 1500 K (T_1) to 2100 K (T_2). Fuel isotopes consist of ^{235}U , ^{236}U , ^{238}U , ^{239}Pu , ^{240}Pu , ^{241}Pu , ^{242}Pu , ^{16}O , and FP. The fuel Doppler coefficient is defined as:

$$K_D^{\text{fuel}} = \frac{k_{\text{eff}}^2 - k_{\text{eff}}^1}{k_{\text{eff}}^2 \cdot k_{\text{eff}}^1} \cdot \frac{1}{\ln\left(\frac{T_2}{T_1}\right)},$$

where $T_1 = 1500$ K and $T_2 = 2100$ K.

The spatial distribution of the fuel Doppler coefficients, integrated over energy and isotopes, is given by subassembly type (see Fig. 3.1), and by axial regions. The axial mesh structure consists of 20.0 cm \times 1 for lower AR, 5.5, 10.0, 19.7 cm for LB, 10.44 cm \times 10 for core, 5.5, 5.0 cm \times 5, 4.7 cm for UB, and 20.0 cm \times 1 for upper AR in the spatial distribution.

3.1.2.3. Steel Doppler coefficient (K_D^{steel})

The steel Doppler coefficient is calculated for a change in steel temperature from 600 K (T_1) to 900 K (T_2). Steel isotopes consist of Fe, Cr, Ni, and Mo. These isotopes are perturbed in all zones. The steel Doppler coefficient is defined as:

$$K_D^{\text{steel}} = \frac{k_{\text{eff}}^2 - k_{\text{eff}}^1}{k_{\text{eff}}^2 \cdot k_{\text{eff}}^1} \cdot \frac{1}{\ln\left(\frac{T_2}{T_1}\right)},$$

where $T_1 = 600$ K and $T_2 = 900$ K.

The spatial distribution of the steel Doppler coefficients, integrated over energy and isotopes, is given as for Section 3.1.2.2.

3.1.2.4. Sodium density coefficient (W_{Na})

The sodium density coefficient is calculated for a 1% change in sodium density in all zones, and is defined as:

$$W_{\text{Na}} = \frac{\partial k}{\partial \rho_{\text{Na}}} \cdot \frac{\rho_{\text{Na}}}{k^2},$$

which is calculated by 1st order perturbation theory.

The spatial distribution, integrated over energy and isotopes, is given as for Section 3.1.2.2.

3.1.2.5.Steel density coefficient (W_{steel})

The steel density coefficient is calculated for a 1% change in steel density in all zones, and is defined as:

$$W_{steel} = \frac{\partial k}{\partial \rho_{steel}} \cdot \frac{\rho_{steel}}{k^2},$$

which are calculated by 1st order perturbation theory.

The spatial distribution, integrated over energy and isotopes, is given as for Section 3.1.2.2.

3.1.2.6.Fuel density coefficient (W_{fuel})

The fuel density coefficient is calculated for a 1% change in fuel density, and is defined as:

$$W_{fuel} = \frac{\partial k}{\partial \rho_{fuel}} \cdot \frac{\rho_{fuel}}{k^2},$$

which is calculated by 1st order perturbation theory.

Fuel isotopes consist of ²³⁵U, ²³⁶U, ²³⁸U, ²³⁹Pu, ²⁴⁰Pu, ²⁴¹Pu, ²⁴²Pu, ¹⁶O, and FP. The spatial distribution, integrated over energy and isotopes, is given as for Section 3.1.2.2.

3.1.2.7.Absorber density coefficient (W_{abs})

The absorber density coefficient is calculated for a 1% change in absorber density, and is defined as:

$$W_{abs} = \frac{\partial k}{\partial \rho_{abs}} \cdot \frac{\rho_{abs}}{k^2},$$

which is calculated by 1st order perturbation theory.

Absorber isotopes consist of ¹⁰B, ¹¹B, and C. The spatial distribution, integrated over energy and isotopes, is given as for Section 3.1.2.2.

3.1.2.8.Expansion coefficients

a) Axial expansion coefficient (R_{ax})

The axial expansion coefficient is calculated for a 1% uniform axial expansion of fuel, steel and absorber within the model. Isotope masses are conserved except for sodium, which is kept at constant number density. The axial expansion coefficient is defined as:

$$R_{ax} = \frac{\partial k_{all}}{k^2} \Big/ \frac{\partial H}{H_0}.$$

Only one value is produced, integrated over energy, isotopes and space.

b) Radial expansion coefficient (R_{rad})

The radial expansion coefficient is calculated for a 1% uniform radial expansion of fuel, steel and absorber within the model. Isotope masses are conserved except for sodium, which is kept at constant number density. The radial expansion coefficient is defined as:

$$R_{\text{rad}} = \frac{\partial k_{\text{all}}}{k^2} \Big/ \frac{\partial R}{R_0}.$$

Only one value is produced, integrated over energy, isotopes and space.

3.1.2.9. Power distribution

Energy is assumed to be deposited at its point of production. The spatial core power distribution, integrated over energy, is given as for Section 3.1.2.2, with normalization to a total power of 1470 MW.

3.1.2.10. β_{eff} — values

The effective delayed neutron fractions in standard 6 groups are calculated by integrating over isotopes including decay constants. The prompt neutron lifetime is also given.

3.1.2.11. Reaction rate distributions

Radial and axial microscopic reaction rates are calculated for ^{235}U fission, ^{238}U fission and ^{238}U capture. Local microscopic cross-sections are used where isotopes are present, and infinite dilution cross sections are used where they are absent.

The radial reaction rates are presented on a radial traverse 10.44 cm below core centre line of the radial mesh regions.

The axial reactions rates are computed at the centre of the first LEZ region (at 23.6 cm), and at the centre of the MOX region, at the centre of the axial mesh structure used for reactivity coefficient edits.

3.1.3. Comparison of results

3.1.3.1. Integral reactivity coefficients

Integral reactivity coefficients obtained by the participants for the Phase 1 benchmark are given in Tables 3.3–3.11, respectively with the mean value and the standard deviation of the results for each coefficient. The comparison of the diffusion and transport results for Phase 1 generally shows good agreement for most parameters. The results of comparisons of each reactivity coefficient are addressed next in more detail.

In Table 3.3, the RZ diffusion and transport theory calculations predicted the k_{eff} as 1.00270 and 1.01460 with relative standard deviations of 0.63% and 0.78%, respectively. In general, the diffusion theory prediction gives the k_{eff} value smaller by 0.86% than that of the transport theory. The k_{eff} values obtained by CEA/SA and KAERI appear to be larger than the mean value. These larger predictions have been recognized partly attributable to their nuclear data library, i.e. JEF-2.2.

The fuel Doppler coefficients were calculated to be -0.00601 and -0.00674 with a relative standard deviations of 13.1% and 9.2% for diffusion and transport theory calculations, respectively. In Table 3.4, the diffusion theory value is in very good agreement with that from transport theory, less than 1% different.

Table 3.5 shows the results for steel Doppler coefficient obtained by diffusion and transport theory calculations. The steel Doppler coefficients were estimated to be -0.00105 and -0.00127 with relative

standard deviations of 25.7% and 9.4% for these two approximations. Diffusion theory predicts a steel Doppler coefficient that is very similar to that from transport theory. From Table 3.5 the diffusion result is only smaller by 2.53% in magnitude relative to that from transport theory.

In considering the comparison of Doppler coefficients, the steel Doppler was evaluated to be $\sim 1/6$ the magnitude of the fuel Doppler coefficient. The steel Doppler coefficient was also predicted with a larger dispersion than the fuel Doppler coefficient. The larger dispersion in the prediction of the steel Doppler is attributable to the sum of its smaller spatial contributions which are widely spread over the entire reactor system.

The sodium density coefficients are 0.0081 and 0.0032 with relative standard deviations of 57.9% and 25.1% for the diffusion and transport theory results, respectively. In Table 3.6, there exists a relatively large dispersion among participants results using the same method approximation, especially between the diffusion results. There also exists a relatively large discrepancy between the diffusion and transport theory results. It is noted that the ANL results were obtained from the calculations with all the flowing sodium removed, instead of 1% of total sodium removed.

As can be seen in Table 3.7, the steel density coefficient has a considerable dispersion among the results obtained by participants. That is, the steel density coefficients were evaluated to be -0.0123 and -0.0128 with relative standard deviations of 91.1% and 21.9% for diffusion and transport theory calculations, respectively.

The results for the sodium and steel density coefficient indicate that the transport theory method is more appropriate for the calculation of the sodium and steel density coefficients. In addition, the results for the steel density coefficient, even calculated by the transport theory method, show a considerable difference between the results obtained by the participants. This is mainly attributed to differences in the spatial coefficient predictions for non-fuelled regions including control rods, which will be discussed in more detail later.

The fuel density coefficients were predicted to be 0.3470 and 0.3446 with relative standard deviations of 2.4% and 1.4% for diffusion and transport theory calculations respectively. Both results given in Table 3.8 show a good agreement in these approximations. The fuel density coefficient was estimated to be ~ 30 times larger than the steel density coefficient in the Phase 1 diffusion results. The reactivity coefficient distributions show that the fuel density coefficient is positive and the steel density is negative in the core zone, and that their signs are reversed in the blanket zone.

TABLE 3.3. EFFECTIVE MULTIPLICATION FACTORS (k_{eff})

Participant	Diffusion		Transport		Rel. Diff. ²⁾ (%)
	Value	Rel. Dev. ¹⁾ (%)	Value	Rel. Dev. (%)	
ANL	0.99684	-0.58	1.00788	-0.66	-1.10
CEA/SA	1.01676	1.40	1.02298	0.83	-0.61
CIAE	0.99808	-0.46	1.01497	0.04	-1.66
IGCAR	1.00360	0.09			
IPPE	1.00140	-0.13	1.00576	-0.87	-0.43
JNC	1.00423	0.15	1.00948	-0.50	-0.52
KAERI			1.02654	1.18	
OKBM	0.99796	-0.47			
Mean	1.00270		1.01460		-0.86
SD +/-	0.00633		0.00777		0.46

* 1) Relative Deviation from the mean = $(\text{Value} - \text{Mean}) / \text{Mean} \times 100$

* 2) Relative Difference = $(\text{Diffusion} - \text{Transport}) / \text{Transport} \times 100$

TABLE 3.4. FUEL DOPPLER COEFFICIENTS (K_D^{fuel})

Participant	Diffusion		Transport		Rel. Diff. (%)
	Value	Rel. Dev.(%)	Value	Rel. Dev. (%)	
ANL	-0.00652	8.45			
CEA/SA	-0.00679	12.94	-0.00671	-0.48	1.23
CIAE	-0.00499	-16.96			
IGCAR	-0.00462	-23.10			
IPPE	-0.00622	3.45	-0.00628	-6.86	-0.93
JNC	-0.00635	5.59	-0.00621	-7.90	2.25
KAERI			-0.00777	15.24	
OKBM	-0.00659	9.64			
Mean	-0.00601		-0.00674		0.85
SD +/-	0.00079		0.00062		1.33

TABLE 3.5. STEEL DOPPLER COEFFICIENTS (K_D^{steel})

Participant	Diffusion		Transport		Rel. Diff. (%)
	Value	Rel. Dev.(%)	Value	Rel. Dev. (%)	
ANL	-0.00110	5.16			
CEA/SA	-0.00134	28.11	-0.00146	14.80	-8.25
CIAE	-0.00049	-53.53			
IGCAR					
IPPE	-0.00122	16.57	-0.00124	-2.19	-2.01
JNC	-0.00116	10.93	-0.00113	-11.15	2.65
KAERI			-0.00125	-1.45	
OKBM	-0.00097	-7.24			
Mean	-0.00105		-0.00127		-2.53
SD +/-	0.00027		0.00012		4.47

TABLE 3.6. SODIUM DENSITY COEFFICIENTS (W_{Na})

Participant	Diffusion		Transport		Rel. Diff. (%)
	Value	Rel. Dev.(%)	Value	Rel. Dev. (%)	
ANL	0.01749	116.60			
CEA/SA	0.00519	-35.69	0.00343	7.52	51.40
CIAE	0.00211	-73.93			
IGCAR	0.00446	-44.78			
IPPE	0.00898	11.19	0.00211	-33.86	325.54
JNC	0.00765	-5.27	0.00403	26.33	89.83
KAERI					
OKBM	0.01065	31.88			
Mean	0.00808		0.00319		155.59
SD +/-	0.00468		0.00080		121.19

TABLE 3.7. STEEL DENSITY COEFFICIENTS (W_{steel})

Participant	Diffusion		Transport		Rel. Diff. (%)
	Value	Rel. Dev. (%)	Value	Rel. Dev. (%)	
ANL	-0.0384	210.90			
CEA/SA	-0.0112	-9.45	-0.0147	14.96	-23.96
CIAE	-0.0055	-55.61			
IGCAR	-0.0021	-82.72			
IPPE	-0.0053	-57.22	-0.0088	-31.49	-39.72
JNC	-0.0126	2.07	-0.0149	16.53	-15.44
KAERI					
OKBM	-0.0114	-7.97			
Mean	-0.0123		-0.0128		-26.37
SD +/-	0.0112		0.0028		10.06

TABLE 3.8. FUEL DENSITY COEFFICIENTS (W_{fuel})

Participant	Diffusion		Transport		Rel. Diff. (%)
	Value	Rel. Dev. (%)	Value	Rel. Dev. (%)	
ANL	0.3343	-3.67			
CEA/SA	0.3423	-1.36	0.3382	-1.86	1.21
CIAE	0.3492	0.62			
IGCAR	0.3410	-1.73			
IPPE	0.3505	1.00	0.3466	0.56	1.14
JNC	0.3491	0.60	0.3491	1.30	0.00
KAERI					
OKBM	0.3628	4.55			
Mean	0.3470		0.3446		0.78
SD +/-	0.0084		0.0047		0.55

The results for absorber density coefficient predicted by diffusion and transport theory calculations are given in Table 3.9. The absorber density coefficients are -0.0287 and -0.0264 with relative standard deviations of 15.0% and 1.5% in the diffusion and transport theory results, respectively. The diffusion theory predicts the absorber density coefficient larger by 2.5% in its magnitude than that of the transport theory.

The axial expansion coefficients given in Table 3.10 were evaluated to be -0.1394 and -0.1344 with relative standard deviations of 3.2% and 3.0% for diffusion and transport theory calculations. The diffusion theory value was estimated to be larger by 2.9% in its magnitude than the transport theory one.

The radial expansion coefficients obtained by diffusion and transport theory calculations are given in Table 3.11. The diffusion and transport theory method predicted the radial expansion coefficient as -0.4729 and -0.4621 with relative standard deviations of 4.5% and 2.1%, respectively. The diffusion theory value is in very good agreement with that from transport theory, less than 1% different.

It can be seen from the result of comparisons of the expansion coefficients that the diffusion theory generally predicts the expansion coefficients larger by in its magnitude than the transport theory. In comparison of uniform expansion effects in the radial and axial directions, the radial expansion coefficient is ~3 times larger than the axial expansion coefficient for a given relative change in dimension.

3.1.3.2. Kinetic parameters

System kinetic parameters such as the effective delayed neutron fraction (β_{eff}), groupwise effective delayed neutron fractions, prompt neutron lifetime (l_p), and decay constants are given in Tables 3.12–3.15, respectively. Most parameters were obtained by the diffusion theory method and show good agreements among the results provided by each participant.

Tables 3.12 and 3.13 show effective delayed neutron fraction and groupwise effective delayed neutron fractions for 6 delayed neutron groups provided by the participants, respectively. The effective delayed neutron fraction is simply the sum of the groupwise delayed neutron fractions over all groups. The groupwise effective delayed neutron fractions for the 6 delayed neutron group structure used by each participant show a reasonable agreement for each group within 10.0% of relative standard deviation, except for the 6th group and, as a result, predicted with 1.5% of relative standard deviation. The diffusion and transport theory methods predict the same value for the effective delayed neutron fraction, $\beta_{\text{eff}} = 0.00588$. The obtained effective delayed neutron fraction, $\beta_{\text{eff}} = 0.00588$ (588 pcm) is representative of a fast reactor system dominated by ^{235}U fission ($\beta = 0.0064$), but with the contribution from ^{239}Pu ($\beta = 0.0020$).

In Table 3.14, the prompt neutron lifetimes for the given benchmark system are given by 4.547×10^{-7} s and 4.645×10^{-7} s for the diffusion and transport theory methods with 3.0% and 0.0% of relative standard deviation respectively, and the diffusion theory predicts the prompt neutron lifetime smaller by 2.1%. The groupwise decay constants for 6 groups provided by each participant show a good agreement within 2.2% of relative standard deviation except for the 6th group.

TABLE 3.9. ABSORBER DENSITY COEFFICIENTS (W_{abs})

Participant	Diffusion		Transport		Rel. Diff. (%)
	Value	Rel. Dev. (%)	Value	Rel. Dev. (%)	
ANL	-0.0266	-7.30			
CEA/SA	-0.0273	-4.55	-0.0263	-0.55	3.98
CIAE	-0.0391	36.38			
IGCAR	-0.0269	-6.02			
IPPE	-0.0274	-4.19	-0.0260	-1.56	5.44
JNC	-0.0265	-7.51	-0.0270	2.10	-1.85
KAERI					
OKBM	-0.0267	-6.80			
Mean	-0.0287		-0.0264		2.52
SD +/-	0.0043		0.0004		3.15

TABLE 3.10. AXIAL EXPANSION COEFFICIENTS (R_{ax})

Participant	Diffusion		Transport		Rel. Diff. (%)
	Value	Rel. Dev. (%)	Value	Rel. Dev. (%)	
ANL	-0.1446	3.75			
CEA/SA	-0.1378	-1.13	-0.1374	2.25	0.29
CIAE	-0.1432	2.75	-0.1341	-0.18	6.76
IGCAR	-0.1395	0.09			
IPPE	-0.1297	-6.94	-0.1267	-5.71	2.37
JNC	-0.1393	-0.05	-0.1361	1.28	2.35
KAERI			-0.1376	2.36	
OKBM	-0.1415	1.53			
Mean	-0.1394		-0.1344		2.94
SD +/-	0.0045		0.0040		2.36

TABLE 3.11. RADIAL EXPANSION COEFFICIENTS (R_{rad})

Participant	Diffusion		Transport		Rel. Diff. (%)
	Value	Rel. Dev.(%)	Value	Rel. Dev. (%)	
ANL	-0.4872	3.03			
CEA/SA	-0.4650	-1.66	-0.4573	-1.03	1.68
CIAE	-0.4232	-10.51	-0.4603	-0.38	-8.07
IGCAR	-0.4840	2.35			
IPPE	-0.4868	2.95	-0.4787	3.60	1.69
JNC	-0.4812	1.76	-0.4647	0.57	3.55
KAERI			-0.4493	-2.76	
OKBM	-0.4827	2.08			
Mean	-0.4729		-0.4621		-0.29
SD +/-	0.0214		0.0097		4.56

TABLE 3.12. EFFECTIVE DELAYED NEUTRON FRACTIONS (β_{eff})

Participant	Diffusion		Transport		Rel. Diff. (%)
	Value	Rel. Dev.(%)	Value	Rel. Dev. (%)	
ANL	569	-3.21			
CEA/SA	597	1.50	594	0.97	0.51
CIAE	604	2.62			
IGCAR	598	1.64			
IPPE	585	-0.53	583	-0.97	0.42
JNC	586	-0.32			
KAERI					
OKBM	578	-1.71			
Mean	588		588		0.46
SD +/-	11.2		5.7		0.04

TABLE 3.13. GROUPWISE EFFECTIVE DELAYED NEUTRON FRACTIONS

Participant	Delayed neutron group						Total
	1	2	3	4	5	6	
ANL							5.693E-03
CEA/SA	1.700E-04	1.020E-03	9.800E-04	2.280E-03	1.080E-03	4.400E-04	5.970E-03
(Transport)	1.700E-04	1.010E-03	9.700E-04	2.270E-03	1.080E-03	4.400E-04	5.940E-03
CIAE	1.909E-04	1.217E-03	1.123E-03	2.331E-03	9.291E-04	2.447E-04	6.036E-03
IGCAR	1.847E-04	1.196E-03	1.100E-03	2.359E-03	9.024E-04	2.357E-04	5.978E-03
IPPE	1.689E-04	9.739E-04	9.381E-04	2.236E-03	1.091E-03	4.417E-04	5.850E-03
(Transport)	1.687E-04	9.724E-04	9.352E-04	2.226E-03	1.084E-03	4.388E-04	5.826E-03
JNC	1.785E-04	1.162E-03	1.072E-03	2.311E-03	8.933E-04	2.375E-04	5.855E-03
KAERI							
OKBM	1.709E-04	9.741E-04	9.373E-04	2.199E-03	1.069E-03	4.311E-04	5.781E-03
Average	1.753E-04	1.066E-03	1.007E-03	2.277E-03	1.016E-03	3.637E-04	5.881E-03
S.D. +/-	8.466E-06	1.067E-04	7.858E-05	5.495E-05	9.010E-05	1.031E-04	1.089E-04

TABLE 3.14. PROMPT NEUTRON LIFETIMES

Participant	Diffusion		Transport		Rel. Diff. (%)
	Value	Rel. Dev.(%)	Value	Rel. Dev. (%)	
ANL	4.423	-2.73			
CEA/SA	4.687	3.08	4.646	0.01	0.88
CIAE	4.277	-5.94			
IGCAR	4.618	1.56			
IPPE	4.586	0.87	4.645	-0.01	-1.26
JNC	4.620	1.61			
KAERI					
OKBM	4.618	1.55			
Mean	4.547		4.645		-0.19
SD +/-	0.134		0.001		1.07

TABLE 3.15. DECAY CONSTANTS

Participant	Delayed neutron group						(Unit: sec ⁻¹)
	1	2	3	4	5	6	
ANL							
CEA/SA	1.291E-02	3.140E-02	1.173E-01	3.133E-01	1.115E+00	3.425E+00	
(Transport)	1.291E-02	3.139E-02	1.173E-01	3.133E-01	1.114E+00	3.424E+00	
CIAE	1.272E-02	3.161E-02	1.171E-01	3.128E-01	1.386E+00	3.758E+00	
IGCAR	1.278E-02	3.169E-02	1.227E-01	3.247E-01	1.395E+00	3.888E+00	
IPPE	1.334E-02	3.217E-02	1.205E-01	3.076E-01	8.708E-01	2.917E+00	
(Transport)	1.334E-02	3.217E-02	1.205E-01	3.075E-01	8.706E-01	2.915E+00	
JNC	1.270E-02	3.170E-02	1.150E-01	3.110E-01	1.400E+00	3.870E+00	
KAERI							
OKBM	1.334E-02	3.214E-02	1.206E-01	3.083E-01	8.733E-01	2.925E+00	
Average	1.300E-02	3.178E-02	1.189E-01	3.123E-01	1.128E+00	3.390E+00	
S.D. +	2.879E-04	3.330E-04	2.563E-03	5.602E-03	2.418E-01	4.280E-01	

3.1.3.3. Power distribution

The core powers were calculated based on a local energy deposition model where energy is deposited at the point of production and the calculated power distribution therefore includes the delayed component due to gamma heating. Isotopic dependent values for the energy release per fission and per capture have been assumed as given in Table 2.2. This local energy deposition model does not allow for gamma transport toward the outer regions of the core, and, as a result, the powers for non-fuelled regions are completely ignored.

The core power distributions calculated with the local energy deposition model by the participants are given in Table 3.16. The SHR region is denoted by SHR1, SHR2 and SHR3 depending on location. Using the core power results given in this table, regionwise normalized power distributions are compared in Fig. 3.4 with their average values. The comparison of regionwise power distributions shows good agreement over the fuel zones for the RZ model. This figure shows the MOX region is the most productive in the fuel regions.

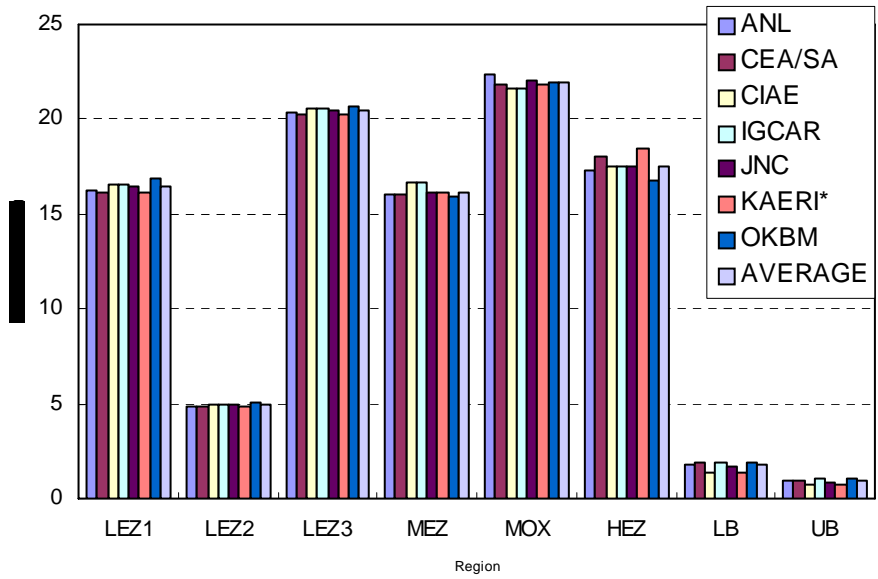
Figure 3.5 illustrates typical regionwise power output distributions for the RZ model, which were obtained from the RZ diffusion theory calculations by ANL. In this figure, the MOX region has the largest power output in the detailed divisions for the enriched fuel regions. Power fractions for LEZ, MEZ and MOX in the core obtained by averaging over the results of each participant are given in Table 3.17, where the results were obtained from the RZ diffusion theory calculations. Most power (97.3% of total power) is produced in the enriched fuel zones, i.e. LEZ, MEZ, HEZ and MOX, and the power fraction of the blanket regions is 2.7%. The MOX region that contains enrichment 21.3wt% with 93.8wt% ²³⁹Pu content for feed fuel, produces 22.0% of total power.

TABLE 3.16. POWER DISTRIBUTIONS

TABLE 3.16. POWER DISTRIBUTIONS (CONTINUED)

(Unit: Watt) (2/2)														
Participant	Region	SHR1	LEZ1	SHR2	LEZ2	SCR	LEZ3	SHR3	MEZ	MOX	HEZ	SSA1	SSA2	RR
JNC	UAR													
	UB	2.1871E+06		5.9824E+05				2.5908E+06				1.8032E+06		
	CORE	2.4240E+08		7.2573E+07				3.0022E+08				2.5736E+08		
	LB	5.2639E+06		1.6624E+06				6.5252E+06				4.6763E+06		
	LAR											3.0899E+06		
	Sum	2.4985E+08		7.4833E+07				3.0934E+08				2.4229E+08	3.3148E+08	2.6226E+08
	Total	1.4701E+09												
KAERI (*)	UAR													
	UB	1.9840E+06		5.3053E+05				2.3507E+06				2.5514E+06		
	CORE	2.3801E+08		7.1804E+07				2.9827E+08				3.2106E+08		
	LB	4.3092E+06		1.3637E+06				5.3911E+06				3.2692E+06		
	LAR											3.9542E+06	2.6371E+06	
	Sum	2.4430E+08		7.3698E+07				3.0601E+08				2.4212E+08	3.2756E+08	2.7624E+08
	Total	1.4699E+09												
OKBM	UAR													
	UB	2.8467E+06		7.4245E+05				3.2673E+06				3.3873E+06		
	CORE	2.4738E+08		7.3871E+07				3.0317E+08				3.2187E+08		
	LB	5.8850E+06		1.8631E+06				7.2730E+06				4.3670E+06	5.2160E+06	3.3870E+06
	LAR													
	Sum	2.5611E+08		7.6477E+07				3.1371E+08				2.4115E+08	3.3047E+08	2.5207E+08
	Total	1.4700E+09												
Mean	UAR													
	UB	2.5328E+06		6.7449E+05				2.9830E+06				2.1282E+06		
	CORE	2.4115E+08		7.2520E+07				3.0017E+08				2.3714E+08		
	LB	5.4307E+06		1.7193E+06				6.7764E+06				4.1080E+06	4.9420E+06	3.1978E+06
	LAR													
	Sum	2.4912E+08		7.4913E+07				3.0993E+08				2.4337E+08	3.3068E+08	2.6199E+08
	Total	1.4700E+09												
SD	UAR													
	UB	3.3364E+05		7.4563E+04				3.6467E+05				2.7246E+05		
	CORE	3.8905E+06		8.5591E+05				2.2706E+06				3.6564E+06		
	LB	5.7442E+05		1.8327E+05				7.1443E+05				4.4375E+05	5.7661E+05	4.3558E+05
	LAR													
	Sum	3.8216E+06		8.3526E+05				2.0349E+06				3.0512E+06	4.2429E+06	6.2950E+06
	Total	3.2108E+04												

* The KAERI results are not included in the averages.



* Transport theory results

FIG. 3.4. Regionwise power distributions (RZ model).

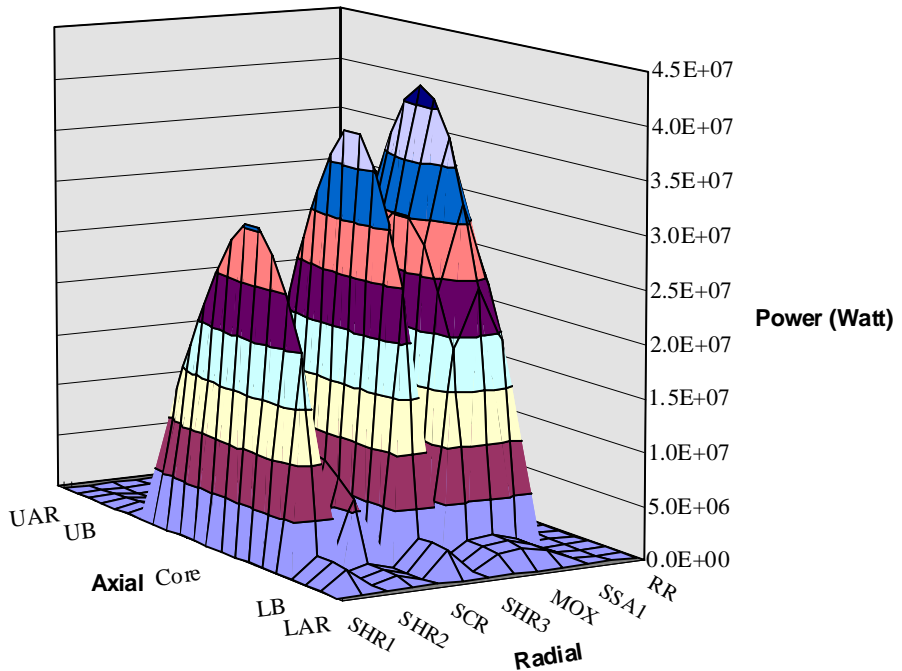


FIG. 3.5. Power output distributions (ANL result) (RZ model).

TABLE 3.17. POWER FRACTIONS FOR FUEL REGIONS

Region	Fraction (%)
LEZ1	16.40
LEZ2	4.93
LEZ3	20.42
MEZ	16.13
MOX	21.95
HEZ	17.46
<u>Core</u>	<u>97.29</u>
LB	1.78
UB	0.93
Total	100.00

3.1.3.4. Reaction rate distributions

Spatially dependent microscopic fission and capture reaction rates ($\sigma \phi$) for ^{235}U fission, ^{238}U fission, and ^{238}U capture on the radial and axial traverses specified in Fig. 3.1 are shown in Figs 3.6–3.23. These figures illustrate spatial reaction rate distributions in the axial and radial directions especially for enriched fuelled regions, i.e. LEZ and MOX respectively, that were obtained from diffusion and transport theory calculations by the participants.

Local microscopic cross-sections were used where isotopes are present in the model regions. For infinite dilution reaction rate calculations, infinite dilution cross sections and arbitrary number densities were used where they are absent. The radial reaction rates are presented on a radial traverse 10.44 cm below core centre line of the radial mesh regions.

Figures 3.6–3.17 show the axial reaction rate distributions for ^{235}U fission, ^{238}U fission, and ^{238}U capture obtained by the participants. It is noted that peak valued locations in the axial reaction rate distributions are shifted lower from the core mid-plane, due to different axial blanket thickness between UB (35.2 cm) and LB (30.2 cm) in the benchmark model. A comparison of the participants' diffusion theory results, the CIAE result shows the largest value in most axial reaction rate distributions. Peak values were obtained within about 13.1% of relative difference in LEZ except the ^{238}U capture rate. The maximum relative difference between the peak values in the ^{238}U capture rate distributions appears to be 32.5%.

Diffusion theory results in MOX show better agreement between the participants' results, as compared with them in LEZ. Peaked values in MOX were calculated to be within 8.4% of relative difference, except 32.7% for the ^{238}U capture rate, similar for LEZ.

Figures 3.12–3.17 compare the axial reaction rate distributions obtained from the diffusion and transport theory calculations, respectively. Both theory results obtained by each participant agree well in the peak values for most reaction rate distributions. Similar for the diffusion theory results, it is observed that the CIAE result has the largest value and the largest relative difference between the diffusion and transport theory results of 21.5% for the ^{238}U capture rate.

In the axial ^{238}U capture rate distributions a hump can commonly be observed at the upper and lower ARs where ^{238}U fertile is absent. This result implies that the ^{238}U capture rate strongly depends on the transitional self-shielding effect resulting from a sudden material composition change near the boundary of the different material compositions, e.g. near the UB-AR and LB-AR interfaces in the benchmark model.

Diffusion results for radial reaction rate distributions calculated by the participants are compared in Figs 3.18–3.23. Most diffusion results show good agreement in the radial reaction rate behaviours and in its magnitudes as well in the fuelled regions of interest on the specified traverses. The IGCAR results have the smallest peak value in most radial reaction rate distributions, smaller by 22.2% in relative difference from the maximum value for the ^{235}U fission rate. It is noted that the CEA/SA result appears to have the largest peak value for the ^{238}U capture rate near the HEZ-SSA interface. Its magnitude is about 50% larger than the others. This large difference is considered to be a self-shielding artifact as there is no ^{238}U present in the non-fuelled regions, i.e. SSA and RR. This effect is not seen for the ^{235}U fission reaction, which also has a zero number density in these regions, but is not subject to significant self-shielding.

Figures 3.21–3.23 compare the radial reaction rate distributions obtained from the diffusion and transport theory calculations, respectively. Similar for the axial distributions, both theory results calculated by each participant agree well both in the radial reaction rate behaviours and in their magnitudes in the fuelled regions of interest for most reaction rate distributions. The KAERI's transport theory result has the largest peak value in the ^{235}U fission rate distributions and for CIAE both results have the largest value in the ^{238}U fission rate distributions. For the ^{238}U capture rate, the CEA/SA results have the largest peak value of all results obtained from the diffusion and transport theory calculations by the participants. This is again due to the same reason as indicated in the comparison of the diffusion results.

In common with the axial reaction rate distributions, a strong transitional self-shielding effect near the HEZ-SSA interface is observed in the radial ^{238}U capture rate distributions.

3.1.3.5. Local reactivity coefficients

Distributions of local reactivity coefficients calculated for the R-Z model by the participants are given in Tables 3.17–3.23. Most reactivity coefficients were determined using the diffusion theory based, first order perturbation method. Using the distribution of results given in these tables, detailed distributions of local reactivity coefficients obtained by each participant are compared in Figs 3.24–3.29.

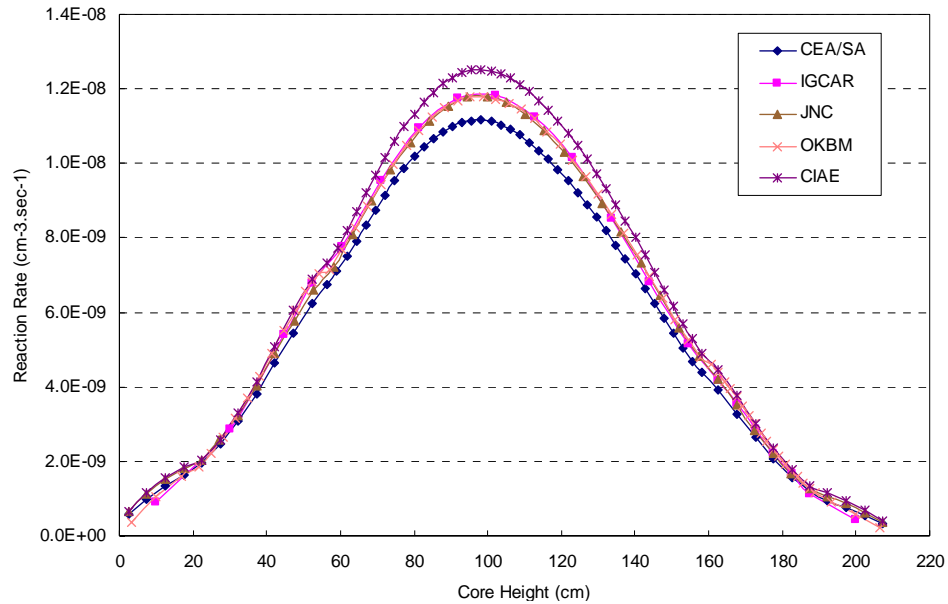


FIG. 3.6. Axial ^{235}U fission rate distributions in LEZ (Phase 1, diffusion).

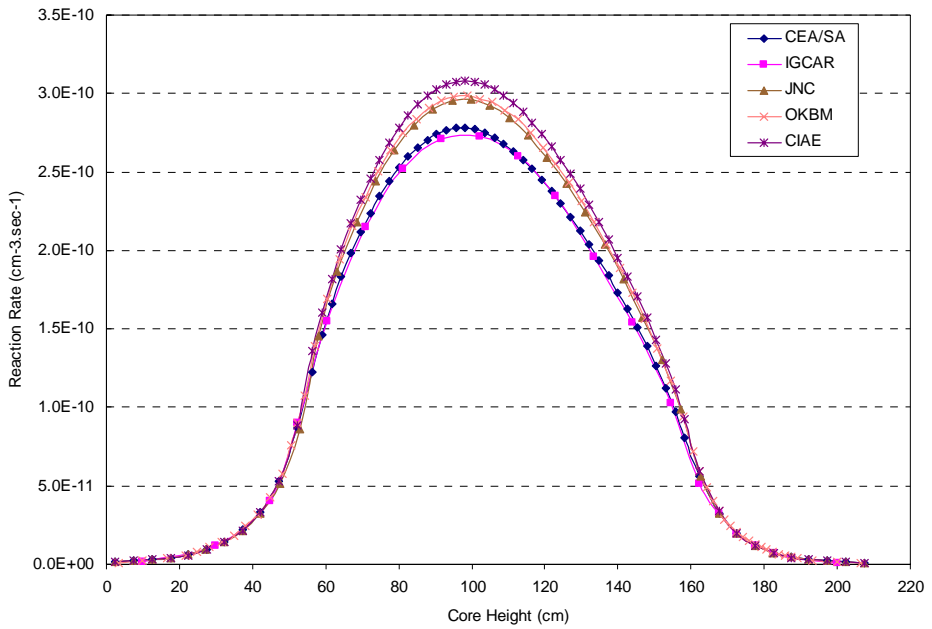


FIG. 3.7. Axial ^{238}U fission rate distributions in LEZ (Phase 1, diffusion).

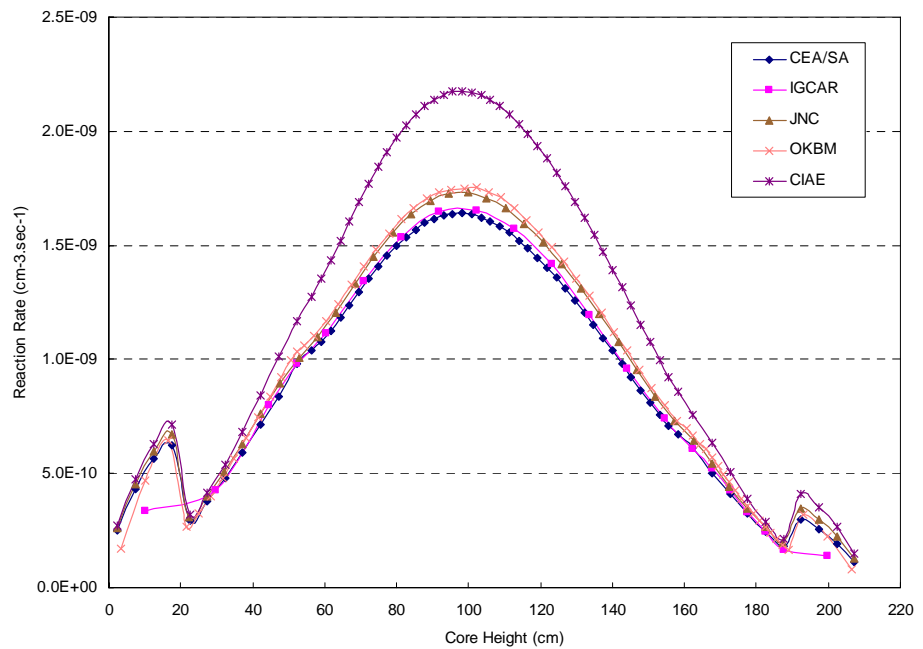


FIG. 3.8. Axial ^{238}U capture rate distributions in LEZ (Phase 1, diffusion).

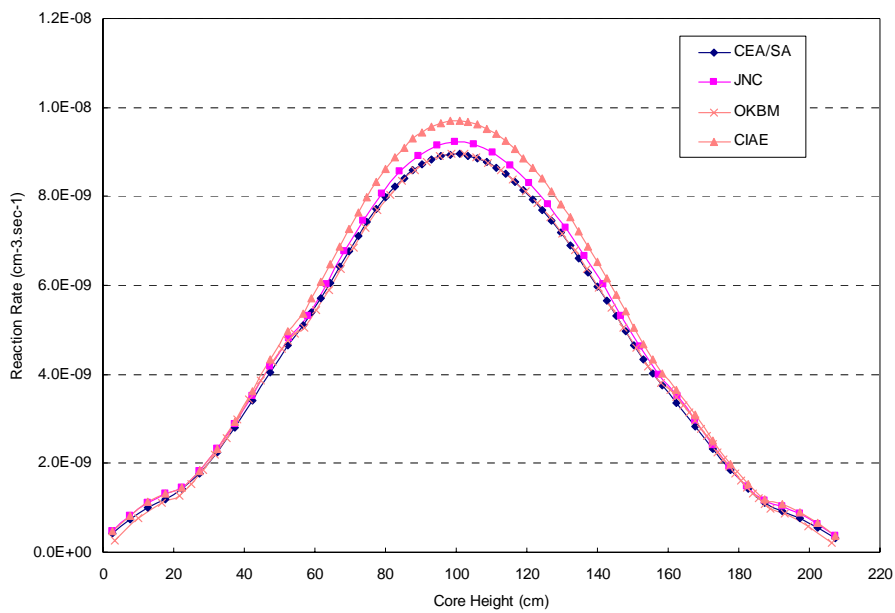


FIG. 3.9. Axial ^{235}U fission rate distributions in MOX (Phase 1, diffusion).

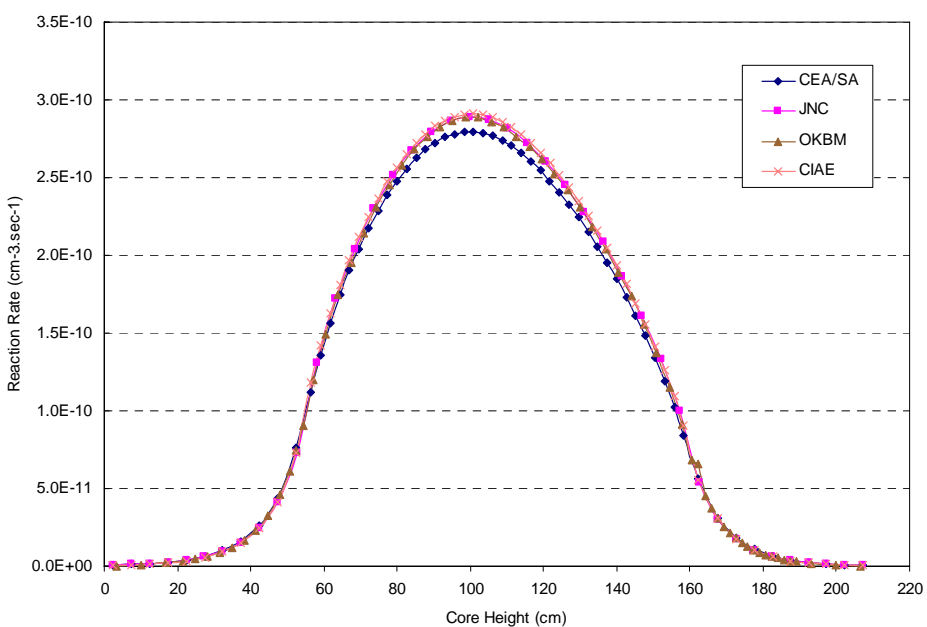


FIG. 3.10. Axial ^{238}U fission rate distributions in MOX (Phase 1, diffusion).

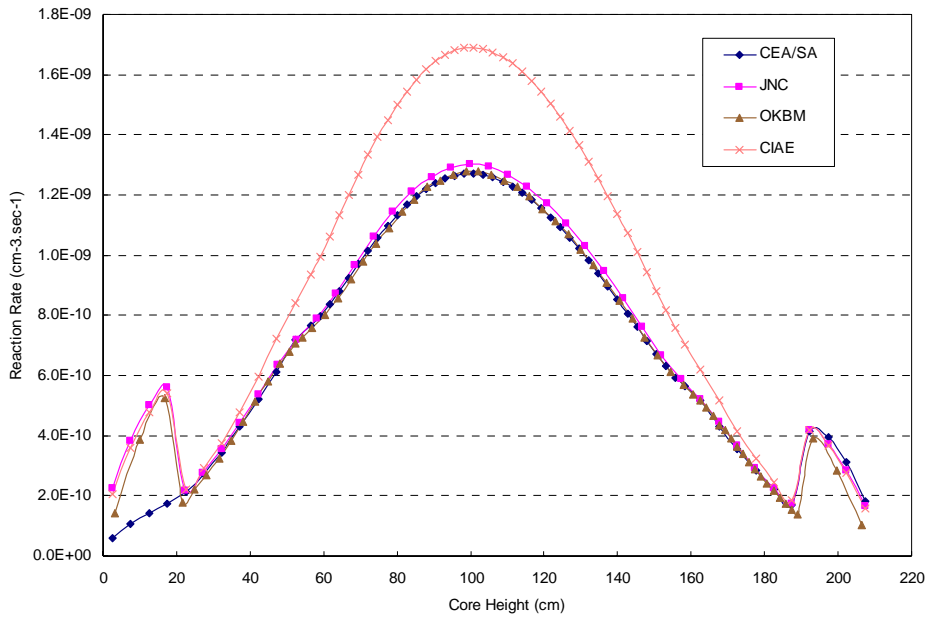


FIG. 3.11. Axial ^{238}U capture rate distributions in MOX (Phase 1, diffusion).

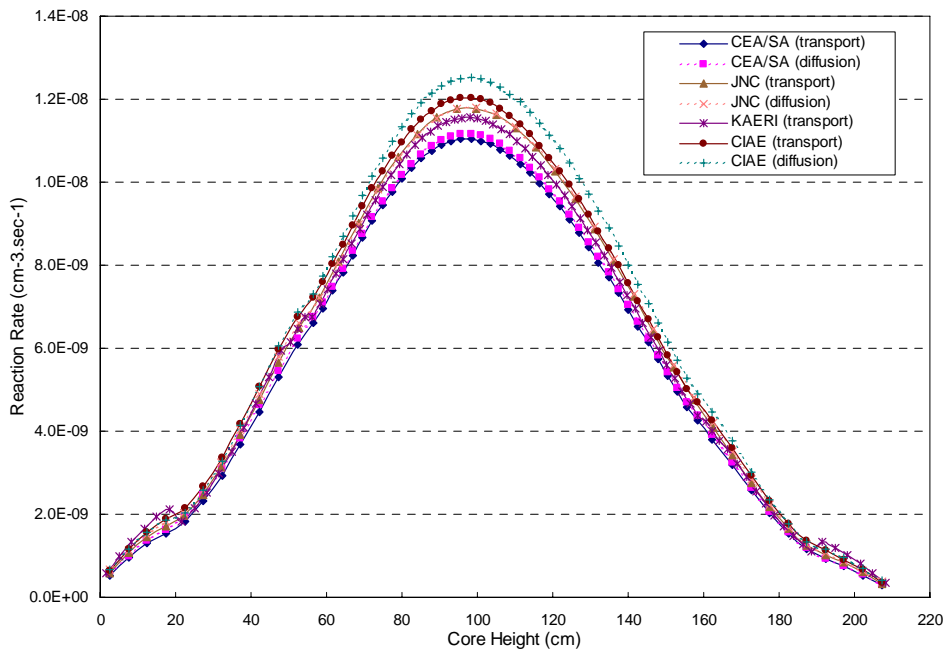


FIG. 3.12. Axial ^{235}U fission rate distributions in LEZ (Phase 1, transport vs. diffusion).

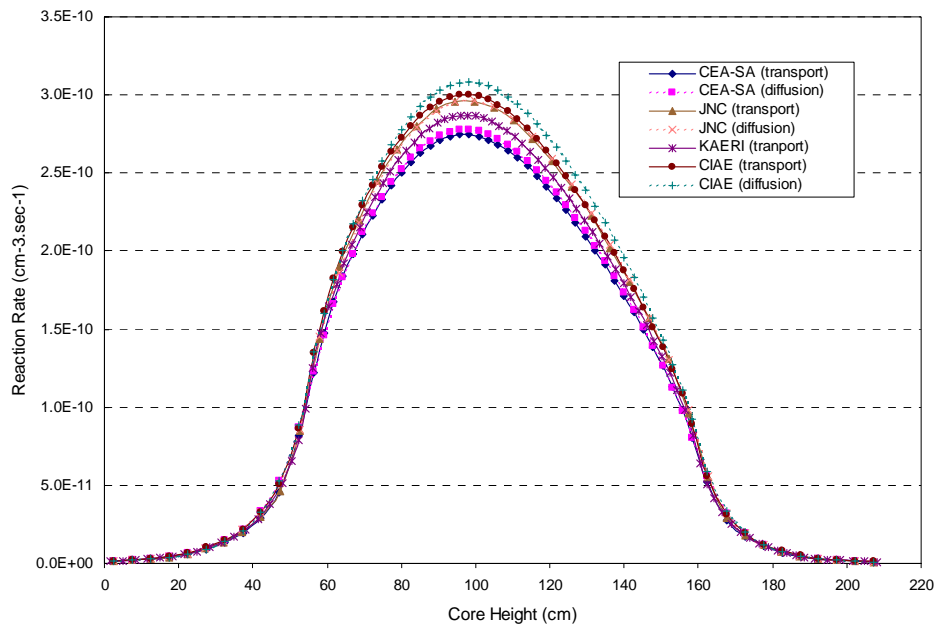


FIG. 3.13. Axial ^{238}U fission rate distributions in LEZ (Phase 1, transport vs. diffusion).

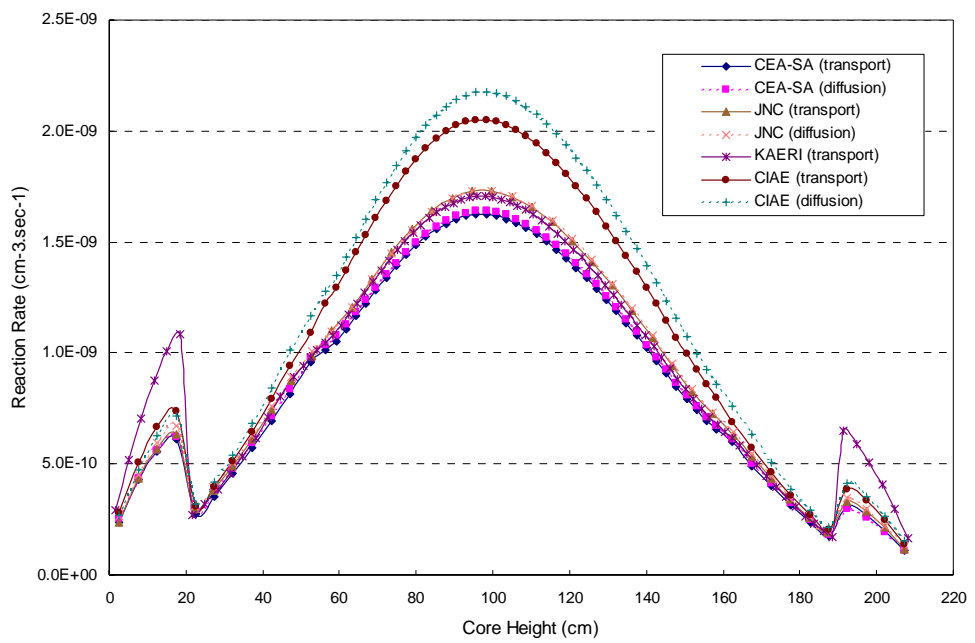


FIG. 3.14. Axial ^{238}U capture rate distributions in LEZ (Phase 1, transport vs. diffusion).

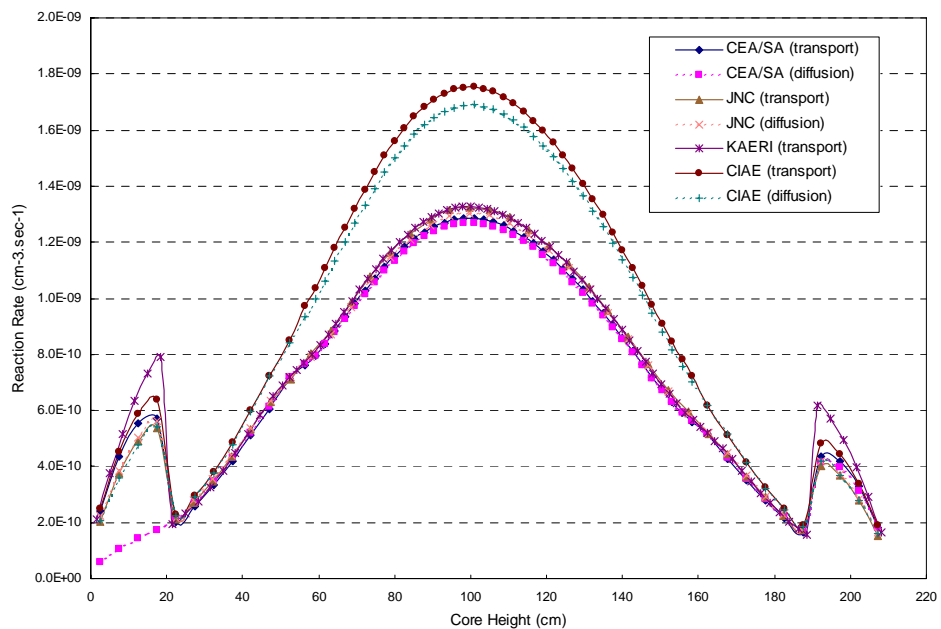


FIG. 3.15. Axial ^{235}U fission rate distributions in MOX (Phase 1, transport vs. diffusion).

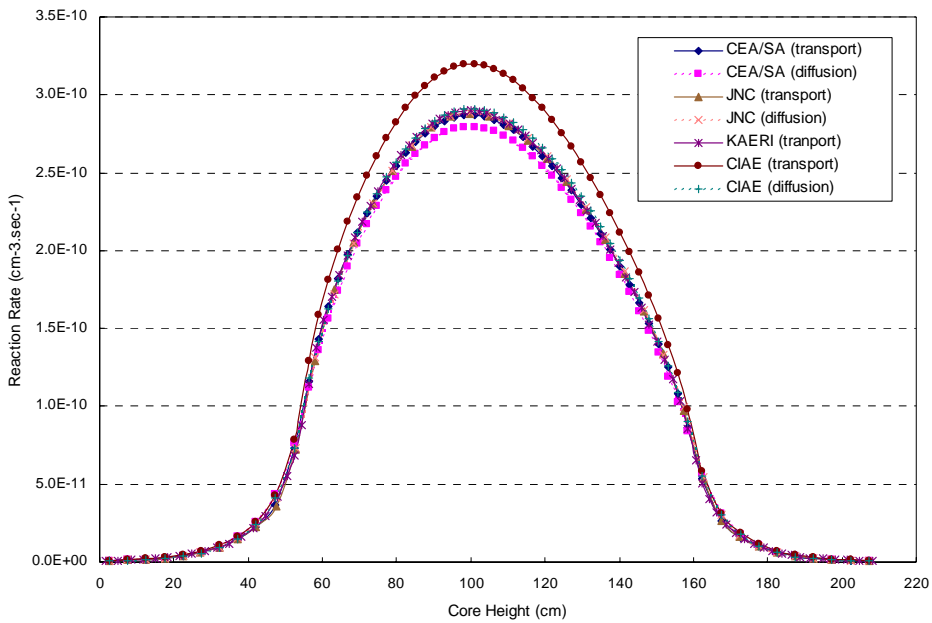


FIG. 3.16. Axial ^{238}U fission rate traverses in MOX (Phase 1, transport vs. diffusion).

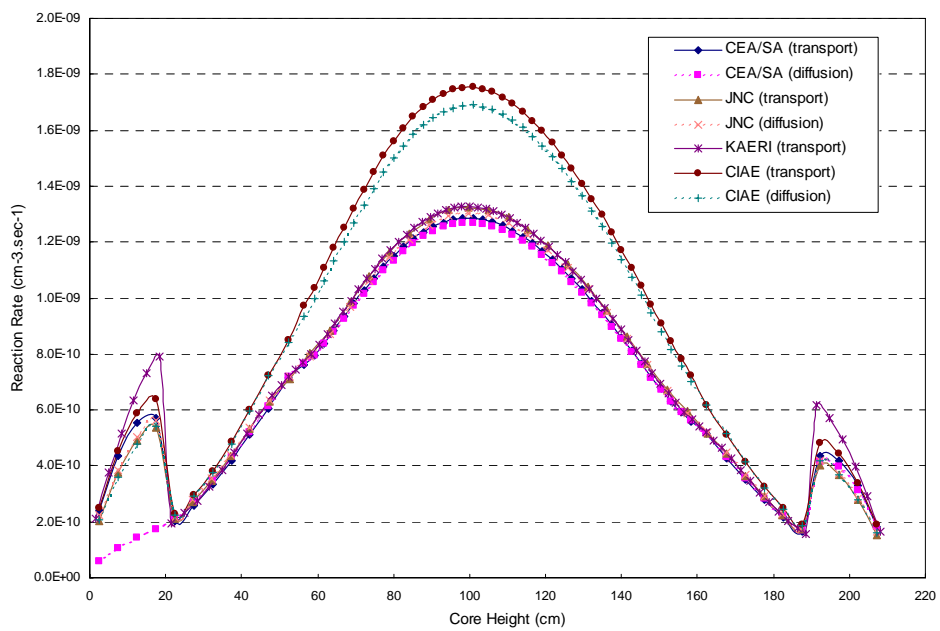


FIG. 3.17. Axial ^{238}U capture rate distributions in MOX (Phase 1, transport vs. diffusion).

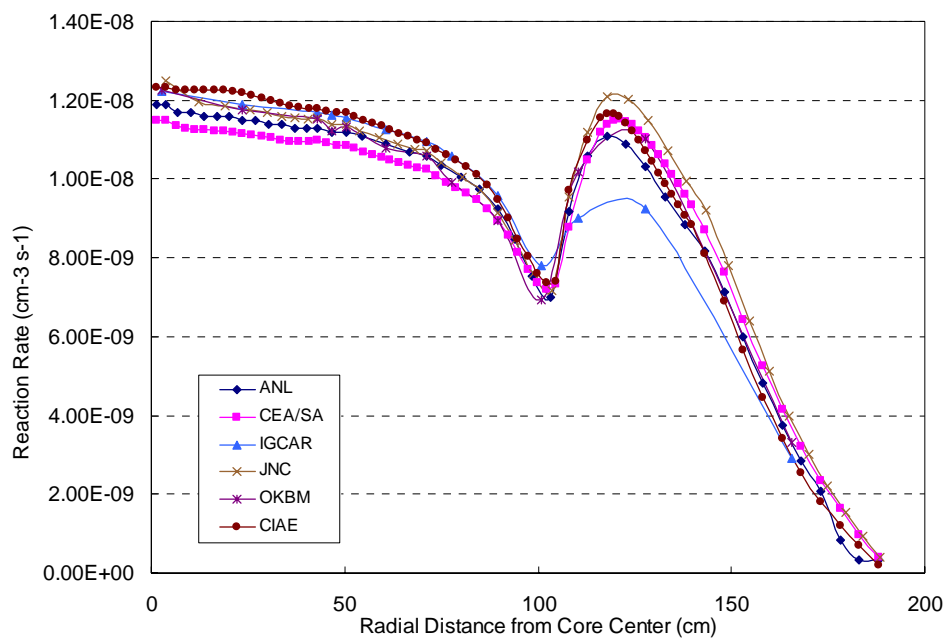


FIG. 3.18. Radial ^{235}U fission rate distributions (Phase 1, diffusion).

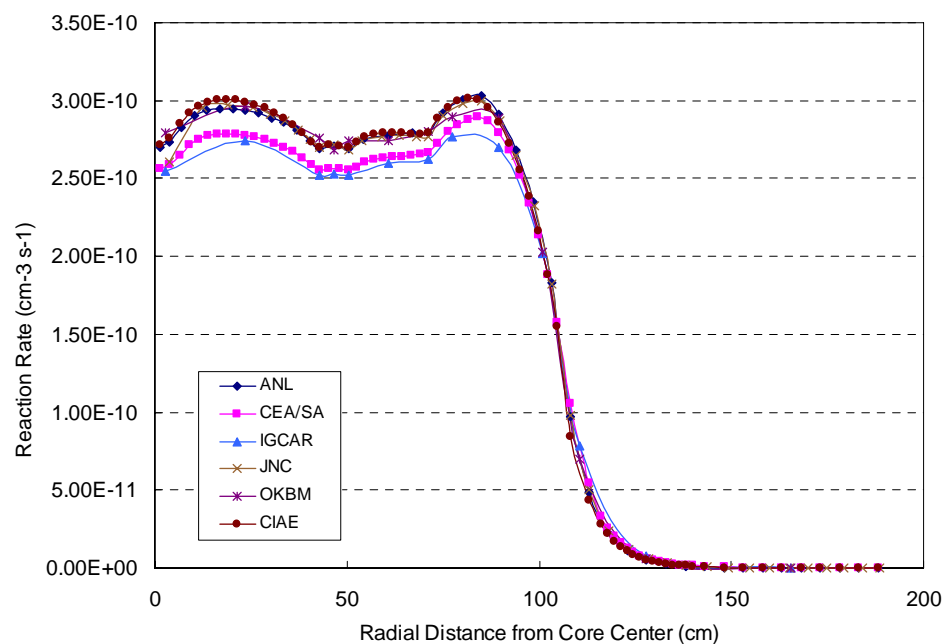


FIG. 3.19. Radial ^{238}U fission rate distributions (Phase 1, diffusion).

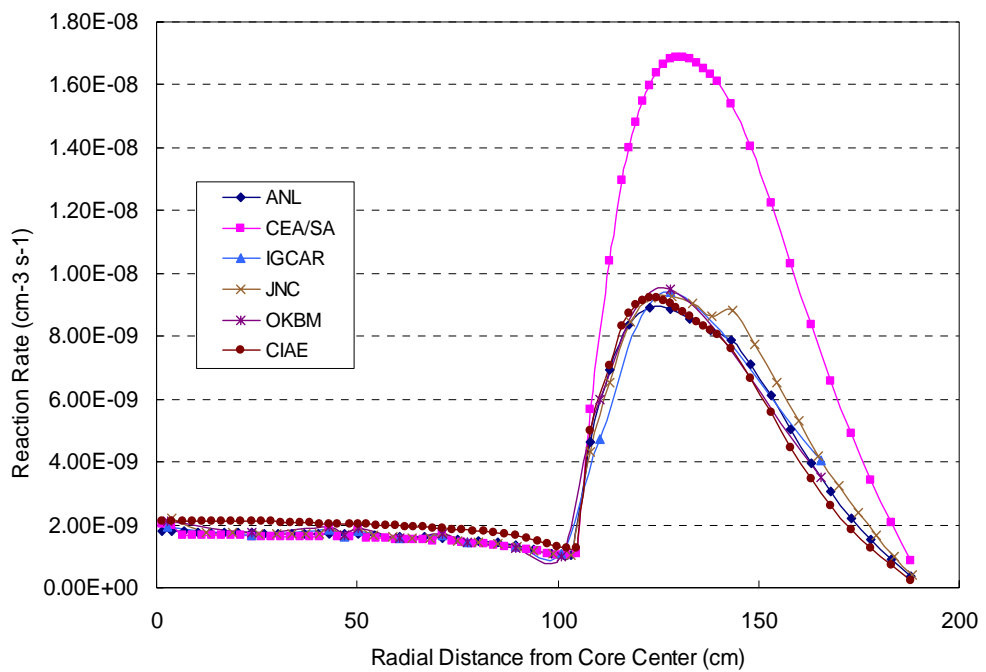


FIG. 3.20. Radial ^{238}U capture rate distributions (Phase 1, diffusion).

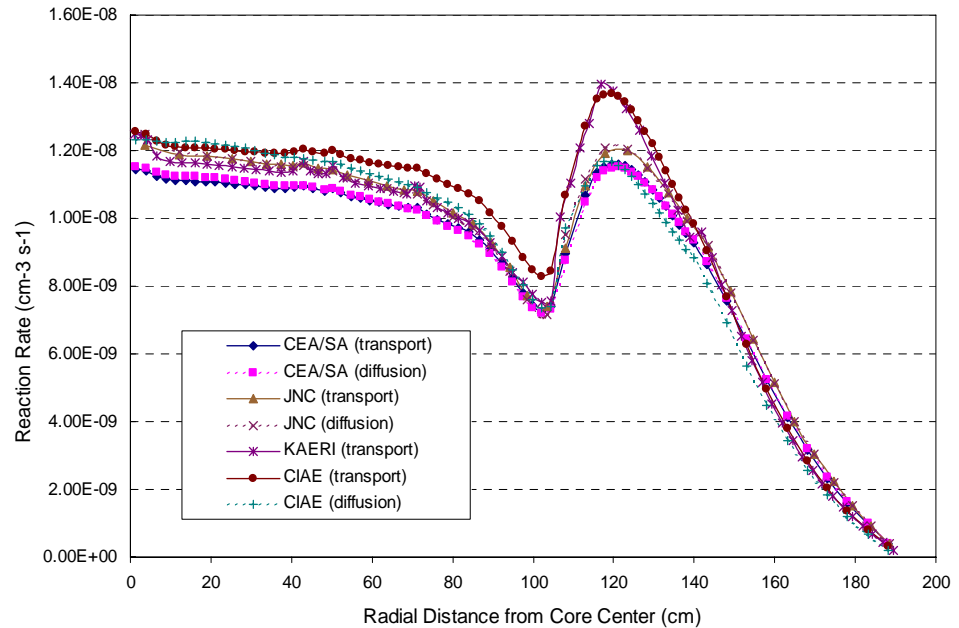


FIG. 3.21. Radial ^{235}U fission rate distributions (Phase 1, transport vs. diffusion).

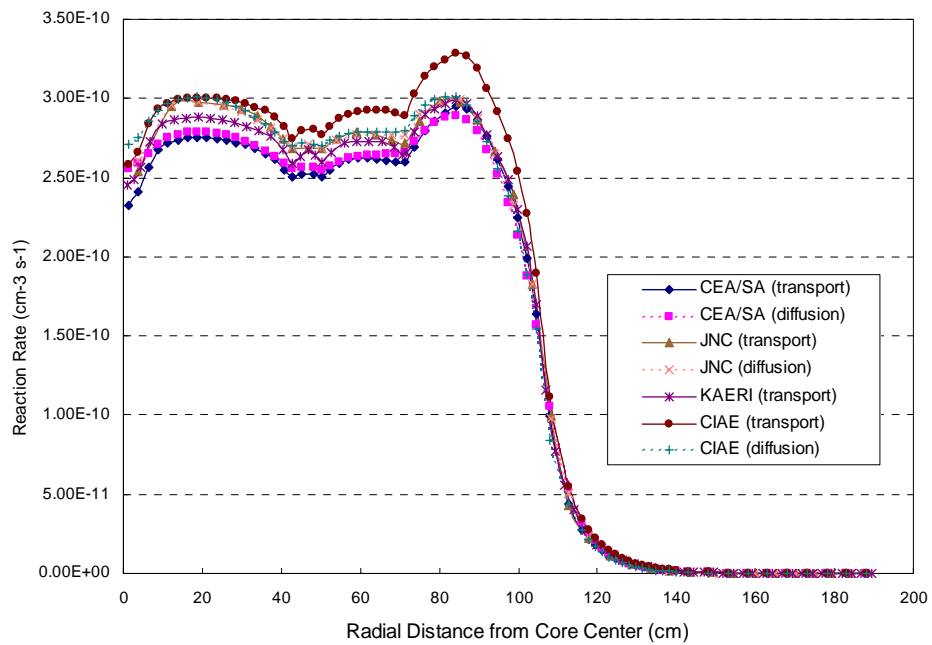


FIG. 3.22. Radial ^{238}U fission rate distributions (Phase 1, transport vs. diffusion).

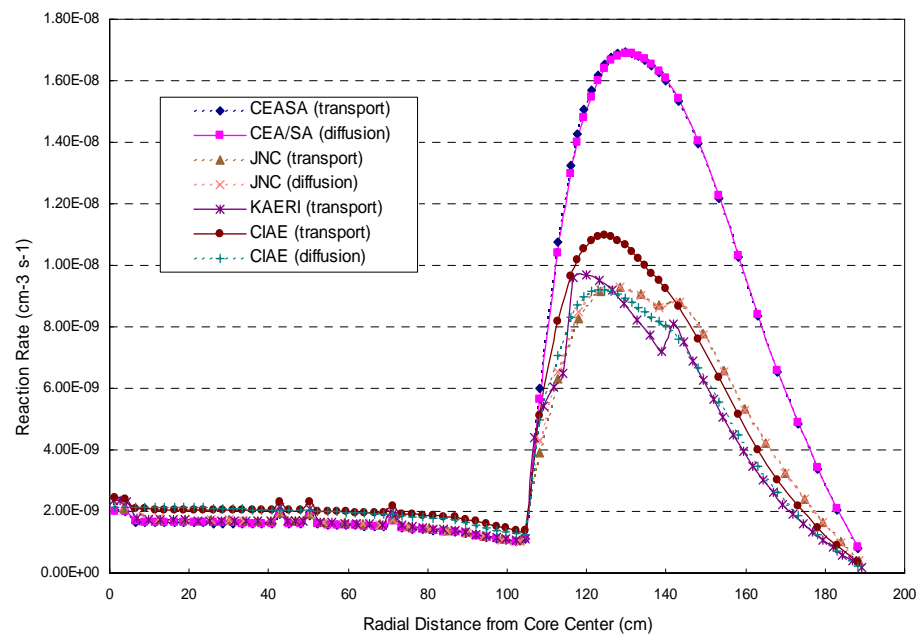


FIG. 3.23. Radial ^{238}U capture rate distributions (Phase 1, transport vs. diffusion).

Table 3.20 presents material-dependent sodium density coefficients for constituent compositions in the whole core system. The resultant sodium density coefficients clearly show spatial distributions that can mainly be characterized by leakage and non-leakage components. LEZ and MEZ contain highly enriched fuel located at the zones near the core centre, the non-leakage component prevails the leakage effect and, as a result, the overall sodium density coefficient is determined to be negative. In the MOX zone, this non-leakage prevailing effect appeared to be valid only for the results obtained by CEA/SA, CIAE and IGCAR. The prevailing non-leakage component becomes smaller with moving toward outer zones. It is clearly observed that the leakage component becomes dominant in HEZ, and, as a result, HEX has the greatest positive worth. Most zones peripheral to the highly enriched fuelled zones have a positive worth except for the outermost zone RR. This indicates that the leakage component is dominant in those zones peripheral to the highly enriched core zones. The comparison of the results for the sodium density coefficients implies that the prediction of the sodium density coefficients for the MOX zone requires further investigation.

Local coefficients are shown for the core plus the upper axial blanket (UB) regions, with the sum of the entire regions for comparison. The integral comparisons using only the core region plus the upper axial blanket regions are given for a better gauge of comparison, since these regions will experience significantly higher temperatures in an accident situation.

In Fig. 3.24, the fuel Doppler coefficients for LEZ3 that has the largest ^{238}U density in the core region appear to be largest in its magnitude. In this figure, the comparison of regional coefficients shows better agreement than the comparison of total coefficients summed over all regions, because discrepancies between the values obtained by the participants in each region are accumulated and, as a result, it leads to the expansion of its magnitude in the total values. For the steel Doppler coefficient case shown in Fig. 3.25, this aspect is more evident, because the total value is a sum of very small positive and small negative contributions from the control regions (SHR, SCR) and other voluminous non-fuelled regions (RR, SSA). The CIAE results for the steel Doppler coefficient appeared to be substantially smaller in its magnitude than those of the other participants.

The regionwise sodium density coefficients for the core plus the upper axial blanket (UB) regions are compared in Fig. 3.26. From the comparison of these figures, it can be inferred that large differences between the values obtained by the participants are due to a net cancellation between the large non-leakage and leakage contributions to the coefficients which also applies in a similar manner to the other coefficients. In this figure, the comparison of regional coefficients shows better agreement than the comparison of total coefficients summed over all regions, because the total value is obtained by summing of very small positive and small negative contributions calculated from a 1% reduction in the sodium density. The resultant aspects are very similar for the steel density coefficients shown in Fig. 3.27. In these figures, the ANL results for the sodium and steel density coefficients were predicted to be relatively larger than those of the other participants, particularly for total values.

TABLE 3.17. FUEL DOPPLER COEFFICIENTS

(1/2)														
Participant	Region	SHR1	LEZ1	SHR2	LEZ2	SCR	LEZ3	SHR3	MEZ	MOX	HEZ	SSA1	SSA2	RR
ANL	UAR	-2.7284E-05		-3.5537E-06		-2.3413E-05		-1.8686E-05	-3.6585E-05	-2.8678E-05				
	UB	-1.3204E-03		-3.9449E-04		-1.5466E-03		-8.3872E-04	-1.0539E-03	-7.3138E-04				
CORE		-1.1555E-04		-3.9229E-05		-1.3869E-04		-7.6911E-05	-7.8387E-05	-4.9844E-05				
LB														
LAR														
Sum		-1.4631E-03			-4.3727E-04		-1.7087E-03		-9.3432E-04	-1.1688E-03	-8.0990E-04			
Total		-6.5221E-03												
CEA/SA	UAR	-2.3314E-05		-2.4314E-06		-1.7903E-05		-1.5705E-05	-3.3807E-05	-3.1712E-05				
	UB	-1.3539E-03		-4.0232E-04		-1.5791E-03		-8.4746E-04	-1.1442E-03	-8.6155E-04				
CORE		-1.0722E-04		-3.6912E-05		-1.3012E-04		-7.2270E-05	-7.5680E-05	-5.6449E-05				
LB														
LAR														
Sum		-1.4844E-03		-4.4186E-04		-1.7271E-03		-9.3543E-04	-1.2537E-03	-9.4971E-04				
Total		-6.7922E-03												
CIAE	UAR	-4.5688E-06		8.9850E-07		4.9390E-07		-1.0325E-06	-5.9553E-06	-4.0985E-06				
	UB	-1.1327E-03		-3.2599E-04		-1.2342E-03		-6.0505E-04	-8.4063E-04	-4.9874E-04				
CORE		-5.3571E-05		-1.8621E-05		-6.2858E-05		-3.1735E-05	-2.4689E-05	-1.1197E-05				
LB														
LAR														
Sum		-1.1908E-03		-3.4371E-04		-1.3466E-03		-7.2782E-04	-8.7127E-04	-5.1404E-04				
Total		-4.9943E-03												
IGCAR	UAR	-2.0140E-05		-2.3190E-06		-1.5930E-05		-1.3693E-05	-2.8574E-05	-2.3084E-05				
	UB	-9.3222E-04		-2.7513E-04		-1.0884E-03		-5.8398E-04	-7.0053E-04	-5.4973E-04				
CORE		-8.8910E-05		-2.9930E-05		-1.0733E-04		-6.0060E-05	-6.3491E-05	-4.1119E-05				
LB														
LAR														
Sum		-1.0413E-03		-3.0740E-04		-1.2117E-03		-6.5773E-04	-7.9260E-04	-6.1393E-04				
Total		-4.6246E-03												
IPPE	UAR	-2.6410E-05		-2.6759E-06		-1.9319E-05		-1.6137E-05	-3.3490E-05	-2.6913E-05				
	UB	-1.3294E-03		-3.8844E-04		-1.4949E-03		-7.7930E-04	-9.7970E-04	-6.3310E-04				
CORE		-1.1730E-04		-3.9300E-05		-1.3730E-04		-7.4300E-05	-7.5200E-05	-4.8070E-05				
LB														
LAR														
Sum		-1.4731E-03		-4.3042E-04		-1.6515E-03		-8.6974E-04	-1.0884E-03	-7.0808E-04				
Total		-6.2213E-03												

TABLE 3.17. FUEL DOPPLER COEFFICIENTS (CONTINUED)

(2/2)														
Participant	Region	SHR1	LEZ1	SHR2	LEZ2	SCR	LEZ3	SHR3	MEZ	MOX	HEZ	SSA1	SSA2	RR
JNC	UAR	-2.4723E-05		-2.9457E-06			-1.9206E-05	-1.6149E-05	-3.3056E-05	-2.9812E-05				
	UB	-1.3228E-03		-3.8785E-04			-1.5116E-03	-8.1335E-04	-1.0276E-03	-8.1306E-04				
CORE		-1.1032E-04		-3.7026E-05			-1.3105E-04	-7.1266E-05	-7.3991E-05	-5.2717E-05				
LB														
LAR														
Sum		-1.4611E-03		-4.2782E-04			-1.6618E-03		-9.0077E-04	-1.1346E-03	-8.9559E-04			
Total		-6.4817E-03												
KAERI (*)	UAR	-2.5101E-05		-3.9485E-06			-2.0306E-05	-1.7204E-05	-3.4690E-05	-3.1588E-05				
	UB	-1.5795E-03		-4.7636E-04			-1.8379E-03	-1.0458E-03	-1.2943E-03	-9.6825E-04				
CORE		-2.8203E-07		-2.8203E-07			-2.8203E-07		-7.9816E-05	-5.5561E-05				
LB														
LAR														
Sum		2.8203E-07	-1.6048E-03	-4.8059E-04			-1.8284E-03		-1.1428E-03	-1.3845E-03	-1.0554E-03			
Total		-7.7452E-03												
CKBM	UAR	-2.5960E-05		-3.0000E-06			-1.9700E-05	-1.3430E-05	-3.0440E-05	-2.5370E-05				
	UB	-1.4390E-03		-4.2500E-04			-1.6200E-03	-8.5190E-04	-9.7260E-04	-6.9130E-04				
CORE		-1.1460E-04		-3.8500E-05			-1.3490E-04		-7.0130E-05	-7.2620E-05	-4.5060E-05			
LB														
LAR														
Sum		-1.5796E-03		-4.6650E-04			-1.7746E-03		-9.3546E-04	-1.0757E-03	-7.6173E-04			
Total		-6.5935E-03												
Mean	UAR	-2.1771E-05		-2.2896E-06			-1.6425E-05	-1.3547E-05	-2.8844E-05	-2.4238E-05				
	UB	-1.26119E-03		-3.7135E-04			-1.4464E-03	-7.7282E-04	-9.5987E-04	-6.8269E-04				
CORE		-1.0107E-04		-3.4220E-05			-1.2032E-04	-6.5239E-05	-6.6294E-05	-4.3494E-05				
LB														
LAR														
Sum		-1.3848E-03		-4.0785E-04			-1.5831E-03		-8.5161E-04	-1.0550E-03	-7.5043E-04			
Total		-6.0328E-03												
SD	UAR	7.9492E-06		1.4644E-06			7.7927E-06	5.7907E-06	1.0411E-05	9.3275E-06				
	UB	1.7189E-04		5.2066E-05			1.9098E-04	9.9634E-05	1.4687E-04	1.3254E-04				
CORE		2.3028E-05		7.5928E-06			2.7447E-05	1.5692E-05	1.8938E-05	1.5085E-05				
LB														
LAR														
Sum		1.9289E-04		5.8558E-05			2.1524E-04		1.1296E-04	1.6478E-04	1.5316E-04			
Total		8.5918E-04												

* transport theory results

TABLE 3.18. STEEL DOPPLER COEFFICIENTS

(1/2)														
Participant	Region	SHR1	LEZ1	SHR2	LEZ2	SCR	LEZ3	SHR3	MEZ	MOX	HEZ	SSA1	SSA2	RR
ANL	UAR	-3.4681E-10	-2.1481E-08	-1.0291E-09	-3.2061E-09	-9.5595E-10	-1.7385E-08	-2.7179E-09	-1.6292E-08	-2.7929E-08	-1.8344E-08	-9.8523E-09	-3.9491E-09	-3.0414E-09
	UB	-9.5562E-09	-1.7786E-06	-6.6417E-08	-3.0556E-07	-2.1269E-08	-1.7027E-06	-1.3285E-07	-1.2666E-06	-2.2110E-06	-1.4802E-06	-3.7836E-06	-2.5932E-06	-1.1113E-07
CORE	-1.3572E-06	-1.4863E-04	-7.8467E-06	-4.4998E-05	-5.9287E-06	-1.7694E-04	-1.3772E-05	-1.0805E-04	-1.3593E-04	-7.1412E-05	-2.0616E-04	-1.1846E-04	-3.8014E-06	
LB	-5.6547E-08	-6.7724E-06	-2.5906E-07	-2.3439E-06	-1.7778E-07	-8.2132E-06	-4.0504E-07	-4.6102E-06	-4.5943E-06	-2.5546E-06	-6.1505E-06	-4.0214E-06	-1.6241E-07	
LAR	-1.6758E-09	-1.1062E-07	-9.2875E-09	-3.5689E-08	-9.0800E-09	-1.2313E-07	-1.2282E-08	-5.7293E-08	-5.5631E-08	-2.7317E-08	-1.4538E-08	-7.3377E-09	-3.3812E-09	
Sum	-1.4223E-06	-1.5731E-04	-8.1825E-06	-4.7687E-05	-6.1378E-06	-1.8700E-04	-1.4325E-05	-1.1400E-04	-1.4282E-04	-7.5493E-05	-2.1611E-04	-1.2508E-04	-4.0814E-06	
Total	-1.0997E-03													
CEA/SA	UAR	-2.0990E-10	-1.3448E-08	-2.7160E-10	-5.4240E-10	-1.1040E-10	-6.3790E-09	-1.3480E-09	-1.0750E-08	-2.5560E-08	-2.1600E-08	-1.6770E-08	-1.3960E-08	-3.3640E-08
	UB	-3.4806E-09	-1.3178E-06	-2.3948E-08	-1.5731E-07	-2.9755E-09	-1.0640E-06	-5.3745E-08	-8.7507E-07	-1.7475E-06	-1.3780E-06	-5.4744E-06	-8.0506E-06	-5.4323E-07
CORE	-3.0905E-07	-1.6266E-04	-2.1184E-06	-4.8975E-05	-6.4907E-07	-1.9211E-04	-3.5278E-06	-1.1501E-04	-1.4750E-04	-8.6332E-05	-2.4247E-04	-2.5371E-04	-1.4742E-05	
LB	-1.0509E-08	-6.0260E-06	-5.0671E-08	-2.1119E-06	-2.1582E-08	-7.3460E-06	-7.8920E-08	-4.0136E-06	-3.9764E-06	-2.4790E-06	-8.9920E-06	-1.2252E-05	-7.9890E-07	
LAR	-1.6770E-09	-1.0160E-07	-9.4460E-09	-3.2750E-08	-9.4360E-09	-1.1370E-07	-1.2920E-08	-5.5260E-08	-5.3320E-08	-3.1810E-08	-2.2140E-08	-1.7080E-08	-3.2630E-08	
Sum	-3.2493E-07	-1.7012E-04	-2.2027E-06	-5.1277E-05	-6.8317E-07	-2.0064E-04	-3.6747E-06	-1.1996E-04	-1.5330E-04	-9.0242E-05	-2.5697E-04	-2.7404E-04	-1.6151E-05	
Total	-1.3396E-03													
CIAE	UAR	5.6386E-09	3.4971E-07	2.9997E-07	1.0382E-07	3.0706E-08	4.3430E-07	6.0230E-08	2.9664E-07	4.2128E-07	3.1574E-07	4.5010E-08	9.3744E-08	2.0866E-08
	UB	2.2075E-08	8.6621E-07	1.1450E-07	3.9558E-07	9.1520E-08	1.4924E-06	2.3264E-07	9.2454E-07	9.7116E-07	4.38811E-07	1.8554E-06	-5.7818E-08	1.3636E-08
CORE	-6.4168E-07	-7.8011E-05	-3.7255E-06	-2.3756E-05	-2.5543E-06	-8.8004E-05	-5.3886E-06	-4.6736E-05	-5.6173E-05	-3.7506E-05	-1.0368E-04	-4.5276E-05	-8.4531E-07	
LB	-2.9216E-08	-1.2513E-06	-1.1624E-07	-5.2470E-07	-4.8464E-08	-1.2840E-06	-1.2288E-07	-5.92558E-07	5.0488E-07	3.5504E-07	-2.2327E-06	-4.0900E-07	1.0916E-08	
LAR	5.2616E-09	3.2926E-07	2.9663E-08	1.0326E-07	3.0568E-08	4.1421E-07	5.5555E-08	2.6150E-07	3.4743E-07	2.5143E-07	1.9608E-08	5.0055E-08	1.2292E-08	
Sum	-6.3792E-07	-7.7717E-05	-3.3976E-06	-2.3678E-05	-2.4500E-06	-8.6947E-05	-5.1633E-06	-4.5547E-05	-5.3929E-05	-3.6096E-05	-1.0399E-04	-4.5599E-05	-7.8760E-07	
Total	-4.8594E-04													
IGCAR	UAR													
	UB													
	CORE													
	LB													
	LAR													
	Sum													
Total														
IPPE	UAR	-3.6900E-10	-2.3100E-08	-1.1600E-09	-3.5800E-09	-1.0000E-09	-1.8100E-08	-2.8600E-09	-1.6800E-08	-2.8300E-08	-1.9900E-08	-1.6900E-08	-2.2500E-08	-1.0700E-08
	UB	-1.845E-08	-2.1881E-06	-1.0760E-07	-3.3706E-07	-7.6579E-08	-1.8957E-06	-2.233E-07	-1.4185E-06	-2.4442E-06	-1.5059E-06	-4.2460E-06	-5.6300E-06	-2.7410E-07
CORE	-1.6067E-06	-1.7801E-04	-9.1070E-06	-5.1040E-05	-6.5050E-06	-2.0004E-04	-1.5624E-05	-1.1791E-04	-1.4481E-04	-7.4850E-05	-1.6820E-04	-1.7053E-04	-7.7590E-06	
LB	-8.5300E-08	-8.4500E-06	-4.1820E-07	-2.7460E-06	-2.8640E-07	-9.7700E-06	-6.8100E-07	-5.3630E-06	-5.3570E-06	-6.7200E-06	-6.9700E-06	-8.6800E-06	-4.0900E-07	
LAR	-1.8300E-09	-9.8400E-08	-9.6900E-09	-3.3400E-08	-9.7100E-09	-1.1300E-07	-1.3600E-08	-5.4000E-08	-5.0500E-08	-2.5500E-08	-1.9000E-08	-2.3200E-08	-1.0600E-08	
Sum	-1.7123E-06	-1.8877E-04	-9.6437E-06	-5.4160E-05	-6.8787E-06	-2.1184E-04	-1.6534E-05	-1.2476E-04	-1.5269E-04	-7.9121E-05	-1.7945E-04	-1.8489E-04	-8.4634E-06	
Total	-1.2189E-03													

TABLE 3.18. STEEL DOPPLER COEFFICIENTS (CONTINUED)

TABLE 3.19. SODIUM DENSITY COEFFICIENTS

(1/2)														
Participant	Region	SHR1	LEZ1	SHR2	LEZ2	SCR	LEZ3	SHR3	MEZ	MOX	HEZ	SSA1	SSA2	RR
ANL	UAR	4.0493E-07	2.6510E-05	1.8181E-06	5.8967E-06	1.7584E-06	2.7639E-05	4.0336E-06	2.1426E-05	3.2209E-05	2.3583E-05	3.0431E-05	4.9969E-05	1.8284E-07
	UB	1.7592E-06	8.9495E-05	1.2240E-05	2.1915E-04	1.0195E-04	2.4615E-05	7.8348E-05	1.4082E-04	7.5680E-05	8.2397E-05	6.3571E-05	4.9969E-05	1.8284E-07
CORE	2.0536E-04	-1.1112E-03	1.1129E-03	-4.4633E-04	3.2828E-03	-1.5726E-03	2.4298E-03	-9.2928E-04	1.3767E-04	3.0493E-03	2.3947E-03	1.4687E-03	-1.5897E-05	
LB	1.9830E-04	1.3951E-04	1.0593E-03	3.8484E-05	1.5301E-03	1.7574E-04	2.0954E-03	1.5334E-04	2.1913E-04	1.1117E-04	1.1822E-04	8.8654E-05	-1.0550E-06	
LAR	2.2075E-06	7.1625E-05	1.0839E-05	2.6499E-05	1.1624E-05	9.0146E-05	1.7618E-05	4.8836E-05	4.4643E-05	2.4498E-05	2.8455E-05	4.6082E-05	1.6128E-07	
Sum	4.0803E-04	-7.8410E-04	2.1970E-03	-3.5297E-04	5.0454E-03	-1.1771E-03	4.5714E-03	-6.2733E-04	5.7448E-04	3.2842E-03	2.6542E-03	1.7170E-03	-1.7334E-05	
Total	1.7493E-02													
CEA/SA	UAR	1.7790E-07	1.2050E-05	7.4440E-07	2.3900E-06	6.7750E-07	1.1770E-05	1.7480E-06	9.8870E-06	1.5660E-05	1.1320E-05	1.9440E-05	2.1550E-07	
	UB	7.8822E-07	7.0418E-05	6.3694E-06	1.6272E-05	1.5097E-04	7.6509E-05	1.2536E-05	6.0022E-05	1.1167E-04	6.5451E-05	4.6279E-05	5.4883E-05	-7.0495E-07
CORE	1.3741E-05	-1.2727E-03	1.1009E-04	-5.1112E-04	6.5453E-04	-1.7658E-03	2.9876E-04	-1.0890E-03	-4.5610E-05	2.4190E-03	1.7757E-03	1.3965E-03	-1.8180E-05	
LB	6.1800E-05	1.0095E-04	3.2820E-04	2.6803E-05	4.1425E-04	1.3050E-04	6.5690E-04	1.2001E-04	1.7582E-04	9.6551E-05	6.8358E-05	7.8460E-05	-1.1462E-06	
LAR	8.1630E-07	3.6140E-05	3.9570E-06	1.3590E-05	4.0610E-06	4.5760E-05	6.2710E-06	2.5010E-05	2.3000E-05	1.2400E-05	1.1180E-05	1.8466E-05	1.9230E-07	
Sum	7.7323E-05	-1.0531E-03	4.4953E-04	-4.5206E-04	1.2245E-03	-1.5013E-03	9.7621E-04	-8.7406E-04	2.8054E-04	2.6047E-03	1.9128E-03	1.5678E-03	-1.9624E-05	
Total	5.1931E-03													
CIAE	UAR	8.0421E-07	2.6003E-05	3.9935E-06	9.6474E-06	4.1965E-06	3.2797E-05	6.3356E-06	1.7551E-05	1.6121E-05	9.0114E-06	1.0399E-05	1.8599E-05	3.2123E-07
	UB	1.9312E-05	3.4074E-05	1.0035E-04	9.4638E-06	1.8383E-04	4.5110E-05	1.9093E-04	4.3898E-05	5.5687E-05	2.3349E-05	4.4434E-05	4.4683E-05	5.7564E-07
CORE	-4.1739E-05	-1.7204E-03	-1.5748E-04	-6.0662E-04	7.1488E-04	-2.1967E-03	-2.3886E-04	-1.3324E-03	-4.3446E-04	2.5421E-03	1.8755E-03	1.2256E-03	1.0787E-05	
LB	3.7419E-06	1.3644E-04	3.0254E-05	2.7730E-05	2.4118E-04	1.4140E-04	5.9980E-05	1.1334E-04	2.2246E-04	1.6481E-04	1.3728E-04	1.0441E-04	1.3487E-06	
LAR	3.4823E-07	2.2840E-05	1.5459E-06	4.8838E-06	1.4580E-06	2.3258E-05	3.4471E-06	1.8173E-05	2.6972E-05	1.8580E-05	2.1435E-05	3.5590E-05	5.7850E-07	
Sum	-1.7532E-05	-1.5010E-03	-2.1346E-05	-5.5490E-04	1.1455E-03	-1.9541E-03	-2.7925E-05	-1.1394E-03	-2.7578E-04	-1.1322E-04	2.0890E-03	1.4289E-03	1.3611E-05	
Total	2.1055E-03													
IGCAR	UAR	3.7140E-07	2.2630E-05	1.6150E-06	5.3200E-06	1.5430E-06	2.3910E-05	3.51160E-06	1.8080E-05	2.6030E-05	1.7510E-05	1.6690E-05	1.7510E-05	1.3210E-07
	UB	1.8324E-06	7.7638E-05	1.2822E-05	1.7910E-05	1.0237E-04	8.3967E-05	2.5786E-05	6.6739E-05	1.2763E-04	7.1844E-05	4.5498E-05	4.4683E-05	-1.7895E-06
CORE	1.9400E-05	-1.2928E-03	1.5038E-04	-5.1376E-04	7.3771E-04	-4.1062E-03	4.1062E-04	-1.1326E-03	-1.9789E-04	2.6252E-03	1.4423E-03	4.0015E-04	-5.3488E-05	
LB	7.3470E-05	1.1408E-04	3.9031E-04	3.1427E-05	4.7670E-04	1.4795E-04	7.8010E-04	1.3422E-04	1.9668E-04	1.0371E-04	6.3060E-05	2.5088E-05	-2.7678E-06	
LAR	1.4050E-06	6.1230E-05	6.8335E-06	2.2690E-05	6.9700E-06	7.6090E-05	1.0670E-05	3.9840E-05	3.6160E-05	1.8830E-05	1.6200E-05	2.2300E-05	1.1590E-07	
Sum	9.6478E-05	-1.0172E-03	5.6196E-04	-4.3641E-04	1.3253E-03	-1.4718E-03	1.2307E-03	-8.7373E-04	1.8861E-04	2.8371E-03	1.5837E-03	4.9202E-04	-5.7797E-05	
Total	4.4589E-03													
IPPE	UAR	4.1100E-07	2.5700E-05	1.8100E-06	6.0000E-06	1.7400E-06	2.6300E-05	3.7400E-06	1.9400E-05	2.8500E-05	2.0600E-05	2.2200E-05	3.6800E-05	5.0100E-07
	UB	1.4879E-06	9.0810E-05	1.0284E-05	1.9541E-05	1.1020E-04	9.2370E-05	1.9706E-05	6.9520E-05	1.2695E-04	7.0030E-05	7.1360E-05	5.3140E-05	1.8150E-08
CORE	5.0295E-05	-9.4420E-04	3.0364E-04	-3.9827E-04	1.0056E-03	-1.2907E-03	6.7530E-04	-7.9470E-04	4.7200E-04	2.7170E-03	1.9563E-03	1.0350E-03	-1.2402E-05	
LB	8.4300E-05	1.5380E-04	4.3800E-04	4.2040E-05	5.2900E-04	1.8480E-04	8.3400E-04	1.4950E-04	2.0360E-04	1.0490E-04	1.0280E-04	7.2800E-05	-2.3900E-07	
LAR	1.6200E-06	7.0200E-05	7.8000E-06	2.5800E-05	7.9100E-06	8.5500E-05	1.1900E-05	4.4200E-05	4.0400E-05	2.2400E-05	2.2000E-05	3.5300E-05	4.7400E-07	
Sum	1.3811E-04	-6.0369E-04	7.6153E-04	-3.0489E-04	1.6545E-03	-9.0173E-03	1.5446E-03	-5.1208E-04	8.7145E-04	2.9349E-03	2.1747E-03	1.2330E-03	-1.1648E-05	
Total	8.9788E-03													

TABLE 3.19. SODIUM DENSITY COEFFICIENTS (CONTINUED)

TABLE 3.20. REGIONWISE SODIUM DENSITY COEFFICIENTS (TOTAL)

Participant	CORE*						Sum
	UB	LEZ	MEZ	MOX	HEZ	LB	
ANL	5.0898E-04	-3.1304E-03	-9.2928E-04	1.3767E-04	3.0493E-03	8.3737E-04	4.7368E-04
CEA/SA	4.0034E-04	-3.5496E-03	-1.0890E-03	-4.5610E-05	2.4190E-03	6.5063E-04	-1.2142E-03
CIAE	2.1158E-04	-4.5237E-03	-1.3324E-03	-4.3446E-04	2.5421E-03	8.0618E-04	-2.7307E-03
IGCAR	4.4572E-04	-3.6103E-03	-1.1326E-03	-1.9789E-04	2.6252E-03	7.2806E-04	-1.1418E-03
IPPE	4.6922E-04	-2.6332E-03	-7.9470E-04	4.7200E-04	2.7170E-03	8.3864E-04	1.0690E-03
JNC	5.2289E-04	-2.3442E-03	-6.8457E-04	1.9578E-04	2.9300E-03	8.3529E-04	1.4552E-03
Participant	Upper AR	Lower AR	SCR	SHR	SSA	RR	Total
ANL	2.2568E-04	4.2307E-04	5.0320E-03	7.1396E-03	4.2163E-03	-1.7334E-05	1.7493E-02
CEA/SA	9.7155E-05	2.0065E-04	1.2197E-03	1.4892E-03	3.4202E-03	-1.9624E-05	5.1931E-03
CIAE	1.5546E-04	1.7851E-04	1.1399E-03	-8.3277E-05	3.4319E-03	1.3611E-05	2.1055E-03
IGCAR	1.6115E-04	3.1922E-04	1.3168E-03	1.8647E-03	1.9966E-03	-5.7797E-05	4.4589E-03
IPPE	1.9320E-04	3.7503E-04	1.6448E-03	2.4170E-03	3.2914E-03	-1.1648E-05	8.9788E-03
JNC	1.6028E-04	3.1324E-04	1.4321E-03	2.0740E-03	3.4874E-03	-1.4715E-05	8.9075E-03

* Each column denotes the value only for the fuelled region.

TABLE 3.21. STEEL DENSITY COEFFICIENTS

TABLE 3.21. STEEL DENSITY COEFFICIENTS (CONTINUED)

(2/2)														
Participant	Region	SHR1	LEZ1	SHR2	LEZ2	SCR	LEZ3	SHR3	MEZ	MOX	HEZ	SSA1	SSA2	RR
JNC	UAR	2.7886E-07	1.8363E-05	1.2754E-06	4.1594E-06	1.2294E-06	1.8896E-05	2.7432E-06	1.4449E-05	2.1576E-05	1.5187E-05	1.6614E-05	2.7495E-05	6.1094E-06
	UB	3.0203E-06	2.4589E-04	2.3426E-05	7.3660E-05	5.7886E-05	2.9214E-04	4.4668E-05	2.0417E-04	3.1653E-04	1.6270E-04	3.9935E-04	3.3085E-04	3.3911E-05
CORE	-4.9466E-05	-7.9668E-03	-2.6869E-04	-2.398E-03	1.3273E-04	-9.6417E-03	-4.9329E-04	-6.2977E-03	-5.6240E-03	2.9589E-03	9.2403E-03	6.3013E-03	7.6480E-04	7.6480E-04
LB	3.0019E-05	3.1101E-04	1.6250E-04	7.7447E-05	1.3885E-04	3.7253E-04	3.1831E-04	3.2985E-04	4.8654E-04	2.4090E-04	5.7574E-04	4.6775E-04	4.8783E-05	4.8783E-05
LAR	1.5365E-06	5.0181E-05	6.6403E-06	1.7427E-05	6.9083E-06	6.0678E-05	1.0454E-05	3.2102E-05	3.1050E-05	1.6979E-05	1.6717E-05	2.6703E-05	5.8211E-06	5.8211E-06
Sum	-1.4611E-05	-7.3414E-03	-7.4851E-05	-2.2181E-03	3.3760E-04	-8.8974E-03	-1.1711E-04	-5.7171E-03	-4.7683E-03	3.3947E-03	1.0249E-02	7.1541E-03	8.5943E-04	8.5943E-04
Total	-7.1544E-03													
KAERI	UAR													
	UB													
CORE														
LB														
LAR														
Sum														
Total														
OKBM	UAR													
	UB													
CORE	-4.1800E-05	-8.6890E-03	-2.8190E-04	-2.5730E-03	1.6730E-04	-1.0140E-02	-4.6650E-04	-6.2160E-03	-5.2780E-03	2.9470E-03	7.7490E-03	5.2370E-03	5.2370E-03	7.2700E-04
LB														
LAR														
Sum	-4.1800E-05	-8.6890E-03	-2.8190E-04	-2.5730E-03	1.6730E-04	-1.0140E-02	-4.6650E-04	-6.2160E-03	-5.2780E-03	2.9470E-03	7.7490E-03	5.2370E-03	5.2370E-03	7.2700E-04
Total	-1.1360E-02													
Mean	UAR	3.2702E-07	1.7206E-05	1.5116E-06	4.4663E-06	1.5029E-06	1.8586E-05	2.9113E-06	1.3068E-05	1.2195E-05	1.2580E-05	2.0443E-05	3.9992E-06	
	UB	9.0593E-06	1.9148E-04	5.9195E-05	5.5303E-05	7.2892E-05	2.3073E-04	9.6704E-05	1.9269E-04	2.5593E-04	1.3279E-04	3.1977E-04	2.7094E-04	2.1975E-05
CORE	-3.9442E-05	-8.1954E-03	-2.3781E-04	-2.4615E-03	1.3312E-04	-9.8456E-03	-4.1614E-04	-6.0619E-03	-5.6371E-03	2.5863E-03	7.6741E-03	5.1043E-03	4.8454E-04	4.8454E-04
LB	2.5156E-05	2.4576E-04	1.3369E-04	6.4191E-05	1.2573E-04	3.1345E-04	2.6283E-04	2.5102E-04	4.2628E-04	2.3229E-04	5.2563E-04	4.1684E-04	3.4036E-05	3.4036E-05
LAR	9.7088E-07	4.0043E-05	4.5611E-06	1.4064E-05	4.6797E-06	4.8521E-05	7.2882E-06	2.6502E-05	2.6173E-05	1.4727E-05	1.4117E-05	2.2166E-05	4.3922E-06	4.3922E-06
Sum	-9.0018E-06	-7.7720E-03	-6.7270E-05	-2.3432E-03	3.0867E-04	-9.3217E-03	-9.9219E-05	-5.6477E-03	-5.0145E-03	2.9223E-03	8.4217E-03	5.7303E-03	5.3974E-04	5.3974E-04
Total	-1.1566E-02													
SD	UAR	2.1742E-07	6.7168E-06	1.1129E-06	2.6037E-06	1.1943E-06	8.3475E-06	1.6167E-06	4.5577E-06	6.1388E-06	4.4751E-06	4.4188E-06	6.9825E-06	2.2617E-06
	UB	1.4050E-05	5.8650E-05	9.2007E-05	1.7203E-05	4.0912E-05	6.5741E-05	1.3460E-04	6.3327E-05	6.5608E-05	4.1869E-05	1.2591E-04	1.1978E-04	1.9488E-05
CORE	2.4707E-05	7.6188E-04	1.3860E-04	2.1191E-04	6.1407E-05	9.1275E-04	3.0210E-04	9.8553E-03	1.2865E-03	1.1887E-03	2.9430E-03	2.5531E-03	4.1512E-04	4.1512E-04
LB	1.1999E-05	9.5879E-05	6.2369E-05	3.0053E-05	3.1653E-05	1.1624E-04	1.2058E-04	9.4537E-05	9.6287E-05	7.2818E-05	2.2847E-04	1.9702E-04	2.9918E-05	2.9918E-05
LAR	4.9103E-07	1.7887E-05	2.2392E-06	7.1920E-06	2.3154E-06	2.2482E-05	3.1746E-06	1.0340E-05	8.5628E-06	4.7115E-06	4.7790E-06	7.9439E-06	2.8116E-06	2.8116E-06
Sum	3.2570E-05	9.4808E-04	1.9975E-04	2.6213E-04	1.0632E-04	1.1155E-03	3.7459E-04	1.0777E-03	1.4153E-03	1.2617E-03	3.2575E-03	2.8494E-03	4.5714E-04	4.5714E-04
Total	1.2275E-02													

TABLE 3.22. FUEL DENSITY COEFFICIENTS

TABLE 3.22. FUEL DENSITY COEFFICIENTS (CONTINUED)

(2/2)														
Participant	Region	SHR1	LEZ1	SHR2	LEZ2	SCR	LEZ3	SHR3	MEZ	MOX	HEZ	SSA1	SSA2	RR
JNC	UAR													
	UB	1.1418E-04		6.0407E-05		1.9039E-04		1.3726E-04	2.2922E-04	5.1091E-05				
	CORE	5.1051E-02		1.4627E-02		6.0438E-02		5.5414E-02	1.0764E-01	5.7271E-02				
	LB	-4.7285E-04		-2.0075E-04		-5.6803E-04		-9.7733E-05	1.5506E-04	2.3945E-05				
	LAR													
	Sum	5.0693E-02		1.4487E-02		6.0061E-02		5.5454E-02	1.0803E-01	5.7346E-02				
KAFERI	Total	3.4607E-01												
	UAR													
	UB													
	CORE													
	LB													
	LAR													
OKBM	Sum													
	Total													
	UAR	1.7690E-04		8.6350E-05		2.6750E-04		1.5230E-04	1.9960E-04	9.4780E-05				
	UB	5.6490E-02		1.5940E-02		6.4770E-02		5.7530E-02	1.0980E-01	5.7890E-02				
	CORE	-2.6960E-04		-1.4740E-04		-3.2750E-04		-2.9700E-05	1.4850E-04	4.7850E-05				
	LB													
SD	LAR													
	Sum	5.6397E-02		1.5879E-02		6.4710E-02		5.7653E-02	1.1015E-01	5.8033E-02				
	Total	3.6282E-01												
	Mean													
	UAR	2.7850E-05		2.5212E-05		7.5867E-05		7.2404E-05	1.3435E-04	-2.1999E-05				
	UB	5.1618E-02		1.4879E-02		6.1274E-02		5.4706E-02	1.0762E-01	5.7321E-02				
SD	CORE	-4.3332E-04		-1.7770E-04		-5.1297E-04		-1.2253E-04	8.0006E-05	2.9341E-05				
	LB													
	LAR													
	Sum	5.1213E-02		1.4727E-02		6.0837E-02		5.4656E-02	1.0783E-01	5.7328E-02				
	Total	3.4659E-01												
	UAR													
SD	UB	1.8401E-04		6.7886E-05		2.3599E-04		1.3381E-04	1.7950E-04	1.5554E-04				
	CORE	3.0920E-03		7.2213E-04		2.4085E-03		2.6691E-03	1.7536E-03	1.6510E-03				
	LB	3.6585E-04		1.2716E-04		4.5649E-04		2.6482E-04	3.1001E-04	1.7128E-04				
	LAR													
	Sum	3.3756E-03		8.1107E-04		2.7713E-03		2.6584E-03	1.5669E-03	1.8458E-03				
	Total	9.0055E-03												

TABLE 3.23. ABSORBER DENSITY COEFFICIENTS

TABLE 3.23. ABSORBER DENSITY COEFFICIENTS (CONTINUED)

(2/2)														
Participant	Region	SHR1	LEZ1	SHR2	LEZ2	SCR	LEZ3	SHR3	MEZ	MOX	HEZ	SSA1	SSA2	RR
JNC	UAR	-3.2752E-05		-2.0401E-04		-2.1340E-04			-4.0777E-04					
	UB	-1.2756E-03		-8.6454E-03					-1.5920E-02					
	CORE													
	LB													
	LAR													
	Sum	-1.3084E-03		-8.8494E-03		-2.1340E-04			-1.6328E-02					
Total		-2.6699E-02												
	UAR													
	UB													
	CORE													
	LB													
	LAR													
KAERI	Sum													
	Total													
	UAR	-3.5890E-05		-1.9750E-04		-2.1400E-04			-3.7250E-04					
	UB	-1.4130E-03		-8.8200E-03					-1.5650E-02					
	CORE													
	LB													
OKBM	LAR													
	Sum	-1.4489E-03		-9.0175E-03		-2.1400E-04			-1.6023E-02					
	Total	-2.6703E-02												
	UAR													
	UB	-3.7770E-05		-2.1061E-04		-3.1520E-04			-4.0026E-04					
	CORE	-1.5416E-03		-9.1903E-03					-1.6984E-02					
Mean	LB													
	LAR													
	Sum	-1.5793E-03		-9.4009E-03		-3.1520E-04			-1.7384E-02					
	Total	-2.8680E-02												
	UAR													
	UB	3.1427E-06		9.3043E-06		1.9764E-04			5.6685E-05					
SD	CORE	4.0654E-04		1.5524E-03					2.5121E-03					
	LB													
	LAR													
	Sum	4.0912E-04		1.5569E-03		1.9764E-04			2.4649E-03					
	Total	4.5955E-03												

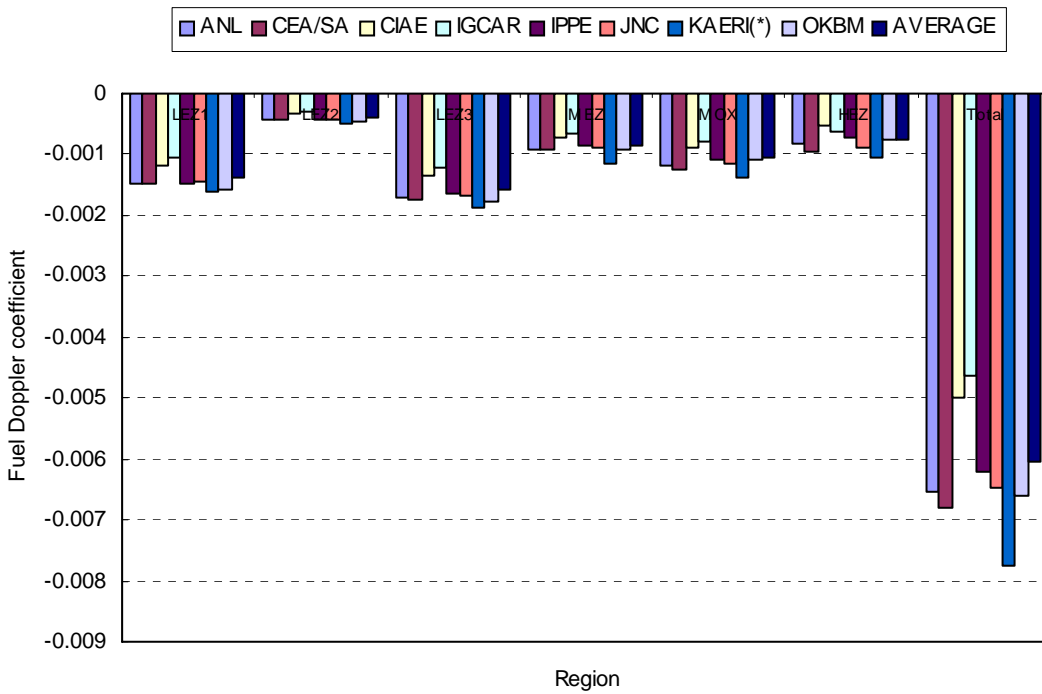


FIG. 3.24. Fuel Doppler coefficients (RZ model).

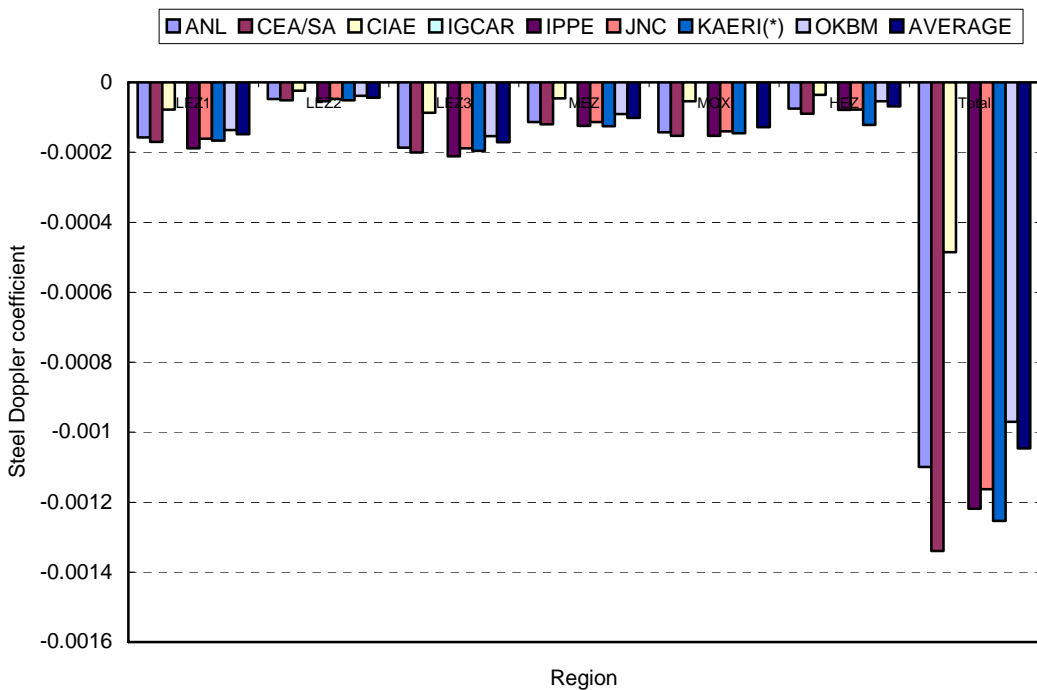


FIG. 3.25. Steel Doppler coefficients (RZ model).

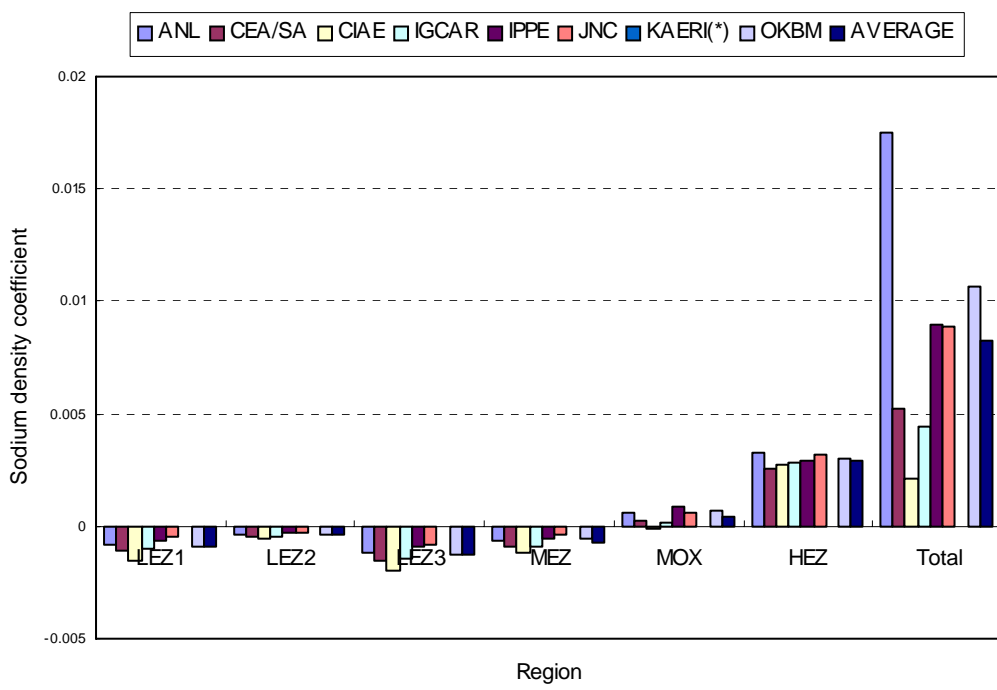


FIG. 3.26. Sodium density coefficients (RZ model).

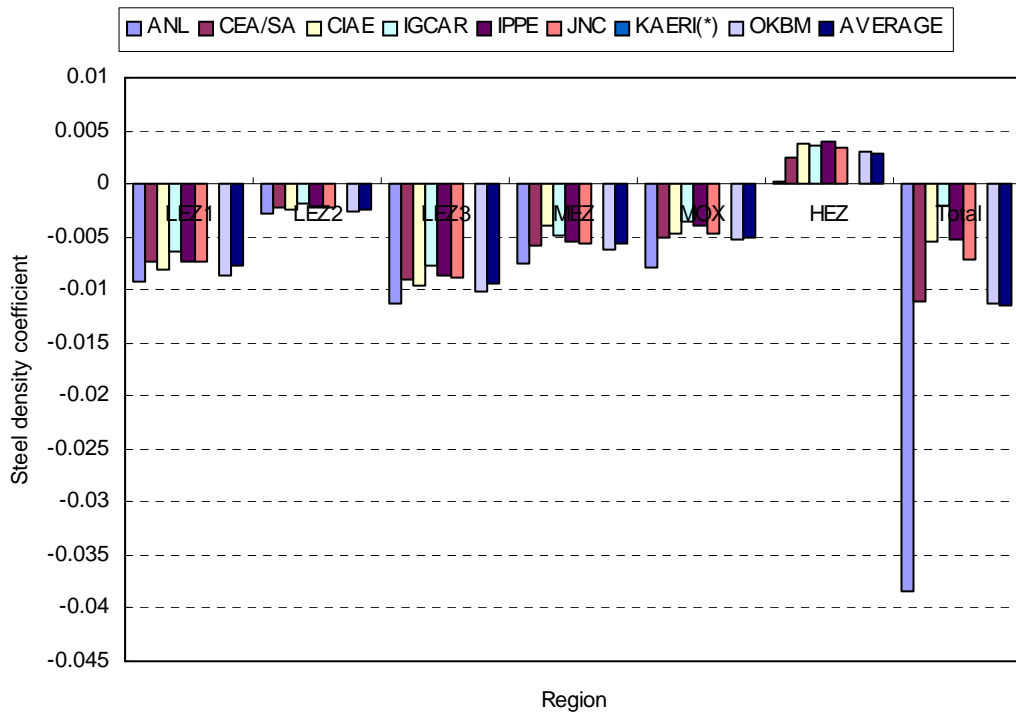


FIG. 3.27. Steel density coefficients (RZ model).

The comparison of the regionwise fuel density coefficients for the core shows good agreement between the results obtained by the participants. In Fig. 3.28 it is observed that the fuel density effect is most effective in the MOX zone in the core. For the absorber density coefficients, most results obtained by the participants show good agreement in their local and total values. The absorber densities for the SHR zones appeared to be substantially larger than those of the SCR zone, due to the control rods loading condition. In the SHR zone the bottom of the absorber is parked at the core midplane whereas in the SCR zone the absorber is parked at the enriched fuel region. It can be inferred in Fig. 3.29 that the absorber control in the outermost zone, i.e. the SHR3 zone is most effective between different SHR locations.

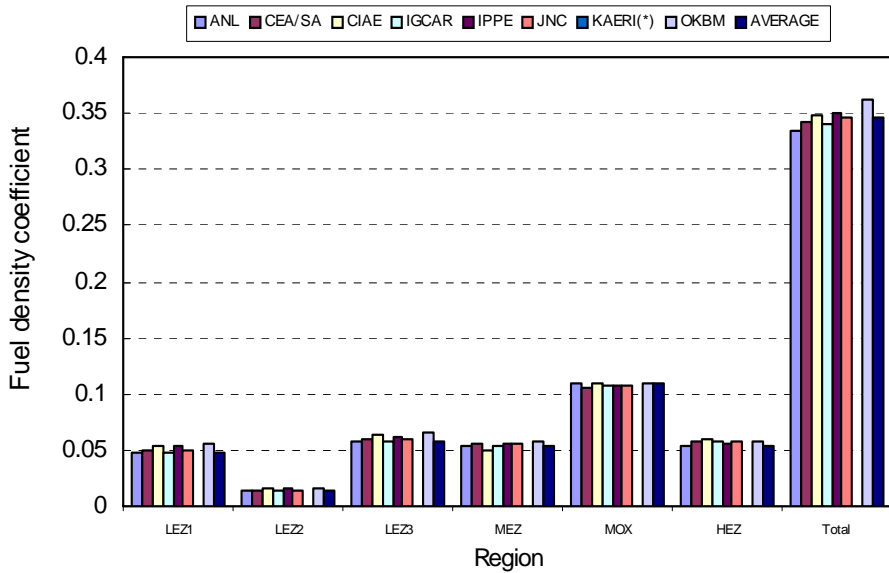


FIG. 3.28. Fuel density coefficients (RZ model).

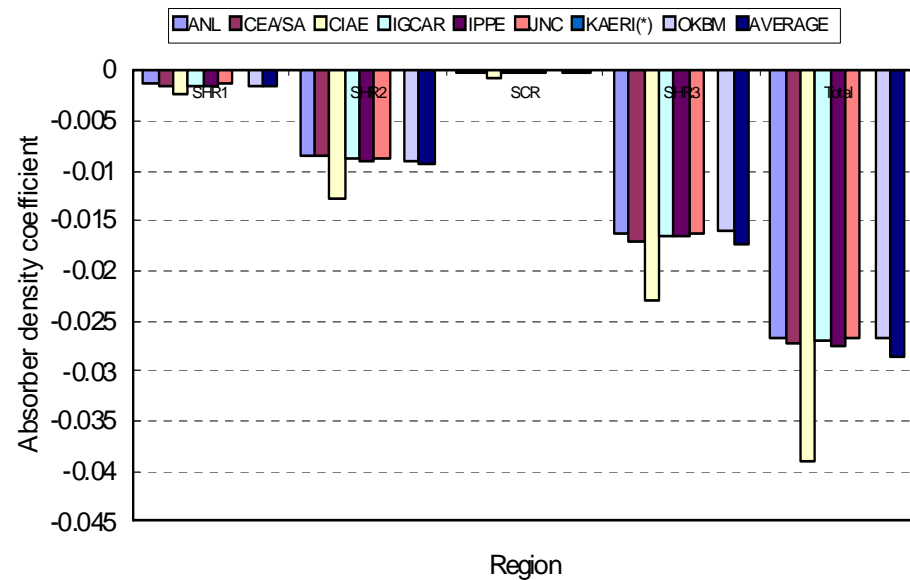


FIG. 3.29. Absorber density coefficients (RZ model).

3.2.Hex-Z homogeneous benchmark (Phase 2)

3.2.1. Hex-Z benchmark model

The three dimensional Hex-Z benchmark has been performed after a simpler two dimensional RZ benchmark (Phase 1).

The subassembly definitions, compositions and temperature conditions are the same as for the two dimensional RZ benchmark, as is the axial mesh. The radial configuration is shown in Fig. 3.1, and the arrangement of compositional regions is given in Fig. 3.2.

3.2.2. Description of the parameters calculated

The items calculated are the same as for the RZ benchmark except:

- The results are presented on the radial regions given in Fig. 3.4 with the axial mesh of the RZ benchmark;
- The radial reaction rates are given for a line 10.44 cm below the core centre line at the centre of each hexagonal mesh for the traverse which are defined in Fig. 3.1;
- The axial reaction rates are computed for a subassembly at the centre of the first LEZ region, and for a subassembly at the centre of the MOX region.

Spatial distributions of local reactivity coefficients and power are given by subassembly type (see Fig. 3.1), and by axial regions (as given in Section 3.1.2.2.). Comparing with the edition of the results for Phase 1, the results for LEZ fuel SAs are edited into LEZ1, LEZ2 types by merging LEZ3 into LEZ2, and for control rods, the results are grouped into one SCR type by merging three SCRs, i.e. SCR1, SCR2 and SCR3 into one SCR type.

3.2.3. Comparison of results

Reactivity parameters the same as those investigated in the calculations for the two-dimensional RZ homogeneous (Phase 1) model were calculated for the three-dimensional Hex-Z model, using first-order perturbation theory and direct k_{eff} differences.

3.2.3.1. Integral reactivity coefficients

Integral reactivity coefficients obtained by the participants for the Phase 2 benchmark are given in Tables 3.24–3.32, respectively with the mean value and the standard deviation of the results for each coefficient. The results of comparison of each reactivity coefficient are discussed in more detail below.

In Table 3.24, the Hex-Z diffusion and transport theory calculations predict the k_{eff} as 1.00451 and 1.01134 with relative standard deviations of 0.71% and 0.89%, respectively. In general, the diffusion theory prediction gives the k_{eff} value smaller by 0.68% than that of the transport theory. The k_{eff} values obtained from the diffusion and transport theory calculations by CEA/SA and KAERI appear to be relatively larger than the mean value. These larger predictions have also been recognised as resulting from the same attribution as in the Phase 1 results, i.e. due to the same nuclear data library JEF-2.2.

The fuel Doppler coefficients were obtained to be -0.00639 and -0.00679 with relative standard deviations of 12.2% and 7.7% for diffusion and transport theory calculations, respectively. In Table 3.25, the diffusion theory value is in good agreement with that from transport theory with 0.8% difference.

The results for the steel Doppler coefficient calculated using diffusion and transport theory are given in Table 3.26. The steel Doppler coefficients were estimated to be -0.00101 and -0.00107 with relative standard deviations of 18.8% and 16.8% for these two approximations. Results given in Table

3.26 show a good agreement between both approximations.

Similar to the Phase 1 results, the steel Doppler coefficient appears to be ~1/6 the magnitude of the fuel Doppler coefficient. The large dispersion in the predictions of the steel Doppler is attributed to the same reason as for the Phase 1 results.

In Table 3.27, the sodium density coefficients are 0.01024 and 0.00487 with relative standard deviations of 44.2% and 41.3% for the diffusion and transport theory results, respectively. Diffusion theory predicts the sodium density coefficient to be 137.4% larger than that of transport theory. Similar to the Phase 1 results, there exists a relatively large dispersion between results even using the same theory approximation, and there is also a relatively large difference between the diffusion and transport theory results.

For the steel density coefficient, there is a considerable dispersion between the results obtained by the different participants, see Table 3.28. That is, the steel density coefficients were evaluated to be 0.0017 and -0.0036 with relative standard deviations of 1354% and 1333% for diffusion and transport theory calculations, respectively. Similarly for the Phase 1 results, a large discrepancy is observed between the diffusion and transport theory results. It is especially noted that the diffusion theory predictions have a substantial dispersion between the results obtained by the participants.

In a comparison of the sodium density coefficients for Phase 1 and 2, there are considerable discrepancies between the RZ and Hex-Z model calculations as well as between the diffusion and transport theory calculations. Substantial discrepancies are also observed in the prediction of the steel density coefficients. The reason for these discrepancies is discussed in more detail in the discussion of spatial coefficient predictions.

The fuel density coefficients were evaluated to be 0.3506 and 0.3427 with relative standard deviations of 2.9% and 0.9% for diffusion and transport theory calculations respectively. Results given in Table 3.29 show a good agreement between both method approximations. Similarly for the Phase 1 results, the fuel density coefficient was estimated to be ~30 times larger than the steel density coefficient in the Phase 2 diffusion results.

The results for absorber density coefficient predicted by diffusion and transport theory calculations are given in Table 3.30. The absorber density coefficients are -0.0238 and -0.0220 with relative standard deviations of 8.4% and 5.0% in the diffusion and transport theory results, respectively. The diffusion theory predicts the absorber density coefficient larger by 2.3% in its magnitude than that of the transport theory.

In Table 3.31, the axial expansion coefficients were evaluated to be -0.1488 and -0.1448 with relative standard deviations of 6.9% and 5.2% for diffusion and transport theory calculations. The diffusion theory estimates the axial expansion coefficient larger by 2.7% in its magnitude than the transport theory. In comparison of the results obtained by the participants for Phase 1 and 2, the RZ diffusion and transport calculations predict the axial expansion coefficient smaller by 6.7% and 7.2% than the Hex-Z calculations, respectively.

Table 3.32 shows the radial expansion coefficients obtained by diffusion and transport theory calculations. The diffusion and transport theory method predict the radial expansion coefficient as -0.4872 and -0.4730 with relative standard deviations of 2.0% and 1.9%, respectively. Diffusion theory predicts a value 2.0% larger in its magnitude than that from transport theory. In the comparison of the results from Phase 1 and 2, for the radial expansion effect results from RZ geometry are similar to those from Hex-Z geometry. In addition, results from diffusion and transport theory calculations are also similar. It is common to the results of Phase 1 and 2 that the radial expansion coefficient is ~3 times larger than the axial expansion coefficient for a given relative change in dimension.

TABLE 3.24. EFFECTIVE MULTIPLICATION FACTORS (K_{EFF})

Participant	Diffusion		Transport		Rel. Diff. ²⁾ (%)
	Value	Rel. Dev. ¹⁾ (%)	Value	Rel. Dev. (%)	
ANL	0.99592	-0.86	0.99802	-1.32	-0.21
CEA/SA	1.01546	1.09	1.02272	1.13	-0.71
CIAE	1.00026	-0.42			
IGCAR	1.00642	0.19			
IPPE	1.00471	0.02			
JNC	1.00713	0.26	1.00967	-0.16	-0.25
KAERI	1.01260	0.81	1.01494	0.36	-0.23
OKBM	0.99357	-1.09			
Mean	1.00451		1.01134		-0.35
SD +/-	0.00714		0.00898		0.21

* 1) Relative Deviation from the mean = (Value - Mean) / Mean × 100 (%)

* 2) Relative Difference = (Diffusion - Transport) / Transport × 100 (%)

TABLE 3.25. FUEL DOPPLER COEFFICIENTS (K_D^{fuel})

Participant	Diffusion		Transport		Rel. Diff. (%)
	Value	Rel. Dev. (%)	Value	Rel. Dev. (%)	
ANL	-0.00665	3.95			
CEA/SA	-0.00686	7.34	-0.00681	0.30	0.78
CIAE	-0.00610	-4.52			
IGCAR	-0.00471	-26.40			
IPPE	-0.00635	-0.65	-0.00638	-6.03	-0.44
JNC	-0.00646	1.04	-0.00633	-6.77	2.05
KAERI	-0.00770	20.39	-0.00764	12.51	0.77
OKBM	-0.00632	-1.14			
Mean	-0.00639		-0.00679		0.79
SD +/-	0.00078		0.00052		0.88

TABLE 3.26. STEEL DOPPLER COEFFICIENTS (K_D^{steel})

Participant	Diffusion		Transport		Rel. Diff. (%)
	Value	Rel. Dev. (%)	Value	Rel. Dev. (%)	
ANL	-0.00106	5.12			
CEA/SA	-0.00131	29.46	-0.00132	23.54	-1.01
CIAE	-0.00067	-33.60			
IGCAR					
IPPE	-0.00080	-21.05	-0.00080	-25.13	-0.40
JNC	-0.00109	7.99	-0.00109	2.01	0.00
KAERI	-0.00108	6.87	-0.00106	-0.43	1.38
OKBM	-0.00106	5.21			
Mean	-0.00101		-0.00107		0.00
SD +/-	0.00019		0.00018		0.88

TABLE 3.27. SODIUM DENSITY COEFFICIENTS (W_{Na})

Participant	Diffusion		Transport		Rel. Diff. (%)
	Value	Rel. Dev. (%)	Value	Rel. Dev. (%)	
ANL	0.02072	102.46			
CEA/SA	0.00771	-24.67	0.00592	21.48	30.24
CIAE	0.00486	-52.52			
IGCAR	0.00668	-34.69			
IPPE	0.00877	-14.31	0.00206	-57.73	325.78
JNC	0.01038	1.41	0.00664	36.25	56.33
KAERI	0.01050	2.55			
OKBM	0.01226	19.76			
Mean	0.01024		0.00487		137.45
SD +/-	0.00453		0.00201		133.60

TABLE 3.28. STEEL DENSITY COEFFICIENTS (W_{steel})

Participant	Diffusion		Transport		Rel. Diff. (%)
	Value	Rel. Dev. (%)	Value	Rel. Dev. (%)	
ANL	-0.0284	-1732.45			
CEA/SA	-0.0022	-228.78	-0.0073	105.25	-69.33
CIAE	-0.0037	-310.04			
IGCAR	0.0107	514.18			
IPPE	0.0019	10.96	0.0032	-189.97	-39.71
JNC	-0.0020	-215.60	-0.0066	84.72	-69.41
KAERI	0.0394	2168.81			
OKBM	-0.0019	-207.07			
Mean	0.0017		-0.0036		-59.48
SD +/-	0.0176		0.0048		13.98

TABLE 3.29. FUEL DENSITY COEFFICIENTS (W_{fuel})

Participant	Diffusion		Transport		Rel. Diff. (%)
	Value	Rel. Dev. (%)	Value	Rel. Dev. (%)	
ANL	0.3339	-4.77			
CEA/SA	0.3435	-2.02	0.3385	-1.22	1.48
CIAE	0.3591	2.41			
IGCAR	0.3691	5.27			
IPPE	0.3477	-0.84	0.3438	0.33	1.13
JNC	0.3466	-1.15	0.3457	0.89	0.26
KAERI	0.3490	-0.46			
OKBM	0.3561	1.55			
Mean	0.3506		0.3427		0.96
SD +/-	0.0100		0.0030		0.51

TABLE 3.30. ABSORBER DENSITY COEFFICIENTS (W_{abs})

Participant	Diffusion		Transport		Rel. Diff. (%)
	Value	Rel. Dev.(%)	Value	Rel. Dev. (%)	
ANL	-0.0241	1.23			
CEA/SA	-0.0258	8.30	-0.0234	6.53	10.16
CIAE	-0.0243	2.07			
IGCAR	-0.0234	-1.81			
IPPE	-0.0217	-8.82	-0.0206	-6.22	5.34
JNC	-0.0200	-15.97	-0.0219	-0.30	-8.68
KAERI	-0.0267	12.24			
OKBM	-0.0245	2.75			
Mean	-0.0238		-0.0220		2.27
SD +/-	0.0020		0.0011		7.99

TABLE 3.31. AXIAL EXPANSION COEFFICIENTS (R_{ax})

Participant	Diffusion		Transport		Rel. Diff. (%)
	Value	Rel. Dev.(%)	Value	Rel. Dev. (%)	
ANL	-0.1598	7.42			
CEA/SA	-0.1463	-1.66	-0.1397	-3.53	4.72
CIAE	-0.1600	7.58			
IGCAR	-0.1461	-1.78			
IPPE	-0.1384	-6.97	-0.1352	-6.64	2.37
JNC	-0.1574	5.80	-0.1530	5.65	2.88
KAERI	-0.1528	2.69	-0.1514	4.51	0.93
OKBM	-0.1293	-13.08			
Mean	-0.1488		-0.1448		2.72
SD +/-	0.0102		0.0076		1.36

TABLE 3.32. RADIAL EXPANSION COEFFICIENTS (R_{rad})

Participant	Diffusion		Transport		Rel. Diff. (%)
	Value	Rel. Dev.(%)	Value	Rel. Dev. (%)	
ANL	-0.4947	1.53			
CEA/SA	-0.4741	-2.69	-0.4605	-2.64	2.95
CIAE	-0.5008	2.79			
IGCAR	-0.4788	-1.72			
IPPE	-0.4904	0.65	-0.4822	1.95	1.70
JNC	-0.4923	1.04	-0.4814	1.78	2.26
KAERI	-0.4726	-3.01	-0.4679	-1.09	1.01
OKBM	-0.4941	1.41			
Mean	-0.4872		-0.4730		1.98
SD +/-	0.0099		0.0092		0.72

In comparison of the results of Phase 1 and 2, the diffusion theory generally predicts the uniform expansion effect in both axial and radial directions larger than the transport theory, however, within acceptable limits. The diffusion and transport calculations predict the uniform expansion effects in both radial and axial directions with a minor relative difference of about 2%. This indicates that both the RZ and Hex-Z model calculations provide an appropriate tool for calculating the uniform expansion coefficients.

3.2.3.2. Kinetic parameters

The system kinetic parameters calculated for Phase 2 were the same as for Phase 1 and are given in Tables 3.33–3.36, respectively. In the Phase 2 study, these parameters were only calculated using the diffusion theory approximation. The Hex-Z diffusion theory results provided by each participant agree well for all parameters except decay constants.

Tables 3.33 and 3.34 show effective delayed neutron fractions and groupwise effective delayed neutron fractions for 6 delayed neutron groups provided by each of the participants, respectively. The total effective delayed neutron fraction is simply the sum of the groupwise delayed neutron fractions over all groups. In a similar manner to Phase 1, the groupwise effective delayed neutron fractions for the 6 delayed neutron group structure show a reasonable agreement for each group. Agreement is within 12.2% of the relative standard deviation about the mean, except for the 6th group and, as a result, the total delayed neutron fraction is predicted with a relative standard deviation of 1.73%. The diffusion theory method gives an effective delayed neutron fraction of 0.00590 (590 pcm) which agrees well with the Phase 1 result, $\beta_{\text{eff}} = 0.00588$ (588 pcm).

In Table 3.35, the prompt neutron lifetime for the benchmark is given as 4.409×10^{-7} s when calculated using diffusion theory with a 3.4% relative standard deviation. Diffusion theory predicts the prompt neutron lifetime as 3.1% smaller in RZ rather than Hex-Z geometry. The 6 group decay constants provided by each participant show good agreement, within a relative standard deviation of 2.3% except for groups 5th and 6th. In comparison to the Phase 1 results, the participants Phase 2 results for the 5th and 6th group show a considerably larger deviation.

TABLE 3.33. EFFECTIVE DELAYED NEUTRON FRACTIONS (β_{eff})

(Unit: pcm)

Participant	Value	Rel. Dev. (%)
ANL	581	-1.62
CEA/SA	598	1.29
CIAE	598	1.29
IGCAR	598	1.34
IPPE	593 (591)*	0.48
JNC	587	-0.57
KAERI	595	0.80
OKBM	573	-3.01
Mean	590	
SD +/-	8.9	

* Transport theory result

TABLE 3.34. GROUPWISE EFFECTIVE DELAYED NEUTRON FRACTIONS

Participant	Delayed neutron group						Total
	1	2	3	4	5	6	
ANL	1.679E-04	9.685E-04	9.320E-04	2.219E-03	1.083E-03	4.383E-04	5.808E-03
CEA/SA	1.700E-04	1.010E-03	9.700E-04	2.270E-03	1.080E-03	4.400E-04	5.980E-03
CIAE	1.863E-04	1.190E-03	1.099E-03	2.361E-03	9.115E-04	2.407E-04	5.988E-03
IGCAR	1.850E-04	1.196E-03	1.101E-03	2.361E-03	9.032E-04	2.369E-04	5.983E-03
IPPE	1.710E-04	9.850E-04	9.500E-04	2.270E-03	1.110E-03	4.490E-04	5.935E-03
JNC	1.791E-04	1.164E-03	1.075E-03	2.317E-03	8.965E-04	2.384E-04	5.870E-03
KAERI							5.951E-03
OKBM	1.600E-04	1.175E-03	1.079E-03	2.213E-03	8.090E-04	2.910E-04	5.726E-03
Average	1.742E-04	1.098E-03	1.029E-03	2.287E-03	9.704E-04	3.335E-04	5.898E-03
S.D. +/-	9.630E-06	1.046E-04	7.505E-05	6.129E-05	1.180E-04	1.036E-04	1.016E-04

TABLE 3.35. PROMPT NEUTRON LIFETIMES

(Unit: 10^{-7} s)

Participant	Value	Rel. Dev.(%)
ANL	4.491	1.87
CEA/SA	4.606	4.48
CIAE	4.239	-3.85
IGCAR		
IPPE	4.467 (4.523)*	1.33
JNC	4.484	1.70
KAERI	4.443	0.79
OKBM	4.130	-6.32
Mean	4.409	
SD +/-	0.152	

* Transport theory result.

TABLE 3.36. DECAY CONSTANTS

(Unit: s^{-1})

Participant	Delayed neutron group					
	1	2	3	4	5	6
ANL	1.337E-02	3.220E-02	1.205E-01	3.075E-01	8.708E-01	2.917E+00
CEA/SA	1.291E-02	3.140E-02	1.173E-01	3.133E-01	1.116E+00	3.428E+00
CIAE	1.272E-02	3.163E-02	1.168E-01	3.125E-01	1.388E+00	3.777E+00
IGCAR	1.278E-02	3.169E-02	1.227E-01	3.247E-01	1.395E+00	3.888E+00
IPPE	1.330E-02	3.220E-02	1.210E-01	3.080E-01	8.710E-01	2.920E+00
JNC	1.270E-02	3.170E-02	1.150E-01	3.110E-01	1.400E+00	3.870E+00
KAERI						
OKBM	1.250E-02	3.070E-02	1.180E-01	3.170E-01	1.240E+00	3.310E+00
Average	1.290E-02	3.164E-02	1.188E-01	3.134E-01	1.183E+00	3.444E+00
S.D. +/-	3.230E-04	5.117E-04	2.718E-03	5.927E-03	2.369E-01	4.204E-01

3.2.3.3. Power distribution

The core power distributions calculated with the local energy deposition model by the participants are given in Table 3.37. Using these power distribution results, regionwise normalized power distributions are compared in Fig. 3.30 with their average values. The comparison of regionwise power distributions shows good agreement over the fuel zones for the Hex-Z model.

Figure 3.31 illustrates typical power output distributions for the Hex-Z model, which were calculated by diffusion theory calculations by ANL. The largest power output is produced in the second half region of LEZ (LEZ2) in the enriched fuel regions.

Table 3.38 shows power fractions for the enriched fuel regions in the core obtained by averaging over the results of each participant, which were calculated from the Hex-Z diffusion calculations. Similar to the RZ diffusion calculational results in Phase 1, 97.5% of total power is produced in the enriched fuel regions, i.e. LEZ, MEZ, HEZ and MOX, and the total power fraction of the blanket regions is 2.5%. The MOX region produces 21.6% of total power, whereas it produces 21.9% in the RZ diffusion calculations. The comparison of diffusion theory calculations for both the RZ and Hex-Z models show good agreement in power distribution predictions.

3.2.3.4. Reaction rate distributions

Spatially dependent microscopic fission and capture reaction rates ($\sigma \phi$) for ^{235}U fission, ^{238}U fission, and ^{238}U capture on the radial and axial traverses specified in Fig. 3.1 are illustrated in Figs 3.32–3.41. These figures show spatial reaction rates distributions in the axial and radial directions which were obtained from diffusion and transport theory calculations by the participants. In the same way as performed for the Phase 1 study, infinite dilution cross sections and arbitrary number densities were used where they are absent. The radial reaction rates are presented on a radial traverse 10.44 cm below core centre line at the centre of each hexagonal mesh which are defined in Fig. 3.1. In the Hex-Z model, the axial reactions rates were computed for a subassembly at the centre of the first LEZ region, and for a subassembly at the centre of the MOX region, at the centre of the axial mesh structure used for reactivity coefficient edits.

Figures 3.32–3.37 show the axial reaction rate distributions for ^{235}U fission, ^{238}U fission, and ^{238}U capture on the axial traverses in LEZ and MOX. Similar for the Phase 1 results, it can also be observed the discordance in the peaked-value positions and the shift of their locations downward from the core mid-plane as well between the participants' results.

In comparison of the diffusion theory results shown in Fig. 3.32, peak values for the ^{235}U fission rates were predicted within 4.4% of relative difference in LEZ. For the ^{238}U fission rate, peak values were obtained within 8.3% of relative difference, where the JNC result has the largest value. The axial ^{238}U capture rate results show worse agreement, as compared with them for the other reaction rates. The CIAE result shows the largest peak value. The maximum relative difference between the peak values in the axial ^{238}U capture rate distributions in LEZ was obtained to be 17.9%. Apparent humps in the ^{238}U capture rates indicate a strong transitional self-shielding effect near the UB-AR and LB-AR interfaces as noted in the Phase 1 study.

Figures 3.36 and 3.37 show the axial reaction rate distributions in MOX obtained from the diffusion and transport theory calculations, respectively. Both theory results obtained by each participant agree well both in the spatial behaviours and in the peak values in the axial reaction rate distributions. More specifically, in Fig. 3.36 the comparison of the KAERI results for the axial ^{235}U fission rate distributions in MOX shows very good agreement between both theory results.

TABLE 3.37. POWER DISTRIBUTIONS

Participant		Region	LEZ1	LEZ2	MEZ	MOX	HEZ	SHR	SCR	SSA1	SSA2	(Unit: Watt) (1/2)
ANL		UAR	1.7837E+06	3.8116E+06	1.8637E+06	2.6618E+06	1.7399E+06					
		UB	1.9857E+08	4.2827E+08	2.3745E+08	3.1938E+08	2.5294E+08					
		CORE	3.7387E+06	8.0023E+06	3.3213E+06	3.9582E+06	2.5016E+06					
		LB										
		LAR										
		Sum	2.0410E+08	4.4008E+08	2.4263E+08	3.2600E+08	2.5719E+08					
		Total	1.4700E+09									
CEA/SA		UAR										
		UB	2.0923E+06	4.3870E+06	2.2254E+06	3.2560E+06	2.2188E+06					
		CORE	1.9365E+08	4.1872E+08	2.3181E+08	3.1433E+08	2.5889E+08					
		LB	4.4995E+06	9.5520E+06	4.0630E+06	4.9730E+06	3.2465E+06					
		LAR										
		Sum	2.0024E+08	4.3266E+08	2.3810E+08	3.2256E+08	2.6435E+08					
		Total	1.4579E+09									
CIAE		UAR										
		UB	1.6868E+06	3.5694E+06	1.8522E+06	2.6888E+06	1.8143E+06					
		CORE	1.9755E+08	4.2601E+08	2.4378E+08	3.1386E+08	2.5505E+08					
		LB	3.5803E+06	7.6857E+06	3.4682E+06	4.4533E+06	2.8722E+06					
		LAR										
		Sum	2.0281E+08	4.3727E+08	2.4910E+08	3.2101E+08	2.5973E+08					
		Total	1.4699E+09									
IGCAR		UAR	3.9750E+04	8.2250E+04	4.1340E+04	6.0780E+04	4.6000E+04	1.2960E+04	3.7990E+03	4.6590E+04	1.0170E+05	4.2130E+04
		UB	2.3560E+06	4.9748E+06	2.4725E+06	3.5745E+06	2.4219E+06	8.2407E+05	1.8166E+05	3.7362E+05	8.0449E+05	1.6935E+05
		CORE	1.9075E+08	4.1417E+08	2.3016E+08	3.1337E+08	2.5342E+08	5.0128E+06	3.2937E+05	3.6867E+06	7.4772E+06	1.4782E+06
		LB	4.8670E+06	1.0339E+07	4.3880E+06	5.3510E+06	3.4660E+06	1.2944E+05	4.1780E+04	5.0380E+05	1.0575E+06	2.1800E+05
		LAR	6.5460E+04	1.3540E+05	5.6480E+04	7.2870E+04	5.0470E+04	2.1408E+04	7.2980E+03	4.9020E+04	1.0380E+05	4.2620E+04
		Sum	1.9808E+08	4.2970E+08	2.3712E+08	3.2243E+08	2.5940E+08	6.0007E+06	5.6391E+05	4.6597E+06	9.5447E+06	1.9503E+06
		Total	1.4695E+09									
IPPE		UAR										
		UB	1.8000E+06	3.8000E+06	1.9000E+06	2.7000E+06	1.8000E+06					
		CORE	2.0120E+08	4.3060E+08	2.3630E+08	3.1470E+08	2.5420E+08					
		LB	3.7000E+06	8.0000E+06	3.4000E+06	4.0000E+06	2.6000E+06					
		LAR										
		Sum	2.0670E+08	4.4240E+08	2.4160E+08	3.2140E+08	2.5860E+08					
		Total	1.4707E+09									

(Note) Regions LEZ2 and SHR in the table correspond to LEZ2 = LEZ2 + LEZ3, SHR = SHR1 + SHR2 + SHR3 in the RZ model respectively.

TABLE 3.37. POWER DISTRIBUTIONS (CONTINUED)

(Unit: Watt) (2/2)											
Participant	Region	LEZ1	LEZ2	MEZ	MOX	HEZ	SHR	SCR	SSA1	SSA2	RR
JNC	UAR	1.8901E+06	3.9937E+06	1.9449E+06	2.7711E+06	1.7895E+06					
	UB	2.0018E+08	4.2804E+08	2.3548E+08	3.2305E+08	2.4928E+08					
	CORE	3.7670E+06	7.9219E+06	3.3353E+06	4.0303E+06	2.5295E+06					
	LB										
	LAR										
	Sum	2.0584E+08	4.3996E+08	2.4076E+08	3.2985E+08	2.5360E+08					
	Total	1.4700E+09									
KAERI	UAR	8.2869E+03	1.6644E+04	8.7213E+03	1.3286E+04	1.0524E+04	2.6282E+03	7.2225E+02	1.1125E+04	2.3940E+04	1.4704E+04
	UB	2.1370E+06	4.4805E+06	2.2442E+06	3.2874E+06	2.2943E+06	3.0708E+05	7.2225E+02	2.0029E+05	4.7755E+05	8.9094E+04
	CORE	1.9444E+08	4.2069E+08	2.3250E+08	3.1016E+08	2.6652E+08	1.7862E+06	7.2225E+02	1.7246E+06	4.2360E+06	6.9046E+05
	LB	4.5145E+06	9.5999E+06	4.0526E+06	4.9439E+06	3.3000E+06	1.9969E+04	7.2225E+02	2.5877E+05	6.0514E+05	9.7527E+04
	LAR	1.4763E+04	3.0570E+04	1.2719E+04	1.6518E+04	1.1799E+04	4.8216E+03	7.2225E+02	1.1912E+04	2.4818E+04	1.4980E+04
	Sum	2.0112E+08	4.3482E+08	2.3882E+08	3.1842E+08	2.6614E+08	2.1207E+06	3.6113E+03	2.2067E+06	5.3674E+06	9.0677E+05
	Total	1.4700E+09									
OKBM	UAR	2.2035E+06	4.6060E+06	2.2447E+06	3.1918E+06	2.1272E+06					
	UB	2.0004E+08	4.2942E+08	2.3540E+08	3.2081E+08	2.4369E+08					
	CORE	4.5785E+06	9.6790E+06	4.0465E+06	4.8624E+06	3.0895E+06					
	LB										
	LAR										
	Sum	2.0682E+08	4.4370E+08	2.4169E+08	3.2887E+08	2.4891E+08					
	Total	1.4700E+09									
Mean	UAR	1.9094E+06	4.0279E+06	2.0052E+06	2.8783E+06	1.9150E+06					
	UB	1.9853E+08	4.2684E+08	2.3670E+08	3.1769E+08	2.5234E+08					
	CORE	3.9773E+06	8.4735E+06	3.6057E+06	4.3795E+06	2.8066E+06					
	LB										
	LAR										
	Sum	2.0442E+08	4.3934E+08	2.4231E+08	3.2495E+08	2.5706E+08					
	Total	1.4681E+09									
SD	UAR	1.9880E+05	3.9323E+05	1.8109E+05	2.7093E+05	2.0353E+05					
	UB	2.7187E+06	4.2628E+06	3.9488E+06	3.9041E+06	5.2380E+06					
	CORE	4.4039E+05	8.9304E+05	3.5174E+05	4.5484E+05	3.1316E+05					
	LB										
	LAR										
	Sum	2.5749E+06	3.9555E+06	3.6677E+06	3.8560E+06	5.3141E+06					
	Total	4.9973E+06									

* The results of IGCAR and KAERI are not included in the averages.

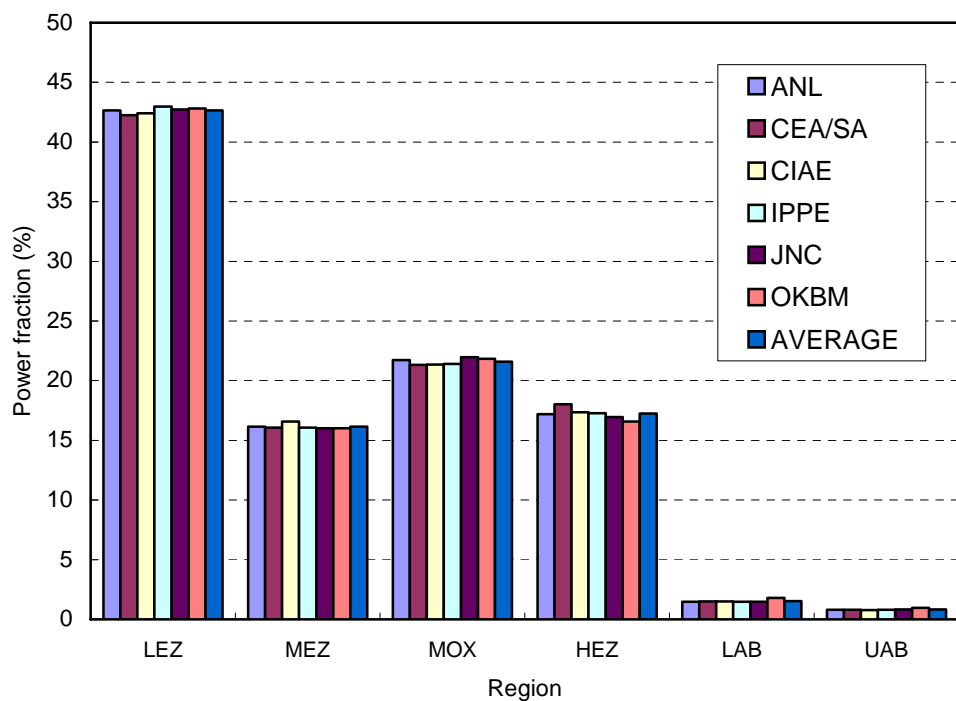


FIG. 3.30. Power distributions (Hex-Z model).

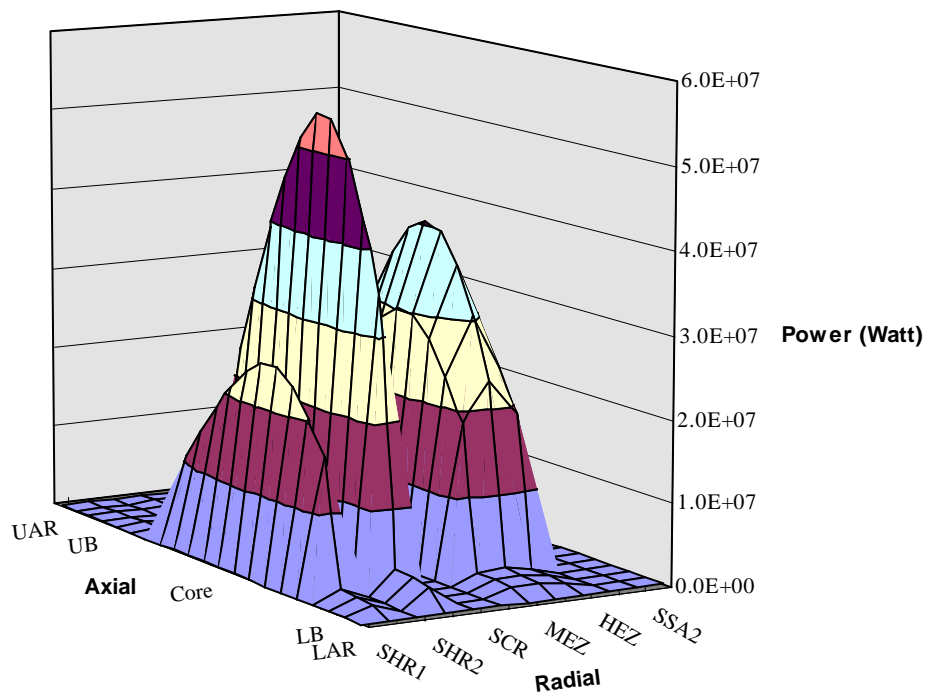


FIG. 3.31. Power output distribution (ANL result) (Hex-Z model).

TABLE 3.38. POWER FRACTIONS FOR FUEL REGIONS

Region	Fraction (%)
LEZ	42.60
MEZ	16.12
MOX	21.64
HEZ	17.19
<i>Core</i>	97.55
LB	1.58
UB	0.87
Total	100.00

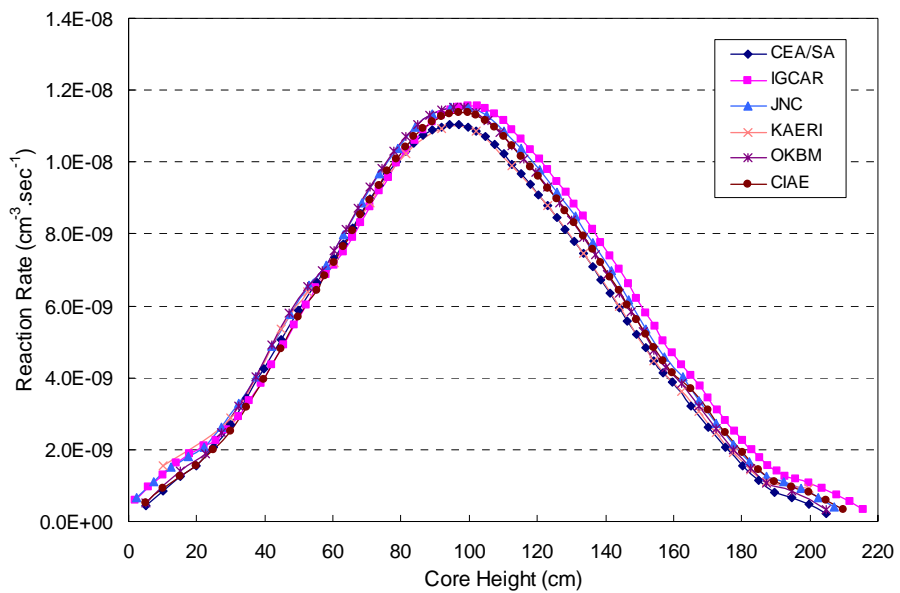


FIG. 3.32. Axial ^{235}U fission rate distributions in LEZ (Phase 2, diffusion).

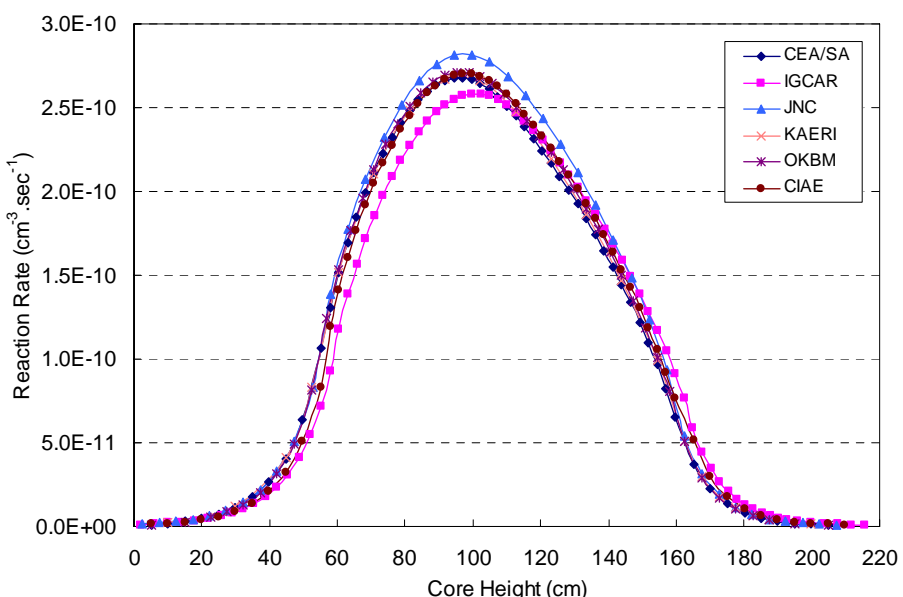


FIG. 3.33. Axial ^{238}U fission rate distributions in LEZ (Phase 2, diffusion).

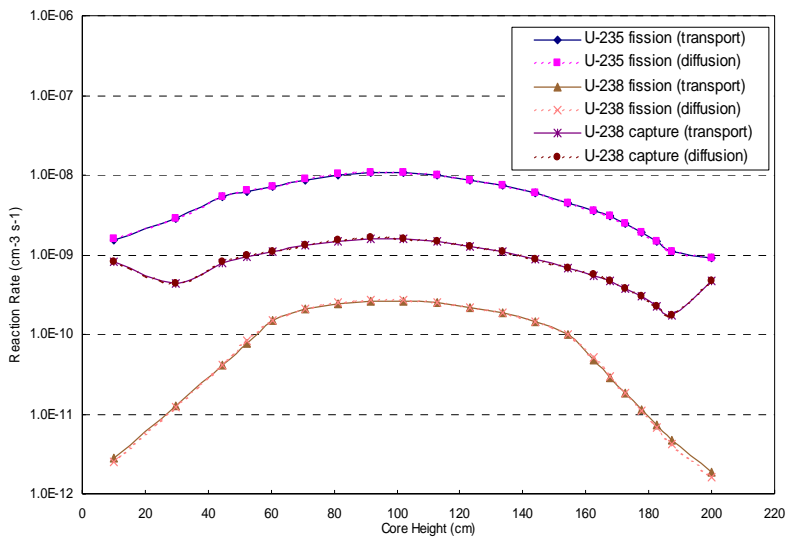


FIG. 3.34. Axial ^{238}U capture rate distributions in LEZ (Phase 2, diffusion).

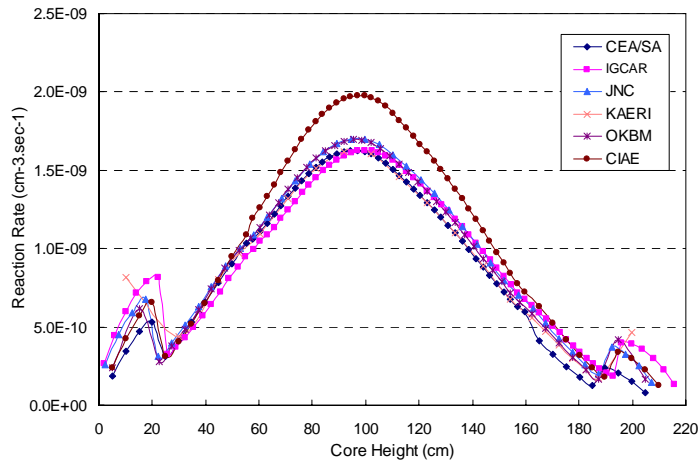


FIG. 3.35. Axial reaction rate distributions in LEZ (Phase 2, transport vs. diffusion) (KAERI results).

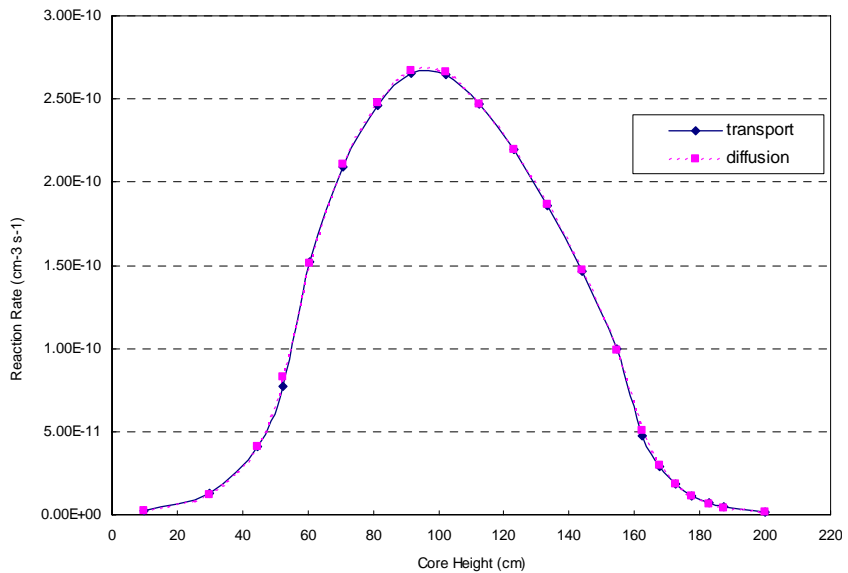


FIG. 3.36. Axial ^{238}U fission rate distributions in MOX (Phase 2, transport vs. diffusion) (KAERI results).

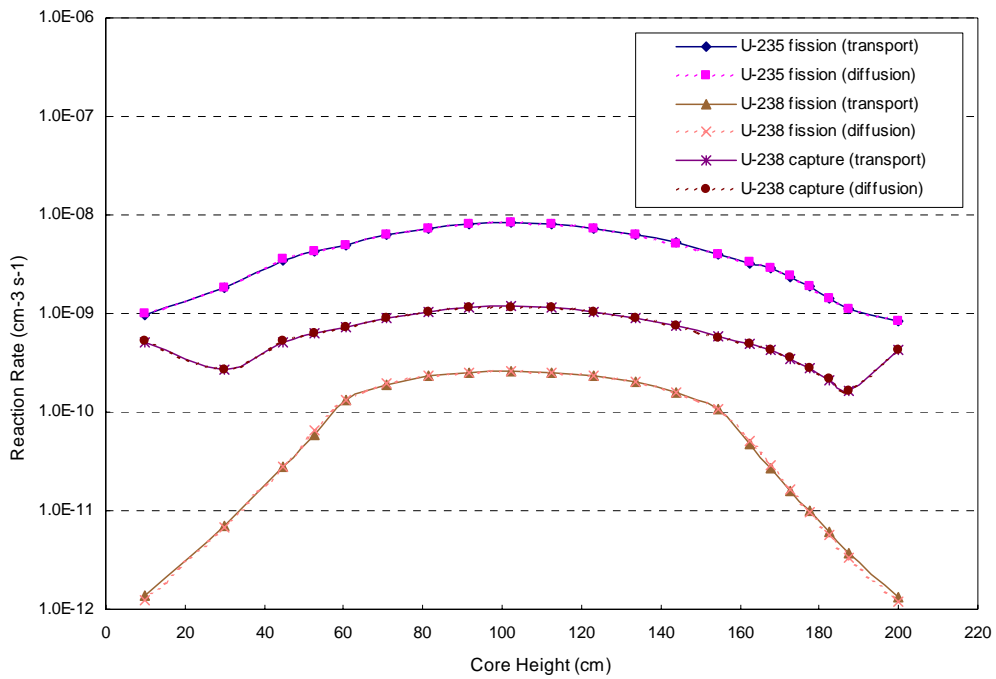


FIG. 3.37. Axial reaction rate distributions in MOX (Phase 2, transport vs. diffusion) (KAERI results).

Diffusion results for radial reaction rate distributions calculated by the participants are compared in Figs 3.38–3.41. Most diffusion results agree well in the radial reaction rate behaviours and in its magnitudes as well in the fuelled regions of interest on the specified traverses. Most radial reaction rates in the fuelled regions were obtained within about 8% of relative difference. Apparently the CEA/SA result has the largest peak value for the ^{238}U capture rate near the HEZ-SSA interface. Its magnitude is about 50% larger than the others and it is attributable again to an artifact of resonance self-shielding when there is a zero nuclide number density. Similarly for the axial reaction rate distributions, there exists a strong transitional self-shielding effect near the HEZ-SSA interface in the radial ^{238}U capture rate distributions.

Figure 3.41 compares the radial reaction rate distributions obtained from the diffusion and transport theory calculations, respectively. Both theory results calculated by each participant agree well both in the radial reaction rate behaviours and in its magnitudes in the fuelled regions of interest in the reaction rate distributions.

In comparison with the RZ calculational results in the Phase 1 study, local dip and rising in the radial reaction rate distributions mainly resulting from different spatial self-shielding are more clearly observable, in comparison with the RZ calculational results in the Phase 1 study. It is attributable to the fact that the Hex-Z model is more descriptive in the actual benchmark model configuration than the RZ model. It is noted that there exist a local dip in the ^{238}U fission rates and a local rising in the ^{235}U fission rates in SHR in the second row.

3.2.3.5. Local reactivity coefficients

Distributions of local reactivity coefficients calculated for the Hex-Z model by participants are given for comparison in Tables 3.39–3.49. Most results were obtained using the diffusion theory based, first order perturbation method. Detailed distributions of local reactivity coefficients obtained by each participant are compared in Figs 3.42–3.47. In these figures, same to the Phase 1 study, local coefficients for the core plus the upper axial blanket (UB) and the entire regions obtained by the participants are compared with corresponding average values.

Similar for Phase 1, the fuel Doppler coefficient for LEZ that has the largest ^{238}U density in the core region was evaluated to be largest in its magnitude in Fig. 3.42. The comparison of regional coefficients can be understood by the similar aspect for discrepancy propagation in the regional values. In Fig. 3.43 this aspect for the steel Doppler coefficient case is more obvious, similar for the Phase 1 results. A substantial under-prediction of the steel Doppler coefficients in its magnitude can also be seen in the CIAE results.

The regionwise sodium density coefficients for the core plus the upper axial blanket (UB) regions are compared for leakage and non-leakage components in Fig. 3.44. The resultant sodium density coefficients obtained by a sum of those two components clearly show spatial distributions that can mainly be characterized by leakage and non-leakage components. In LEZ and MEZ that are highly enriched fuelled and located at the zones near the core centre, the non-leakage component prevails the leakage effect and, as a result, the overall sodium density coefficient is determined to be negative. In the MOX zone, this non-leakage prevailing effect appeared to be valid for all results. The dominance of the non-leakage component reduces when moving toward the outer zone. It is clearly observed that the leakage component becomes dominant in HEZ, and, as a result, HEZ has the greatest positive worth in the core.

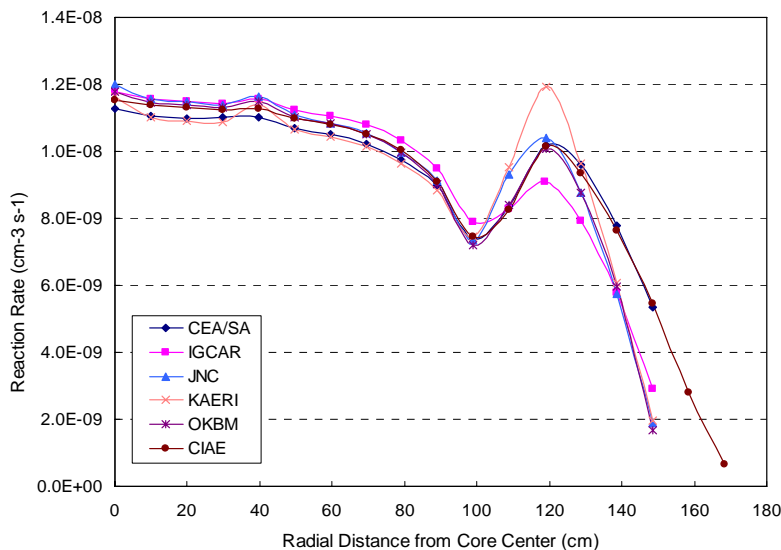


FIG. 3.38. Radial ^{235}U fission rate distributions (Phase 2, diffusion).

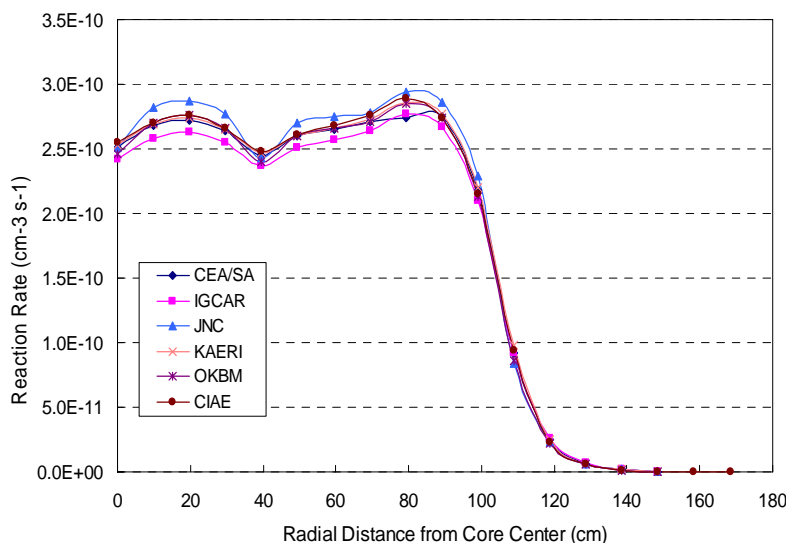


FIG. 3.39. Radial ^{238}U fission rate distributions (Phase 2, diffusion).

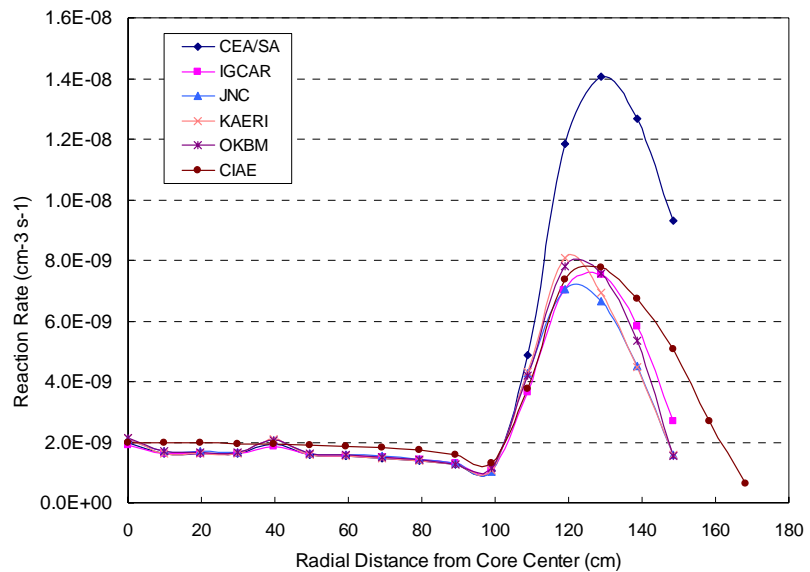


FIG. 3.40. Radial ^{238}U capture rate distributions (Phase 2, diffusion).

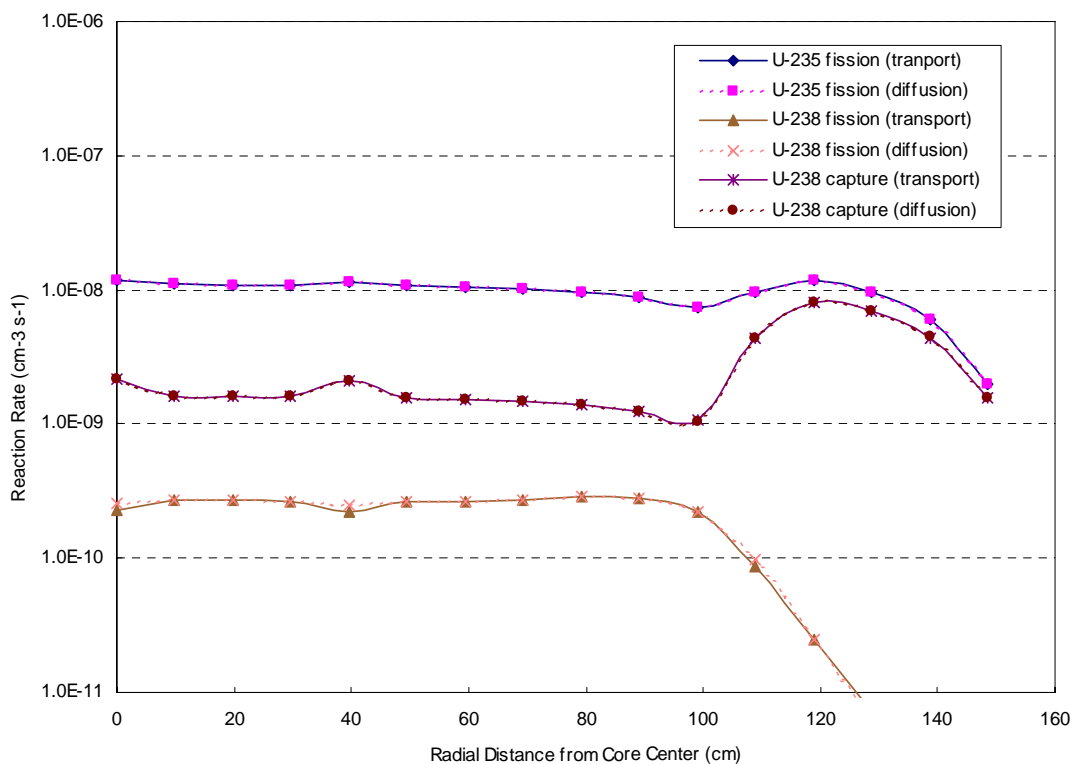


FIG. 3.41. Radial reaction rate distributions (Phase 2, transport vs. diffusion) (KAERI results).

TABLE 3.39. FUEL DOPPLER COEFFICIENTS

(1/2)											
Participant	Region	LEZ1	LEZ2	MEZ	MOX	HEZ	SHR	SCR	SSA1	SSA2	RR
ANL	UAR	-2.4746E-05	-4.5387E-05	-2.3086E-05	-3.7805E-05	-2.8032E-05			-2.6492E-12	6.8238E-14	3.2079E-14
	UB	-1.1012E-03	-2.3095E-03	-8.5049E-04	-1.0408E-03	-6.9628E-04			-1.0155E-10	-3.6811E-12	7.1625E-13
	CORE	-9.5624E-05	-1.9764E-04	-7.2967E-05	-7.5495E-05	-4.7013E-05			-4.2254E-12	6.7204E-14	4.6262E-14
	LB										
	LAR										
	Sun	-1.2216E-03	-2.5523E-03	-9.4655E-04	-1.1541E-03	-7.7133E-04			-1.0843E-10	-3.5456E-12	7.9459E-13
Total											
CEA/SA	UAR										
	UB	-1.8762E-05	-3.1704E-05	-1.8357E-05	-3.3463E-05	-2.9650E-05					
	CORE	-1.1153E-03	-2.3369E-03	-8.6030E-04	-1.1440E-03	-8.1554E-04					
	LB	-8.7019E-05	-1.8049E-04	-6.7451E-05	-7.2257E-05	-5.2181E-05					
	LAR										
	Sun	-1.2210E-03	-2.5491E-03	-9.4610E-04	-1.2497E-03	-8.9737E-04					
Total											
CIAE	UAR										
	UB	-1.9236E-05	-3.1980E-05	-1.8776E-05	-3.1132E-05	-2.2673E-05					
	CORE	-1.0433E-03	-2.1437E-03	-7.9832E-04	-9.8165E-04	-6.0884E-04					
	LB	-7.8359E-05	-1.6072E-04	-6.0954E-05	-6.5502E-05	-3.9764E-05					
	LAR										
	Sun	-1.1409E-03	-2.3364E-03	-8.7805E-04	-1.0783E-03	-6.7128E-04					
Total											
IGCAR	UAR										
	UB	-1.8421E-05	-3.3827E-05	-1.7892E-05	-3.0374E-05	-2.3183E-05					
	CORE	-7.6468E-04	-1.6156E-03	-5.9774E-04	-6.9564E-04	-5.2286E-04					
	LB	-7.4000E-05	-1.5320E-04	-5.7580E-05	-6.1750E-05	-3.9212E-05					
	LAR										
	Sun	-8.5710E-04	-1.8026E-03	-6.7321E-04	-7.8776E-04	-5.8525E-04					
Total											
IPPE	UAR										
	UB	-2.2270E-05	-4.0240E-05	-2.0000E-05	-3.3230E-05	-2.6330E-05					
	CORE	-1.0830E-03	-2.2380E-03	-7.8880E-04	-9.1330E-04	-7.2490E-04					
	LB	-9.1030E-05	-1.8490E-04	-6.6660E-05	-7.0050E-05	-4.6300E-05					
	LAR										
	Sun	-1.1963E-03	-2.4631E-03	-8.7546E-04	-1.0166E-03	-7.9753E-04					
Total											

TABLE 3.39. FUEL DOPPLER COEFFICIENTS (CONTINUED)

(2/2)											
Participant	Region	LEZ1	LEZ2	MEZ	MOX	HEZ	SHR	SCR	SSA1	SSA2	RR
JNC	UAR	-2.5389E-05	-4.7690E-05	-2.2943E-05	-3.5160E-05	-2.7749E-05					
	UB	-1.1112E-03	-2.2854E-03	-8.3824E-04	-1.0214E-03	-7.3115E-04					
	CORE	-8.8693E-05	-1.7926E-04	-6.5673E-05	-6.8760E-05	-4.5838E-05					
	LB										
	LAR										
	Sum	-1.2253E-03	-2.5124E-03	-9.2686E-04	-1.1253E-03	-8.0473E-04					
	Total	-6.5945E-03									
KAERI	UAR	-2.2065E-05	-3.9090E-05	-2.1083E-05	-3.6026E-05	-3.0682E-05					
	UB	-1.2743E-03	-2.6656E-03	-1.0161E-03	-1.2158E-03	-9.0029E-04					
	CORE	-9.1719E-05	-1.8784E-04	-6.9975E-05	-7.4391E-05	-5.2387E-05					
	LB										
	LAR										
	Sum	-1.3881E-03	-2.8925E-03	-1.1072E-03	-1.3262E-03	-9.8336E-04					
	Total	-7.6973E-03									
OKBM	UAR	-1.9384E-05	-3.5031E-05	-1.7486E-05	-2.9309E-05	-2.3116E-05					
	UB	-1.0170E-03	-2.1399E-03	-7.7594E-04	-1.0542E-03	-7.9074E-04					
	CORE	-8.1721E-05	-1.6740E-04	-6.1113E-05	-6.4911E-05	-4.3588E-05					
	LB										
	LAR										
	Sum	-1.1181E-03	-2.3424E-03	-8.5454E-04	-1.1484E-03	-8.5744E-04					
	Total	-6.3209E-03									
Mean	UAR	-2.1284E-05	-3.8118E-05	-1.9953E-05	-3.3312E-05	-2.6427E-05					
	UB	-1.0637E-03	-2.2168E-03	-8.1574E-04	-1.0083E-03	-7.2383E-04					
	CORE	-8.6021E-05	-1.7633E-04	-6.5297E-05	-6.9139E-05	-4.5785E-05					
	LB										
	LAR										
	Sum	-1.1710E-03	-2.4314E-03	-9.0099E-04	-1.1108E-03	-7.9604E-04					
	Total	-6.4106E-03									
SD	UAR	2.7458E-06	6.0554E-06	2.2135E-06	2.9376E-06	3.1261E-06					
	UB	1.4295E-04	2.9332E-04	1.1587E-04	1.5688E-04	1.1859E-04					
	CORE	7.3641E-06	1.4853E-05	5.1167E-06	4.8457E-06	4.9361E-06					
	LB										
	LAR										
	Sum	1.5023E-04	3.0729E-04	1.2101E-04	1.6190E-04	1.2525E-04					
	Total	8.4180E-04									

* The result for the SSA2 region in IPPE includes the result for the RR region.

TABLE 3.40. STEEL DOPPLER COEFFICIENTS

(1/2)										
Participant	Region	LEZ1	LEZ2	MEZ	MOX	HEZ	SHR	SCR	SSA1	SSA2
ANL	UAR	-2.1693E-08	-3.7059E-08	-1.9986E-08	-2.9770E-08	-1.7915E-08	-5.1934E-09	-1.2908E-09	-8.9086E-09	-8.5960E-10
	UB	-1.5734E-06	-3.0280E-06	-1.4888E-06	-2.2791E-06	-1.4575E-06	-1.5660E-07	-1.9613E-08	-3.5130E-06	-3.1085E-07
	CORE	-1.2319E-04	-2.6018E-04	-1.0856E-04	-1.3393E-04	-6.9573E-05	-2.2243E-05	-7.5577E-06	-1.8961E-04	9.1011E-06
	LB	-5.5910E-06	-1.1655E-05	-4.3562E-06	-4.4321E-06	-2.4237E-06	-8.9607E-07	-2.2799E-07	-5.5257E-06	4.3776E-07
	LAR	-9.3095E-08	-1.7956E-07	-5.4393E-08	-5.2712E-08	-2.4916E-08	-2.4421E-08	-9.4987E-09	-1.2405E-08	-3.5457E-09
	Sum	-1.3047E-04	-2.7508E-04	-1.1448E-04	-1.4072E-04	-7.3497E-05	-2.3326E-05	-7.8161E-06	-1.9867E-04	-1.0681E-04
	Total	-1.0610E-03								9.8768E-06
CEA/SA	UAR	1.6782E-09	1.0002E-08	1.4265E-09	-2.6882E-09	-2.9594E-09	1.7516E-09	8.8535E-10	-4.3512E-10	5.8466E-09
	UB	-1.0571E-06	-1.8257E-06	-1.0038E-06	-1.7215E-06	-1.2785E-06	-6.1291E-08	-3.9948E-10	-4.8661E-06	-7.3214E-06
	CORE	-1.3391E-04	-2.8257E-04	-1.1605E-04	-1.4634E-04	-8.4361E-05	-5.2771E-06	-7.9945E-07	-2.1814E-04	-2.3920E-04
	LB	-4.8960E-06	-1.0197E-05	-3.7324E-06	-3.7900E-06	-2.2799E-06	-1.5043E-07	-2.3258E-08	-7.3664E-06	-1.0995E-05
	LAR	-3.1396E-08	-5.9956E-08	-1.6097E-08	-1.5370E-08	-7.4797E-09	-8.3814E-09	-3.4837E-09	-2.8691E-09	4.0555E-09
	Sum	-1.3989E-04	-2.9464E-04	-1.2080E-04	-1.5187E-04	-8.7930E-05	-5.4954E-06	-8.2570E-07	-2.3087E-04	-2.5751E-04
	Total	-1.3067E-03								-1.6869E-05
CIAE	UAR	2.5388E-08	5.2231E-08	2.5580E-08	3.2957E-08	2.3831E-08	9.7058E-09	3.0655E-09	3.3121E-08	6.7350E-08
	UB	-5.9755E-07	-6.9416E-07	-5.1531E-07	-1.0612E-06	-1.1170E-06	3.1461E-08	1.6487E-07	-1.0896E-06	-4.6454E-07
	CORE	-9.2508E-05	-1.9324E-04	-7.5071E-05	-8.8623E-05	-4.9126E-05	-1.4514E-05	-5.3880E-06	-9.6140E-05	-3.7991E-05
	LB	-3.6504E-06	-7.4998E-06	-2.5730E-06	-2.5644E-06	-1.9618E-06	5.9928E-07	1.5930E-07	-2.0614E-06	-2.4937E-08
	LAR	2.6191E-08	6.5828E-08	2.7904E-08	1.0732E-08	1.6875E-08	3.3607E-08	1.1824E-08	2.7802E-08	6.1148E-08
	Sum	-9.6705E-05	-2.0131E-04	-7.8106E-05	-9.2205E-05	-5.2164E-05	-1.3840E-05	-5.0490E-06	-9.9230E-05	-3.8351E-05
	Total	-6.7016E-04								6.8019E-06
IGCAR	UAR									
	UB									
	CORE									
	LB									
	LAR									
	Sum									
	Total									
IPPE	UAR	-1.9120E-06	-3.6160E-06	-1.7380E-06	-2.5670E-06	-1.5270E-06	5.3740E-04		-4.1430E-06	-3.4740E-06
	UB	-1.4440E-04	-2.9250E-04	-1.2050E-04	-1.4620E-04	-7.9170E-05	-1.8058E-03		-1.9730E-04	-1.4100E-04
	CORE	-6.8381E-06	-1.3668E-05	-5.0764E-06	-7.7140E-07	-2.6516E-06	1.6571E-03		-6.6884E-06	-5.3382E-06
	LB									
	LAR									
	Sum	-1.5315E-04	-3.0978E-04	-1.2731E-04	-1.4954E-04	-8.3349E-05	3.8870E-04		-2.0813E-04	-1.4981E-04
	Total	-7.9682E-04								

TABLE 3.40. STEEL DOPPLER COEFFICIENTS (CONTINUED)

(2/2)								
Participant	Region	LEZ1	LEZ2	MEZ	MOX	HEZ	SHR	SCR
JNC	UAR	-2.4150E-08	-4.2522E-08	-2.0459E-08	-2.8479E-08	-1.7010E-08	-3.8931E-09	-8.4426E-09
	UB	-1.6101E-06	-3.1095E-06	-1.4669E-06	-2.0867E-06	-1.2563E-06	-9.2136E-08	-3.7269E-06
	CORE	-1.2684E-04	-2.6352E-04	-1.0844E-04	-1.3256E-04	-6.8910E-05	-1.6455E-05	-8.0314E-06
	LB	-5.2216E-06	-1.0594E-05	-3.9386E-06	-3.9927E-06	-2.0745E-06	-6.8112E-07	-2.1728E-07
	LAR	-8.5515E-08	-1.6330E-07	-4.8175E-08	-4.5401E-08	-2.1376E-08	-1.4049E-08	-8.4766E-09
	Sum	-1.3378E-04	-2.7743E-04	-1.1391E-04	-1.3871E-04	-7.2280E-05	-1.7247E-05	-8.2628E-06
Total		-1.0894E-03						
KAERI	UAR	-6.2298E-09	-8.8515E-09	-6.8792E-09	-1.4071E-08	-1.1401E-08	-1.2027E-09	-1.9242E-10
	UB	-1.2281E-06	-2.2970E-06	-1.1424E-06	-1.7689E-06	-1.2085E-06	-1.0514E-07	-1.6140E-08
	CORE	-1.2257E-04	-2.5853E-04	-1.0811E-04	-1.3106E-04	-7.1360E-05	-2.1773E-05	-7.0572E-06
	LB	-4.6982E-06	-9.6676E-06	-3.5848E-06	-3.6027E-06	-2.0737E-06	-5.4091E-07	-1.2055E-07
	LAR	-4.5316E-08	-8.1636E-08	-2.4197E-08	-2.8046E-08	-1.6140E-08	-5.9892E-09	-2.1407E-09
	Sum	-1.2855E-04	-2.7058E-04	-1.1287E-04	-1.3647E-04	-7.4670E-05	-2.2426E-05	-7.1639E-06
Total		-1.0786E-03						
OKBM	UAR	-1.1626E-08	-2.1601E-08	-9.5529E-09	-1.4519E-08	-1.1717E-08	-2.8302E-09	-7.3352E-10
	UB	-9.9383E-07	-1.8829E-06	-8.9573E-07	-1.3420E-06	-8.1839E-07	-1.0131E-07	-3.0946E-08
	CORE	-1.2191E-04	-2.4890E-04	-1.0312E-04	-1.2542E-04	-7.6174E-05	-1.7994E-05	-5.3154E-06
	LB	-3.6992E-06	-7.4716E-06	-2.7810E-06	-2.8370E-06	-1.4775E-06	-7.7982E-07	-1.8209E-07
	LAR	-4.6627E-08	-8.9230E-08	-2.8714E-08	-2.9075E-08	-1.3676E-08	-1.5234E-08	-5.7158E-09
	Sum	-1.2666E-04	-2.5836E-04	-1.0683E-04	-1.2964E-04	-7.8495E-05	-1.8893E-05	-5.5349E-06
Total		-1.0619E-03						
Mean	UAR	-6.1055E-09	-7.9667E-09	-4.9785E-09	-9.4234E-09	-6.1924E-09	-2.7699E-10	-6.2687E-11
	UB	-1.2817E-06	-2.3505E-06	-1.1778E-06	-1.8323E-06	-1.2376E-06	-7.6702E-05	-2.0958E-08
	CORE	-1.2362E-04	-2.5706E-04	-1.0569E-04	-1.2916E-04	-7.1239E-05	-2.7201E-04	-5.6915E-06
	LB	-4.9421E-06	-1.0108E-05	-3.7203E-06	-3.1415E-06	-2.1347E-06	-2.3638E-04	-1.0198E-07
	LAR	-4.5960E-08	-8.4643E-08	-2.3945E-08	-2.6645E-08	-1.1119E-08	-5.7447E-09	-2.9153E-09
	Sum	-1.2989E-04	-2.6960E-04	-1.1062E-04	-1.3417E-04	-7.4626E-05	-4.1067E-05	-5.7754E-06
Total		-1.0092E-03						
SD	UAR	1.8774E-08	3.5139E-08	1.7113E-08	2.3092E-08	1.5646E-08	5.4478E-09	1.6878E-09
	UB	4.4619E-07	9.8970E-07	4.1716E-07	5.2527E-07	2.3283E-07	2.0315E-04	7.2342E-08
	CORE	1.5918E-05	3.1885E-05	1.4676E-05	1.9497E-05	1.1230E-05	6.7636E-04	2.6453E-06
	LB	1.1082E-06	2.2082E-06	8.6682E-07	1.2293E-06	3.7438E-07	6.2648E-04	1.4859E-07
	LAR	4.2907E-08	8.7725E-08	2.9281E-08	2.2642E-08	1.4995E-08	2.0314E-08	7.7496E-09
	Sum	1.7176E-05	3.4456E-05	1.5730E-05	2.0000E-05	1.1397E-05	1.5341E-04	2.7333E-06
Total		2.1027E-04						

TABLE 3.41. SODIUM DENSITY COEFFICIENTS

(1/2)											
Participant	Region	LEZ1	LEZ2	MEZ	MOX	HEZ	SHR	SCR	SSA1	SSA2	RR
ANL	UAR	2.3268E-05	4.5642E-05	2.3652E-05	3.4056E-05	2.4335E-05	6.7519E-06	1.8112E-06	2.9768E-05	4.5875E-05	1.2941E-06
	UB	7.5470E-05	1.7187E-04	8.9608E-05	1.4607E-04	7.8186E-05	3.2227E-05	2.5478E-04	8.8188E-05	8.8947E-05	2.7814E-05
	CORE	-8.5624E-04	-1.7581E-03	-6.6576E-04	4.1473E-04	3.1242E-03	3.5930E-03	3.3414E-03	2.6684E-03	2.4264E-03	8.6349E-04
	LB	1.1434E-04	2.5276E-04	1.5237E-04	2.1507E-04	1.1111E-04	3.3105E-03	1.4776E-03	1.2325E-04	1.2290E-04	3.9290E-05
	LAR	5.9849E-05	1.2941E-04	4.6325E-05	4.3504E-05	2.4028E-05	3.6692E-05	1.4224E-05	2.6189E-05	4.0383E-05	1.1293E-06
	Sum	-5.8331E-04	-1.1585E-03	-3.5380E-04	8.5344E-04	3.3619E-03	6.9792E-03	5.0898E-03	2.8753E-03	2.7245E-03	9.3302E-04
Total											
CEA/SA	UAR	1.6200E-05	3.1928E-05	1.7178E-05	2.5171E-05	1.7503E-05	4.8735E-06	1.2928E-06	1.6391E-05	2.4127E-05	4.9905E-07
	UB	5.9839E-05	1.3530E-04	7.2164E-05	1.2038E-04	7.0291E-05	1.8067E-05	2.0806E-04	5.2373E-05	7.5501E-05	1.0778E-05
	CORE	-1.0365E-03	-2.1672E-03	-8.5157E-04	2.2467E-04	2.4289E-03	3.3731E-04	7.6180E-04	1.8908E-03	2.0874E-03	3.3678E-04
	LB	9.3206E-05	2.0560E-04	1.2748E-04	1.8234E-04	1.0104E-04	1.0692E-03	4.1460E-04	7.5447E-05	1.0707E-04	1.5728E-05
	LAR	4.6099E-05	9.7208E-05	3.4082E-05	3.3339E-05	1.8312E-05	1.7736E-05	6.6738E-06	1.5625E-05	2.2178E-05	4.5156E-07
	Sum	-8.2115E-04	-1.6971E-03	-6.0067E-04	5.8589E-04	2.6360E-03	1.4835E-03	1.3924E-03	2.0506E-03	2.3163E-03	3.6424E-04
Total											
CIAE	UAR	1.0946E-05	2.0618E-05	1.1481E-05	1.6837E-05	1.2199E-05	3.6379E-06	1.0336E-06	1.3753E-05	2.3295E-05	4.9405E-06
	UB	5.6106E-05	1.2517E-04	6.6965E-05	1.1202E-04	5.9411E-05	2.8986E-05	1.0853E-04	6.8042E-05	6.6311E-05	7.7125E-06
	CORE	-1.3431E-03	-2.8606E-03	-1.2802E-03	-2.3680E-04	2.5522E-03	3.1791E-04	5.2281E-04	2.0176E-03	1.5632E-03	2.0391E-04
	LB	7.7051E-05	1.6716E-04	1.1202E-04	1.6616E-04	8.5846E-05	1.1862E-03	3.7471E-04	9.7959E-05	9.2766E-05	1.0900E-05
	LAR	2.9925E-05	6.2556E-05	2.2795E-05	2.2954E-05	1.2939E-05	1.6824E-05	6.0160E-06	1.3446E-05	2.2133E-05	4.6688E-06
	Sum	-1.1695E-03	-2.4851E-03	-1.0669E-03	8.1173E-05	2.7722E-03	1.5536E-03	1.0131E-03	2.2108E-03	2.1767E-03	2.3214E-04
Total											
IGCAR	UAR	-2.7170E-07	-1.2550E-06	4.4100E-08	5.6140E-07	2.6130E-07	-3.8178E-07	-2.2180E-07	5.5100E-07	2.6120E-07	2.0740E-07
	UB	1.3775E-04	3.1415E-04	1.6266E-04	2.5329E-04	1.3635E-04	3.2649E-05	4.3412E-05	4.4434E-05	2.5258E-05	4.3528E-06
	CORE	-6.2870E-04	-1.3066E-03	-4.0978E-04	8.7799E-04	3.6822E-03	-1.0337E-03	-1.5145E-04	1.5618E-03	7.9533E-04	1.4862E-04
	LB	2.3808E-04	5.1365E-04	2.8359E-04	3.9378E-04	2.0151E-04	1.8906E-04	5.7720E-05	6.1194E-05	3.3362E-05	6.2960E-06
	LAR	1.3890E-06	5.5390E-06	2.3590E-06	1.0240E-06	5.6340E-08	2.4772E-06	9.5130E-07	2.2490E-07	4.7300E-08	1.8340E-07
	Sum	-2.5175E-04	-4.7451E-04	-4.0873E-05	1.5266E-03	4.0209E-03	-8.0986E-04	-4.9590E-05	1.6682E-03	8.5416E-04	1.5966E-04
Total											
IPPE	UAR	0.0000E+00	0.0000E+00	0.0000E+00	0.0000E+00	0.0000E+00	0.0000E+00	0.0000E+00	0.0000E+00	0.0000E+00	0.0000E+00
	UB	6.7260E-05	1.5210E-04	7.7040E-05	1.2740E-04	6.3970E-05	1.2520E-04	0.0000E+00	6.2500E-05	4.6352E-05	0.0000E+00
	CORE	-8.3180E-04	-1.6460E-03	-5.9540E-04	3.7440E-04	2.8260E-03	1.4740E-03	0.0000E+00	2.2490E-03	1.6589E-03	0.0000E+00
	LB	9.5570E-05	2.0570E-04	1.2430E-04	1.8640E-04	9.0170E-05	1.6990E-03	0.0000E+00	8.9070E-05	4.9910E-05	0.0000E+00
	LAR	0.0000E+00	0.0000E+00	0.0000E+00	0.0000E+00	0.0000E+00	0.0000E+00	0.0000E+00	0.0000E+00	0.0000E+00	0.0000E+00
	Sum	-6.6897E-04	-1.2882E-03	-3.9406E-04	6.8820E-04	2.9801E-03	3.2982E-03	0.0000E+00	2.4006E-03	1.7552E-03	0.0000E+00
Total											

* The results for axial reflectors (UAR and LAR) of IPPE are not included in regionwise averages.

TABLE 3.41. SODIUM DENSITY COEFFICIENTS (CONTINUED)

2/2

TABLE 3.42. SODIUM DENSITY COEFFICIENTS (LEAKAGE COMPONENT)

(1/2)											
Participant	Region	LEZ1	LEZ2	MEZ	MOX	HEZ	SHR	SCR	SSA1	SSA2	RR
ANL	UAR	2.8137E-05	5.6051E-05	2.8545E-05	4.0668E-05	2.9114E-05	8.4297E-06	2.3364E-06	3.4544E-05	5.4338E-05	1.4830E-06
	UB	1.6861E-04	3.7882E-04	1.8697E-04	2.6273E-04	1.3725E-04	8.2420E-05	2.7560E-04	1.2255E-04	1.4744E-04	3.1824E-05
	CORE	1.1200E-03	2.3692E-03	1.2396E-03	2.8978E-03	3.7660E-03	5.3799E-03	3.7884E-03	2.9467E-03	3.6840E-03	9.6671E-04
	LB	3.2936E-04	6.8317E-04	3.2874E-04	4.2296E-04	2.0869E-04	3.4697E-03	1.5327E-03	1.7610E-04	2.0861E-04	4.5016E-05
	LAR	6.9410E-05	1.4862E-04	5.3206E-05	5.1165E-05	2.8839E-05	3.9794E-05	1.5335E-05	3.1203E-05	4.8223E-05	1.3013E-06
	Sum	1.7156E-03	3.6359E-03	1.8370E-03	3.6754E-03	4.1699E-03	8.9802E-03	5.6143E-03	3.3111E-03	4.1427E-03	1.0463E-03
	Total	3.8128E-02									
CEA/SA (Transport)	UAR	1.7910E-05	2.3083E-05	1.4710E-05	2.2160E-05	1.5770E-05	4.2627E-06	1.1890E-06	1.5710E-05	2.8020E-05	8.7080E-07
	UB	1.8389E-04	2.7600E-04	1.5939E-04	2.2176E-04	1.2972E-04	6.4384E-05	2.5622E-04	8.1571E-05	1.2032E-04	1.1016E-05
	CORE	1.2911E-03	1.9005E-03	1.1646E-03	2.4393E-03	3.4024E-03	1.9647E-03	1.2869E-03	2.2859E-03	2.9260E-03	2.3326E-04
	LB	5.6951E-04	3.1632E-04	4.0695E-04	2.1151E-04	1.2143E-03	4.5985E-04	1.2713E-04	1.7995E-04	1.6080E-05	2.1151E-04
	LAR	7.7740E-05	3.2730E-05	3.1450E-05	1.7450E-05	1.4188E-05	6.0190E-05	1.5820E-05	2.7120E-05	8.3310E-07	1.7450E-05
	Sum	2.1402E-03	2.5480E-03	1.7771E-03	2.9122E-03	4.7763E-03	2.5533E-03	1.6873E-03	2.5903E-03	3.0913E-03	4.7411E-04
	Total	2.4752E-02									
CIAE	UAR	1.4865E-05	2.8817E-05	1.5332E-05	2.2016E-05	1.5828E-05	4.9591E-06	1.4690E-06	1.7256E-05	2.8777E-05	5.7081E-06
	UB	1.5005E-04	3.3330E-04	1.6469E-04	2.2928E-04	1.1803E-04	7.1253E-05	1.2844E-04	9.4774E-05	1.0677E-04	1.2563E-05
	CORE	1.0374E-03	2.1848E-03	1.1241E-03	2.6743E-03	3.4745E-03	2.3171E-03	1.1368E-03	2.5930E-03	2.6209E-03	3.2755E-04
	LB	3.0557E-04	6.2933E-04	2.9892E-04	3.7749E-04	1.8290E-04	1.3414E-03	4.2762E-04	1.3957E-04	1.5318E-04	1.7933E-05
	LAR	3.8115E-05	7.9541E-05	2.8779E-05	2.9569E-05	1.6939E-05	1.9539E-05	6.9913E-06	1.7065E-05	2.7604E-05	5.4242E-06
	Sum	1.5461E-03	3.2558E-03	1.6318E-03	3.3327E-03	3.8082E-03	3.7542E-03	1.7013E-03	2.8617E-03	2.9372E-03	3.6918E-04
	Total	2.5198E-02									
IGCAR	UAR										
	UB										
	CORE										
	LB										
	LAR										
	Sum										
	Total										
IPPE	UAR										
	UB										
	CORE										
	LB										
	LAR										
	Sum										
	Total										

TABLE 3.42. SODIUM DENSITY COEFFICIENTS (LEAKAGE COMPONENT) (CONTINUED)

(2/2)										
Participant	Region	LEZ1	LEZ2	MEZ	MOX	HEZ	SHR	SCR	SSA1	SSA2
JNC	UAR	2.4800E-05	4.9000E-05	2.3700E-05	2.1400E-05	6.9030E-06	1.9600E-06	2.2500E-05	3.2200E-05	4.6000E-06
	UB	1.7378E-04	3.7792E-04	1.8423E-04	2.6139E-04	1.3396E-04	7.1137E-05	1.3740E-04	9.5690E-05	1.1824E-05
	CORE	1.0831E-03	2.2435E-03	1.1895E-03	2.8310E-03	3.5270E-03	2.4563E-03	1.2866E-03	2.6160E-03	3.5770E-04
	LB	3.2170E-04	6.5450E-04	3.1330E-04	4.0880E-04	1.9940E-04	1.3033E-03	4.8800E-04	1.3690E-04	1.6830E-05
	LAR	5.5300E-05	1.1350E-04	4.0000E-05	3.9800E-05	2.1500E-05	3.1350E-05	1.1900E-05	2.0800E-05	4.1300E-06
	Sum	1.6587E-03	3.4384E-03	1.7507E-03	3.5737E-03	3.9033E-03	3.8689E-03	1.9259E-03	2.8919E-03	3.1316E-03
Total		2.6538E-02								3.9508E-04
KAERI	UAR	1.5156E-04	3.3952E-04	1.6738E-04	2.3522E-04	1.1840E-04				
	UB	1.0063E-03	2.1226E-03	1.0790E-03	1.9549E-03	2.0215E-03				
	CORE	3.0979E-04	6.3820E-04	3.0135E-04	3.8093E-04	1.7892E-04				
	LB									
	LAR									
	Sum	1.4676E-03	3.1003E-03	1.5477E-03	2.5711E-03	2.3188E-03				
Total		1.1006E-02								
OKBM	UAR	2.4766E-05	4.8653E-05	2.4400E-05	3.4051E-05	2.3239E-05	7.3328E-06	2.1015E-06	2.6060E-05	3.5075E-05
	UB	1.6854E-04	3.7434E-04	1.7973E-04	2.5026E-04	1.2842E-04	7.4491E-05	1.4465E-04	1.7180E-04	1.9501E-04
	CORE	1.0978E-03	2.2950E-03	1.1911E-03	2.8493E-03	3.8291E-03	2.3697E-03	1.4521E-03	4.5954E-03	5.4440E-04
	LB	7.3570E-04	3.4101E-04	4.2759E-04	2.0743E-04	1.3883E-03	5.0663E-04	2.5982E-04	2.9322E-04	2.4987E-05
	LAR	1.2186E-04	4.2400E-05	4.1680E-05	2.3067E-05	3.1654E-05	1.1733E-05	2.3936E-05	3.2269E-05	5.3333E-07
	Sum	2.1487E-03	3.1014E-03	1.8645E-03	3.3641E-03	5.4006E-03	2.9698E-03	1.8826E-03	4.8188E-03	5.2554E-03
Total		3.1784E-02								7.9273E-04
Mean	UAR	2.3142E-05	4.5630E-05	2.2994E-05	3.2339E-05	2.2395E-05	6.9062E-06	1.9667E-06	2.5090E-05	3.7597E-05
	UB	1.6525E-04	3.6609E-04	1.7891E-04	2.5092E-04	1.2941E-04	7.4825E-05	1.7152E-04	1.2120E-04	1.3836E-05
	CORE	1.0846E-03	2.2731E-03	1.1860E-03	2.8131E-03	3.6491E-03	3.1307E-03	1.9160E-03	3.1128E-03	5.4909E-04
	LB	4.2308E-04	5.7702E-04	3.4214E-04	3.5417E-04	4.9481E-04	1.6553E-03	6.7703E-04	1.8645E-04	7.1802E-05
	LAR	7.1172E-05	9.6014E-05	4.0916E-05	3.5900E-05	2.4738E-05	2.5604E-05	1.4541E-05	2.5334E-05	2.6390E-05
	Sum	1.7672E-03	3.3579E-03	1.7710E-03	3.4865E-03	4.3205E-03	4.8933E-03	2.7810E-03	3.4708E-03	3.8667E-03
Total		3.0412E-02								6.5083E-04
SD	UAR	5.7401E-06	1.1716E-05	5.5375E-06	7.7243E-06	5.4763E-06	1.4485E-06	3.6634E-07	7.2663E-06	1.1453E-05
	UB	1.0421E-05	2.1950E-05	9.9358E-06	1.5469E-05	8.4166E-06	5.2964E-06	6.9703E-05	3.6108E-05	4.2106E-05
	CORE	3.4908E-05	7.8293E-05	4.7397E-05	9.6728E-05	1.7457E-04	1.5005E-03	1.2549E-03	8.0481E-04	1.0837E-03
	LB	2.0865E-04	1.5883E-04	5.8255E-05	9.9656E-05	5.9573E-04	1.2694E-03	5.7855E-04	7.3396E-05	7.7612E-05
	LAR	3.6136E-05	4.5529E-05	9.9964E-06	1.2288E-05	6.7362E-06	1.2430E-05	7.1385E-06	7.5601E-06	1.9618E-05
	Sum	2.6386E-04	2.3093E-04	1.0469E-04	1.6524E-04	7.3618E-04	2.7538E-03	1.8914E-03	9.2172E-04	1.0660E-03
Total		5.8769E-03								3.2726E-04

* The results of CEA/SA and KAERI are not included in the averages.

TABLE 3.43. SODIUM DENSITY COEFFICIENTS (NON-LEAKAGE COMPONENT)

(1/2)											
Participant	Region	LEZ1	LEZ2	MEZ	MOX	HEZ	SHR	SCR	SSA1	SSA2	RR
ANL	UAR	-4.8689E-06	-1.0408E-05	-4.8924E-06	-6.6125E-06	-4.7790E-06	-1.6778E-06	-5.224E-07	-5.2761E-06	-8.4626E-06	-1.8883E-07
	UB	-9.3138E-05	-2.0655E-04	-9.7364E-05	-1.1666E-04	-5.9061E-05	-5.0153E-05	-2.0823E-05	-3.4359E-05	-5.8492E-05	-4.0100E-06
CORE		-1.9763E-03	-4.1274E-03	-1.9053E-03	-2.4831E-03	-6.4174E-04	-1.7869E-03	-4.4695E-04	-3.3830E-04	-1.2577E-03	-1.0322E-04
LB		-2.1502E-04	-4.3042E-04	-1.7636E-04	-2.0789E-04	-9.7572E-05	-1.5917E-04	-5.5125E-05	-5.2846E-05	-8.5704E-05	-5.7260E-06
LAR		-9.5607E-06	-1.9211E-05	-6.8815E-06	-7.6608E-06	-4.8311E-06	-3.1013E-06	-1.1103E-06	-5.0142E-06	-7.8406E-06	-1.7199E-07
Sum		-2.2989E-03	-4.7944E-03	-2.1908E-03	-2.8219E-03	-8.0798E-04	-2.0010E-03	-5.2454E-04	-4.3580E-04	-1.4182E-03	-1.1331E-04
Total		-1.7407E-02									
CEA/SA (Transport)	UAR	-5.8540E-06	-8.9210E-06	-4.8270E-06	-6.4960E-06	-4.4790E-06	-1.5920E-06	-5.1190E-07	-4.3920E-06	-8.5770E-06	-6.5530E-07
	UB	-1.1346E-04	-1.4780E-04	-9.9368E-05	-1.1909E-04	-6.4258E-05	-4.5242E-05	-1.0526E-04	-3.5273E-05	-6.5427E-05	-1.1721E-05
CORE		-2.5636E-03	-4.1774E-03	-2.1854E-03	-2.4847E-03	-9.8326E-04	-1.4546E-03	-5.3712E-04	-6.1052E-04	-1.5294E-03	-2.7801E-04
LB		-2.8127E-04	-4.1209E-04	-1.9638E-04	-2.3122E-04	-1.1496E-04	-1.6731E-04	-6.0500E-05	-5.8770E-05	-1.0149E-04	-1.7277E-05
LAR		-1.2290E-05	-1.8389E-05	-7.7210E-08	-8.4500E-06	-5.0420E-06	-3.1448E-06	-1.1570E-06	-4.6410E-06	-8.6640E-06	-6.4090E-07
Sum		-2.9765E-03	-4.7646E-03	-2.4861E-03	-2.8500E-03	-1.1720E-03	-1.6718E-03	-7.0455E-04	-7.1360E-04	-1.7136E-03	-3.0830E-04
Total		-1.9361E-02									
CIAE	UAR	-3.9186E-06	-8.1987E-06	-3.8515E-06	-5.1786E-06	-3.6294E-06	-1.3212E-06	-4.3540E-07	-3.5035E-06	-5.4823E-06	-7.6757E-07
	UB	-9.3948E-05	-2.0813E-04	-9.7725E-05	-1.1726E-04	-5.8623E-05	-4.2267E-05	-1.9909E-05	-2.6731E-05	-4.0462E-05	-4.8509E-06
CORE		-2.3806E-03	-5.0454E-03	-2.4043E-03	-2.9111E-03	-9.2235E-04	-1.9992E-03	-6.1397E-04	-5.7537E-04	-1.0577E-03	-1.2363E-04
LB		-2.2852E-04	-4.6218E-04	-1.8690E-04	-2.1134E-04	-9.7054E-05	-1.5517E-04	-5.2908E-05	-4.1608E-05	-6.0417E-05	-7.0327E-06
LAR		-8.5900E-06	-1.6980E-05	-5.9838E-06	-6.6146E-06	-4.0001E-06	-2.7147E-06	-9.7531E-07	-3.6194E-06	-5.4707E-06	-7.5537E-07
Sum		-2.7155E-03	-5.7409E-03	-2.6987E-03	-3.2515E-03	-1.0837E-03	-2.2007E-03	-6.8820E-04	-6.5083E-04	-1.1695E-03	-1.3704E-04
Total		-2.0339E-02									
IGCAR	UAR										
	UB										
CORE											
LB											
LAR											
Sum											
Total											
IPPE	UAR										
	UB										
CORE											
LB											
LAR											
Sum											
Total											

TABLE 3.43. SODIUM DENSITY COEFFICIENTS (NON-LEAKAGE COMPONENT) (CONTINUED)

(2/2)											
Participant	Region	LEZ1	LEZ2	MEZ	MOX	HEZ	SHR	SCR	SSA1	SSA2	RR
JNC	UAR	-5.0900E-06	-1.0460E-05	-4.8200E-06	-6.3900E-06	-4.2900E-06	-1.7010E-06	-5.1700E-07	-4.1500E-06	-5.6800E-06	-3.6800E-07
	UB	-8.8504E-05	-1.8770E-04	-8.7190E-05	-1.1030E-04	-5.3880E-05	-4.6161E-05	-1.8760E-05	-2.9100E-05	-4.3090E-05	-2.1840E-06
CORE	-1.6420E-03	-3.3604E-03	-1.4550E-03	-2.4790E-03	-5.5540E-04	-1.7225E-03	-3.5970E-04	-4.4850E-04	-9.8870E-04	-5.5640E-05	-3.1380E-06
LB	-2.0720E-04	-4.1040E-04	-1.6520E-04	-1.9510E-04	-8.7910E-05	-1.4129E-04	-4.6900E-05	-4.8500E-05	-6.3300E-05	-6.3300E-05	-3.4300E-07
LAR	-9.6200E-06	-1.9000E-05	-6.7400E-06	-7.4200E-06	-4.3800E-06	-3.3120E-06	-1.1900E-06	-4.0300E-06	-5.3800E-06	-5.3428E-04	-6.1673E-05
Sum	-1.9526E-03	-3.9880E-03	-1.7190E-03	-2.7982E-03	-7.0586E-04	-1.9150E-03	-4.2707E-04	-5.3428E-04	-1.1062E-03	-6.1673E-05	
Total	-1.5208E-02										
KAERI	UAR										
	UB	-9.7087E-05	-2.1240E-04	-1.0008E-04	-1.2230E-04	-6.1516E-05	-3.3930E-04	-6.1516E-05	-2.8209E-06	-3.9055E-06	-5.2537E-08
CORE	-1.7443E-03	-3.6580E-03	-1.5752E-03	-2.0123E-04	-2.2946E-04	-1.0496E-04			-3.6155E-05	-5.3240E-05	-2.0306E-06
LB	-2.4781E-04	-5.0314E-04									
LAR											
Sum	-2.0892E-03	-4.3735E-03	-1.8765E-03	-2.4032E-03	-5.0578E-04						
Total	-1.1248E-02										
OKBM	UAR	-3.0348E-06	-6.4706E-06	-3.0239E-06	-3.8856E-06	-3.0119E-06	-7.9552E-07	-3.8308E-07	-2.8209E-06	-3.9055E-06	-5.2537E-08
	UB	-1.0076E-04	-2.2002E-04	-1.0083E-04	-1.2085E-04	-6.1037E-05	-5.1892E-05	-2.0146E-05	-3.6155E-05	-5.3240E-05	-2.0306E-06
CORE	-2.2989E-03	-4.7512E-03	-2.1714E-03	-2.8113E-03	-8.6911E-04	-1.8981E-03	-4.7889E-04	-4.5188E-04	-1.1772E-03	-5.0136E-05	-1.1772E-03
LB	-2.6687E-04	-5.3758E-04	-2.1182E-04	-2.3921E-04	-1.1155E-04	-1.5256E-04	-5.4225E-05	-6.6168E-05	-9.2851E-05	-2.8446E-06	-2.8446E-06
LAR	-5.5433E-06	-1.1986E-05	-4.1791E-06	-4.5532E-06	-2.8398E-06	-1.8445E-06	-6.4179E-07	-2.5910E-06	-3.9493E-06	-7.2040E-08	
Sum	-2.6751E-03	-5.5272E-03	-2.4913E-03	-3.1798E-03	-1.0476E-03	-2.1052E-03	-5.5428E-04	-5.5962E-04	-1.3311E-03	-5.5136E-05	
Total	-1.9526E-02										
Mean	UAR	-4.5533E-06	-8.8917E-06	-4.2829E-06	-5.7125E-06	-4.0379E-06	-1.4175E-06	-4.7453E-07	-4.0285E-06	-6.4215E-06	-4.0645E-07
	UB	-9.7961E-05	-1.9412E-04	-9.6495E-05	-1.1683E-04	-5.9372E-05	-4.7143E-05	-3.6979E-05	-3.2324E-05	-5.2142E-05	-4.9594E-06
CORE	-2.1723E-03	-4.2923E-03	-2.0243E-03	-2.6338E-03	-7.9437E-04	-1.7723E-03	-4.8733E-04	-4.8911E-04	-1.2021E-03	-1.2213E-04	-1.2213E-04
LB	-2.3978E-04	-4.5055E-04	-1.8733E-04	-2.1695E-04	-1.0181E-04	-1.5510E-04	-5.3932E-05	-5.3578E-05	-8.0752E-05	-7.2036E-06	-7.2036E-06
LAR	-9.1208E-06	-1.7114E-05	-4.7723E-06	-6.9397E-06	-4.2186E-06	-2.8235E-06	-1.0149E-06	-3.9791E-06	-6.2609E-06	-3.9666E-07	
Sum	-2.5237E-03	-4.9630E-03	-2.3172E-03	-2.9803E-03	-9.6381E-04	-1.9787E-03	-5.7973E-04	-5.7882E-04	-1.3477E-03	-1.3509E-04	
Total	-1.8368E-02										
SD	UAR	1.2468E-06	1.6560E-06	8.6852E-07	1.2238E-06	6.6839E-07	4.0416E-07	6.4421E-08	7.0515E-07	1.9465E-06	3.2001E-07
	UB	1.0765E-05	3.1689E-05	6.1899E-06	4.6216E-06	4.3720E-06	4.0264E-06	4.2831E-05	4.6192E-06	1.1343E-05	4.5384E-06
CORE	4.0172E-04	7.4220E-04	4.1333E-04	2.2280E-04	1.9055E-04	2.3854E-04	1.0719E-04	8.3669E-05	2.4041E-04	1.0617E-04	
LB	3.4109E-05	5.9722E-05	1.9508E-05	1.9897E-05	1.2637E-05	1.0680E-05	5.5787E-06	1.0869E-05	2.0724E-05	6.7450E-06	
LAR	2.7884E-06	3.1831E-06	2.9790E-06	1.6515E-06	9.2359E-07	6.5647E-07	2.5123E-07	8.6197E-07	1.9912E-06	3.0766E-07	
Sum	4.3903E-04	7.9717E-04	4.3139E-04	2.2894E-04	2.0467E-04	2.3337E-04	1.2979E-04	8.2839E-05	2.7264E-04	1.1786E-04	
Total	2.3071E-03										

* The results of CEA/SA and KAERI are not included in the averages.

TABLE 3.44. REGIONWISE SODIUM DENSITY COEFFICIENTS (TOTAL)

Participant	CORE*					
	UB	LEZ	MEZ	MOX	HEZ	LB
ANL	5.6121E-04	-2.6144E-03	-6.6576E-04	4.1473E-04	3.1242E-03	8.4566E-04
CEA/SA	4.5797E-04	-3.2037E-03	-8.5157E-04	2.2467E-04	2.4289E-03	7.0966E-04
CIAE	4.1968E-04	-4.2037E-03	-1.2802E-03	-2.3680E-04	2.5522E-03	6.0823E-04
IGCAR	1.0042E-03	-1.9353E-03	-4.0978E-04	8.7799E-04	3.6827E-03	1.6326E-03
IPPE	4.8777E-04	-2.4778E-03	-5.9540E-04	3.7440E-04	2.8260E-03	7.0214E-04
JNC	6.0362E-04	-1.6771E-03	-2.6649E-04	3.5125E-04	2.9705E-03	8.3340E-04
KAERI	-6.2511E-05	-3.2102E-03	-6.9444E-04	1.1715E-03	5.3592E-03	-2.5458E-04
OKBM	4.9780E-04	-3.6574E-03	-9.8035E-04	3.7970E-05	2.9600E-03	7.0217E-04
Participant	Upper AR	Lower AR	SCR	SHR	SSA	RR
ANL	2.3466E-04	4.2060E-04	5.0738E-03	6.9358E-03	5.4580E-03	9.3302E-04
CEA/SA	1.5466E-04	2.9125E-04	1.3845E-03	1.4609E-03	4.2885E-03	3.6424E-04
CIAE	1.1380E-04	2.0919E-04	1.0060E-03	1.5331E-03	3.9059E-03	2.3214E-04
IGCAR	-4.5128E-07	1.3973E-05	-5.0319E-05	-8.1195E-04	2.5214E-03	1.5966E-04
IPPE	0.0000E+00	0.0000E+00	0.0000E+00	3.2982E-03	4.1557E-03	0.0000E+00
JNC	1.7069E-04	2.9282E-04	1.4842E-03	1.3046E-03	4.3031E-03	3.3324E-04
KAERI	3.3796E-05	7.6889E-05	4.2753E-04	-3.5985E-04	7.5463E-03	4.6288E-04
OKBM	1.9835E-04	3.4900E-04	1.5502E-03	1.7298E-03	8.3376E-03	5.3262E-04

* Each column denotes the value only for the fuelled region.

TABLE 3.45. REGIONWISE SODIUM DENSITY COEFFICIENTS (LEAKAGE COMPONENT)

Participant	CORE ¹⁾						Sum
	UB	LEZ	MEZ	MOX	HEZ	LB	
ANL	1.1344E-03	3.4893E-03	1.2396E-03	2.8978E-03	3.7660E-03	1.9729E-03	1.4500E-02
CEA/SA ²⁾	9.7075E-04	3.1916E-03	1.1646E-03	2.4393E-03	3.4024E-03	2.7185E-03	1.3887E-02
CIAE	9.9536E-04	3.2223E-03	1.1241E-03	2.6743E-03	3.4745E-03	1.7942E-03	1.3285E-02
JNC	1.1313E-03	3.3266E-03	1.1895E-03	2.8310E-03	3.5270E-03	1.8977E-03	1.3903E-02
KAERI	1.0121E-03	3.1289E-03	1.0790E-03	1.9549E-03	2.0215E-03	1.8092E-03	1.1006E-02
OKBM	1.1013E-03	3.3927E-03	1.1911E-03	2.8493E-03	3.8291E-03	3.1001E-03	1.5464E-02
Participant	Upper AR	Lower AR	SCR	SHR	SSA	RR	Total
ANL	2.8216E-04	4.8581E-04	5.5967E-03	8.9320E-03	7.2854E-03	1.0463E-03	3.8128E-02
CEA/SA	1.4281E-04	2.7752E-04	1.6703E-03	2.4890E-03	5.6098E-03	4.7411E-04	2.4551E-02
CIAE	1.4932E-04	2.6414E-04	1.6928E-03	3.7297E-03	5.7082E-03	3.6918E-04	2.5198E-02
JNC	2.1516E-04	3.6335E-04	1.9120E-03	3.8307E-03	5.9188E-03	3.9508E-04	2.6538E-02
KAERI							
OKBM	2.2568E-04	3.2914E-04	1.8566E-03	2.9508E-03	9.9802E-03	7.9273E-04	3.1599E-02

1) Each column denotes the value only for the fuelled region.
 2) Transport theory calculations.

TABLE 3.46. REGIONWISE SODIUM DENSITY COEFFICIENTS (NON-LEAKAGE COMPONENT)

Participant	CORE ¹⁾						Sum
	UB	LEZ	MEZ	MOX	HEZ	LB	
ANL	-5.7317E-04	-6.1037E-03	-1.9053E-03	-2.4831E-03	-6.4174E-04	-1.1273E-03	-1.2834E-02
CEA/SA ²⁾	-5.4397E-04	-6.7410E-03	-2.1854E-03	-2.4847E-03	-9.8326E-04	-1.2359E-03	-1.4174E-02
CIAE	-5.7568E-04	-7.4260E-03	-2.4043E-03	-2.9111E-03	-9.2235E-04	-1.1860E-03	-1.5425E-02
JNC	-5.2757E-04	-5.0024E-03	-1.4550E-03	-2.4790E-03	-5.540E-04	-1.0658E-03	-1.1085E-02
KAERI	-5.9338E-04	-5.4022E-03	-1.5752E-03	-2.0514E-03	-3.3930E-04	-1.2866E-03	-1.1248E-02
OKBM	-6.0349E-04	-7.0501E-03	-2.8113E-03	-2.8113E-03	-8.6911E-04	-1.3670E-03	-1.4872E-02
Participant	Upper AR	Lower AR	SCR	SHR	SSA	RR	Total
ANL	-4.7503E-05	-6.5212E-05	-5.2290E-04	-1.9962E-03	-1.8274E-03	-1.1331E-04	-1.7407E-02
CEA/SA*	-4.5650E-05	-6.1855E-05	-7.0288E-04	-1.6671E-03	-2.4009E-03	-3.0830E-04	-1.9361E-02
CIAE	-3.5519E-05	-5.4954E-05	-6.8679E-04	-2.1966E-03	-1.8022E-03	-1.3704E-04	-2.0339E-02
JNC	-4.3098E-05	-6.1072E-05	-4.2536E-04	-19100E-03	-1.6212E-03	-6.1673E-05	-1.5208E-02
KAERI							
OKBM	-2.7332E-05	-3.8128E-05	-5.5326E-04	-2.1026E-03	-1.8775E-03	-5.5136E-05	-1.9526E-02

1) Each column denotes the value only for the fuelled region.

2) Transport theory calculations

TABLE 3.47. STEEL DENSITY COEFFICIENTS

TABLE 3.47. STEEL DENSITY COEFFICIENTS (CONTINUED)

Participant	Region	LEZ1	LEZ2	MEZ	MOX	HEZ	SHR	SCR	SSA1	SSA2	RR
JNC	UAR	1.7406E-05	3.4022E-05	1.6633E-05	2.3169E-05	1.5127E-05	4.7045E-06	1.3295E-06	1.5924E-05	2.2876E-05	3.4519E-06
	UB	2.0430E-04	4.6250E-04	2.2790E-04	3.4107E-04	1.7349E-04	6.7264E-05	8.5049E-05	4.1718E-04	4.1737E-04	1.0964E-04
CORE	-6.4632E-03	-1.3194E-02	-5.6625E-03	-5.1795E-03	3.0346E-03	-3.6413E-04	1.3250E-04	1.0966E-02	1.0667E-02	3.3803E-03	
LB	2.5072E-04	5.2944E-04	3.2573E-04	4.8140E-04	2.4128E-04	4.8309E-04	1.2807E-04	5.7598E-04	5.7424E-04	1.5593E-04	
LAR	4.0471E-05	8.3461E-05	2.9374E-05	2.8873E-05	1.5403E-05	2.4131E-05	9.2035E-06	1.4799E-05	2.0755E-05	3.1028E-06	
Sum	-5.9503E-03	-1.2088E-02	-5.0628E-03	-4.3050E-03	3.4799E-03	2.1507E-04	3.5615E-04	1.1987E-02	1.1703E-02	3.6524E-03	
Total	3.9908E-03										
KAERI	UAR	3.6071E-06	7.2558E-06	3.8486E-06	6.0002E-06	4.5980E-06	1.0173E-06	2.4568E-07	5.2683E-06	1.1699E-05	6.9603E-06
	UB	1.0669E-06	2.3202E-05	1.4119E-05	5.6902E-05	8.2190E-05	3.2307E-06	2.5464E-05	3.2701E-04	5.1385E-04	1.5386E-04
CORE	-6.7850E-03	-1.4193E-02	-6.1455E-03	-2.8227E-03	9.4617E-03	-1.3203E-03	-8.5542E-05	2.7916E-02	2.4942E-02	5.2054E-03	
LB	-9.8341E-05	-1.8228E-04	2.4474E-05	1.4472E-04	1.6388E-04	2.3367E-04	6.1336E-05	5.5658E-04	8.0005E-04	2.2576E-04	
LAR	1.0386E-05	2.4877E-05	1.1042E-05	1.0493E-05	5.6980E-06	7.0517E-06	2.5820E-06	5.6492E-06	1.1167E-05	6.2767E-06	
Sum	-6.8683E-03	-1.4320E-02	-6.0921E-03	-2.6046E-03	9.7180E-03	-1.0753E-03	-4.0851E-06	2.8811E-02	2.6279E-02	5.5983E-03	
Total	3.9449E-02										
OKBM	UAR	1.4617E-05	2.7929E-05	1.4207E-05	2.0193E-05	1.3212E-05	4.0677E-06	1.1312E-06	1.4071E-05	1.8868E-05	4.5076E-06
	UB	1.5465E-04	3.6891E-04	1.7780E-04	2.6533E-04	1.2676E-04	5.8662E-05	6.4770E-05	3.5841E-04	3.8656E-04	1.2464E-04
CORE	-7.1560E-03	-1.4780E-02	-6.3762E-03	-5.4738E-03	3.1132E-03	-8.7334E-04	1.0046E-04	9.6615E-03	1.0380E-02	3.9957E-03	
LB	1.5701E-04	3.3961E-04	2.4410E-04	3.7235E-04	1.7674E-04	4.4285E-04	1.1071E-04	5.1552E-04	5.4380E-04	1.8109E-04	
LAR	3.5363E-05	7.4408E-05	2.5830E-05	2.5039E-05	1.3461E-05	1.9778E-05	7.4075E-06	1.2792E-05	1.6449E-05	3.9196E-06	
Sum	-6.7944E-03	-1.3969E-02	-5.9143E-03	-4.7909E-03	3.4428E-03	-3.4799E-04	2.8448E-04	1.0572E-02	1.1345E-02	4.3098E-03	
Total	-1.8617E-03										
Mean	UAR	8.3823E-06	1.6283E-05	8.4769E-06	1.2238E-05	8.3565E-06	2.4242E-06	6.6431E-07	8.6927E-06	1.5153E-05	4.7093E-06
	UB	1.6133E-04	3.7870E-04	1.8676E-04	2.8437E-04	1.5292E-04	7.3669E-05	5.1136E-05	3.5220E-04	3.6285E-04	1.0973E-04
CORE	-6.5315E-03	-1.3526E-02	-5.9379E-03	-4.8591E-03	3.7666E-03	-9.0984E-04	2.6111E-05	1.1349E-02	1.0558E-02	3.4150E-03	
LB	1.9805E-04	4.2443E-04	2.8339E-04	4.2521E-04	2.2449E-04	4.1043E-04	8.9257E-05	5.0700E-04	5.1797E-04	1.8050E-04	
LAR	2.1586E-05	4.5946E-05	1.6584E-05	1.6146E-05	8.7835E-06	1.1736E-05	4.3728E-06	8.2629E-06	1.3891E-05	4.2464E-06	
Sum	-6.1421E-03	-1.2660E-02	-5.4427E-03	-4.1212E-03	4.1612E-03	-4.1158E-04	1.7155E-04	1.2225E-02	1.1468E-02	3.7142E-03	
Total	2.4889E-03										
SD	UAR	6.5014E-06	1.2648E-05	6.3447E-06	8.9247E-06	5.8964E-06	1.8677E-06	5.3785E-07	5.9567E-06	7.0356E-06	1.1611E-06
	UB	9.0740E-05	2.0298E-04	9.8867E-05	1.3671E-04	6.4793E-05	6.2941E-05	2.8225E-05	1.0014E-04	1.1958E-04	2.4939E-05
CORE	8.0872E-04	1.7249E-03	8.8628E-04	1.6911E-03	2.5914E-03	3.3117E-04	1.2153E-04	7.3094E-03	6.8850E-03	9.8287E-04	
LB	1.7796E-04	3.6827E-04	1.6802E-04	2.0375E-04	9.3824E-05	1.8697E-04	5.8448E-05	1.4792E-04	1.8919E-04	5.7892E-05	
LAR	1.6115E-05	3.3009E-05	1.1306E-05	1.1236E-05	6.0046E-06	8.3329E-06	3.1353E-06	5.5977E-06	6.5082E-06	1.0208E-06	
Sum	1.0268E-03	2.1948E-03	1.1018E-03	1.8361E-03	2.6008E-03	5.2733E-04	1.9782E-04	7.4182E-03	7.1533E-03	1.0201E-03	
Total	1.8776E-02										

TABLE 3.48. FUEL DENSITY COEFFICIENTS

(1/2)								
Participant	Region	LEZ1	LEZ2	MEZ	MOX	HEZ	SHR	SCR
ANL	UAR	-2.3682E-04	-4.2729E-04	-1.9700E-04	-2.3567E-04	-1.6651E-04		
	UB	3.9811E-02	8.4329E-02	5.5021E-02	1.0800E-01	5.2476E-02		
	CORE	-9.7028E-04	-1.9717E-03	-6.4802E-04	-5.8153E-04	-2.9850E-04		
	LB							
	LAR							
	Sum	3.8604E-02	8.1920E-02	5.4176E-02	1.0719E-01	5.2011E-02		
Total		3.3391E-01						
CEA/SA	UAR	8.3333E-05	2.6851E-04	1.3585E-04	2.1828E-04	-1.9814E-04		
	UB	4.0849E-02	8.6262E-02	5.5176E-02	1.0385E-01	5.7485E-02		
	CORE	-2.8168E-04	-5.6371E-04	-1.8135E-05	1.6999E-04	8.0205E-05		
	LB							
	LAR							
	Sum	4.0651E-02	8.5967E-02	5.5293E-02	1.0424E-01	5.7367E-02		
Total		3.4352E-01						
CIAE	UAR	9.7170E-05	3.4571E-04	1.5665E-04	2.4137E-04	6.0962E-05		
	UB	4.2511E-02	8.9566E-02	6.0856E-02	1.0830E-01	5.7544E-02		
	CORE	-3.0152E-04	-5.9660E-04	-1.5290E-06	2.2323E-04	5.3621E-05		
	LB							
	LAR							
	Sum	4.2307E-02	8.9315E-02	6.1011E-02	1.0877E-01	5.7658E-02		
Total		3.5906E-01						
IGCAR	UAR	5.0147E-04	1.2258E-03	6.2473E-04	9.3120E-04	4.5390E-04		
	UB	4.0653E-02	8.8110E-02	5.6694E-02	1.1246E-01	6.2987E-02		
	CORE	5.1970E-04	1.1184E-03	8.4580E-04	1.3322E-03	6.5257E-04		
	LB							
	LAR							
	Sum	4.1674E-02	9.0454E-02	5.8165E-02	1.1472E-01	6.4093E-02		
Total		3.6911E-01						
IPPE	UAR	1.2000E-04	3.6000E-04	1.8700E-04	3.0100E-04	8.2100E-05		
	UB	4.2620E-02	8.7920E-02	5.5290E-02	1.0600E-01	5.5390E-02		
	CORE	-3.1000E-04	-6.2200E-04	8.3100E-06	2.6300E-04	6.5500E-05		
	LB							
	LAR							
	Sum	4.2430E-02	8.7638E-02	5.5485E-02	1.0656E-01	5.5538E-02		
Total		3.4767E-01						

TABLE 3.48. FUEL DENSITY COEFFICIENTS (CONTINUED)

(2/2)							
Participant	Region	LEZ1	LEZ2	MEZ	MOX	HEZ	SHR
INC	UAR						
	UB	6.2946E-05	2.2285E-04	1.3705E-04	2.5589E-04	8.4078E-05	
	CORE	4.1094E-02	8.5175E-02	5.4379E-02	1.0788E-01	5.4983E-02	
	LB	-3.7992E-04	-7.4621E-04	-5.1661E-05	1.9370E-04	7.3011E-05	
	LAR						
	Sum	4.0777E-02	8.4651E-02	5.4464E-02	1.0833E-01	5.5140E-02	
Total							
KAERI	UAR						
	UB	-3.3449E-04	-6.4263E-04	-3.0867E-04	-3.6393E-04	-1.4935E-04	
	CORE	3.9851E-02	8.3968E-02	5.4539E-02	1.0877E-01	6.8697E-02	
	LB	-1.1482E-03	-2.3411E-03	-7.5006E-04	-6.1531E-04	-1.7825E-04	
	LAR						
	Sum	3.8368E-02	8.0984E-02	5.3480E-02	1.0779E-01	6.8369E-02	
Total							
OKBM	UAR						
	UB	1.3457E-04	3.8360E-04	1.9851E-04	3.1940E-04	1.2633E-04	
	CORE	4.2857E-02	8.9383E-02	5.6511E-02	1.0966E-01	5.6387E-02	
	LB	-2.1258E-04	-4.2850E-04	7.9403E-05	3.2473E-04	1.4555E-04	
	LAR						
	Sum	4.2779E-02	8.9339E-02	5.6789E-02	1.1030E-01	5.6859E-02	
Total							
Mean	UAR						
	UB	5.3522E-05	2.1706E-04	1.1670E-04	2.0844E-04	3.6673E-05	
	CORE	4.1281E-02	8.6839E-02	5.6058E-02	1.0812E-01	5.8269E-02	
	LB	-3.8556E-04	-7.6893E-04	-6.6987E-05	1.6375E-04	7.4213E-05	
	LAR						
	Sum	4.0949E-02	8.6287E-02	5.6108E-02	1.0849E-01	5.8380E-02	
Total							
SD	UAR						
	UB	2.5337E-04	5.6558E-04	2.8068E-04	3.9125E-04	2.1315E-04	
	CORE	1.2313E-03	2.2150E-03	2.1113E-03	2.5189E-03	5.1770E-03	
	LB	5.0661E-04	1.0481E-03	4.8864E-04	6.0567E-04	2.7846E-04	
	LAR						
	Sum	1.6984E-03	3.5378E-03	2.4821E-03	3.0742E-03	5.2838E-03	
Total							

TABLE 3.49. ABSORBER DENSITY COEFFICIENTS

(1/2)							
Participant	Region	LEZ1	LEZ2	MEZ	MOX	HEZ	SHR
ANL	UAR					0.0000E+00	0.0000E+00
	UB					-6.5206E-04	-1.9224E-04
	CORE					-2.3249E-02	0.0000E+00
	LB					0.0000E+00	0.0000E+00
	LAR					0.0000E+00	0.0000E+00
	Sum					-2.3901E-02	-1.9224E-04
	Total	-2.4093E-02					
CEA/SA	UAR					0.0000E+00	0.0000E+00
	UB					-6.5131E-04	-2.4406E-04
	CORE					-2.4881E-02	0.0000E+00
	LB					0.0000E+00	0.0000E+00
	LAR					0.0000E+00	0.0000E+00
	Sum					-2.5532E-02	-2.4406E-04
	Total	-2.5776E-02					
CIAE	UAR					0.0000E+00	0.0000E+00
	UB					-5.6229E-04	-1.9091E-04
	CORE					-2.3539E-02	0.0000E+00
	LB					0.0000E+00	0.0000E+00
	LAR					0.0000E+00	0.0000E+00
	Sum					-2.4101E-02	-1.9091E-04
	Total	-2.4292E-02					
IGCAR	UAR					0.0000E+00	0.0000E+00
	UB					-5.9677E-04	-1.9951E-04
	CORE					-2.2574E-02	0.0000E+00
	LB					0.0000E+00	0.0000E+00
	LAR					0.0000E+00	0.0000E+00
	Sum					-2.3170E-02	-1.9951E-04
	Total	-2.3370E-02					
IPPE	UAR						
	UB						
	CORE						
	LB						
Sum	LAR						
	Total	-2.3370E-02					
	Total	-2.1700E-02					

TABLE 3.49. ABSORBER DENSITY COEFFICIENTS (CONTINUED)

(2/2)											
Participant	Region	LEZ1	LEZ2	MEZ	MOX	HEZ	SHR	SCR	SSA1	SSA2	RR
JNC	UAR						0.0000E+00	0.0000E+00			
	UB						-4.9553E-04	-1.1997E-04			
	CORE						-1.9574E-02	0.0000E+00			
	LB						0.0000E+00	0.0000E+00			
	LAR						0.0000E+00	0.0000E+00			
	Sum						-2.0069E-02	-1.1997E-04			
KAERI	Total	-2.0189E-02									
	UAR						0.0000E+00	0.0000E+00			
	UB						-7.4866E-04	-2.5941E-04			
	CORE						-2.5713E-02	0.0000E+00			
	LB						0.0000E+00	0.0000E+00			
	LAR						0.0000E+00	0.0000E+00			
OKBM	Sum						-2.6462E-02	-2.5241E-04			
	Total	-2.6714E-02									
	UAR						0.0000E+00	0.0000E+00			
	UB						-5.8316E-04	-1.4374E-04			
	CORE						-2.3728E-02	0.0000E+00			
	LB						0.0000E+00	0.0000E+00			
Mean	LAR						0.0000E+00	0.0000E+00			
	Sum						-2.4311E-02	-1.4374E-04			
	Total	-2.4455E-02									
	UAR						0.0000E+00	0.0000E+00			
	UB						-6.1283E-04	-1.9184E-04			
	CORE						-2.3322E-02	0.0000E+00			
SD	LB						0.0000E+00	0.0000E+00			
	LAR						0.0000E+00	0.0000E+00			
	Sum						-2.3935E-02	-1.9184E-04			
	Total	-2.3824E-02									
	UAR						0.0000E+00	0.0000E+00			
	UB						8.0540E-05	4.8193E-05			
Total	CORE						1.9568E-03	0.0000E+00			
	LB						0.0000E+00	0.0000E+00			
	LAR						0.0000E+00	0.0000E+00			
	Sum						2.0262E-03	4.8193E-05			
	Total	2.0970E-03									

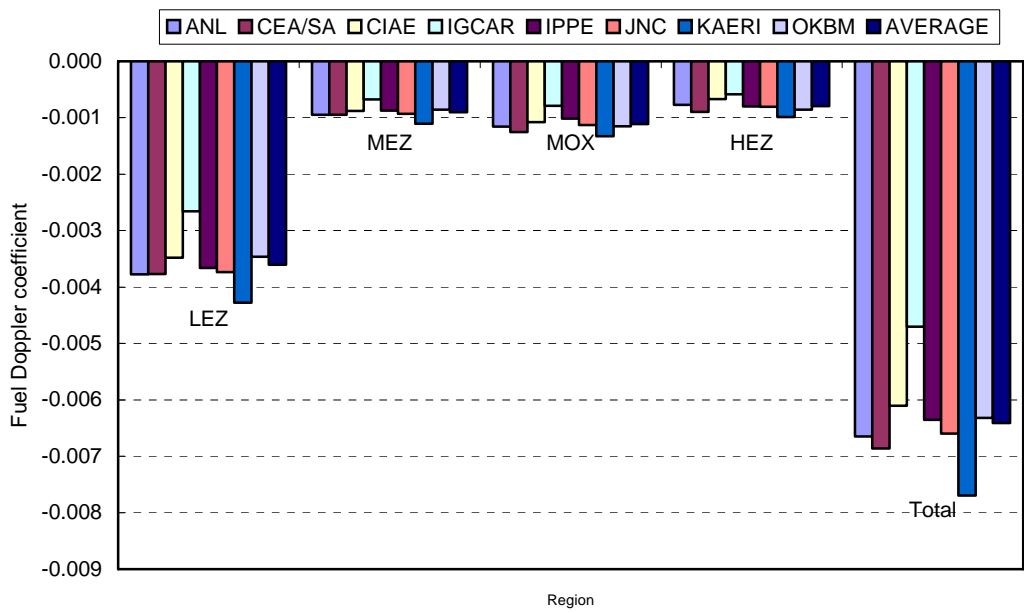


FIG. 3.42. Fuel Doppler coefficients (Hex-Z model).

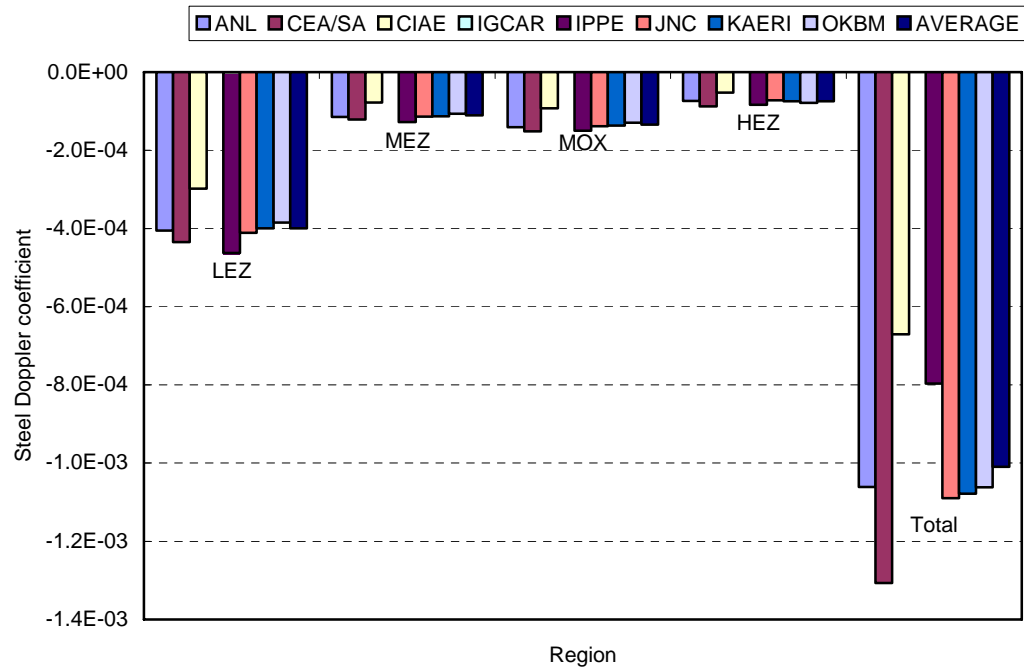


FIG. 3.43. Steel Doppler coefficients (Hex-Z model).

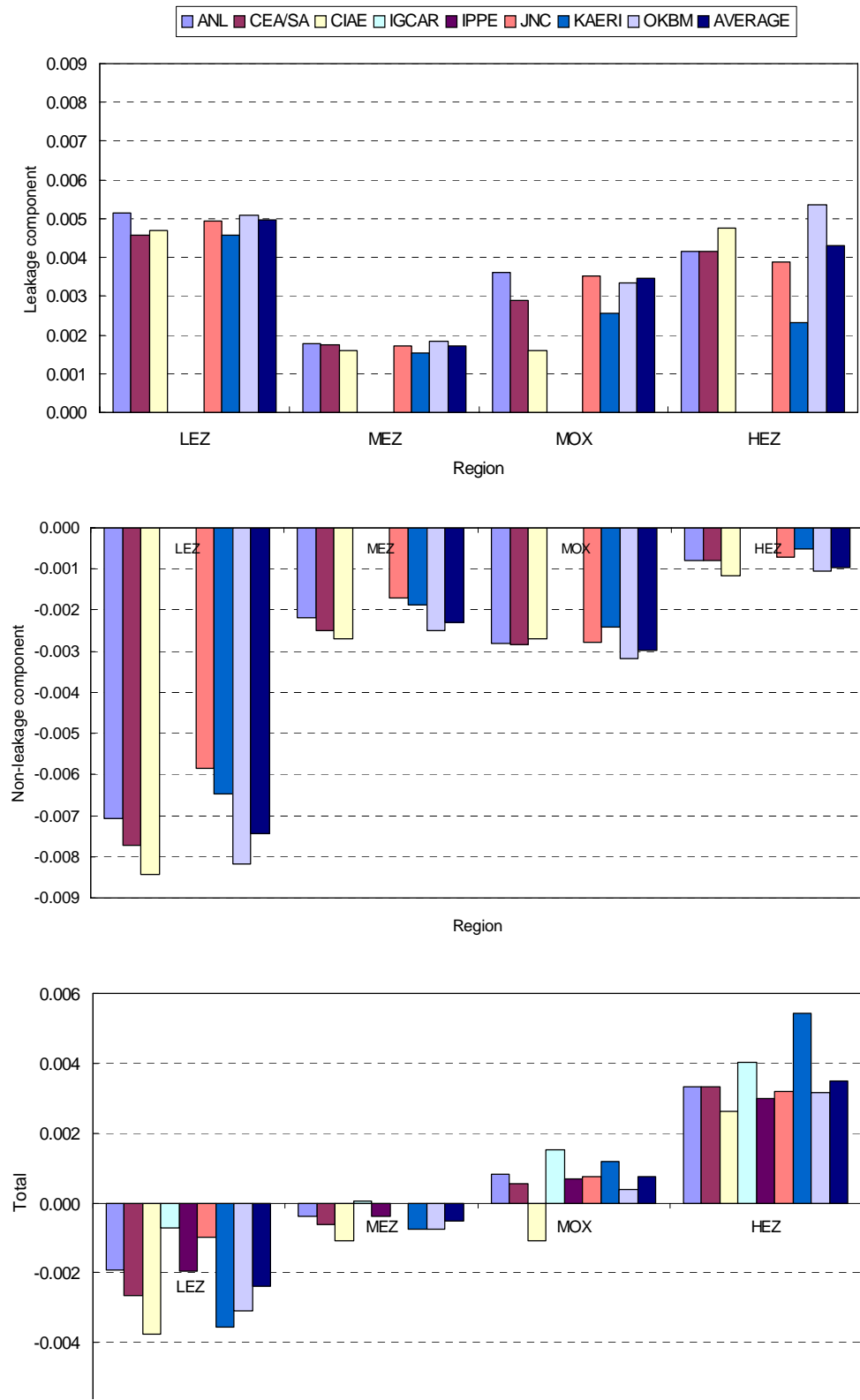


FIG. 3.44. Componentwise sodium density coefficients for the core and upper axial blanket region (Hex-Z model.)

In Fig. 3.44 the regional coefficients in general show better agreement than the comparison of the total coefficients summed over all regions in the core. This is attributed to the same reason as indicated in the Phase 1 study: the net coefficient resulting from the difference in large positive and negative contributions from the non-leakage and leakage components respectively.

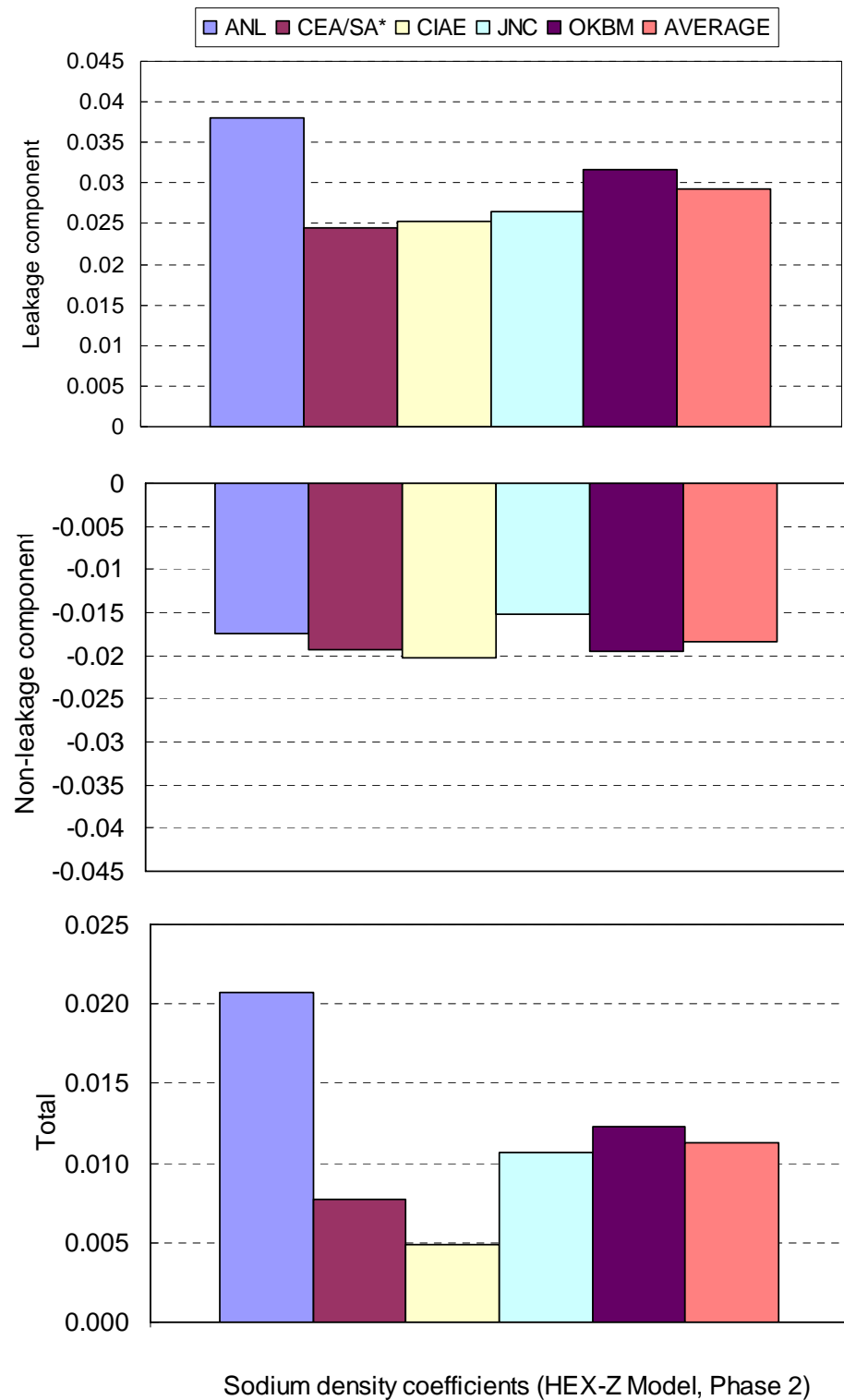
Figure 3.45 compares the leakage and non-leakage components of the sodium density coefficients for the whole core system. Due to dominance of the leakage effect, the resultant total sodium density coefficient was found to be positive for the whole core system. The ANL results give the largest leakage and total core sodium density coefficient values among the participants' results.

The resultant aspects are very similar for the steel density coefficients shown in Fig. 3.47, where the regional values for the fuelled regions show better agreement than the total value for the whole core system. In this figure, the ANL and KAERI results for the steel density coefficients were predicted to be relatively larger than those of the other participants, particularly for total core values.

The comparison of the regionwise fuel density coefficients for the core shows good agreement between the results obtained by the participants. In Fig. 3.46 it is observed that the fuel density effect is most effective in the LEZ and MOX zones of the core. For the absorber density coefficients, Fig. 3.48, the results obtained by the participants show good agreement in their local and total values. The absorber densities for the SHR zones are substantially larger than those of the SCR zone, due to the control rod insertion in the benchmark loading. In the SHR zone the rods are inserted to the core midplane whereas in the SCR zone the absorber is inserted to the upper blanket core interface. It can be inferred from Fig. 3.48 that the absorber control in the outermost zone, i.e. the SHR3 zone is most effective between the different SHR regions.

Tables 3.44–3.46 present material-dependent sodium density coefficients for constituent compositions in the whole core system. In these tables, the spatial distributions of the resultant sodium density coefficients are shown along with those of the leakage and non-leakage components. In the LEZ and MEZ zones which contain highly enriched fuel and for zones located near the core centre, the non-leakage component dominates the leakage effect and, as a result, the overall sodium density coefficient is negative. In the MOX zone, the domination of the non-leakage effect is only apparent for the result obtained by CIAE. The domination of the non-leakage component becomes smaller when moving toward the outer zones. It is clearly observed that the leakage component becomes dominant in the HEZ zone, where it has the greatest positive worth in the core. Most zones peripheral to the highly enriched fuelled zones have a positive worth due to prevalence of the leakage component in those zones.

The comparison of the results for the sodium density coefficients obtained from the Phase 1 and 2 studies, shows the existence of large discrepancies in the predictions of both spatial and total values depending on the geometrical model employed, i.e. the two-dimensional RZ model for Phase 1 and the three-dimensional Hex-Z model for Phase 2. The Hex-Z model calculation is assumed to give a more appropriate and realistic spatial representation of the benchmark core.



* Transport theory results

FIG. 3.45. Componentwise sodium density coefficients for the whole core (Hex-Z model).

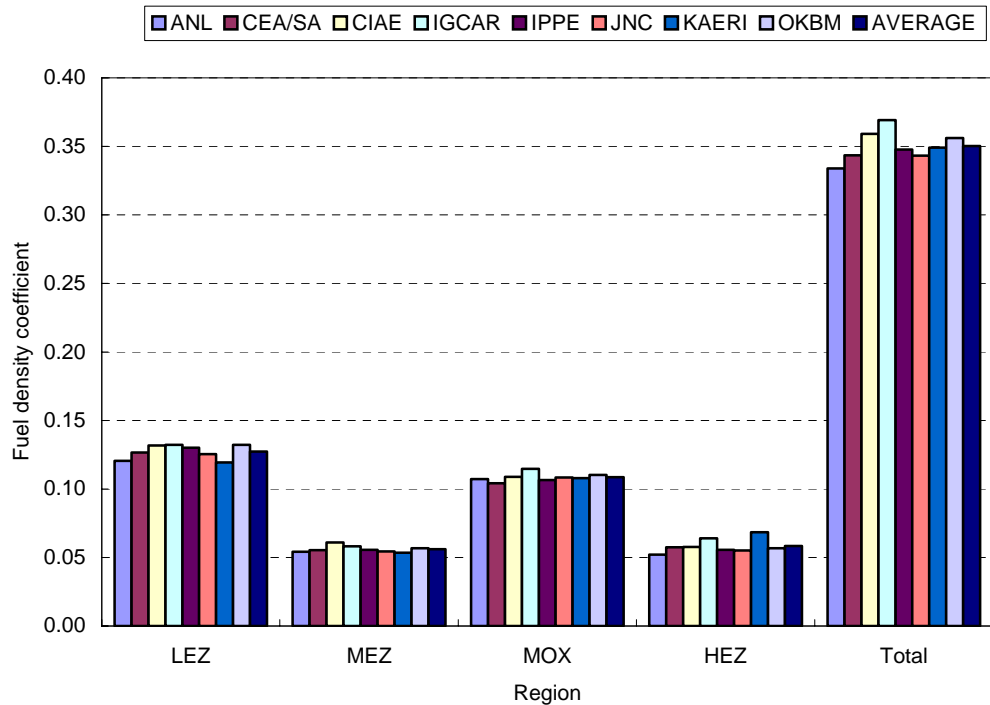


FIG. 3.46. Fuel density coefficients (Hex-Z model).

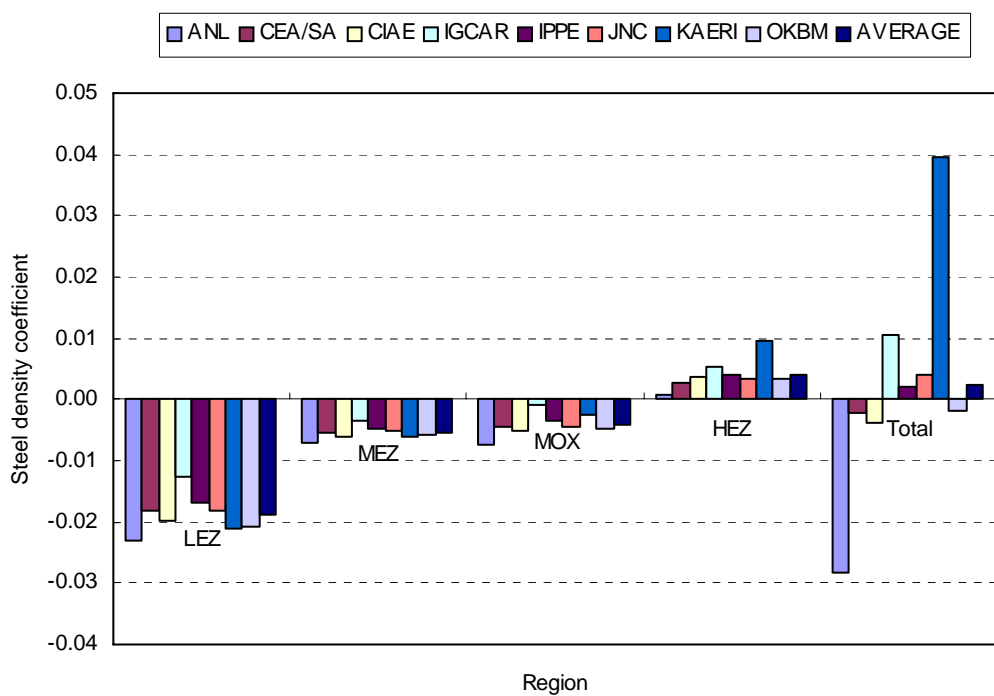


FIG. 3.47. Steel density coefficients (Hex-Z model).

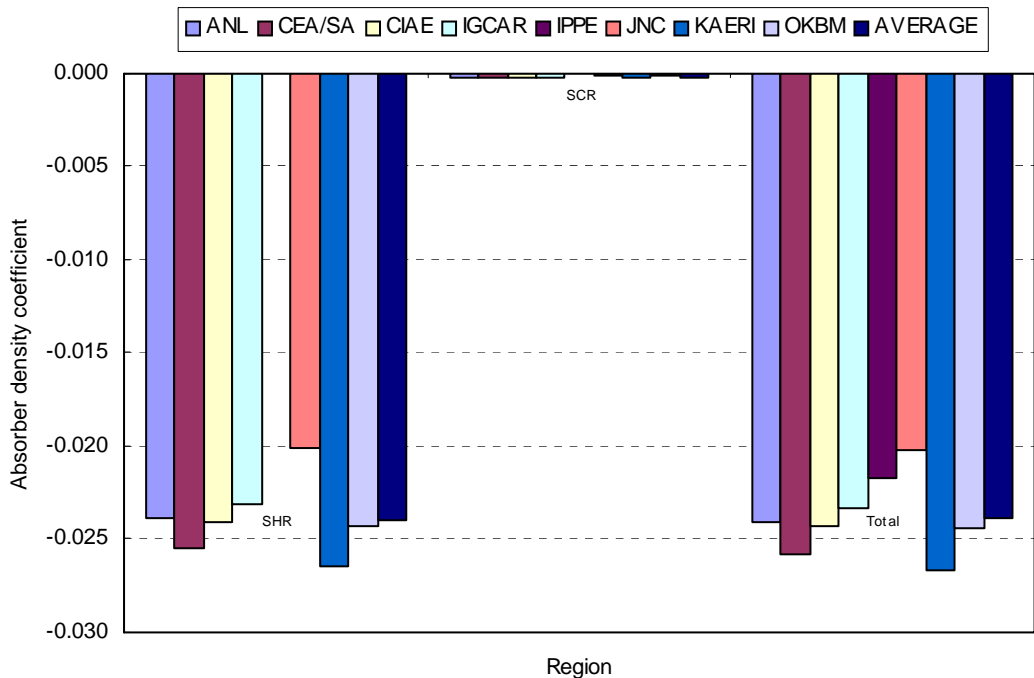


FIG. 3.48. Absorber density coefficients (Hex-Z model).

3.2.4. Summary of homogeneous benchmarks (Phase 1 and 2)

Integral reactivity parameters obtained by the participants for the Phase 1 and 2 benchmarks are summarized in Tables 3.50 and 3.51, respectively, with the mean value and relative standard deviation of the results for each coefficient.

The comparison of the diffusion and transport theory results for Phase 1 and 2 generally shows good agreement for most parameters between the RZ and Hex-Z models. The results for the sodium and steel density coefficients show large discrepancies both in the diffusion theory approximation and between the diffusion and transport theory approximations. Such large differences arise as the net coefficient results from the cancellation of large non-leakage terms and leakage terms of opposite sign.

The effective delayed neutron fraction (β_{eff}) and prompt neutron lifetime (l_p) for system kinetics parameters are given in Table 3.52. The results for Phase 1 and 2 show good agreement between the diffusion and transport theory results with the RZ and Hex-Z models. The effective delayed neutron fraction was calculated to be 0.0059 for the partially MOX fuelled hybrid BN-600 core. The prompt neutron lifetime for the hybrid BN-600 benchmark core was evaluated to be 4.55×10^{-7} s and 4.40×10^{-7} s for the RZ and Hex-Z models respectively. The Hex-Z model predicts a 3.0% smaller prompt neutron lifetime than the RZ model.

TABLE 3.50. REACTIVITY PARAMETERS (RZ MODEL, PHASE 1)

Participant	k_{eff}		K_D^{fuel}		K_D^{steel}		W_{Na}		W_{steel}		W_{fuel}		W_{abs}		R_{rad}		
	Diffusion	Transport	Diffusion	Transport	Diffusion	Transport	Diffusion	Transport	Diffusion	Transport	Diffusion	Transport	Diffusion	Transport	Diffusion	Transport	
ANL	0.99684	1.00788	-0.00652	-0.00110	0.01749	-0.0384	-0.0112	-0.0147	0.3343	-0.0266	-0.1446	-0.1378	-0.0263	-0.1374	-0.4872	-0.4573	
CEA/SA	1.01676	1.02298	-0.00679	-0.00134	0.00519	0.00343	-0.0055	-0.0021	0.3423	-0.0273	-0.1378	-0.1432	-0.0391	-0.1341	-0.4650	-0.4603	
CIAE	0.99808	1.01497	-0.00499	-0.00049	0.00211	0.00446	-0.0021	-0.0021	0.3492	-0.0269	-0.1395	-0.1297	-0.0274	-0.1267	-0.4868	-0.4840	
IGCAR	1.00360	1.00462	-0.00622	-0.00028	-0.00124	0.00898	0.00201	-0.0053	0.3505	0.3466	-0.0260	-0.0270	-0.0265	-0.1267	-0.4868	-0.4787	
IPPE	1.00140	1.00576	-0.00622	-0.00021	-0.00122	0.00765	0.00403	-0.0126	0.3491	-0.0270	-0.1361	-0.1376	-0.0270	-0.1376	-0.4812	-0.4647	
JNC	1.00423	1.00948	-0.00635	-0.00021	-0.00116	0.00125	0.01065	-0.0114	0.3628	-0.0287	-0.1415	-0.1415	-0.0287	-0.1415	-0.4827	-0.4493	
KAERI	1.02654	1.02777	-0.00659	-0.00097	-0.00125	0.01065	0.01065	-0.0114	0.3628	-0.0287	-0.1415	-0.1415	-0.0287	-0.1415	-0.4827	-0.4493	
OKBM	0.99796	-	-	-	-	-	-	-	-	-	-	-	-	-	-	-	
Mean	1.00270	1.01460	-0.00601	-0.00054	-0.00127	0.00808	0.00319	-0.0123	0.3470	0.3446	-0.0264	-0.1394	-0.0264	-0.1394	-0.4729	-0.4621	
SD (\pm) (Rel. %)	0.00623 (0.62)	0.00777 (0.77)	0.00079 (0.31)	0.00062 (9.2)	0.00027 (25.7)	0.00012 (9.4)	0.00468 (57.9)	0.00080 (25.1)	0.0112 (91.1)	0.0028 (21.9)	0.0047 (2.4)	0.0045 (15.0)	0.0044 (1.5)	0.0044 (3.2)	0.0044 (3.0)	0.0214 (4.5)	0.0097 (2.1)

TABLE 3.51. REACTIVITY PARAMETERS (HEX-Z MODEL, PHASE 2)

Participant	k_{eff}		K_D^{fuel}		K_D^{steel}		W_{Na}		W_{steel}		W_{fuel}		W_{abs}		R_{rad}	
	Diffusion	Transport	Diffusion	Transport	Diffusion	Transport	Diffusion	Transport	Diffusion	Transport	Diffusion	Transport	Diffusion	Transport	Diffusion	Transport
ANL	0.99592	0.99802	-0.00665	-0.00106	0.00771	0.02072	-0.0284	-0.0022	0.3339	0.3385	-0.0241	-0.1598	-0.0258	-0.1397	-0.4947	-0.4605
CEA/SA	1.01546	1.02272	-0.00686	-0.00131	-0.00067	0.00486	-0.0037	-0.0073	0.3435	0.3591	-0.0243	-0.1463	-0.0234	-0.1397	-0.4741	-0.5008
CIAE	1.00026	-0.00610	-0.00471	-0.00132	-0.00132	0.00668	0.0107	0.0032	0.3435	0.3691	-0.0234	-0.1461	-0.0217	-0.1384	-0.4788	-0.4822
IGCAR	1.00642	-0.00635	-0.00080	-0.00080	-0.00087	0.00206	0.0019	0.0032	0.3477	0.3438	-0.0206	-0.1352	-0.0219	-0.1352	-0.4904	-0.4814
IPPE	1.00471	-0.00646	-0.00033	-0.00109	0.01038	0.00664	-0.0020	-0.0066	0.3466	0.3437	-0.0200	-0.1574	-0.0219	-0.1530	-0.4923	-0.4814
JNC	1.00713	1.00967	-0.00770	-0.00166	-0.00106	0.01050	0.01226	-0.0019	0.3490	0.3561	-0.0267	-0.1528	-0.0245	-0.1293	-0.4726	-0.4679
KAERI	1.01260	1.01494	-0.00632	-0.00106	-0.00106	0.01024	0.00487	-0.0017	0.3506	0.3427	-0.0220	-0.1488	-0.0220	-0.1448	-0.4872	-0.4730
OKBM	0.99357	-	-	-	-	-	-	-	-	-	-	-	-	-	-	-
Mean	1.00451	1.01134	-0.00639	-0.00079	-0.00101	0.01024	0.00487	-0.0017	0.3506	0.3427	-0.0228	-0.1488	-0.0220	-0.1448	-0.4872	-0.4730
SD (\pm) (Rel. %)	0.00714 (0.71)	0.00898 (0.89)	0.00078 (12.2)	0.00052 (7.7)	0.00018 (18.8)	0.00019 (44.1)	0.00453 (41.3)	0.0176 (13.3)	0.00201 (29.9)	0.0048 (8.4)	0.0102 (5.0)	0.0011 (6.9)	0.0020 (5.2)	0.0011 (6.9)	0.0099 (2.0)	0.0092 (1.9)

TABLE 3.52. KINETICS PARAMETERS

Participant	RZ Model (Phase 1)		Hex-Z Model (Phase 2)	
	β_{eff} (pcm)	$l_p (10^{-7} \text{ s})$	β_{eff} (pcm)	$l_p (10^{-7} \text{ s})$
ANL	569	4.423	581	4.491
CEA/SA	597 (594)*	4.687	598	4.606
CIAE	604	4.277	598	4.239
IGCAR	598	4.618	598	
IPPE	585 (583)*	4.586	593 (591)*	4.467 (4.523)*
JNC	586	4.620	587	4.484
KAERI			595	4.443
OKBM	578	4.618	573	4.130
Mean	588	4.547	590	4.409
SD (\pm) (Rel. %)	11.2 (1.9)	0.134 (2.9)	8.9 (1.5)	0.152 (3.4)

* Transport theory results.

3.2.5. Influence of mesh size and number of energy groups

As previously mentioned, various planar and axial mesh sizes were used in the benchmark calculations, even though the axial mesh sizes were specified for desired result edit. It is generally recognized that the impact of mesh size is not negligible in diffusion theory solutions computed by employing a finite difference scheme. In addition, some results were obtained using relatively low group numbered cross-sections in few group calculations. The value of a corresponding additional uncertainty strongly depends on the number of energy groups and the choice of the energy group boundaries. Therefore, probable additional uncertainties due to the coarse mesh and the few group calculations could inherently be included in the benchmark calculational results.

The OKBM participant devoted to investigate the possible uncertainties due to coarse mesh and few group calculations of the reactivity coefficients [37]. This parametric study was performed based on the Phase 2 results obtained using the finite difference option of the JARFR code in Hex-Z/triangular-Z diffusion approximations. In this study, few group calculations were performed for 26 to 9 energy groups with axial mesh sizes being varied from 2.61 to 10.0 cm for the core and from 2.5 to 5.0 cm for the axial blankets, respectively.

In summary, among the examined parameters, the planar mesh size appeared to be most influential. The Hex-Z option has a coarse planar mesh configuration, i.e. one mesh point per hexagon, compared with six points per hexagon of the triangular-Z option. The results show that the use of the Hex-Z option having a larger planar mesh, results in the following additional uncertainties; overestimation of the fuel and steel Doppler coefficients by up to ~10-15% in the upper blanket, some shift of the sodium worth to positive by up to ~20% in LEZ, and significant underestimation of the absorber worth by 20%. The use of a larger axial mesh leads to some overestimation by 4-8% of all reactivity coefficients in axial blankets.

It has also been revealed that the few group schemes, used by some participants, may result in significant uncertainties by up to -45% in the core and by up to -24 % in the axial blankets for the sodium ‘worth’. The principle of the choice of the energy scale optimal division has been proposed for

the few group calculations. That is, the optimal collapsing of the initial 26 groups into 9 groups has been provided by grouping adjacent groups with similar sodium ‘worth’ so that the error originated from the cross section averaging in case of coupling groups with different neutron fluxes can be minimized. The sodium worth in the core (except for the MOX core), obtained from 9 group calculation, agrees well with that obtained from 26 group calculation. More details about the results are addressed in Appendix I

3.3.Hex-Z heterogeneous and burnup benchmark (Phase 3)

3.3.1. Hex-Z heterogeneous and burnup model

During the second RCM held in 20-24 November 2000, Vienna, the motivation for continuing the Phase 2 studies into Phase 3 was discussed and the following items were identified as important:

- Heterogeneity will affect absolute core reactivity;
- Rod worths could be considerably reduced by heterogeneity effects depending on their detailed design;
- Heterogeneity effects will affect the resonance self-shielding in the treatment of fuel Doppler, steel Doppler and sodium density effects. However, it was considered more important to concentrate on the sodium density effect in order to reduce the calculational effort required;
- It was also recognized that burnup effects will have an influence on fuel Doppler and sodium worths.

Based on the above recognitions, a benchmark for the assessment of heterogeneity effect for Phase 3 was defined by the following [38].

3.3.1.1. Homogeneous burnup model

The burnup calculation is performed as a single stage calculation with no recalculation of the flux or resonance self-shielding for sub time steps. The burnup period is 140 full power days with the assumption of 100% load factor (burnup for 140 days at a power of 1470 MW thermal). The core power is normalized at the start of the burnup, assuming all power is deposited at the point of fission using an energy per fission of 200 MeV for all nuclides and 0 MeV per capture for all nuclides. No depletion is included for boron isotopes. The definitions of rod raised and rod inserted for SHR are given in Table 3.53, using the composition numbers. The Phase 3 calculations are performed at the fixed insertion (mid-core insertion).

TABLE 3.53. AXIAL COMPOSITION NUMBERS FOR SHR CONFIGURATIONS

Axial height (cm)	Phase 2 definition	Phase 3 definition	
		Rod raised (fully withdrawn)	Rod inserted (fully inserted)
189.8–209.8	34	34	34
165.1–189.8	26	26	26
159.6–165.1	26	27	26
107.4–159.6	26	27	26
55.2–107.4	27	27	26
49.7–55.2	27	27	27
20.0–49.7	27	27	27
0.0–20.0	34	34	34

The following parameters are evaluated, where possible, by diffusion and transport theory by direct reactivity difference or perturbation theory for the Hex-Z model only, with the SHR control rods mid-core insertion and the end of cycle (EOC) with the SHR rods fully withdrawn:

- k_{eff} ;
- Fuel Doppler for core and blanket;
- Sodium density (1% density change for direct calculation);
- Other parameters from the Phase 2 studies are optional;
- No distributions are required.

3.3.1.2. Heterogeneous burnup model

a) Heterogeneity calculation

A heterogeneous treatment is applied to both the core fuel regions and the control rods. Subassemblies LEZ, MEZ, MOX, and HEZ use the same heterogeneous geometry description. A separate geometry description is defined for the SHR absorber region.

In more details, subassemblies LEZ, MEZ, MOX, HEZ have the identical geometry, where 127 fuel pins are located with triangular pitch of 7.95 mm inside hexagonal wrapper. The cross section of SHR is shown in Fig. 3.49. The detailed heterogeneous geometry description of FSA and SHR is presented in Table 3.54.

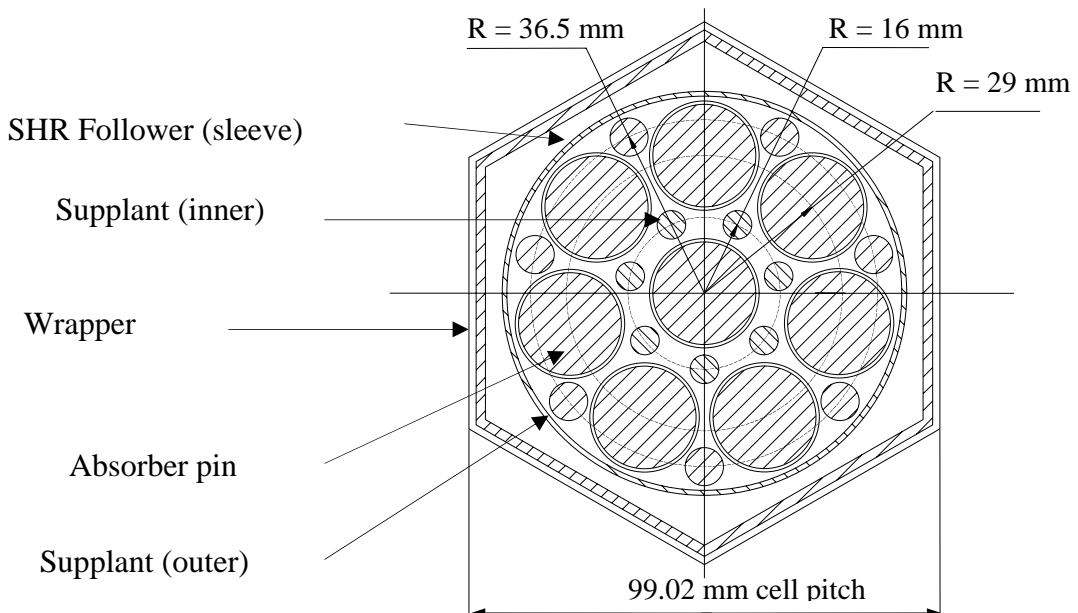


FIG. 3.49. SHR cross section.

TABLE 3.54. HETEROGENEOUS GEOMETRY DESCRIPTION FOR FUEL SA AND SHR

SA type	Homogeneous composition No	Structural element	Heterogeneous composition No
FSA	1–25	<i>Hexagonal wrapper</i> • external size across flats – 96.0 mm • thickness – 2.0 mm	26
	1–25	<i>Fuel pin (127)</i>	27
	1–25	Cladding: • external diameter – 6.9 mm • thickness – 0.4 mm	
	1–5	Fuel	1–5 respectively
	6–25	Fertile material	6–25 respectively
SHR	1–25	<i>Coolant (sodium)</i>	28
	26	<i>Hexagonal follower</i> • external size across flats – 96.0 mm • thickness – 2.0 mm	26
		<i>Rod wrapper</i> • external diameter – 85.0 mm • thickness – 1.0 mm	29
		<i>Absorber pin (7)</i> Cladding: • external diameter – 23.0 mm • thickness – 0.7 mm Absorbing material (B_4C)	30 31
		<i>Inner supplant (7)</i> • diameter – 6.0 mm	29
		<i>Outer supplant (7)</i> • diameter – 8.0 mm	29
		<i>Coolant (sodium)</i>	32

The following insignificant simplifications of real geometry description have been assumed in the heterogeneous geometry descriptions:

- Fuel pin spacer wire is omitted and cladding steel density is increased respectively;
- The dimensions of structural elements (wrapper, cladding, etc) in SA cross section are taken without regard to thermal expansion (at 20°C);
- The dimension of fuel/absorber pellet equals to cladding internal diameter, no hole in fuel pellet is considered.

Nuclear densities for heterogeneous compositions are listed in Table 3.55. The value of nuclear density for inter-assembly sodium is taken the same as for sodium inside SA. For each isotope the amount of nuclei in heterogeneous model has been retained as in homogeneous model.

The following parameters are calculated at the start of cycle using the heterogeneous core description, where possible, by diffusion and transport theory, either by direct reactivity difference or perturbation theory:

- k_{eff} ;
- Control rod worth;
- Sodium density (1% density change for direct calculation);
- The sodium density distribution, calculated by first-order perturbation theory is desirable but optional;
- Other parameters from the Phase 2 studies are optional.

b) Heterogeneous burnup calculation

The heterogeneous model is normalized and the burnup performed in the same manner as for the homogenous burnup calculation. The calculation of k_{eff} only (optional) with rods at their Phase 2 insertion is suggested.

3.3.2. Comparison of results

In this section the BOC results for ANL, JNC and IPPE have been taken from the results for Phase 2. Those for CEA/SA, IGCAR and KAERI are new analyses specifically for Phase 3. For CIAE homogeneous results have been taken from Phase 2 but new results are presented for heterogeneous geometries.

3.3.2.1. Burnup effect

To evaluate the burnup effect, k_{eff} , Doppler coefficients for fuel and steel, density coefficients for fuel, sodium and absorber, and a control rod worth were calculated at the beginning of cycle (BOC) with the SHR control rods mid-core insertion and the end of cycle (EOC) with the SHR rods fully ‘withdrawn’ for the homogeneous core model. Burnup calculations were performed for 140 effective full power days at 1470 MW•th in the equilibrium cycle with SHR control rods mid-core insertion. The k_{eff} at EOC with the SHR rods mid-core position was calculated to evaluate the reactivity loss with burnup.

TABLE 3.55. ISOTOPIC DENSITY FOR HETEROGENEOUS COMPOSITIONS
 (Unit: 10^{24} nuclei / cm³)

Isotope	Heterogeneous composition No.				
	1	2	3	4	5
²³⁵ U	.2674E-02*	.2699E-02	.3397E-02	.3857E-04	.4420E-02
²³⁶ U	.1218E-03	.1165E-03	.1284E-03	.1328E-05	.1180E-03
²³⁸ U	.1527E-01	.1530E-01	.1459E-01	.1459E-01	.1376E-01
²³⁹ Pu	.3184E-03	.3040E-03	.2599E-03	.3441E-02	.1736E-03
²⁴⁰ Pu	.1002E-04	.8947E-05	.6584E-05	.3072E-03	.3136E-05
²⁴¹ Pu	.2633E-06	.1839E-06	.1349E-06	.1961E-04	.8700E-07
²⁴² Pu	.0000E+00	.0000E+00	.0000E+00	.1570E-05	.0000E+00
FP**	.5552E-03	.5296E-03	.5788E-03	.5099E-03	.4861E-03
O	.3793E-01	.3793E-01	.3793E-01	.3781E-01	.3793E-01
Na	-	-	-	-	-
Fe	-	-	-	-	-
Cr	-	-	-	-	-
Ni	-	-	-	-	-
Mo	-	-	-	-	-
¹⁰ B	-	-	-	-	-
¹¹ B	-	-	-	-	-
C	-	-	-	-	-
Isotope	6	7	8	9	10
²³⁵ U	.5696E-04	.5696E-04	.5765E-04	.5856E-04	.5856E-04
²³⁶ U	.1373E-05	.1373E-05	.1144E-05	.9151E-06	.9151E-06
²³⁸ U	.2036E-01	.2036E-01	.2039E-01	.2043E-01	.2043E-01
²³⁹ Pu	.1757E-03	.1757E-03	.1480E-03	.1169E-03	.1169E-03
²⁴⁰ Pu	.3431E-05	.3431E-05	.2288E-05	.1601E-05	.1601E-05
²⁴¹ Pu	.6863E-07	.6863E-07	.4575E-07	.4575E-07	.4575E-07
²⁴² Pu	.0000E+00	.0000E+00	.0000E+00	.0000E+00	.0000E+00
FP	.1876E-04	.1876E-04	.1510E-04	.1052E-04	.1052E-04
O	.4125E-01	.4125E-01	.4125E-01	.4125E-01	.4125E-01
Na	-	-	-	-	-
Fe	-	-	-	-	-
Cr	-	-	-	-	-
Ni	-	-	-	-	-
Mo	-	-	-	-	-
¹⁰ B	-	-	-	-	-
¹¹ B	-	-	-	-	-
C	-	-	-	-	-

TABLE 3.55. ISOTOPIC DENSITY FOR HETEROGENEOUS COMPOSITIONS
 (Unit: 10^{24} nuclei / cm³)

Isotope	Heterogeneous composition No.				
	11	12	13	14	15
²³⁵ U	.5353E-04	.5399E-04	.5490E-04	.5582E-04	.5673E-04
²³⁶ U	.2059E-05	.1830E-05	.1601E-05	.1373E-05	.1373E-05
²³⁸ U	.2019E-01	.2021E-01	.2025E-01	.2030E-01	.2035E-01
²³⁹ Pu	.3059E-03	.2892E-03	.2532E-03	.2189E-03	.1773E-03
²⁴⁰ Pu	.8693E-05	.7549E-05	.5719E-05	.4118E-05	.3203E-05
²⁴¹ Pu	.2059E-06	.1601E-06	.1144E-06	.9151E-07	.1373E-06
²⁴² Pu	.0000E+00	.0000E+00	.0000E+00	.0000E+00	.0000E+00
FP**	.5902E-04	.5490E-04	.4827E-04	.4049E-04	.2882E-04
O	.4125E-01	.4125E-01	.4125E-01	.4125E-01	.4125E-01
Na	-	-	-	-	-
Fe	-	-	-	-	-
Cr	-	-	-	-	-
Ni	-	-	-	-	-
Mo	-	-	-	-	-
¹⁰ B	-	-	-	-	-
¹¹ B	-	-	-	-	-
C	-	-	-	-	-
Isotope	16	17	18	19	20
²³⁵ U	.5582E-04	.5628E-04	.5650E-04	.5696E-04	.5742E-04
²³⁶ U	.1373E-05	.1373E-05	.1144E-05	.1144E-05	.1144E-05
²³⁸ U	.2029E-01	.2031E-01	.2033E-01	.2034E-01	.2038E-01
²³⁹ Pu	.2265E-03	.2137E-03	.1960E-03	.1819E-03	.1533E-03
²⁴⁰ Pu	.4346E-05	.3660E-05	.2974E-05	.2745E-05	.2288E-05
²⁴¹ Pu	.6863E-07	.4575E-07	.4575E-07	.4575E-07	.9151E-07
²⁴² Pu	.0000E+00	.0000E+00	.0000E+00	.0000E+00	.0000E+00
FP	.3912E-04	.3683E-04	.3523E-04	.3248E-04	.2425E-04
O	.4125E-01	.4125E-01	.4125E-01	.4125E-01	.4125E-01
Na	-	-	-	-	-
Fe	-	-	-	-	-
Cr	-	-	-	-	-
Ni	-	-	-	-	-
Mo	-	-	-	-	-
¹⁰ B	-	-	-	-	-
¹¹ B	-	-	-	-	-
C	-	-	-	-	-

TABLE 3.55. ISOTOPIC DENSITY FOR HETEROGENEOUS COMPOSITIONS

(Unit: 10^{24} nuclei / cm³)

Isotope	Heterogeneous composition No.				
	21	22	23	24	25
²³⁵ U	.5856E-04	.5856E-04	.5879E-04	.5902E-04	.5902E-04
²³⁶ U	.9151E-06	.9151E-06	.6863E-06	.6863E-06	.6863E-06
²³⁸ U	.2043E-01	.2043E-01	.2044E-01	.2044E-01	.2046E-01
²³⁹ Pu	.1201E-03	.1201E-03	.1114E-03	.1059E-03	.9448E-04
²⁴⁰ Pu	.1373E-05	.1373E-05	.1144E-05	.1144E-05	.1144E-05
²⁴¹ Pu	.0000E+00	.0000E+00	.0000E+00	.0000E+00	.4575E-07
²⁴² Pu	.0000E+00	.0000E+00	.0000E+00	.0000E+00	.0000E+00
FP**	.1121E-04	.1121E-04	.1029E-04	.9608E-05	.7778E-05
O	.4125E-01	.4125E-01	.4125E-01	.4125E-01	.4125E-01
Na	-	-	-	-	-
Fe	-	-	-	-	-
Cr	-	-	-	-	-
Ni	-	-	-	-	-
Mo	-	-	-	-	-
¹⁰ B	-	-	-	-	-
¹¹ B	-	-	-	-	-
C	-	-	-	-	-
Isotope	26	27	28	29	30
²³⁵ U	-	-	-	-	-
²³⁶ U	-	-	-	-	-
²³⁸ U	-	-	-	-	-
²³⁹ Pu	-	-	-	-	-
²⁴⁰ Pu	-	-	-	-	-
²⁴¹ Pu	-	-	-	-	-
²⁴² Pu	-	-	-	-	-
FP	-	-	-	-	-
O	-	-	-	-	-
Na	-	-	.2074E-01	-	-
Fe	.7064E-01	.6097E-01	-	.5377E-01	.5477E-01
Cr	.1096E-01	.1643E-01	-	.1347E-01	.1444E-01
Ni	.1580E-03	.1322E-01	-	.7619E-02	.1255E-01
Mo	.9238E-03	.1201E-02	-	.1648E-02	.1844E-02
¹⁰ B	-	-	-	-	-
¹¹ B	-	-	-	-	-
C	-	-	-	-	-

TABLE 3.55. ISOTOPIC DENSITY FOR HETEROGENEOUS COMPOSITIONS
(Unit: 10^{24} nuclei / cm³)

Isotope	Heterogeneous composition No.	
	31	32
²³⁵ U	-	-
²³⁶ U	-	-
²³⁸ U	-	-
²³⁹ Pu	-	-
²⁴⁰ Pu	-	-
²⁴¹ Pu	-	-
²⁴² Pu	-	-
FP**	-	-
O	-	-
Na	-	.2214E-01
Fe	-	-
Cr	-	-
Ni	-	-
Mo	-	-
¹⁰ B	.1481E-01	-
¹¹ B	.5924E-01	-
C	.1852E-01	-

* read as .2674E-02 = $.2674 \times 10^{-2}$.

** For all compositions, ²³⁵U fission products will be used.

The control rod worth for the whole bank of rods was calculated only for the homogeneous model, one with the SHR rods fully ‘withdrawn’ and the other with the rods fully ‘inserted’. Core power calculations assumed a local energy deposition model using an energy 200 MeV per fission for fissionable isotopes and 0 MeV per capture for all nuclides.

The reactivity parameters at BOC and EOC obtained by the homogeneous core model are given in Tables 3.56–3.64. Most burnup effects on the reactivity parameters show good agreement for diffusion and transport theory results.

Results for the reactivity loss with burnup in an equilibrium fuel cycle are given in Table 3.56 together with the k_{eff} values at BOC and EOC in an equilibrium cycle. Basically the k_{eff} values at BOC are the results obtained in the Phase 2 study. The burnup effects defined by a k_{eff} difference during an equilibrium fuel cycle were predicted to be -2502 pcm and -2528 pcm with relative standard deviations of 4.4% and 5.7% for the diffusion and transport theory calculations, respectively. Both results show good agreement between the diffusion and transport theory predictions.

Table 3.57 shows the burnup reactivity loss for an equilibrium cycle, which was evaluated by using the k_{eff} values given in Table 3.56. This table also shows the values obtained from the heterogeneous calculations. The heterogeneous results will be discussed later. The burnup reactivity loss during an equilibrium fuel cycle was evaluated to be 0.0256 and 0.0251 with relative standard deviations of 5.5% and 4.0% for diffusion and transport theory calculations, which are equivalent to 4.4\$ and 4.3\$ respectively with $\beta_{\text{eff}} = 588$ pcm for the BN-600 hybrid benchmark core. Both predictions show good agreement for the burnup reactivity loss.

Tables 3.58 shows that the fuel Doppler coefficient is more negative by 6.3% and 7.7% at EOC with relative standard deviations of 49.5% and 30.0% for diffusion and transport theory calculations, respectively. This is counterintuitive since the ^{238}U content in the core is reduced at EOC. It is conjectured that this change is caused either the absorption of low-energy neutrons by the control rods with mid-core insertion at BOC (instead fully withdrawn at EOC) or by the power shift toward LEZ. The burnup effect estimated by KAERI is the smallest and has the largest discrepancy between the results. The rod motion effect and the burnup effect on the fuel Doppler coefficients appeared to be negligibly small in the ANL study [39]. It has also been reported in the ANL study that the differences between the reactivity difference method using the Hex-Z nodal diffusion methods and the trigonal-z diffusion theory perturbation method are small for the fuel Doppler coefficient.

The burnup effect on the steel Doppler coefficient was estimated to be -28.0% and -1.9% for diffusion and transport theory calculations, respectively in Table 3.59. Even with a few results and a large standard deviation for the diffusion theory results, it can be inferred that burnup does not affect the steel Doppler effect during an equilibrium fuel cycle.

In Table 3.60 the burnup effects on the sodium density coefficient show a conflicting aspect between the diffusion and transport theory results, i.e. -3.7% and 5.2% respectively. The sodium density coefficients for the whole core system were predicted with a large standard deviation by the participants. The ANL results were obtained only for the core (LEZ, MEZ, MOX and HEZ) and the upper axial blanket (UB) instead for the whole core system. The sodium density coefficient becomes more positive (corresponding to more negative in sodium void worth) at EOC by 55% at maximum in the CEA/SA result. However, in details, the sodium density coefficient is observed to be less positive in most results. This is attributed to the build up of fission products leading to a harder spectrum in the core, and is partly exacerbated by the power shift into the low leakage LEZ. This power redistribution with burnup is clearly supported by the ANL results [39].

TABLE 3.56. EFFECTIVE MULTIPLICATION FACTORS (k_{eff})

Participant	BOC		EOC		Burnup Effect* (pcm)	
	Diffusion	Transport	Diffusion	Transport	Diffusion	Transport
ANL	0.9959	0.9980	0.9716		-2430	
CEA/SA	1.0154	1.0227	0.9891	0.9964	-2632	-2630
CIAE	1.0002		0.9742		-2606	
IGCAR	1.0013		0.9767		-2465	
IPPE	1.0047					
JNC	1.0071	1.0096	0.9832	0.9854	-2390	-2426
KAERI	1.0146		0.9905		-2416	
OKBM	0.9948		0.9681		-2670	
Mean	1.0043	1.0101	0.9790	0.9909	-2516	-2528
SD +/-	0.0072	0.0100	0.0080	0.0055	116	144

* Burnup Effect = (EOC - BOC) $\times 10^5$ (pcm)

TABLE 3.57. BURNUP REACTIVITY LOSS

Participant	Homogeneous		Heterogeneous		Heterogeneity Effect** (pcm)	
	Diffusion	Transport	Diffusion	Transport	Diffusion	Transport
ANL	0.02511					
CEA/SA	0.02621	0.02581	0.02624	0.02583	3.2	2.0
CIAE	0.02674		0.02666		-7.7	
IGCAR	0.02520					
IPPE						
JNC	0.02414	0.02438				
KAERI	0.02404					
OKBM	0.02773					
Mean	0.02559	0.02510	0.02645	0.02583	-2.2	2.0
SD +/-	0.00137	0.00101				

* Burnup reactivity loss = $(k_{\text{eff}}^{\text{BOC}} - k_{\text{eff}}^{\text{EOC}}) / k_{\text{eff}}^{\text{BOC}} / k_{\text{eff}}^{\text{EOC}}$ (dk/k.k')

* Heterogeneity Effect = (Hete. - Homo.) x 105 (pcm)

TABLE 3.58. FUEL DOPPLER COEFFICIENTS (K_D^{fuel})

Participant	BOC		EOC		Burnup Effect* (%)	
	Diffusion	Transport	Diffusion	Transport	Diffusion	Transport
ANL**	-0.00665		-0.00689			
CEA/SA	-0.00683	-0.00682	-0.00732	-0.00724	7.11	6.15
CIAE	-0.00610					
IGCAR	-0.00684		-0.00731		6.87	
IPPE	-0.00635					
JNC	-0.00646	-0.00633	-0.00703	-0.00692	8.82	9.32
KAERI	-0.00770	-0.00764	-0.00777		0.98	
OKBM	-0.00632		-0.00682		7.90	
Mean	-0.00666	-0.00693	-0.00725	-0.00708	6.34	7.73
SD +/-	0.00046	0.00054	0.00036	0.00016	3.09	2.24

* Burnup Effect = [(EOC - BOC) / BOC] x 100 (%)

** EOC value for (core + UB); omitted from mean and standard deviation calculations

TABLE 3.59. STEEL DOPPLER COEFFICIENTS (K_D^{steel})

Participant	BOC		EOC		Burnup Effect (%)	
	Diffusion	Transport	Diffusion	Transport	Diffusion	Transport
ANL	-0.00106					
CEA/SA	-0.00128	-0.00132	-0.00129	-0.00129	1.25	-1.90
CIAE	-0.00067		-0.00029		-57.17	
IGCAR						
IPPE	-0.00080					
JNC	-0.00109	-0.00109				
KAERI	-0.00108	-0.00106				
OKBM	-0.00106					
Mean	-0.00100	-0.00116	-0.00079	-0.00129	-27.96	-1.90
SD +/-	0.00019	0.00011	0.00050		41.32	

TABLE 3.60. SODIUM DENSITY COEFFICIENTS (W_{Na})

Participant	BOC		EOC		Burnup Effect (%)	
	Diffusion	Transport	Diffusion	Transport	Diffusion	Transport
ANL*	0.00080	-0.00087	-0.00195		-343.74	
CEA/SA	0.00610	0.00592	0.00943	0.00762	54.53	28.78
CIAE	0.00487		0.00386		-20.74	
IGCAR	0.01090		0.00920		-15.60	
IPPE	0.00877					
JNC	0.01038	0.00664	0.00937	0.00542	-9.73	-18.37
KAERI	0.01050		0.00831		-20.80	
OKBM	0.01226		0.01105		-9.87	
Mean	0.00911	0.00628	0.00854	0.00652	-3.70	5.20
SD +/-	0.00254	0.00036	0.00483	0.00110	28.95	33.34

* Values for (core + UB), Monte Carlo result for transport (omitted from mean and standard deviation calculations).

TABLE 3.61. STEEL DENSITY COEFFICIENTS (W_{steel})

Participant	BOC		EOC		Burnup Effect (%)	
	Diffusion	Transport	Diffusion	Transport	Diffusion	Transport
ANL	-0.0037					
CEA/SA	-0.0039	-0.0073	-0.0041	-0.0088	5.89	19.96
CIAE	-0.0037		-0.0060		64.28	
IGCAR	0.0007		-0.0087		-1342.86	
IPPE	0.0019					
JNC	-0.0020	-0.0066				
KAERI	-0.0395					
OKBM	-0.0019					
Mean	-0.0065	-0.0069	-0.0063	-0.0088	-424.23	19.96
SD +/-	0.0126	0.0004	0.0019		796.09	

The different results between the diffusion and transport theory predictions arise due to the compensation of large leakage and non-leakage components of opposite sign. Therefore, the conflicting results cause a large standard deviation in determining the sodium density coefficient. This fact is partly supported by the results from the comparison of the reactivity difference method using nodal diffusion theory methods and the Monte Carlo method performed by ANL. The results imply that the reactivity difference method employing the subtraction of deterministic eigenvalues obtained from nodal diffusion theory methods has very high standard deviations to finally obtain the sodium density coefficient in the low coolant removal cases [32]. In a check on calculational methodology, the sodium density coefficient differences between the reactivity difference method using Hex-Z nodal diffusion methods and the trigonal-Z diffusion theory perturbation method appeared to be small in the ANL study.

In the Phase 3 study, a limited number of results of density coefficients (material worths) for steel and fuel at EOC were provided by the participants. No results for absorber were provided by the participants. Hence the burnup effect on these density coefficients should be evaluated based on the limited number of results available. In Table 3.61 the steel density coefficient is more negative at EOC, but the burnup effects have a large standard deviation between the results. The fuel density coefficient apparently has no difference in its value between BOC and EOC during an equilibrium fuel cycle in Table 3.62.

In the Phase 2 definition, the total 19 SHR rods are positioned at the core-midplane bank location. The control rod worths for the whole bank of rods at BOC and EOC were calculated for the homogeneous model, one with the SHR rods fully ‘withdrawn’ and the other with the rods fully ‘inserted’. From the Phase 3 benchmark definition, the fully ‘withdrawn’ configuration is defined as the axial position of the bottom of the B4C absorber is 5.5 cm above the top of the core, and the fully ‘inserted’ configuration is defined as the axial position of the B4C absorber is at the bottom of the core.

For the burnup effect on control rod worth, only one data set was provided by IGCAR for the diffusion theory calculations. The control rod worth for the whole bank of rods at BOC was evaluated to be 0.0661 and 0.0652 with relative standard deviations of 4.4% and 0.2% for the diffusion and transport theory calculations, respectively. The control rod worth at EOC was estimated to be 0.0716 for the diffusion theory calculations. It is observed in Table 3.63 that the control rod worth is more positive (more effective in neutron absorption) at EOC by 4.9% for the diffusion theory calculations. In comparison of the diffusion and transport theory results at BOC, the transport theory method predicts the control rod worth less by 1.4% in its magnitude (less effective in neutron absorption) than the diffusion theory method.

ANL and CIAE additionally provided the Monte Carlo results. The CIAE’s Monte Carlo results show the same aspect observed from the diffusion theory results, that is, the control rod worth is more positive at EOC. In addition, the comparison of the CIAE results at BOC shows that the Monte Carlo method predicts the control rod worth less by 3.6% in its magnitude than the diffusion theory method.

TABLE 3.62. FUEL DENSITY COEFFICIENTS (W_{fuel})

Participant	BOC		EOC		Burnup Effect (%)	
	Diffusion	Transport	Diffusion	Transport	Diffusion	Transport
ANL	0.3339					
CEA/SA	0.3444	0.3385				
CIAE	0.3591		0.3568		-0.63	
IGCAR	0.3691					
IPPE	0.3477					
JNC	0.3466	0.3457				
KAERI	0.3490					
OKBM	0.3561					
Mean	0.3507	0.3421	0.3568		-0.63	
SD +/-	0.0099	0.0036				

TABLE 3.63. CONTROL ROD WORTH

Participant	BOC		EOC		Burnup Effect (%)	
	Diffusion	Transport	Diffusion	Transport	Diffusion	Transport
ANL*	0.0653	0.0628		0.0598		-4.78
CEA/SA	0.0697	0.0652				
CIAE	0.0662	0.0638		0.0672*		5.33
IGCAR	0.0682		0.0716		4.91	
IPPE						
JNC	0.0603	0.0653				
KAERI						
OKBM	0.0667					
Mean	0.0661	0.0652	0.0716		4.91	
SD +/-	0.0029	0.0001				

* Monte Carlo result for transport (omitted from mean and standard deviation calculations).

Power fractions for each region in the core at BOC and EOC are compared in Table 3.64. These regionwise power fractions were obtained by averaging the power distribution data provided by the participants for the Phase 2 and 3 studies. For the Phase 3 study, power distributions at BOC were given by all participants, CEA/SA, however, in addition provided distributions at EOC. It is noted that the control rods stay at the mid-plane bank position ('mid-core insertion') in the depletion calculations and are non-depleted. In Table 3.64 the reduction of power fraction in the core region (LEZ, MEZ, MOX and HEZ) and the increase in the axial blanket region (LB and UB) reflect the burnup of fissile material in the core region and the build-up of fissile material in the axial blanket region, respectively. In more details, the power fraction for HEZ increases with burnup even with the decrease of total power fraction in the core region. These results indicate the power shift to outer core region HEZ and the axial blanket regions LB and UB. The resultant sodium density coefficient of being less positive at EOC is attributed to the power behavior with burnup.

The power behaviour with burnup has been investigated based on the CEA/SA results only. However, a different power behaviour showing a power shift to low leakage LEZ in the core region has been provided by the participant, even the obtained result supports the resultant sodium density coefficient. Considering the importance of knowledge of power behaviours with burnup, a more detailed investigation with more results provided by the participants will be needed to examine the sodium density coefficient.

TABLE 3.64. POWER FRACTIONS FOR FUEL REGIONS AT BOC AND EOC

Region	Fraction (%)		
	BOC	EOC	Change
LEZ	42.64	42.46	-0.18
MEZ	16.15	15.77	-0.38
MOX	21.60	21.05	-0.45
HEZ	17.23	17.61	+0.38
<u>Core</u>	<u>97.63</u>	<u>96.89</u>	<u>-0.74</u>
LB	1.53	2.08	+0.55
UB	0.84	1.03	+0.19
Total	100.00	100.00	0.00

3.3.2.2. Heterogeneity effect

The k_{eff} and the same reactivity parameters investigated for the burnup effect were calculated with the heterogeneous treatment of the core fuel regions (LEZ, MEZ, HEZ, and MOX, core and axial blanket) and the SHR control rods in the heterogeneous core model. Several insignificant simplifications of real geometry description have been assumed in the heterogeneous geometry descriptions. Fuel subassemblies for LEZ, MEZ, MOX, HEZ have the identical geometry, where 127 fuel pins are located with triangular pitch of 7.95 mm inside hexagonal wrapper. A separate geometry description was defined for the SHR absorber region.

To consider the heterogeneous geometry of fuel subassemblies, cell calculations were performed by applying various approximation methods such as the Bell method, an interface current method, and the Tone's background cross-section method to the heterogeneous cell model for fuel subassembly [40-43]. To specifically evaluate the heterogeneity effect of control rods, the heterogeneous geometry of the SHR control rods has been treated by employing various specific heterogeneous modeling

methods with specific procedures for reaction rate preservation. The heterogeneous treatments of the control rods include a specific set of procedures for enabling homogeneous equivalent cross sections prepared using the reactivity equivalence technique, two-dimensional transport solutions by first collision probability method, the one-dimensional Bell modification method to the rational approximation and one-dimensional super-cell model with the reaction rate distribution preservation method. The control rod worth for the whole bank of rods was calculated for the heterogeneous core model in the same manner performed for the homogeneous core model.

The reactivity parameters calculated by the homogeneous and heterogeneous core models with the SHR rods mid-core insertion at BOC are given in Tables 3.65–3.72.

In Table 3.65 the heterogeneity effect on k_{eff} at BOC was evaluated to be the increase of 92 pcm and 40 pcm for the diffusion and transport theory calculations, respectively. The heterogeneity effect itself was predicted to be negligibly small, but estimated with large standard deviations. Most results indicate that the heterogeneity treatment results in an increase of reactivity except for the CEA/SA data. The obtained results appeared to differ depending on the heterogeneity treatment method and, as a result, it leads to a large standard deviation in the heterogeneity prediction.

Table 3.65 shows that with the heterogeneous core model the fuel Doppler coefficient is more negative by 6.1% and 5.9% for the diffusion and transport theory calculations with a relative standard deviation of 31.4% for the diffusion theory result. The heterogeneity effect evaluated by the transport theory method appeared to be larger by 4.0% and 5.1% in its magnitude than that by the diffusion theory method.

In Table 3.66 the heterogeneity effect on the steel Doppler coefficient appeared to be negligibly small (based on the transport results). The heterogeneous core model increases the steel Doppler coefficient by 69.0% and 12.9% in its magnitude for the diffusion and transport theory calculations. However, the diffusion theory predictions show a large standard deviation in heterogeneous core model calculations. The heterogeneity effect evaluated by IGCAR appeared to be notably large.

The sodium density coefficient appeared to be more positive for the heterogeneous core model. In Table 3.67 the heterogeneity effect was estimated to be 12.9% and 53.5% for the diffusion and transport theory calculations, but with substantially large standard deviations for both calculations. There exist a large standard deviation and even an opposite aspect as well in the heterogeneity predictions based on the diffusion results. The large standard deviation in the predictions is conjectured to come from the summation over its very small spatial contributions from non-fuelled regions in determining the sodium density coefficient for the heterogeneous core model.

Even with the limited number of results and a large standard deviation between the results in Table 3.69, it can be presumed that the steel density coefficient is more negative for the heterogeneous core model. The large standard deviation in evaluating the steel density coefficient is also attributable to the summation over its very small spatial contributions from the whole core system as indicated in previous phase studies.

As can be seen in Table 3.70, the heterogeneity effect on the fuel density coefficient is negligibly small. Both diffusion and transport theory show good agreement in predicting the fuel density coefficients even with the heterogeneous treatment of fuel subassemblies.

In Table 3.71 the absorber density coefficient is less negative by 3.5% and 2.6% for the diffusion and transport theory calculations respectively for the heterogeneous core model. The results indicate that the absorber density coefficient (absorber worth) is smaller in its magnitude for the heterogeneous core model.

It can be summarized that the heterogeneity effect on the fuel and absorber density coefficients appeared to be negligibly small. It can be conjectured that the sodium density coefficient is more positive and that the steel density coefficient is more negative for the heterogeneous core model even with large standard deviations in the predicted values.

TABLE 3.65. EFFECTIVE MULTIPLICATION FACTORS (k_{eff})

Participant	Homogeneous		Heterogeneous		Heterogeneity Effect (pcm)	
	Diffusion	Transport	Diffusion	Transport	Diffusion	Transport
ANL	0.99592	0.99802				
CEA/SA	1.01546	1.02272	1.01474	1.02211	-72	-61
CIAE	1.00026		1.00214		188	
IGCAR	1.00136		1.00188		52	
IPPE	1.00471					
JNC	1.00713	1.00967	1.00913	1.01109	200	142
KAERI	1.01467					
OKBM	0.99486					
Mean	1.00430	1.01014	1.00697	1.01660	92	40
SD +/-	0.00729	0.01009	0.00534	0.00551	111	102

* Heterogeneity Effect = (Hete. - Homo.) (pcm)

TABLE 3.66. FUEL DOPPLER COEFFICIENTS (K_D^{fuel})

Participant	Homogeneous		Heterogeneous		Heterogeneity Effect (%)	
	Diffusion	Transport	Diffusion	Transport	Diffusion	Transport
ANL	-0.00665					
CEA/SA	-0.00683	-0.00682	-0.00734	-0.00722	7.48	5.93
CIAE	-0.00610		-0.00640		4.77	
IGCAR	-0.00684					
IPPE	-0.00635					
JNC	-0.00646	-0.00633				
KAERI	-0.00770	-0.00764				
OKBM	-0.00632					
Mean	-0.00666	-0.00693	-0.00687	-0.00722	6.12	5.93
SD +/-	0.00046	0.00054	0.00047		1.92	

* Heterogeneity Effect = (Hete. - Homo.) x 105 (pcm)

TABLE 3.67. STEEL DOPPLER COEFFICIENTS (K_D^{steel})

Participant	Homogeneous		Heterogeneous		Heterogeneity Effect (%)	
	Diffusion	Transport	Diffusion	Transport	Diffusion	Transport
ANL	-0.00106					
CEA/SA	-0.00128	-0.00132	-0.00128	-0.00131	0.55	-1.06
CIAE	-0.00067		-0.00211		214.25	
IGCAR						
IPPE	-0.00080					
JNC	-0.00109	-0.00109				
KAERI	-0.00108	-0.00106				
OKBM	-0.00106					
Mean	-0.00100	-0.00116	-0.00169	-0.00131	107.40	-1.06
SD +/-	0.00019	0.00011	0.00041		151.11	

TABLE 3.68. SODIUM DENSITY COEFFICIENTS (W_{Na})

Participant	Homogeneous		Heterogeneous		Heterogeneity Effect (%)	
	Diffusion	Transport	Diffusion	Transport	Diffusion	Transport
ANL*	0.00080		0.00080		0.12	
CEA/SA	0.00610	0.00592	0.01062	0.00984	73.99	66.29
CIAE	0.00486		0.00529		8.88	
IGCAR	0.01090		0.00838		-23.12	
IPPE	0.00877					
JNC	0.01038	0.00664	0.01280	0.00934	23.31	40.66
KAERI	0.01050		0.00858		-18.30	
OKBM	0.01226					
Mean	0.00911	0.00628	0.00913	0.00959	12.95	53.48
SD +/-	0.00254	0.00036	0.00449	0.00025	39.14	18.12

* Values for (core + UB); omitted from mean and standard deviation calculations.

TABLE 3.69. STEEL DENSITY COEFFICIENTS (W_{steel})

Participant	Homogeneous		Heterogeneous		Heterogeneity Effect (%)	
	Diffusion	Transport	Diffusion	Transport	Diffusion	Transport
ANL	-0.0037					
CEA/SA	-0.0039	-0.0073	0.0027	-0.0015	-169.35	-80.16
CIAE	-0.0037				-0.086	
IGCAR	0.0007					
IPPE	0.0019					
JNC	-0.0020	-0.0066				
KAERI	-0.0395					
OKBM	-0.0019					
Mean	-0.0065	-0.0069	0.0027	-0.0015	-169.35	-80.16
SD +/-	0.0126	0.0004				

TABLE 3.70. FUEL DENSITY COEFFICIENTS (W_{fuel})

Participant	Homogeneous		Heterogeneous		Heterogeneity Effect (%)	
	Diffusion	Transport	Diffusion	Transport	Diffusion	Transport
ANL	0.3339					
CEA/SA	0.3444	0.3385	0.3431	0.3369	-0.40	-0.46
CIAE	0.3591		0.3560			
IGCAR	0.3691					
IPPE	0.3477					
JNC	0.3466	0.3457				
KAERI	0.3490					
OKBM	0.3561					
Mean	0.3507	0.3421	0.3495	0.3369	-0.63	-0.46
SD +/-	0.0099	0.0036	0.0065		0.33	

Table 3.72 shows that the control rod worth becomes less positive by 2.3% (2.3% decrease in the control rod worth) and 3.3% for the diffusion and transport theory calculations, respectively. The control rod worth was predicted to be 0.0646 and 0.0631 with relative standard deviations of 6.2% and 1.6% for the diffusion and transport theory calculations for the heterogeneous core model. Both diffusion and transport results clearly show that the heterogeneous treatment of the control rods reduces the control rod worth. From the comparison of the participants' results obtained with the heterogeneous treatment, it has been observed that the prediction of heterogeneity effect strongly depends on the heterogeneous modeling and the heterogeneity treatment methodology.

Power fractions for fuel regions at BOC calculated with the homogeneous and heterogeneous core model are given in Table 3.73. The power fractions were obtained with the CEA/SA and CIAE results. Apparently the heterogeneity effect in the power distribution is negligibly small. There can be seen a small change in each fuel region. However, the total power in the fuel regions is increased by 0.03% for the heterogeneous core model and the increased power is compensated and makes even by the reduction in the axial blanket regions.

TABLE 3.71. ABSORBER DENSITY COEFFICIENTS (W_{abs})

Participant	Homogeneous		Heterogeneous		Heterogeneity Effect (%)	
	Diffusion	Transport	Diffusion	Transport	Diffusion	Transport
ANL	-0.0241					
CEA/SA	-0.0275	-0.0234	-0.0265	-0.0228	-3.54	-2.60
CIAE	-0.0243					
IGCAR	-0.0234					
IPPE	-0.0217					
JNC	-0.0200	-0.0219				
KAERI	-0.0267					
OKBM	-0.0245					
Mean	-0.0240	-0.0226	-0.0265	-0.0228	-3.54	-2.60
SD +/-	0.0023	0.0007				

TABLE 3.72. CONTROL ROD WORTHS (W_{CR})

Participant	Homogeneous		Heterogeneous		Heterogeneity Effect (%)	
	Diffusion	Transport	Diffusion	Transport	Diffusion	Transport
ANL*	0.0653	0.0628		0.0598		-4.78
CEA/SA	0.0697	0.0652	0.0683	0.0641	-1.94	-1.69
CIAE*	0.0662	0.0638*	0.0664	0.0603*	0.33	-5.49
IGCAR	0.0682		0.0656		-3.77	
IPPE						
JNC	0.0603	0.0653	0.0579	0.0621	-3.98	-4.90
KAERI						
OKBM	0.0667					
Mean	0.0661	0.0652	0.0646	0.0631	-2.34	-3.30
SD +/-	0.0029	0.0001	0.0040	0.0010	2.00	2.27

* Monte Carlo result for transport (omitted from mean and standard deviation calculations).

TABLE 3.73. POWER FRACTIONS FOR FUEL REGIONS AT BOC

Region	Fraction (%)		
	Homogeneous	Heterogeneous	Difference
LEZ	42.64	42.57	-0.07
MEZ	16.15	16.31	+0.16
MOX	21.60	21.25	-0.35
HEZ	17.23	17.52	+0.29
<i>Core</i>	97.63	97.66	+0.03
LB	1.53	1.53	0.00
UB	0.84	0.81	-0.03
Total	100.00	100.00	0.00

3.3.3. Summary of Hex-Z heterogeneous and burnup benchmark (Phase 3)

Integral reactivity coefficients obtained by the participants for the Phase 3 benchmark are summarized in Tables 3.74 and 3.75. The reactivity parameters at BOC and EOC obtained with the homogeneous core model are compared in Table 3.74. The reactivity parameters calculated by the homogeneous and heterogeneous core models with the SHR rods mid-core insertion at BOC are summarized in Table 3.75. The burnup effect and the heterogeneity effect on most reactivity parameters show good agreement for diffusion and transport theory results. The heterogeneity effect on most reactivity parameters was evaluated to be small. The heterogeneity effect on k_{eff} and control rod worth appeared to be strongly dependent on the heterogeneity treatment method.

3.4. BFS-62-3A experimental data analysis benchmark (Phase 5)

3.4.1. Benchmark model

3.4.4.1. BFS-62-3A critical experiment

The BFS-62 critical experiments are currently used as benchmarks for the verification of IPPE codes and nuclear data, and in particular for the loading of a significant amount of plutonium in fast reactors [44, 45]. The BFS-62 experiments have been performed in the BFS-2 critical facility at IPPE, Obninsk. The BFS-2 critical facility was designed for the full size simulation of the core and shielding of large reactors with a unit power up to 3000 MW(e). A top side view of the BFS-2 facility is shown in Fig. 3.50. The experimental program has been arranged in such a way that the effect of replacement of uranium dioxide (UO_2) blanket by the steel reflector as well as the effect of replacing UOX by MOX on the main characteristics of the reactor model was studied. A series of four BFS-62 critical assemblies have been designed to study the changes in the reactor physics behavior of the BN-600 core from its existing state to that of a hybrid core containing MOX fuel.



FIG. 3.50. Top side view of the BFS-62 facility.

TABLE 3.74. BURNUP EFFECTS

Participant	k_{eff}			K_D fuel			K_D steel			W_{Na}		
	BOC	EOC	Burnup reactivity loss ¹⁾	BOC	EOC	Burnup effect (%) ²⁾	BOC	EOC	Burnup effect (%)	BOC	EOC	Burnup effect (%)
ANL	0.99592	0.97162	0.02511	-0.00665	-0.00689 ⁴⁾	3.37	-0.00106			[0.00080 ⁴⁾ (0.0087) ₅₎	[-0.00195]	
CEA/SA	1.01546 (1.02272) ³⁾	0.98914 (0.99642)	0.02621 (0.02581)	-0.00683 (-0.00682)	-0.00732 (-0.00724)	7.11 (6.15)	-0.00128 (-0.00132)	-0.00129 (-0.00129)	1.25 (-1.90)	0.00610 (0.00592)	0.00943 (0.00762)	54.53 (28.78)
CIAE	1.00026	0.97420	0.02674	-0.00610			-0.00067		-57.17	0.00486	0.00386	-20.58
IGCAR	1.00136 (1.00188)	0.97671	0.02520	-0.00684	-0.00731	6.87				0.01090	0.00920	-15.60
JNC	1.00713 (1.00967)	0.98323 (0.98542)	0.02414 (0.02438)	-0.00646 (-0.00633)	-0.00703 (-0.00692)	8.82 (9.32)	-0.00109 (-0.00109)			0.01038 (0.00664)	0.00937 (0.00542)	-9.73 (-18.37)
KAERI	1.01467	0.99051	0.02404	-0.00770 (-0.00764)	-0.00777 (-0.00764)	0.98 (-0.00106)	-0.00108 (-0.00106)			0.01050	0.00831	-20.80
OKBM	0.99486	0.96815	0.02773	-0.00632	-0.00682	7.90	-0.00106			0.01226	0.01105	-9.87
Mean	1.00430 (1.01014)	0.97989 (0.99091)	0.02540 (0.02510)	-0.00666 (-0.0693)	-0.00725 (-0.00708)	5.89 (7.73)	-0.00100 (-0.00116)	-0.00079 (-0.00129)	-27.96 (-1.90)	0.00911 (0.00628)	0.00854 (0.00652)	-3.70 (5.20)
SD (\pm)	(0.01099)	(0.00843)	(0.00139)	(0.00054)	(0.00046)	0.00036 (0.00016)	3.36 (2.24)	0.00019 (0.00011)	0.00050 (0.00)	41.32 (0.00)	0.00254 (0.00036)	0.00449 (0.00110)
Participant	W_{steel}			W_{fuel}			W_{abs}			Control rod worth		
	BOC	EOC	Burnup effect (%)	BOC	EOC	Burnup effect (%)	BOC	EOC	Burnup effect (%)	BOC	EOC	Burnup effect (%)
CEA/SA	-0.0039 (-0.0073)	-0.0041 (-0.0088)	5.89 (19.96)	0.3344 (0.3385)			-0.0275 (-0.0234)			0.0697 (0.0652)		
CIAE	-0.0037	-0.0060	64.28	0.3591	0.3568	-0.63				0.0662 (0.0638) ₅₎	0.0672 (0.0716)	(5.33)
IGCAR	0.0007	-0.0087	-1342.86	0.3691						0.0682		4.91
Mean	-0.0065 (-0.0069)	-0.0063 (-0.0088)	-424.23 (19.96)	0.3507 (0.3421)	0.3568	-0.63	-0.0240 (-0.0226)			0.0661 (0.0652)	0.0706 (0.0652)	4.91 (5.33)
SD (\pm)	0.0126 (0.0004)	0.0019 (0.00)	796.09 (0.00)	0.0096 (0.0036)			0.0023 (0.0007)			0.0029 (0.00)	0.0009 (0.00)	0.00 (0.00)

Notes: 1) Burnup reactivity loss = $(k_{\text{eff}}^{\text{BOC}} - k_{\text{eff}}^{\text{EOC}}) / k_{\text{eff}}^{\text{BOC}}$ based on diffusion results, and transport results denoted by parenthesis.

2) Burnup effect = $(\text{BOC} - \text{EOC}) / \text{BOC} \times 100$ (%) based on diffusion results, and transport results denoted by parenthesis.

3) Values in parentheses denote transport results.

4) Value only for the core and upper axial blanket regions.

5) Monte Carlo results.

TABLE 3.75. HETEROGENEITY EFFECTS

Participant	k_{eff}			K_D^{fuel}			K_D^{steel}			W_{Na}		
	Diffusion	Transport	Hete. effect (pcm) ¹⁾	Diffusion	Transport	Hete. effect (%) ²⁾	Diffusion	Transport	Hete. effect (%)	Diffusion	Transport	Hete. effect (%)
ANL	(0.99592) ³⁾	(0.99802)	(-0.00665)	-0.00722	7.48	(-0.00106)	-0.00131	0.55	[0.00080] ⁴⁾	0.00984	73.99	[0.12]
CEA/SA	1.01474 (1.01546)	1.02211 (1.02272)	-72 (-61)	-0.00734 (-0.00683)	(5.93)	(-0.00128)	(-0.00132)	(-1.06)	[0.00800]	0.01062	(66.29)	
CIAE	1.00214 (1.0026)		188	-0.00640 (-0.00610)	4.77	(-0.00211)	214.25	(0.00529)			8.65	
IGCAR	1.00188 (1.00136)		52	(-0.00684)		(-0.00067)		(0.00487)		0.00838		-23.12
JNC	1.00913 (1.00713)	1.01109 (1.00967)	200 (142)	(-0.00646)	(-0.00633)	(-0.00109)	(-0.00109)	(0.01090)	0.01280 (0.01038)	0.00934 (0.00664)	23.31 (40.66)	
KAERI		(1.01260)		(-0.00770)	(-0.00764)	(-0.00108)	(-0.00106)	(0.01050)	0.00858		-18.30	
Mean	1.00697	1.01660	92 (40)	-0.00687	-0.00722	6.12 (5.93)	-0.00169	-0.00131 (-1.06)	107.40	0.00913	0.00959 (53.48)	12.91
SD (\pm)	0.00534	0.00551	111 (102)	0.00047	0.00	1.92 (0.00)	0.00041	0.00 (0.00)	151.11 (0.00)	0.00449	0.00025 (18.12)	39.14 (18.12)
Participant	W_{steel}			W_{fuel}			W_{abs}			Control rod worth		
	Diffusion	Transport	Hete. effect (%)	Diffusion	Transport	Hete. effect (%)	Diffusion	Transport	Hete. effect (%)	Diffusion	Transport	Hete. effect (%)
ANL	(-0.0037)			(0.3339)			(-0.0241)			(0.0653)	0.0598 ⁵⁾	(-4.78)
CEA/SA	0.0027 (-0.0041)	-0.0015 (-0.0088)	-165.44 (-83.49)	0.3431 (0.3444)	0.3369 (0.3385)	-0.40 (-0.46)	-0.0265 (-0.0275)	-3.54 (-2.60)	0.0683 (0.0697)	0.0641 (0.0652)	(0.0628) ⁴⁾	-1.94 (-1.69)
CIAE	(-0.0037)			0.3560 (0.3591)		-0.85	(-0.0243)		0.0664	(0.0662)	0.0656 (0.0682)	0.33
IGCAR	(0.0007)								0.0579	0.0579	0.0621 (0.0653)	-3.77
JNC	(-0.0020)	(-0.0066)		(0.3466)	(0.3457)	(-0.0200)	(-0.0219)					-3.98 (4.90)
Mean	0.0027	-0.0015	-165.44 (-83.49)	0.3495	0.3369	-0.63 (-0.46)	-0.0265	0.10 (0.06)	0.0646	0.0631	-2.34 (-3.30)	
SD (\pm)	0.00	0.00	(0.00)	0.0065	0.00	0.32 (0.00)	0.00	0.00 (0.00)	0.0040	0.0010	2.00 (2.27)	

Notes: 1) Heterogeneity effect = (Hete. - Homo.) $\times 10^5$ (pcm) based on diffusion results, and transport results denoted by parenthesis.2) Heterogeneity effect = (Hete. - Homo.) / Homo. $\times 100$ (%) based on diffusion results, and transport results denoted by parenthesis.

3) Values in parentheses denote homogeneous results at BOC.

4) Values in brackets denote only for the core and upper axial blanket regions.

5) Monte Carlo results.

The first assembly in the series, BFS-62-1, is an analogue of the BN-600 reactor in operation. There are three fuelled regions in the core: Inner Core (IC), Middle Core (MC) and Outer Core (OC), consisting of UO_2 fuel with different enrichments. The core is surrounded by radial and axial blankets consisting of depleted uranium dioxide. The BFS-62-2 assembly differs from BFS-62-1 by the structure of the radial blanket. In the BFS-62-2 assembly, a 120° sector of the radial blanket outside the core has been replaced by stainless steel, with naturally enriched boron carbide being located behind this sector.

The third assembly, BFS-62-3A, is a full-scale model of the BN-600 reactor hybrid core. A MOX fuelled zone has been added like a ring between the MC and OC zones. The radial blanket is similar to that in the BFS-62-2 assembly. The layout of the BFS-62-3A assembly is shown in Fig. 3.51. The main characteristics of fuel zones in the BFS-62-3A core are shown in Table 3.76.

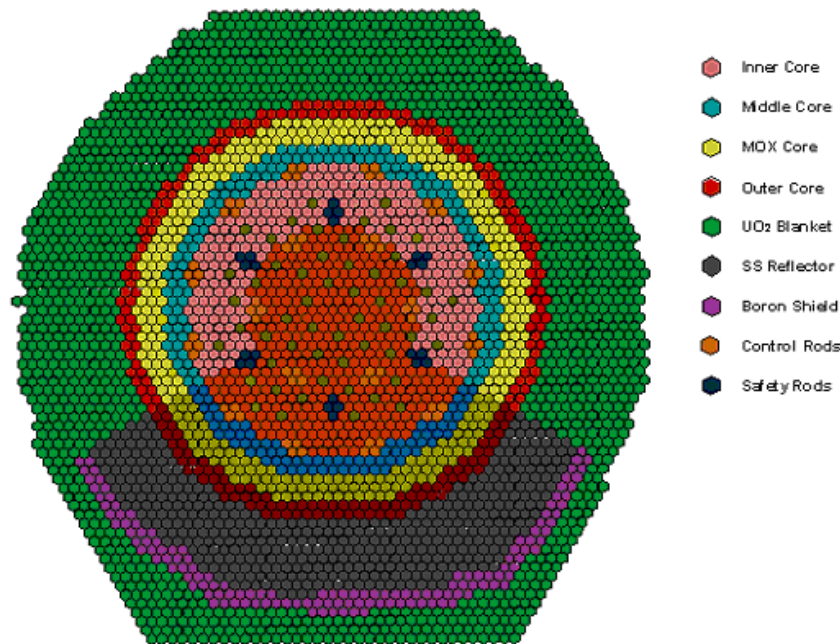


FIG. 3.51. Layout of the BFS-62-3A assembly.

TABLE 3.76. PARAMETERS OF BFS-62-3A ASSEMBLY

Parameter	Zone			
	IC*	MC	MOX	OC
Fuel	UO_2	UO_2	MOX	UO_2
Enrichment, at. %	15	18	17	21
Number of FAs (fuel tubes)	595 ^{*)}	222	336	237

* Besides, there are 54 tubes in the IC zone, which contain no fissile material.

All of the fuelled subassemblies in the BFS-62 core are made of a matrix of vertical steel tubes or rods as shown in Fig. 3.52. Each subassembly (tube) is located within a hexagonal mesh with a pitch of 5.1 cm. Each tube is composed of fuel and structural material pellets, 4.7 cm in diameter, which are combined into standard cells. The fuel cells have a ‘mirror symmetry’ relative to the core midplane. An axial structure of each type of fuel subassembly (FA) is shown in Fig. 3.53.

Six Control Rods (CRs) and six Safety Rods (SRs) are located in the low enrichment zone (IC). The remaining twelve control rods are located on the border between the IC and MC zones. Each control or safety rod consists of four BFS tubes.

During the sodium void reactivity effect (SVRE) measurements, sodium pellets were replaced with empty boxes, in the 60° sector of IC, MC, MOX and OC zones and the upper axial blanket. Sodium was not removed from the control rod mock-ups and from the standard control rods of the assembly. In total, 259 fuel rods (FAs) were reassembled during the SVRE measurements. In the SVRE measurements the regions were voided consecutively with the previously voided regions remaining voided, although SVRE experimental values are presented for each region as itself. The interaction effect between the voided regions has been shown to be negligible.

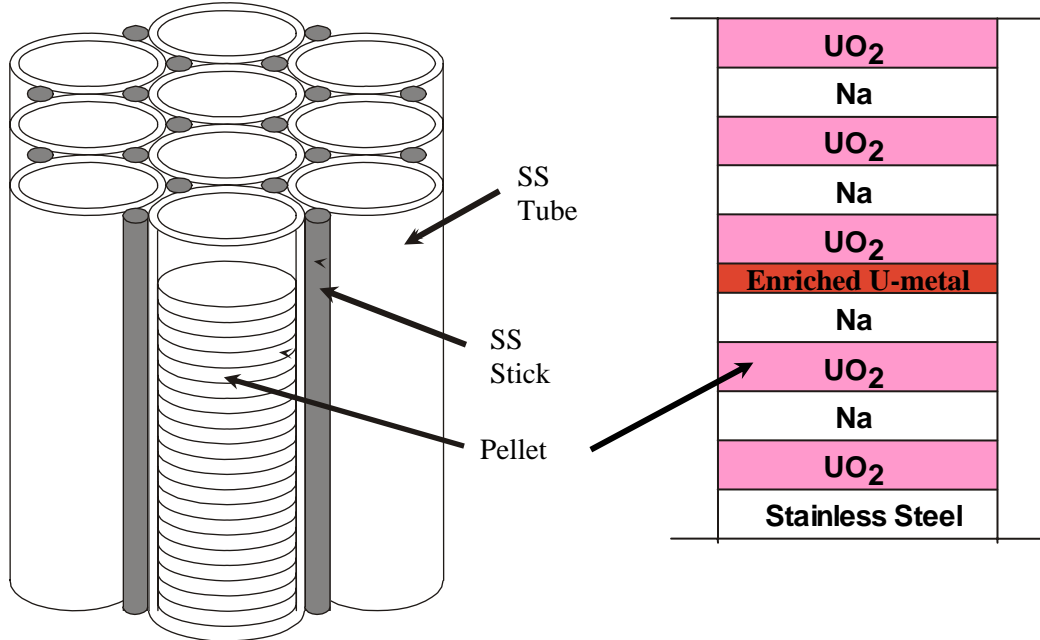


FIG. 3.52. Example structure of BFS subassembly.

3.4.4.2. Benchmark model

Figure 3.54. shows the radial layout of the benchmark model. This benchmark model for the reference core is developed as a three-dimensional (3D) homogeneous model for the BFS-62-3A critical experiment as the mock-up of the BN-600 reactor with a hybrid zone and a steel reflector [46].

The compositions of the BFS-62-3A benchmark model are given as the following:

- Low Enrichment Zone (LEZ) consists of:
- 595 fuel rods (FAs) of LEZ type
- 54 empty rods (without fissile materials)
- 18 mock-ups of reactivity compensators (1 CR = 4 BFS tubes)
- 6 mock-ups of safety rods (1 SR = 4 BFS tubes)
- Medium Enrichment Zone (MEZ) consists of 222 FAs of MEZ type
- Plutonium Enrichment Zone (MOX) consists of 336 FAs of MOX type
- High Enrichment Zone (HEZ) consists of 237 FAs of HEZ type
- Radial Reflector consists of:
 - i) 1478 rods of uranium oxide in radial blanket (RB)
 - ii) 1172 rods of empty tubes
 - iii) 433 rods of stainless steel (SS) in the sector 120°
 - iv) 137 rods containing boron carbide (B₄C) powder in the sector 120°.

The FAs are positioned in hexagonal lattice pitch of 5.1 cm.

Cu	Steel	50.0
Cu	1.0	1.0
Steel	25.0	↑
Cu	1.0	↓
LAB	35.40	↑
IC	103.81	↑
UAB	29.5	↓
UAS	39.86	↑

Inner Core (IC)

Middle Core (MC)

Cu	Steel	LAB	OC	UAB	UAS	39.86
Cu	Steel	LAB	OC	UAB	UAS	29.5
Cu	Steel	LAB	OC	UAB	UAS	103.30
Cu	Steel	LAB	OC	UAB	UAS	35.40
Cu	Steel	LAB	OC	UAB	UAS	1.0
Cu	Steel	LAB	OC	UAB	UAS	25.0
Cu	Steel	LAB	OC	UAB	UAS	50.0
Cu	Steel	LAB	OC	UAB	UAS	1.0

Outer Core (OC)

MOX Core (MOX)

(unit: cm)

FIG. 3.53. Fuel rods of the BFS-62-3A assembly.

Figure 3.55 examples an axial description of each type of FAs. More detailed axial descriptions of FAs are shown in Appendix VII in Figs G.1.1 for the reference (unvoided) state and in Figs G.1.2 for the voided states. The radial core layouts of the assembly configurations for the reference core and the voided cores are shown in Appendix VII in Fig. G.2.1 and Figs G.2.2 to G.2.5 with all fuel rods (FAs) being numbered from No.1 to No.30 corresponding to its core layout.

Atomic densities for nuclear materials in all zones of FAs, illustrated in Figs G.1.1 and G.1.2, are given in Table G.1. The reference core consists of total 30 material zones. Material zones 31 to 38 are specified for the voided cores. All material data are specified at room temperature 293 K.

The constituent material descriptions for each fuel rod (FA) in the reference (unvoided) benchmark core shown in Figs G.1.1 and G.1.2, in accordance with the material data given in Table 3.77, are given in the following:

- Low Enrichment Zone (LEZ) FAs: material No. 1, 2, 19, 20, 21, 29 and 30 (FAs 1, 2, 16, 17, 19 and 20);
- Medium Enrichment Zone (MEZ) FAs: material No. 3, 19, 20, 21 and 29 (FAs 3 and 4);
- Plutonium Enrichment Zone (MOX) FAs: material No. 7, 8, 19, 20, 21, 29 and 30 (FAs 12 and 13);
- High Enrichment Zone (HEZ) FAs: material No. 5, 6, 19, 20, 21, 29 and 30 (FAs 5, 6, 21 and 22).
- Radial (Stainless Steel) Reflector: material No. 16 (FAs 14);
- Boron carbide shield: material No. 17 and 18 (FAs 15 and 18);
- Radial Blanket: material No. 26 and 28 (FAs 7 and 23);
- Control Rods: material No. 11, 12, 15, 27 and 29 (FAs 8, 9, 10, 11).

In more detail, descriptions of fuel rod loads in Figs G.1.1 and G.1.2 are given in Table 3.77.

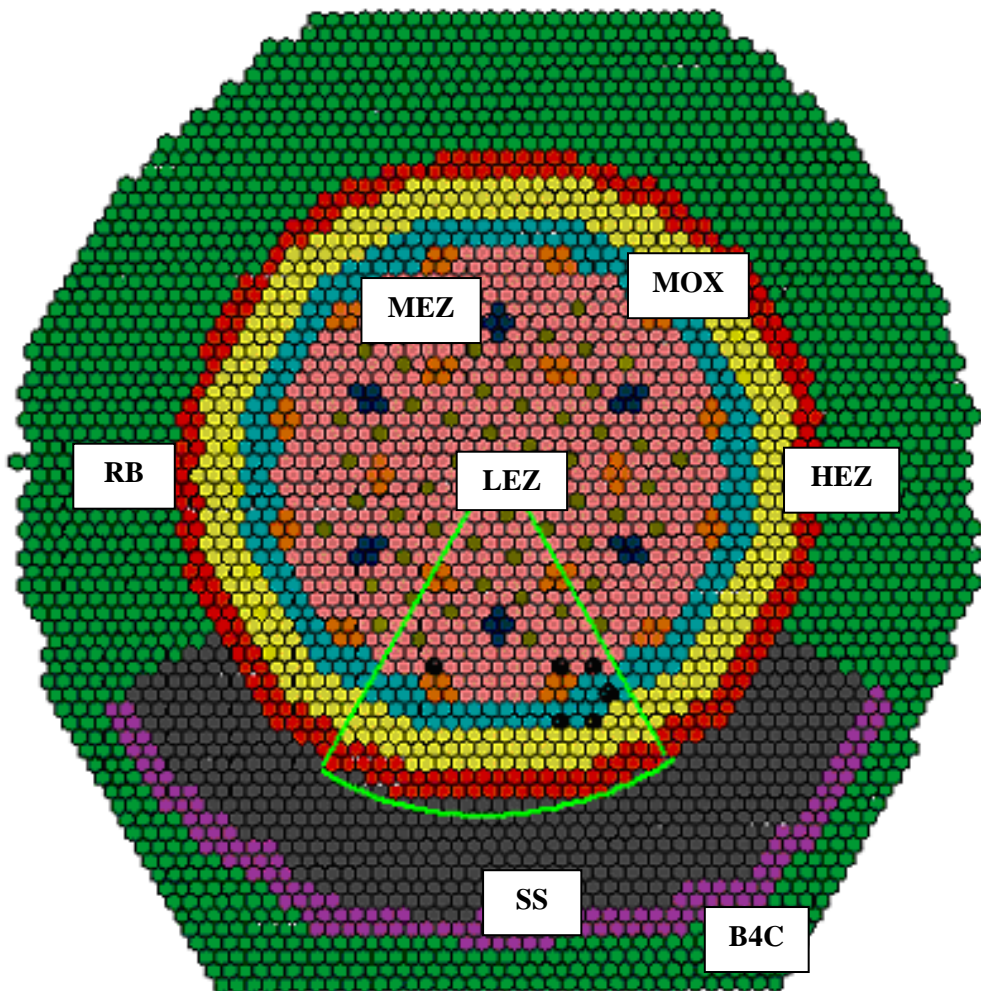
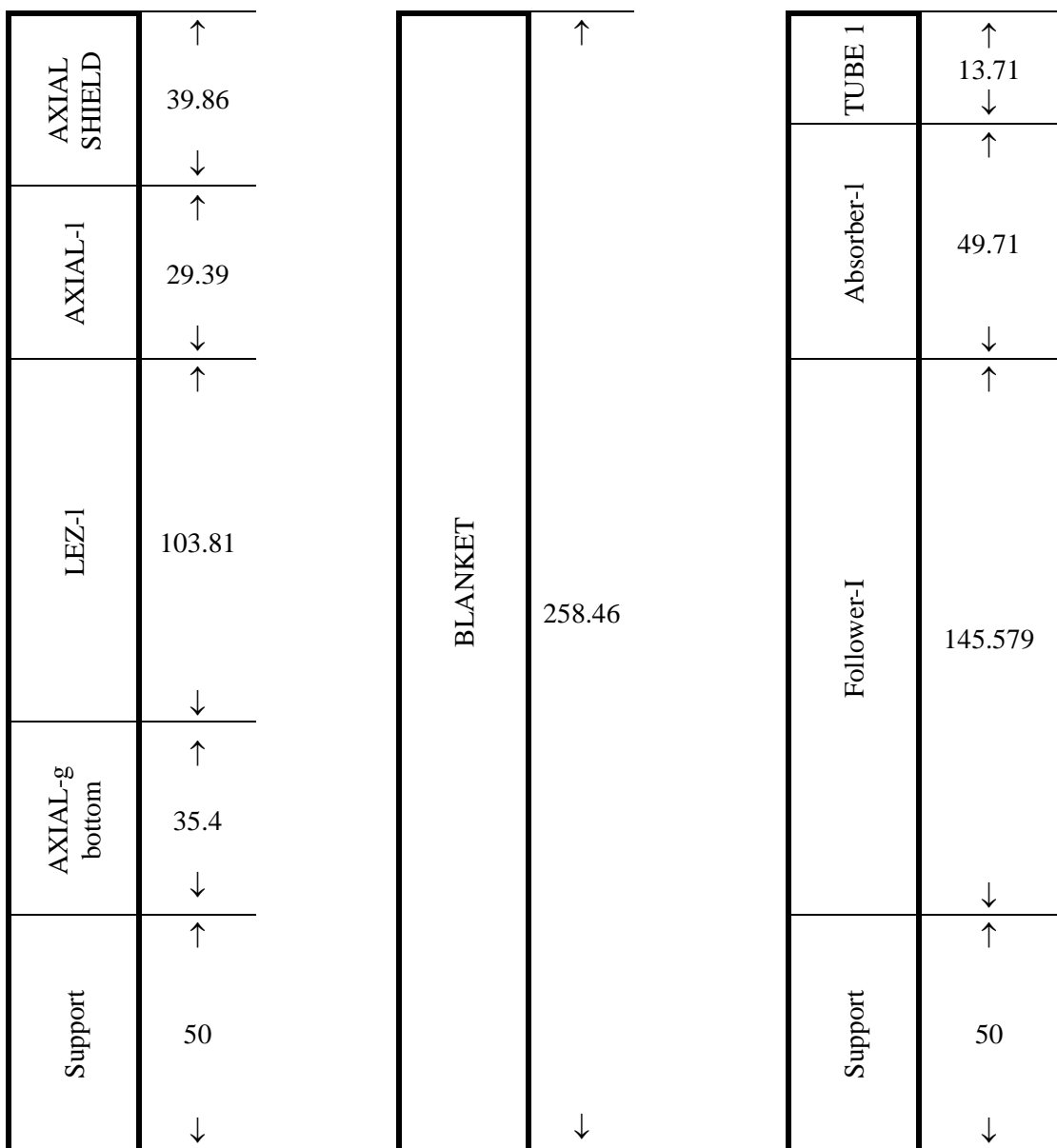


FIG. 3.54. Layout of the benchmark core and location of the voided sector.



(unit: cm)

FIG. 3.55. Axial description of the fuel rods of the reference (unvoided) benchmark core.

TABLE 3.77. FUEL ROD LOADS OF THE BFS-62-3A BENCHMARK CORE

FA No.	FA Type		Constituent material No.
1	LEZ	LEZ-l	29, 20, 1, 19, 21
2		LEZ-g	29, 20, 2, 30, 21
3	MEZ	MEZ-l	29, 20, 3, 19, 21
4		MEZ-g	29, 20, 4, 30, 21
5	HEZ	HEZ-l	29, 20, 5, 19, 21
6		HEZ-g	29, 20, 6, 30, 21
7	Radial blanket	Radial blanket	26
8	CR	CR-l	29, 11, 13, 27
9		CR-g	29, 12, 14, 27
10	SR	SR-l	29, 11, 15, 27
11		SR-1	29, 12, 15, 27
12	MOX	MOX-l	29, 20, 7, 19, 21
13		MOX-g	29, 20, 8, 30, 21
14	Radial reflector	Radial reflector	16
15	B4C	B4C-l	17
16	Modified LEZ	Modified LEZ-l	29, 20, 9, 19, 21
17		Modified LEZ-g	29, 20, 10, 30, 21
18	B4C	B4C-2	18
19	LEZ-brig	LEZ brig-l	29, 20, 22, 19, 21
20		LEZ brig-g	29, 20, 23, 30, 21
21	HEZ-brig	HEZ brig-l	29, 20, 22, 19, 21
22		HEZ brig-g	29, 20, 25, 30, 21
23	Empty tube	Empty tube	28
24	LEZ void	LEZ-l void	29, 20, 31, 38, 21
25		Modified LEZ-l void	29, 20, 32, 38, 21
26		LEZ brig-l void	29, 20, 33, 38, 21
27	MEZ void	MEZ-l void	29, 20, 34, 38, 21
28	HEZ void	HEZ-l void	29, 20, 35, 38, 21
29		HEZ brig-l void	29, 20, 36, 38, 21
30	MOX void	MOX-l void	29, 20, 37, 38, 21

1) Sodium void reactivity effect (SVRE)

SVRE values are determined for four states when the sodium is removed in fuel rods in (i) LEZ (118 FAs), (ii) MEZ (37 FAs), (iii) HEZ (47 FAs) and (iv) MOX (58 FAs), within the 60° sector of the key-regions, based on the reference (unvoided) state as they are shown in Fig. G.2.1. Sodium is removed in the core regions LEZ, MEZ, HEZ and MOX, and the upper axial blanket (AB) region. Sodium is not removed from control rod mock-ups and regular control rods in the core. Figures G.2.2 to G.2.5 in Appendix VII show the layout of core models for each state for SVRE calculations.

The SVRE value is determined as the difference between two states (with and without sodium) by the following formula:

$$RE_i = \frac{k_{\text{eff}}^0 - k_{\text{eff}}^i}{k_{\text{eff}}^0 \times k_{\text{eff}}^i}.$$

Here the index i means perturbed (voided) state and index 0 is related to the initial (reference) state of the core.

2) Equivalent measured values

For the purpose of the benchmark analysis, equivalent experimental data have been determined for the criticality and SVRE values of the BFS-62-3A core. The equivalent experimental data represent the data which are adjusted to the specified benchmark model and include the following corrections to the actually obtained experimental results for simplifications: (a) 3D model simplification effect and (b) heterogeneity effect.

The equivalent experimental data and the associated corrections, provided by IPPE, are based on calculations performed with the 3D Hex-Z diffusion code TRIGEX, the discrete ordinate code TWODANT, and the Monte Carlo code MMKKENO. The calculated β_{eff} value of 0.00623 was used to convert the SVRE experimental data to values in pcm unit. Full details of the evaluation of the equivalent data are given in Ref. 38.

To start with a ‘reference’ or ‘as built’ heterogeneous model was specified for the BFS-62-3A core. The heterogeneous model fully represents the real structure of the critical assembly without any simplification, and specifically represents each single pellet and its can as well as the BFS tubes and the inter-tube sticks. An ‘exact’ homogeneous model was then constructed, based on the geometry of the ‘as built’ heterogeneous model by averaging the pellet compositions with their volumes so that the net material balance was preserved. Finally a ‘simplified’ homogeneous model was constructed so that all axial sizes of the fuel and control rods were adjusted to one consistent value, and the bottom part of the core support, grid plate and upper (empty) part of the tubes were removed. Using these homogeneous models the total heterogeneity and modelling effects were determined.

Monte Carlo calculations were used to evaluate the adjusted correction for whole core reactivity while the 1D collision probability code FFCP was used to evaluate heterogeneity corrections for the SVRE values. The results for the criticality and the SVRE values are presented in Tables 3.78 and 3.79 respectively, together with the resulting equivalent measured values.

TABLE 3.78. EQUIVALENT EXPERIMENTAL CRITICALITY VALUE FOR BENCHMARK MODEL

Value	k_{eff}
Adjusted correction factor	-0.012
Equivalent measured value	0.9887 ± 0.0030

TABLE 3.79. EQUIVALENT EXPERIMENTAL SVRE VALUES FOR BENCHMARK MODEL

Voided Region	Heterogeneity Correction Correction Factor (pcm)	Equivalent Measured Values (pcm)
LEZ	-37	-20±9
MEZ	-5	-11±4
MOX	-18	-14±6
HEZ	-15	-57±6
Total effect	-75	-102±20

It is noted that the uncertainty for the equivalent measured data for the criticality and SVRE values is taken to be the square root from the sum of the squares of the experimental uncertainty and the uncertainty associated with the bias estimated as one fourth of the applied correction factor.

3.4.2. Comparison of results

The (C-E) values, differences between the experimental (E) and calculated (C) values of the diffusion and transport results obtained with the three-dimensional Hex-Z equivalent homogeneous calculational model are given in Tables 3.80 and 3.81, respectively.

The calculated (C) values were obtained by the participants with their own state-of-the-art basic data, codes and methods to check the capability of predicting main parameters. The validation efforts were extended to include corrections by mesh size, ultra-fine energy group and transport theory approximation in some participants' results. For the SVRE values, a detailed investigation by separating those values into leakage and non-leakage components was additionally performed by several participants.

The uncertainties on the measured values comprise two components, the measurement uncertainty and a modelling uncertainty. The dominant uncertainty is that from modelling which, by expert judgement, has been assumed to be one quarter of the correction due to heterogeneity. This judgement is supported by a comparison of independent heterogeneity assessments by IPPE and JNC [47].

3.4.2.1. Criticality

Table 3.80 shows the (C-E) values for the criticality based on diffusion theory calculations with employing a finite-difference method. The mean calculated (C-E) value is -214 pcm with a standard deviation of ±387 pcm. In the case of including more extensive results calculated using various nuclear data libraries, the mean calculated (C-E) value is obtained to be -72 pcm with a standard deviation of ±397 pcm in Table 3.82. The difference of these two results given in Tables 3.80 and 3.82 is estimated to be 142 pcm with a similar standard deviation of about ±400 pcm, which indicates that the difference between the calculated values results from the difference between different nuclear data libraries.

The comparison between JEF2.2 results from JNC and CEA/SA shows an uncertainty in the generation of broad group cross-sections for treating the solution of the fine group homogeneous cell calculations of about ±50 pcm. This is supported by the difference in fine and ultra-fine group calculations by JNC where there was a difference of 60 pcm [39].

In Table 3.82 the difference of the mean (C-E) values between the cases for all nuclear libraries and only for JEF-2.2, 377 pcm (249 pcm + 128 pcm) supports that the major component of the difference of the analyses between measurement and calculation is attributed to the difference between different nuclear data libraries.

Table 3.81 shows that the mean calculated (C-E) value for the criticality obtained from transport theory calculations, 285 pcm, is similar to the uncertainty in the adjusted experimental reactivity, \pm 300 pcm. The difference associated with the nuclear data is estimated to be about \pm 400 pcm, similar to that in the diffusion results. In Table 3.83 the mean transport correction on the criticality evaluated from the comparison between the diffusion and transport results is evaluated to be 481 pcm with a standard deviation of \pm 100 pcm.

In more specific investigation performed by the CEA/SA result, the transport theory (C-E) value of +643 pcm is consistent with the expected over-estimation of k_{eff} that arises when using cross-section data from the JEF-2.2 nuclear data evaluation for uranium fuelled systems. It is envisaged that a calculation using the cross-section data derived from the more recent JEFF3.1 nuclear data evaluation will lead to a reduction in the observed (C-E) value by approximately 500 pcm.

FZK/IKET used two different data libraries for Phase 5. The new FZK 30-group library – based on JEFF 3.0 data – gives rather accurate criticality results [(C-E) is less than the experimental uncertainty], provided that the transport theory option is used. The additionally employed (because it was used in Phase 4) ‘old’ 11-group SIMMER library gives less accurate criticality values [(C-E) is larger than the experimental uncertainty by a factor of 2.5] with the transport option due to rather old (more than 30 years) evaluations employed for major nuclides like ^{238}U and ^{239}Pu as well as due to the small energy group number (11).

3.4.2.2. Sodium void reactivity effect (SVRE)

The (C-E) values of the diffusion and transport results for the sodium void reactivity effect (SVRE) in four different core regions are given in Tables 3.80 and 3.81, respectively. In these tables, the CIAE results are given only for the comparison and are not included in the mean value estimation.

Sodium voiding effects in the core are relatively small as the voided region was limited to one sixth of the core in this benchmark. As previously noted in the benchmark description, although the benchmark considers the voiding of four separate regions, in practice, the regions were voided consecutively, the previously voided region remaining voided. However, the interaction effect between the voided regions has been shown to be negligible, less than one pcm on total void according to calculations by JNC [48].

In Table 3.80 the uncertainties in the diffusion calculated values for the SVRE are estimated to be similar in magnitude to the experimental uncertainties except for the MOX region. The (C-E) diffusion calculated values for the MOX region show a relatively large uncertainty, nearly double the size of the uncertainty in the adjusted experimental value. The KAERI result for the MOX region is obtained to be positive, differing from the other participants’ results. It has been clarified from the analytic comparison that the difference in the SVRE values results from the use of ^{239}Pu cross-sections from old JEF-2.2. A cautious treatment of the SVRE is particularly suggested for the MOX region in this kind of benchmark study.

The comparison of the IPPE and IGCAR values for the diffusion results, both using similar nuclear data, shows only small differences, which indicates that the influence of methods for cross-section processing is small. This is supported by the small differences in the JNC and CEA/SA values obtained based on the JEF2.2 cross-sections.

In Table 3.81 the mean calculated (C-E) transport values for SVRE are generally less than the uncertainty in the adjusted measured values. Table 3.83 shows that uncertainties in the transport correction are relatively small compared to the experimental uncertainty.

In general, the standard deviation between the calculated values for SVRE is similar to or less in magnitude than the experimental uncertainty. However, it is important that appropriate methods (diffusion/transport) and data are used in reactivity coefficient evaluations.

Table 3.84 compares the CEA/SA and JNC results for the separated non-leakage and leakage components of the SVRE values. These results were obtained with some corrections by mesh size,

transport theory or ultra-fine energy group, based on the diffusion results. The mesh correction in the CEA/SA results is taken from the sample calculations performed by IPPE with the 3D diffusion code TRIGEX [46]. This procedure is certainly not the best one but as the mesh correction is negligible with respect to SVRE, this has not a significant impact on the results. JNC corrected the diffusion results by ultra-fine group calculations with approximately 100,000 group constants below 50 keV and ABBN type 175 group constants with shielding factors above 50 keV. It is observed that the SVRE values are evaluated within the uncertainty in the adjusted experimental values except in the MOX region. From these results the effect from mesh size and transport theory approximation appears to be relatively small compared to that from the ultra-fine group treatment. It is noteworthy in the JNC results that the correction by the ultra-fine energy group treatment strongly affects the non-leakage components of the SVRE values by –6 to –15%. Regarding the non-leakage and leakage terms of the SVRE values, detailed investigations of the similarity and relevance for the sodium void reactivity effect (SVRE) in the BFS mockup and BN-600 hybrid cores are separately addressed in Chapter 5.

3.4.2.3. Conclusions on BFS-62-3A analyses

For the BFS-62-3A core the mean diffusion theory result underestimates k_{eff} by about 500 pcm relative to the mean transport theory result and the total (120 degree sector) sodium void effect by a relative value of between 10% and 20% compared to transport theory. Depending on the specific transport and diffusion codes employed, as well as the nuclear data libraries, deviations for sodium void can be larger, by up to a factor of 2, relative to the corresponding experimental uncertainties

In conclusion, most analytical results for the criticality and the sodium void reactivity, obtained by the participants with their own basic data and computer codes system, consistently agree with equivalent measured values within the associated uncertainty. This finding confirms each participant's reliable prediction capability using standard nuclear data, techniques and computer codes basically employing the diffusion theory approximation. For both the criticality and the sodium void worth, the main uncertainties in the calculated values result from differences in nuclear data between libraries. The uncertainty associated with the nuclear data is of the same size as the uncertainty in the simplified adjusted homogeneous benchmark experimental values.

3.5. Influence of basic nuclear data

As part of the BN-600 hybrid core benchmark analysis effort, the JNC participant performed sensitivity analysis of the difference between the JENDL-3.2, JENDL-3.3 or JEF-2.2 libraries [47, 49, 50]. Using the cross-section sensitivity coefficients, the nuclide-wise and reaction-wise contributions to the effect of the library change were analyzed for their effect on important reactivity parameters.

From the sensitivity analysis, the dominant nuclides and reactions were identified for the investigated reactivity parameters. For example, Fig. 3.56 shows that the ^{235}U and iron cross-sections largely contribute to the k_{eff} difference between JEF and JENDL. It can be seen in Fig. 3.57 that the ^{235}U capture and iron elastic reactions are the largest components of the sodium density reactivity difference. The ^{235}U capture and ^{238}U capture reactions are observed to be main contributors to the burnup reactivity loss difference in Fig. 3.58. The major findings observed from the results of the sensitivity analysis are given as follows:

- The criticality and sodium density reactivity effect are very sensitive to cross-section changes and show strong non-linearities;
- The steel density reactivity effect has large sensitivity coefficients arising from a few specific reactions;
- The fuel and absorber density reactivity are relatively easy to predict.

More details of the sensitivity analysis methodology and the results are addressed in Appendix II.

TABLE 3.80. (C-E) VALUES OF DIFFUSION RESULTS (Unit: pcm)

Participants	Nuclear Data	Core Reactivity		LEZ		MEZ		MOX		SVRE	
		Value	Uncertainty	Value	Uncertainty	Value	Uncertainty	Value	Uncertainty	Value	Uncertainty
CEA/SA	JEFF-2.2	26	300	-1	9	-45	4	-12	6	9	6
	ENDF/B-IV	-512	300	-125	9	2	4	-77	6	-58	6
Clae	JEFF 3.0	-345	300	5	9	2	4	-16	6	4	6
FZK/KET	XSET-98	-390	300	-8	9	0	4	-14	6	6	6
ICGCAR	ABBN-93	-650	300	-13	9	-1	4	-13	6	2	6
IPPE	JENDL-3.2	-230	300	-17	9	-3	4	-13	6	2	6
JNC	JEFF-2.2	602	300	-10	9	0	4	-4	6	22	6
KAERI											
Mean		-214	300	-7	9	0	4	-11	6	8	6
Standard Deviation		387		7		2		7		7	

TABLE 3.81. (C-E) VALUES OF TRANSPORT RESULTS (Unit: pcm)

Participants	Nuclear Data	Core Reactivity		LEZ		MEZ		MOX		SVRE	
		Value	Uncertainty	Value	Uncertainty	Value	Uncertainty	Value	Uncertainty	Value	Uncertainty
CEA/SA	JEFF-2.2	643	300	-7	9	5	4	-2	6	11	6
	ENDF/B-IV	71	300	9	9	4	4	-11	6	6	6
Clae	JEFF 3.0	70	300	9	9	4	4	-11	6	5	5
FZK/KET	XSET-98	-220	300	-10	9	0	4	-7	6	4	6
ICGCAR	ABBN-93	129	300	-13	9	-2	4	-8	6	3	6
IPPE	JENDL-3.2	1019	300	-2	9	0	4	10	6	24	6
JNC	JEFF-2.2										
KAERI*											
Mean		285	300	-5	9	1	4	-4	6	9	6
Standard Deviation		416		8		3		7		8	

* Transport correction calculated with a 2D RZ core model

TABLE 3.82. (C-E) VALUES OF DIFFUSION RESULTS BASED ON DIFFERENT NUCLEAR DATA (Unit: pcm)

Participants	Nuclear Data	Core Reactivity		LEZ		MEZ		MOX		SVRE		HEZ		Total	
		Value	Uncertainty	Value	Uncertainty	Value	Uncertainty	Value	Uncertainty	Value	Uncertainty	Value	Uncertainty	Value	Uncertainty
CEA/SA	JEF-2.2	26	300	-1	9	2	4	-12	6	9	6	-58	6	-2	20
CIAE	ENDFB-IV	-512	300	-125	9	-45	4	-77	6	6	6	-306	6	-306	20
FZK/IKET	JEFF 3.0	-345	300	5	9	2	4	-16	6	4	6	-5	6	-5	20
11-group	431	300	-9	9	2	4	-13	6	4	6	6	-16	6	-16	20
XSET-98	390	300	-8	9	0	4	-14	6	6	6	6	-16	6	-16	20
ICGCAR	ABBN-93	-650	300	-13	9	-1	4	-13	6	2	6	-26	6	-26	20
IPPE	JENDL-3.2	-230	300	-17	9	-3	4	-13	6	2	6	-31	6	-31	20
JNC	JEF-2.2	120	300	-4	9	2	4	-7	6	9	6	0	6	0	20
KAERI	JEF-2.2	602	300	-10	9	0	4	-4	6	22	6	15	6	15	20
	ENDFB-VI	230	300	17	9	3	4	13	6	-2	6	31	6	31	20
Mean for all		-72	300	-4	9	1	4	-8	6	6	6	-6	6	-6	20
Standard Deviation		397		10		2		9		6		19		19	
Mean for JEF-2.2		249	300	-5	9	1	4	-5	6	13	6	4	4	4	20
Standard Deviation		252		4		1		7		6		8		8	

TABLE 3.83. (C-E) VALUES OF TRANSPORT CORRECTION RESULTS (Unit: pcm)

Participants	Nuclear Data	Core Reactivity		LEZ		MEZ		MOX		SVRE		HEZ		Total	
		Value	Uncertainty	Value	Uncertainty	Value	Uncertainty	Value	Uncertainty	Value	Uncertainty	Value	Uncertainty	Value	Uncertainty
CEA/SA	JEF-2.2	617	300	-6	9	3	4	10	6	2	6	6	6	22	20
CIAE	ENDFB-IV	583	300	4	9	2	4	5	6	1	6	6	6	12	20
FZK/IKET	JEFF 3.0	415	300	4	9	2	4	5	6	1	6	6	6	12	20
ICGCAR	XSET-98	300	3	9	1	4	6	6	6	2	6	6	6	13	20
IPPE	ABBN-93	430	300	4	9	1	4	5	6	1	6	6	6	11	20
JNC	JENDL-3.2	359	300	8	9	0	4	6	6	2	6	6	6	17	20
KAERI	JEF-2.2	417	300	3	9	1	4	6	6	2	6	6	6	15	20
Mean		481	300	5	9	1	4	6	6	0	6	6	6	4	20
Standard Deviation		100		5		1		2		0		0		0	

* Transport correction calculated with a 2D RZ core model

TABLE 3.84. SVRE VALUES

Voided region	CEA/SA			JNC			Equi. value (E) (pcm)					
	Perturbation theroy (diffusion) (JEFF-2.2, 33g) (pcm)			Diffusion (JENDL- 3.2, 70g) (pcm)								
	Non- leakage	Leakage	Mesh correct.	Total	Non- leakage	Leakage	Non- leakage	Leakage	Non- leakage	Leakage	Total	
LEZ	63	-82	-2	-21	57	-85	0.865	1.017	1.024	0.969	51	-84
MEZ	17	-26	0	-9	15	-27	0.870	1.016	1.042	0.959	14	-26
MOX	26	-51	-1	-26	30	-55	0.937	1.010	1.097	0.953	31	-53
HEZ	10	-59	-1	-50	7	-62	0.853	0.977	1.048	0.999	6	-60
Total	116	-218	-4	-106	109	-229	0.885	1.004	1.048	0.971	101	-223
												-102

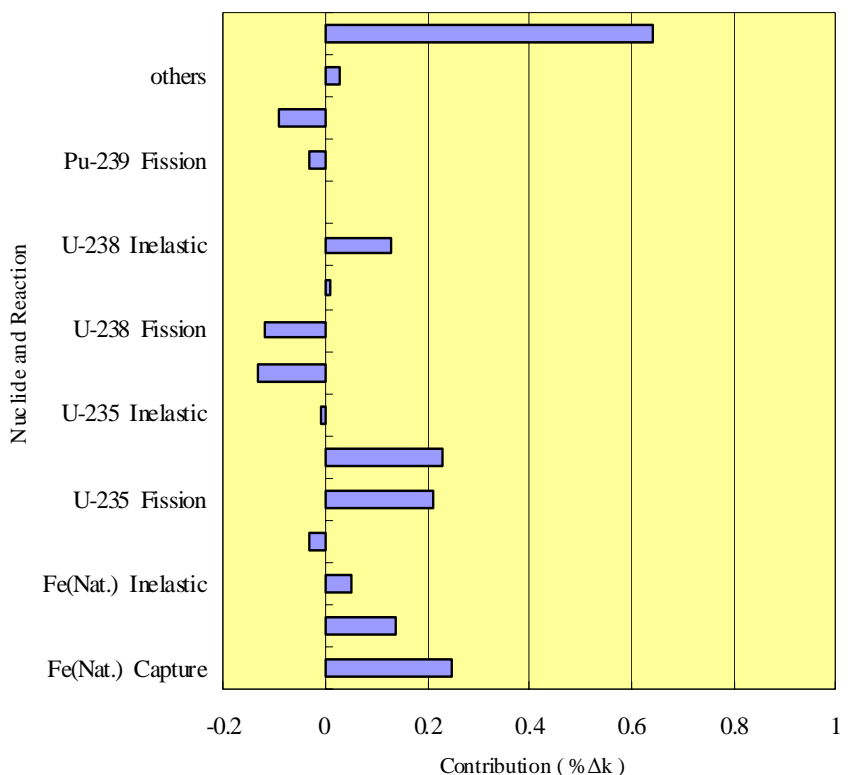


FIG. 3.56. Nuclide-wise contributions to k_{eff} difference due to cross-section difference between JEF-2.2R and JENDL-3.2 for BN-600 hybrid core.

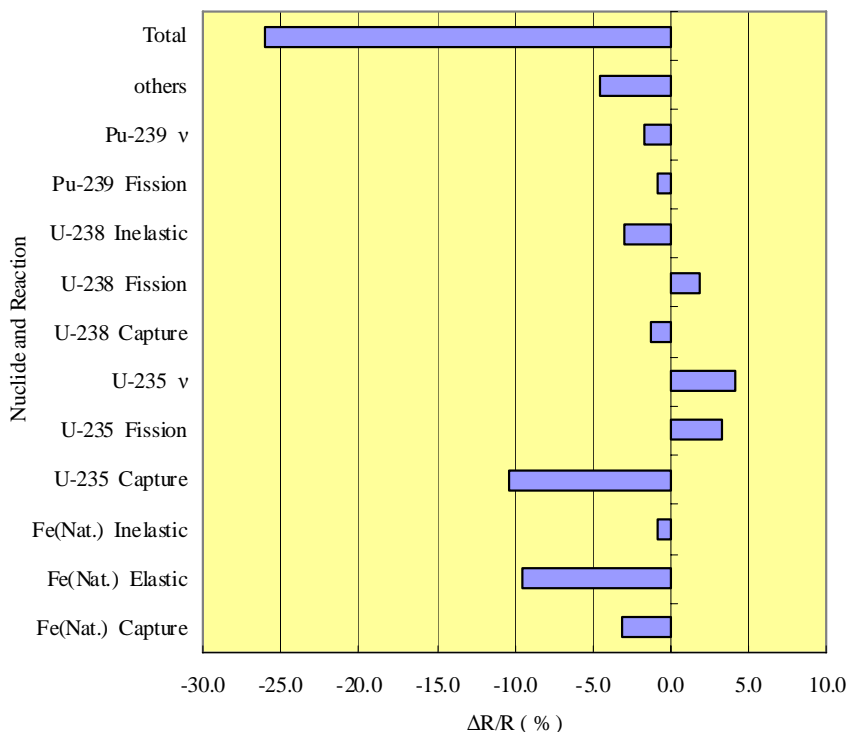


FIG. 3.57. Nuclide-wise contributions to sodium density reactivity difference due to cross-section difference between JEF-2.2R and JENDL-3.2 for BN-600 hybrid core.

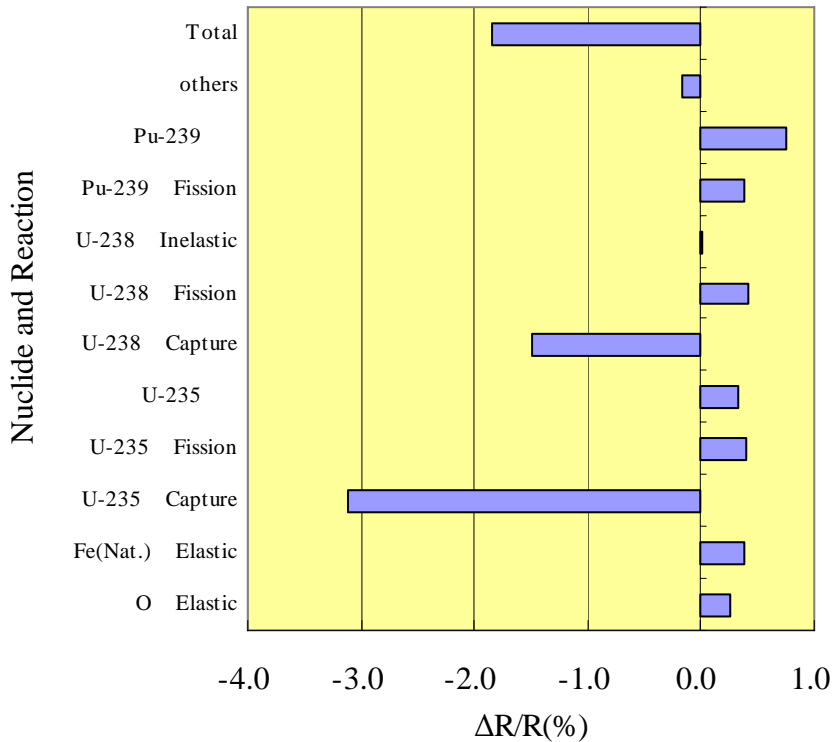


FIG. 3.58. Nuclide-wise contributions to burnup reactivity loss difference due to cross-section difference between JEF-2.2R and JENDL-3.2 for BN-600 hybrid core.

In 2002, JNC generated and released a revised version of JFS set based on JENDL-3.2, named JFS-3-J3.2R, in which a weighting function for processing group-wise constants, and the energy distribution of the secondary neutron by the inelastic and ($n,2n$) scattering reaction were corrected. In the present IAEA CRP, JNC used the JFS-3-J3.2 in Phase 1, 2 and 3, and changed it to JFS-3-J3.2R from Phase 4. JNC evaluated the effect of cross-section set change from JFS-3-J3.2 to JFS-3-J3.2R for the typical parameters of Phase 1, 2 and 3. In the comparison of Phase 1 and 2 results, the effect of cross-section change appeared to be insignificant for most reactivity parameters except for the criticality and the fuel Doppler coefficient. The effect on criticality and fuel Doppler reactivity in the Phase 3 results was almost the same as that of Phases 1 and 2. The effect on criticality in the Phase 4 results was the same as that in the previous cases. The effect on control rod worth was negligible in the heterogeneous calculation. More details are addressed in Appendix VI.

Figures 3.59 and 3.60 show that a significant influence on the prediction of criticality and sodium void reactivity in the BFS-62-3A core is caused by the differences of ^{235}U capture, v and fission, iron capture and elastic scattering between JEF and JENDL. The sodium void reactivity is sensitive to cross-section changes from more various nuclide-wise reactions with a strong non-linearity, which makes more difficulty in precisely predict it for design work. These figures also illustrate results similar to those for the BN-600 hybrid core shown in Figs 3.56 and 3.57. Figures 3.61 and 62 show the cross-section sensitivity for nuclide-wise reactions evaluated based on JENDL-3.2 for the prediction of these two parameters. In these figures, the nuclides and reactions can be identified for which the cross-sections should be treated carefully for precise predictions. More detailed results are available in Appendix VIII.

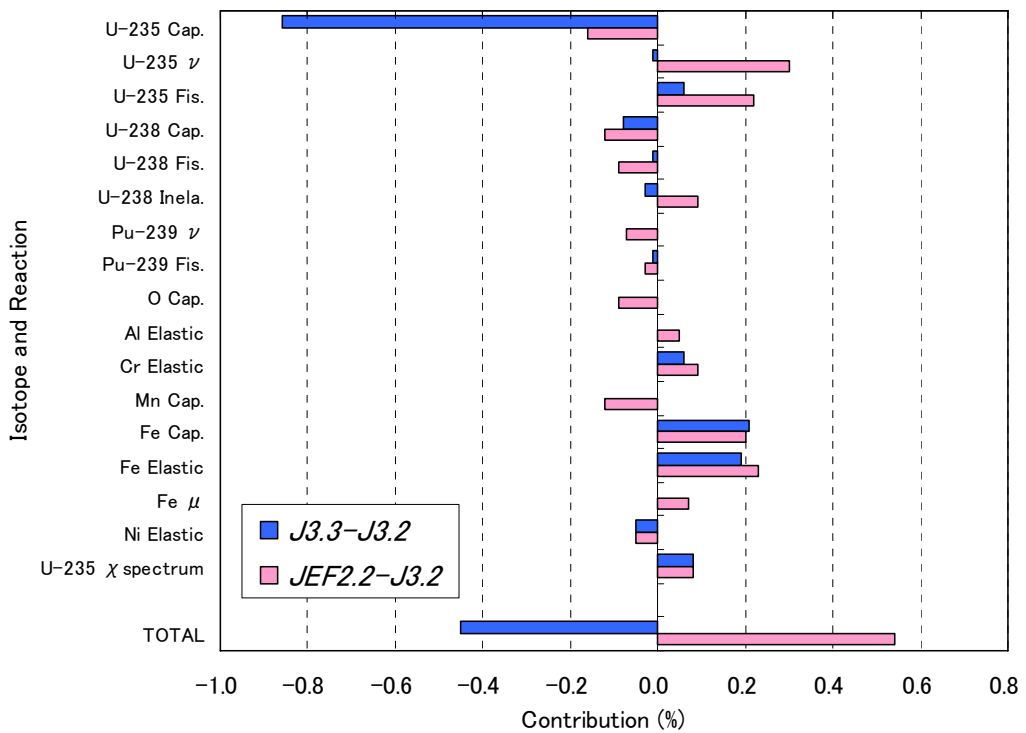


Fig. A.3.1 Sensitivity Analysis for BFS-62-3A Experiment – Criticality –

FIG. 3.59. Nuclide-wise contributions to k_{eff} difference due to cross-section differences between JEF-2.2 and JENDL-3 for BFS-62-3A core.

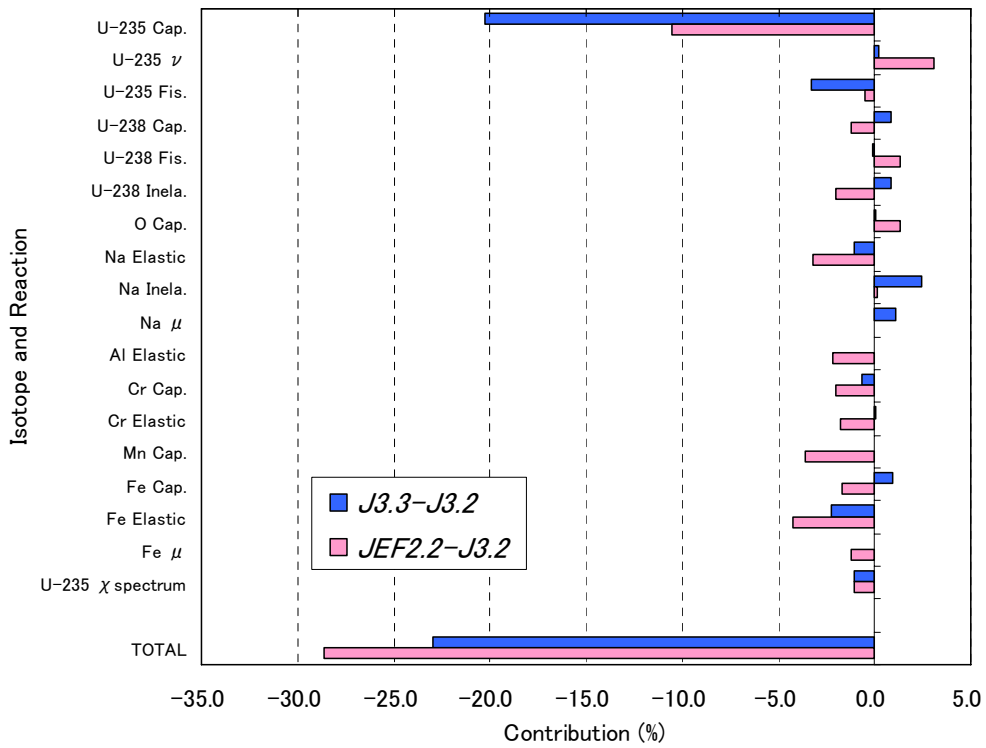


Fig. A.3.6 Sensitivity Analysis for BFS-62-3A Experiment
– Sodium Void Reactivity (Total Effect) –

FIG. 3.60. Nuclide-wise contributions to sodium void reactivity due to cross-section differences between JEF-2.2 and JENDL-3 for BFS-62-3A core.

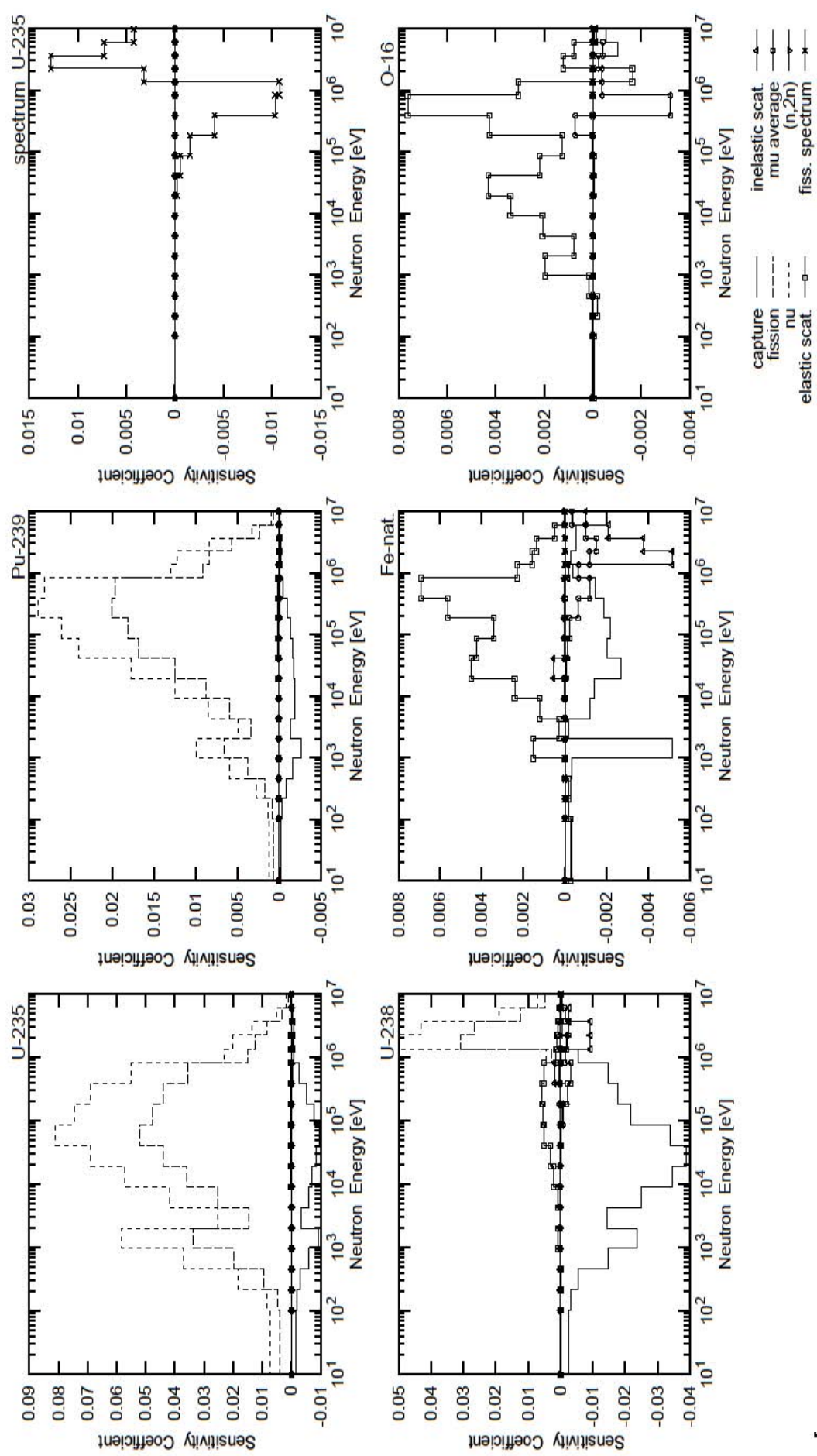


FIG. 3.61. Cross-section sensitivity coefficients for criticality of BFS-62-3A core based on JENDL-3.2.

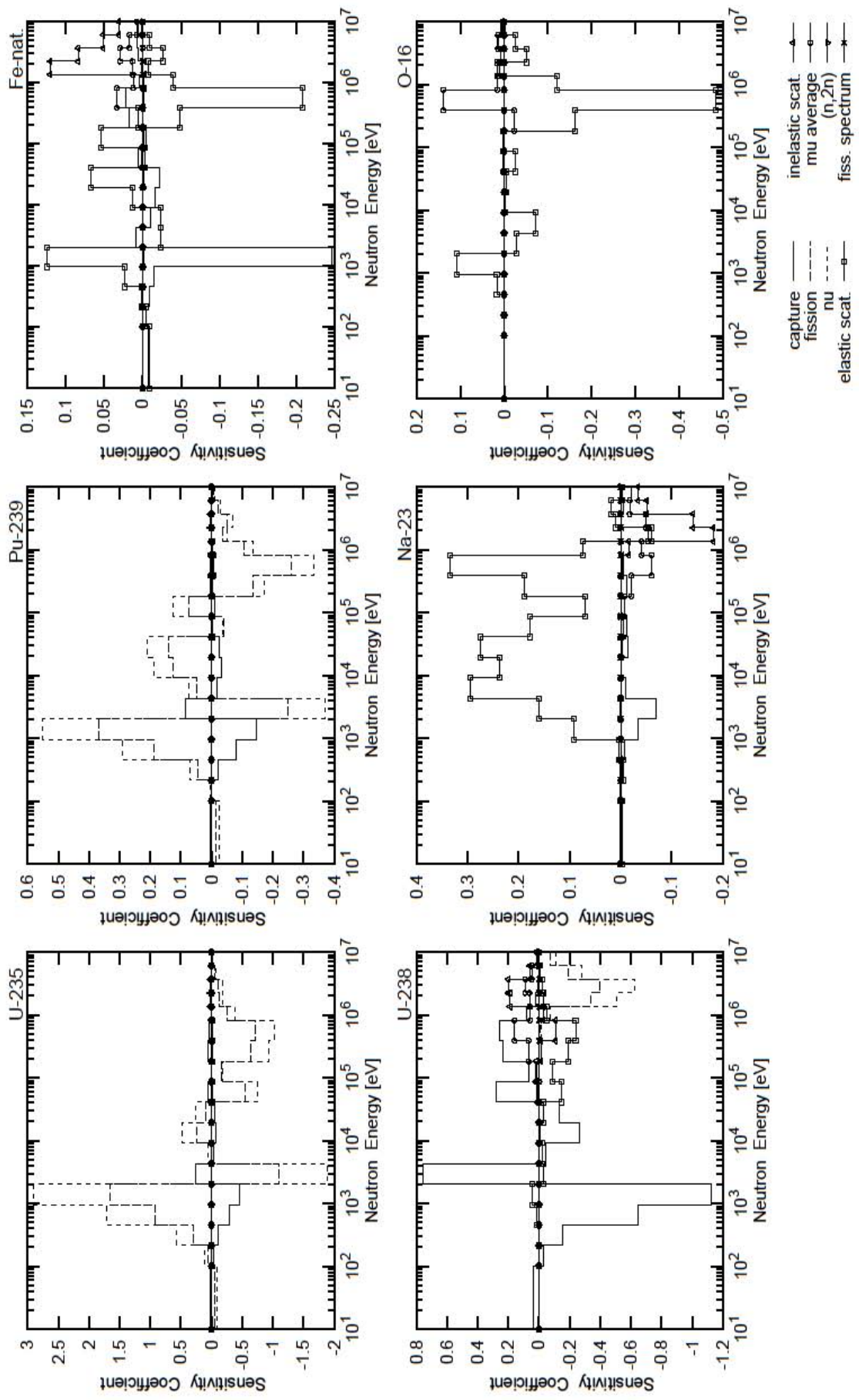


FIG. 3.62. Cross-section sensitivity coefficients for sodium void reactivity of BFS-62-3A core based on JENDL-3.2.

4. ULOF TRANSIENT ANALYSES

The Russian participants, OKBM and IPPE, performed ULOF transient studies using the results prepared by the participants in Phases 1 and 2. These transient analyses have been proposed for a preliminary evaluation of the effect of possible uncertainties present in the reactivity coefficient calculations by comparing reactor dynamics behavior under several different accident conditions. IPPE performed a simplified transient analysis up to the onset of sodium boiling and OKBM carried out SAS4A transient analysis up to and beyond sodium boiling with a more detailed reactor model. The transient analysis performed by IPPE is described in Appendix IV. More details on the results of the transient analyses are addressed in Refs [51, 52].

IPPE performed simplified transient analyses on the ULOF accident in the hybrid BN-600 benchmark core using the results provided by the CRP participants in Phases 1 and 2. The simplified transient analysis employs point kinetics approximation without taking into account phase transitions of core materials and sodium boiling. In these simplified transient analyses, the contribution of individual reactivity feedback components (e.g. sodium void, radial expansion, etc.) to the transient is determined by the magnitudes of the other feedback components in the reactivity balance and are dependent on the specific algorithm in which they are used in a given transient analysis code. The simplified ULOF ($G = 30\% G_0$) transient analysis shows that flow of ULOF is characterized by the reactivity balance mainly due to the fuel Doppler effect and the radial expansion. No principal differences in the ULOF flow were found in cases of using the Phase 2 diffusion results of different participants, especially for reactivity coefficients due to thermal expansion of materials (see Fig. 4.1). The advanced methods used for obtaining reactivity coefficients give the following changes in the ULOF flow: ~14 MW in maximum power, ~8% in total reactivity, ~7°C in sodium temperature, and less than 10°C in fuel temperature. For the hybrid BN-600 core the influence of reactivity due to sodium density change on the accident process appeared to be negligible. The sodium density effect differs from one participant to the other but variation is of small magnitude and therefore the total reactivity effect is not significantly affected. As a consequence, the predicted onset of sodium boiling is not significantly affected.

The SAS4A transient analysis used a simplified channel model for the BN-600 reactor hybrid core. A total of eight input data sets were prepared for SAS4A code calculations using the reactivity coefficients and power distributions obtained by different participants using the diffusion theory approximation. These take into account the energy release at the point of neutron capture in the Phase 2 study. The ULOF transient analyses used the primary pump rundown characteristics for the BN-600 reactor (see Fig. 4.2), where the initial flow rate is reduced by a half within 7.3 s and to 10% in ~50 s after the primary pump trip. Core deformation reactivity coefficients require a complex mechanical study which has been provided by OKBM and IPPE for SAS4A transient studies that are reported in Appendix IV. Results of these reactivity coefficients are reported in Table 2 of Appendix IV and have been used in place of those of the participants in the SAS4A analysis only.

The results of the inter-comparison of the ULOF transient analyses show that the existing spread in the reactivity coefficients is insignificant from the viewpoint of consequent spread in the basic integrated parameters of the initial ULOF accident stage. A current total reactivity was estimated to be ~6.0 cents at ~83.0% relative power at the onset of sodium boiling with small spread in the time dependences of the current reactivity and its components. Using the individual coefficient sets supplied by half of the participants the first bubble generation was obtained 22.2 s after the start of the transient. The spread in reactivity coefficients correlates with the spread (up to the sign reverse for the sodium density component) of the values of corresponding full current reactivity components.

However, after the onset of sodium boiling, the spread in the reactivity coefficient distributions of the Doppler effect and the sodium worth in association with the power distributions causes a significant divergence in the characteristics of the accident progress. Variations of the reactivity components obtained based on the IGCAR data and the OKBM data are illustrated in Figs 4.3 and 4.4 for exemplifying the spreads. The sodium density component shows the most significant relative spread among the components of the current reactivity balance. Up to the onset of sodium boiling, this large spread causes the current reactivity ranging from -66% to 59%. At the sodium boiling stage, the impact of a large uncertainty in the sodium worth becomes much more substantial. A significant contribution

of the components from core radial deformation and the large uncertainty of its value have been noticed.

It is noteworthy that the results of the inter-comparison of the ULOF transient analyses using the reactivity coefficients and power distributions of the different participants show good agreement up to the onset of sodium boiling in spite of a substantial spread noticed for several reactivity coefficients. This is due to compensating effects between several reactivity effects and the specific design of the hybrid core mainly loaded with UOX fuel. On the other hand, beyond sodium boiling there exist significant differences in the transient behaviors resulting mainly from differences in Doppler, sodium void and power distributions.

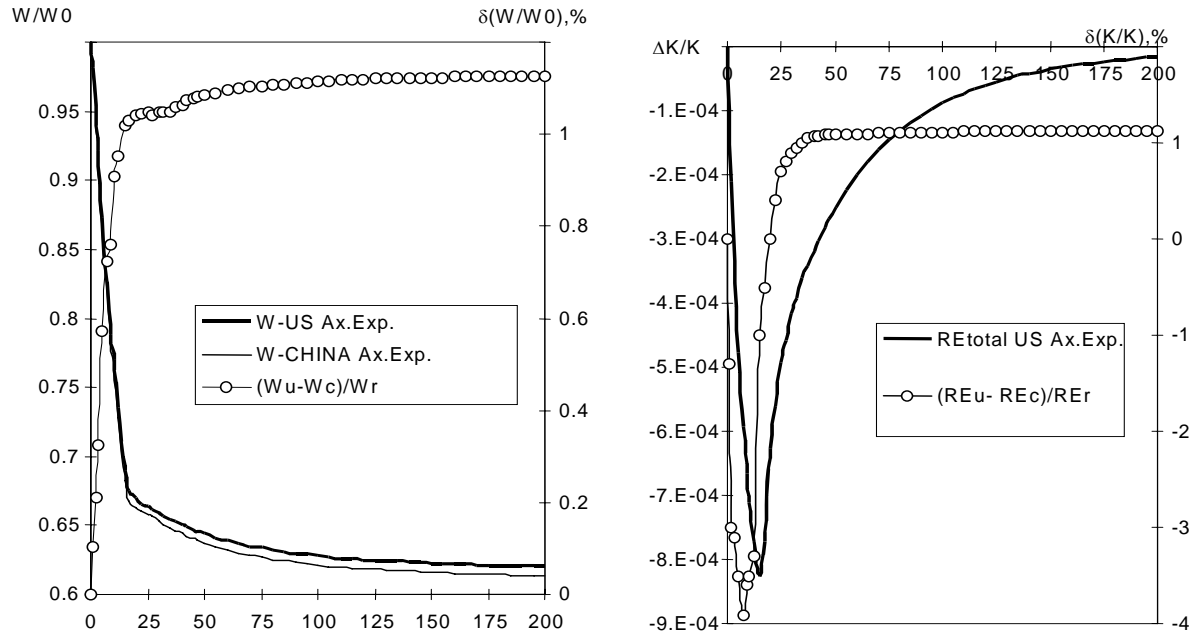


FIG. 4.1. Influence of axial -expansion on power and reactivity in ULOF.

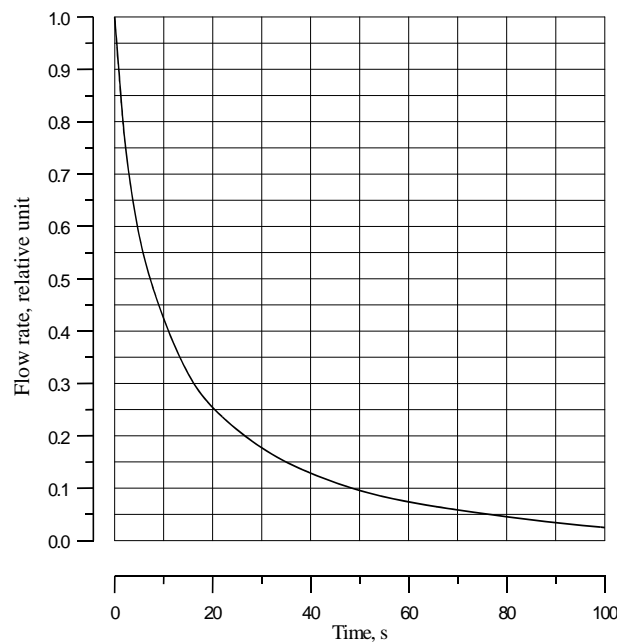


FIG. 4.2. Primary pump rundown for BN-600.

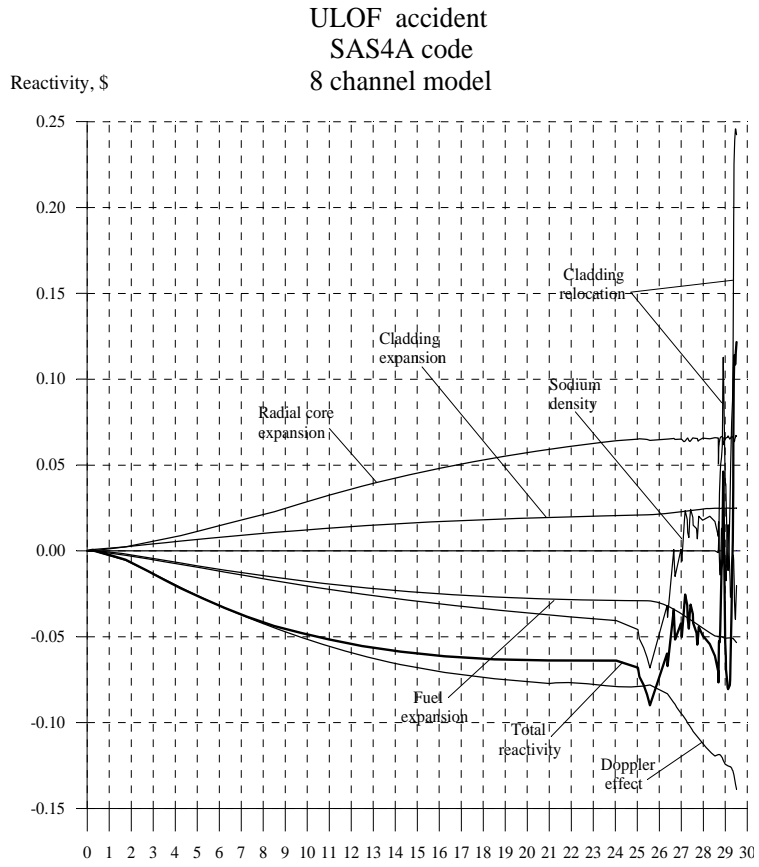


FIG. 4.3. Time dependence of reactivity components based on IGCAR data.

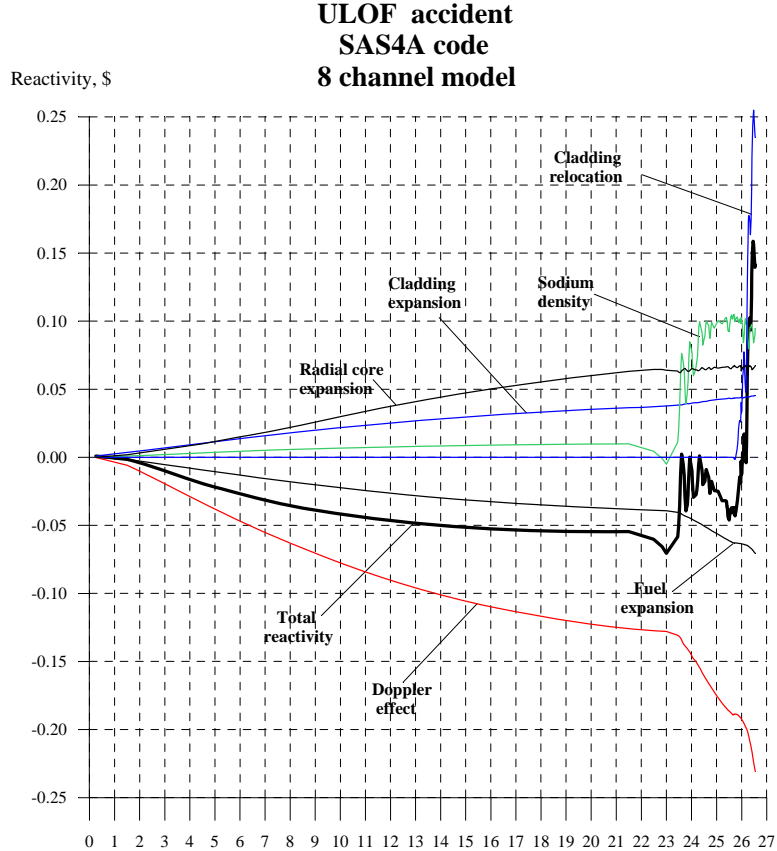


FIG. 4.4. Time dependence of reactivity components based on OKBM data.

5. RELATIONSHIP OF BFS-62-3A AND BN-600 HYBRID CORES

5.1. Sodium void reactivity effect in BFS-62-3A and BN-600 hybrid cores

The BFS-62-3A assembly was designed to be as close as possible to the BN-600 hybrid core. It is the reason for which the BFS-62-3A assembly was entitled a BFS mockup of the BN-600 hybrid core. Most of the neutronic measurements performed within the BFS-62-3A assembly were representative of BN-600 hybrid core characteristics. However, for the Sodium Void Reactivity Effect (SVRE), improving the SVRE prediction of the BN-600 hybrid core with the analysis of BFS-62-3A experiments is a difficult task [53]. The objective of this section is to study the similarity and relevance for the sodium void reactivity effect (SVRE) in the BFS mockup and BN-600 hybrid cores. This task has been investigated by CEA/SA, using the data provided by JNC. The JNC data, details of which are described in Appendices I, J and K, provide the SVRE values by region for those two cores particularly breaking down those values into non-leakage and leakage terms, and sensitivity coefficients for major isotopes and reactions.

The breakdown of the SVRE values into leakage and non-leakage terms in the two cores improves the understanding of the values of the two cores (Appendix I). It appears for instance that the SVRE leakage terms in both cores have similar sign and magnitude, and hence with the other arguments, e.g. similarities in composition and geometry, associated with the similarity between the two cores on the SVRE leakage components validate the connection of the BFS-62-3A assembly with the BN-600 hybrid core. However, some larger differences exist on the non-leakage components. That is, ratios of the non-leakage terms between the BFS-62-3A and BN-600 hybrid cores are in the range of 0.30 to 0.47.

In order to better understand the possible reasons which lead to differences on the SVRE between the BN-600 hybrid core and the BFS-62-3A assembly, JNC performed a step-by-step analysis on the possible reasons for the differences by investigating LEZ and MOX region voiding (Appendix X).

Effects of the following parameters on SVRE were investigated:

- Sodium density difference;
- Temperature difference;
- Pu presence in LEZ, MEZ, and HEZ (1.0 ~ 1.7 wt% only in BN-600);
- Fission product (FP) presence (only in BN-600);
- Control rod partially inserted (only in BN-600).

This detailed analysis performed by JNC has the advantage of describing in details the major source of differences on the SVRE between the BFS-62-3A and BN-600 cores. Among all these sources of differences, only the temperature difference is under control for the computation of the SVRE. All the other effects lead to less similarity of the BFS-62-3A SVRE experiments for the BN-600 SVRE.

Ratios between the BFS-62-3A and BN-600 leakage terms are in the range of 0.82–0.96. In the course of these investigations (Appendix X), the ratio went up to 0.91–1.17 with fuel temperature change. This ratio for the leakage term of the SVRE in the MOX zone, is equal to 1.19 (from 0.86) (Appendix X).

The differences in region-wise SVRE values between the BFS-62-3A and BN-600 hybrid cores lead to ratios of the non-leakage terms in the range of 0.30 to 0.47 [53]. Applying the BFS-62-3A temperatures to the BN-600 hybrid core confirmed the significant temperature influence on the non-leakage terms of SVRE. The ratios of the non-leakage terms of both cores under the same fuel temperature conditions (1500 K for fuel, and 600 K for sodium and structure material) are raised up to 0.68–1.04. The increased ratios come out resulting from changes in fuel temperature even in the MOX region where the value becomes 0.79 (from 0.40).

The reaction component-wise comparison of the non-leakage terms of SVRE for the LEZ region, where the difference appears most clearly, shows that the previous difference is halved by equalizing the temperature condition. This is mainly attributed to the increase in the scattering term resulting from the decrease of ^{238}U resonance capture mostly contributing to the Doppler effect. The ^{238}U capture has a significant effect on the adjoint flux shape and this explains the difference in the slowing down contribution to the non-leakage terms of SVRE. An adjoint flux shape has been studied in a paper of Mr. Hazama, et al. [54], but only for method related problems, i.e. the necessity of using ultra-fine

group scheme for reducing method approximations in the calculations of the slowing down contribution to the non-leakage terms. The adjoint fluxes for the LEZ zone (see Fig. 9 of Appendix XI) are significantly changed in the ^{238}U resonance region, where the adjoint flux shape is roughly given by the ratio of the fission rate and the capture rate. The change induces a significant reduction of the positive contribution of the slowing down component as part of the non-leakage term to the SVRE. Similar effects are observed on the adjoint fluxes for the MOX zone (see Fig. 11 of Appendix XI) but normalization effects are hiding the obvious convergence. Here also, the change induces a significant reduction of the positive contribution of the slowing down component as part of the non-leakage term to the SVRE.

JNC also performed a sensitivity analysis of the SVRE to cross-sections of different isotopes. It would have been better to calculate the sensitivity for each component for both the BFS-62-3A and BN-600 hybrid cores in an attempt to calculate representative factors which make use of variance-covariance matrices on nuclear data (see Appendix XII). Although the theoretical approach to calculate representative factors is very powerful, it is of significant help to understand the reasons for which the SVRE values are different between the two cores, since it is a physical understanding that makes the connection possible.

Based on the data and relevant issues addressed above, the similarity and the relevance of the BFS-62-3A and BN-600 hybrid cores are concluded and an attempt of quantifying them, is performed in the following section.

5.2. Similarity and relevance of BFS-62-3A and BN-600 hybrid cores

The detailed values of SVRE of the BFS-62-3A and BN-600 hybrid cores provided by JNC are given for comparison in Table 5.1. From the comparison of three sets of data in this table, two main parameters that bring about the differences between the two cores have been identified:

- Different temperature conditions for fuel and structure material;
- Different sodium density.

As can be seen in Table 5.1, these two parameters have a different impact on the leakage and non-leakage terms. In the last column of the table, the ratios of the SVRE values between the BFS-62-3A and BN-600 cores are given for each region.

Some correlations can be observed in previous columns where the ratios are quoted for the non-leakage term and the leakage term respectively. The reasons for the remaining differences, especially in the MOX zone, are identified, and an attempt made to quantify the similarity and relevance of the BFS-62-3A results to the BN-600 core presented below. The ratio between different breakdowns of void contributions between the cores is in itself only a weak measure of the representativity factor, since a sensitivity could be coming from different compensating sources of errors with no constant factor which would appear in the representativity factor formulation. As the sources of the differences are known (see Appendix VII), we know that additional compensations do not exist and that, as a result, no bias is introduced into the representativity factor itself. This comes from the fact that the non-leakage component has positive and negative group contributions associated directly to the importance of the neutrons. The importance of neutrons is very different in the UOX zones (LEZ, MEZ and HEZ) and in the MOX zone due to the energy dependency of the production relative to capture in ^{235}U and ^{239}Pu . This view is supported by a plotting of the different adjoint fluxes in the different core regions. Hence, differences are only region-wise variations which are coming from the difficulty of the computational tools to represent the region interactions. Although the ratio of reactivity contributions is different between different core regions (LEZ, MEZ, MOX, HEZ) of the reactors, a knowledge of these ratios allows an accurate estimation of the representativity of the experimental values.

Since a change due to the Doppler effect, for example, is a well-known phenomenon, it can be assumed that computer codes will compute the change in a satisfactory manner. Any other changes, however, might affect the transferability of the analysis from one core to the other. This presumption is applicable to the case for a change in sodium density and also for other changes due to composition modifications.

Hence the values to consider are the ones of the second part of Table 5.1, i.e. the ratios of leakage terms

of the SVRE between the two cores which range from 0.91 to 1.17, and the ratios of non-leakage terms of SVRE which range from 0.61 to 0.79. From these values one can deduce a representativity factor that is almost identical for the two components of 0.70 (roughly approximated as = $(2^* \text{ minimum value} - \text{maximum value of the ratio}) / \text{minimum value}$). The representativity factor should in practice be applied independently to each component to derive independent uncertainties. The uncertainty in the SVRE will be determined by a combination of the uncertainties of the two components: leakage and non-leakage terms. This way of proceeding could be further enhanced by using the energy shape of the different components. It is suggested this approach is applied to the MOX region, since a large uncertainty in the SVRE in the MOX region, compared to that of the UOX regions, in the hybrid core configuration has been commonly observed in the first three phase studies of the CRP and possible reasons for the uncertainty need to be examined.

The approach and representativity factor applied to this investigation are well supported by the fact that the nuclear characteristics of the two cores are quite similar after allowance for the increase of fuel temperature in the BFS-62-3A core to those specified in the BN-600 hybrid core. This view is again supported by a plotting of the different direct and adjoint fluxes in the other core regions, in particular in the MOX region (Appendix XI). In conclusion, the BFS-62-3A SVRE experiments provide useful data to improve the prediction accuracy of the BN-600 SVRE, subject to the condition that the BN-600 designer uses the BFS results with specific consideration of region-dependent and component-dependent effects.

6. CONCLUSIONS

A series of four benchmark analyses for the UOX/MOX hybrid BN-600 reactor containing three different uranium enrichment zones and one plutonium zone in the core, have been performed within the frame for the IAEA sponsored Co-ordinated Research Project on 'Updated Codes and Methods to Reduce the Calculational Uncertainties of the LMFTR Reactivity Effects'. The general objective of the CRP to validate, verify and improve methodologies and computer codes used for the calculation of reactivity coefficients in fast reactors aiming at enhancing the utilization of plutonium and minor actinides for energy production in a MOX core of the BN-600 reactor.

Phases 1, 2 and 3 of the benchmark analysis in the CRP were devoted to benchmark analyses focusing on safety related reactivity effects and their influence on transient analysis. Phase 1 considered RZ homogeneous core studies, Phase 2 extended these studies to include Hex-Z geometry modelling and in Phase 3 heterogeneous modelling was introduced as well as a consideration of core burnup. This step by step approach had the aim of trying to identify any possible geometrical effects or method approximations along with their resulting biases on predictions. The first consideration of the studies was for the prediction of individual reactivity coefficient values acting within the course of a core transient. Secondly, an assessment was performed of the integral effect of these coefficients acting together within the transient and the resulting outcome. Phase 4 results are not discussed in this report and are available in a separate report. Phase 5 analyzed an experiment for the validation of calculated sodium void coefficient distributions and integral reactivity coefficients. A comparison was performed between experimental measurements taken from the BFS-62-3A critical assembly and calculated values. This comparison was performed in support of the validation of the calculated results from the first three phases.

The comparison of the diffusion and transport results for Phase 1 and 2, obtained for the homogeneous representation, generally show good agreement between RZ and Hex-Z prediction for parameters other than sodium and steel density coefficients. The results for the absolute core reactivity as well as the sodium and steel density coefficients, however, show relatively large differences between participants both in the diffusion approximation, and between the diffusion and transport theory approximations. The differences in the integral reactivity coefficient for sodium arise from the compensation between large positive and negative non-leakage and leakage contributions respectively. It is therefore sufficient to use the diffusion theory approximation in RZ geometry for the calculation of all reactivity coefficients except those for sodium and steel. For these coefficients and the absolute core reactivity it is necessary to use a minimum of Hex-Z geometry transport theory to reduce uncertainties to the required level.

Table 5.1. Results of SVRE in BFS-62-3A and BN-600 hybrid cores

		BFS-62-3A (pcm)			BN-600 (pcm)			Ratio (BFS-62-3A/BN-600)		
		Non-leakage	Leakage	Total	Non-leakage	Leakage	Total	Non-leakage	Leakage	Total
LEZ + AB*		42.2	-87.2	-45.0	141.3	-99.8	41.5	0.299	0.874	-1.084
MEZ + AB		15.5	-28.8	-13.3	36.5	-32.2	4.3	0.425	0.894	-3.093
MOX + AB		25.6	-59.2	-33.6	54.1	-65.2	-11.1	0.473	0.908	3.027
HEZ + AB		5.4	-69.3	-63.9	15.9	-72.3	-56.4	0.340	0.959	1.133
All (Fuel + AB)		85.9	-222.7	-136.8	248.4	-270.3	-21.9	0.346	0.824	6.247
		BFS-62-3A (High Temperature) (pcm)			BN-600 (pcm)			Ratio (BFS-62-3A/BN-600)		
		Non-leakage	Leakage	Total	Non-leakage	Leakage	Total	Non-leakage	Leakage	Total
LEZ + AB		86.1	-91.0	-4.9	141.3	-99.8	41.5	0.609	0.912	-0.118
MEZ + AB		27.6	-31.2	-2.6	36.5	-32.2	4.3	0.756	0.969	-0.837
MOX + AB		42.6	-66.9	-24.3	54.1	-65.2	-11.1	0.787	1.026	2.189
HEZ + AB		11.9	-84.5	-72.6	15.9	-72.3	-56.4	0.748	1.169	1.287
All (Fuel + AB)		164.2	-269.5	-105.3	248.4	-270.3	-21.9	0.661	0.997	4.808
		BFS-62-3A (High Temperature) (pcm)			BN-600 (Sodium reduced) (pcm)			Ratio (BFS-62-3A/BN-600)		
		Non-leakage	Leakage	Total	Non-leakage	Leakage	Total	Non-leakage	Leakage	Total
LEZ + AB		86.1	-91.0	-4.9	126.8	-89.6	37.2	0.679	1.016	-0.132
MEZ + AB		27.6	-31.2	-3.6	28.6	-25.3	3.3	0.965	1.233	-1.091
MOX + AB		42.6	-66.9	-24.3	40.8	-49.2	-8.4	1.044	1.360	2.893
HEZ + AB		11.9	-84.5	-72.6	11.9	-54.1	-42.2	1.000	1.562	1.720
All (Fuel + AB)		164.2	-269.5	-105.3	203.9	-221.8	-17.9	0.805	1.215	5.883

* AB: Axial Blanket

In the Phase 3 study, the burnup effect and the heterogeneity effect on most reactivity parameters show good agreement for both diffusion and transport theory results. The burnup reactivity loss per 140 EFPD cycle at the nominal thermal power of 1470 MW was predicted to be 0.025 (4.3\$) with a 5.5% standard deviation among participants. Also, in the Phase 3 study, heterogeneity effects on most reactivity parameters were evaluated to be small; the control rod worth is decreased by a few percent using a heterogeneous treatment. The calculated heterogeneity effect on absolute k_{eff} and control rod worth is observed to be strongly dependent on the method used to treat the heterogeneity effect.

In Phase 5, it was concluded that transport theory must be used to obtain accurate results. In this case, for most participants, analytical results for the criticality and the sodium void reactivity effect, obtained using their own basic data and computer code systems agreed with equivalent measured values within the range of uncertainties. The transferability of the BFS-62-3A sodium void reactivity effect to that of the BN-600 hybrid core is possible by taking into account a detailed breakdown of the individual reactivity contributions. The breakdown should be considered by region as well as leakage and non-leakage components. This finding confirms the reliability of each of the participant's results for BN-600 hybrid core using standard nuclear data, techniques and computer codes.

The substantial spread between the different participants noticed for some of the reactivity coefficients and power distributions along with their associated uncertainties, did not have a significant impact on the ULOF transient behaviour prediction, especially up to the onset of sodium boiling. This result is attributable to compensating effects between several different reactivity contributions in the specific design of the hybrid core, mainly loaded with UOX fuel. This gives confidence that the outcome of this type of transient can be understood and predicted reasonably well in the partially MOX fuelled hybrid core.

Appendix I

THE INFLUENCE OF AN ENERGY GROUPS NUMBER AND MESH SIZE ON RESULTS OF REACTIVITY COEFFICIENTS CALCULATIONS FOR BN-600 BENCHMARK CORE

M.Farakshin, B.Vasilyev
OKBM, Russian Federation

1. INTRODUCTION

This document presents the OKBM contribution to the analysis of a benchmark of BN-600 reactor hybrid core with simultaneous loading of uranium fuel and MOX fuel within the framework of the international IAEA Co-ordinated Research Project (CRP) on ‘Updated Codes and Methods to Reduce the Calculational Uncertainties of the LMFTR Reactivity Effects’ [1].

The purpose of the present document is the comparison of some obtained for the Phase 2 results using the different energy groups number and the different mesh point size.

The CRP participants at calculation of a benchmark used different planar mesh point sizes. The axial mesh point size was not stipulated, but the mesh sizes were specified for the desired results representation. Therefore in some cases there was possible the application of rather large axial mesh size. The discrepancy in results because the different mesh point size using should be estimated.

The results of some participants were obtained using the relatively small energy groups number — 6, 9, and 12. The influence of the energy group number on value of the obtained reactivity coefficients is analyzed in case of the OKBM calculations results.

Besides in case of the sodium density reactivity coefficient the OKBM used method of the choice for the few group optimal division of the energy scale is shown. The probable additional uncertainties as the consequence of the baseless group division are estimated by the comparison of the group division schemes applied by different CRP participants

2. THE USED METHODS AND MODELS FOR CALCULATIONS

2.1. The used code and cross sections

The same methods as used one for the preparation of already published results for Phase 2 are applied for the described calculations. The finite difference option of the JARFR code in HEX-Z diffusion approximation is used. As is mentioned below, in this case were used both the hexagonal and triangular calculating cells. The 26-group initial constants library BNAB-78 was used for cross sections processing in 26, 12, 9 and 6 groups. The cross section processing in all cases is performed using the previously defined intrinsical 26-group spectrum for the each calculational model zone.

All reactivity coefficients are received using the first order perturbation theory. It is necessary to note the increased uncertainty in results for the axial reflector and (in some cases) for the axial blankets, where because of processing technique features of the results the additional absolute error comes to ~0.001 from the peak value over the whole height of considered radial zone.

2.2. The used mesh point size and energy group divisions for the Phase 2 calculations

The used mesh point size and number of the used groups to obtain reactivity coefficients distribution are presented in Table 1. As one can see from Table 1, the planar mesh point size ranges from 3.3 cm up to 9.9 cm. The axial mesh point size ranges from 2.61 cm up to 10 cm. The energy group number ranges from 6 up to 230.

TABLE 1. THE USED MESH POINT SIZE AND THE NUMBER OF GROUPS

Participant	Method of the diffusion equation solution	The calculating cell geometry	The axial mesh points size for the core /for the axial blankets, cm	The number of energy groups
ANL	Finite difference	Triangle	?	230
CEA&AEAT	Finite difference	Hexagon	2.61? / ~5?	33
CIAE	Nodal	Hexagon	~10 / ~ 5	6, 12
IGCAR	Finite difference ?	Triangle ?	2.61? / ~2.5?	25?
IPPE	Nodal	Hexagon	?	18
JNC	?	Hexagon	~5 / ~ 5?	18
KAERI	Nodal	Hexagon	?	9
OKBM	Finite difference	Hexagon	3.48 / ~ 5	9,26

3. DEPENDENCES OF THE CALCULATION RESULTS ON A MESH POINT SIZE

3.1. Dependence of results on the planar calculation mesh point size

The changes in reactivity coefficients distributions due to the transition from the hexagonal calculating cell to the triangular one with respective change of the mesh point size are presented in Tables 2-7. The most essential changes are highlighted in the tables with the shading.

From Table 2 one can see, that the most change of the Doppler constant occurred in UB, especially above LEZ and MEZ, i.e. in the regions with the high absorber content. Taking into account the features of detailed axial distribution changes in such a character of the Doppler constant change indicates to some spectral hardening in the fuel zones, inside which there are cells with an absorber.

From Table 3 one can see, that due to decrease of the planar mesh point size the change characteristic of the steel Doppler constant is similar to that of the fuel Doppler constant (see Table 2). Taking into account of the more detailed axial distribution analysis, one can see the substantial increase of the Doppler constant inside the absorbing parts of SHR and SCR cells.

From Table 4 one can see, that the most sodium ‘worth’ change occurred in LEZ1, LEZ2, MEZ, MOX zone and also in SHR cells and UB regions. The additional analysis of more detailed axial distribution has shown the connection of the most of these changes with leakage changes in the vicinities of absorbing rods in SHR cells and in these cells. The relatively large decrease of the negative sodium ‘worth’ in MOX zone concerned with the affinity to zero of the sodium ‘worth’, that has caused its large sensitivity to the minor increase of a leakage in peripheral (HEZ and MOX) zones.

From Table 5 one can see, that the change of the steel ‘worth’ at decrease of the mesh point size is similar on the character to the change of the sodium ‘worth’, but is much less evident. It is possible to note relatively large change of the total coefficient, but it only indicates to its origin as the very small difference of relatively large values.

From Table 6 one can see, that the maximal changes have taken place in LEZ1, LEZ2 and in UB above them. The additional analysis of the more detailed axial distribution also has shown connection of these changes with the vicinity of SHR and SCR cells. Thus fuel ‘worth’ to the greatest degree has increased in a lower half of core and in the adjacent to the core UB regions.

From Table 7 one can see, that the absorber ‘worth’ is considerably increased at the decrease of the mesh point size which is corresponding to the hexagon division on the six triangles.

TABLE 2. THE CHANGE OF THE FUEL DOPPLER CONSTANT DISTRIBUTION, %rel.

Layer	LEZ1	LEZ2	MEZ	MOX	HEZ
UB	-10.8	-16.1	-11.7	-4.6	0.1
Core	0.4	0.1	-0.9	-2.1	1.9
LB	4.2	4.3	3.3	1.8	3.9
Total	-0.1				

TABLE 3. THE CHANGE OF THE STEEL DOPPLER CONSTANT DISTRIBUTION, %rel.

Layer	LEZ1	LEZ2	MEZ	MOX	HEZ	SHR	SCR	SSA1	SSA2	RR
UR	2.6	-31.4	-24.4	-20.5	3.4	-2.3	-27.3	1.2	7.1	23.7
UB	-8.4	-11.4	-10.4	-3.7	-0.4	48.3	-1.2	-1.1	3.9	23.3
Core	0.4	0.7	-1.5	-1.1	3.2	9.6	-3.6	1.2	6.9	23.6
LB	4.0	4.5	2.1	2.3	3.1	-4.7	-4.7	1.9	6.5	25.7
LR	2.6	2.9	0.8	13.5	3.4	-8.4	-9.1	1.2	7.1	23.7
Total	1.5									

TABLE 4. THE CHANGE OF THE SODIUM DENSITY COEFFICIENT DISTRIBUTION, %rel.

Layer	LEZ1	LEZ2	MEZ	MOX	HEZ	SHR	SCR	SSA1	SSA2	RR
UR	-5.9	-7.5	-4.9	-2.5	0.9	3.1	9.7	-3.5	1.0	-2.7
UB	-5.6	-5.0	-7.5	-4.1	-4.1	10.7	-5.1	3.5	5.8	-2.0
Core	7.3	7.8	24.0	-71.0	0.7	-6.2	3.8	3.9	4.6	-2.6
LB	2.8	2.7	1.2	0.2	-1.7	5.3	5.2	5.7	7.4	-0.9
LR	4.3	4.2	3.4	3.6	4.6	-12.1	-11.7	-0.7	3.1	6.5
Total	1.4									

TABLE 5. THE CHANGE OF THE STEEL ‘WORTH’ DISTRIBUTION, %rel.

Layer	LEZ1	LEZ2	MEZ	MOX	HEZ	SHR	SCR	SSA1	SSA2	RR
UR	1.8	-5.1	-4.4	-3.5	-3.5	-4.1	-3.5	-3.0	-0.4	-0.6
UB	-2.2	-3.1	-2.9	-2.6	-4.2	-0.9	-1.2	-2.3	-1.7	-2.3
Core	0.6	-0.1	-0.6	-0.7	-0.2	-5.4	-0.6	-0.6	-0.7	-0.6
LB	0.2	-1.7	-0.9	-2.4	-2.8	0.7	0.7	-1.2	-1.1	-0.5
LR	-2.3	-1.7	-3.4	-3.2	-1.1	-2.5	-2.4	-3.2	2.0	-0.6
Total	24.2									

TABLE 6. THE CHANGE OF THE FUEL ‘WORTH’ DISTRIBUTION, %rel.

Layer	LEZ1	LEZ2	MEZ	MOX	HEZ
UB	7.4	11.3	-0.3	-4.6	-10.0
Core	3.6	3.3	1.7	-1.7	1.3
LB	4.3	5.3	-4.1	-4.5	-6.9
Total	1.2				

TABLE 7. THE CHANGE OF THE ABSORBER ‘WORTH’ DISTRIBUTION, %rel.

Layer	SHR	SCR
UB	19.8	33.2
Core	18.7	
LB		
Total	18.8	

3.2. Dependence of results on the axial mesh points size

The OKBM calculations of all reactivity coefficients and the power distributions were carried out with the axial calculational pitch 3.48 cm for the core, because the adopted for results representation mesh size 10.44 cm seems to be too large. The mesh size in UB and LB amounts to ~5cm. The evaluation of the reactivity coefficients change at transition from the fine mesh size 3.48 cm to the too large size 10.44 cm seems to be expedient, as some results of other CRP participants were obtained with the large pitch size.

The changes of the axial reactivity coefficients distribution due to the increase of the mesh point size are presented in Tables 8-13. The most essential changes are highlighted in the tables with shading.

From Table 8 one can see, that the Doppler constant changes are insignificant and are expressed mainly in decrease of its values in the axial blankets, especially in upper ones — on 3.5%rel. From Table 9 one can see, that character and scale of the steel Doppler constant change are similar to those of the fuel Doppler constant change (see Table 8).

From Table 10 one can see, that the most sodium ‘worth’ changes occurred in axial blankets and in the MOX and SHR cells on the core level. The additional analysis of more detailed axial distribution has shown, that evident change in SHR cells concerned with the changes of the axial sodium ‘worth’ distribution near the lower absorber tip at the level of the core central plane.

From Table 11 one can see, that the change of the steel ‘worth’ due to the mesh point size increase on a character is similar to change of the sodium ‘worth’, but is much less evident. The relatively large change in the SHR cells also concerned with by redistribution of steel ‘worth’ near the absorber tip. The relatively large change of the total coefficient simply indicates to its origin as the very small difference of the relatively large values.

From Table 12 one can see, that the changes of the fuel ‘worth’ in the core are very small. The changes in axial blankets are a little bit more, but here it is necessary to mean the mentioned large processing uncertainty at the relatively small values.

From Table 13 one can see, that the absorber ‘worth’ due to the increase of the axial mesh size slightly decreases. From the analysis of detailed distribution follows, that the basic part of the change concerned with the decrease of the lower tip ‘worth’ in SHR cells.

TABLE 8. THE CHANGE OF THE FUEL DOPPLER CONSTANT DISTRIBUTION, %rel.

Layer	LEZ1	LEZ2	MEZ	MOX	HEZ
UB	-3.3	-4.4	-3.8	-3.4	-5.0
Core	1.0	0.5	0.5	-0.1	-0.3
LB	-1.5	-2.0	-2.3	-2.7	-3.8
Total	-0.1				

TABLE 9. THE CHANGE OF THE STEEL DOPPLER CONSTANT DISTRIBUTION, %rel.

Layer	LEZ1	LEZ2	MEZ	MOX	HEZ	SHR	SCR	SSA1	SSA2	RR
UR	-0.4	-0.5	-25.6	-40.3	-14.3	-17.6	-25.5	-100.0	49.0	-0.5
UB	-4.0	-2.9	-5.3	-4.9	-4.7	-5.1	-2.5	-3.8	-2.1	-1.1
Core	0.5	0.3	-0.2	-0.4	-0.1	1.9	-0.2	-0.4	-0.6	-0.5
LB	-2.3	-2.1	-3.4	-3.9	-4.1	-1.6	-1.3	-2.6	-2.3	-0.8
LR	-18.5	-13.5	-0.8	-14.7	-25.0	2.5	2.5	-100.0	49.0	4.5
Total	-0.2									

TABLE 10. THE CHANGE OF THE SODIUM DENSITY COEFFICIENT DISTRIBUTION, %rel.

Layer	LEZ1	LEZ2	MEZ	MOX	HEZ	SHR	SCR	SSA1	SSA2	RR
UR	-3.7	-3.7	-3.3	-3.8	-3.5	6.4	9.0	-2.5	-2.5	-1.1
UB	-4.0	-4.9	-5.3	-5.0	-6.4	-3.7	-0.2	-2.5	-1.6	-2.3
Core	-0.5	-1.5	-2.4	-10.5	0.1	20.0	0.2	-0.4	-0.6	-1.1
LB	-8.3	-7.6	-5.0	-4.4	-6.3	0.6	0.8	-1.8	-0.7	-1.6
LR	-1.3	-2.3	-2.9	-3.0	-3.6	-2.9	-2.5	-2.1	-0.4	-1.1
Total	0.3									

TABLE 11. THE CHANGE OF THE STEEL ‘WORTH’ DISTRIBUTION, %rel.

Layer	LEZ1	LEZ2	MEZ	MOX	HEZ	SHR	SCR	SSA1	SSA2	RR
UR	1.8	-5.1	-4.4	-3.5	-3.5	-4.1	-3.5	-3.0	-0.4	-0.6
UB	-2.2	-3.1	-2.9	-2.6	-4.2	-0.9	-1.2	-2.3	-1.7	-2.3
Core	0.6	-0.1	-0.6	-0.7	-0.2	-5.4	-0.6	-0.6	-0.7	-0.6
LB	0.2	-1.7	-0.9	-2.4	-2.8	0.7	0.7	-1.2	-1.1	-0.5
LR	-2.3	-1.7	-3.4	-3.2	-1.1	-2.5	-2.4	-3.2	2.0	-0.6
Total	24.2									

TABLE 12. THE CHANGE OF THE FUEL ‘WORTH’ DISTRIBUTION, %rel.

Layer	LEZ1	LEZ2	MEZ	MOX	HEZ
UB	-0.4	-3.6	-4.1	-5.1	-4.2
Core	0.9	0.0	-0.6	-0.4	-0.6
LB	-1.6	5.8	-6.5	1.2	-2.1
Total	-0.2				

TABLE 13. THE CHANGE OF THE ABSORBER ‘WORTH’ DISTRIBUTION, %rel.

Layer	SHR	SCR
UB	-1.6	-2.9
Core	-2.0	0.0
LB		
Total	-2.0	

4. THE INFLUENCE OF THE ENERGY GROUPS NUMBER AND THE CHOICE OF BOUNDARIES FOR THE GROUP DIVISION ON THE RESULTS

4.1 The comparison of calculations results in 26 and in 9 groups

The published earlier OKBM results for Phase 2 were obtained at the calculations in 9 energy groups with one planar mesh point on a hexagonal cell. The changes in reactivity coefficients distributions at transition from 9 energy groups to 26 groups are presented in Tables 14-19. The presented results are obtained at the comparison on the model with the hexagon division on six triangular cells. The most essential changes are highlighted in the tables with the shading.

From Table 14 one can see, that at the transition to 26 groups the Doppler constant mainly has increased in MOX and HEZ, and in their axial blankets. The increase amounts to 3.1%, 4.4% and ~6.5%, respectively.

From Table 15 one can see, that at the transition to 26 groups the steel Doppler constant most considerably varies in the peripheral row of the core (HEZ) and in the first row of the radial steel blanket (SSA1). From the analysis of more detailed axial distribution one can see relatively large increase of the Doppler constant inside the absorbing parts of SHR and SCR cells.

From Table 16 one can see, that sodium ‘worth’ is most significant (up to the sign reverse) has changed in MOX zone and in SHR cells. From the analysis of more detailed axial distribution one can see the shift of the sodium ‘worth’ toward positivity almost on all height of the MOX zone and on the absorber height in SHR. However the relatively minor increase of negative sodium ‘worth’ in LEZ and MEZ and decrease of the positive sodium ‘worth’ in the radial steel blanket have resulted to decrease of the total effect.

From Table 17 one can see, that change of the steel ‘worth’ distribution at transition to 26 energy groups is negligible except of the minor shift of the steel ‘worth’ toward the positivity in the SHR absorbing part. The relatively large change of the total coefficient only indicates to its origin as the very small difference of the relatively large values.

From Table 18 one can see, that at the transition to 26 energy groups the changes of the fuel ‘worth’ distribution in the core are very small. The minor increase (~0.4%) in the core is completely compensated by decrease of the fissile materials ‘worth’ in the axial blankets. From Table 19 one can see, that the absorber ‘worth’ at transition to 26 energy groups changes very little, and only at a level of the upper blanket its decrease by 3-4 % is evident.

TABLE 14. THE CHANGE OF THE FUEL DOPPLER CONSTANT DISTRIBUTION, %rel.

Layer	LEZ1	LEZ2	MEZ	MOX	HEZ
UB	2.5	2.1	2.9	5.8	6.0
Core	1.2	0.9	0.8	3.1	4.4
LB	3.6	3.2	3.9	6.0	6.5
Total	1.9				

TABLE 15. THE CHANGE OF THE STEEL DOPPLER CONSTANT DISTRIBUTION, %rel.

Layer	LEZ1	LEZ2	MEZ	MOX	HEZ	SHR	SCR	SSA1	SSA2	RR
UR	0.6	37.9	0.8	0.0	-7.7	0.6	33.5	5.5	3.0	-20.9
UB	0.6	1.3	1.5	2.6	14.8	10.2	2.0	4.5	-2.0	-18.2
Core	0.5	0.6	0.9	0.2	7.6	2.4	0.2	5.6	2.9	-13.0
LB	1.7	1.6	2.5	4.4	10.9	2.2	1.1	4.8	-1.2	-17.9
LR	9.8	0.9	0.8	0.0	-5.8	6.1	3.5	5.5	3.0	-21.3
Total	2.3									

TABLE 16. THE CHANGE OF THE SODIUM DENSITY COEFFICIENT DISTRIBUTION, %rel.

Layer	LEZ1	LEZ2	MEZ	MOX	HEZ	SHR	SCR	SSA1	SSA2	RR
UR	-8.3	-8.2	-8.1	-8.6	-9.4	-1.3	-8.9	-8.9	-12.2	-21.8
UB	-1.2	-1.6	-2.0	-2.1	-0.4	17.0	-1.0	-8.3	-14.9	-19.1
Core	2.6	1.1	2.1	-153.8	-0.8	22.4	-1.4	-0.2	-8.2	-15.2
LB	3.9	5.0	1.9	-0.6	-0.3	-1.6	-1.1	-7.1	-14.4	-18.8
LR	-5.7	-6.4	-7.0	-8.4	-9.4	-5.6	-4.7	-9.6	-13.2	-29.5
Total	-4.1									

TABLE 17. THE CHANGE OF THE STEEL ‘WORTH’ DISTRIBUTION, %rel.

Layer	LEZ1	LEZ2	MEZ	MOX	HEZ	SHR	SCR	SSA1	SSA2	RR
UR	-6.5	-6.7	-5.7	-4.8	-8.5	-8.4	-5.3	-11.2	-12.5	-13.8
UB	-0.7	0.0	-0.7	-1.3	-2.6	2.4	-1.1	-1.7	-5.5	-10.8
Core	0.0	0.1	0.4	-0.6	-2.8	-8.4	-0.1	-0.7	-1.6	-6.8
LB	0.8	2.0	0.4	-0.7	-2.9	-1.8	-1.9	-0.8	-4.7	-10.6
LR	-4.3	-4.0	-3.2	-5.6	-8.3	-4.5	-3.6	-12.2	-18.1	-18.5
Total	58.6									

TABLE 18. THE CHANGE OF THE FUEL ‘WORTH’ DISTRIBUTION, %rel.

Layer	LEZ1	LEZ2	MEZ	MOX	HEZ
UB	0.5	-0.5	-0.9	-2.0	-2.5
Core	0.5	0.3	0.4	-0.4	-0.4
LB	-3.9	-1.7	0.4	-3.5	-5.7
Total	0				

TABLE 19. THE CHANGE OF THE ABSORBER ‘WORTH’ DISTRIBUTION, %rel.

Layer	SHR	SCR
UB	-3.3	-4.6
Core	-0.5	
LB		
Total	-0.6	

4.2 The influence on results of sodium ‘worth’ calculation of the boundaries choice for the energy group division

Some CRP participants have obtained the results using the few group calculations. The value of a corresponding additional uncertainty strongly depends on number of the used energy groups and the choice of the boundaries for the energy group division.

It was decided to compare the used few group divisions at the analysis of the sodium ‘worth’ calculation results. The calculations were carried out on the OKBM method used for the earlier published results, but in all now considered cases the calculations with the triangular cell was used. Among themselves calculations differed only with few group divisions.

The energy scale and the energy groups boundaries location on it for compared cases is presented in Table 20. In addition to the real energy boundaries for the foreign participants the assumed boundaries are presented. These assumed boundaries were adopted to bring the energy division to used 26 group initial library BNAB-78. This discrepancy slightly limits the direct application of the proposed comparison results, but should not influence character of the received uncertainties and the subsequent conclusions relative to the calculation method.

The calculational results of the sodium ‘worth’ obtained for the examined energy divisions, are presented in Table 21 for the basic model zones. In this table the shading highlight the results closest to results 26 group calculations.

TABLE 20. THE BOUNDARIES OF ENERGY GROUPS

Upper energy, eV	Real KAERI 9 group	Real CIAE 6 group	Real CIAE 12 group	OKBM 9 group	OKBM 26 group scale	Assumed KAERI 9 group	Assumed CIAE 6 group	Assumed CIAE 12 group
2.000E+07	1							
1.492E+07		1	1					
1.050E+07				1	1	1	1	1
6.500E+06					2			2
6.065E+06	2		2					
4.000E+06					3	2		
2.500E+06					4			3
2.231E+06			3					
1.400E+06				2	5	3	2	
1.353E+06	3	2						
8.209E+05			4					
8.000E+05					6		3	4
4.979E+05	4	3						
4.000E+05				3	7	4		
2.000E+05					8	5		5
1.832E+05	5		5					
1.000E+05				4	9			
6.738E+04	6							
4.650E+04				5	10	6	4	6
4.087E+04		4	6					
2.479E+04	7							
2.150E+04					11	7		
1.033E+04				6	12	8	5	7
9.119E+03	8	5	7					
5.531E+03			8					
4.650E+03				7	13	9		8
3.355E+03	9							
2.150E+03				8	14			9
2.035E+03			9					
1.234E+03			10					
1.000E+03				9	15			10
4.540E+02		6			16		6	
2.150E+02					17			
1.013E+02					18			
6.144E+01			11					
4.650E+01					19			11
2.150E+01					20			
1.000E+01					21			
4.650E+00					22			
2.150E+00					23			12
1.860E+00			12					
1.000E+00					24			
4.650E-01					25			
2.530E-02				26				

From Table 21, one can see that with the increase of the group number the results come close to the 26 group calculational results. It is necessary to note, that at the OKBM 9 group division scheme the sodium ‘worth’ in a core (except for MOX zone) practically agrees with the obtained by 26 group ‘worth’ calculations. Besides it is necessary to stress that sodium ‘worth’ in the MOX zone is lower about 100 times than values for other core zones, i.e. the absolute uncertainty here is very small (except for the 6 group calculations).

TABLE 21. DISTRIBUTION OF SODIUM 'WORTH' ON THE BASIC MODEL ZONES

The scheme of energy groups		Value for zone / deviation from the 26 group OKBM results, % rel.						
		LEZ+MEZ	MOX	HEZ	Core	Blankets	SSA1+SSA2	Whole model
KAERI 9 group	4.28E-05 -8.3	-5.41E-07 +40.0	-3.14E-05 +5.2	1.08E-05 -34.0	-9.75E-06 -19.2	-8.03E-05 -4.1	-1.19E-04 -3.6	
CIAE 6 group	3.88E-05 -16.8	2.74E-06 -807.9	-3.23E-05 +8.2	9.24E-06 -43.7	-9.24E-06 -23.5	-8.83E-05 +5.5	-1.29E-04 +4.7	
CIAE 12 group	4.52E-05 -3.2	-2.73E-07 -29.5	-3.06E-05 2.4	1.43E-05 -12.7	-1.14E-05 -5.6	-8.73E-05 +4.3	-1.27E-04 +3.0	
OKBM 9 group	4.58E-05 -1.7	7.06E-07 -283	-2.99E-05 +0.3	1.66E-05 +1.1	-1.20E-05 -0.7	-8.82E-05 +5.3	-1.28E-04 +4.2	
OKBM 26 group	4.66E-05	-3.86E-07	-2.98E-05	1.64E-05	-1.21E-05	-8.37E-05	-1.23E-04	

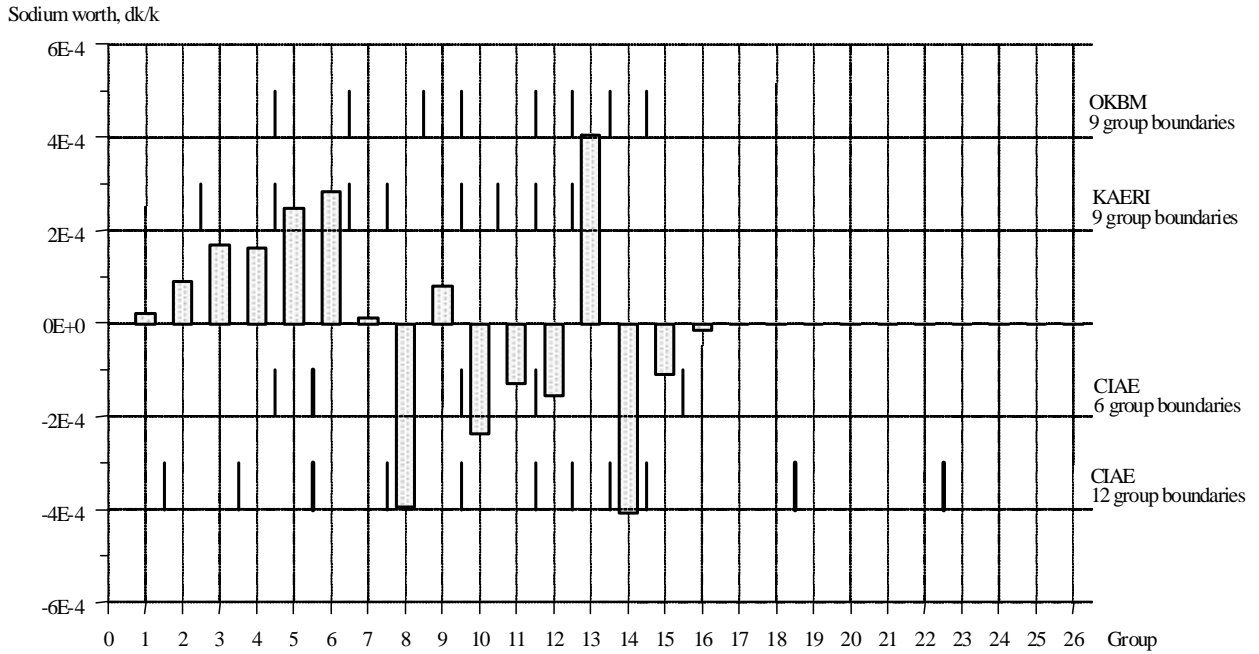


FIG. 1. Sodium worth distribution on energy groups (for fissile zones).

For the explanation of the principle of the optimal group division choice, let's consider the sodium 'worth' distribution presented in Fig. 1 on 26 energy groups. The optimal collapsing of the initial 26 groups is provided at the grouping of the adjacent groups only with the close sodium 'worth', i.e. the boundaries for the collapsed groups on distribution of sodium 'worth' should be chosen in terms of essential change of its value. It is especially important to divide the groups with opposite signs and the comparable absolute values of the sodium 'worth'. At such group division the mistake of the sodium 'worth' originated from the cross sections averaging in case of the coupling of groups with different value of the neutron flux will be minimal. From Fig. 1 one can see, that the OKBM with 9 groups and CIAE with 12 groups few group division schemes well correspond to the proposed principle, but in the CIAE scheme with 12 groups the desirable boundaries 4/5, 6/7 and 8/9 groups are not established. On the other hand, in this scheme there are useless boundaries 18/19 and 22/23 groups. The considered principle can be proposed for the group division choice for calculation of any other neutron flux functionals with the strong dependence on neutron energy.

5. CONCLUSIONS

1. Among the examined calculation method parameters most essential is the planar mesh points size. The use of the one point in hexagon instead of the mesh with one point in the triangular cell causes the following additional uncertainties:
 - overestimation of the fuel Doppler effect by 5-15% in the upper blanket;
 - overestimation of the steel Doppler effect by 4-11% in the upper blanket and underestimation by 10-33 % in SHR cells;
 - underestimation of negative sodium 'worth' in LEZ and MEZ by 7-20% and overestimation of positive sodium 'worth' in the upper blanket by 4-7%.
 - overestimation of positive steel 'worth' by 2-4% in the upper blanket;
 - insignificant redistribution of the fuel 'worth' with its underestimation by ~3% at the core centre;
 - significant underestimation (by ~15-20%) of the absorber 'worth'.
2. The use of the large axial mesh size (~10.5 cm instead of ~3.5 cm) leads to the following possible errors:

- underestimation of the steel and fuel Doppler constant by 1.5-4% in the lower axial blanket and by 3-5 % in the upper axial blanket;
 - underestimation in axial blankets of the sodium ‘worth’ by 4-8% and ‘worths’ of steel by 0-4%;
 - underestimation of the absorber ‘worth’ by 2%.
3. The principle of the choice of the energy scale optimum division is proposed for the few group calculations. The using of the optimal few group division scheme instead of the fine group calculation can lead to the following additional uncertainties:
- underestimation of the fuel Doppler constant by 3-4% in HEZ and MOX zone and by 2-6% in axial blankets;
 - underestimation of the steel Doppler constant by 8-15% in HEZ and by ~5% in the first SSA1 row;
 - overestimation by 0-15% of the sodium ‘worth’ in SSA1 and SSA2 zones.
4. Depending on group division scheme the use of few group calculation for the sodium ‘worth’ determination may cause the uncertainty in range from +1% rel. up to -45% rel. for the core and from -1% rel. up to -24% rel. for the axial blankets.

REFERENCE TO APPENDIX I

- [1] DANILYTCHEV, A., et al., ‘INPUT DATA FOR BN-600 HYBRID CORE BENCHMARK CALCULATIONS’ paper presented in the first Research Co-ordination Meeting of the Co-ordinated Research Project ‘in the First Research Co-ordination Meeting of the Research Co-ordination Project ‘Updated Codes and Methods to Reduce the Calculational Uncertainties of the LMFR Reactivity Effects’, Vienna, 24-26 November 1999.

Appendix II

SENSITIVITY ANALYSIS OF JEF AND JENDL

M. Ishikawa
 O-arai Engineering Center
 Japan Nuclear Cycle Development Institute (JNC), Japan

1. INTRODUCTION

The present work is corresponding to the Action 3.6 in the 3rd meeting report, that is, ‘JNC to provide a sensitivity analysis of cross-section for the Summary Report.’ Here, The effects of cross-section differences between two libraries, JEF-2.2R (Pu-239 is revised to be the same as that used by CEA/SA) and JENDL-3.2 were evaluated for three core parameters, k_{eff} , sodium density coefficient and burnup reactivity loss, of BN-600 3-D Hex-Z homogeneous benchmark model.

2. ANALYTICAL METHOD

Sensitivity of a core parameter R to cross-sections are defined as follows:

$$S_{m,x,g} = \frac{dR / R}{d\sigma_{m,x,g} / \sigma_{m,x,g}},$$

where R: core parameter,

m: nuclide,

x: reaction type, and

g: energy group number.

Sensitivity was evaluated by the SAGEP code based on the generalized perturbation theory.

$$\frac{R_{\text{JEF}} - R_{\text{JENDL}}}{R_{\text{JENDL}}} = \sum_{m,x} \sum_g \left[S_{m,x,g} \times \frac{\sigma_{m,x,g,\text{JEF}} - \sigma_{m,x,g,\text{JENDL}}}{\sigma_{m,x,g,\text{JENDL}}} \right]$$

Contribution of each cross-section to the effect of library difference is calculated as follow:

- Relative differences of the cross-sections between JEF-2.2R and JENDL-3.2 are shown in Table 1. Sensitivity values of BN-600 core parameters can be found in the 2nd CRP meeting material, Nov. 2000, presented by JNC.
- The sensitivity study used a 18-group cross-sections, the energy group structure of which are given by (denoted by Group No./Upper energy boundary):

1/ 10.0MeV	2/ 6.07MeV,	3/ 3.68MeV,	4/ 2.23MeV,	5/ 1.35MeV,
6/ 821keV,	7/ 388keV	8/ 183keV	9/ 86.5keV	10/ 40.9keV,
11/ 19.3keV	12/ 9.12keV,	13/ 4.31keV,	14/ 2.03keV,	15/ 961eV,
16/ 454eV,	17/ 214eV,	18/ 101eV (Lowest energy boundary/1.0E-5eV)		

- Effective microscopic cross-sections treated are given for the following nuclides: B-10, B-11, C-12, O-16, Na-23, Cr(Nat.), Fe(Nat.), Ni(Nat.), U-235, U-238, Pu-239, Pu-240, Pu-241, FP(U-235);
- Reactions are considered for the following types: capture, fission, v, elastic, inelastic, (n,2n), μ -avg. (scattering reactions are matrix-wise);
- Other nuclear parameters taken into account are:
Fission spectrum (18 groups): χ (U-235), χ (Pu-239) (\otimes delayed neutron is not needed in this survey).

3. RESULTS

3.1. k_{eff}

The nuclide and reaction-wise contribution to k_{eff} difference are summarized in Fig.1. The k_{eff} of JEF-2.2R is larger than that of JENDL-3.2 by 0.6%dk according to the sensitivity summation, while the k_{eff} value of the diffusion-based direct calculation by JEF-2.2R (CEA) was 1.0155 and that of JENDL-3.2 (JNC) was 1.0071 in the synthesis report, Nov. 2001 by IAEA, see Table 3.24. The coincidence between sensitivity and direct calculation is satisfactory.

The large contribution to k_{eff} difference between JEF and JENDL came from the cross-sections of U-235 and iron.

3.2. Sodium density reactivity

The nuclide and reaction-wise contribution to sodium density reactivity difference are shown in Fig.2. The relative difference by sensitivity analysis is -26%, while that of direct calculation was -42%. (In the Table 3.27 of the synthesis report, the sodium density coefficient by JEF-2.2R (CEA) was 0.00601, and that of JENDL-3.2. (JNC) was 0.01038.). In spite of the complicated mechanism of sodium density reactivity, the agreement between sensitivity and direct calculation is rather excellent.

The largest components of sodium density reactivity difference between JEF and JENDL were U-235 capture reaction and Iron elastic reaction.

3.3. Burnup reactivity loss

The nuclide- and reaction-wise contribution to burnup reactivity loss difference are shown in Fig. 3. Regarding these results, more details of the contributions and sensitivity coefficients are given in Tables 2 and 3, respectively. The relative difference by sensitivity analysis is -2%, while that of direct calculation was +9%. (In the 3rd Meeting report, the burnup reactivity loss by JEF-2.2R (CEA) was 2.62%dk/kk', and that of JENDL-3.2. (JNC) was 2.41%dk/kk'.) Though the absolute difference of burnup reactivity loss by two libraries is small, the agreement between sensitivity and direct calculation does not seem to be good. Further investigation may be needed for the difference of analytical method such as burnup chain.

The large contribution to the difference between two libraries came from the major heavy nuclides, that is, U-235 capture and U-238 capture reactions.

4. CONCLUSIONS

The nuclide- and reaction-wise contribution to the effect of the library change was analyzed by the sensitivity method for the important core parameters of BN-600 Hex-Z benchmark model, which include k_{eff} , sodium density reactivity and burnup reactivity loss. The difference of the evaluated values between CEA and JNC was found to be mainly the results of the library difference between JEF-2.2R and JENDL-3.2, and the dominant nuclides were identified.

TABLE 1. DIFFERENCE OF CROSS SECTIONS BETWEEN JEF-2.2R AND JENDL-3.2 (1/2)

$[(JEF-2.2R)-(JENDL-3.2)]/(JENDL-3.2)*100(\%)$											
Nuclide Reaction		Pu-239	C-12	O-16	O-16	Na-23	Na-23	Na-23	Cr(Nat.)	Fe(nat.)	Fe(nat.)
Group	Upper E. (eV)	χ	CAP	Elastic	Inelastic	μ	Capture	Elastic	Inelastic	μ	Elastic
1	1.00E+07	1.2	-2.9	-7.6	3.0	-45.3	-1.3	-10.8	0.0	-1.8	0.8
2	6.07E+06	1.8	11.8	2.1	-6.6	-6.6	-7.6	0.0	0.0	-8.6	1.2
3	3.68E+06	0.5	-44.4	-0.8	0.0	52.1	0.1	-5.3	0.0	-0.1	0.8
4	2.23E+06	-0.8	-80.3	1.3	0.0	23.7	-0.1	-3.8	-0.7	-0.5	-2.3
5	1.35E+06	-0.9	-92.8	0.5	0.0	2.1	0.1	-1.4	-3.2	0.0	3.3
6	8.21E+05	-2.0	-95.2	0.4	0.0	-2.3	1.0	-0.8	-2.9	-0.4	-46.8
7	3.88E+05	1.4	-95.7	0.6	0.0	-0.7	-0.1	0.2	0.0	-0.5	-30.1
8	1.83E+05	6.5	-95.1	1.9	0.0	11.8	4.9	0.1	0.0	-0.2	15.9
9	8.65E+04	7.5	-93.4	2.5	0.0	-10.8	4.1	0.9	0.0	5.6	6.1
10	4.09E+04	8.6	-91.6	2.7	0.0	-8.9	0.8	0.0	0.0	42.9	3.4
11	1.93E+04	10.4	-89.8	2.8	0.0	-11.0	2.1	0.3	0.0	-0.4	-4.1
12	9.12E+03	10.0	-86.8	2.8	0.0	-5.0	6.5	-1.3	0.0	-0.3	-37.4
13	4.31E+03	11.9	-11.8	2.8	0.0	-2.7	0.6	0.1	0.0	-0.2	9.1
14	2.04E+03	10.9	-2.5	2.9	0.0	-1.4	-1.5	-1.7	0.0	-0.1	-12.4
15	9.61E+02	0.0	-9.7	2.9	0.0	-0.6	-0.1	-0.2	0.0	-0.1	8.8
16	4.54E+02	0.0	-7.2	2.9	0.0	-0.4	0.3	-0.1	0.0	-0.2	6.2
17	2.14E+02	0.0	-4.8	2.9	0.0	-0.2	0.4	-0.1	0.0	-0.2	3.3
18	1.01E+02	0.0	-2.8	2.9	0.0	0.0	0.8	-0.1	0.0	-0.2	1.9

$[(JEF-2.2R)-(JENDL-3.2)]/(JENDL-3.2)*100(\%)$											
Nuclide Reaction		Fe(nat.)	Fe(nat.)	Ni(Nat.)	U-235	U-235	U-235	U-238	U-238	U-238	U-238
Group	Upper E. (eV)	INEL	26	26	28	925	925	925	928	928	928
1	1.00E+07	0.4	2.2	4.1	**	**	**	**	**	**	**
2	6.07E+06	-4.7	-1.1	3.6	-254.5	-1.4	-1.7	2.8	-56.1	-0.8	-0.2
3	3.68E+06	-15.8	-4.5	1.8	62.8	-1.6	-1.4	3.1	9.6	-2.1	0.0
4	2.23E+06	2.4	-8.4	-2.8	22.2	-2.1	-0.9	10.7	24.7	-2.2	0.0
5	1.35E+06	10.4	-15.5	-22.3	3.2	-2.4	-0.3	13.8	1.6	-2.7	0.0
6	8.21E+05	19.8	-20.6	-10.6	-3.7	-0.3	-0.2	6.5	-1.0	0.3	-1.1
7	3.88E+05	16.0	-17.9	-15.0	5.4	0.5	0.0	6.4	-6.4	0.0	1.4
8	1.83E+05	-26.1	-16.5	-14.4	-12.7	-0.3	-0.3	-1.0	186.6	0.0	-7.7
9	8.65E+04	-12.0	7.9	-36.3	-9.3	0.2	0.9	-8.8	-0.3	6.1	4.7
10	4.09E+04	-35.6	-0.6	-21.5	-3.7	1.9	1.0	-39.3	1.6	-30.9	0.0
11	1.93E+04	-15.2	23.0	9.1	7.4	3.8	0.6	-59.6	2.6	344.9	0.0
12	9.12E+03	0.0	10.4	3.2	4.3	0.9	0.6	-59.8	-0.9	7.3	0.0
13	4.31E+03	0.0	3.1	1.2	1.8	2.7	0.9	-42.4	0.4	0.1	0.0
14	2.04E+03	0.0	0.7	1.8	23.8	-1.8	0.6	***	0.3	3.3	0.0
15	9.61E+02	0.0	-0.2	1.5	1.25	3.2	0.8	***	0.1	1.1	0.0
16	4.54E+02	0.0	-0.1	1.3	-2.6	2.3	1.3	***	1.1	0.0	0.0
17	2.14E+02	0.0	-0.1	1.2	-4.7	2.7	2.0	***	-1.7	0.0	0.0
18	1.01E+02	0.0	-0.1	1.1	-0.1	0.7	1.2	***	2.2	1.2	0.0

$[(\text{JEF-2.2R}) - (\text{JENDL-3.2})]/(\text{JENDL-3.2}) \times 100[\%]$

Group	Nuclide	Upper E. (eV)	U-238 μ	Pu-239 Capture	Pu-239 Fission	Pu-239 ν	Pu-239 Inelastic	Pu-239 μ	Pu-239 NU	Pu-240 Capture	Pu-240 Fission	Pu-240 ν	Pu-241 Capture	Pu-241 Fission	Pu-241 CAP	Pu-241 NU	Pu-241 o
1	1.00E+07		-0.2	228.7	-3.9	-0.3	21.1	1.6	0.4	-2.8	-0.2	62.2	-3.6	-1.1			
2	6.07E+06	-0.1	82.9	-1.0	-0.4	2.6	1.1	3.4	-0.9	-0.2	128.5	-2.8	-0.9				
3	3.68E+06	-0.2	52.8	-0.4	-0.5	0.4	1.9	0.8	0.1	-0.1	187.2	-2.5	-0.5				
4	2.23E+06	-0.1	53.0	0.8	0.3	-4.0	4.0	0.2	-0.2	0.0	148.5	-2.8	-0.3				
5	1.35E+06	0.1	32.3	0.5	-0.1	-9.5	0.4	0.1	1.3	0.0	92.4	-0.1	-0.2				
6	8.21E+05	-0.2	11.5	1.9	0.0	-17.9	7.6	0.3	4.4	0.0	59.3	0.1	-0.1				
7	3.88E+05	-0.4	4.3	-0.5	-0.1	-23.0	-10.1	0.3	10.0	0.0	41.9	0.4	0.0				
8	1.83E+05	-0.3	1.6	1.2	-0.2	-29.7	-13.5	0.3	-1.9	0.0	41.4	1.3	0.0				
9	8.65E+04	-0.3	2.2	0.6	-0.4	-27.0	-23.8	-8.0	-12.6	0.0	16.7	3.1	0.0				
10	4.09E+04	-0.6	-2.5	-4.1	0.5	-30.8	-12.2	-13.8	0.0	5.2	-0.9	0.0	0.0				
11	1.93E+04	-3.2	2.0	-2.8	-1.3	1.4	-3.5	-30.8	-11.3	0.0	-1.4	-2.2	0.0				
12	9.12E+03	-32.7	-2.1	-2.6	-1.5	49.5	-30.0	-1.2	-37.1	0.0	-8.8	-4.3	0.0				
13	4.31E+03	113.0	-8.4	-2.4	-1.6	0.0	12.4	0.2	157.3	0.0	-7.3	-3.0	0.0				
14	2.04E+03	51.9	-4.3	4.4	-1.6	0.0	16.0	0.2	47.9	0.0	-12.4	-0.9	0.0				
15	9.61E+02	24.4	-1.1	-2.5	-1.4	0.0	0.0	-0.1	25.4	0.0	-8.8	9.0	0.0				
16	4.54E+02	9.5	1.9	-1.9	-0.3	0.0	0.0	-0.1	342.9	0.0	-16.9	0.1	0.0				
17	2.14E+02	2.4	2.3	-2.9	-0.4	0.0	0.0	1.0	578.4	0.0	-5.4	2.4	0.0				
18	1.01E+02	0.0	2.6	-2.6	0.1	0.0	0.0	1.0	492.7	0.0	-3.6	2.8	0.0				

Group	Nuclide	Upper E. (eV)	U-235 χ	FPU-235 Capture	B-10 (n, α)	B-11 Capture
1	1.00E+07		2.9	0.0	8.5	-50.0
2	6.07E+06	2.0	0.5	7.3	-69.5	
3	3.68E+06	1.1	-0.2	6.1	-54.6	
4	2.23E+06	0.3	-0.1	-9.5	-59.8	
5	1.35E+06	-0.7	-0.2	-17.3	-76.2	
6	8.21E+05	-1.8	0.1	-1.6	-27.4	
7	3.88E+05	-2.1	0.0	2.8	-39.3	
8	1.83E+05	-2.0	0.0	2.3	-45.4	
9	8.65E+04	-2.5	-0.1	1.0	-38.2	
10	4.09E+04	-2.5	0.1	2.2	25.4	
11	1.93E+04	-2.1	0.1	1.2	294.2	
12	9.12E+03	-2.6	-0.9	1.0	-10.0	
13	4.31E+03	-2.5	0.2	1.7	-3.8	
14	2.04E+03	-2.1	0.2	1.4	-1.4	
15	9.61E+02	0.0	0.3	1.2	0.6	
16	4.54E+02	0.0	0.0	1.2	3.0	
17	2.14E+02	0.0	0.5	1.1	4.6	
18	1.01E+02	0.0	1.5	1.2	6.2	

No.	Nuclide and Reaction	$\Delta R/R\ (%)$	Contribution (%)
1	Pu-239 χ	0.01	1.6
2	C-12 Capture	0	0.0
3	O-16 Elastic	-0.09	-14.1
4	O-16 Inelastic	0	0.0
5	O-16 μ	-0.01	-1.6
6	Na-23 Capture	0	0.0
7	Na-23 Elastic	-0.06	-9.4
8	Na-23 Inelastic	0.02	3.1
9	Na-23 μ	0	0.0
10	Cr(Nat.) μ	0	0.0
11	Fe(Nat.) Capture	0.25	39.1
12	Fe(Nat.) Elastic	0.14	21.9
13	Fe(Nat.) Inelastic	0.05	7.8
14	Fe(Nat.) μ	0.11	17.2
15	Ni(Nat.) μ	0.01	1.6
16	U-235 Capture	-0.03	-4.7
17	U-235 Fission	0.21	32.8
18	U-235 v	0.23	35.9
19	U-235 Inelastic	-0.01	-1.6
20	U-238 Capture	-0.13	-20.3
21	U-238 Fission	-0.12	-18.8
22	U-238 v	-0.01	-1.6
23	U-238 Elastic	0.01	1.6
24	U-238 Inelastic	0.13	20.3
25	U-238 μ	0	0.0
26	Pu-239 Capture	0	0.0
27	Pu-239 Fission	-0.03	-4.7
28	Pu-239 v	-0.09	-14.1
29	Pu-239 Inelastic	-0.01	-1.6
30	Pu-239 μ	0	0.0
31	Pu-240 Capture	0.01	1.6
32	Pu-240 Fission	0	0.0
33	Pu-240 v	0	0.0
34	Pu-241 Capture	0	0.0
35	Pu-241 Fission	0	0.0
36	Pu-241 v	0	0.0
37	U-235 χ	0.08	12.5
38	FP(U-235) Capture	0	0.0
39	B-10 (N,g)	-0.03	-4.7
40	B-11 Capture	0	0.0
Total		0.64	100.0

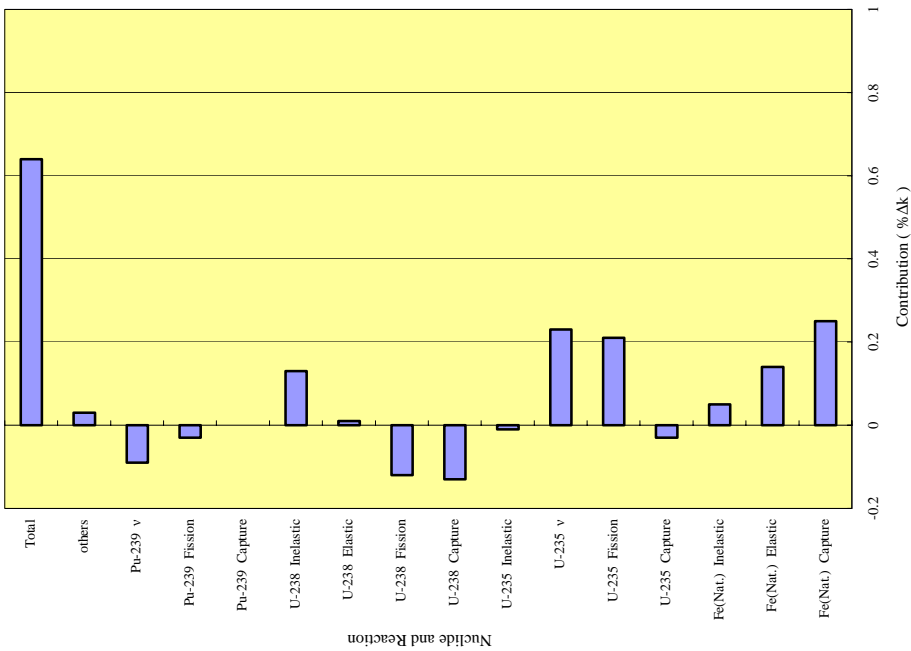


FIG. 1. Nuclide-wise contribution (k_{eff} difference) (cross-section difference between JEF-2.2R and JENDL-3.2).

No.	Nuclide and Reaction	$\Delta R/R$ (%)	Contribution (%)
1	Pu-239 γ	-0.2	0.7
2	C-12 Capture	0.0	-0.7
3	O-16 Elastic	2.9	-0.0
4	O-16 Inelastic	0.0	-11.1
5	O-16 μ	0.2	-0.1
6	Na-23 Capture	-0.1	-0.6
7	Na-23 Elastic	-5.5	0.2
8	Na-23 Inelastic	2.2	21.1
9	Na-23 μ	0.0	-8.5
10	Cr(Nat.) μ	0.3	U-235 Capture
11	Fe(Nat.) Capture	-3.1	U-235 Fission
12	Fe(Nat.) Elastic	-9.5	U-235 v
13	Fe(Nat.) Inelastic	-0.9	U-238 Capture
14	Fe(Nat.) μ	-4.5	U-238 Fission
15	Ni(Nat.) μ	-0.3	U-238 v
16	U-235 Capture	-10.4	Pu-239 Capture
17	U-235 Fission	3.3	Pu-239 Fission
18	U-235 v	4.1	Pu-239 v
19	U-235 Inelastic	0.2	Total
20	U-238 Capture	-1.2	others
21	U-238 Fission	1.8	
22	U-238 v	0.1	
23	U-238 Elastic	-0.1	
24	U-238 Inelastic	-3.1	
25	U-238 μ	-0.1	
26	Pu-239 Capture	0.7	
27	Pu-239 Fission	-0.9	
28	Pu-239 v	-1.7	
29	Pu-239 Inelastic	0.2	
30	Pu-239 μ	-0.1	
31	Pu-240 Capture	0.0	
32	Pu-240 Fission	0.0	
33	Pu-240 v	0.0	
34	Pu-241 Capture	0.0	
35	Pu-241 Fission	0.0	
36	Pu-241 v	0.0	
37	U-235 χ	-1.0	
38	FP(U-235) Capture	0.0	
39	B-10 ($N\alpha$)	0.2	
40	B-11 Capture	0.0	
	Total	-26.1	100.0

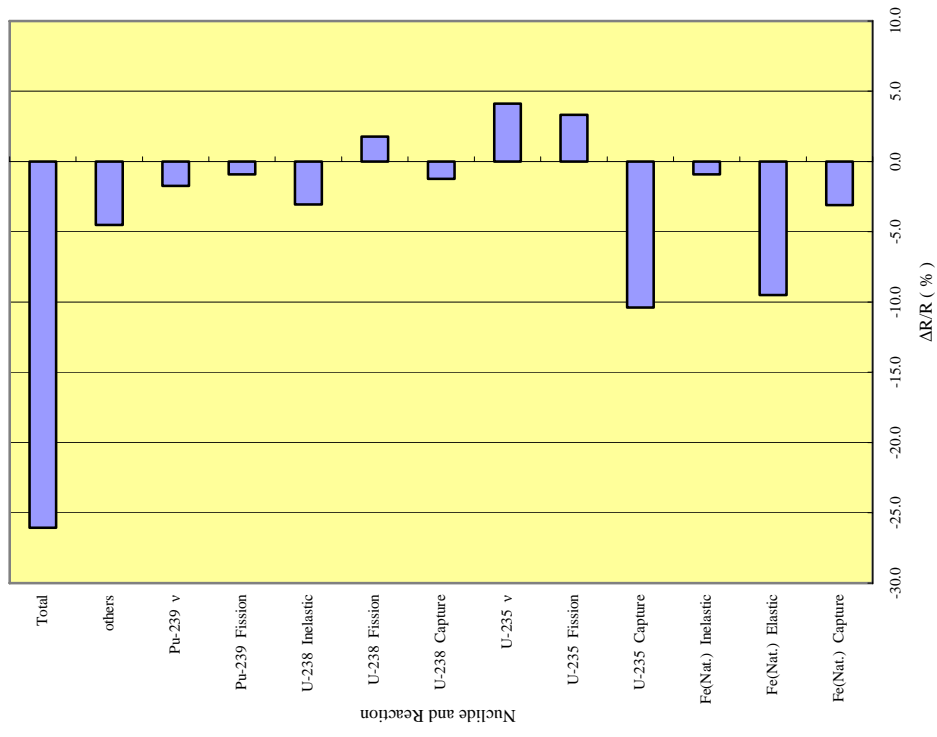


FIG. 2. Nuclide-wise contribution (sodium reactivity difference) (cross-section difference between JEF-2.2R and JENDL-3.2).

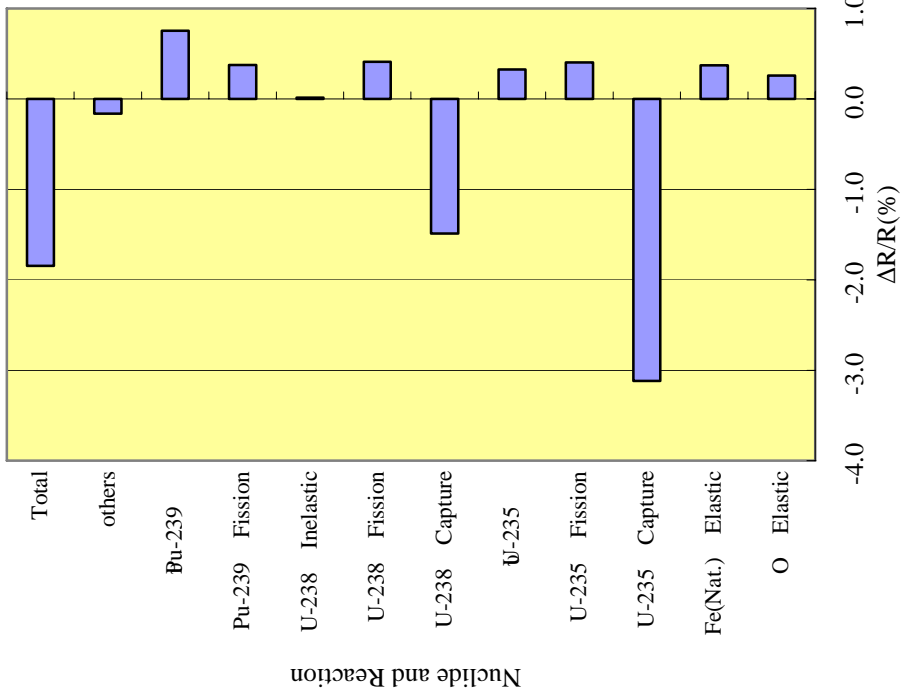


FIG. 3. Nuclide-wise contribution (burnup reactivity differences) (cross-section difference between JEF-2.2R and JENDL-3.2).

No.	Nuclide and Reaction	$\Delta R/R(\%)$	Contribution(%)	Nuclide and Reaction	$\Delta R/R(\%)$	Contribution(%)
1	O Elastic	0.26	-14.0	O Elastic	0.26	0.26
2	O Inelastic	0.00	-0.1	Fe(Nat.) Elastic	0.37	0.37
3	ϕ	0.01	-0.4	U-235 Capture	-3.12	-3.12
4	Na Capture	0.00	0.0	U-235 Fission	0.40	0.40
5	Na Elastic	0.02	-1.3	U-235 U	0.33	0.33
6	Na Inelastic	-0.05	2.5	U-238 Capture	-1.49	-1.49
7	Na	0.00	0.0	U-238 Fission	0.41	0.41
8	Cr(Nat.) Elastic	0.00	0.0	U-238 Fission	0.02	0.02
9	Cr(Nat.) Inelastic	0.00	0.0	Pu-239 Elastic	0.38	0.38
10	Fe(Nat.) Capture	-0.11	5.7	Pu-239 Fission	0.76	0.76
11	Fe(Nat.) Elastic	0.37	-20.2	Pu-239 U	-0.16	-0.16
12	Fe(Nat.) Inelastic	-0.07	3.9	Total	-1.85	-1.85
13	Re(Nat.)	-0.02	0.9	U-238 Inelastic		
14	Ni(Nat.)	0.00	0.1	U-238 Capture		
15	U-235 Capture	-3.12	168.9	U-238 Fission		
16	U-235 Fission	0.40	-21.9	U-235 Capture		
17	U-235	0.33	-17.7	U-235 Fission		
18	U-235 Inelastic	0.02	-0.9	U-235		
19	U-238 Capture	-1.49	80.5	O		
20	U-238 Fission	0.41	-22.2	Elastic		
21	U-238	0.01	-0.5	Capture		
22	U-238 Elastic	0.02	-1.1	Fission		
23	U-238 Inelastic	0.20	-10.6	Fe(Nat.)		
24	U-238	0.00	0.0	Capture		
25	Pu-239 Capture	-0.06	3.4	Fission		
26	Pu-239 Fission	0.38	-20.4	Elastic		
27	Pu-239	0.76	-41.0	Total	-1.85	-1.85
28	Pu-239 Inelastic	-0.09	5.1	Total	100.0	100.0
29	Pu-239	-0.01	0.5			
30	Pu-240 Capture	0.00	0.0			
31	Pu-240 Fission	-0.06	3.2			
32	Pu-240	0.00	-0.1			
33	Pu-241 Capture	0.04	-2.1			
34	Pu-241 Fission	0.00	-0.3			
35	Pu-241	0.00	0.0			
36	FPU-235 Capture	0.00	-0.3			
37	FPU-235 Inelastic	0.00	0.0			
Total		-1.85	100.0			

TABLE 2. NUCLIDE AND REACTION-WISE SENSITIVITY COEFFICIENTS FOR BURNUP REACTIVITY LOSS (1/2)

		(UNIT : 1.0E-4)																		
NUCLIDE	REACTION	TOTAL	1G	2G	3G	4G	5G	6G	7G	8G	9G	10G	11G	12G	13G	14G	15G	16G	17G	18G
U-235	CAPTURE	1511	-7	-1	1	7	16	64	123	209	229	205	158	126	66	176	94	33	12	0
NU		12632	52	163	417	583	633	1483	1795	2012	1788	1376	926	532	228	359	134	62	24	59
FUSION		12373	46	146	372	540	609	1442	1736	1941	1704	1305	833	537	245	432	194	74	22	28
ELASTIC,SCT		86	0	1	3	4	4	12	18	20	16	10	3	0	0	-1	-1	0	0	-1
INEL,SCT		42	-2	-9	-25	-12	10	25	29	20	6	0	0	0	0	0	0	0	0	0
N2N		9	7	1	0	0	0	0	0	0	0	0	0	0	0	0	0	0	0	0
MU-AVE		-44	-1	-5	-9	-7	-4	-6	-3	-1	0	0	0	0	0	0	0	0	0	0
U-238	CAPTURE	-15758	65	-7	-36	-123	-343	-938	-1155	-1628	-2396	-2851	-2331	-1492	-666	-1085	-526	-130	-50	-40
NU		-1683	-90	-240	-575	-709	-60	-6	-1	0	0	0	0	0	0	0	-1	0	0	0
FISSION		-2328	-120	-335	-807	-968	-84	-9	-1	-1	-1	-1	-1	0	0	0	-1	0	0	0
ELASTIC,SCT		37	0	-1	-2	-1	-3	-22	45	36	4	-15	-11	-5	-15	-7	-3	-2	-1	
INEL,SCT		1433	8	65	266	340	259	127	135	168	65	0	0	0	0	0	0	0	0	0
N2N		3	3	0	0	0	0	0	0	0	0	0	0	0	0	0	0	0	0	0
MU-AVE		41	1	4	3	7	3	9	6	3	1	0	0	0	0	0	0	0	0	0
Pu-239	CAPTURE	2701	-1	0	2	8	82	169	241	269	310	319	314	198	400	222	103	25	23	
NU		-19632	-61	-221	-590	-897	-943	-2243	-2509	-2704	-2460	-2001	-1436	-970	-474	-1105	-614	-233	-86	-79
FISSION		-10480	-31	-105	-261	-397	-439	-1063	-1244	-1425	-1388	-1179	-856	-573	-276	-653	-358	-133	-53	-49
ELASTIC,SCT		-35	0	0	-1	-2	-1	-5	-5	-5	-4	-3	-1	0	-1	0	0	0	0	0
INEL,SCT		86	1	7	17	21	9	16	8	9	3	0	-4	0	0	0	0	0	0	0
N2N		3	0	0	0	0	0	0	0	0	0	0	0	0	0	0	0	0	0	0
MU-AVE		23	1	2	4	3	2	4	3	2	1	0	0	0	0	0	0	0	0	0
Pu-240	CAPTURE	22	0	0	0	0	0	0	1	1	0	0	1	2	2	5	4	2	1	2
NU		-619	-10	-34	-89	-123	-126	-135	-27	-18	-18	-15	-9	-4	-1	-6	-4	0	0	0
FISSION		-459	-7	-26	-64	-89	-94	-101	-101	-21	-14	-14	-12	-7	-3	-1	-4	-3	-1	0
ELASTIC,SCT		-8	0	0	0	0	0	-1	-1	-1	-1	-1	-1	0	0	0	0	0	0	0
INEL,SCT		13	0	1	3	4	1	1	1	1	0	0	0	0	0	0	0	0	0	0
N2N		0	0	0	0	0	0	0	0	0	0	0	0	0	0	0	0	0	0	0
MU-AVE		3	0	0	0	1	0	0	1	0	0	0	0	0	0	0	0	0	0	0
Pu-241	CAPTURE	21	0	0	0	0	0	2	2	3	3	3	2	2	1	2	1	0	0	0
NU		-249	-1	-2	-6	-9	-10	-23	-30	-35	-33	-28	-22	-16	-8	-16	-7	-3	-1	0
FISSION		-1666	-1	-3	-9	-13	-14	-20	-16	-18	-18	-18	-12	-8	-4	-8	-4	-1	0	0
ELASTIC,SCT		0	0	0	0	0	0	0	0	0	0	0	0	0	0	0	0	0	0	0
INEL,SCT		1	0	0	0	0	0	0	0	0	0	0	0	0	0	0	0	0	0	0
N2N		0	0	0	0	0	0	0	0	0	0	0	0	0	0	0	0	0	0	0
MU-AVE		0	0	0	0	0	0	0	0	0	0	0	0	0	0	0	0	0	0	0
Pu-242	CAPTURE	1	0	0	0	0	0	0	0	0	0	0	0	0	0	0	0	0	0	0
NU		-2	0	0	0	0	0	-1	0	0	0	0	0	0	0	0	0	0	0	0
FISSION		-2	0	0	0	0	0	0	0	0	0	0	0	0	0	0	0	0	0	0
ELASTIC,SCT		0	0	0	0	0	0	0	0	0	0	0	0	0	0	0	0	0	0	0
INEL,SCT		0	0	0	0	0	0	0	0	0	0	0	0	0	0	0	0	0	0	0
N2N		0	0	0	0	0	0	0	0	0	0	0	0	0	0	0	0	0	0	0
MU-AVE		0	0	0	0	0	0	0	0	0	0	0	0	0	0	0	0	0	0	0
Am-241	CAPTURE	3	0	0	0	0	0	-1	-1	0	0	0	0	0	0	0	0	0	0	0
NU		-3	0	0	0	0	-1	-1	0	0	0	0	0	0	0	0	0	0	0	0
FISSION		-2	0	0	0	0	-1	0	0	0	0	0	0	0	0	0	0	0	0	0
ELASTIC,SCT		0	0	0	0	0	0	0	0	0	0	0	0	0	0	0	0	0	0	0
INEL,SCT		0	0	0	0	0	0	0	0	0	0	0	0	0	0	0	0	0	0	0
N2N		0	0	0	0	0	0	0	0	0	0	0	0	0	0	0	0	0	0	0
MU-AVE		0	0	0	0	0	0	0	0	0	0	0	0	0	0	0	0	0	0	0

														(UNIT : 1.0E-4)						
NUCLIDE	REACTION	TOTAL	1G	2G	3G	4G	5G	6G	7G	8G	9G	10G	11G	12G	13G	14G	15G	16G	17G	18G
O	CAPTURE	23	7	14	0	0	0	0	0	0	0	0	0	0	0	0	0	0	0	
	ELASTIC SCT	2279	1	-4	-3	98	74	543	601	726	475	73	-99	-66	-33	-67	-34	-7	-3	
	INEL.SCT	4	4	0	0	0	0	0	0	0	0	0	0	0	0	0	0	0	0	
Ni	N2N	0	0	0	0	0	0	0	0	0	0	0	0	0	0	0	0	0	0	
MU-AVE		29	1	3	2	3	2	22	-5	0	0	0	0	0	0	0	0	0	0	
Na	CAPTURE	21	2	1	0	0	0	1	1	1	1	1	1	1	1	7	4	1	0	
	ELASTIC SCT	525	0	-3	-2	21	17	84	252	249	176	24	-57	-87	-99	-34	-13	-3	-1	
	INEL.SCT	206	6	17	43	56	32	112	0	0	0	0	0	0	0	0	0	0	0	
N2N		0	0	0	0	0	0	0	0	0	0	0	0	0	0	0	0	0	0	
MU-AVE		35	1	2	7	8	5	7	3	1	0	0	0	0	0	0	0	0	0	
Cr	CAPTURE	40	1	1	1	1	1	2	2	3	1	2	1	8	2	14	1	0	0	
	ELASTIC SCT	38	0	-1	-1	4	2	10	49	21	8	2	-17	-28	-3	-4	-2	-1	0	
	INEL.SCT	92	4	16	34	32	4	3	0	0	0	0	0	0	0	0	0	0	0	
N2N		0	0	0	0	0	0	0	0	0	0	0	0	0	0	0	0	0	0	
MU-AVE		7	0	1	3	2	0	0	0	0	0	0	0	0	0	0	0	0	0	
Fe	CAPTURE	177	4	6	6	3	13	14	17	11	7	10	1	64	3	2	1	1	1	
	ELASTIC SCT	478	0	-2	-5	9	12	84	219	245	135	3	-62	-32	-18	-56	-13	-5	-1	
	INEL.SCT	574	20	76	136	169	142	7	4	4	15	2	-2	0	0	0	0	0	0	
N2N		0	0	0	0	0	0	0	0	0	0	0	0	0	0	0	0	0	0	
MU-AVE		26	1	5	8	6	1	3	0	0	0	0	0	0	0	0	0	0	0	
Ni	CAPTURE	64	4	10	4	2	3	5	5	4	4	8	2	1	2	1	0	0	0	
	ELASTIC SCT	32	0	0	-1	2	1	2	18	32	20	8	-15	-14	-4	-9	-5	-1	0	
	INEL.SCT	43	2	6	17	16	0	0	1	0	0	0	0	0	0	0	0	0	0	
N2N		0	0	0	0	0	0	0	0	0	0	0	0	0	0	0	0	0	0	
MU-AVE		5	0	1	1	1	0	1	0	0	0	0	0	0	0	0	0	0	0	
	ELASTIC SCT	1668	0	1	6	13	19	63	104	151	181	201	197	166	94	215	136	75	19	
	INEL.SCT	-123	0	-2	-6	-9	-11	-26	-19	-11	-10	-14	-9	-5	-1	-4	-1	2	1	
		236	11	31	83	64	13	14	7	3	0	0	0	0	0	0	0	0	0	
N2N		0	0	0	0	0	0	0	0	0	0	0	0	0	0	0	0	0	0	
MU-AVE		69	1	4	10	13	9	16	4	2	0	0	0	0	0	0	0	0	0	
	U-238FP CAPTURE	322	0	0	1	2	4	13	22	32	38	41	39	32	18	39	24	12	3	
	ELASTIC SCT	-22	0	0	-1	-1	-2	-4	-3	-2	-2	-1	0	-1	0	0	0	0	0	
	INEL.SCT	33	2	5	13	10	2	2	1	0	0	0	0	0	0	0	0	0	0	
N2N		0	0	0	0	0	0	0	0	0	0	0	0	0	0	0	0	0	0	
MU-AVE		11	0	1	2	1	3	2	1	0	0	0	0	0	0	0	0	0	0	
	Pu-239FP CAPTURE	806	0	0	3	7	9	34	59	85	101	108	100	79	42	89	53	25	6	
	ELASTIC SCT	-57	0	-1	-2	-4	-4	-12	-9	-8	-6	-5	-3	-1	0	-1	0	0	0	
	INEL.SCT	81	5	11	30	24	4	4	2	1	0	0	0	0	0	0	0	0	0	
N2N		0	0	0	0	0	0	0	0	0	0	0	0	0	0	0	0	0	0	
MU-AVE		29	0	1	4	6	4	7	4	2	1	0	0	0	0	0	0	0	0	

TABLE 3. NUCLIDE AND REACTION-WISE CONTRIBUTIONS TO BURNUP REACTIVITY LOSS DIFFERENCES DUE TO CROSS-SECTION DIFFERENCE BETWEEN JEF-2.2R AND JENDL-3.2 (1/2)

NUCLIDE	REACTION	TOTAL	1G	2G	3G	4G	5G	6G	7G	8G	9G	10G	11G	12G	13G	14G	15G	16G	17G	18G	
U-235	CAPTURE	-3.12%	-3.29%	-0.023%	0.008%	0.015%	0.0055%	-0.023%	-0.067%	-0.265%	-0.213%	-0.075%	0.116%	0.054%	0.119%	0.419%	0.118%	-0.009%	-0.006%	0.000%	
NU	FUSION	0.33%	-0.001%	-0.027%	-0.060%	-0.051%	-0.021%	-0.022%	-0.005%	0.057%	0.153%	0.141%	0.055%	0.034%	0.020%	0.022%	0.011%	0.008%	0.005%	0.007%	
	ELASTIC SCT	0.40%	-0.007%	-0.020%	-0.061%	-0.111%	-0.145%	-0.066%	0.091%	-0.053%	0.041%	0.248%	0.339%	0.048%	0.066%	0.063%	0.082%	0.063%	0.017%	0.006%	0.002%
	INEL SCT	0.02%	-0.001%	-0.003%	-0.008%	-0.012%	-0.013%	-0.017%	0.019%	-0.002%	-0.001%	0.000%	0.000%	0.000%	0.000%	0.000%	0.000%	0.000%	0.000%	0.000%	0.000%
N2N	MU-AVE	0.00%	0.000%	0.000%	0.000%	0.000%	0.000%	0.000%	0.000%	0.000%	0.000%	0.000%	0.000%	0.000%	0.000%	0.000%	0.000%	0.000%	0.000%	0.000%	
U-238	CAPTURE	-1.49%	-0.49%	-0.037%	-0.034%	-0.303%	-0.054%	-0.064%	0.171%	-0.002%	-0.003%	-0.001%	0.000%	0.000%	0.000%	0.000%	0.000%	0.000%	0.000%	0.000%	
NU	FUSION	0.01%	0.001%	0.004%	0.002%	0.001%	0.000%	0.000%	0.000%	0.000%	0.000%	0.000%	0.000%	0.000%	0.000%	0.000%	0.000%	0.000%	0.000%	0.000%	
	ELASTIC SCT	0.02%	0.000%	0.000%	0.000%	0.000%	0.000%	0.000%	0.000%	0.000%	0.000%	0.000%	0.000%	0.000%	0.000%	0.000%	0.000%	0.000%	0.000%	0.000%	
	INEL SCT	0.20%	0.000%	0.033%	0.066%	0.054%	0.032%	-0.059%	-0.104%	0.079%	0.097%	0.000%	0.000%	0.000%	0.000%	0.000%	0.000%	0.000%	0.000%	0.000%	
N2N	MU-AVE	0.00%	0.000%	0.000%	0.000%	0.000%	0.000%	0.000%	0.000%	0.000%	0.000%	0.000%	0.000%	0.000%	0.000%	0.000%	0.000%	0.000%	0.000%	0.000%	
Pu-239	CAPTURE	-0.06%	-0.027%	0.00%	0.012%	0.043%	0.053%	0.094%	0.073%	0.038%	0.060%	-0.077%	0.063%	-0.064%	-0.167%	-0.170%	-0.024%	0.019%	0.006%	0.006%	
NU	FUSION	0.76%	0.002%	0.010%	0.027%	-0.029%	0.005%	0.005%	0.019%	0.050%	0.090%	-0.098%	0.186%	0.141%	0.076%	0.175%	0.088%	0.006%	0.003%	0.000%	
	ELASTIC SCT	0.38%	0.012%	0.000%	0.000%	0.000%	0.000%	0.000%	0.000%	0.000%	0.000%	0.000%	0.000%	0.000%	0.000%	0.000%	0.000%	0.000%	0.000%	0.000%	
	INEL SCT	-0.09%	0.002%	0.002%	0.001%	-0.008%	-0.009%	-0.028%	-0.018%	-0.028%	-0.007%	0.000%	0.000%	0.000%	0.000%	0.000%	0.000%	0.000%	0.000%	0.000%	
N2N	MU-AVE	-0.01%	0.000%	0.000%	0.000%	0.000%	0.000%	0.000%	0.000%	0.000%	0.000%	0.000%	0.000%	0.000%	0.000%	0.000%	0.000%	0.000%	0.000%	0.000%	
Pu-240	CAPTURE	0.00%	0.000%	0.000%	0.000%	0.000%	0.000%	0.000%	0.000%	0.000%	0.000%	0.000%	0.000%	0.000%	0.000%	0.000%	0.000%	0.000%	0.000%	0.000%	
NU	FUSION	0.00%	0.000%	0.001%	0.000%	0.000%	0.000%	0.000%	0.000%	0.000%	0.000%	0.000%	0.000%	0.000%	0.000%	0.000%	0.000%	0.000%	0.000%	0.000%	
	ELASTIC SCT	0.00%	0.000%	0.000%	0.000%	0.000%	0.000%	0.000%	0.000%	0.000%	0.000%	0.000%	0.000%	0.000%	0.000%	0.000%	0.000%	0.000%	0.000%	0.000%	
	INEL SCT	0.00%	0.000%	0.000%	0.000%	0.000%	0.000%	0.000%	0.000%	0.000%	0.000%	0.000%	0.000%	0.000%	0.000%	0.000%	0.000%	0.000%	0.000%	0.000%	
N2N	MU-AVE	0.00%	0.000%	0.000%	0.000%	0.000%	0.000%	0.000%	0.000%	0.000%	0.000%	0.000%	0.000%	0.000%	0.000%	0.000%	0.000%	0.000%	0.000%	0.000%	
Pu-241	CAPTURE	0.04%	0.000%	0.000%	0.000%	0.000%	0.000%	0.000%	0.000%	0.000%	0.000%	0.000%	0.000%	0.000%	0.000%	0.000%	0.000%	0.000%	0.000%	0.000%	
NU	FUSION	0.00%	0.000%	0.000%	0.000%	0.000%	0.000%	0.000%	0.000%	0.000%	0.000%	0.000%	0.000%	0.000%	0.000%	0.000%	0.000%	0.000%	0.000%	0.000%	
	ELASTIC SCT	0.00%	0.000%	0.000%	0.000%	0.000%	0.000%	0.000%	0.000%	0.000%	0.000%	0.000%	0.000%	0.000%	0.000%	0.000%	0.000%	0.000%	0.000%	0.000%	
	INEL SCT	0.00%	0.000%	0.000%	0.000%	0.000%	0.000%	0.000%	0.000%	0.000%	0.000%	0.000%	0.000%	0.000%	0.000%	0.000%	0.000%	0.000%	0.000%	0.000%	
N2N	MU-AVE	0.00%	0.000%	0.000%	0.000%	0.000%	0.000%	0.000%	0.000%	0.000%	0.000%	0.000%	0.000%	0.000%	0.000%	0.000%	0.000%	0.000%	0.000%	0.000%	

TABLE 3. NUCLIDE AND REACTION-WISE CONTRIBUTIONS TO BURNUP REACTIVITY LOSS DIFFERENCES DUE TO CROSS-SECTION DIFFERENCE BETWEEN JEF-2.2R AND JENDL-3.2 (2/2)

Appendix III

EFFECT OF JFS SET CHANGES

M. Ishikawa
Japan Nuclear Cycle Development Institute, Japan

1. INTRODUCTION

It has been proposed to make preliminary evaluation of the effect of possible error of reactivity coefficient calculation when comparing reactor dynamics under different accident conditions. This study is supposed to be carried out with the common dynamic code available, in which the sets of reactivity coefficients obtained by the researchers from different countries are variable input data (on the initial stage of study).

Ramified dynamic codes, which are often used for the design analysis (such as SAS4A code), provide rather large scope of information, thus hindering analytical process. These codes require using complete thermo-hydraulic model for at least the primary circuit. Simplification or cutting off of this model can result in the contradictory evaluations. Taking into account boiling and melting processes would significantly complicate analysis of the effect of supposed error of reactivity coefficient calculation on the accident. That is why it has been proposed to make preliminary analysis using simplified dynamic code. DINCOR code especially designed at the IPPE for this purpose realizes point kinetics approximation without taking into account phase transitions of the core materials. Owing to the possibility to change rapidly input data, this code provides results, which are sufficiently evident for preliminary analysis. Such (preliminary) evaluations will make it possible to choose the range of calculated values of the main reactivity coefficients, within which minimum variations of maximum temperature values will be assured. As regards values beyond this range, it is reasonable to carry out calculations using full-scale dynamic codes used for design studies. Neither boiling nor melting processes are taken into account in the simplified code DIN COR. Therefore, accident dynamics simulation requires to choose perturbations (in the flow rate or reactivity) that should not result in exceeding maximum temperature values. The following conditions can be taken as limiting points:

- No sodium boiling;
- Fuel cladding temperature is below maximum permissible level (<870°C).

These limitations simulate maximum perturbations in the coolant flow rate and inserted reactivity (considered as ULOF and UTOP accident analogues). It should be also demonstrated that point kinetics can be used for analysis of dynamics of reactor with heterogeneous arrangement of different fuel s (uranium and MOX fuel).

2. PARAMETERS OF ELEMENTARY THERMAL CHANNEL (FUEL ELEMENT)

In the DIN COR code, the core is represented as a system of parallel channels having independent flow supply. The channels connecting core diagrid and upper reactor plenum are separated from each other over their length. Channels belonging to one radial physical zone (LEZ, MEZ, etc.) are considered equivalent with respect to then thermo-hydraulic parameters. Temperature field inhomogeneity in the SA cross section is neglected. Thermo-hydraulic processes in two chambers are described within the framework of simplified common thermal capacity model. Thus, single channel (fuel element) with radius-averaged axial power profile is studied in each fuel zone. The main dimensions of the channel are as follows (at 20°C):

- Diameter of steel tube 6.9×0.4 mm;
- Fuel element spacing 7.95 mm;

- Spacer wire diameter 1.05 mm;
- Fuel column diameter 5.9 mm (fresh fuel);
- Central hole diameter 1.8 mm (according to experts estimate);
- Coolant inlet temperature 365°C;
- Coolant outlet temperature 550°C.

Initial coolant flow rate is evaluated on the basis of rated sodium temperature rise and average power rates obtained by TRIGEX code. Reactivity feedback dynamics is calculated taking into account changes of axial average power rate $Q(z, t)$ (and material temperatures $T(z, t_i)$). Current maximum over zone power rates are used for determining maximum temperatures of materials in the hottest channel.

3. THERMO-HYDRAULIC MODEL OF ACCIDENT WITH PARTIAL LOSS OF FLOW

Under real ULOF accident conditions, sodium boiling onset in the hottest channels occurs in ~15 s (Fig. 2). Accident model in the DFNCOR code gives only partial description of the process of the primary pump shutdown (specified flow mode does not result in exceeding permissible temperature level). In order to choose permissible flow rate, real pump coast-down halftime value (~6.5 s) was kept as a reference point in all options (Fig. 2).

Based on maximum permissible temperature of the fuel element cladding, 30% flow rate of coolant was chosen as minimum level. Corresponding time of the pump coast-down was $\tau = 12.07$ s. For this flow rate, possible variations of maximum temperatures depending on the choice of the flow rate smoothing range AT are presented in Fig. 3. In the subsequent studies, three sets of reactivity coefficients were used for ULOF accident analysis. These sets were obtained at the IPPE for the following geometry options:

- R-Z geometry (diffusion and transport analysis);
- HEX-Z geometry (diffusion analysis).

With respect to the main reactivity coefficients (both integral values and space distribution), such approach covers the majority of the results presented by other researchers for the area within the core boundaries.

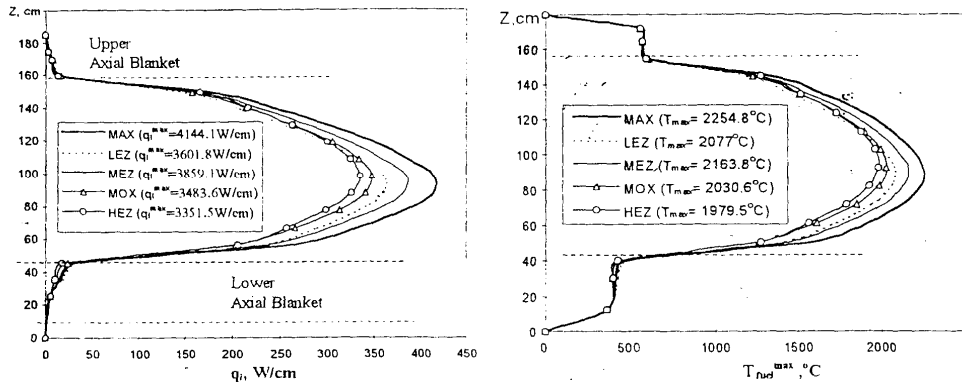


FIG. 1. Axial distribution of $<q_i>^{max}$, $<q_i>$ and the maximal temperatures of fuel in various channels (MAX is the hottest channel) at stationary condition.

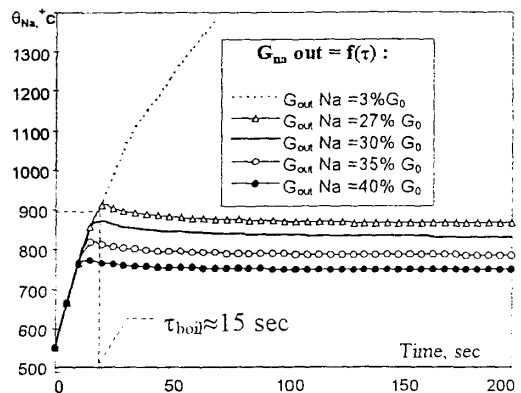


FIG. 2. Maximum sodium outlet temperature as a function of coolant flow rate in the core.

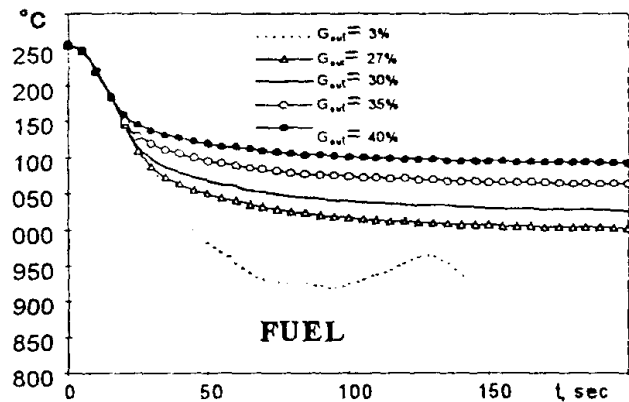
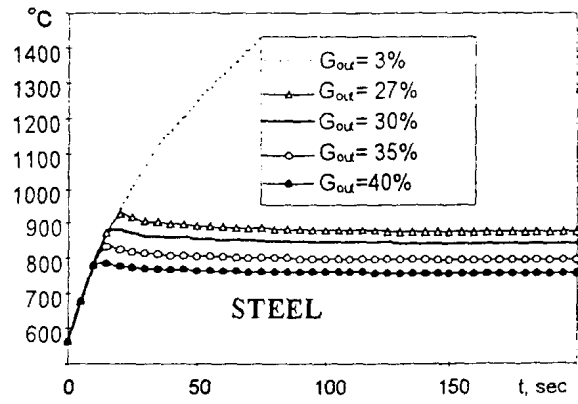
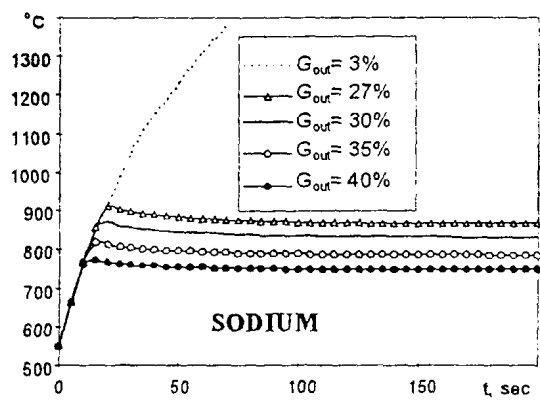


FIG. 3. Maximum temperatures of materials- under conditions of ULOF accident analogue.

4. REACTIVITY PERTURBATION MODEL

Spontaneous control rod withdrawal is considered as initial event. Under real conditions, with AM and N/G preliminary settings, accident is terminated in ~5 s on the overpower signal (115% of rated power level). In this problem model for UTOP type accident analogue, the inserted reactivity value should be limited by DICOR code capability on condition that temperature and power values are within permissible limits.

Similarly to the previous section, unauthorized withdrawal of control rod having 0.1% worth during 7.5 s was taken as reactivity perturbation. Preliminary analysis has shown that this perturbation would not result in exceeding maximum permissible temperature values. Two sets of reactivity coefficients obtained at the IPPE for R-Z model in diffusion and transport approximation were used for this accident analysis.

5. NEUTRONICS INITIAL DATA AND REACTIVITY COEFFICIENTS

Under simplified dynamics calculations the averaged delayed neutron parameters were used. Under averaging maximum and minimum values were not rejected; the role of maximum deviations will be analyzed below (Table 1).

TABLE 1. AVERAGE VALUES (β and $\bar{\lambda}_i$)

Group	1	2	3	4	5	6	$\bar{\beta}_{eff}$
$\bar{\beta}_i$	1.758E-04	1.085E-03	1.019E-03	2.292E-03	9.916E-04	3.393E-04	5.904E-03
$\bar{\lambda}_i$, s^{-1}	1.280E-02	3.161E-02	1.199E-01	3.189E-01	1.322	3.747	

For assessment of influence of variations of calculational values of the reactivity coefficients (obtained in different countries) on description of the dynamic process it is necessary to average those data. Existence of such influence at the first stage of the simplified calculations of analogous of the accident processes is demonstrated by the choice as the basis of the two reactivity coefficients sets, obtained for the R-Z model at the IPPE: calculations in diffusion and transport approximations — base calculation. Since in the DIN COR computer code 5 independent channels are used, reactivity coefficients are used in their axial distribution as integrals over zones LEZ, MEZ, MOX and HEZ.

For further calculations 3 sets of reactivity coefficients obtained in Russia (IPPE) are used: for R-Z model — diffusion and transport approximations and for HEX-Z model -diffusion approximation. Averaged between different countries the values of reactivity coefficients for 3D calculations obtained under exclusion of minimum values are rather close to the TRIGEX code calculation results. Thus, 3 sets considered practically totally (excluding minimum values of the parameters submitted) encompass the diapason of calculational values obtained by different researches. Importance of deviations in reactivity coefficients values including deviations in coefficient values in different reactor zones has to be determined by the end of Year 2001. Allowable diapason of deviations will be determined by the difference between initial temperatures (undisturbed state;) and transient process utmost temperatures obtained in the corresponding calculations.

6. ACCIDENT WITH COOLANT WITH COOLANT FLOW RATE DECREASE (ANALOGUE OF ULOF ACCIDENT)

For preliminary assessment of influence of a method of calculation on accident process description, calculations of full scale ULOF accident were performed (up to the coolant flow rate of natural circulation $G \sim 5\%$ Go with reactivity coefficients obtained in diffusion and transport approximations for Phase 1 (R-Z model). The calculation results are displayed on Figs 4-7. From Fig. 8 it is visible that the maximal contribution in negative reactivity of a feedback brings in of a component of radial expansion. In Fig. 8A the behaviour of characteristic temperatures is submitted with:

$$TCR_{Rad}^{Diff, Transp}(r, z) = TCR_{Rad}^{Total}(r, z) = \{TCR_{Rad}^{Fuel}(r, z) + TCR_{Rad}^{Steel}(r, z)\}^{Diff, Transp}$$

and Fig. 8B with:

$$TCR_{Rad}^{Diff, Transp}(r, z) = \{TCR_{Rad}^{Total}(r, z) - TCR_{Rad}^{Fuel}(r, z)\}^{Diff, Transp}$$

(artificial variant determining the contribution of an error other components).

For such accident the results displayed have only attribute character since boiling of sodium and connected with it change of reactivity balance are not taken into account. However even in this attribute consideration it is seen that under 3 sets of reactivity coefficients chosen (RHEIN, TWODANT, TRIGEX) inconsistency (difference) of values obtained can reach:

- ~ 2.5% (~9 MW) — for power level;
- ~ 2% (-0.00002 $\Delta K/K$) -for reactivity;
- ~ 20% — for average temperature of fuel;
- ~ 5% — uncertainty of sodium temperature at the moment of boiling.

For the analogue of ULOF type accident considered ($G = 30\%$ Go) the results of calculations are given in Figs. 8–9. Deviations of thermal-technical parameters for such accident are as follows (without the account of the contribution components of radial expansion / with by the account of the contribution of radial expansion):

- ~ 14 MW/ — for power level;
- ~ 8% / — difference in total reactivity between 2D and 3D calculations (difference between transport and diffusion calculations for R-Z geometry does not exceed 1%, that is defined, in first turn, by the sodium density component value which in 3D calculations changes its sign, see further in the text);
- ~ Sodium temperature deviations are less than 7°C and less than 10°C for fuel temperature under transition to 3D coefficients of reactivity.

Change of outlet sodium temperature from different channels under transition from diffusion to transport approximation when calculating reactivity coefficients (analogue of ULOF accident under $G = 30\%$ Go) is given in Fig. 10.

Resulting values show weak influence of method of reactivity coefficients calculation in the framework of the same geometry for reactors with traditional core design, in particular for considered test model of the BN-600 reactor. Model error — transition to the HEX-Z geometry for such reactor design will be determinative.

In the considered thermal-hydraulic model of the accident taking course during 50 seconds it was not taken into account change of temperatures in the control rods-channels and in the steel blanket. Contribution of those zones and also influence of accuracy of reactivity coefficients calculation on reactor dynamics with sodium boiling ($G = 3\%$) could be estimated later with the usage of more sophisticated dynamic codes (for instance, SAS4A).

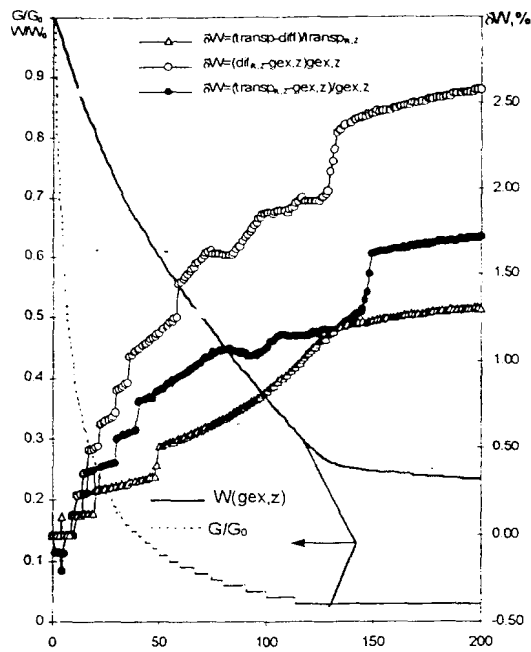


FIG. 4a. Capacity and total reactivity in ULOF accident ($G=3\% G_{NOm}$).

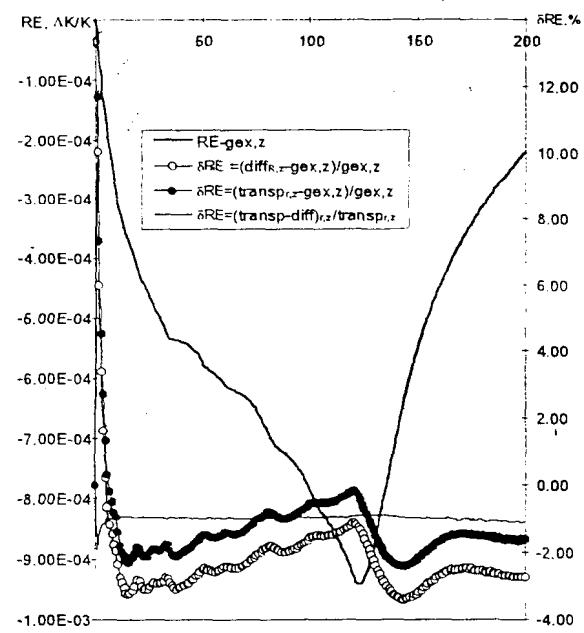


FIG. 4b. The maximum temperatures of sodium and steel in ULOF accident ($G \sim 3\% G_0$).

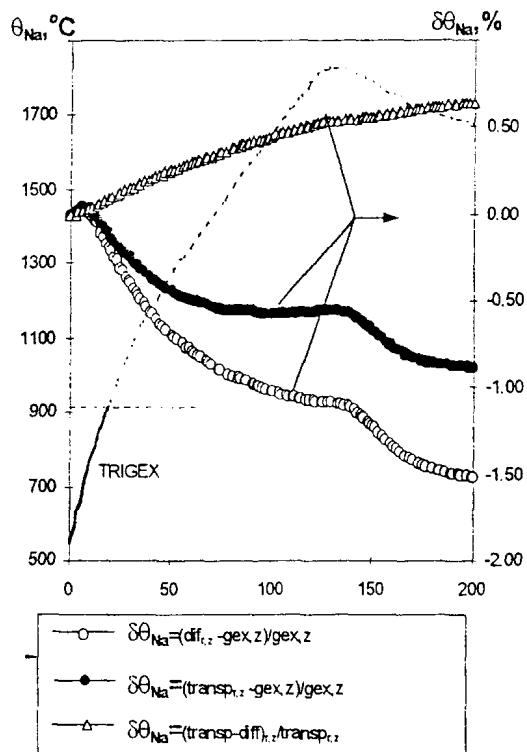
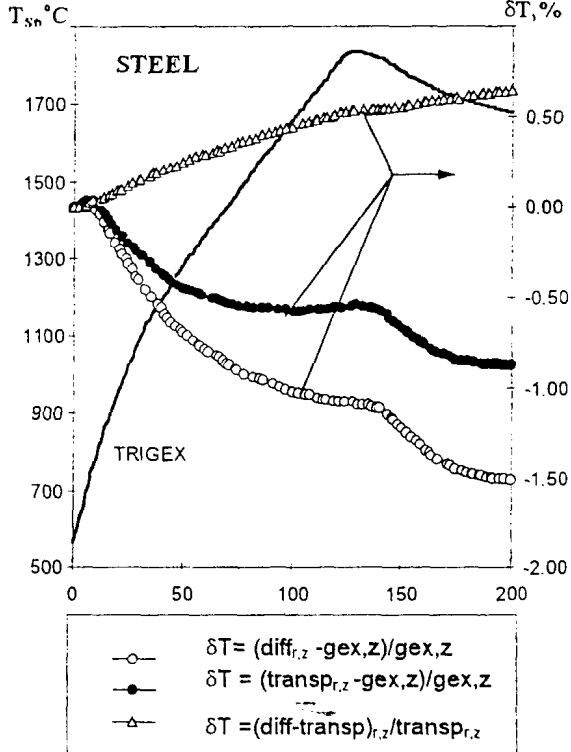


FIG. 5. The maximal temperatures of sodium and steel in ULOF accident ($G = 30\% G_0$).



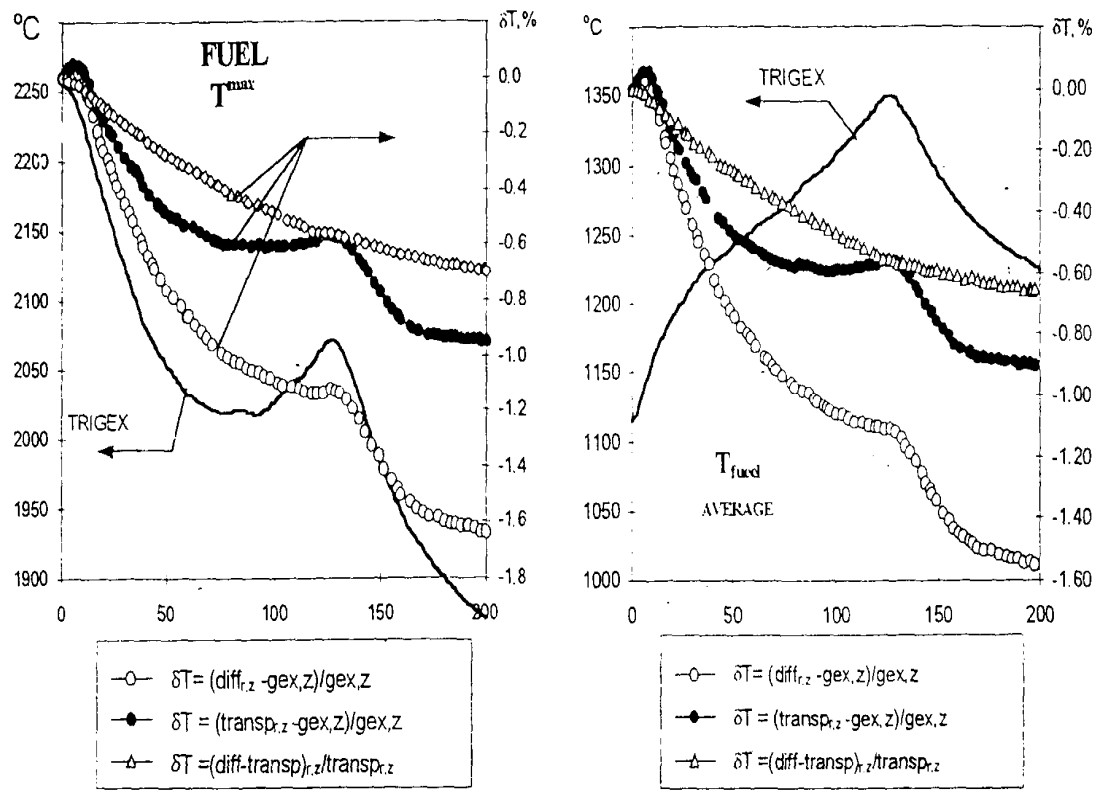


FIG. 6. Behaviour of temperature of fuel in ULOF accident (reactivity coefficients calculated by various methods).

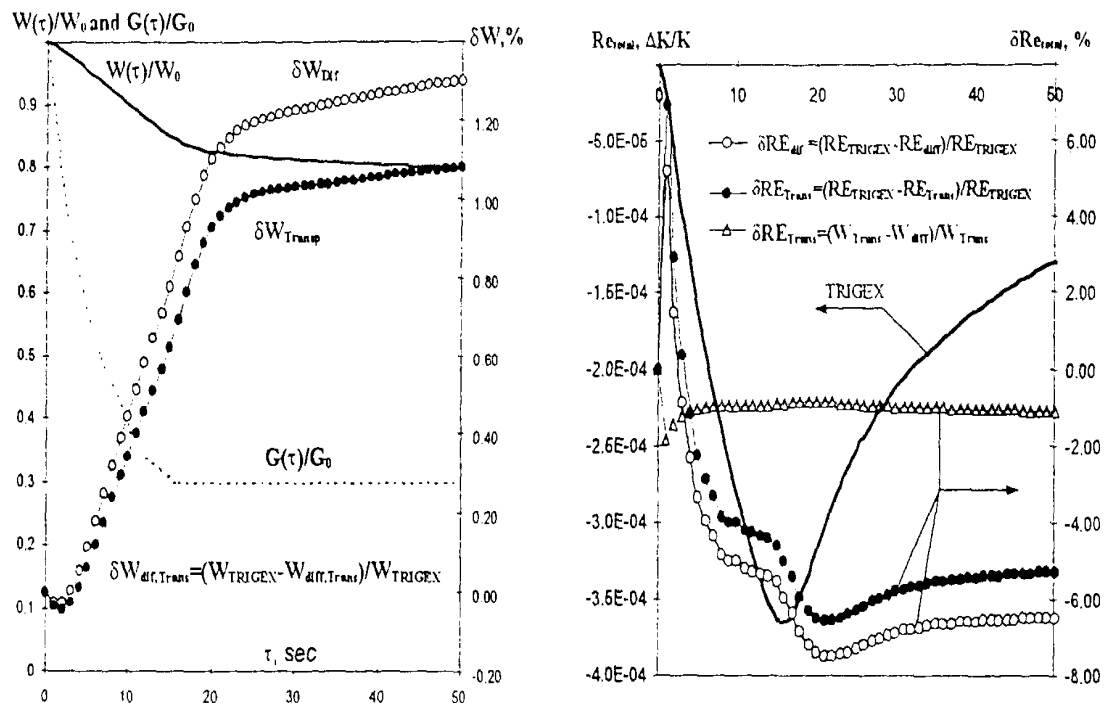


FIG. 7. Change of relative power, flow rate (A) and total feedback reactivity (B) in the accident with decrease of coolant flow rate (different ways of calculation of reactivity coefficient).

7. UTOP TYPE ACCIDENT

For the UTOP type accident insertion of outer reactivity $0.1\%\Delta K/K$ during 7.5 s (imitation of automatic regulator rod ‘self-driven’) was considered. The results given in Figs 11-13 for the reactivity coefficients obtained at IPPE for Phase 1 (R-Z geometry) demonstrate weak dependence of maximum values of thermal-technical parameters from the set of reactivity coefficients used. Thus, at the stage of preliminary simplified dynamic calculations seen distinctions in reactivity coefficients does not lead to any essential change in description of accidents processes. It is owing to the design of the reactor considered -traditional design with thick axial blankets. For reactors with sodium plenum influence of the model non-diffusiveness appears to be more significant.

Maximum resulting influence is displayed in Fig. 14 for fuel maximum temperature and in the most tense channel.

Changes of sodium temperatures appear to be essentially less and are comparable with the calculation error ($\sim 1^\circ\text{C}$). Negligible calculational fluctuations of temperatures are manifested in non-principle change of feedback reactivity and power (see Fig. 15).

8. INFLUENCE OF PARAMETERS OF DELAYED NEUTRONS

Assessment of influence of accuracy of neutron kinetics parameters calculation was carried out on the example of ULOF ($G = 30\% G_0$) accident with reactivity coefficients obtained from diffusion calculation of R, Z model. Base variant — averaged parameters of delayed neutrons (Table 1)

- Variant with λ_i values convoluted with all over the nuclides taking into account fission contribution only (without $(\beta_i$ factor of a nuclide);
- Variant with group β_i values which are forming minimum β_{eff} value from provided (USA-ANL results).

9. INFLUENCE OF VALUE REACTIVITY COEFFICIENT FROM THERMAL EXPANSION OF MATERIALS

Assessment of influence of accuracy of value reactivity coefficient from thermal expansion of materials calculation was carried out on the example of ULOF ($G = 30\% G_0$) accident with reactivity coefficients obtained from diffusion calculation of R-Z model. Base variant — Russian reactivity coefficients, received in 2D account.

Variants are considered:

- Variant with maximal value from axial expansion reactivity coefficient (meaning of China in Table 2 is used), see Figs 18-19;
- Variant with maximal and minimum values from Radial expansion reactivity coefficient (meanings of China and USA is used), see Fig. 20.

8. INFLUENCE OF VALUE SODIUM DENSITY COEFFICIENT

Depending on a mark these components of fluctuation of the maximal temperatures do not surpass 1%(10°C), see Figs 16-17.

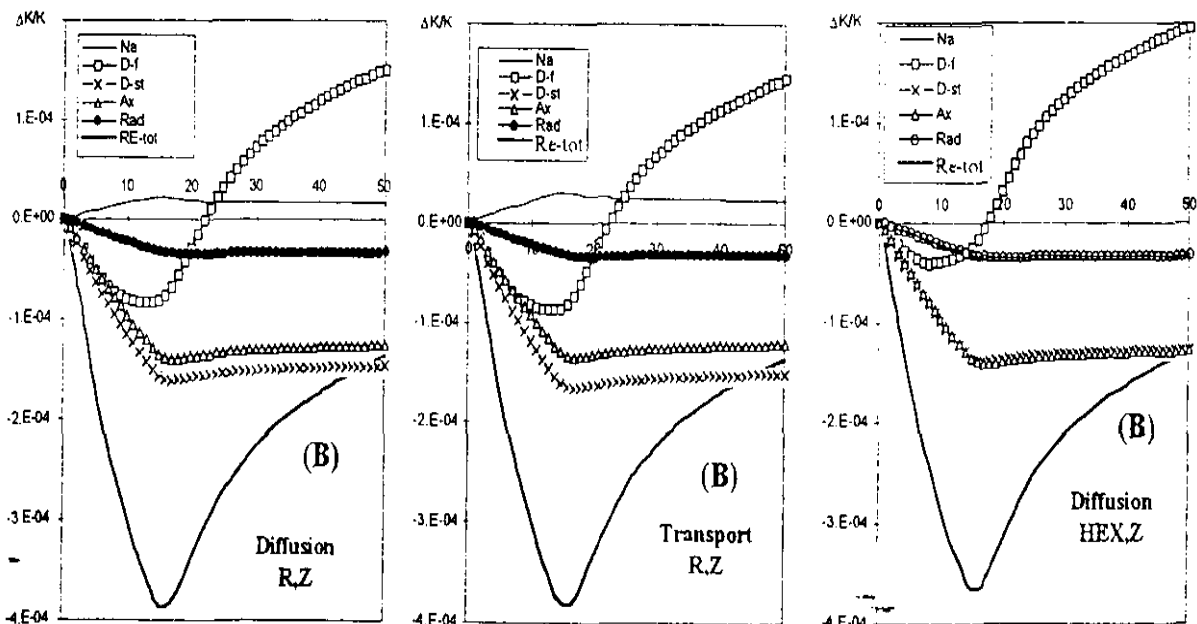
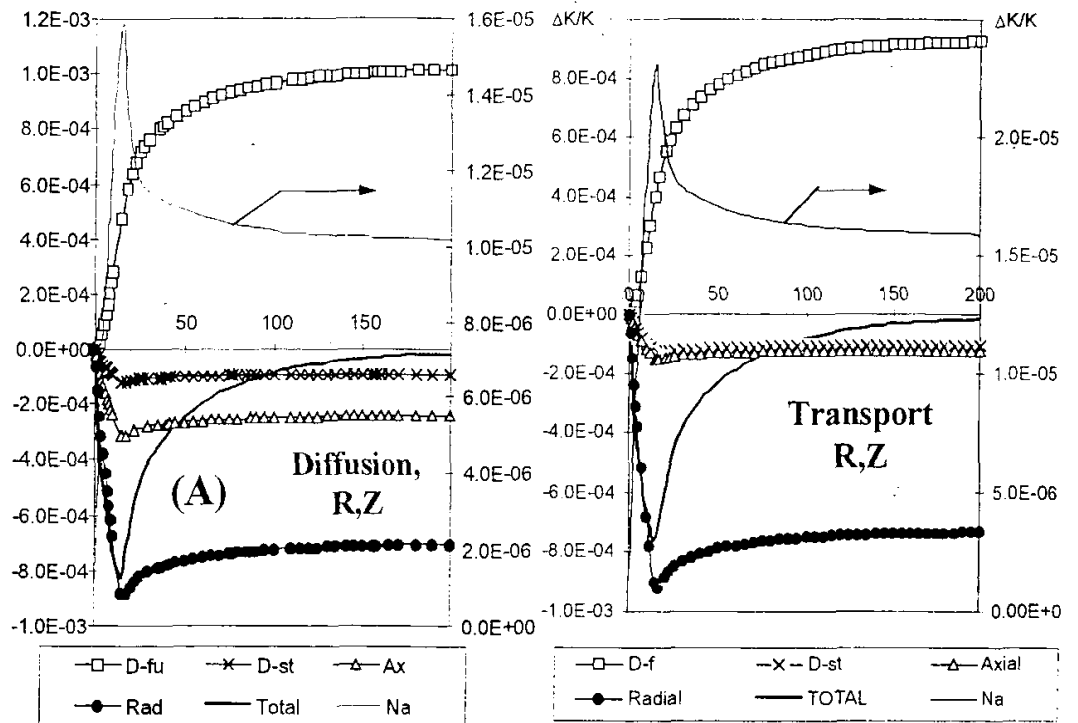


FIG. 8. Reactivity balance in analogue of ULOF type accident ($G = 30\% G_0$) A — $TCR_{Rad}^{Diff, Transp}(r, z) = TCR_{Rad}^{Total}(r, z) = \{TCR_{Rad}^{Fuel}(r, z) + TCR_{Rad}^{Steel}(r, z)\}^{Diff, Transp}$ B — $TCR_{Rad}^{Diff, Transp}(r, z) = TCR_{Rad}^{Total}(r, z) - TCR_{Rad}^{Fuel}(r, z)\}^{Diff, Transp}$ (see also Appendix, Fig. A. 1).

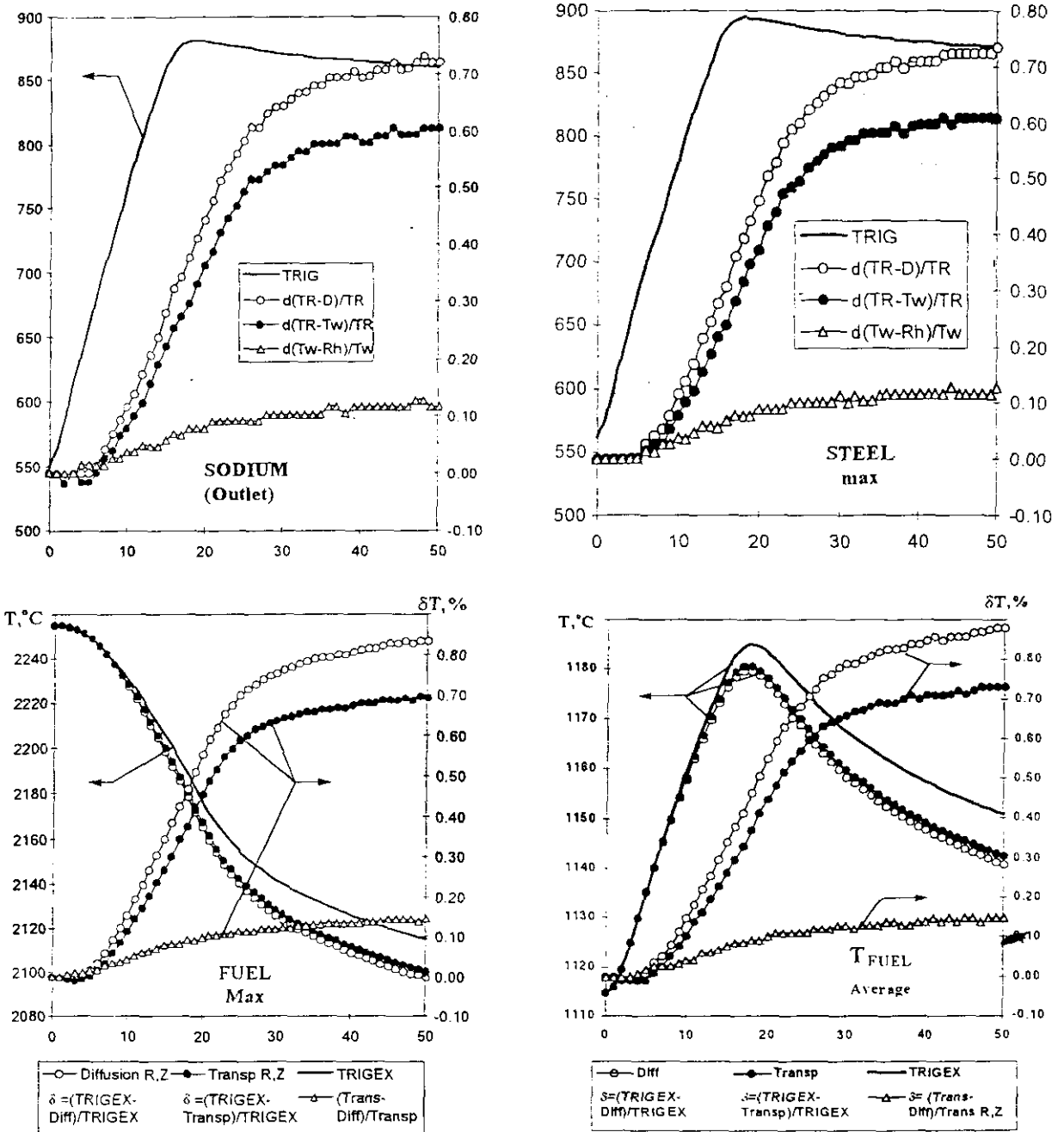


FIG. 9. Behavior of materials temperature in analogue of ULOF type accident ($G = 30\% G_0$).

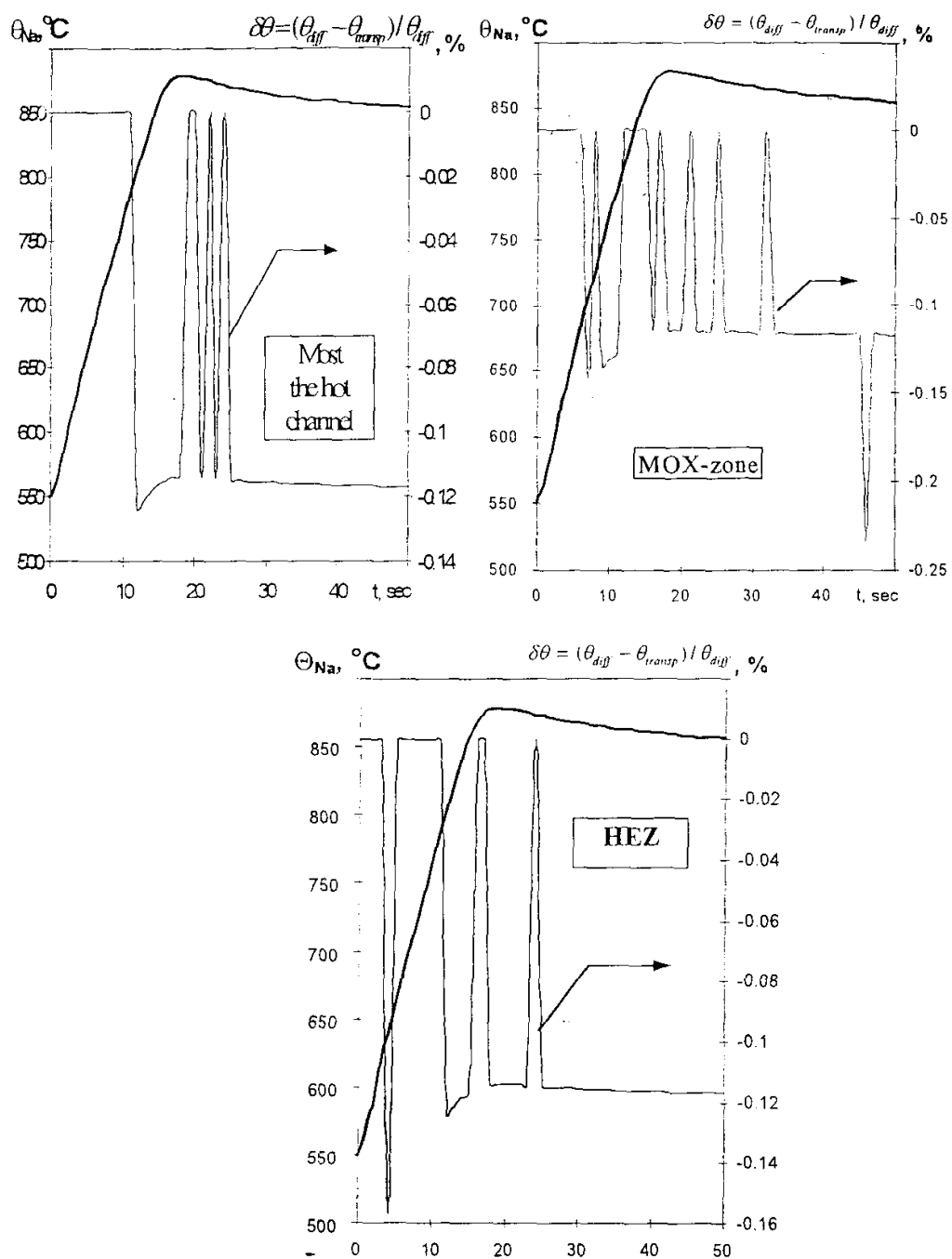
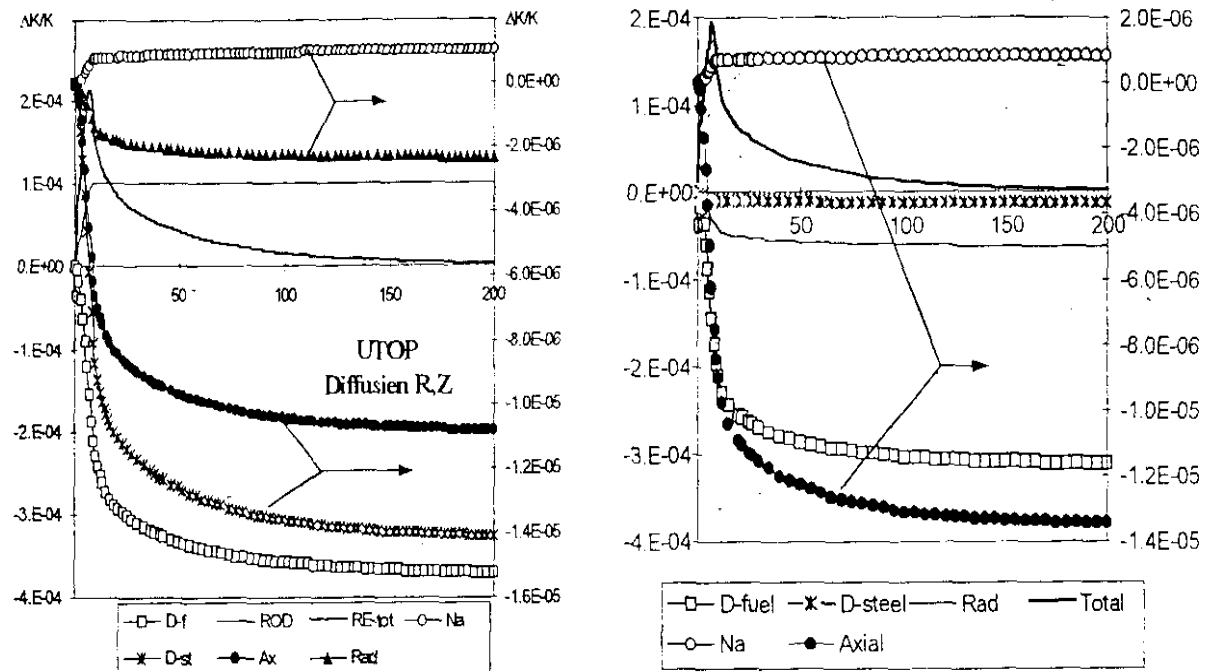


FIG. 10. Change of sodium temperature on an output from various channels with transition from diffusion to transport approach with account of reactivity coefficients. Analogue of ULOF type accident ($G = 30\% G_0$).



Radial expansion reactivity without the contribution
of fuel
Diffusion approach

Radial expansion reactivity = 100%
Diffusion approach

FIG. 11. Reactivity balance in UTOP accident.

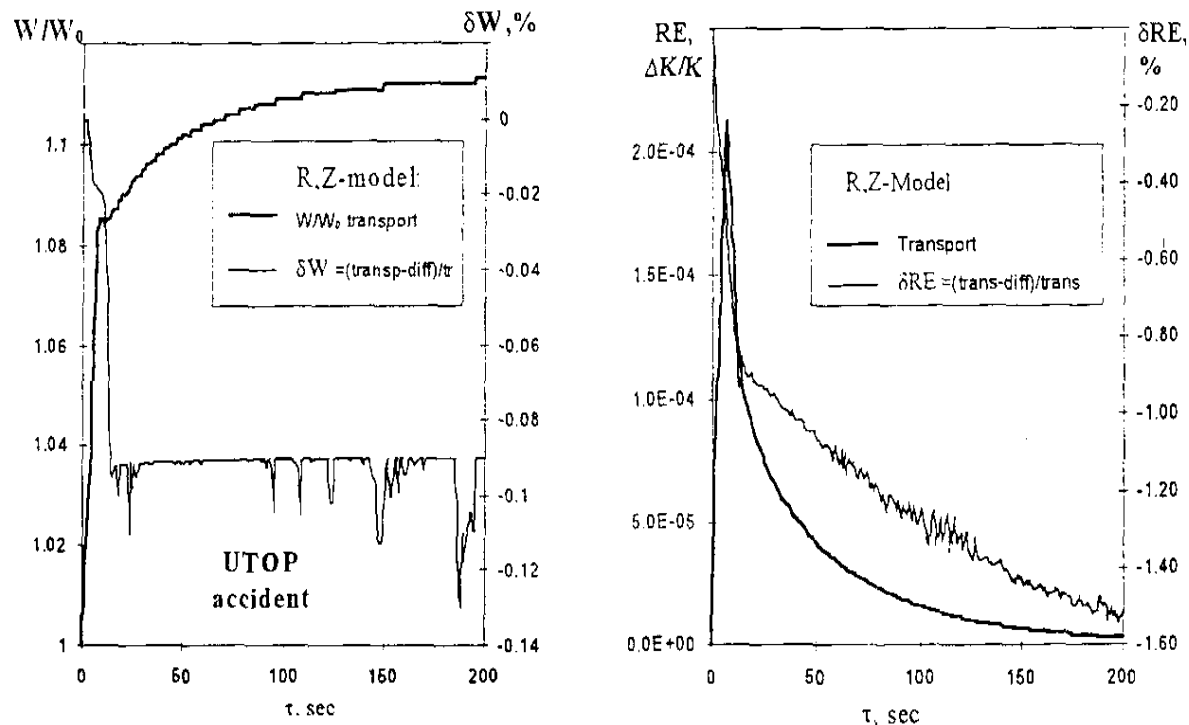


FIG. 12. Relative power and total reactivity in UTOP accident (different ways of calculation of reactivity).

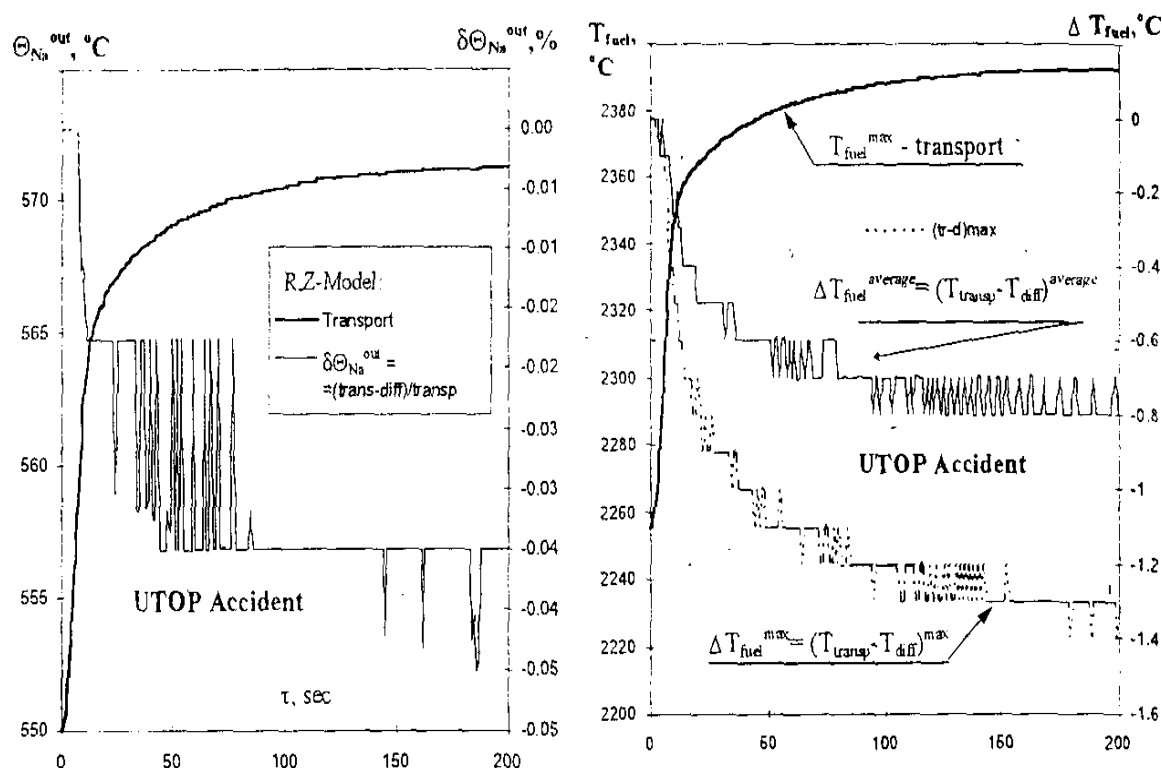


FIG. 13. Behaviour of temperature of sodium and fuel in UTOP accident (different ways of calculation of reactivity).

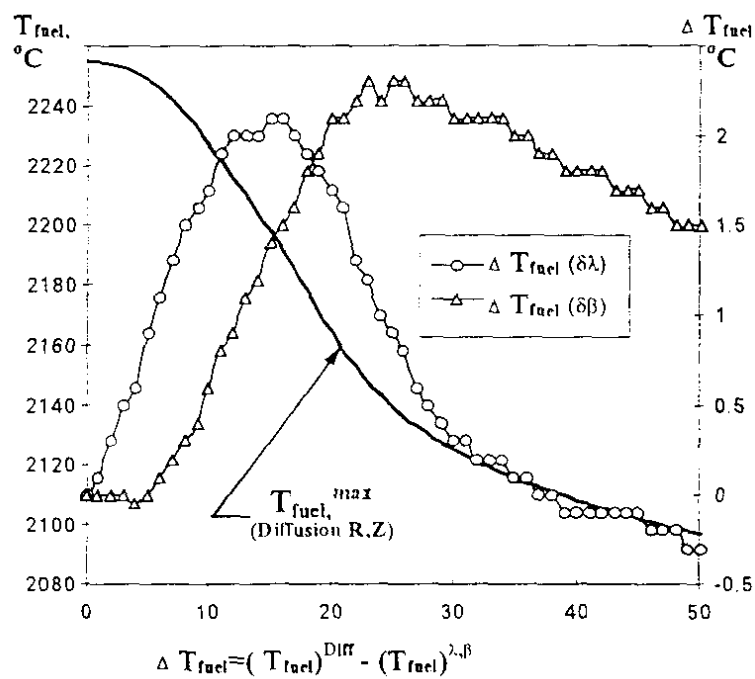


FIG. 14. Change of maximum fuel temperature under variation of neutron kinetics parameter, ULOF accident.

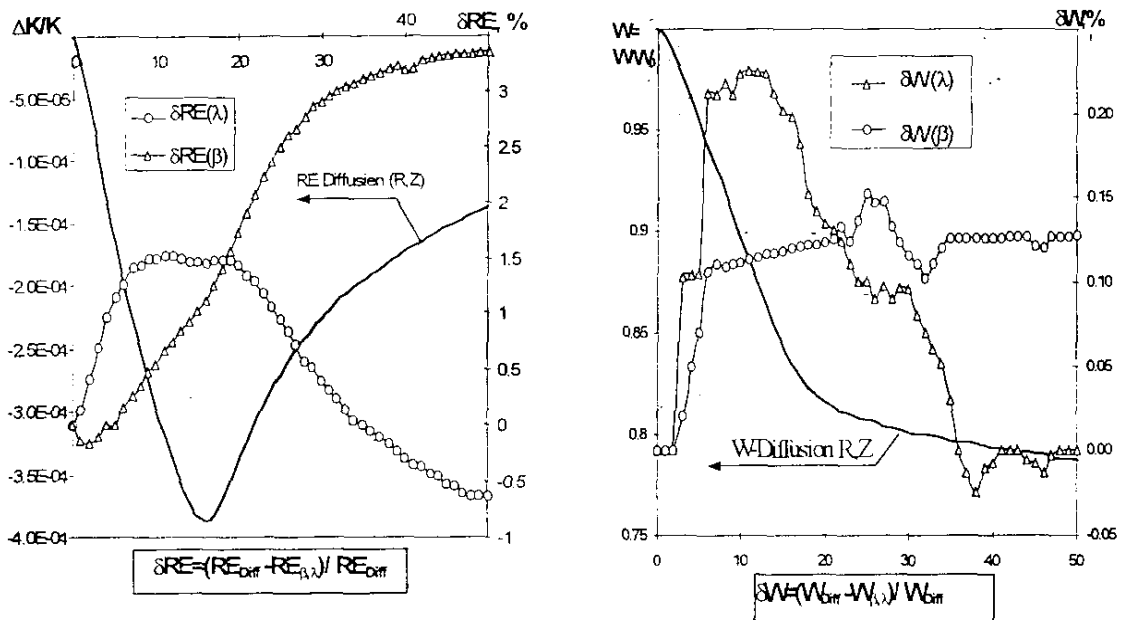


FIG. 15. Total reactivity and relative power in ULOF accident ($G = 30\% \text{ Go}$) and influence of parameters of delayed neutrons.

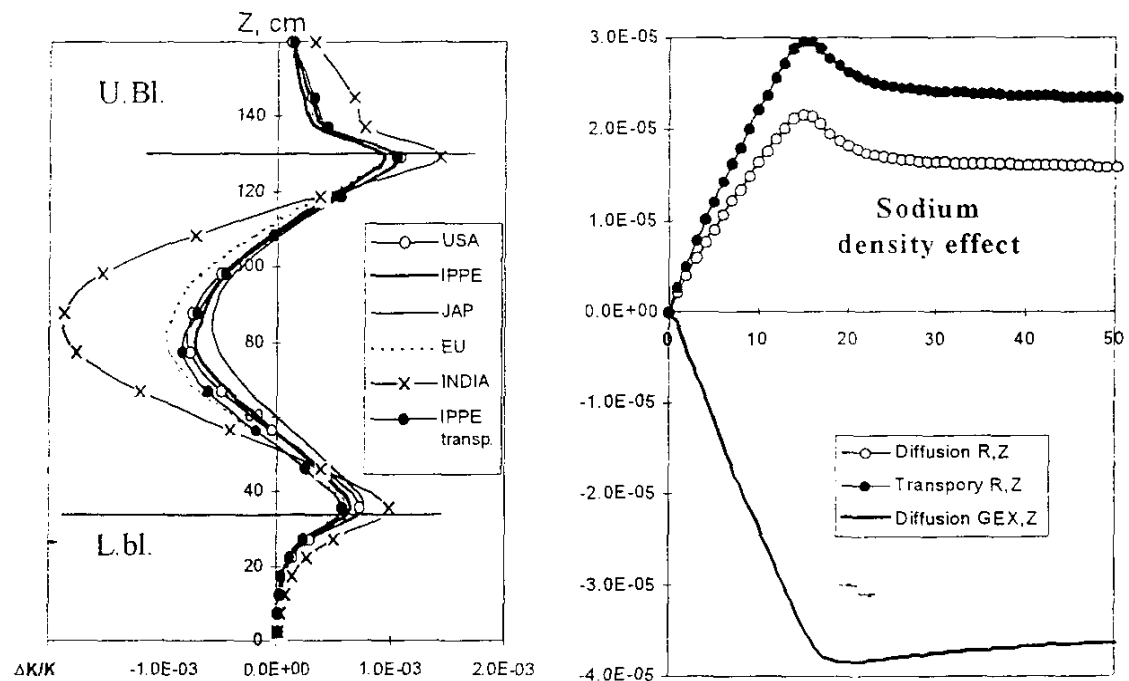


FIG. 16. Integral of sodium efficiency on fuel SA (A) u and sodium density reactivity (B) in UTOP accident (different -ways of calculation of reactivity) $G = 30\%$.

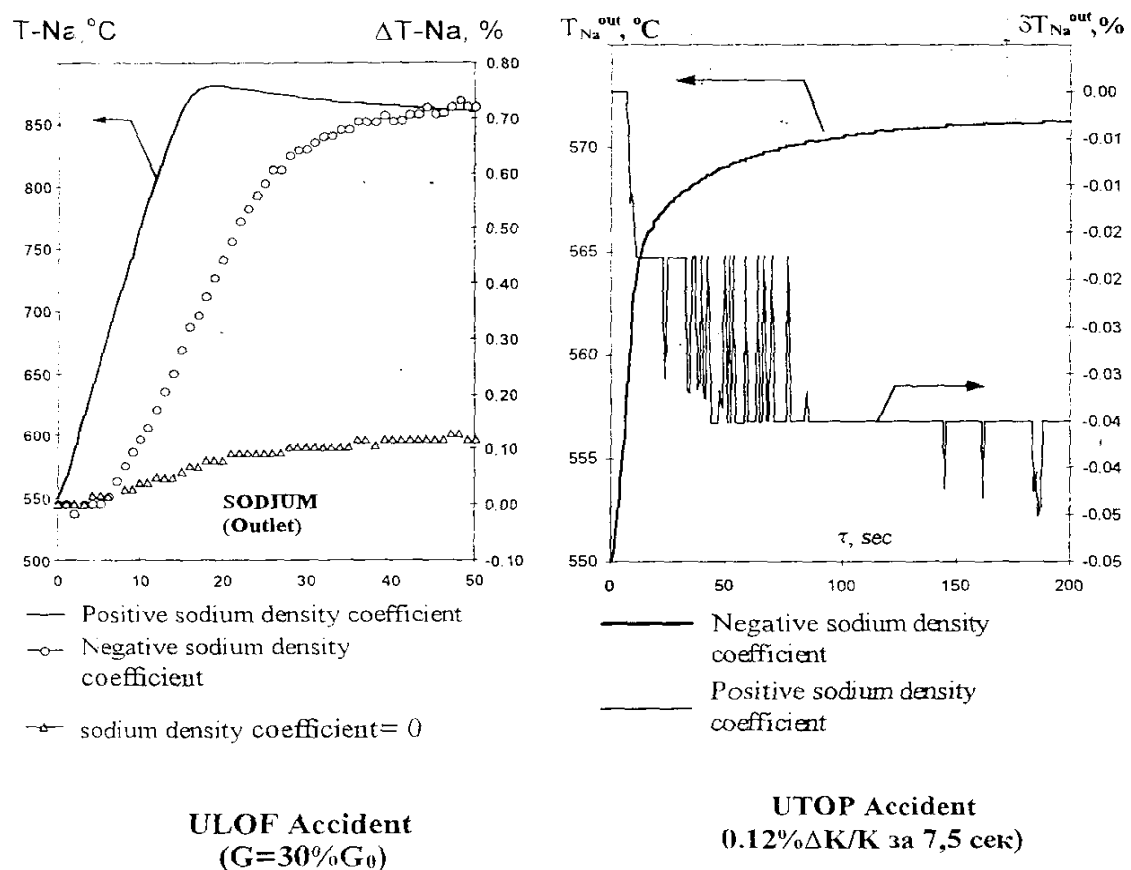


FIG. 17. Change of sodium outlet temperature in typical accidents with a variation of value sodium density components.

TABLE 2. REACTIVITY COEFFICIENTS DUE TO THERMAL EXPANSION OF MATERIALS

	2D Direct calculation on k_{eff}	
	Axial Expansion	Radial Expansion
OKBM (Diffusion)	-0.1415	-0.4827
IPPE (Diffusion)	-0.134	-0.478
China	-0.16779	-0.51048
EU	-0.1378	-0.465
India	-0.1395	-0.4837
Korea	-0.13755	-0.44929
Japan	-0.1395	-0.4812
USA	-0.1327	-0.4360

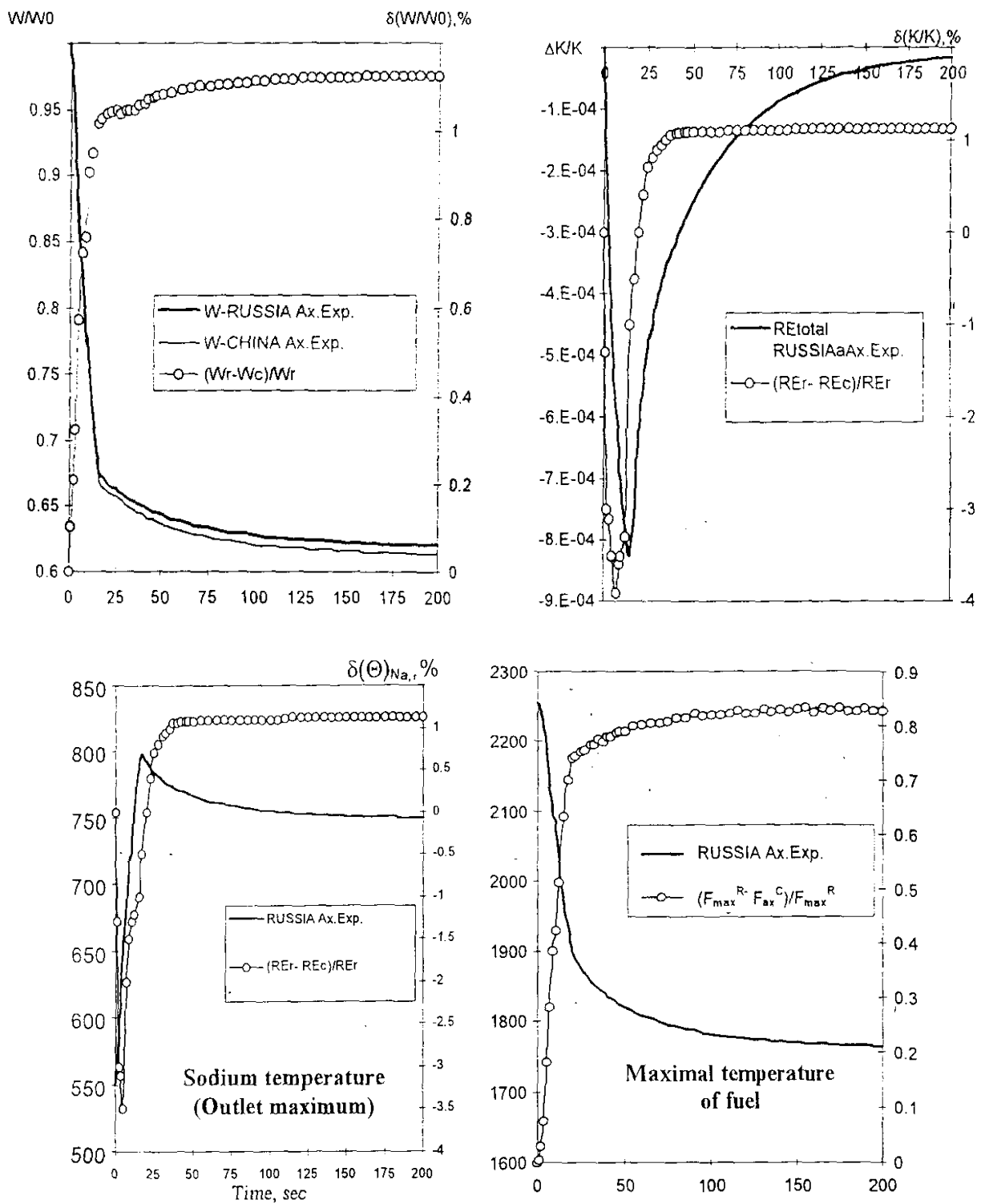


FIG. 19. Influence of components from axial expansion value on power and reactivity (ULOF, 30% G_{NOM}).

10. CONCLUSIONS

In the results of calculational studies the following was received:

- 1) The differences observed in integral values of reactivity coefficients and in their spatial distributions (in relative units) are great in the regions where the leakage component is definitive. At the same time contribution of those regions into total value of reactivity coefficient is negligible, especially taking into account temperature change of the reactor state.
- 2) For the results obtained by different methods the proposed method of the results comparison was used; the method is based on studying of accidents dynamics with the usage of different sets of calculational values of reactivity coefficients. Such comparison was based on specially created for this purpose simplified dynamic code DICOR. The code enables to determine allowable limits of reactivity coefficient variations using for that purpose changes of maximum temperatures. On this stage 3 sets of reactivity coefficients obtained in Russia were chosen: diffusion and transport calculation in R-Z geometry and diffusion calculation in HEX-Z geometry. Such choice was substantiated by the fact that practically all the rest basic results are embraced by this set. From the other side such set allows estimate both methodological error in the same geometry and preliminary model error in the same calculation approximation (in diffusion).
- 3) The differences observed in integral values of reactivity coefficients and in their spatial distributions (in relative units) are great in the regions where the leakage component is definitive. At the same time contribution of those regions into total value of reactivity coefficient is negligible, especially taking into account temperature change of the reactor state.
- 4) For the results obtained by different methods the proposed method of the results comparison was used; the method is based on studying of accidents dynamics with the usage of different sets of calculational values of reactivity coefficients. Such comparison was based on specially created for this purpose simplified dynamic code DICOR. The code enables to determine allowable limits of reactivity coefficient variations using for that purpose changes of maximum temperatures. On this stage 3 sets of reactivity coefficients obtained in Russia were chosen: diffusion and transport calculation in R-Z geometry and diffusion calculation in HEX-Z geometry. Such choice was substantiated by the fact that practically all the rest basic results are embraced by this set. From the other side such set allows estimate both methodological error in the same geometry and preliminary model error in the same calculation approximation (in diffusion).
- 5) Analogues of typical accident situations (ULOF and UTOP types accidents) were developed which allow to use code D1COR in which boiling and melting processes are not envisaged. For full scale ULOF accident the results are qualitative only.
- 6) The results of simplified dynamic studies carried out give evidence of weak influence of method of reactivity coefficients calculation in the framework of the same R-Z geometry for reactors with traditional core design, in particular for considered test model of the BN-600 reactor. Model error — transition to HEX-Z geometry — will be determinative.
- 7) For full scale ULOF accident (qualitative estimate only) it is seen that for 3 sets of reactivity coefficients chosen (RHETN, TWODANT, TR1GEX) deviations of the results could reach: ~ 2.5% (~ 9 MW) for power, ~ 2% (-0.00002 $\Delta K/K$) for reactivity, ~ 20°C for mean temperature of fuel and – 5°C uncertainty in sodium temperature in the moment of boiling. For the considered analogue of the ULOF ($G = 30\% G_0$) type accident the deviations of thermal-technical parameters will be, respectively: -14 MW for power, -8% difference in total reactivity between 2D and 3D calculations (difference between transport and diffusion calculations for R-Z geometry does not exceed 1%, and it is explained in first turn by the value of sodium density component which in 3D calculation changes its sign); deviations in sodium temperature are < 7°C and less than 10°C for fuel temperature under transition to 3D reactivity coefficients.

- 8) For the UTOP type accident (insertion of reactivity $0.1\% \Delta K/K$) the results also demonstrate weak dependence of maximum values of thermal-technical parameters from the set of reactivity coefficients used.
- 9) At the stage of preliminary dynamic calculations the observed differences in reactivity coefficients does not lead to essential change in description of accident processes. It is connected with the design of the reactor considered — traditional design with thick axial blankets. For reactors with sodium plenum the influence of model non-diffusiveness demonstrate more strong character. In the considered thermal-hydraulic model of the accident it was not taken into account change of temperatures in the control rods channels — and in the steel blanket. Contribution of those zones and also influence of accuracy of reactivity coefficients calculation on reactor dynamics with sodium boiling ($G = 3\%$) could be estimated later with the usage of more sophisticated dynamic codes (for instance, SAS4A). Sufficient reliability of the results obtained with the usage of Russian computer codes being employed in the practice of the design assessments of reactivity coefficients was demonstrated. Nevertheless the problem of accuracy of calculations in such regions for reactors with sodium plenum and steel blankets is evident; in the first turn it is related to neutron fluxes calculation and connected with the fluxes functionals (for instance, power distribution).

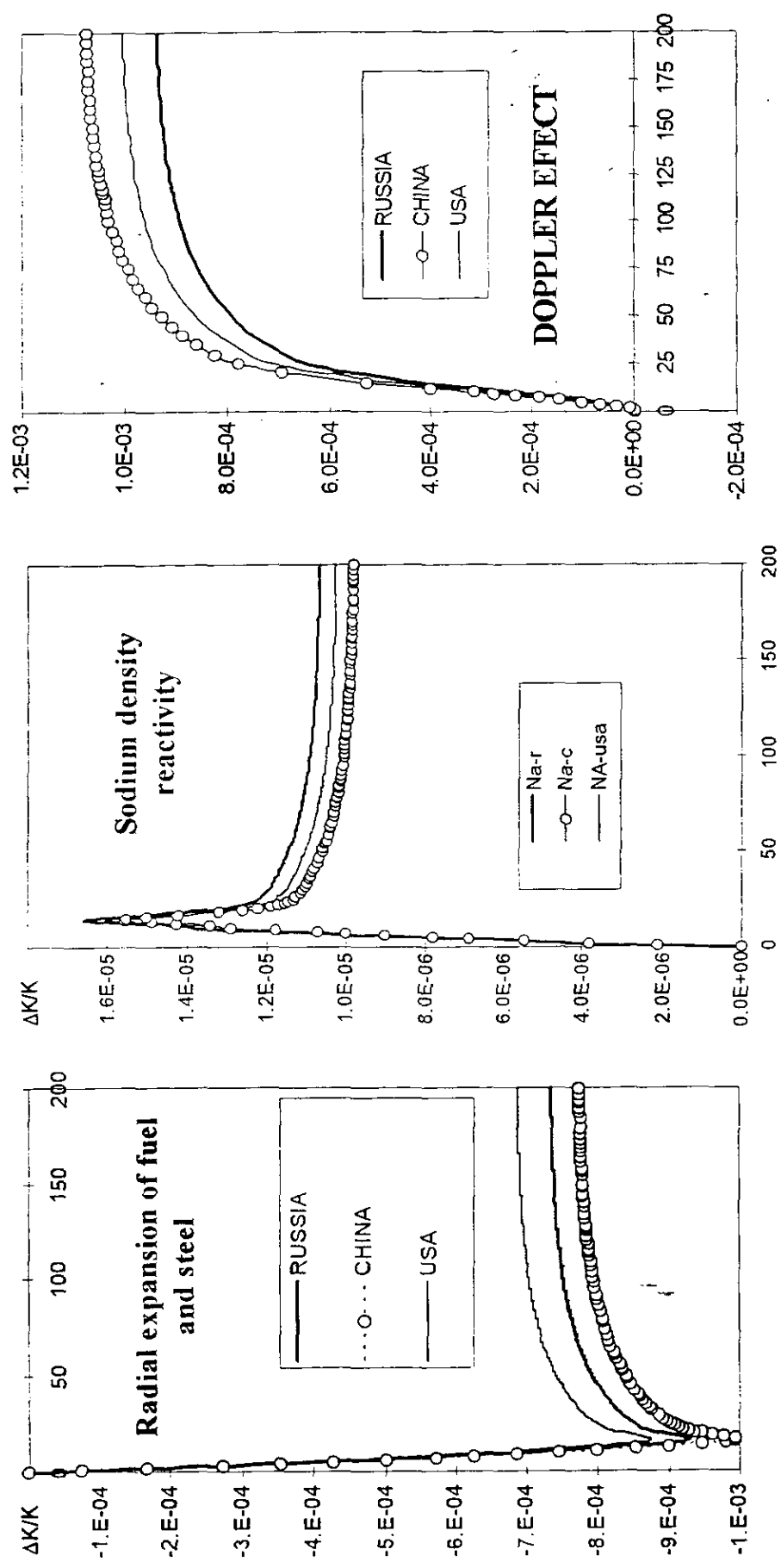


FIG. 21. The basic reactivity components of a feedback with a variation TCR_{RAD} ULOF accident $G = 30\% G_0$

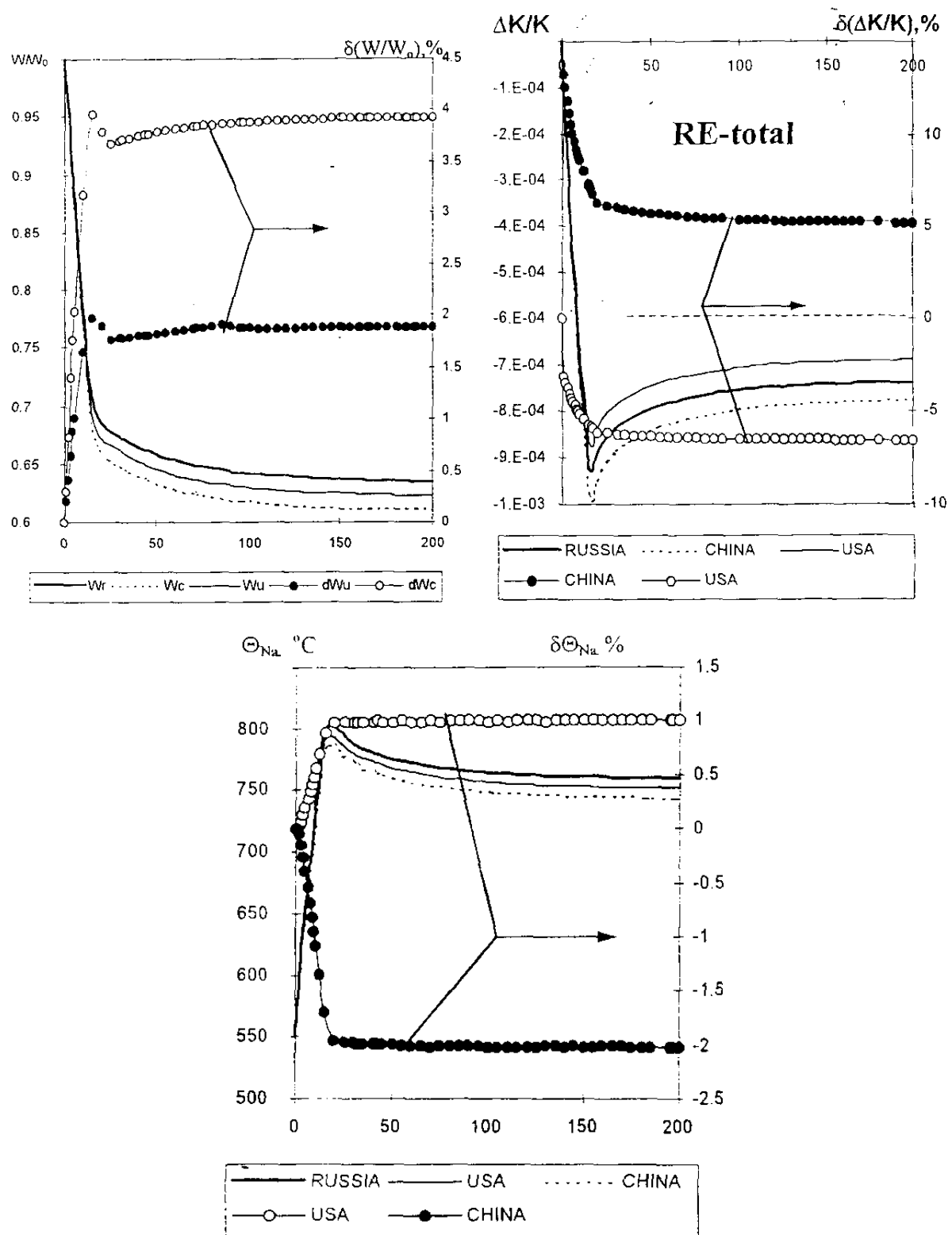
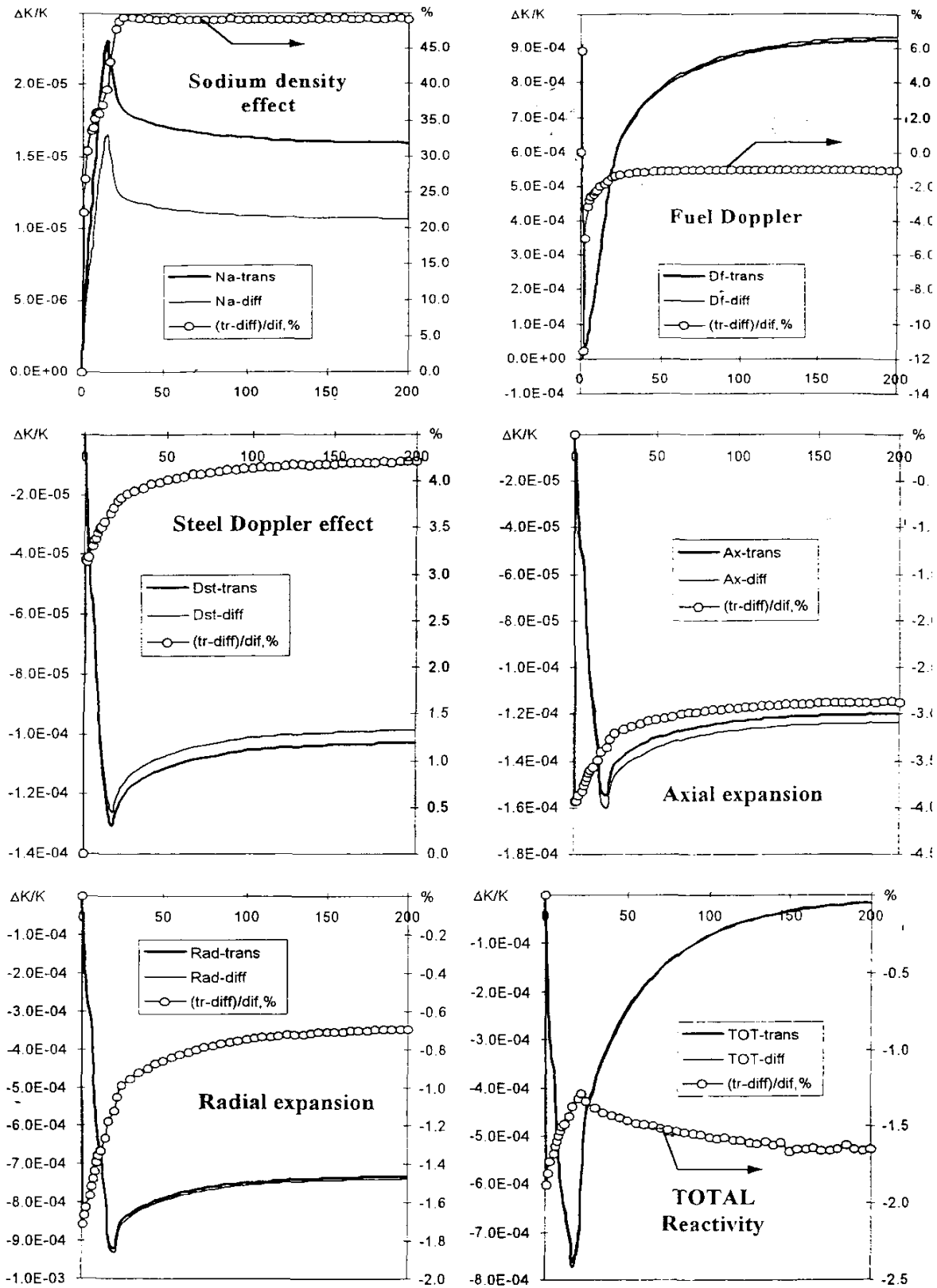


FIG. 22. Change of the basic parameters with a variation reactivity coefficient from radial expansion.



APPENDIX: FIG .A.1. Reactivity components in ULOF accident ($G = 30\%G_0$)
 $A - TCR_{Rad}^{Diff,Transp}(r,z)$
 $= TCR_{Rad}^{Total}(r,z) = \{TCR_{Rad}^{Fuel}(r,z) + TCR_{Rad}^{Steel}(r,z)\}^{Diff,Transp}$

Appendix IV

SIMPLIFIED APPROACH TO DYNAMIC PROCESS MODELING

A. Danilytchev, D. Elistratov, V. Stogov
Institute of Physics and Power Engineering, Russian Federation

1. INTRODUCTION

This document presents the OKBM contribution to the analysis of a benchmark of BN-600 reactor hybrid core with simultaneous loading of uranium fuel and MOX within the framework of the international IAEA Co-ordinated Research Project ‘Updated Codes and Methods to Reduce the Calculational Uncertainties of the LMFR Reactivity Effects’. In accordance with Action 12 defined during the second RCM, the simplified transient analysis was carried out on the basis of the reactivity coefficients sets, presented by all CRP participants. Purpose of present comparison is the evaluation of spread in the basic transient parameters in connection with spread in the used reactivity coefficients. A ULOF accident initial stage on the simplified model was calculated by using the SAS4A code.

2. CALCULATION METHOD

2.1 Used code

For calculations SAS4A REF96R0.1 code was used. The code was received from ANL specialists in 1997 for safety analysis of the BN-600 reactor hybrid core within the framework of the Russia-USA cooperation. For the present calculations the code is applied by approbation of ANL specialists.

The code is intended for a transients analysis and provides simultaneous calculation of the point neutron kinetics, the heat exchange and the mass transfer of the basic materials for the sodium cooled LMFRs. The core is simulated by several (up to 35) channels, for each of which the axial distribution of necessary parameters is assigned.

2.2 Adopted preconditions and used model

The evaluation of reactivity coefficients spread effect on accident consequences was made on the base of ULOF accident analysis. The set of reactivity coefficients obtained within the framework of the CRP, just suits the calculation of initial stage of this accident up to a sodium boiling. For this accident stage the volume of the required information is not too bulky yet and it is possible to use the model with moderate number of channels.

The model for calculation was created by simplification of the existing full scale 22 channels model of the BN-600 reactor hybrid core. The main difference is the reduction of channels quantity in the model. Taking into account of parameters of the CRP benchmark 8 channels were accepted for calculations using SAS4A code. Their description is listed in Table 1.

The comparison of these calculation results with the results based on the 22 channel models has shown the sufficient consistency of both models.

2.3 Requirement to input data

Considerable volume of the input data with the reactor design description, the geometry of channels and the basic materials properties was adopted on the base of the reference 22 channel model and subsequently was not changed.

TABLE 1. CHANNEL DESCRIPTION

Channel No	Group of the benchmark assemblies
1	LEZ-1 FSAs
2	LEZ-2 FSAs
3	MEZ FSAs
4	MOX fueled FSAs
5	HEZ FSAs
6	1 st row SSAs
7	Others SSA and radial reflector
8	SHR, SCR

The distributions of power and reactivity coefficients obtained in the CRP frameworks only were changed during carried out comparison. The following axial distributions for each channel are required for calculations:

- The distribution of a Doppler constant at presence and at absence of sodium. Taking into account of expected termination of calculation at the sodium boiling onset these both distributions were taken identical;
- The distributions for worth of steel, sodium and fuel in terms of dk/k/kg.;
- The power distribution.

These distributions were prepared in the certain format.

For correct temperatures calculation by the SAS4A code the power distributions for all model channels, including the channels without fuel are required.

In addition to the mentioned reactivity effects in model the reactivity effect from the core radial expansion was described also. This effect was earlier calculated in the OKBM and was set here by an identical way for all calculations. In correspondence with one of SAS4A code options this effect is set as the following tabulated relation to the average sodium temperature at core outlet (see Table 2).

TABLE 2. REACTIVITY EFFECT DUE TO THE CORE RADIAL DEFORMATION

Relative power to relative flow rate ratio (N/G)	Average temperature on core outlet, K	Value, \$
1	823	0
1.5	916	9.50E-03
2.0	1008	2.22E-02
2.5	1101	3.90E-02
3.0	1193	5.57E-02
3.5	1286	7.30E-02

3. VARIED INPUT DATA

3.1 Input data origin

For comparative calculations the input data from IAEA site for the CRP on the moment 19.10.2001 were adopted. Some of data was taken from spreadsheets, another data was taken from the initial textual documents. The data on the Phase 2 obtained in diffusion approximation were used.

Eight input data sets (according to the number of the CRP participants groups) were prepared.

3.2 Complementary data processing

All obtained data were brought together into the book consisting of Excel spreadsheets for cross check and analysis for mutual correspondence and self-consistency. By results of such check some technical mistakes in data (misprint in a exponent number, erroneous addition of rows or columns in the tables, etc.) were revealed and corrected. The most essential corrections were coordinated with the interested party. On occasion as a consequence of incompleteness or inaccessibility in the convenient form a data were filled by the special way. It is mentioned further.

The updated tables were used for the preparation of input data for the SAS4A code in a necessary format.

Contents of these tables, taking into account of their very large volume, and their comparison in a present document are not presented and they will be a subject of consideration in the other documents.

At the input data analysis their incompleteness has come to light:

- The power distribution with taking into account energy releases in non-fueled benchmark zones was presented only from ANL, IGCAR, KAERI and OKBM. The power distribution from OKBM was substituted for data sets of the other participants;
- In IGCAR data there was no distribution of the Doppler constant for steel. The data averaged over other CRP participants in appropriate way were taken.

4. CALCULATION RESULTS OF ULOF ACCIDENT INITIAL STAGE

4.1 Adopted parameters for results comparison

Calculations results using SAS4A code are the time dependence graphs for set of parameters — total current reactivity and its components, current reactor power, temperature of the basic materials in key positions, sodium flow rate, velocities and boundaries location of the basic moving mediums. For the evaluation and the comparisons of ULOF accident calculation results were chosen the following parameters:

- Graphs of time dependence for the current reactivity and its components;
- The time of first bubble generation in sodium;
- Value of the current reactivity and current power on the moment of the first bubble generation.

4.2 Results as integrated parameters

The integrated results are presented in Table 3.

4.3 Graphs of the current reactivity and its component

In Figures 1-8 the time dependences of the current reactivity and its components starting with the beginning of accident up to the moment ~23 s from the beginning are presented. This time point approximately corresponds to the first bubble generation time according to data of the participants majority, that allows to draw the graphs in identical scale for convenient comparison.

In Figures 9-16 the time dependences of the current reactivity and its components are presented from the beginning of accident up to the moment which was achieved in each particular calculation. It is necessary to stress, that to obtain of correct results of calculation with the sodium boiling both steel and fuel relocation models with a plenty of channels are required, and after the boiling onset the updating input data are required. The last eight figures are presented only for an illustration of an increased discrepancy in the calculational results in case of accident progress.

TABLE 3. INTEGRATED PARAMETERS ON THE MOMENT OF A FIRST BUBBLE GENERATION

Participant	Time from the beginning of accident, s	The channel	The current total reactivity, cents	The current relative power, %
ANL	22.22	3	-5.3	84.5
CEA&SA	22.29	3	-5.7	83.6
CIAE	21.09	3	-5.0	86.2
IGCAR	24.55	3	-6.6	80.5
IPPE	22.21	3	-5.5	83.9
JNC	23.66	3	-6.6	80.9
KAERI	24.52	5	-7.0	79.9
OKBM	22.06	3	-5.5	84.1

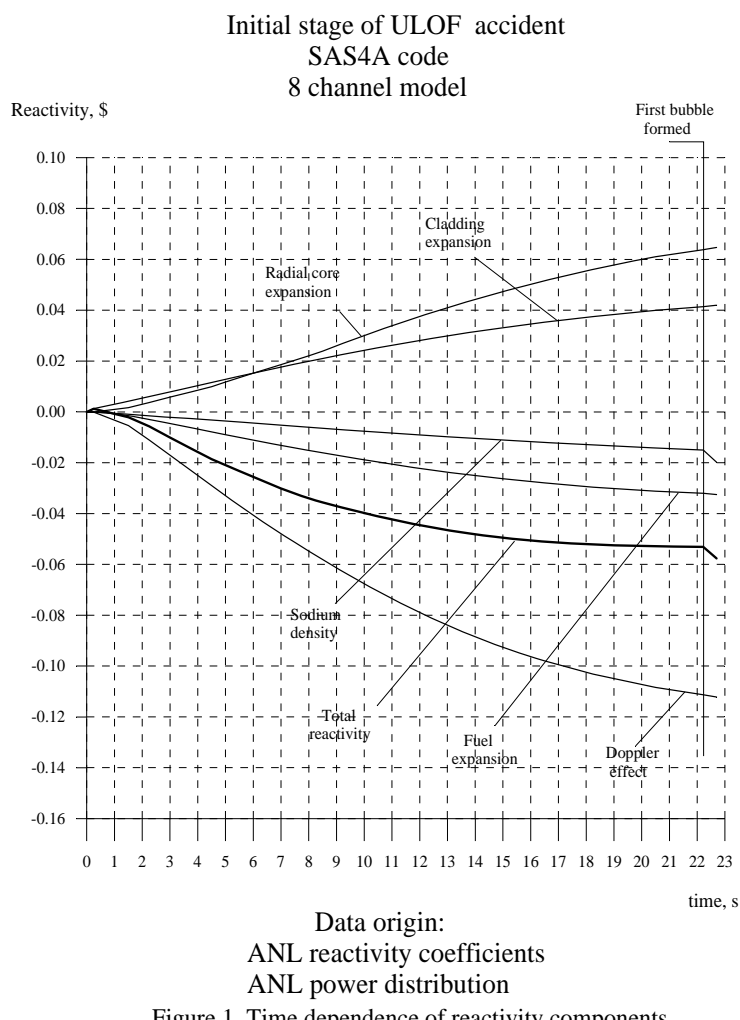


Figure 1 Time dependence of reactivity components based on ANL data

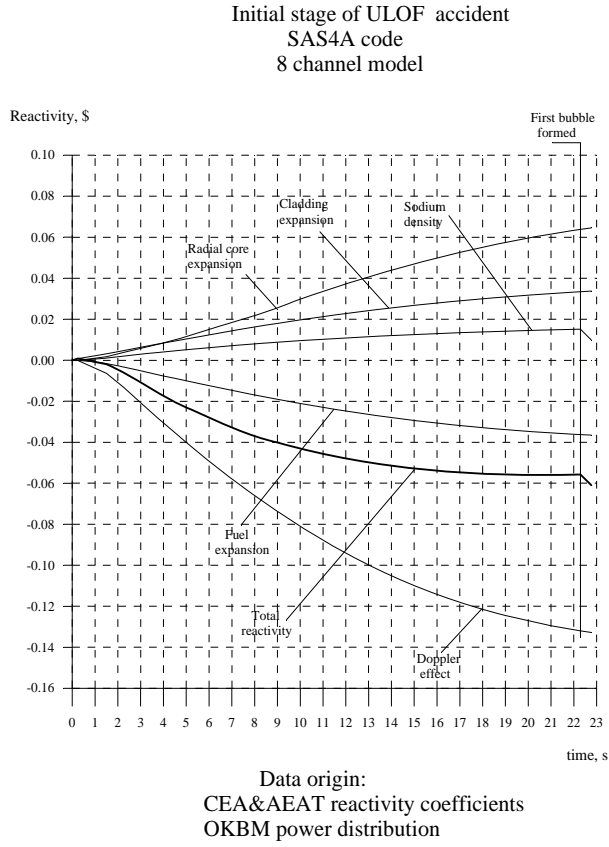


Figure 2 Time dependence of reactivity components based on CEA&AEAT data

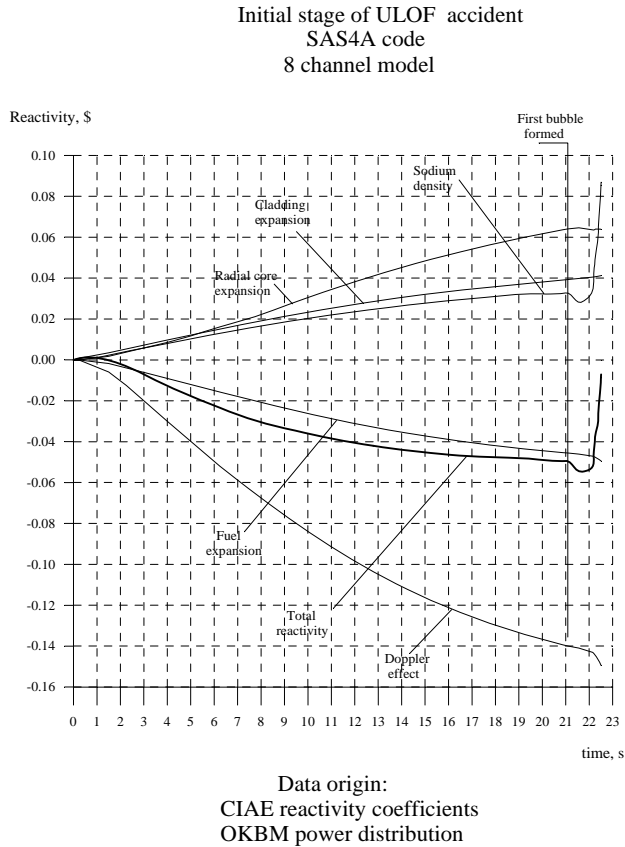


Figure 3 Time dependence of reactivity components based on CIAE data

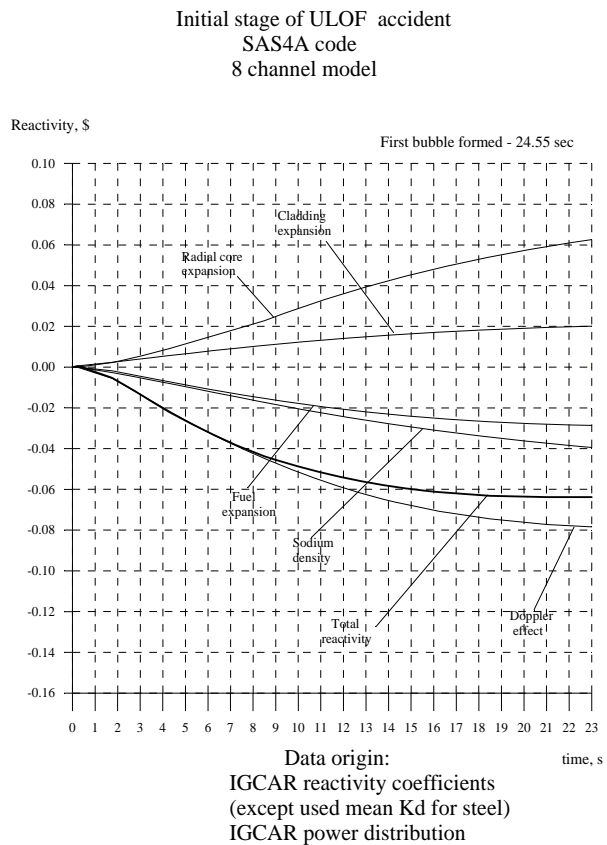


Figure 4 Time dependence of reactivity components based on IGCAR data

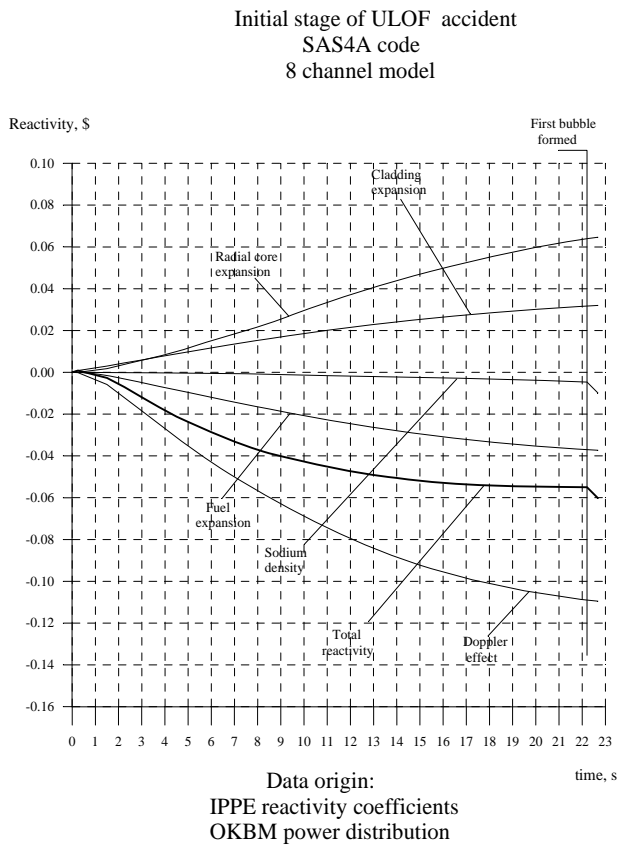


Figure 5 Time dependence of reactivity components based on IPPE data

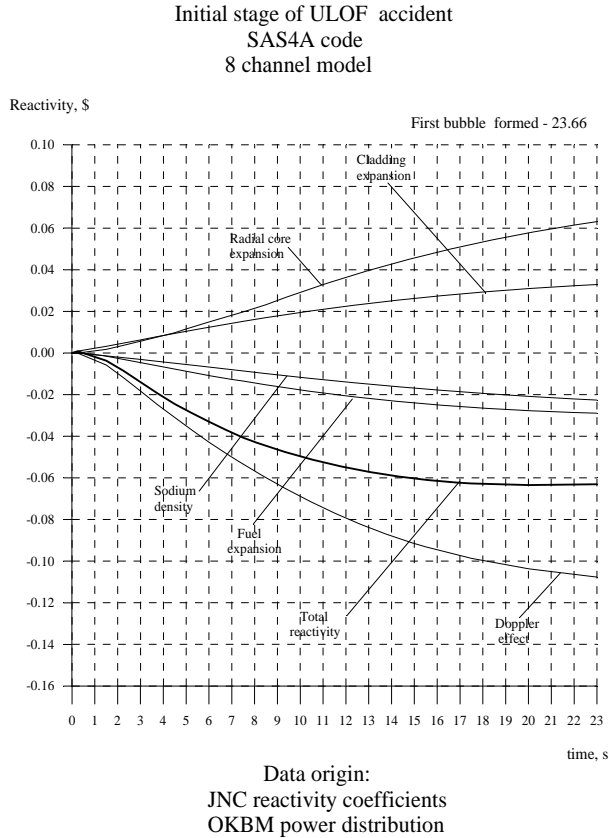


Figure 6 Time dependence of reactivity components based on JNC data

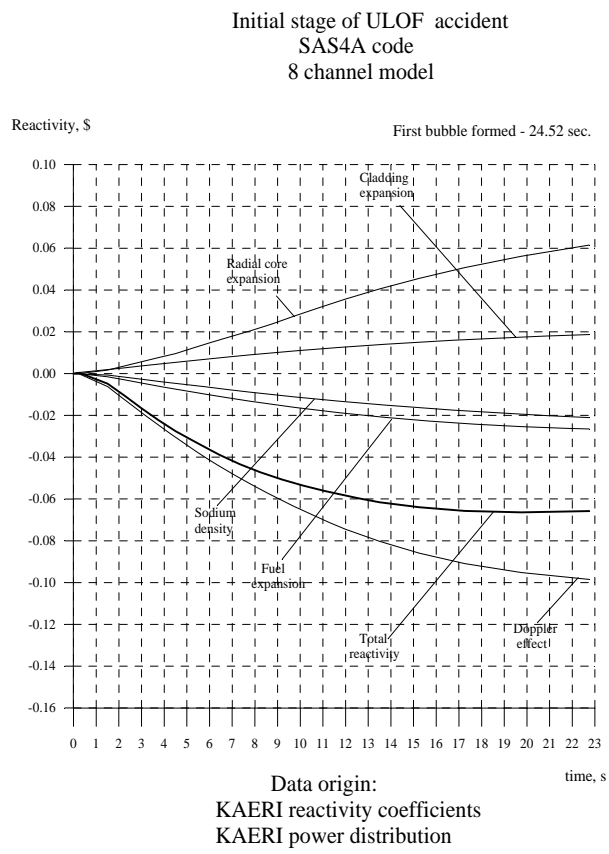


Figure 7 Time dependence of reactivity components based on KAERI data

Initial stage of ULOF accident

SAS4A code

8 channel model

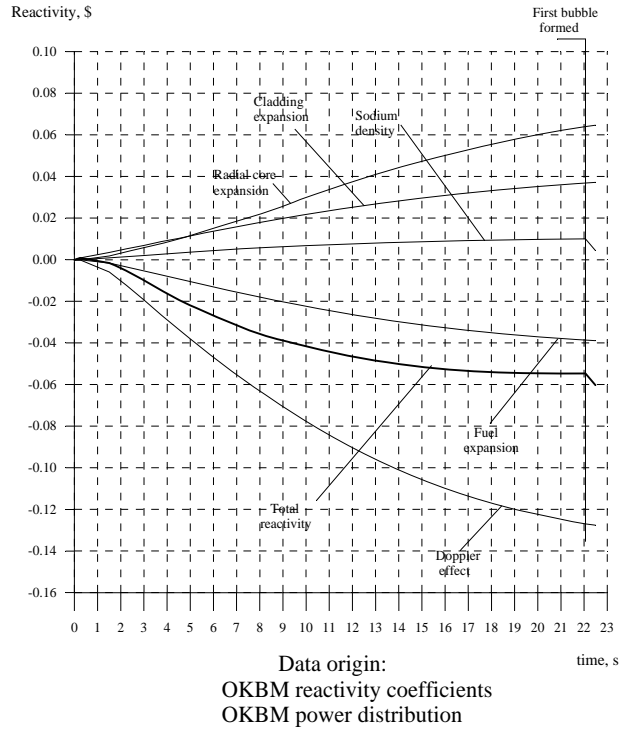


Figure 8 Time dependence of reactivity components based on OKBM data

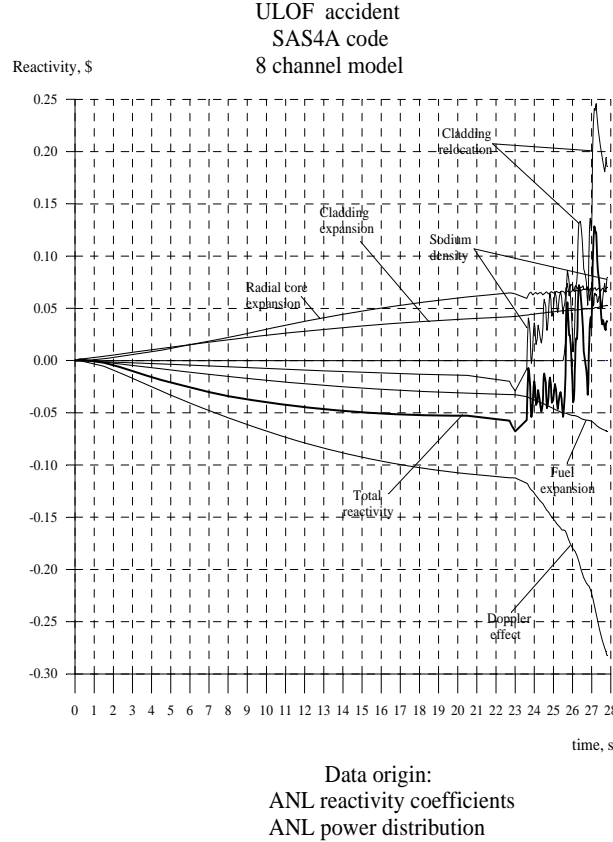


Figure 9 Time dependence of reactivity components based on ANL data

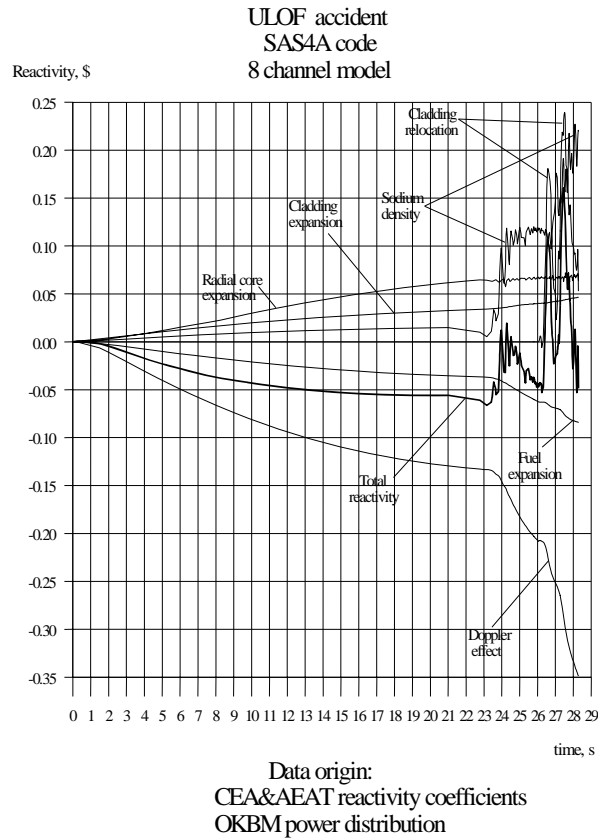


Figure 10 Time dependence of reactivity components based on CEA&AEAT data

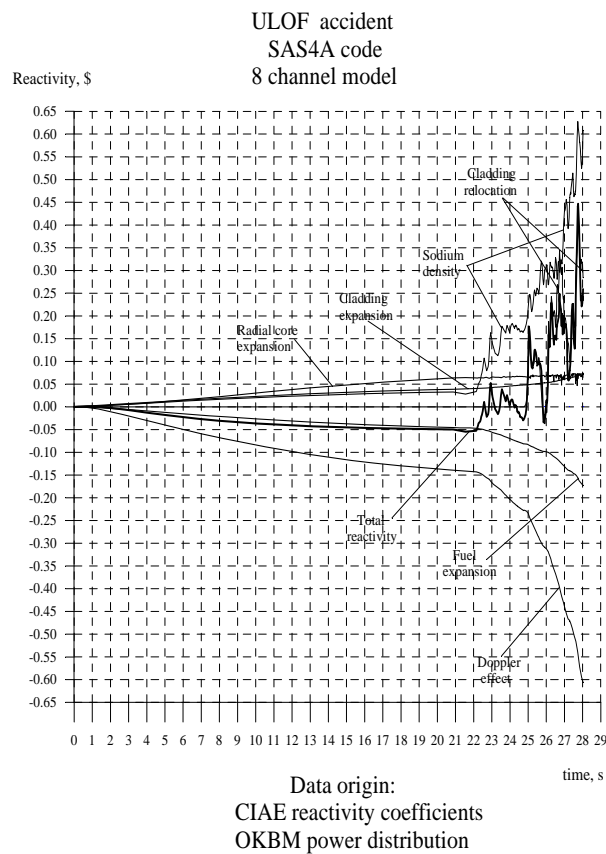


Figure 11 Time dependence of reactivity components based on CIAE data

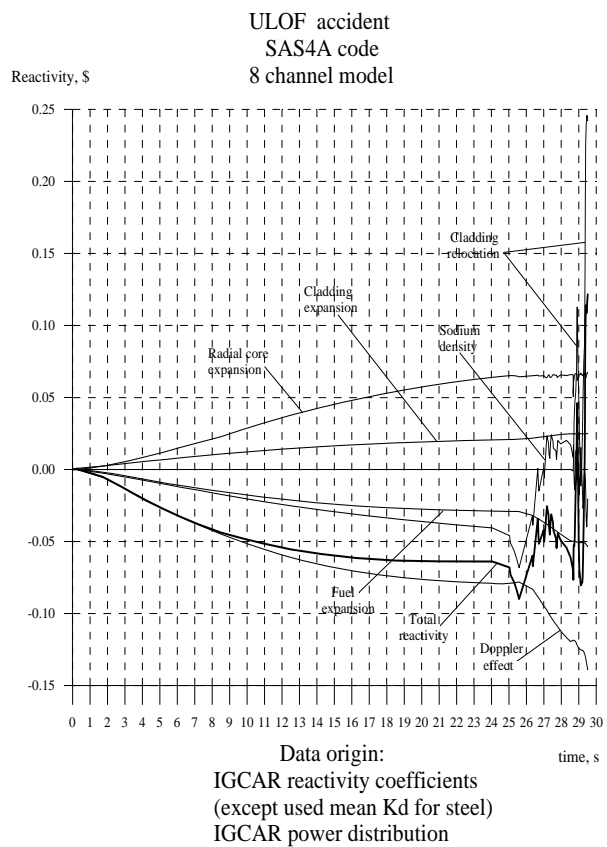


Figure 12 Time dependence of reactivity components based on IGCAR data

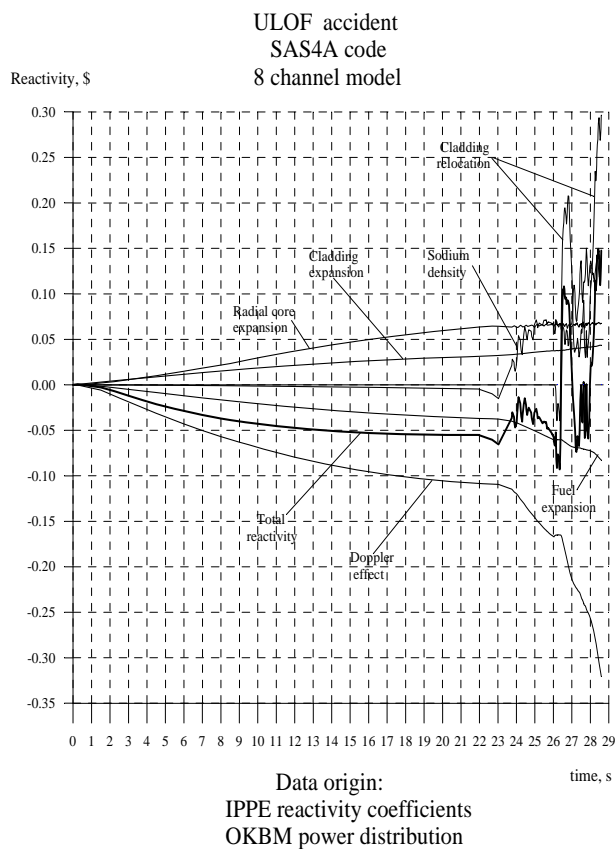


Figure 13 Time dependence of reactivity components based on IPPE data

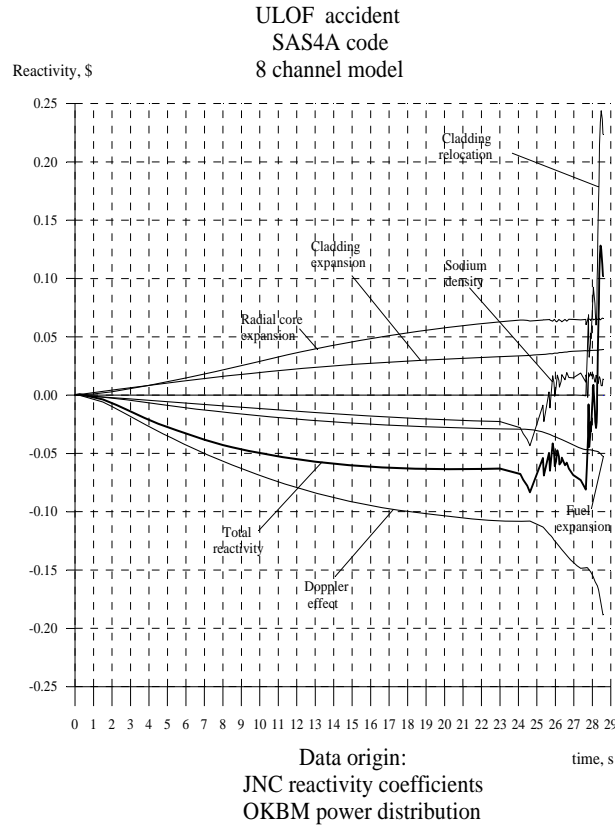


Figure 14 Time dependence of reactivity components based on JNC data

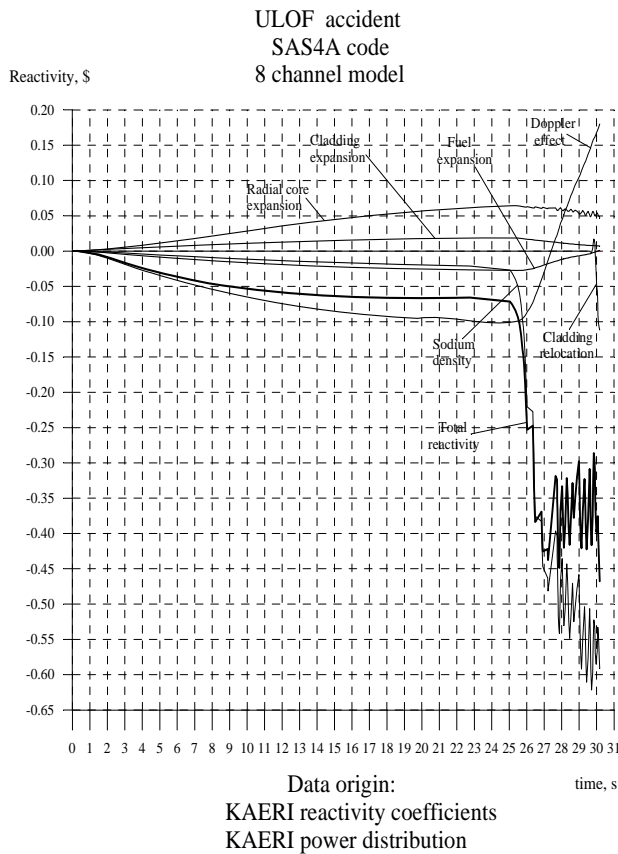


Figure 15 Time dependence of reactivity components based on KAERI data

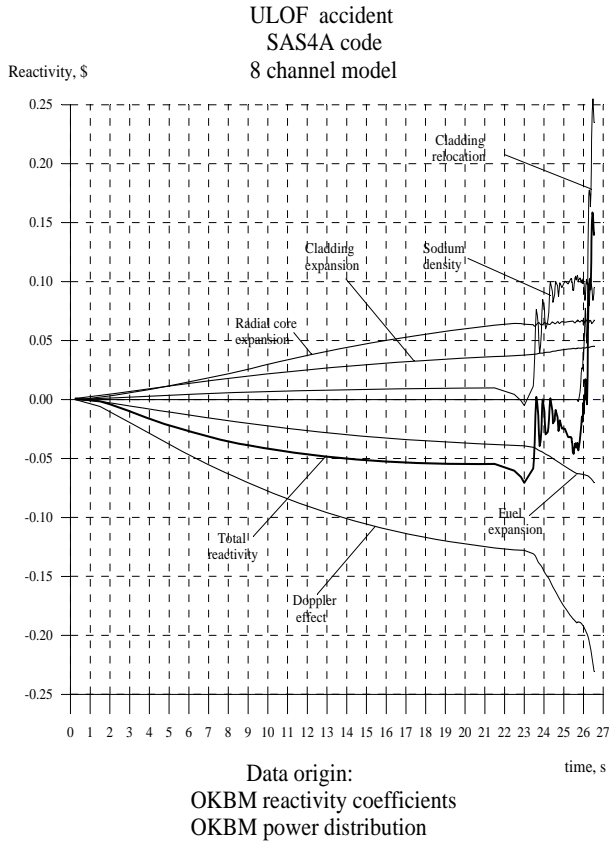


Figure 16 Time dependence of reactivity components based on OKBM data

4.4 Preliminary analysis of calculations results

From Table 3 one can see, that for the half of participants the first bubble generation time with very small spread comes to 22.2 s. For other participants this parameter has evident spread. The values of the current reactivity and current power well correlate among themselves and with a first bubble generation time.

The consecutive analysis of the obtained results for each participant in comparison to the published reactivity coefficient distributions allows to note the following differences of these results in contrast to the average values.

The ANL results are on the whole close to the average results. The sodium component is slightly too negative, which correlates with evident overestimation of positive sodium worth in axial blankets and in the MOX fueled zones. The component of steel expansion is apparently overestimated, and it concerns with by the overestimated negative steel worth in the majority of fuel zones and underestimated positive steel worth in axial blankets and in HEZ.

The results of the EU participants also are close to the average results. It may be noted that a little bit overestimated Doppler effect, which correlates with its small excess above the average effect in fuel parts of the core. Besides the sodium component is slightly more positive, and it correlates with the sodium worth slightly shifted in fuel zones to the negativity.

The CIAE results evidently differ from the average results by large positive sodium component. They correlate with the sodium worth, strongly shifted to the negativity in all fuel zones and in axial blankets. The effect from fuel expansion is a little overestimated and it correlates with the overestimated fuel worth in MEZ.

In IGCAR results the large negative sodium component stands out against mean values. From the published tables it could be found that it concerned with the negative sodium worth in LEZ and MEZ, and with the overestimation of the positive sodium worth in other fuel zones and axial blankets.

The similar character of a deviation from the average in some degree is observed in the steel worth distribution. It has also caused some shift to the negativity of the steel expansion components. The Doppler effect component in a reactivity balance is evidently underestimated. As follows from the analysis of the published tables, it correlates with significant underestimation of the Doppler constant in all fuel zones.

The IPPE results to the greatest degree correlates with the average results, and it corresponds with the minor difference of distributions of reactivity coefficients from average ones.

The JNC results differ from the average results by slightly more negative value of the sodium components. It correlates with the negative sodium worth, underestimated relative to average distribution in LEZ and MEZ and overestimated positive sodium worth in axial blankets.

The KAERI results show that the steel expansion component is slightly underestimated, which can be concerned with the strongly overestimated positive steel worth in HEZ. The sodium component of reactivity is slightly shifted to negativity, that could be explained by the evidently overestimated positive sodium worth in HEZ and in MOX fueled zone. The importance of these specified features in the reactivity coefficients distribution becomes more significant taking into account some overestimation of power in HEZ. As a result, sodium begins to boil in HEZ, instead of in MEZ, as by results of the other participants.

The OKBM results differ from the average results by slightly more positive value of the sodium component. The analysis of reactivity coefficients distributions has revealed corresponding significant shift to negativity of sodium worth in MOX fueled zone relative to the average values.

5. CONCLUSIONS

The existing nowadays spread in reactivity coefficients appeared to be insignificant from the point of view that consequent spread in the basic integrated parameters of an initial ULOF accident stage is insignificant.

Time of the sodium boiling onset, the current reactivity and the reactor power to this moment determined on data all participants, are very close.

The current reactivity to this moment ranges from -5.0 cents up to ~7.0 cents. The current power value ranges from 79.9% up to 86.2% relative to initial value.

The sodium density component shows the most significant relative spread among the components of the current reactivity balance. To the moment of boiling the value of this effect, taking into account the sign distinctions of its value, ranges from -66% up to +59% of the current reactivity. Correct analysis of the further accident progress needs considerably more high level of its simulation. However from existing comparison of accident progress after the sodium boiling onset it could be marked, that at a stage of a sodium boiling the impact of uncertainty of effect due to the sodium density change becomes much more essential.

The Doppler effect brings into the current reactivity balance the most significant contribution. Therefore relatively minor spread in its value can strongly influence the reactivity balance. To the moment of boiling the value of a Doppler effect ranges from 120% up to 280% relative to the current reactivity

The components from the fuel and steel axial expansion have different signs and are close on absolute value. This value to the moment of boiling ranges from 38% up to 90% relative to current reactivity. The contribution of the core radial expansion component is assumed determined by identical way to all participants and the corresponding value practically has no spread. However, it is necessary to mean, as this component has a significant uncertainty due to the complexity of the determination, both detailed distribution of the core deformations, and reactivity effect caused by such deformation. Taking into account of designated scale of this effect (~ 110% relative to current reactivity), its uncertainty can essentially affect scale of uncertainty in the transient progress.

Appendix V

EFFECT OF JFS SET CHANGES

(JNC'S RESPONSE TO ACTION 4.3 IN THE 4th CRP MEETING)

M. Ishikawa
Japan Nuclear Cycle Development Institute (JNC), Japan

1. REVISION OF JFS GROUP-CONSTANT SE

In the analysis of the present IAEA CRP, JNC used the Japanese standard 70-group constant set for fast reactors, JFS-3-J3.2, which was based on the Japanese evaluated nuclear data library, JENDL-3.2. The original JFS-3-J3.2 set was generated and released by JAERI in 1995 [1].

Recently, JNC found that two errors were included in the procedure to generate the original JFS set [2]. The major error was the mistreatment of the weighting function to process the group-wise constants from JENDL. The JFS was supposed to use the collision density spectra of a typical prototype fast reactor core as the weighting function, so called ‘REMO correction’, but the actual one used was much hardened than intended as shown in Fig. 1. The reason of this mistake is guessed as the confusion of the energy-unit integral and the lethargy-unit integral. The effect of this error was found to make the neutron spectrum of the calculated core too hard. Other minor error was related to the energy distribution of the secondary neutron by the inelastic and (n,2n) scattering reaction. The effect of the second error was found to make the neutron spectrum a little too soft, and somewhat to relieve the effect of the first error.

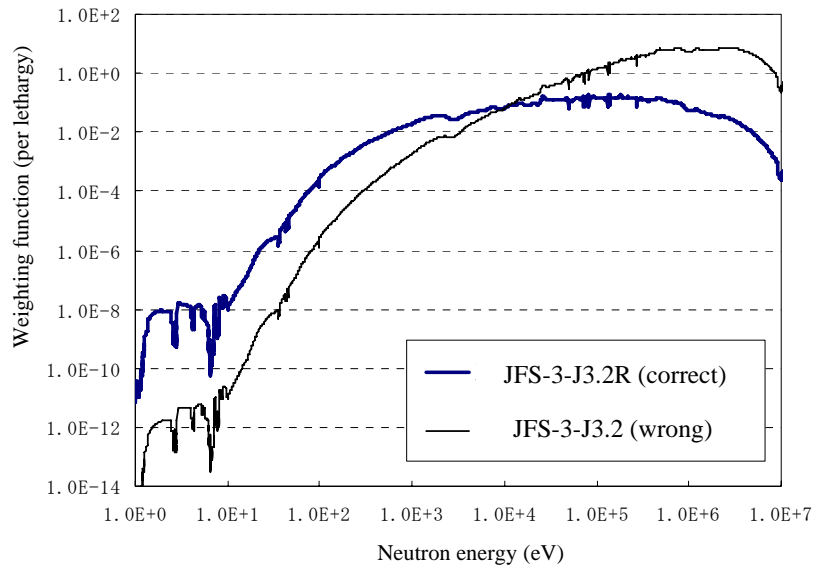


Fig. 1. Weighting function used to generate JFS-3-J3.2 and JFS-3-J3.2R.

In 2002, JNC generated and released a revised version of JFS set based on JENDL-3.2, named JFS-3-J3.2R, which was corrected the above problems. In the present IAEA CRP, JNC used the JFS-3-J3.2 in Phase 1, 2 and 3, and changed it to JFS-3-J3.2R from Phase 4. This report was submitted to estimate the effect of the JFS change in Phase 1, 2 and 3.

2. EFFECT OF JFS REVISION TO PHASE 1, 2 AND 3

According to the agreement in the 4th CRP meeting, JNC evaluated the effect of cross-section set change from JFS-3-J3.2 to JFS-3-J3.2R for the typical parameters of Phase 1, 2 and 3.

Table 1 shows the results for Phase 1: 2D RZ homogeneous model and Phase 2: 3D Hex-Z homogeneous model. In this survey, only basic diffusion calculations were performed, since the effect of the cross-section change to the transport correction factor is considered negligible. Main conclusions are:

- 1) The criticality was decreased by 0.2-0.3%dk. It is reasonable because the neutron spectrum of the core became softer by the cross-section change.
- 2) The absolute value of the fuel Doppler reactivity increased by 8-9%, which is also reasonable because the major energy of the fuel Doppler is rather lower, that is, keV to several-tens keV. On the other hand, the absolute value of the steel Doppler reactivity decreased by 7-8%, the reason of which is considered as the resonance of high energy region such as several-hundreds keV may give large contribution for the steel Doppler reactivity.
- 3) For other core parameters, the effects of cross-section change were not so significant. However it should be noticed that the small changed value of sodium density reactivity might be only the result of the cancellation of large positive and negative energy components, considering the JNC's experience of other cores.
- 4) The increase of neutron lifetime by 3% can be considered as the evidence of the spectrum softening by the cross-section change.

Table 2 showed the results for Phase 3: homogeneous burnup model. The influence to burnup reactivity by JFS change is not significant.

Table 3 summarized the result for Phase 3: EOC of homogeneous model. The effect to criticality and fuel Doppler reactivity was almost the same with Phase 1 and 2. On the other hand, the effect to sodium density reactivity was quite emphasized since the energy cancellation was not balanced like Phase 1 and 2. Table 4 is the result for Phase 3: BOC of heterogeneous model. The effect to criticality was the same with the previous cases, and the effect to control rod worth was negligible.

TABLE 1. BN-600 HYBRID CORE BENCHMARK CALCULATION RESULTS (BASIC DIFFUSION CALCULATION)

Item	Phase1 (RZ homogeneous model)			Phase2 (Hex-Z homogeneous model)		
	JFS-3-J3.2	JFS-3-J3.2R	Change ^{*1)} (%)	JFS-3-J3.2	JFS-3-J3.2R	Change ^{*1)} (%)
1 k_{eff}	1.00423	1.00165	-0.26	1.00713	1.00504	-0.21
2 Fuel doppler coefficient $k_{\text{eff}}(\text{Fuel_2100K})$ Coefficient (dk/kk'/dlnK)	1.00208 -0.00635	0.99933 -0.00688		1.00493 -0.00646	1.00267 -0.00701	8.6
3 Steel doppler coefficient $k_{\text{eff}}(\text{Steel_900K})$ Coefficient (dk/kk'/dlnK)	1.00376 -0.00116	1.00121 -0.00107	-7.5	1.00668 -0.00109	1.00463 -0.00102	-7.2
4 Sodium density coefficient $k_{\text{eff}}(\text{Sodium dens.}*1.01)$ Coefficient (dk/kk'/dp/p)	1.00431 0.00765	1.00173 0.00767	0.3	1.00724 0.01038	1.00515 0.01024	-1.4
5 Fuel density coefficient $k_{\text{eff}}(\text{Fuel dens.}*1.01)$ Coefficient (dk/kk'/dp/p)	1.00777 0.3491	1.00517 0.3490	0.0	1.01066 0.3466	1.00855 0.3459	-0.2
6 Absorber density coefficient $k_{\text{eff}}(\text{Abs. dens.}*1.01)$ Coefficient (dk/kk'/dp/p)	1.00397 -0.0265	1.00138 -0.0266	0.4	1.00693 -0.0200	1.00484 -0.0199	-0.5
7 Expansion coefficients Axial Coefficient (dk/kk'/dcm/cm)	1.00283 -0.1393	1.00026 -0.1392		1.00554 -0.1574	1.00347 -0.1560	
Radial Coefficient (dk/kk'/dcm/cm)	0.99940 -0.4812	0.99686 -0.4799	-0.1 -0.3	1.00216 -0.4923	1.00014 -0.4878	-0.9 -0.9
8 Beta-eff Prompt neutron life time (10^{-7} sec)	5.863 4.620	5.853 4.744	-0.2 2.7	5.870 4.484	5.867 4.616	-0.1 2.9

*1) $(J3.2R-J3.2)/J3.2 \times 100$

TABLE 2. BN-600 HYBRID CORE BENCHMARK CALCULATION RESULTS (PHASE 3) (END OF CYCLE, HOMOGENEOUS BURNUP, DIFFUSION CALCULATION) <** CORRESPONDING TO TABLES 3.56 AND 3.57 IN THE SYNTHESIS REPORT.>

Item		JFS-3-J3.2	JFS-3-J3.2R	Change ^{*1)} (%)
1	k_{eff} (EOC)	0.98323	0.98002	
	k_{eff} (BOC)	1.00713	1.00417	
	Reactivity loss (%dk/kk')	2.414	2.455	1.7

TABLE 3. BN-600 HYBRID CORE BENCHMARK CALCULATION RESULTS (PHASE 3) (END OF CYCLE, HOMOGENEOUS BURNUP AND CONTROL RODS WITHDRAWN, DIFFUSION CALCULATION) <** CORRESPONDING TO TABLES 3.58 AND 3.60 IN THE SYNTHESIS REPORT.>

Item		JFS-3-J3.2	JFS-3-J3.2R	Change ^{*1)} (%)
1	k_{eff}	1.01332	1.0106015	-0.27
2	Fuel Doppler coefficient			
	k_{eff} (Fuel_2100K)	1.01090	1.00798	
3	Coefficient (dk/kk'/dlnK)	-0.00703	-0.00765	8.8
	Sodium density coefficient			
	k_{eff} (Sodium dens.*1.01)	1.01342	1.010693	
	Coefficient (dk/kk'/dp/p)	0.00937	0.00896	-4.4

TABLE 4. BN-600 HYBRID CORE BENCHMARK CALCULATION RESULTS (PHASE 3) (BEGINNING OF CYCLE, HETEROGENEOUS, DIFFUSION CALCULATION) <** CORRESPONDING TO TABLES 3.65 AND 3.72 IN THE SYNTHESIS REPORT.>

Item		JFS-3-J3.2	JFS-3-J3.2R	Change ^{*1)} (%)
1	k_{eff}	1.00913	1.00719	-0.19
2	k_{eff} with Control Rods Withdrawn	1.03845	1.03650	
	k_{eff} with Control Rods Inserted	0.97955	0.97754	
	Rods worth (dk/kk')	0.0579	0.0582	0.5

*1) $(J3.2R - J3.2) / J3.2 \times 100$

REFERENCES TO APPENDIX VI

- [1] TAKANO, H., et al., "Generation of Group Constants for JENDL-3.2", JAERI-memo 07-03 (1995).
- [2] CHIBA, G., HAZAMA, T. and ISHIKAWA, M., "The Revision of Nuclear Constant Set for Fast Reactor, JFS-3-J3.2", Trans. Atom. Energy Soc. Japan, Vol. 1, No.4, pp. 335-340 (2002).

Appendix VI

DESCRIPTION OF BENCHMARK MODEL FOR PHASE 5

G. Manturov, M. Semenov, A. Seregin, L. Lykova
 Institute of Physics and Power Engineering, Russian Federation

VI.1. Description of Fuel Loads

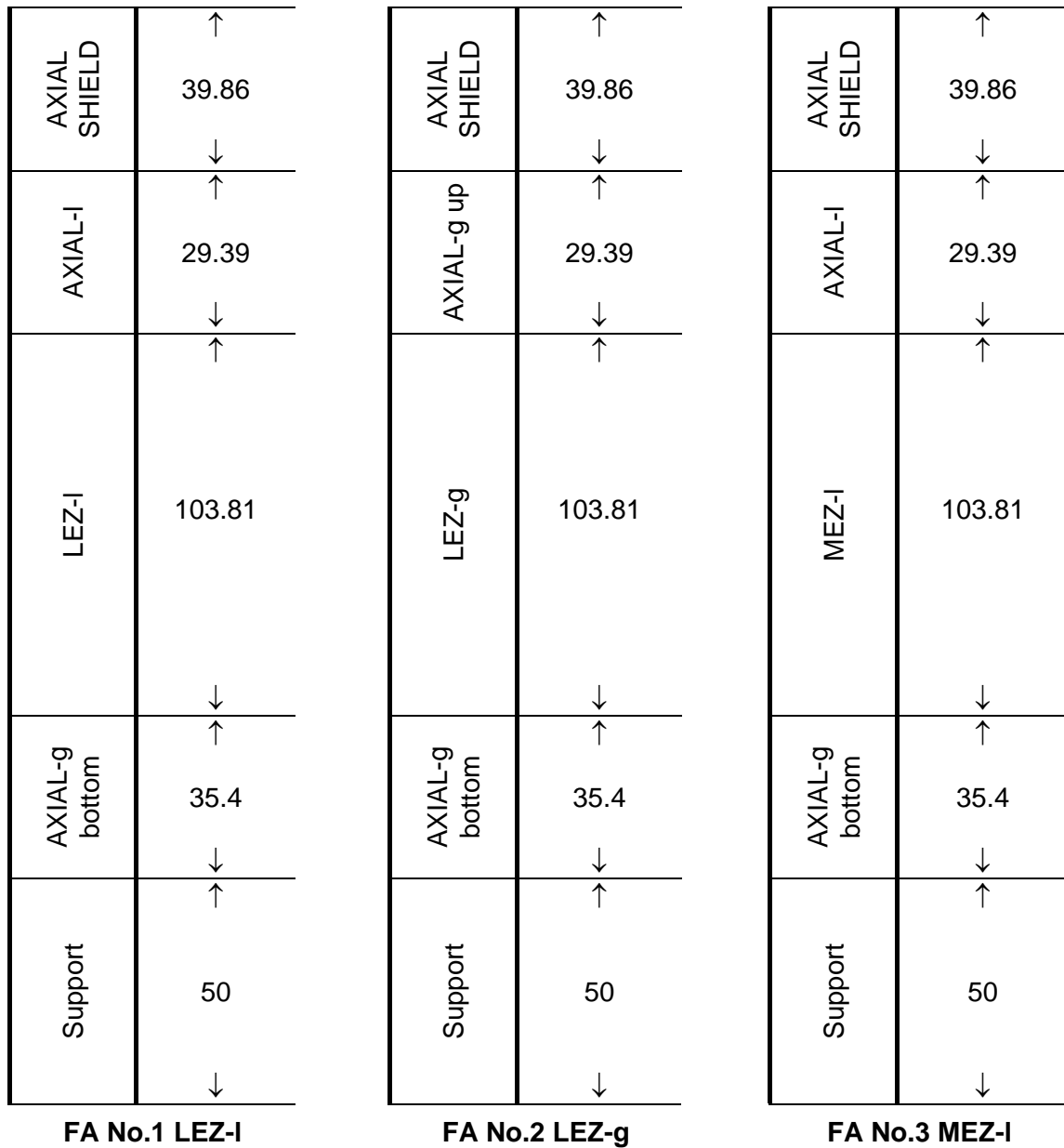


FIG. VI.1.1. Fuel Rods of the Basic Unvoided Benchmark Core (all sizes are given in cm).

	AXIAL-g up	AXIAL SHIELD
	↑	39.86
	↓	
	↑	
	29.39	
	↓	
	↑	
Support	MEZ-g	103.81
	↓	
	↑	
	35.4	
	↓	
	↑	
	50	
	↓	

FA No.4 LEZ-g

	AXIAL-I	AXIAL SHIELD
	↑	39.86
	↓	
	↑	
	29.39	
	↓	
	↑	
Support	HEZ-I	103.81
	↓	
	↑	
	35.4	
	↓	
	↑	
	50	
	↓	

FA No.5 HEZ-I

	AXIAL-g up	AXIAL SHIELD
	↑	39.86
	↓	
	↑	
	29.39	
	↓	
	↑	
Support	HEZ-g	103.81
	↓	
	↑	
	35.4	
	↓	
	↑	
	50	
	↓	

FA No.6 HEZ-g

FIG. VI.1.1 (continued).

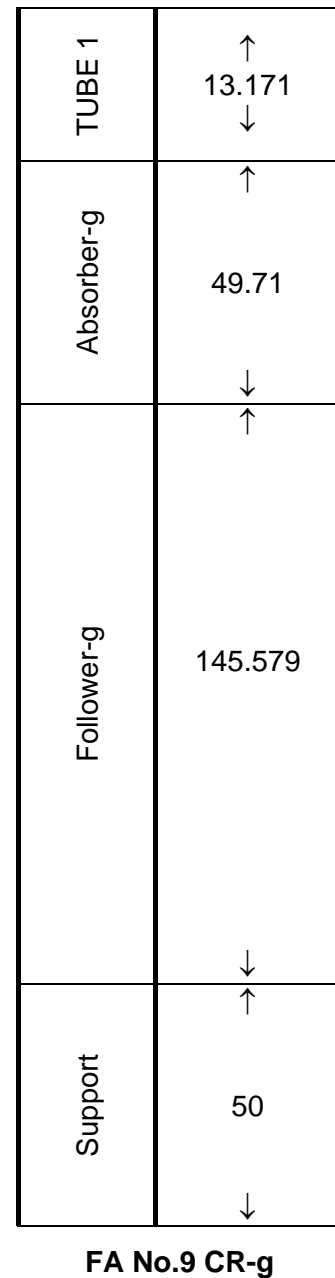
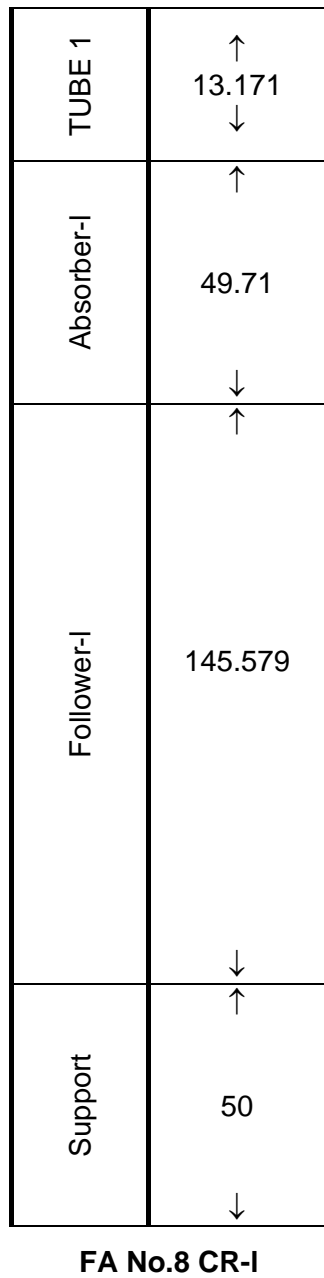
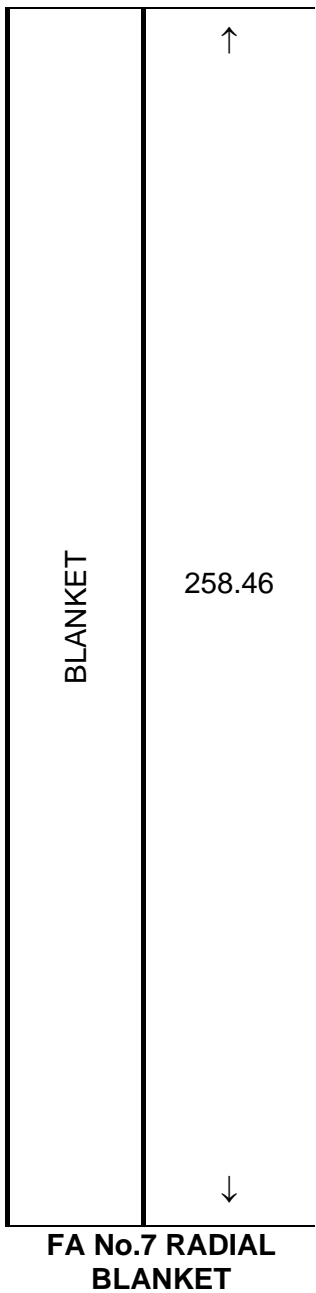


FIG.VI.1.1 (continued).

	TUBE 1	↑ 13.171 ↓
	B4C	↑ 49.71
		↓
		↑
Follower-I		145.579
		↓
		↑
Support		50
		↓

FA No.10 SR-I

	TUBE 1	↑ 13.171 ↓
	B4C	↑ 49.71
		↓
		↑
Follower-g		145.579
		↓
		↑
Support		50
		↓

FA No.11 SR-I

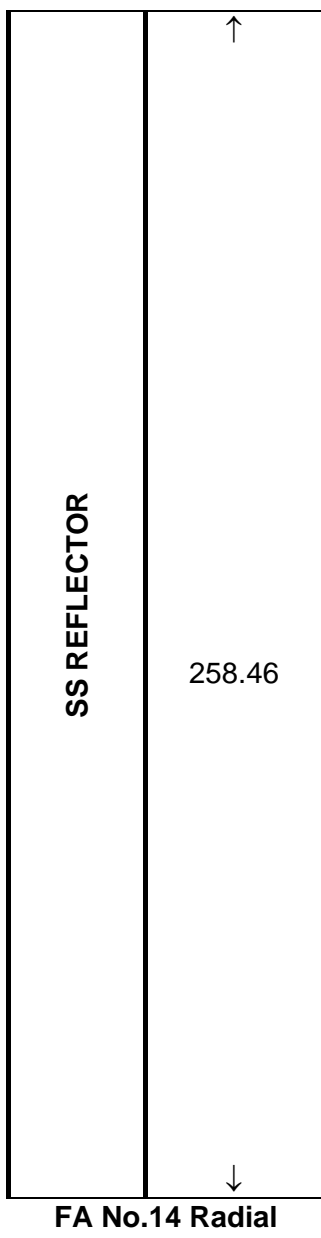
	AXIAL SHIELD	↑ 39.86 ↓
	AXIAL-I	↑ 29.39 ↓
		↑
		↓
Support	MOX-I	103.81
		↓
	AXIAL-g bottom	35.4
		↓
		↑
Support		50
		↓

FA No.12 MOX-I

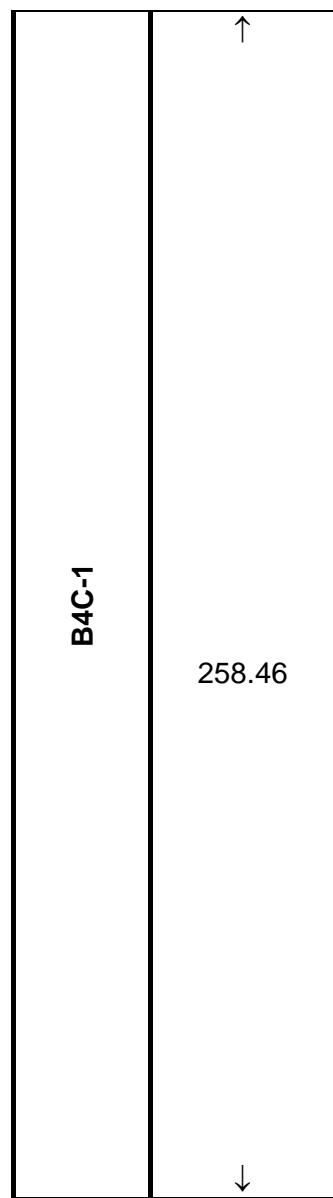
FIG. VI.1.1 (continued).

	AXIAL-g up	AXIAL SHIELD
		↑ 39.86
		↓ ↑
		29.39
		↓ ↑
Support	MOX-g	103.81
		↓ ↑
	AXIAL-g bottom	35.4
		↓ ↑
		50
		↓

FA No.13 MOX-g



FA No.14 Radial
REFLECTOR



FA No.15 B4C-1

FIG. VI.1.1 (continued).

		AXIAL SHIELD	
			↑
		39.86	↓
			↑
		29.39	↓
			↑
			↓
Support	LEZ-I hom w/o U5		↑
		103.81	
			↓
		35.4	↑
			↓
		50	↑
			↓

FA No.16 Modified
LEZ-I

	AXIAL-g up	AXIAL-g bottom	
			↑
	39.86		↓
			↑
	29.39		↓
			↑
	103.81		
			↓
		35.4	↑
			↓
		50	↑
			↓

FA No.17 Modified
LEZ-g

			↑
B4C-2			258.46
			↓

FA No.18 B4C-2

FIG. VI.1.1 (continued).

	AXIAL-g bottom		
Support			
	LEZ-I brig		
		39.86	↑
		29.39	↓
		29.39	↑
		103.81	↓
		35.4	↑
		35.4	↓
		50	↑
		50	↓

FA No.19 LEZ brig-I

	AXIAL-g bottom		
Support			
	LEZ-g brig		
		39.86	↑
		29.39	↓
		29.39	↑
		103.81	↓
		35.4	↑
		35.4	↓
		50	↑
		50	↓

FA No.20 LEZ brig-g

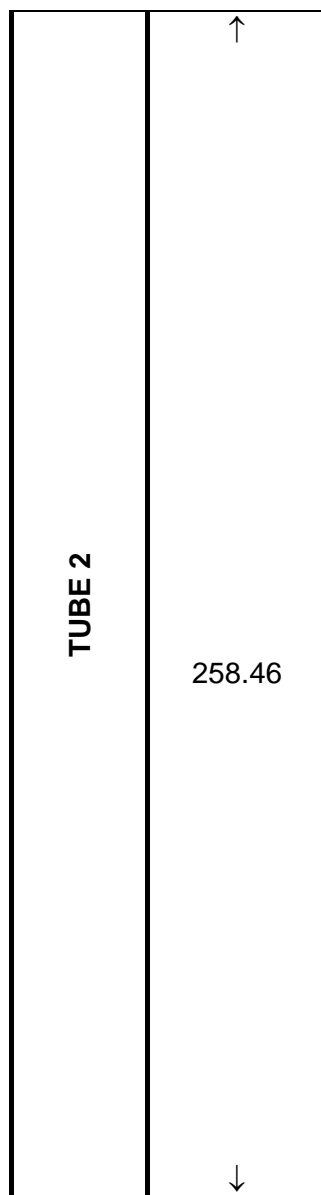
	AXIAL-g bottom		
Support			
	HEZ-I brig		
		39.86	↑
		29.39	↓
		29.39	↑
		103.81	↓
		35.4	↑
		35.4	↓
		50	↑
		50	↓

FA No.21 HEZ brig-I

FIG. VI.1.1 (continued).

		AXIAL SHIELD	↑
			39.86
		↓	
		↑	
		29.39	
		↓	
		↑	
	HEZ-g brig		103.81
		↓	
		↑	
	AXIAL-g bottom	35.4	
		↓	
		↑	
Support		50	
		↓	

FA No.22 HEZ brig-g



FA No.23 Empty tube

FIG. VI.1.1 (continued).

Support	AXIAL-g bottom	LEZ-I void	AXIAL-I void	AXIAL SHIELD
				39.86 ↑
			↑ ↓	29.39
			↓ ↑	103.81
			↓ ↑	35.4
			↓ ↑	50
			↓	

FA No.24 LEZ-I void

Support	AXIAL-g bottom	LEZ-I hom w/o U5 void	AXIAL-I void	AXIAL SHIELD
				39.86 ↑
			↑ ↓	29.39
			↓ ↑	103.81
			↓ ↑	35.4
			↓ ↑	50
			↓	

FA No.25 Modified
LEZ-I void

Support	AXIAL-g bottom	LEZ-I brig void	AXIAL-I void	AXIAL SHIELD
				39.86 ↑
			↑ ↓	29.39
			↓ ↑	103.81
			↓ ↑	35.4
			↓ ↑	50
			↓	

FA No.26 LEZ brig-I
void

FIG. VI.1.2. Voided FAs (all sizes are given in cm).

FA No.27
MEZ-I void

			AXIAL SHIELD	
			39.86	↑ ↓ →
			29.39	↑ ↓ →
			103.81	↑ ↓ →
		HEZ-I void		
	AXIAL-g bottom		35.4	↑ ↓ →
Support			50	↓

**FA No.28 HEZ-
I void**

				→
			39.86	↓
		AXIAL-SHIELD		→
			29.39	↓
				→
		HEZ-I brig void	103.81	↓
	AXIAL-g bottom			→
			35.4	↓
			50	→
				↓

**FA No.29 HEZ
brig-I void**

FA No.30 MOX-I
void

FIG. VI.1.2 (continued).

VI.2.Benchmark Core Layouts

FIG. VI.2.1. FA's layout of the basic unvoided benchmark core.

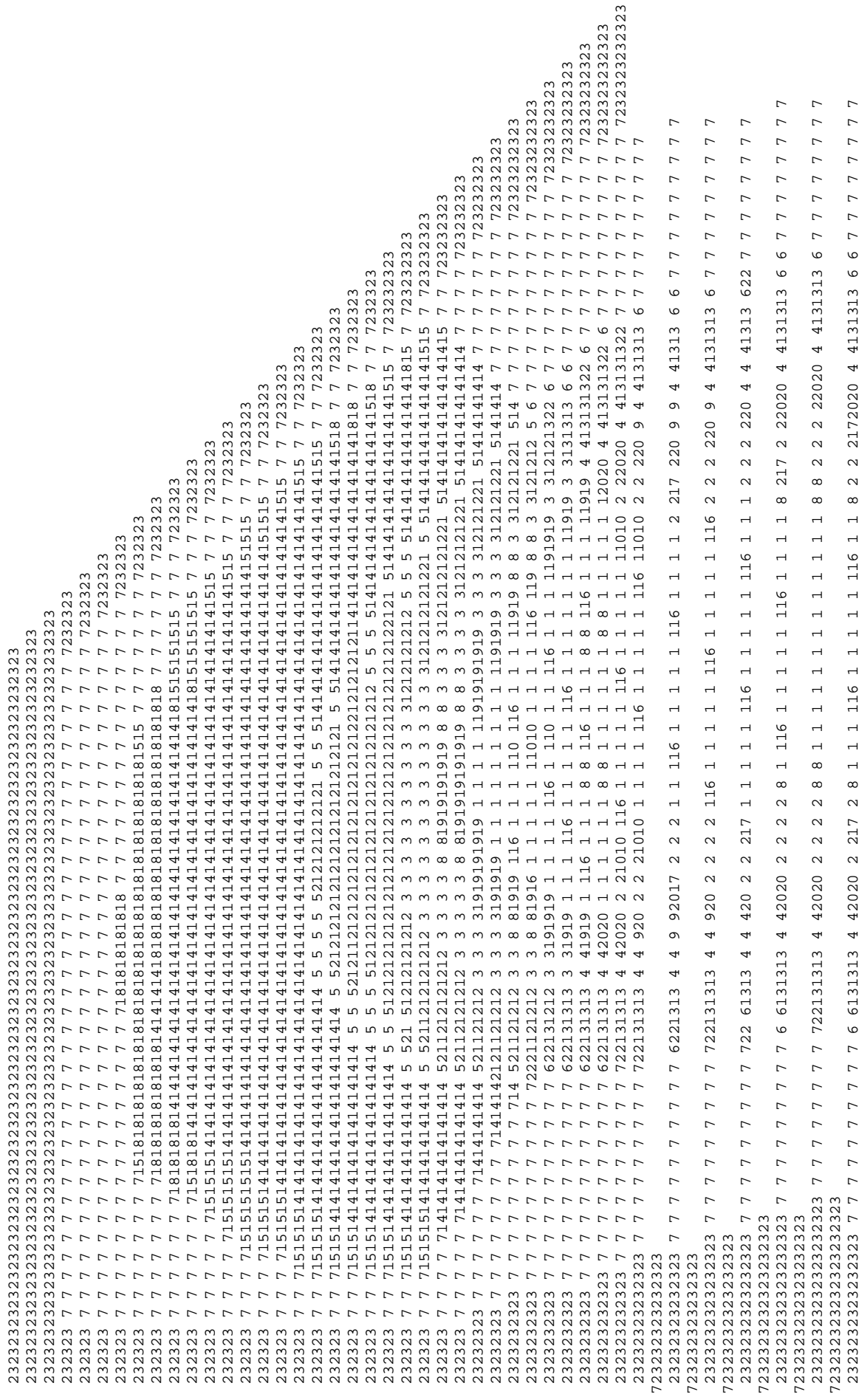


FIG. VI.2.2. FA's layout for SVRE calculation in LEZ region.

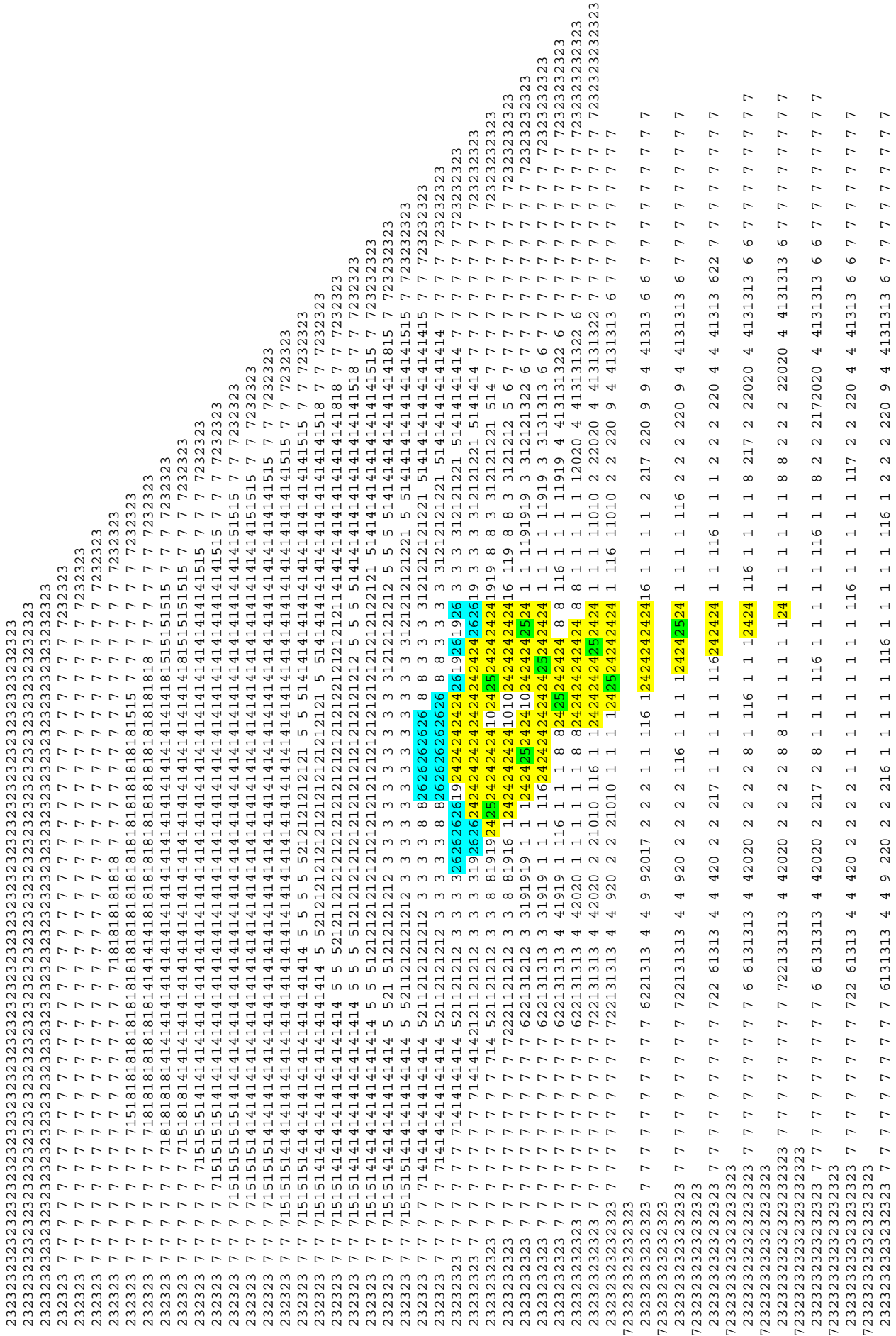


FIG. VI.2.3. FA's layout for SVRE calculation in MEZ region.

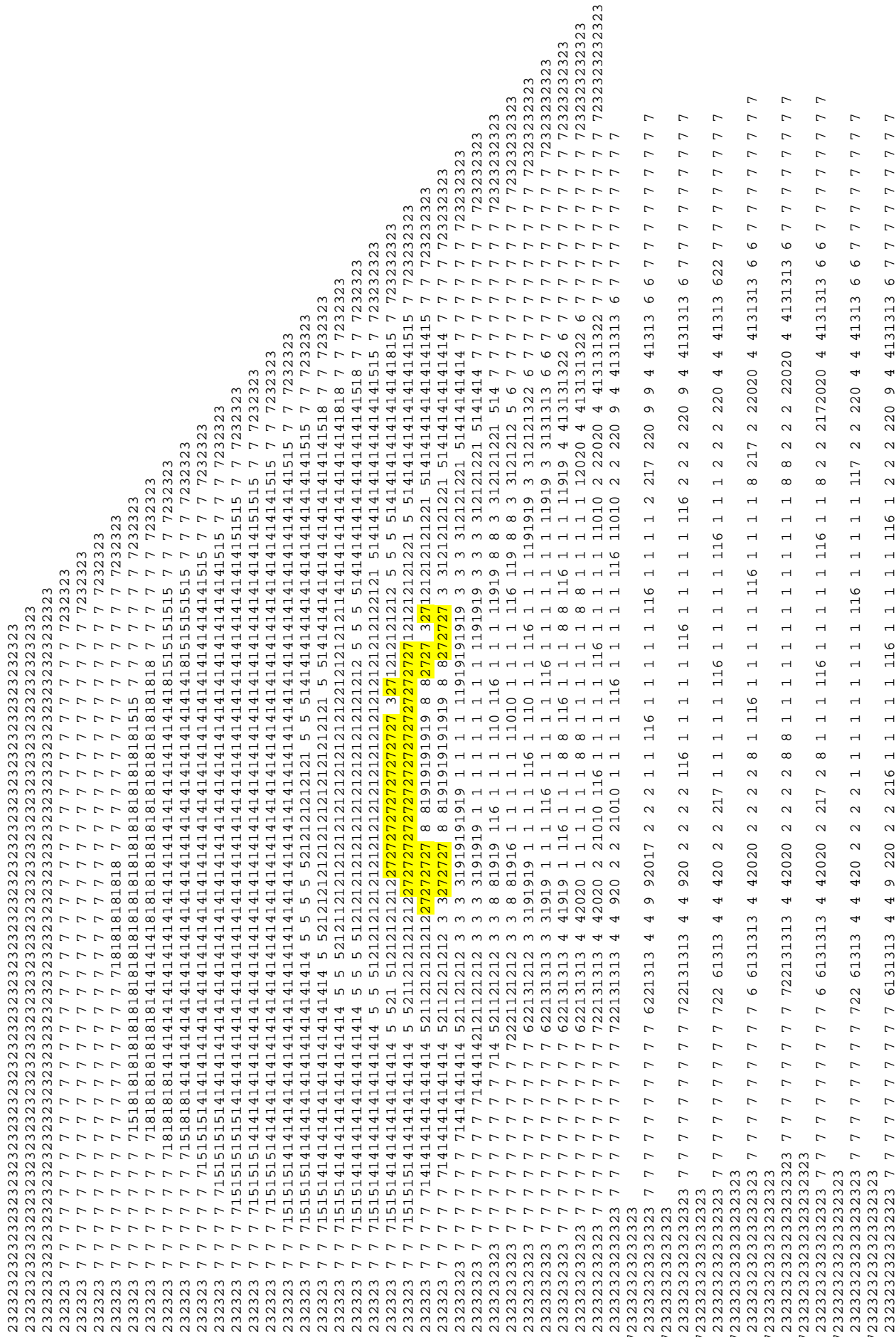
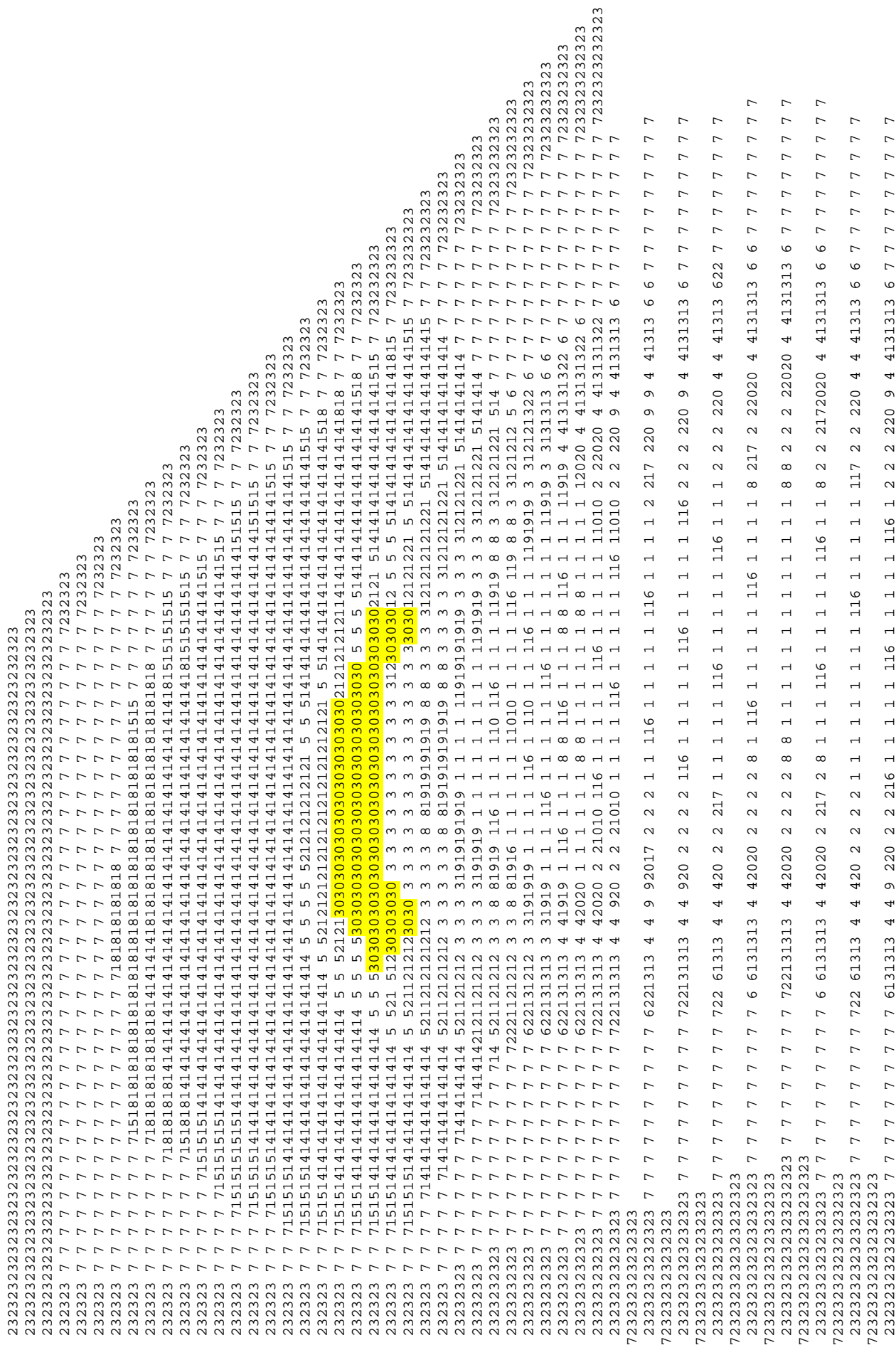


FIG. VII.2.4. FA's layout for SVRE calculation in HEZ region.

FIG. VI.2.5. FA's layout for SVRE calculation in MOX region.



VI.3. Atom Densities

TABLE VI.1. ATOMIC DENSITIES BY NUCLIDES IN MATERIAL ZONES (UNIT: BARN⁻¹ CM⁻¹)

	H	NA	C	AL	TI	CR
1 LEZ-l	1.5820E-05	6.5728E-03	3.0195E-04	5.0196E-03	1.1997E-04	3.1507E-03
2 LEZ-g	3.0062E-04	6.5652E-03	3.0215E-04	5.0204E-03	1.2028E-04	3.1591E-03
3 MEZ-l	5.0247E-06	6.2598E-03	4.0190E-04	2.4161E-03	1.3688E-04	3.6349E-03
4 MEZ-g	2.7626E-04	6.2526E-03	4.0209E-04	2.4169E-03	1.3718E-04	3.6429E-03
5 HEZ-l	1.0623E-05	5.6338E-03	3.6591E-04	4.0036E-03	1.3132E-04	3.4462E-03
6 HEZ-g	2.5474E-04	5.6273E-03	3.6609E-04	4.0043E-03	1.3159E-04	3.4534E-03
7 MOX-l	5.4267E-06	5.6338E-03	4.2824E-04	2.5889E-03	1.3838E-04	3.6993E-03
8 MOX-g	2.4954E-04	5.6273E-03	4.2841E-04	2.5895E-03	1.3865E-04	3.7065E-03
9 LEZ-l w/o u5	3.6178E-06	6.5728E-03	3.0727E-04	4.9902E-03	1.2823E-04	3.3718E-03
10 LEZ-g w/o u5	2.8842E-04	6.5652E-03	3.0747E-04	4.9910E-03	1.2855E-04	3.3802E-03
11 Follower-l	0.0000E+00	1.0936E-02	1.6468E-04	6.2311E-04	2.5612E-04	6.8472E-03
12 Follower-g	4.7386E-04	1.0924E-02	1.6501E-04	6.2438E-04	2.5665E-04	6.8612E-03
13 Absorber-l	0.0000E+00	9.8043E-03	6.0934E-03	2.4029E-04	9.8771E-05	2.6405E-03
14 Absorber-g	4.2482E-04	9.7931E-03	6.0937E-03	2.4144E-04	9.9241E-05	2.6531E-03
15 B4C	0.0000E+00	0.0000E+00	1.5003E-02	1.7229E-04	7.0817E-05	1.8932E-03
16 SS REFLECTOR	0.0000E+00	0.0000E+00	2.4180E-04	9.1493E-04	3.7607E-04	1.0054E-02
17 B4C-1	0.0000E+00	0.0000E+00	1.0892E-02	1.0477E-04	4.3066E-05	1.1513E-03
18 B4C-2	0.0000E+00	0.0000E+00	1.1414E-02	1.0477E-04	4.3066E-05	1.1513E-03
19 AXIAL-l	7.0993E-06	5.5276E-03	4.9949E-04	3.1570E-03	8.6577E-05	2.3146E-03
20 AXIAL-g bot	2.4569E-04	5.5007E-03	4.9780E-04	3.1458E-03	8.6518E-05	2.3130E-03
21 AXIAL SHIELD	3.5320E-04	8.1420E-03	2.0820E-04	7.8779E-04	3.2381E-04	8.6569E-03
22 LEZ-l brig	1.5820E-05	6.5728E-03	3.0195E-04	5.0196E-03	1.1997E-04	3.1507E-03
23 LEZ-g brig	3.0062E-04	6.5652E-03	3.0215E-04	5.0204E-03	1.2028E-04	3.1591E-03
24 HEZ-l brig	1.0623E-05	5.6338E-03	3.6591E-04	4.0036E-03	1.3132E-04	3.4462E-03
25 HEZ-g brig	2.5474E-04	5.6273E-03	3.6609E-04	4.0043E-03	1.3159E-04	3.4534E-03
26 BLANKET	1.0700E-05	0.0000E+00	6.9662E-04	4.5454E-03	4.3066E-05	1.1513E-03
27 TUBE 1	0.0000E+00	0.0000E+00	4.5532E-05	1.7229E-04	7.0817E-05	1.8932E-03
28 TUBE 2	0.0000E+00	0.0000E+00	2.7690E-05	1.0477E-04	4.3066E-05	1.1513E-03
29 SUPPORT	0.0000E+00	0.0000E+00	9.2259E-05	3.4909E-04	1.4349E-04	3.8361E-03
30 AXIAL-g up	2.4661E-04	5.5213E-03	4.9966E-04	3.1576E-03	8.6842E-05	2.3216E-03
31 LEZ-l void	1.5820E-05	0.0000E+00	3.0195E-04	5.0196E-03	1.1997E-04	3.1507E-03
32 LEZ-l wo u5 void	3.6178E-06	0.0000E+00	3.0727E-04	4.9902E-03	1.2823E-04	3.3718E-03
33 LEZ-l brig void	1.5820E-05	0.0000E+00	3.0195E-04	5.0196E-03	1.1997E-04	3.1507E-03
34 MEZ-l void	5.0247E-06	0.0000E+00	4.0190E-04	2.4161E-03	1.3688E-04	3.6349E-03
35 HEZ-l void	1.0623E-05	0.0000E+00	3.6591E-04	4.0036E-03	1.3132E-04	3.4462E-03
36 HEZ-l brig void	1.0623E-05	0.0000E+00	3.6591E-04	4.0036E-03	1.3132E-04	3.4462E-03
37 MOX-l void	5.4267E-06	0.0000E+00	4.2824E-04	2.5889E-03	1.3838E-04	3.6993E-03
38 AXIAL-l void	7.0993E-06	0.0000E+00	4.9949E-04	3.1570E-03	8.6577E-05	2.3146E-03

TABLE VI.1. ATOMIC DENSITIES BY NUCLIDES IN MATERIAL ZONES (CONTINUED) (UNIT: BARN⁻¹ CM⁻¹)

	MN	FE	NI	U235	U238	O
1 LEZ-l	2.4850E-04	1.1429E-02	1.4732E-03	1.1876E-03	6.7809E-03	1.3282E-02
2 LEZ-g	2.4916E-04	1.1459E-02	1.4771E-03	1.1876E-03	6.7809E-03	1.3282E-02
3 MEZ-l	2.8976E-04	1.3168E-02	1.7017E-03	1.4786E-03	6.7585E-03	1.3240E-02
4 MEZ-g	2.9039E-04	1.3196E-02	1.7055E-03	1.4786E-03	6.7585E-03	1.3240E-02
5 HEZ-l	2.7457E-04	1.2513E-02	1.6133E-03	1.8646E-03	7.0132E-03	1.4148E-02
6 HEZ-g	2.7514E-04	1.2539E-02	1.6167E-03	1.8646E-03	7.0132E-03	1.4148E-02
7 MOX-l	2.9177E-04	1.3410E-02	1.7297E-03	2.9720E-05	7.1145E-03	1.4299E-02
8 MOX-g	2.9234E-04	1.3436E-02	1.7331E-03	2.9720E-05	7.1145E-03	1.4299E-02
9 LEZ-l w/o u5	2.6593E-04	1.2196E-02	1.5766E-03	1.9814E-05	4.7430E-03	1.2502E-02
10 LEZ-g w/o u5	2.6660E-04	1.2227E-02	1.5805E-03	1.9814E-05	4.7430E-03	1.2502E-02
11 Follower-l	5.4004E-04	2.4590E-02	3.2016E-03	0.0000E+00	0.0000E+00	0.0000E+00
12 Follower-g	5.4115E-04	2.4640E-02	3.2082E-03	0.0000E+00	0.0000E+00	0.0000E+00
13 Absorber-l	2.0826E-04	9.4828E-03	1.2347E-03	0.0000E+00	0.0000E+00	0.0000E+00
14 Absorber-g	2.0925E-04	9.5280E-03	1.2405E-03	0.0000E+00	0.0000E+00	0.0000E+00
15 B4C	1.4932E-04	6.7990E-03	8.8523E-04	0.0000E+00	0.0000E+00	0.0000E+00
16 SS REFLECTOR	7.9296E-04	3.6106E-02	4.7010E-03	0.0000E+00	0.0000E+00	0.0000E+00
17 B4C-1	9.0806E-05	4.1347E-03	5.3834E-04	0.0000E+00	0.0000E+00	0.0000E+00
18 B4C-2	9.0806E-05	4.1347E-03	5.3834E-04	0.0000E+00	0.0000E+00	0.0000E+00
19 AXIAL-l	1.8255E-04	8.4758E-03	1.0822E-03	3.8880E-05	9.3072E-03	1.8706E-02
20 AXIAL-gbot	1.8243E-04	8.4695E-03	1.0815E-03	3.8735E-05	9.2725E-03	1.8636E-02
21 AXIAL SHIELD	6.8278E-04	3.1089E-02	4.0478E-03	0.0000E+00	0.0000E+00	0.0000E+00
22 LEZ-l brig	2.4850E-04	1.1467E-02	1.4732E-03	1.2222E-03	6.8447E-03	1.3282E-02
23 LEZ-g brig	2.4916E-04	1.1497E-02	1.4771E-03	1.2222E-03	6.8447E-03	1.3282E-02
24 HEZ-l brig	2.7457E-04	1.2513E-02	1.6133E-03	1.8610E-03	7.0090E-03	1.4148E-02
25 HEZ-g brig	2.7514E-04	1.2539E-02	1.6167E-03	1.8610E-03	7.0091E-03	1.4148E-02
26 BLANKET	9.0806E-05	4.3813E-03	5.3834E-04	5.8599E-05	1.4028E-02	2.8194E-02
27 TUBE 1	1.4932E-04	6.7990E-03	8.8523E-04	0.0000E+00	0.0000E+00	0.0000E+00
28 TUBE 2	9.0806E-05	4.1347E-03	5.3834E-04	0.0000E+00	0.0000E+00	0.0000E+00
29 SUPPORT	3.0256E-04	1.3776E-02	1.7937E-03	0.0000E+00	0.0000E+00	0.0000E+00
30 AXIAL-g up	1.8311E-04	8.5012E-03	1.0856E-03	3.8880E-05	9.3072E-03	1.8706E-02
31 LEZ-l void	2.4850E-04	1.1429E-02	1.4732E-03	1.1876E-03	6.7809E-03	1.3282E-02
32 LEZ-l wo u5	2.6593E-04	1.2196E-02	1.5766E-03	1.9814E-05	4.7430E-03	1.2502E-02
33 LEZ-l brig void	2.4850E-04	1.1467E-02	1.4732E-03	1.2222E-03	6.8447E-03	1.3282E-02
34 MEZ-l void	2.8976E-04	1.3168E-02	1.7017E-03	1.4786E-03	6.7585E-03	1.3240E-02
35 HEZ-l void	2.7457E-04	1.2513E-02	1.6133E-03	1.8646E-03	7.0132E-03	1.4148E-02
36 HEZ-l brig void	2.7457E-04	1.2513E-02	1.6133E-03	1.8610E-03	7.0090E-03	1.4148E-02
37 MOX-l void	2.9177E-04	1.3410E-02	1.7297E-03	2.9720E-05	7.1145E-03	1.4299E-02
38 AXIAL-l void	1.8255E-04	8.4758E-03	1.0822E-03	3.8880E-05	9.3072E-03	1.8706E-02

TABLE VI.1. ATOMIC DENSITIES BY NUCLIDES IN MATERIAL ZONES (CONTINUED) (UNIT: BARN⁻¹ CM⁻¹)

	B-10	B-11	PU39	PU40	PU41
1 LEZ-l	0.0000E+00	0.0000E+00	0.0000E+00	0.0000E+00	0.0000E+00
2 LEZ-g	0.0000E+00	0.0000E+00	0.0000E+00	0.0000E+00	0.0000E+00
3 MEZ-l	0.0000E+00	0.0000E+00	0.0000E+00	0.0000E+00	0.0000E+00
4 MEZ-g	0.0000E+00	0.0000E+00	0.0000E+00	0.0000E+00	0.0000E+00
5 HEZ-l	0.0000E+00	0.0000E+00	0.0000E+00	0.0000E+00	0.0000E+00
6 HEZ-g	0.0000E+00	0.0000E+00	0.0000E+00	0.0000E+00	0.0000E+00
7 MOX-l	0.0000E+00	0.0000E+00	1.4501E-03	7.0234E-05	8.0423E-07
8 MOX-g	0.0000E+00	0.0000E+00	1.4501E-03	7.0233E-05	8.0422E-07
9 LEZ-l w/o u5	0.0000E+00	0.0000E+00	0.0000E+00	0.0000E+00	0.0000E+00
10 LEZ-g w/o u5	0.0000E+00	0.0000E+00	0.0000E+00	0.0000E+00	0.0000E+00
11 Follower-l	0.0000E+00	0.0000E+00	0.0000E+00	0.0000E+00	0.0000E+00
12 Follower-g	0.0000E+00	0.0000E+00	0.0000E+00	0.0000E+00	0.0000E+00
13 Absorber-l	4.8000E-03	1.9320E-02	0.0000E+00	0.0000E+00	0.0000E+00
14 Absorber-g	4.8000E-03	1.9320E-02	0.0000E+00	0.0000E+00	0.0000E+00
15 B4C	1.1907E-02	4.7925E-02	0.0000E+00	0.0000E+00	0.0000E+00
16 SS REFLECTOR	0.0000E+00	0.0000E+00	0.0000E+00	0.0000E+00	0.0000E+00
17 B4C-1	8.6478E-03	3.4810E-02	0.0000E+00	0.0000E+00	0.0000E+00
18 B4C-2	9.0632E-03	3.6481E-02	0.0000E+00	0.0000E+00	0.0000E+00
19 AXIAL-l	0.0000E+00	0.0000E+00	0.0000E+00	0.0000E+00	0.0000E+00
20 AXIAL-gbot	0.0000E+00	0.0000E+00	0.0000E+00	0.0000E+00	0.0000E+00
21 AXIAL SHIELD	0.0000E+00	0.0000E+00	0.0000E+00	0.0000E+00	0.0000E+00
22 LEZ-l brig	0.0000E+00	0.0000E+00	0.0000E+00	0.0000E+00	0.0000E+00
23 LEZ-g brig	0.0000E+00	0.0000E+00	0.0000E+00	0.0000E+00	0.0000E+00
24 HEZ-l brig	0.0000E+00	0.0000E+00	0.0000E+00	0.0000E+00	0.0000E+00
25 HEZ-g brig	0.0000E+00	0.0000E+00	0.0000E+00	0.0000E+00	0.0000E+00
26 BLANKET	0.0000E+00	0.0000E+00	0.0000E+00	0.0000E+00	0.0000E+00
27 TUBE 1	0.0000E+00	0.0000E+00	0.0000E+00	0.0000E+00	0.0000E+00
28 TUBE 2	0.0000E+00	0.0000E+00	0.0000E+00	0.0000E+00	0.0000E+00
29 SUPPORT	0.0000E+00	0.0000E+00	0.0000E+00	0.0000E+00	0.0000E+00
30 AXIAL-g up	0.0000E+00	0.0000E+00	0.0000E+00	0.0000E+00	0.0000E+00
31 LEZ-l void	0.0000E+00	0.0000E+00	0.0000E+00	0.0000E+00	0.0000E+00
32 LEZ-l wo u5 void	0.0000E+00	0.0000E+00	0.0000E+00	0.0000E+00	0.0000E+00
33 LEZ-l brig void	0.0000E+00	0.0000E+00	0.0000E+00	0.0000E+00	0.0000E+00
34 MEZ-l void	0.0000E+00	0.0000E+00	0.0000E+00	0.0000E+00	0.0000E+00
35 HEZ-l void	0.0000E+00	0.0000E+00	0.0000E+00	0.0000E+00	0.0000E+00
36 HEZ-l brig void	0.0000E+00	0.0000E+00	0.0000E+00	0.0000E+00	0.0000E+00
37 MOX-l void	0.0000E+00	0.0000E+00	1.4501E-03	7.0234E-05	8.0423E-07
38 AXIAL-l void	0.0000E+00	0.0000E+00	0.0000E+00	0.0000E+00	0.0000E+00

Appendix VII

SENSITIVITY ANALYSIS OF JENDL-3.2, JEDL-3.3 AND JEF-2.2 FOR BFS-62-3A CRITICAL EXPERIMENTS

M. Ishikawa

Japan Nuclear Cycle Development Institute, Japan

VII.1. Cross-section Sensitivity Coefficients of BFS-62-3A VII.1.1 Criticality

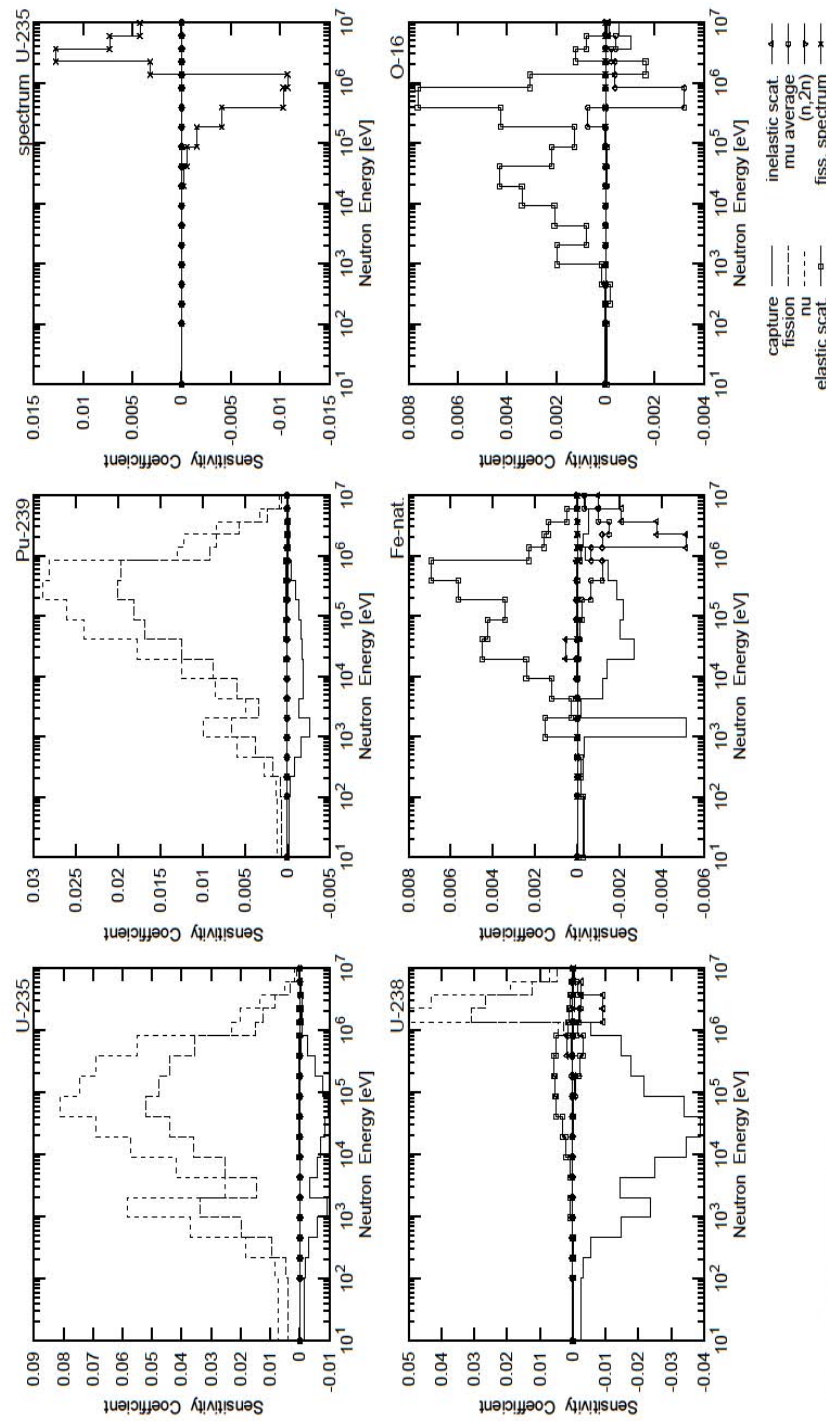


Fig. BFS-62-3A KEFF

TABLE BFS-62-3A KEFF (HEAVY METAL) UNIT:1.0E-4

NUCL.	REACTION	TOTAL	18G	17G	16G	15G	14G	13G	12G	11G	10G	9G	8G	7G	6G	5G	4G	3G	2G	1G
U-235	CAPTURE	-735	-16	-19	-32	-60	-91	-35	-58	-72	-86	-98	-79	-51	-27	-7	-4	-1	0	0
U-235	NU	6666	74	85	182	369	585	254	419	573	688	813	747	691	550	231	201	135	51	16
U-235	FISSION	4109	39	46	96	199	336	148	254	358	439	520	476	441	354	149	125	84	34	11
U-235	ELAS. SCT	23	0	0	0	1	0	1	2	3	4	4	3	1	1	1	0	0	0	0
U-235	INEL. SCT	-19	0	0	0	0	0	0	0	0	0	0	0	0	0	0	0	0	0	0
U-235	(n, 2n)	0	0	0	0	0	0	0	0	0	0	0	0	0	0	0	0	0	0	0
U-235	MU-AVE.	-12	0	0	0	0	0	0	0	0	0	-1	-2	-2	-1	-2	-2	-1	0	0
U-238	CAPTURE	-2592	-26	-33	-55	-148	-235	-145	-251	-347	-388	-339	-217	-177	-147	-55	-21	-6	-1	0
U-238	NU	1237	0	0	0	0	0	0	0	0	0	1	4	43	496	431	190	71	0	0
U-238	FISSION	779	0	0	0	0	0	0	0	0	0	0	3	28	310	266	124	47	0	0
U-238	ELAS. SCT	311	-1	-1	1	8	2	8	19	31	51	53	57	51	13	10	7	2	1	1
U-238	INEL. SCT	-206	0	0	0	0	0	0	0	0	0	0	-6	3	17	-1	-93	-27	-6	1
U-238	(n, 2n)	1	0	0	0	0	0	0	0	0	0	0	0	0	0	0	0	0	0	0
U-238	MU-AVE.	-145	0	0	0	0	0	0	-1	-4	-9	-21	-33	-14	-20	-25	-14	-3	0	0
Pu-239	CAPTURE	-176	-3	-9	-17	-27	-14	-19	-19	-18	-16	-13	-11	-5	-1	0	0	0	0	0
Pu-239	NU	2101	12	14	27	60	99	49	86	125	178	240	261	290	282	130	122	84	33	9
Pu-239	FISSION	1452	7	8	17	38	66	33	59	88	126	169	182	201	197	91	83	57	23	6
Pu-239	ELAS. SCT	8	0	0	0	0	0	0	0	0	1	1	2	1	0	0	0	0	0	0
Pu-239	INEL. SCT	-3	0	0	0	0	0	0	0	0	0	0	0	0	0	-2	-2	-1	0	0
Pu-239	(n, 2n)	0	0	0	0	0	0	0	0	0	0	0	0	0	0	0	0	0	0	0
Pu-239	MU-AVE.	-4	0	0	0	0	0	0	0	0	0	-1	-1	0	-1	0	-1	0	0	0

TABLE BFS-62-3A KEFF (FISSION SPECTRUM) UNIT:1.0E-4

	FISSION SPECTRUM	TOTAL	18G	17G	16G	15G	14G	13G	12G	11G	10G	9G	8G	7G	6G	5G	4G	3G	2G	1G
SPEC.	U-235	0.05	-1	0	0	0	0	0	0	-2	-6	-16	-41	-103	-108	32	128	73	42	0
SPEC.	Pu-239	0.05	0	0	0	0	0	0	0	-1	-2	-5	-13	-33	-32	11	39	22	13	0

NUCL.	REACTION	TOTAL	18G	17G	16G	15G	14G	13G	12G	11G	10G	9G	8G	7G	6G	5G	4G	3G	2G	1G
-------	----------	-------	-----	-----	-----	-----	-----	-----	-----	-----	-----	----	----	----	----	----	----	----	----	----

Na-23	CAPTURE	-17	0	0	-1	-3	-6	-1	0	-1	0	0	0	-2		
Na-23	ELAS. SCT	162	0	0	0	8	16	23	18	20	15	8	18	31	7	
Na-23	INEL. SCT	-31	0	0	0	0	0	0	0	0	0	0	0	-1	-4	-3
Na-23	(n, 2n)	0	0	0	0	0	0	0	0	0	0	0	0	0	0	0
Na-23	MU-AVE.	-23	0	0	0	0	0	0	0	-1	-2	-6	-4	-4	-1	0

AL-27	CAPTURE	-14	0	0	0	0	-4	0	-2	-1	-2	-1	0	0	-1	-1		
AL-27	ELAS. SCT	60	0	0	0	1	0	1	2	6	5	12	19	5	-1	2	1	0
AL-27	INEL. SCT	-18	0	0	0	0	0	0	0	0	0	0	0	0	-6	-7	-3	-2
AL-27	(n, 2n)	0	0	0	0	0	0	0	0	0	0	0	0	0	0	0	0	0
AL-27	MU-AVE.	-23	0	0	0	0	0	0	0	0	-1	-2	-5	-3	-5	-4	-1	0

Cr CAPTURE	-62	-1	0	-1	-15	-4	-13	-2	-4	-3	-4	-2	-1	-1	-1			
Cr ELAS.	SCT	124	0	0	0	1	1	13	8	6	11	24	19	22	9	5	3	1
Cr INEL.	SCT	-31	0	0	0	0	0	0	0	0	0	0	0	-8	-14	-5	-3	
Cr (n, 2n)	0	0	0	0	0	0	0	0	0	0	0	0	0	0	0	0	0	
Cr MU-AVE.	-20	0	0	0	0	0	0	0	0	-1	-1	-2	-2	-4	-6	-3	-1	

Mn-55 CAPTURE -29 0 0 -1 -1 -8 -1 -2 -1 -1 0 0 0 0 0 0
Mn-55 ELAS, SCT 17 0 0 -1 0 2 3 1 2 3 2 2 2 1 0 0 0 0

Mn-55	INEL. SCT	-2 0 0 0 0 0 0 0 0 0 0 0 0 0 0 -1 -1 0 0
Mn-55	(n, 2n)	0 0
Mn-55	MU-AVE.	-2 0

Fe	CAPTURE	-214 -3 -2 -3 -3 -52 -2 -12 -14 -27 -21 -22 -19 -15 -4 -3 -5 -6 -4
Fe	ELAS. SCT	353 -3 -2 -2 0 15 3 12 24 45 43 34 56 69 23 16 14 5 0
Fe	INEL. SCT	-115 0 0 0 0 0 0 0 1 5 0 0 0 0 -2 -52 -38 -21 -10
Fe	(n, 2n)	0 0
Fe	MU-AVE.	-70 0 0 0 0 0 0 0 -1 -1 -2 -7 -12 -7 -12 -15 -10 -3

Ni	CAPTURE	-79 -1 0 0 -1 -2 -2 -2 -14 -8 -7 -7 -5 -3 -2 -3 -9 -9 -3
Ni	ELAS. SCT	99 -1 0 0 0 4 1 6 14 16 13 9 16 12 5 3 2 1 0
Ni	INEL. SCT	-12 0 0 0 0 0 0 0 0 0 0 0 0 0 0 -3 -6 -2 -1
Ni	(n, 2n)	0 0 0 0 0 0 0 0 0 0 0 0 0 0 0 0 0 0 0 0
Ni	MU-AVE.	-11 0 0 0 0 0 0 0 0 -1 -2 -2 -1 -2 -2 -1 0

VII.1.2 Sodium Void Reactivity — Inner Core

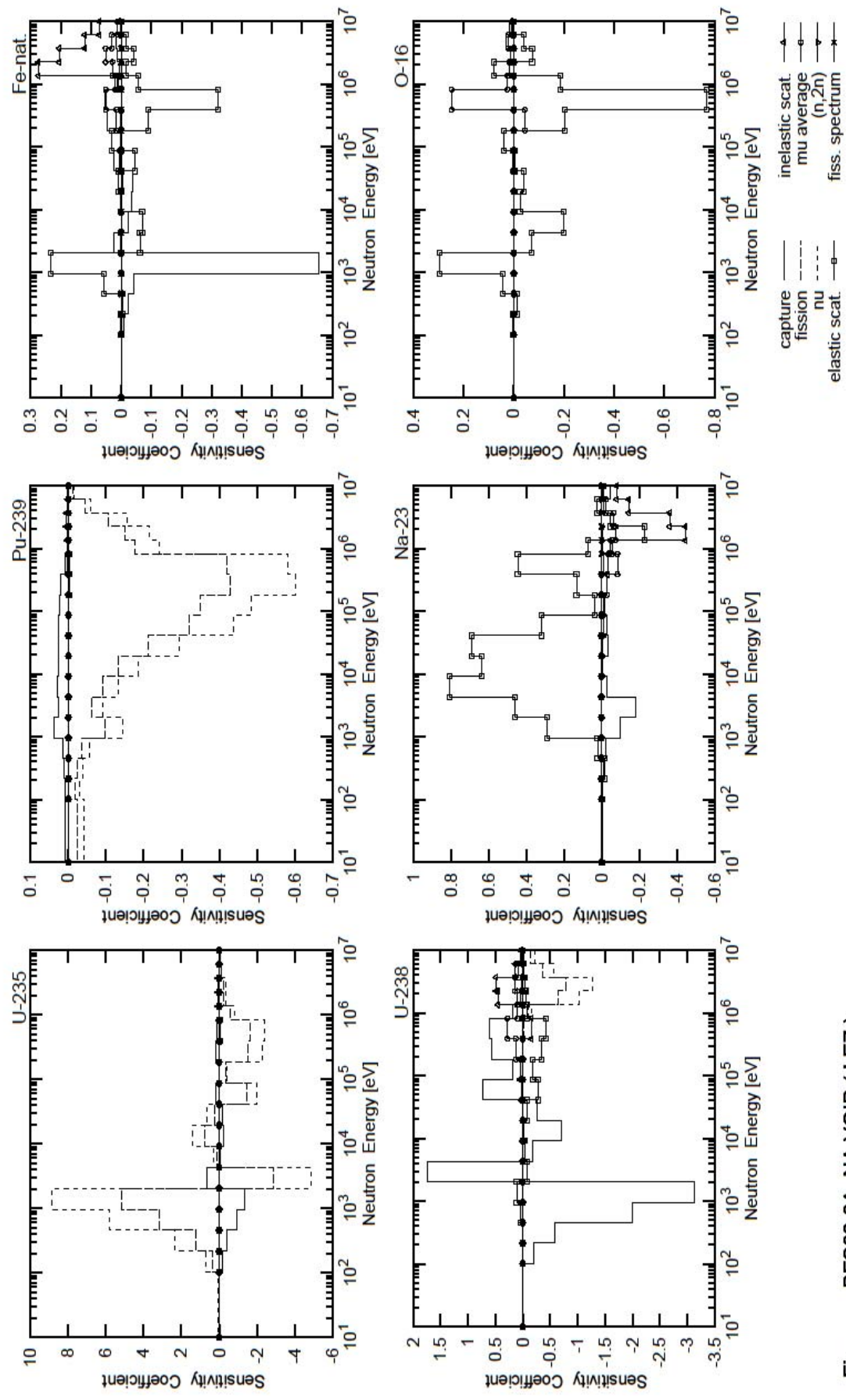


Fig. BES62-3A NAVOID (LEZ)

TABLE BFS62-3A NA VOID (LEZ) (HEAVY METAL) UNIT:1.0E-4

NUCL.	REACTION	TOTAL	18G	17G	16G	15G	14G	13G	12G	11G	10G	9G	8G	7G	6G	5G	4G	3G	2G	1G	
U-235	CAPTURE	-22032	-124	-1466	-4012	-9438	-13790	6608	-803	-2238	-1459	1791	88	1506	996	227	58	25	1	0	
U-235	NU	64361	546	6787	23259	58164	88677	-48761	3186	14361	6739	-20219	-3981	-22889	-24089	-8383	-3413	-3721	-1418	-484	
U-235	FISSION	20282	280	3740	12313	31546	51453	-28639	1142	7674	2602	-14690	-3716	-15550	-16467	-5751	-2163	-2286	-918	-286	
U-235	ELAS. SCT	-850	0	1	2	43	130	-65	-27	23	-11	-183	-75	-229	-296	-69	-42	-37	-12	-2	
U-235	INEL. SCT	1051	0	0	0	0	0	0	0	0	-13	67	91	-198	-2	389	500	180	39		
U-235	(n, 2n)	-4	0	0	0	0	0	0	0	0	0	0	0	0	0	0	0	0	0	-4	
U-235	MU-AVE.	689	0	0	0	0	0	0	1	19	17	92	215	79	80	113	59	16			
U-238	CAPTURE	-29462	32	-2017	-5877	-19903	-31255	17470	-1885	-6964	-2600	7376	1858	5732	6070	1861	415	188	33	5	
U-238	NU	-32577	0	0	39	20	0	1	1	-1	-9	-3	-18	-266	-1508	-10236	-12763	-5615	-2220		
U-238	FISSION	-20644	0	0	21	12	0	0	-1	-6	-2	-12	-180	-1042	-6543	-7860	-3671	-1360			
U-238	ELAS. SCT	-14756	18	40	45	389	1114	-776	-435	-174	-699	-2883	-1817	-3485	-4175	-885	-502	-382	-122	-28	
U-238	INEL. SCT	10151	0	0	0	0	0	0	0	0	203	505	7	-1595	-59	4530	4794	1366	401		
U-238	(n, 2n)	-57	0	0	0	0	0	0	0	0	0	0	0	0	0	0	0	0	-57		
U-238	MU-AVE.	8906	0	0	-1	-2	2	3	3	24	235	325	1274	2774	929	1011	1397	738	195		
Pu-239	NU	-38096	-425	-309	-383	-568	-1448	-902	-1313	-1842	-2929	-4396	-4853	-6014	-5819	-2426	-2157	-1549	-604	-160	
Pu-239	FISSION	-27018	-235	-185	-236	-358	-961	-609	-909	-1314	-2127	-3199	-3502	-4307	-4202	-1758	-1505	-1071	-429	-111	
Pu-239	ELAS. SCT	-79	0	0	1	4	3	-1	0	1	-3	-12	-13	-27	-22	-4	-3	-2	-1	0	
Pu-239	INEL. SCT	84	0	0	0	0	0	-1	-8	-4	-3	1	-2	-9	3	41	45	18	3		
Pu-239	(n, 2n)	0	0	0	0	0	0	0	0	0	0	0	0	0	0	0	0	0	0		
Pu-239	MU-AVE.	60	0	0	0	0	0	0	0	0	1	3	12	17	6	6	9	5	1		

TABLE BFS62-3A NA VOID (LEZ) (FISSION SPECTRUM) UNIT:1.0E-4

	FISSION SPECTRUM	TOTAL	18G	17G	16G	15G	14G	13G	12G	11G	10G	9G	8G	7G	6G	5G	4G	3G	2G	1G
SPEC.	U-235	0.05	12	0	0	0	-1	0	6	23	71	169	370	844	2966	2832	-1584	-2797	-1409	-1479
SPEC.	Pu-239	0.05	-3	0	0	0	0	0	3	13	42	113	291	762	768	-221	-906	-535	-332	

TABLE BFS62-3A NA VOID (LEZ) (STRUCTURE , COOLANT) UNIT:1.0E-4

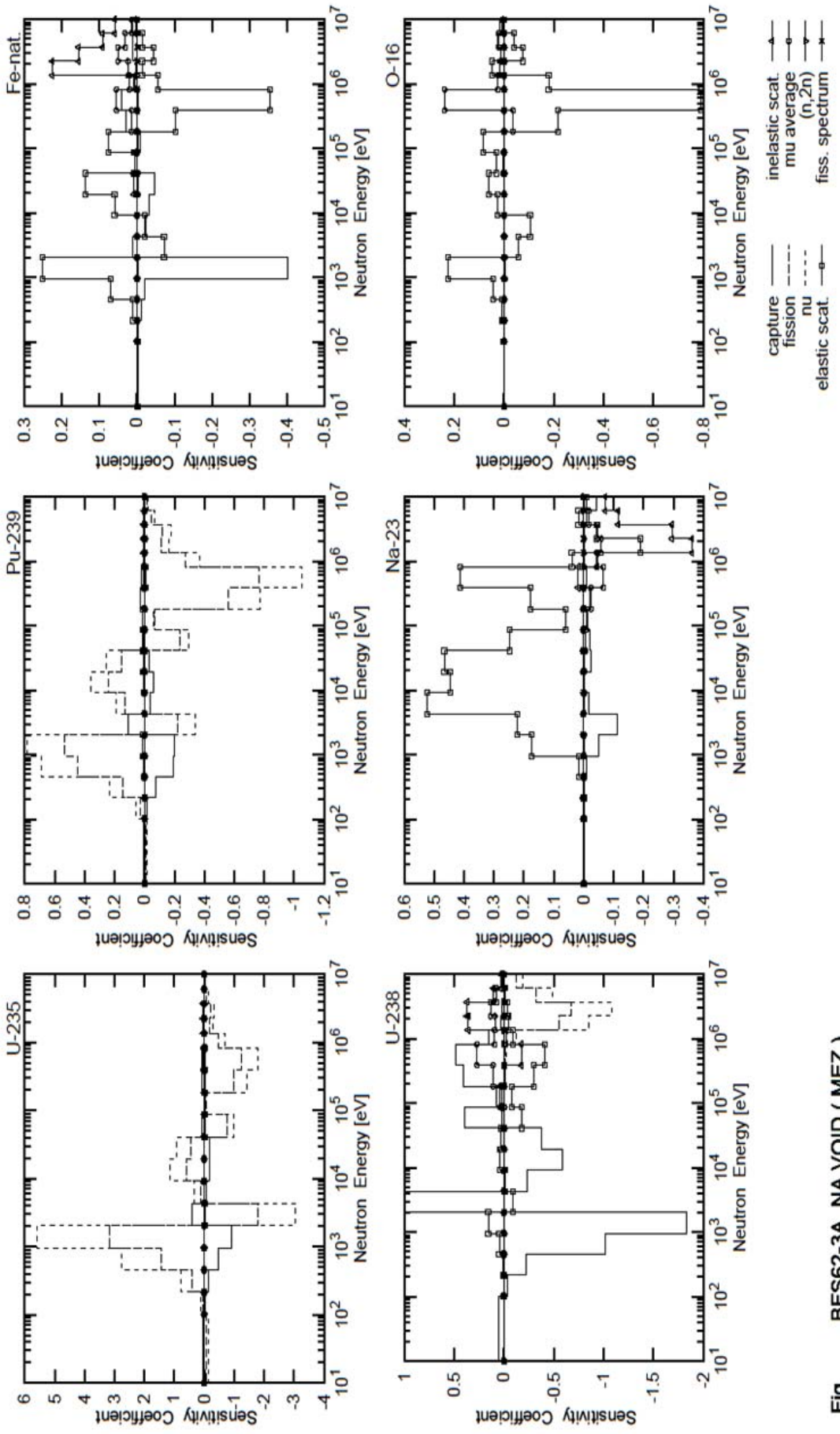
NUCL.	REACTION	TOTAL	186	176	166	156	146	136	126	116	106	96	86	76	66	56	46	36	26	16
H-1	CAPTURE	2	0	0	0	0	0	0	0	0	0	0	0	0	0	0	0	0	0	
H-1	ELAS. SCT	-2692	0	-11	6	-7	-221	-202	-441	-711	-848	-494	-58	67	-3	16	123	74	13	5
H-1	INEL. SCT	0	0	0	0	0	0	0	0	0	0	0	0	0	0	0	0	0	0	
H-1	(n, 2n)	0	0	0	0	0	0	0	0	0	0	0	0	0	0	0	0	0	0	
H-1	MU-AVE.	268	-1	-1	-3	-2	3	4	9	20	45	41	52	51	18	17	11	4	1	
C-12	CAPTURE	2	0	0	0	0	0	0	0	0	0	0	0	0	0	0	0	0	0	
C-12	ELAS. SCT	-46	0	2	-5	18	124	-29	-81	-11	-8	35	51	7	-141	-23	38	-11	-12	2
C-12	INEL. SCT	5	0	0	0	0	0	0	0	0	0	0	0	0	0	0	0	0	2	
C-12	(n, 2n)	0	0	0	0	0	0	0	0	0	0	0	0	0	0	0	0	0	0	
C-12	MU-AVE.	62	0	0	0	-1	-1	0	0	1	5	4	11	23	8	5	1	4	1	
0-16	CAPTURE	529	0	0	0	0	0	0	0	0	0	0	2	1	6	10	3	2	312	192
0-16	ELAS. SCT	-11568	12	41	-132	451	2950	-710	-1985	-248	-396	-59	405	-2036	-7680	-1870	785	-736	-409	50
0-16	INEL. SCT	92	0	0	0	0	0	0	0	0	0	0	0	0	0	0	0	0	92	
0-16	(n, 2n)	0	0	0	0	0	0	0	0	0	0	0	0	0	0	0	0	0	0	
0-16	MU-AVE.	2931	-1	-1	-2	-10	-17	16	5	5	16	49	-10	-438	2479	251	189	131	223	45
Na-23	CAPTURE	-5346	-7	-24	-78	-250	-978	-1838	-282	-17	-358	-305	-170	-262	-116	-25	-23	-14	-125	-474
Na-23	ELAS. SCT	36168	-21	1	-156	209	2863	4597	8071	6331	6871	3200	375	1325	4443	702	-2284	-483	220	-96
Na-23	INEL. SCT	-11115	0	0	0	0	0	0	0	0	0	-321	-461	-4449	-3621	-1446	-817			
Na-23	(n, 2n)	0	0	0	0	0	0	0	0	0	0	0	0	0	0	0	0	0	0	
Na-23	MU-AVE.	-3685	1	1	-2	-13	-30	-46	-97	-116	-301	-844	-558	-736	-643	-232	-55			
AL-27	CAPTURE	-21	0	-2	-6	-13	-20	13	-130	-5	-50	10	7	33	26	7	3	8	41	57
AL-27	ELAS. SCT	-2710	1	3	-10	40	246	-67	-137	-1	-66	-75	442	-628	-1962	-339	43	-144	-63	6
AL-27	INEL. SCT	1006	0	0	0	0	0	0	0	0	0	0	0	5	310	395	153	143		
AL-27	(n, 2n)	0	0	0	0	0	0	0	0	0	0	0	0	0	0	0	0	0	0	
AL-27	MU-AVE.	1553	0	0	-1	1	0	0	2	17	32	113	478	251	280	280	83	19		
Cr	CAPTURE	-1224	-11	-24	-63	-140	-1645	551	-79	-42	-90	34	14	85	86	27	11	20	21	20
Cr	ELAS. SCT	-2818	-1	-4	-42	227	-311	-956	-9	12	-187	-52	-267	-943	-225	-6	-100	-39	1	
Cr	INEL. SCT	1699	0	0	0	0	0	0	0	0	0	0	3	7	426	780	293	189		
Cr	(n, 2n)	0	0	0	0	0	0	0	0	0	0	0	0	0	0	0	0	0	0	
Cr	MU-AVE.	576	0	0	0	-1	4	1	0	0	6	5	25	82	45	93	190	94	34	
Mn-55	CAPTURE	-2180	-4	-21	-1113	-87	-975	39	-25	-24	-14	19	3	10	8	2	1	0	1	

Mn-55 ELAS. SCT -174 0 0 49 36 306 -434 -26 -10 7 4 8 -22 -66 -15 -2 -8 -3 0
Mn-55 INEL. SCT 141 0 0 0 0 0 0 0 0 0 0 0 0 0 0 0 1 9 -19 0 43 66 26 16
Mn-55 (n, 2n) 0
Mn-55 MU-AVE. 54 0 0 -1 0 -2 2 0 0 0 1 0 3 14 6 8 13 7 3

Fe CAPTURE -6210 -34 -90 -246 -402 -6542 227 -237 -338 -384 246 14 470 517 112 49 146 153 128
Fe ELAS. SCT -3938 -11 19 -44 556 2320 -622 -697 28 84 -471 322 -895 -3222 -584 -147 -423 -153 2
Fe INEL. SCT 6819 0 0 0 0 0 0 -15 -42 48 6 6 -24 141 2739 2049 1198 714
Fe (n, 2n) 0
Fe MU-AVE. 2108 0 0 -1 -6 -10 5 1 -2 -2 26 14 153 509 194 288 515 308 117

Ni CAPTURE 467 -8 -17 -47 -101 -194 184 -19 -347 -106 117 23 143 120 49 52 244 260 114
Ni ELAS. SCT -983 -2 4 -8 128 560 -233 -461 144 31 -200 40 -287 -492 -116 -10 -59 -21 0
Ni INEL. SCT 666 0
Ni (n, 2n) 0
Ni MU-AVE. 312 0 0 0 -1 -3 2 0 -2 -1 9 3 35 75 32 41 65 39 17

VII.1.3. Sodium Void Reactivity – Middle Core



BFS62-3A NAVOID (MEZ)

Fig.

TABLE BFS62-3A NA VOID (MEZ) (HEAVY METAL) UNIT:1.0E-4

NUCL.	REACTION	TOTAL	18G	17G	16G	15G	14G	13G	12G	11G	10G	9G	8G	7G	6G	5G	4G	3G	2G	1G
U-235	CAPTURE	-12865	282	-271	-1447	-4639	-8986	4119	-825	-1789	-1596	740	-257	910	685	187	49	21	1	0
U-235	NU	28155	-1360	1109	7911	27646	56026	-30501	3413	11342	9138	-9917	175	-14284	-17816	-6896	-2932	-3212	-1260	-428
U-235	FISSION	3680	-764	528	3974	14515	31690	-17925	1266	5997	4591	-7552	-736	-9842	-12345	-4736	-1883	-2008	-829	-261
U-235	ELAS. SCT	-839	-1	1	6	50	177	-110	-8	59	50	-162	-66	-273	-366	-84	-52	-43	-14	-3
U-235	INEL. SCT	623	0	0	0	0	0	0	0	0	0	2	6	66	31	-272	-21	281	368	132
U-235	(n, 2n)	-5	0	0	0	0	0	0	0	0	0	0	0	0	0	0	0	0	0	0
U-235	MU-AVE.	805	0	0	0	0	0	-1	-1	16	15	106	267	95	92	130	67	20		
U-238	CAPTURE	-16979	531	-327	-2214	-10110	-18356	9993	-2317	-5915	-3809	3911	773	4019	4775	1539	340	156	28	4
U-238	NU	-27500	0	0	0	19	11	0	1	1	0	-5	-2	-13	-222	-1247	-8517	-10784	-4828	-1916
U-238	FISSION	-17597	0	0	0	10	7	0	1	0	-4	-1	-9	-151	-864	-5486	-6716	-3193	-1191	
U-238	ELAS. SCT	-9788	11	23	79	469	1567	-928	-155	378	298	-1819	-792	-2993	-4030	-880	-453	-366	-118	-29
U-238	INEL. SCT	7099	0	0	0	0	0	0	0	0	197	442	-119	-1740	-272	3574	3672	1027	318	
U-238	(n, 2n)	-59	0	0	0	0	0	0	0	0	0	0	0	0	0	0	0	0	0	
U-238	MU-AVE.	8141	0	0	0	-1	-4	3	0	-7	-8	151	153	1082	2706	925	899	1328	713	200
Pu-239	CAPTURE	-4407	40	-132	-753	-1892	-2008	1066	-394	-587	-333	131	-14	253	177	28	7	3	0	0
Pu-239	NU	-7743	-176	537	2354	6902	7825	-3372	1872	3582	2519	-2977	-605	-7738	-10536	-3671	-1617	-1754	-685	-203
Pu-239	FISSION	-7490	-103	314	1467	4436	5335	-2185	1319	2403	1544	-2396	-689	-5629	-7688	-2703	-1114	-1188	-482	-131
Pu-239	ELAS. SCT	306	0	1	6	42	108	-26	8	60	87	29	96	-17	-62	-15	0	-7	-3	-1
Pu-239	INEL. SCT	148	0	0	0	0	0	-23	-4	1	16	6	-36	-1	76	78	29	6		
Pu-239	(n, 2n)	-1	0	0	0	0	0	0	0	0	0	0	0	0	0	0	0	0	0	
Pu-239	MU-AVE.	93	0	0	0	0	0	-1	-4	-3	-20	9	47	19	3	24	14	6		

TABLE BFS62-3A NA VOID (MEZ) (FISSION SPECTRUM) UNIT:1.0E-4

	FISSION SPECTRUM	TOTAL	18G	17G	16G	14G	13G	12G	11G	10G	9G	8G	7G	6G	5G	4G	3G	2G	1G	
SPEC.	U-235	0.05	12	0	0	0	0	2	7	21	55	123	252	606	2367	2003	-1204	-2077	-1068	-1074
SPEC.	Pu-239	0.05	-3	0	0	0	0	-1	-1	4	19	54	132	307	983	970	-400	-1037	-540	-493

TABLE BFS62-3A NA VOID (MEZ) (STRUCTURE , COOLANT) UNIT:1.0E-4
NUCL. REACTION TOTAL 18G 17G 16G 15G 14G 13G 12G 11G 10G 9G 8G 7G 6G 5G 4G 3G 2G 1G

H-1	ELAS.	SCT	-2563	0	-12	10	-7	-276	-150	-381	-652	-773	-463	-77	34	-17	12	109	65	12	4
H-1	INEL.	SCT	0	0	0	0	0	0	0	0	0	0	0	0	0	0	0	0	0	0	0
H-1	(n,2n)		0	0	0	0	0	0	0	0	0	0	0	0	0	0	0	0	0	0	0
H-1	MU-AVE.		235	-1	-1	-1	-1	2	3	8	17	37	36	46	45	16	15	10	3	1	
<hr/>																					
C-12	ELAS.	SCT	-9	0	1	3	19	112	-25	-50	15	37	42	57	-23	-174	-23	29	-18	-13	2
C-12	INEL.	SCT	4	0	0	0	0	0	0	0	0	0	0	0	0	0	0	0	0	0	3
C-12	(n,2n)		0	0	0	0	0	0	0	0	0	0	0	0	0	0	0	0	0	0	0
C-12	MU-AVE.		57	0	0	-1	-2	1	0	0	-1	3	1	10	25	8	5	1	4	1	
<hr/>																					
0-16	ELAS.	SCT	-9329	7	18	66	455	2251	-585	-1041	254	601	306	848	-2166	-7903	-1793	487	-757	-407	31
0-16	INEL.	SCT	74	0	0	0	0	0	0	0	0	0	0	0	0	0	0	0	0	0	74
0-16	(n,2n)		0	0	0	0	0	0	0	0	0	0	0	0	0	0	0	0	0	0	0
0-16	MU-AVE.		2805	0	0	-2	-12	-31	19	1	-8	-4	31	-4	-369	2386	248	167	125	215	46
<hr/>																					
Na-23	CAPTURE	-3438	1	-6	-27	-109	-512	-1141	-168	-10	-257	-216	-129	-204	-93	-21	-19	-12	-106	-409	
Na-23	ELAS.	SCT	25555	-14	-8	-23	167	1729	2228	5240	4447	4658	2476	594	1783	4114	399	-1888	-423	174	-97
Na-23	INEL.	SCT	-8742	0	0	0	0	0	0	0	0	0	0	0	181	-455	-3634	-2946	-1157	-730	
Na-23	(n,2n)		0	0	0	0	0	0	0	0	0	0	0	0	0	0	0	0	0	0	
Na-23	MU-AVE.		-2882	0	0	-2	-14	9	-9	-21	-34	-70	-100	-239	-663	-436	-584	-482	-172	-40	
<hr/>																					
Al-27	CAPTURE	66	1	0	-1	-4	-6	4	-43	-2	-17	6	11	22	17	5	2	6	28	37	
Al-27	ELAS.	SCT	-1217	0	1	4	28	116	-40	-40	11	95	26	536	-386	-1271	-203	36	-92	-41	3
Al-27	INEL.	SCT	620	0	0	0	0	0	0	0	0	0	0	0	2	194	244	94	85		
Al-27	(n,2n)		0	0	0	0	0	0	0	0	0	0	0	0	0	0	0	0	0	0	
Al-27	MU-AVE.		947	0	0	-1	-1	1	0	0	-2	6	8	65	304	160	163	178	54	13	
<hr/>																					
Cr	CAPTURE	-969	-7	-9	-27	-77	-1076	324	-139	-39	-112	4	-13	54	66	22	9	16	18	17	
Cr	ELAS.	SCT	-1719	-3	-1	8	54	263	-423	-410	164	161	-47	252	-314	-1042	-220	-10	-110	-40	-1
Cr	INEL.	SCT	1346	0	0	0	0	0	0	0	0	0	0	-2	4	347	614	225	157		
Cr	(n,2n)		0	0	0	0	0	0	0	0	0	0	0	0	0	0	0	0	0	0	
Cr	MU-AVE.		549	0	0	-1	-2	5	-1	-2	-2	-2	-7	24	89	45	77	187	95	39	
<hr/>																					
Mn-55	CAPTURE	-1199	-3	-8	-472	-47	-626	5	-31	-22	-19	9	-1	7	6	1	0	0	1		
Mn-55	ELAS.	SCT	92	0	0	71	44	389	-436	-2	28	73	27	-26	-73	-15	-2	-9	-3	0	

Mn-55	INEL. SCT	103	0	0	0	0	0	0	0	0	0	1	5	-23	0	35	51	20	13
Mn-55	(n, 2n)	0	0	0	0	0	0	0	0	0	0	0	0	0	0	0	0	0	0
Mn-55	MU-AVE.	52	0	0	-1	0	-4	4	0	0	-1	0	0	3	15	6	7	13	7
Fe	CAPTURE	-4137	-21	-34	-107	-220	-4037	127	-242	-311	-463	66	-87	304	399	92	38	121	130
Fe	ELAS. SCT	-723	-33	-7	104	708	2532	-725	-208	599	1379	69	760	-1023	-3560	-572	-137	-448	-156
Fe	INEL. SCT	5484	0	0	0	0	0	-4	82	46	11	2	-34	53	2253	1562	920	592	
Fe	(n, 2n)	0	0	0	0	0	0	0	0	0	0	0	0	0	0	0	0	0	
Fe	MU-AVE.	2018	0	-1	-8	-19	8	-2	-6	-24	10	-17	140	552	197	239	507	309	133
Ni	CAPTURE	224	-5	-7	-20	-56	-128	98	-29	-320	-133	48	-10	94	92	40	41	202	221
Ni	ELAS. SCT	421	-7	-1	23	165	636	-288	-218	608	434	-35	156	-296	-544	-113	-11	-64	-21
Ni	INEL. SCT	530	0	0	0	0	0	0	0	0	0	2	1	-2	0	131	256	89	
Ni	(n, 2n)	0	0	0	0	0	0	0	0	0	0	0	0	0	0	0	0	0	
Ni	MU-AVE.	287	0	0	0	-2	-5	3	0	-7	-5	4	-4	32	82	33	34	64	40

VII.1.4. Sodium Void Reactivity – MOX Core –

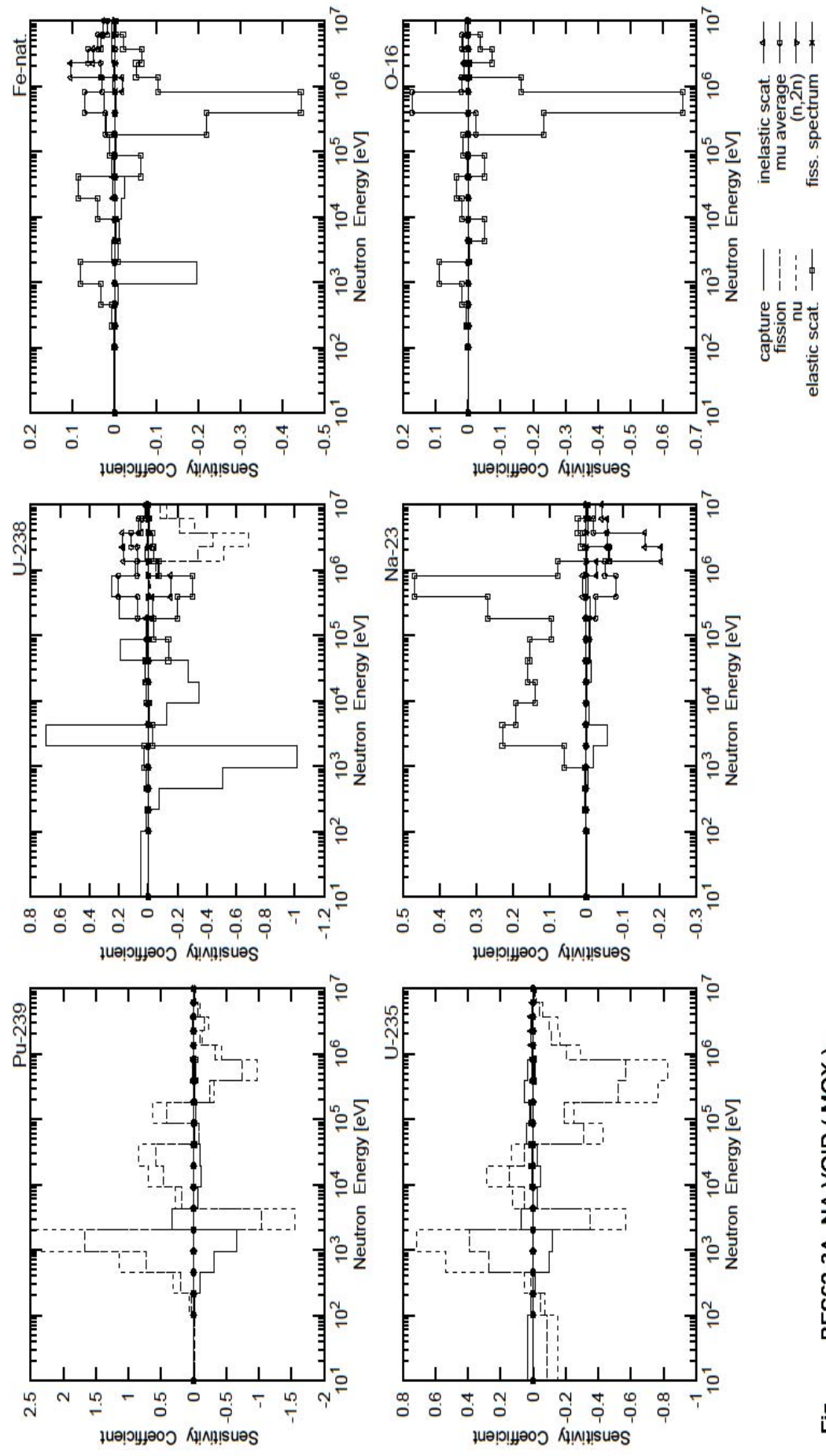


Fig. BFS62-3A VOID (MOX)

TABLE BFS62-3A NA VOID (MOX) (HEAVY METAL) UNIT:1.0E-4

NUCL.	REACTION	TOTAL	18G	17G	16G	15G	14G	13G	12G	11G	10G	9G	8G	7G	6G	5G	4G	3G	2G	1G	
	U-235 CAPTURE	-485	320	143	-127	-960	-1156	733	-250	-454	-279	399	178	504	353	74	26	9	0	0	
U-235 NU	-19134	-1531	-744	511	5351	7149	-5703	1249	2839	1355	-4299	-2508	-7688	-8245	-2926	-1649	-1519	-583	-194		
U-235 FISSION	-16031	-850	-454	162	2691	3905	-3490	536	1482	551	-3102	-1893	-5230	-5690	-2044	-1098	-985	-397	-126		
U-235 ELAS. SCT	175	-2	-1	15	21	-1	13	55	101	26	116	-21	-86	-28	-9	-18	-6	-2			
U-235 INEL. SCT	182	0	0	0	0	0	0	0	0	-1	12	-8	-98	-23	104	138	47	10			
U-235 (n, 2n)	-3	0	0	0	0	0	0	0	0	0	0	0	0	0	0	0	0	-3			
U-235 MU-AVE.	185	0	0	0	0	0	0	0	-1	-4	-2	-21	7	60	32	19	53	32	12		
	U-238 CAPTURE	-8398	506	114	-757	-5064	-10181	6983	-1286	-3467	-2757	1861	10	1962	2509	863	191	94	17	2	
U-238 NU	-17244	0	0	11	7	0	1	1	-3	0	-6	-129	-722	-3141	-6858	-3155	-1250				
U-238 FISSION	-11379	0	0	6	4	0	0	0	-2	0	-4	-89	-510	-3430	-4404	-2144	-806				
U-238 ELAS. SCT	-7999	4	5	21	110	294	-274	-103	111	180	-1381	-370	-2001	-3038	-722	-383	-320	-104	-27		
U-238 INEL. SCT	1701	0	0	0	0	0	0	0	0	70	128	-324	-1524	-686	1661	1740	473	163			
U-238 (n, 2n)	-53	0	0	0	0	0	0	0	0	0	0	0	0	0	0	0	0	-53			
U-238 MU-AVE.	6335	0	0	0	-1	1	-2	-5	108	66	698	2021	754	736	1150	628	179				
	Pu-239 CAPTURE	-10285	28	-162	-1014	-3150	-6606	3341	-577	-1084	-893	-19	-353	80	82	34	5	4	0	0	
Pu-239 NU	25983	-101	669	3134	11352	24937	-15465	2782	6891	8378	-799	6237	-3166	-9665	-4356	-1325	-2262	-968	-289		
Pu-239 FISSION	14925	-72	388	1950	7270	16655	-10379	1866	4707	5728	-792	4153	-2504	-7380	-3255	-949	-1572	-699	-192		
Pu-239 ELAS. SCT	-735	0	1	1	9	37	-37	-14	8	7	-144	-42	-170	-247	-60	-38	-33	-10	-2		
Pu-239 INEL. SCT	-138	0	0	0	0	0	1	-5	3	-8	-1	-40	-180	-38	44	57	22	5			
Pu-239 (n, 2n)	-1	0	0	0	0	0	0	0	0	0	0	0	0	0	0	0	0	-1			
Pu-239 MU-AVE.	609	0	0	0	0	0	0	0	15	9	69	196	72	69	107	56	16				
	TABLE BFS62-3A NA VOID (MOX) (FISSION SPECTRUM) UNIT:1.0E-4																				
	FISSION SPECTRUM TOTAL	18G	17G	16G	15G	14G	13G	12G	11G	10G	9G	8G	7G	6G	5G	4G	3G	2G	1G		
	SPEC.	U-235	0.05	5	0	0	0	0	0	1	4	13	34	90	269	1128	1162	-314	-1194	-650	
	SPEC.	Pu-239	0.05	-3	0	0	0	0	-1	0	1	5	9	6	126	1061	732	-607	-624	-263	
	TABLE BFS62-3A NA VOID (MOX) (STRUCTURE , COOLANT) UNIT:1.0E-4																				
	NUCL.	REACTION	TOTAL	18G	17G	16G	15G	14G	13G	12G	11G	10G	9G	8G	7G	6G	5G	4G	3G	2G	1G

H-1	ELAS.	SCT	-2198	0	-9	-7	-239	-122	-304	-523	-626	-397	-95	-7	-34	6	86	52	9	3	
H-1	INEL.	SCT	0	0	0	0	0	0	0	0	0	0	0	0	0	0	0	0	0	0	
H-1	(n, 2n)		0	0	0	0	0	0	0	0	0	0	0	0	0	0	0	0	0	0	
H-1	MU-AVE.		179	0	0	0	1	2	6	13	28	27	34	33	12	12	8	3	1		
C-12	ELAS.	SCT	-227	0	0	3	8	46	-2	-22	13	21	-9	10	-72	-167	-27	6	-24	-12	0
C-12	INEL.	SCT	2	0	0	0	0	0	0	0	0	0	0	0	0	0	0	0	1	1	
C-12	(n, 2n)		0	0	0	0	0	0	0	0	0	0	0	0	0	0	0	0	0	0	
C-12	MU-AVE.		55	0	0	0	0	0	0	0	3	2	10	23	8	4	1	4	1		
C-12	CAPTURE	1	0	0	0	0	0	0	0	0	0	0	1	0	2	4	2	1	163	99	
0-16	ELAS.	SCT	-10948	2	6	67	179	890	-29	-510	190	356	-505	148	-2339	-6611	-1636	-41	-744	-372	1
0-16	INEL.	SCT	41	0	0	0	0	0	0	0	0	0	0	0	0	0	0	0	0	41	
0-16	(n, 2n)		0	0	0	0	0	0	0	0	0	0	0	0	0	0	0	0	0	0	0
0-16	MU-AVE.		2183	0	0	0	-3	-4	7	1	-2	-3	23	-2	-240	1722	204	138	110	191	42
Na-23	CAPTURE	-1769	1	-2	-8	-42	-208	-584	-79	-5	-133	-119	-70	-116	-53	-12	-11	-7	-66	-255	
Na-23	ELAS.	SCT	18070	-19	-9	21	36	590	2279	1907	1377	1588	1525	938	2684	4673	765	-614	148	225	-43
Na-23	INEL.	SCT	-4901	0	0	0	0	0	0	0	0	0	0	0	86	-298	-2057	-1614	-584	-433	
Na-23	(n, 2n)		0	0	0	0	0	0	0	0	0	0	0	0	0	0	0	0	0	0	
Na-23	MU-AVE.		-3295	1	1	0	0	-3	-9	-7	-15	-29	-69	-101	-271	-813	-509	-651	-570	-203	-47
AL-27	CAPTURE	43	1	0	0	-1	-3	-3	-19	-1	-9	3	5	11	9	3	1	3	17	22	
AL-27	ELAS.	SCT	-1856	0	0	3	11	39	-6	-19	8	75	-98	136	-455	-1081	-238	-61	-125	-43	-2
AL-27	INEL.	SCT	262	0	0	0	0	0	0	0	0	0	0	0	-8	94	107	29	40		
AL-27	(n, 2n)		0	0	0	0	0	0	0	0	0	0	0	0	0	0	0	0	0	0	
AL-27	MU-AVE.		857	0	0	0	0	0	0	-2	5	1	48	258	152	151	175	55	14		
Cr	CAPTURE	-388	5	-1	-9	-34	-537	199	-64	-19	-59	6	-2	36	43	13	5	10	10	10	
Cr	ELAS.	SCT	-2961	0	0	6	24	81	-97	-117	113	94	-164	20	-745	-1374	-410	-161	-170	-52	-8
Cr	INEL.	SCT	552	0	0	0	0	0	0	0	0	0	0	-5	-7	151	266	75	73		
Cr	(n, 2n)		0	0	0	0	0	0	0	0	0	0	0	0	0	0	0	0	0	0	
Cr	MU-AVE.		752	0	0	0	0	-1	-1	-1	-4	0	42	122	71	110	237	122	48		
Mn-55	CAPTURE	-476	2	-1	-144	-20	-303	8	-15	-11	-10	6	0	5	4	1	0	0	0	0	
Mn-55	ELAS.	SCT	-18	0	0	26	21	112	-7	3	22	44	-27	2	-61	-97	-27	-12	-13	-4	0

Mn-55	INEL. SCT	13 0 0 0 0 0 0 0 0 0 0 0 0 -3 -24 -7 12 20 7 6											
Mn-55	(n, 2n)	0 0											
Mn-55	MU-AVE.	74 0 0 0 0 -1 1 0 0 0 1 0 6 21 10 9 16 9 4											
<hr/>													
Fe	CAPTURE	-1748 17 -4 -33 -96 -1957 80 -121 -154 -246 57 -34 201 259 56 23 70 76 62											
Fe	ELAS. SCT	-7228 -5 7 76 320 816 -97 -31 391 873 -621 112 -2193 -4449 -1030 -512 -655 -202 -27											
Fe	INEL. SCT	1962 0 0 0 0 0 1 42 6 1 -11 -40 -182 1044 517 315 267											
Fe	(n, 2n)	0 0											
Fe	MU-AVE.	2751 0 0 0 -3 -4 2 -1 -4 -15 20 0 220 719 295 332 634 394 164											
<hr/>													
Ni	CAPTURE	238 4 -1 -6 -24 -62 64 -14 -162 -69 36 1 62 60 24 118 129 55											
Ni	ELAS. SCT	-1191 -1 1 16 74 200 -50 -68 352 248 -220 16 -610 -724 -212 -85 -96 -28 -4											
Ni	INEL. SCT	221 0 0 0 0 0 0 0 0 0 0 0 0 -1 -2 -1 55 113 31 25											
Ni	(n, 2n)	0 0											
Ni	MU-AVE.	425 0 0 0 -1 -1 0 -4 -4 7 0 59 112 52 49 81 51 23											

VII.1.5. Sodium Void Reactivity — Outer Core

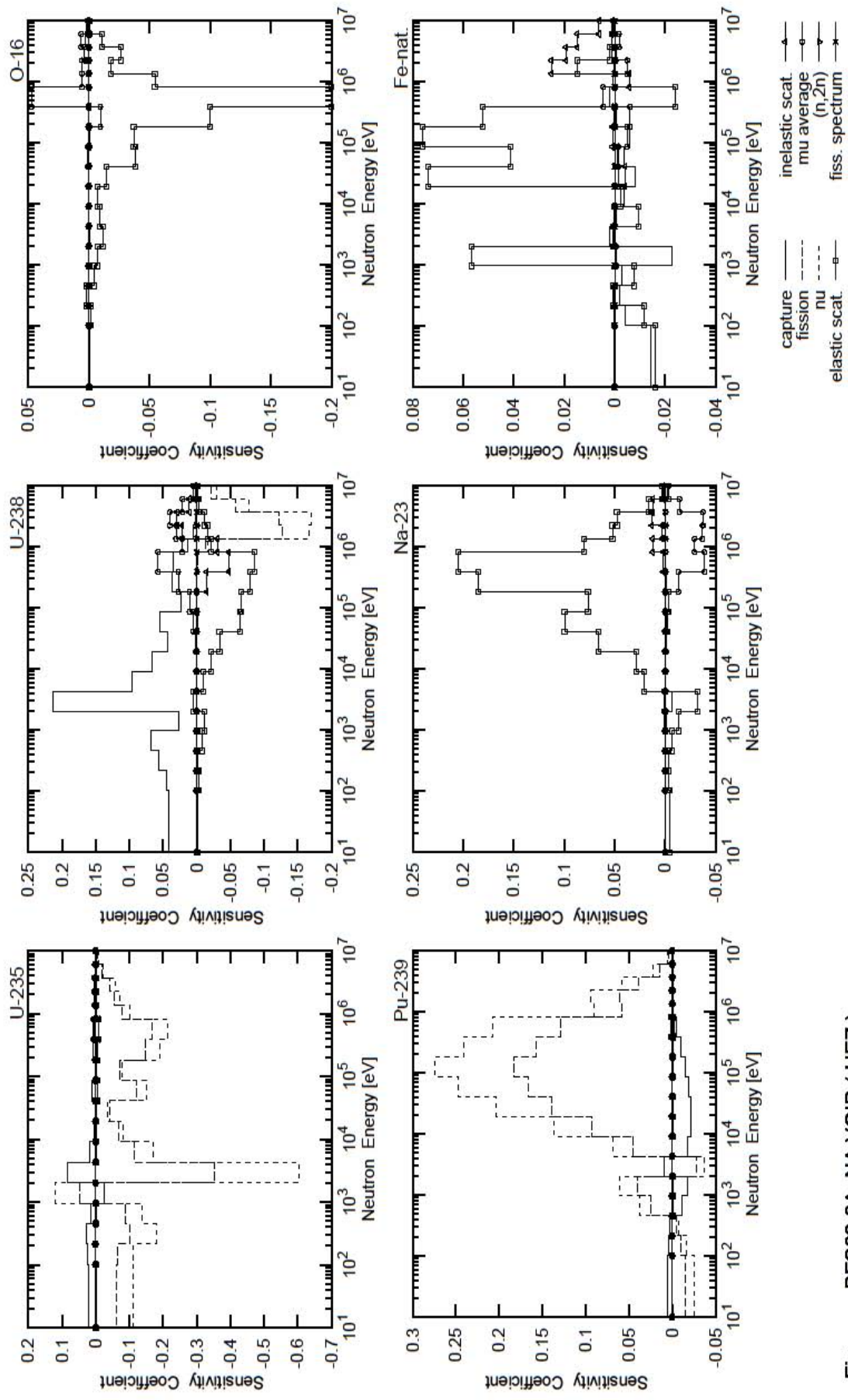


Fig. BFS62-3A NAVOID (HEZ)

TABLE BFS62-3A NA VOID (HEZ) (HEAVY METAL) UNIT:1.0E-4

Na-23	CAPTURE	-166	-2	0	-1	-12	-71	-6	0	-12	-12	-6	-11	-5	-1	-1	-5	-20	
Na-23	ELAS. SCT	8168	-48	-31	-30	-70	-137	-318	204	282	662	995	763	1852	2050	802	522	477	166 28
Na-23	INEL. SCT	444	0	0	0	0	0	0	0	0	0	0	0	17	125	32	131	122	18
Na-23	(n, 2n)	0	0	0	0	0	0	0	0	0	0	0	0	0	0	0	0	0	
Na-23	MU-AVE.	-1790	1	1	2	5	13	-1	-4	-9	-27	-37	-132	-390	-291	-369	-375	-142	-36

Mn-55 CAPTURE -144 -9 -57 -7 -48 7 -1 -3 -5 -2 -2 0 0 0 0 0
 Mn-55 ELAS. SCT 223 -1 -1 -27 -11 86 80 -4 -16 43 15 39 18 -4 0 4 1 0 0

Mn-55 INEL. SCT 14 0 0 0 0 0 0 0 0 0 0 0 0 0 0 0 0 0 0 4 6 3 1
Mn-55 (*n*, 2*n*) 0
Mn-55 MU-AVE. -5 0 0 0 -1 1 0 0 -1 -1 -1 -2 1 0 -2 0 0 0

Fe CAPTURE -613 -145 -40 -21 -30 -230 19 -6 -37 -81 -36 -58 -6 21 5 2 9 11 9
Fe ELAS. SCT 2480 -161 -118 5 -76 569 6 -94 -23 740 412 761 523 -240 -4 146 21 11 1
Fe INEL. SCT 551 0 0 0 0 0 0 0 -2 -42 -12 9 2 -2 -57 252 192 148 63
Fe (*n*, 2*n*) 0
Fe MU-AVE. -163 2 1 0 -1 -5 2 0 -2 -14 -15 -49 -61 45 -1 -49 -5 -18 6

Ni CAPTURE -96 -33 -8 -4 -8 -12 17 -1 -37 -27 -15 -20 -2 5 2 15 19 8
Ni ELAS. SCT 865 -33 -24 0 -16 147 -15 -57 126 196 142 217 177 -32 2 30 4 2 0
Ni INEL. SCT 57 0 6
Ni (*n*, 2*n*) 0
Ni MU-AVE. -48 0 0 0 -1 1 0 -2 -5 -5 -13 -18 6 -1 -8 -1 -3 1

VII.1.6. Sodium Void Reactivity – Total Effect -

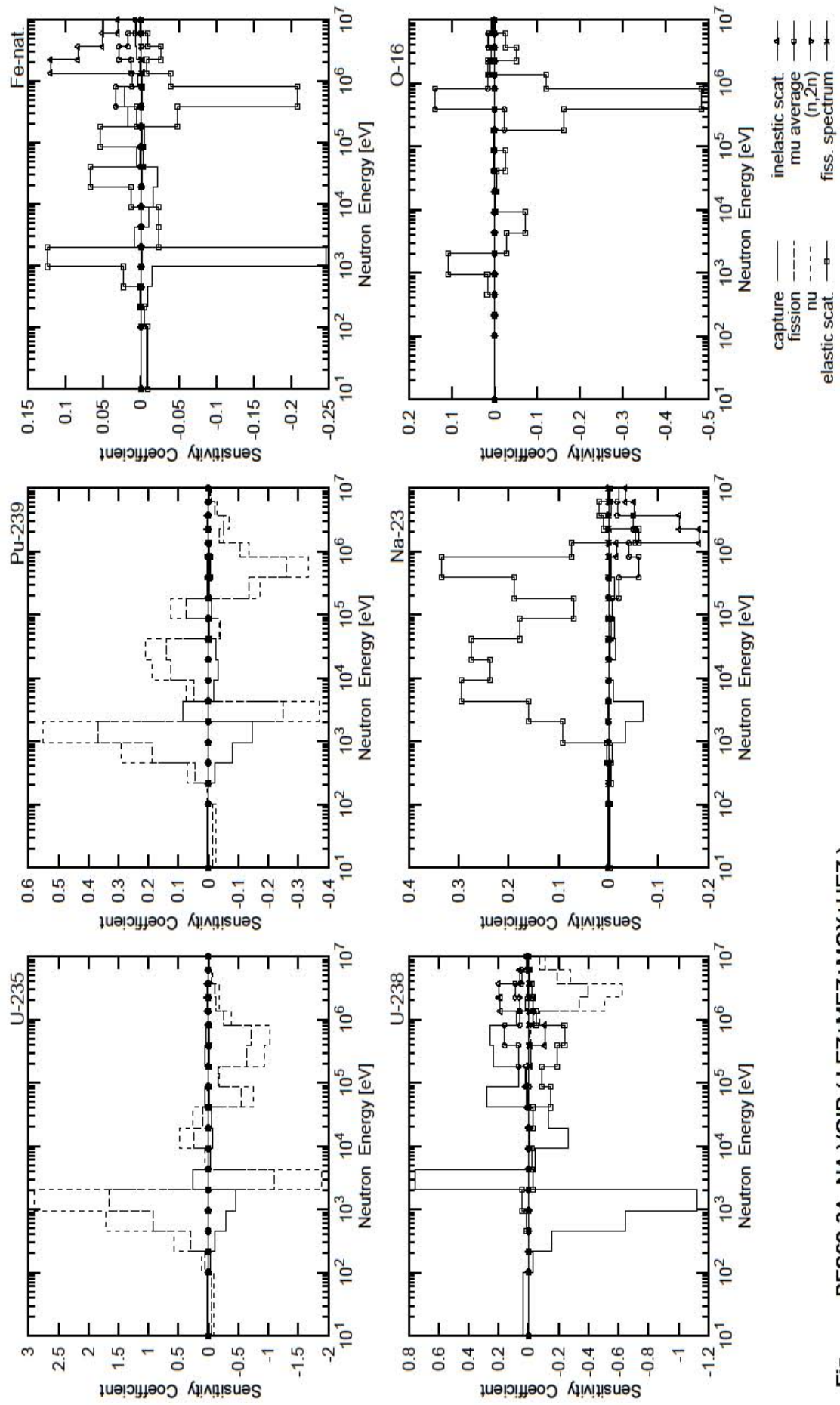


Fig. BFS62-3A NAVOID (LEZ+MEZ+MOX+HEZ)

TABLE BFS62-3A NA VOID (LEZ+MEZ+MOX+HEZ) (HEAVY METAL) UNIT:1.0E-4

NUCL.	REACTION	TOTAL	18G	17G	16G	15G	14G	13G	12G	11G	10G	9G	8G	7G	6G	5G	4G	3G	2G	1G
U-235	CAPTURE	-5770	164	-245	-1003	-2858	-4575	2545	-237	-785	-576	630	36	591	405	98	28	11	0	0
U-235	NU	4298	-809	1081	5662	17189	28983	-18794	547	4767	2638	-7421	-1785	-9330	-10196	-3157	-1772	-1784	-689	-232
U-235	FISSION	-5099	-466	565	2931	9172	16580	-11048	-38	2423	1005	-5473	-1672	-6444	-7093	-2621	-1175	-1140	-462	-145
U-235	ELAS.	SCT	-400	-2	-1	0	15	59	-18	-7	20	18	-80	-14	-118	-168	-43	-27	-24	-8
U-235	INEL.	SCT	302	0	0	0	0	0	0	0	0	-4	23	10	-131	-20	146	194	70	15
U-235	(n, 2n)	-3	0	0	0	0	0	0	0	0	0	0	0	0	0	0	0	0	-3	
U-235	MU-AVE.	397	0	0	0	0	0	0	-1	8	3	46	123	48	48	73	38	11		
U-238	CAPTURE	-6508	351	-287	-1524	-6470	-11215	7578	-479	-2624	-1336	2792	638	2340	2596	833	192	87	16	2
U-238	NU	-16117	0	0	0	12	7	0	0	-4	-1	-8	-121	-705	-5101	-6280	-2811	-1106		
U-238	FISSION	-10553	0	0	0	7	4	0	0	0	-3	-1	-5	-84	-497	-3388	-3996	-1888	-702	
U-238	ELAS.	SCT	-8123	-1	2	14	124	428	-299	-190	-88	-265	-1450	-900	-1897	-2403	-539	-318	-243	-78
U-238	INEL.	SCT	3346	0	0	0	0	0	0	0	74	189	-143	-1075	-315	1870	1997	576	172	
U-238	(n, 2n)	-37	0	0	0	0	0	0	0	0	0	0	0	0	0	0	0	-37		
U-238	MU-AVE.	5224	0	0	0	-1	1	2	10	116	158	679	1598	563	621	880	471	127		
Pu-239	CAPTURE	-2307	58	-6	-227	-810	-1460	858	-163	-307	-242	-12	-87	43	36	10	2	1	0	
Pu-239	NU	2879	-260	30	716	2923	5525	-3707	733	1885	2118	-346	1262	-1704	-3346	-1364	-494	-707	-297	
Pu-239	FISSION	775	-149	15	447	1875	3700	-2498	484	1267	1402	-380	750	-1348	-2597	-1049	-372	-497	-214	
Pu-239	ELAS.	SCT	-137	0	0	4	12	-8	-2	6	5	-25	-8	-40	-53	-12	-7	-6	-2	
Pu-239	INEL.	SCT	-1	0	0	0	0	0	-2	0	-3	1	-9	-47	-7	23	29	12		
Pu-239	(n, 2n)	0	0	0	0	0	0	0	0	0	0	0	0	0	0	0	0	3		
Pu-239	MU-AVE.	125	0	0	0	0	0	0	0	3	2	16	41	15	14	21	11	3		

H-1	ELAS. SCT	-2398	0	-10	7	-11	-248	-144	-343	-576	-689	-434	-96	3	-31	8	94	57	10	3
H-1	INEL. SCT	0	0	0	0	0	0	0	0	0	0	0	0	0	0	0	0	0	0	0
H-1	(n, 2n)	0	0	0	0	0	0	0	0	0	0	0	0	0	0	0	0	0	0	0
H-1	MU-AVE.	198	-1	0	-1	0	1	1	3	8	15	31	31	37	36	13	13	8	3	1
C-12	CAPTURE	1	0	0	0	0	0	0	0	0	0	0	0	0	0	0	0	0	0	0
C-12	ELAS. SCT	-95	0	0	0	6	51	-10	-31	0	4	8	19	-20	-99	-16	13	-12	-7	1
C-12	INEL. SCT	2	0	0	0	0	0	0	0	0	0	0	0	0	0	0	0	0	0	1
C-12	(n, 2n)	0	0	0	0	0	0	0	0	0	0	0	0	0	0	0	0	0	0	0
C-12	MU-AVE.	36	0	0	0	0	0	0	0	0	0	0	0	2	1	6	15	5	3	1
0-16	CAPTURE	249	0	0	0	0	0	0	0	0	1	0	3	4	1	1	148	90		
0-16	ELAS. SCT	-8365	0	5	-3	168	1076	-284	-726	-34	-39	-260	34	-1627	-4845	-1202	143	-520	-263	12
0-16	INEL. SCT	41	0	0	0	0	0	0	0	0	0	0	0	0	0	0	0	0	0	41
0-16	(n, 2n)	0	0	0	0	0	0	0	0	0	0	0	0	0	0	0	0	0	0	0
0-16	MU-AVE.	1706	0	0	0	-3	-7	6	3	7	24	-5	-233	1391	152	116	82	142	29	
Na-23	CAPTURE	-2054	-2	-7	-23	-80	-333	-704	-103	-6	-143	-124	-71	-111	-50	-11	-10	-6	-56	-214
Na-23	ELAS. SCT	18559	-33	-17	-50	41	914	1592	2940	2373	2744	1780	689	1883	3331	731	-614	93	192	-28
Na-23	INEL. SCT	-4297	0	0	0	0	0	0	0	0	0	0	0	-36	-156	-1820	-1419	-520	-345	
Na-23	(n, 2n)	0	0	0	0	0	0	0	0	0	0	0	0	0	0	0	0	0	0	0
Na-23	MU-AVE.	-2646	1	1	-3	5	-6	-14	-24	-56	-75	-210	-607	-412	-535	-489	-179	-43		
Al-27	CAPTURE	32	0	0	-1	-4	-6	5	-32	-1	-14	5	6	14	11	3	1	4	19	25
Al-27	ELAS. SCT	-1585	0	0	-1	12	77	-22	-45	-2	-6	-69	134	-364	-973	-187	-17	-90	-34	1
Al-27	INEL. SCT	392	0	0	0	0	0	0	0	0	0	0	-2	125	156	58	55			
Al-27	(n, 2n)	0	0	0	0	0	0	0	0	0	0	0	0	0	0	0	0	0	0	0
Al-27	MU-AVE.	782	0	0	0	0	0	0	0	0	0	0	0	11	51	234	128	145	150	45
Cr	CAPTURE	-543	-26	-12	-22	-53	-646	224	-48	-20	-54	6	-6	32	37	12	5	9	10	9
Cr	ELAS. SCT	-1046	-7	-4	1	17	126	-159	-354	20	75	-20	264	-140	-620	-153	-5	-64	-22	-1
Cr	INEL. SCT	722	0	0	0	0	0	0	0	0	0	0	-1	0	181	334	125	83		
Cr	(n, 2n)	0	0	0	0	0	0	0	0	0	0	0	0	0	0	0	0	0	0	0
Cr	MU-AVE.	310	0	0	0	-1	2	0	-1	-1	-9	10	55	28	43	108	53	22		
Mn-55	CAPTURE	-808	-10	-10	-372	-33	-379	15	-13	-11	-9	6	0	4	3	1	0	0	0	0
Mn-55	ELAS. SCT	73	0	-1	11	12	176	-109	-8	-3	38	6	24	-11	-43	-10	-1	-5	-2	0

VII.2. Comparison of Direct Calculation and Sensitivity Analysis for BFS-62-3A Experiment

Library		Difference of JENDL-3.3 Result from JENDL-3.2		Difference of JEF-2.2 Result from JENDL-3.2	
Method	Core Parameter	Direct Calculation	Sensitivity Analysis	Direct Calculation	Sensitivity Analysis
Sodium Void Reactivity	Criticality	-0.50 %dk	-0.45 %dk	+0.35 %dk	+0.54 %dk
	Inner Core	+22 pcm	+21 pcm	+13 pcm	+18 pcm
	Middle Core	+6 pcm	+5 pcm	+5 pcm	+5 pcm
	MOX Core	0 pcm	+2 pcm	+6 pcm	+7 pcm
	Outer Core	0 pcm	-2 pcm	+7 pcm	+3 pcm
	Total Effect	+28 pcm	+26 pcm	+31 pcm	+33 pcm

VII.3. Sensitivity Analysis for BFS-62-3A Experiment

VII.3.1. Criticality

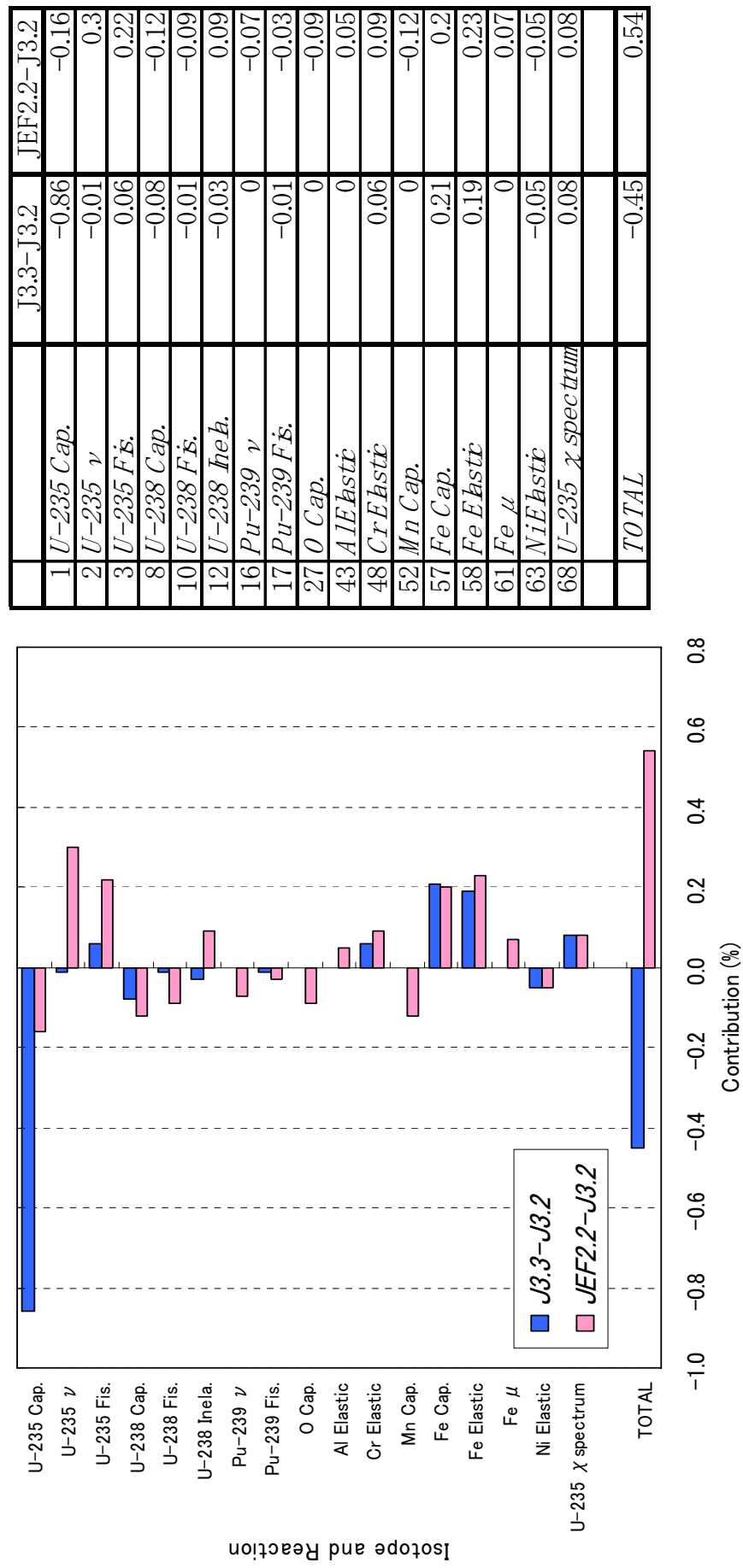


Fig. A.3.1 Sensitivity Analysis for BFS-62-3A Experiment – Criticality –

VII.3.2. Sodium Void Reactivity – Inner Core –

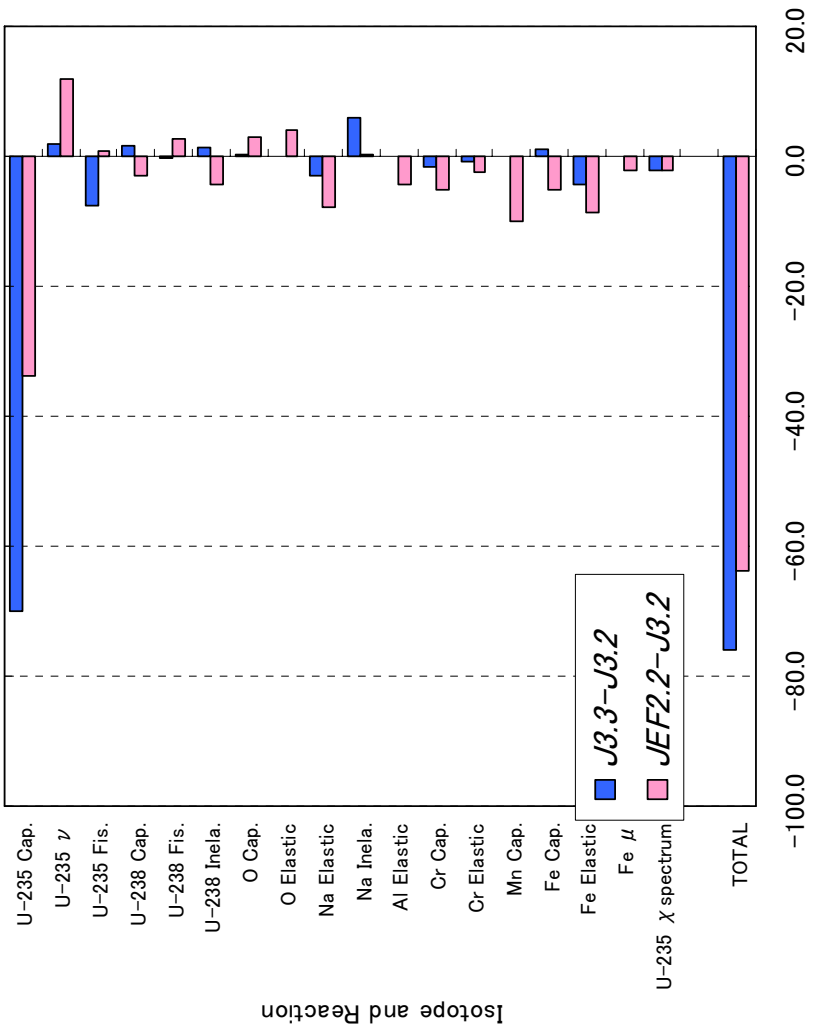


Fig. A.3.2 Sensitivity Analysis for BFS-62-3A Experiment
– Sodium Void Reactivity (Inner Core) –

NO.		J3.3-J3.2	JEF2.2-J3.2
1	$U-235\ Cap.$	-70.0	-33.8
2	$U-235\ \nu$	1.9	12.0
3	$U-235\ Fis.$	-7.6	0.9
8	$U-238\ Cap.$	1.7	-3.1
10	$U-238\ Fis.$	-0.3	2.7
12	$U-238\ Inela.$	1.2	-4.4
27	$O\ Cap.$	0.2	2.9
28	$O\ Elastic$	-0.1	3.9
38	$Na\ Elastic$	-3.0	-7.9
39	$Na\ Inela.$	5.9	0.3
43	$Al\ Elastic$	-0.1	-4.3
47	$Cr\ Cap.$	-1.7	-5.2
48	$Cr\ Elastic$	-0.7	-2.3
52	$Mn\ Cap.$	-0.1	-10.0
57	$Fe\ Cap.$	1.0	-5.2
58	$Fe\ Elastic$	-4.4	-8.7
61	$Fe\ \mu$	0.0	-2.1
68	$U-235\ \chi\ spectrum$	-2.1	-2.1
	TOTAL	-75.8	-63.7

VII.3.3. Sodium Void Reactivity – Middle Core –

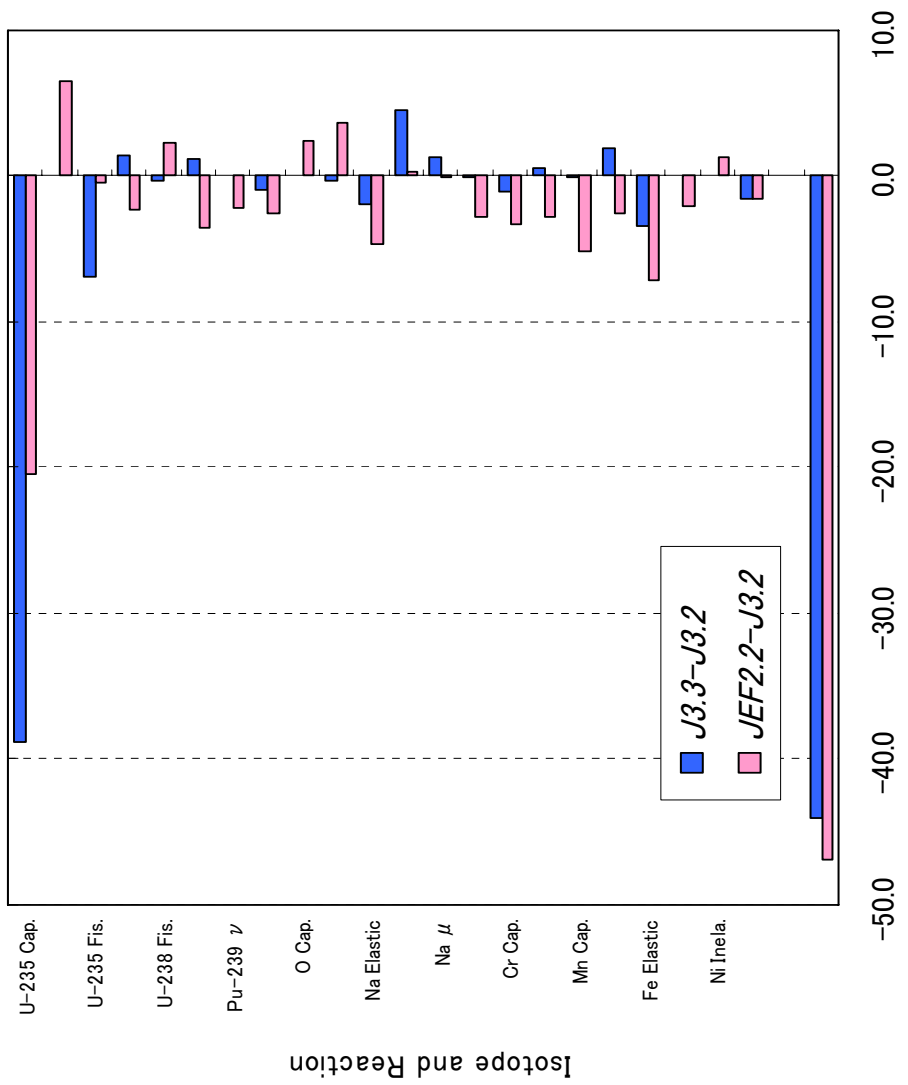


Fig. A.3.3 Sensitivity Analysis for BFS-62-3A Experiment
– Sodium Void Reactivity (Middle Core) –

	J3.3-J3.2	JEF2.2-J3.2
1 <i>U-235 Cap.</i>	-38.8	-20.4
2 <i>U-235 ν</i>	0.0	6.5
3 <i>U-235 Fis.</i>	-6.9	-0.4
8 <i>U-238 Cap.</i>	1.5	-2.4
10 <i>U-238 Fis.</i>	-0.3	2.3
12 <i>U-238 Inel.</i>	1.2	-3.6
16 <i>Pu-239 ν</i>	0.0	-2.1
17 <i>Pu-239 Fis.</i>	-1.0	-2.6
27 <i>O Cap.</i>	0.1	2.4
28 <i>O Elastic</i>	-0.3	3.6
38 <i>Na Elastic</i>	-2.0	-4.7
39 <i>Na Inel.</i>	4.6	0.4
41 <i>Na μ</i>	1.3	0.0
43 <i>Al Elastic</i>	-0.1	-2.8
47 <i>Cr Cap.</i>	-1.1	-3.3
48 <i>Cr Elastic</i>	0.6	-2.8
52 <i>Mn Cap.</i>	0.0	-5.1
57 <i>Fe Cap.</i>	2.0	-2.6
58 <i>Fe Elastic</i>	-3.4	-7.2
61 <i>Fe μ</i>	0.0	-2.1
64 <i>Ni Inel.</i>	0.1	1.3
68 <i>U-235 χ spectrum</i>	-1.6	-1.6
<i>TOTAL</i>	-44.0	-46.9

VII.3.4. Sodium Void Reactivity – MOX Core –

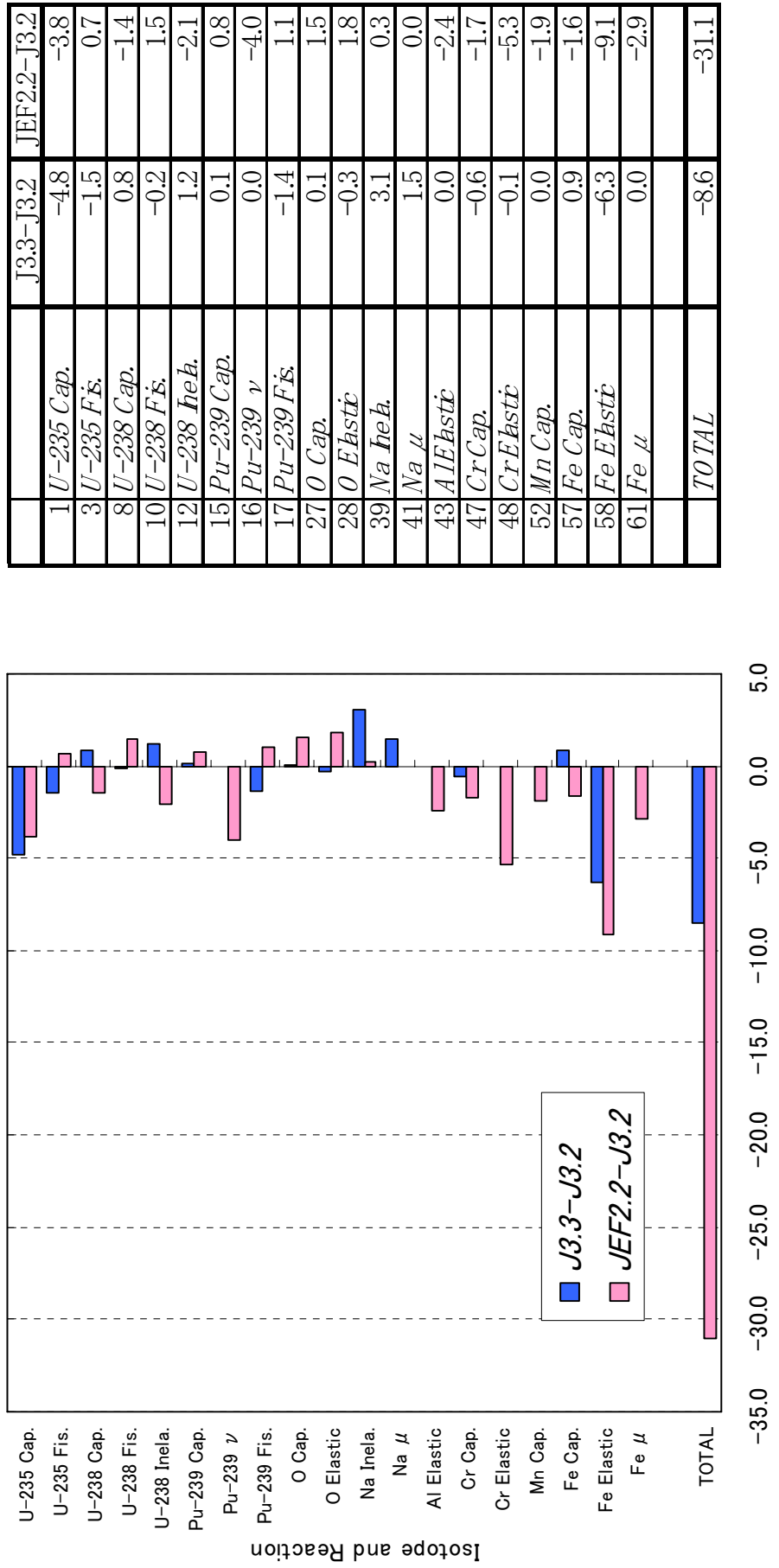


Fig. A.3.4 Sensitivity Analysis for BFS-62-3A Experiment
– Sodium Void Reactivity (MOX Core) –

VII.3.5. Sodium Void Reactivity – Outer Core –

	J3.3–J32	JEF2.2–J3.2
1 U-235 Cap.	3.1	0.9
2 U-235 ν	-0.4	-1.2
3 U-235 Fis.	-1.1	-1.6
8 U-238 Cap.	0.2	0.1
10 U-238 Fis.	0.0	0.4
11 U-238 Elastic	0.0	-0.4
12 U-238 Inela.	0.4	-0.5
16 Pu-239 ν	0.0	-0.4
27 O Cap.	0.0	0.3
38 Na Elastic	-0.1	-0.8
41 Na μ	0.7	0.0
43 Al Elastic	0.0	-0.8
52 Mn Cap.	0.0	-0.6
57 Fe Cap.	0.6	0.3
58 Fe Elastic	0.7	0.7
63 Ni Elastic	-0.6	-0.7
68 U-235 χ spectrum	-0.4	-0.4
<i>TOTAL</i>	3.0	-5.7

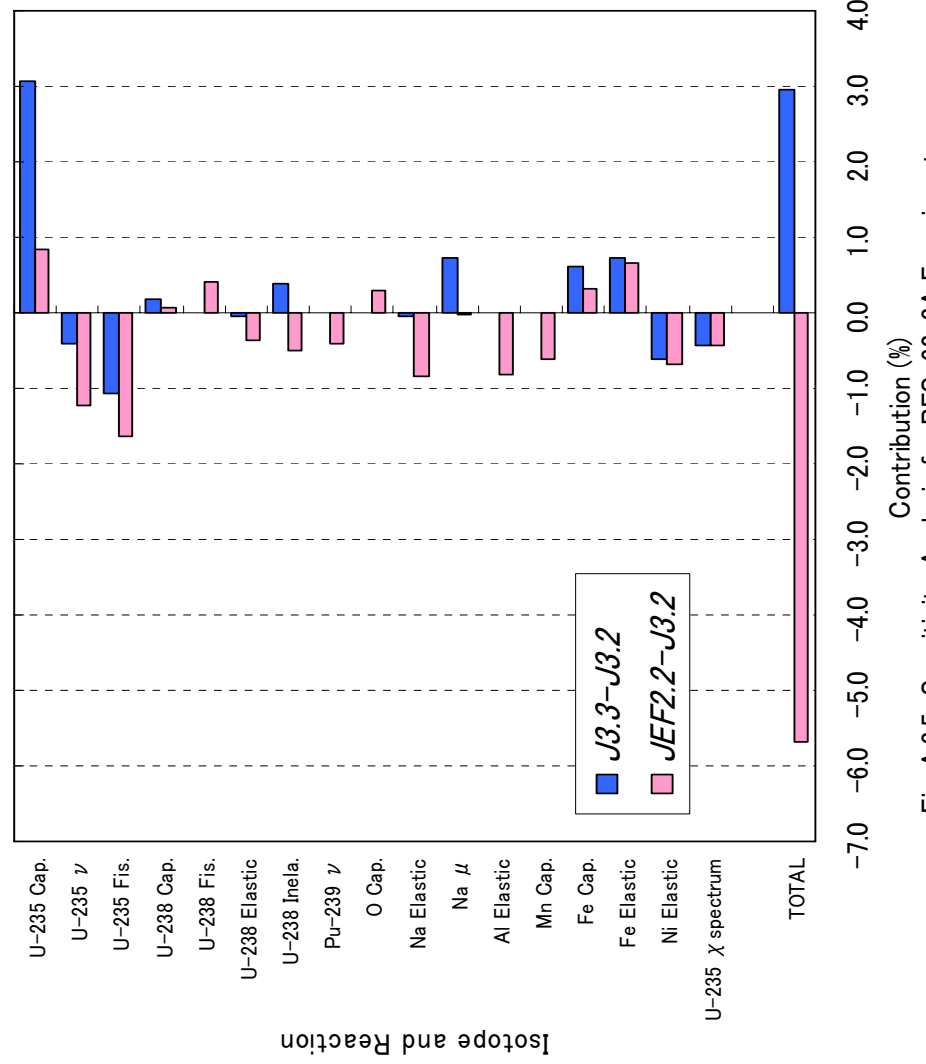


Fig. A.3.5 Sensitivity Analysis for BFS-62-3A Experiment
– Sodium Void Reactivity (Outer Core) –

VII.3.6. Sodium Void Reactivity – Total Effect –

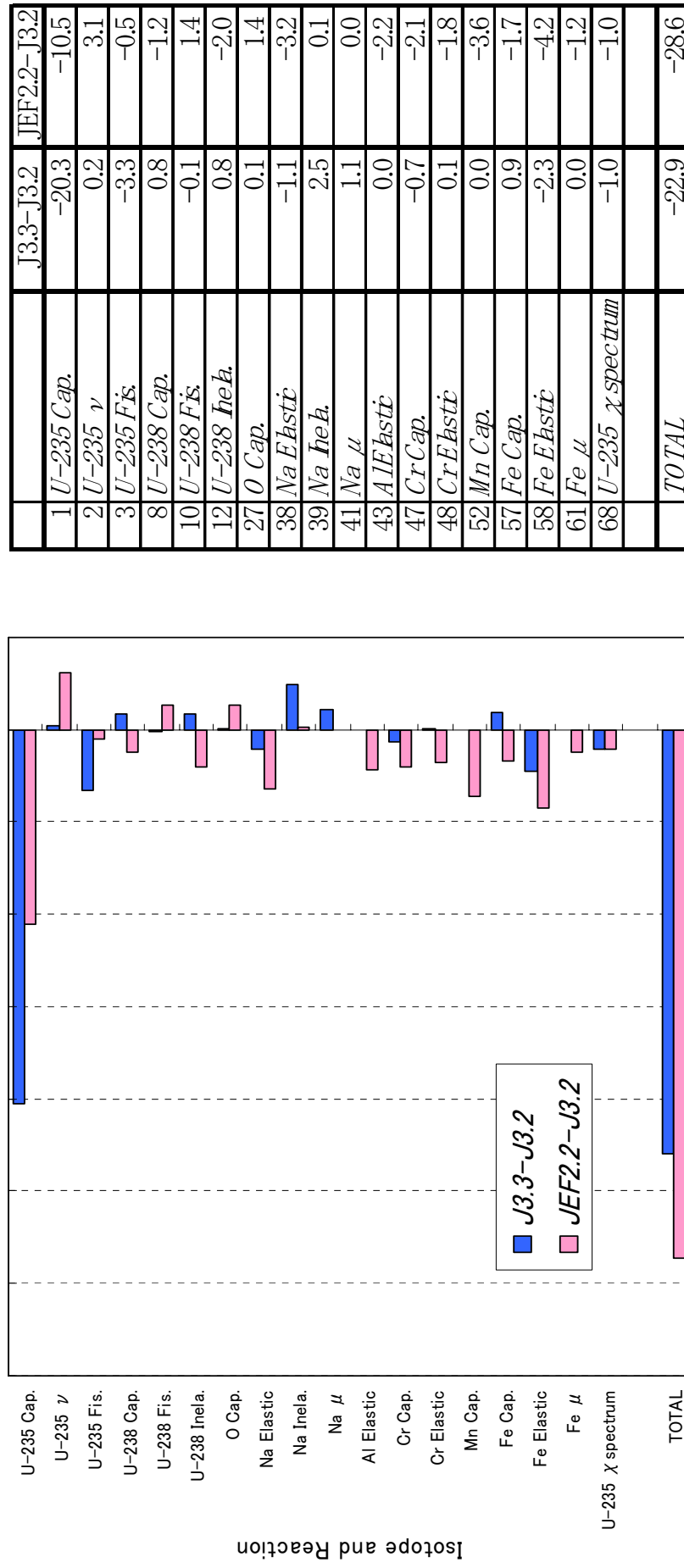


Fig. A.3.6 Sensitivity Analysis for BFS-62-3A Experiment
– Sodium Void Reactivity (Total Effect) –

Appendix VIII

POSSIBLE REMAINING REASONS OF THE DIFFERENCES ON SVRW BETWEEN BFS-62-3A AND BN-600 HYBRID CORE

T. Hazama

Japan Nuclear Cycle Development Institute, Japan

The document Action 5.12v1 prepared by Dr. G.Rimpault mentions that there are unknown reasons on the differences of SVRW between the BN-600 hybrid core and BFS-62-3A.

In this note possible reasons are investigated for LEZ and MOX region voiding.

Calculations were based on heterogeneous cell calculation in fuel zones, and SVRW in BN-600 hybrid core was calculated by voiding all fuel assemblies in each zone and subsequently divided by 6 to obtain equivalent values to those in BFS-62-3A.

Effects of the following parameters on SVRW were investigated.

1. Na density difference
2. Temperature difference
3. Pu presence in LEZ, MEZ, and HEZ (1.0~1.7wt% only in BN-600)
4. FP presence (only in BN-600)
5. Control rod partially inserted (only in BN-600)

The investigation was made in a step-by-step manner by removing the differences from BN-600 hybrid core model, except that the difference in Na density was removed by changing BFS-62-3A results. Since what is of interest in IAEA CRP Phase 3 (BN-600 hybrid core benchmark model analysis) is the sodium density coefficient, the difference was adjusted at first. The difference of the 3rd parameters was roughly removed by changing Pu in the UO₂ regions to U-235.

Obtained reactivity data are compared in Table 1 and Figure 1, in a form of upper, lower, and total energy integrated values with a energy boundary of 31.8 keV, since the most influential scattering (slowing down) components has change sign around 30-40 keV. The effect of the 5th parameter is found to be negligible and not shown.

In Figures 2 and 3, the scattering components are compared in the 70 energy group structure, for LEZ and MOX, respectively.

It is clearly found in LEZ region case that the differences are reduced as steps proceed. The 3rd parameter affects the higher energy region. In MOX region, temperature effect is found but the other 2 parameters are not clear. The other differences such as Pu concentration in the region may affect the remaining difference.

TABLE 1. EFFECT OF TEMPERATURE ON SVRW FOR EACH REGION

LEZ region void reactivity in pcm

Case	Production	Absorption	Scattering	Non-leakage	Leakage	Total
BFS-62-3A (Na density adjusted)	-23.8	16.4	85.7	78.4	-74.6	3.8
	13.9	31.2	-81.8	-36.7	-11.3	-48.0
	-9.9	47.6	3.9	41.7	-85.9	-44.2
BN-600 hybrid core	-5.2	10.1	148.9	153.8	-90.1	63.7
	-5.6	39.6	-46.5	-12.5	-9.8	-22.2
	-10.8	49.7	102.4	141.3	-99.8	41.5
BN-600 hybrid core (300K)	-5.2	11.0	128.1	133.9	-88.8	45.0
	-7.9	51.6	-73.0	-29.3	-10.6	-39.9
	-13.1	62.5	55.1	104.6	-99.4	5.1
BN-600 hybrid core (300K, Pu -> U235)	-4.9	10.7	110.1	115.9	-86.4	29.4
	-8.3	51.1	-72.1	-29.3	-10.4	-39.7
	-13.2	61.8	37.9	86.5	-96.8	-10.3
BN-600 hybrid core (300K, Pu -> U235, noFP)	-4.9	10.8	102.1	108.0	-87.6	20.4
	-8.7	53.8	-79.6	-34.5	-10.9	-45.4
	-13.6	64.6	22.5	73.5	-98.5	-25.0

Ratio BFS-62-3A/BN-600

BN-600 hybrid core	4.55	1.62	0.58	0.51	0.83	0.06
	-2.50	0.79	1.76	2.94	1.16	2.16
	0.92	0.96	0.04	0.29	0.86	-1.07
BN-600 hybrid core (300K)	4.59	1.50	0.67	0.59	0.84	0.08
	-1.76	0.60	1.12	1.25	1.07	1.20
	0.75	0.76	0.07	0.40	0.86	-8.65
BN-600 hybrid core (300K, Pu -> U235)	4.84	1.54	0.78	0.68	0.86	0.13
	-1.68	0.61	1.13	1.25	1.09	1.21
	0.75	0.77	0.10	0.48	0.89	4.30
BN-600 hybrid core (300K, Pu -> U235, noFP)	4.87	1.53	0.84	0.73	0.85	0.19
	-1.60	0.58	1.03	1.07	1.04	1.06
	0.73	0.74	0.18	0.57	0.87	1.77

MOX region void reactivity in pcm

Case	Production	Absorption	Scattering	Non-leakage	Leakage	Total
BFS-62-3A (Na density adjusted)	-19.0	9.1	50.6	40.6	-69.2	-28.6
	-2.6	13.3	-18.2	-7.5	-6.6	-14.1
	-21.6	22.4	32.4	33.1	-75.7	-42.6
BN-600 hybrid core	-2.9	4.0	52.6	53.7	-60.8	-7.1
	-2.8	11.1	-7.8	0.5	-4.5	-4.0
	-5.8	15.1	44.8	54.1	-65.2	-11.1
BN-600 hybrid core (300K)	-2.8	4.1	45.6	46.9	-58.8	-11.8
	-4.2	15.0	-15.9	-5.1	-4.7	-9.8
	-7.0	19.2	29.7	41.9	-63.5	-21.6
BN-600 hybrid core (300K, Pu -> U235)	-3.0	4.3	44.9	46.2	-60.8	-14.6
	-4.3	15.7	-16.6	-5.3	-4.8	-10.1
	-7.3	20.0	28.2	41.0	-65.6	-24.6
BN-600 hybrid core (300K, Pu -> U235, noFP)	-2.9	4.3	41.6	43.0	-60.6	-17.5
	-4.5	16.4	-18.6	-6.7	-5.0	-11.7
	-7.4	20.6	23.0	36.3	-65.5	-29.2

Ratio BFS-62-3A/BN-600

BN-600 hybrid core	6.52	2.28	0.96	0.76	1.14	4.00
	0.92	1.20	2.32	-15.65	1.48	3.54
	3.76	1.48	0.72	0.61	1.16	3.84
BN-600 hybrid core (300K)	6.79	2.19	1.11	0.86	1.18	2.41
	0.63	0.89	1.14	1.48	1.39	1.44
	3.11	1.17	1.09	0.79	1.19	1.97
BN-600 hybrid core (300K, Pu -> U235)	6.42	2.09	1.13	0.88	1.14	1.96
	0.60	0.85	1.09	1.42	1.37	1.39
	2.96	1.12	1.15	0.81	1.15	1.73
BN-600 hybrid core (300K, Pu -> U235, noFP)	6.59	2.12	1.21	0.94	1.14	1.63
	0.58	0.81	0.98	1.11	1.33	1.20
	2.93	1.08	1.41	0.91	1.16	1.46

Upper: above 31.8 keV, Middle: below 31.8 keV, Lower: Energy total.

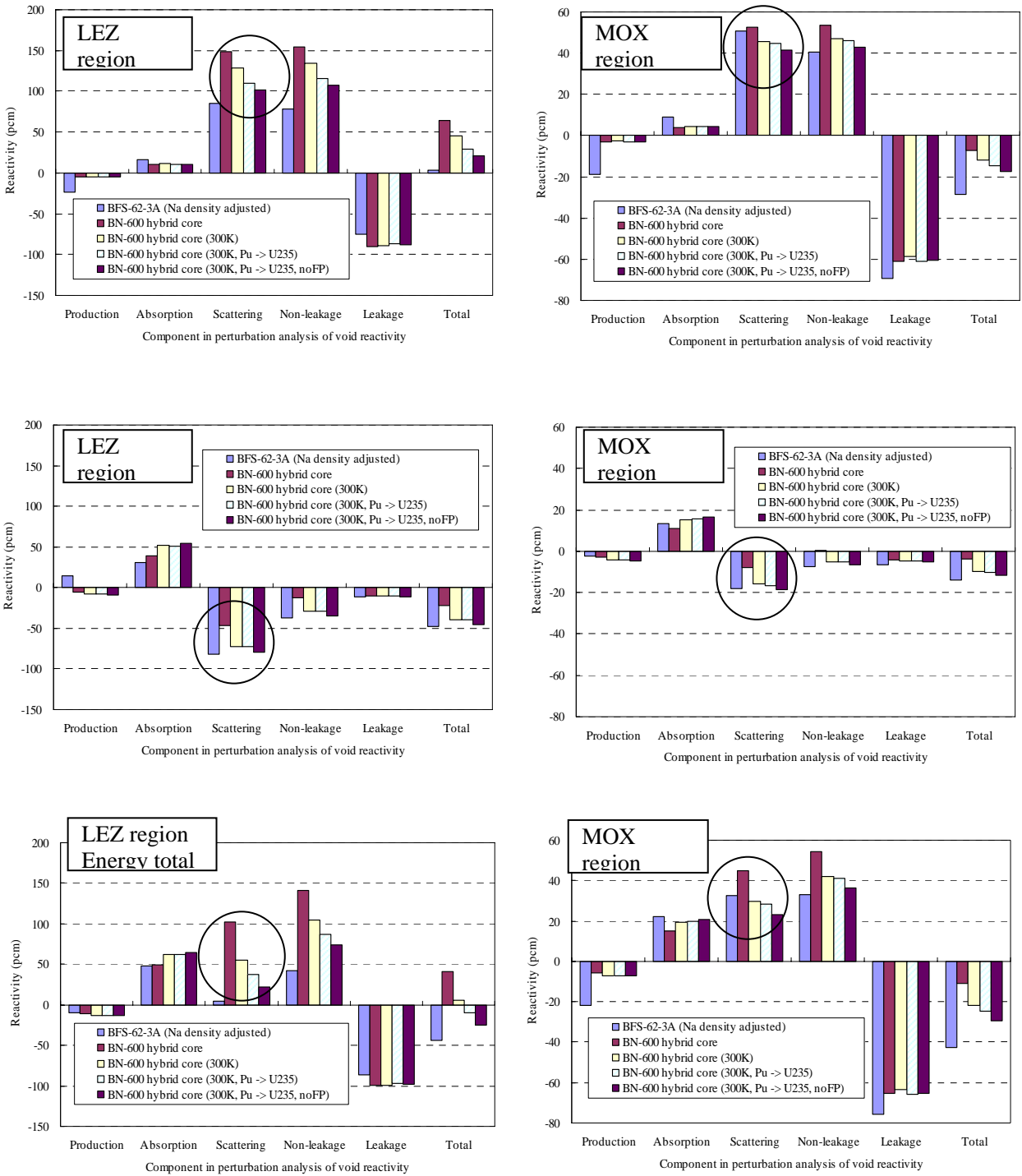


FIG. 1. Effect of removing the differences on SVRW analysis.

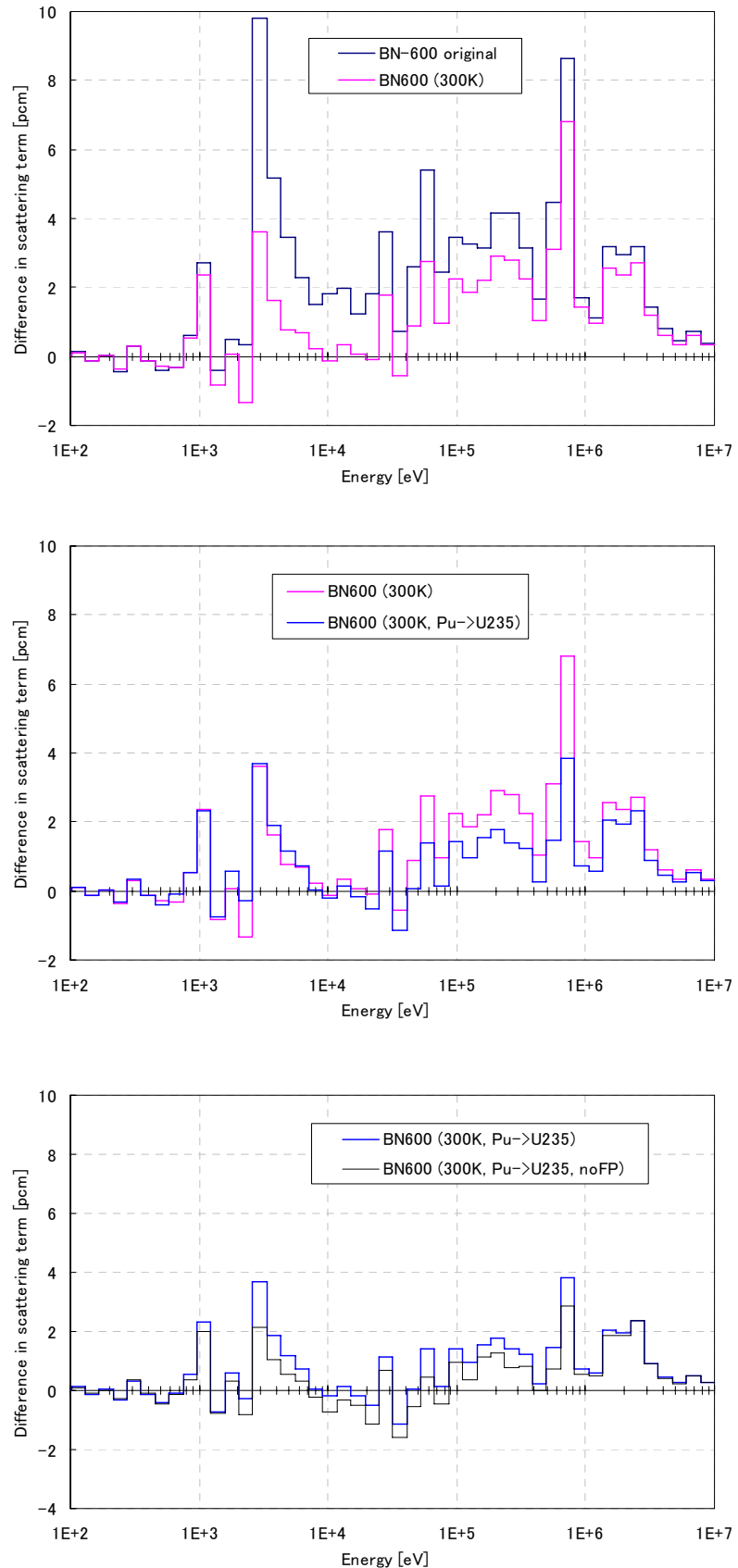


FIG. 2. Transition of the differences in the scattering component of SVRW for LEZ region (difference from BFS-62-3A data with Na density adjusted).

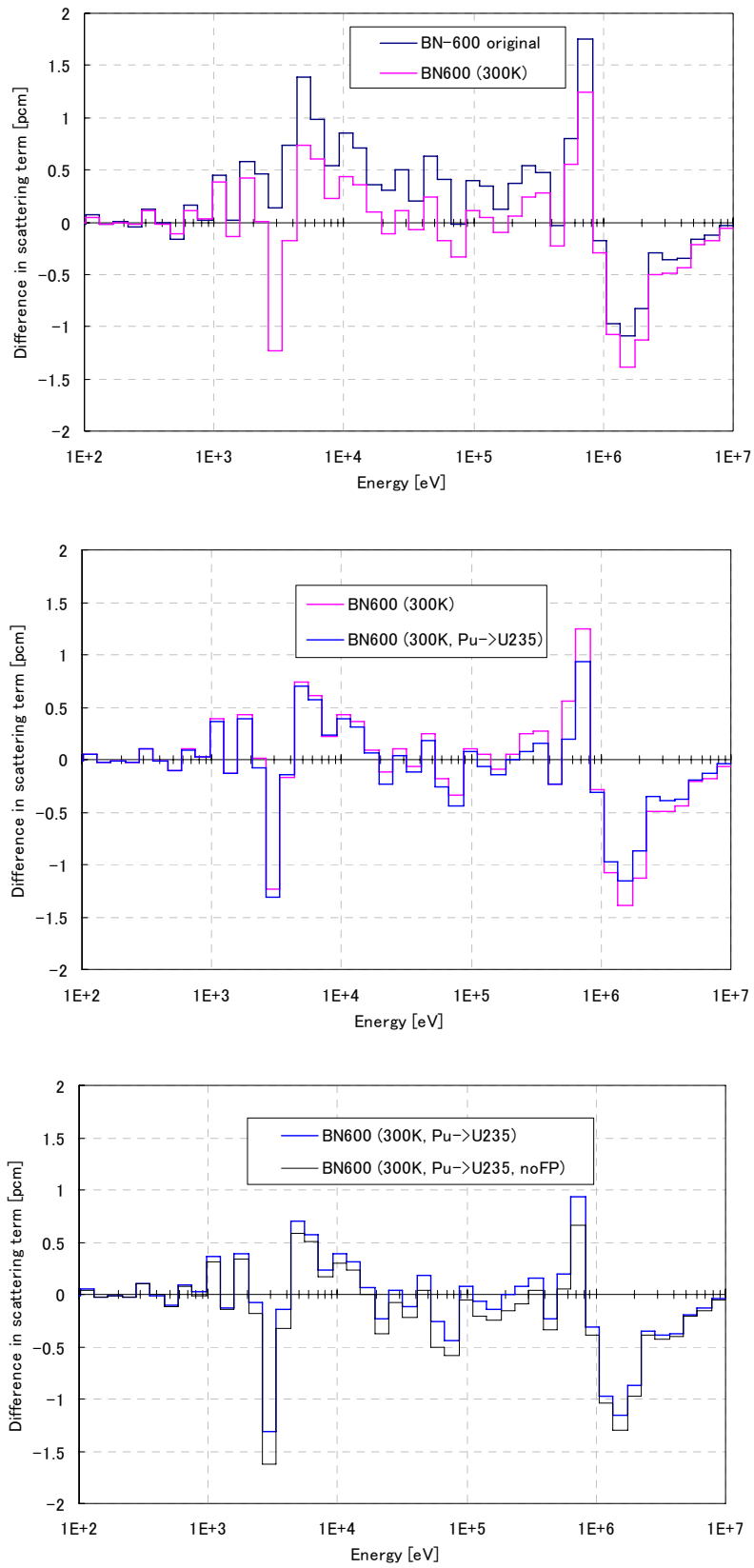


FIG. 3. Transition of the differences in the scattering component of SVRW for MOX region (difference from BFS-62-3A data with Na density adjusted).

Appendix IX

COMPARISON OF NON-LEAKAGE AND LEAKAGE TERMS OF SVRW IN BFS-62-3A AND BN-600 HYBRID CORE

A. Shono

Japan Nuclear Cycle Development Institute, Japan

As was presented in PHYSOR2004 (see Table 2 below), there exists a difference in region-wise SVRW values between BFS-62-3A and BN-600 hybrid core. Here shows the breakdown into non-leakage and leakage terms for both the cores. Please note that SVRW in BN-600 hybrid core was calculated by voiding all fuel assemblies in each zone and subsequently divided by 6 to obtain an equivalent value to those in BFS-62-3A. Another point to be noted is that all the results were based on heterogeneous cell calculation in fuel zones, which is different from the condition discussed in IAEA CRP.

Table 1.

**Comparison of SVRE components between BN-600 hybrid core and BFS-62-3A
(3-D Hex-Z model, Exact perturbation based on diffusion calculation results)
(60 degree sector is voided as the measurement in BFS-62-3A)**

BFS-62-3A core				BN600 hybrid core			
	Non-leakage	Leakage	Total		Non-leakage	Leakage	Total
LEZ+Ax. blanket	6.8	-14.1	-7.3	24.1	-17.0	7.1	
MEZ+Ax. Blanket	2.5	-4.6	-2.1	6.2	-5.5	0.7	
MOX+Ax. Blanket	4.1	-9.6	-5.4	9.2	-11.1	-1.9	
HEZ+Ax. Blanket	0.9	-11.2	-10.3	2.7	-12.3	-9.6	
All FUEL+Ax. blanket	13.9	-36.0	-22.1	42.3	-46.0	-3.7	
(Unit in cent)				(Unit in cent)			
β_{eff}				β_{eff}			
6.19E-03				5.87E-03			

BFS-62-3A core				BN600 hybrid core			
	Non-leakage	Leakage	Total		Non-leakage	Leakage	Total
LEZ+Ax. blanket	42.2	-87.2	-45.0	141.3	-99.8	41.4	
MEZ+Ax. Blanket	15.5	-28.8	-13.2	36.5	-32.2	4.2	
MOX+Ax. Blanket	25.6	-59.2	-33.7	54.1	-65.2	-11.1	
HEZ+Ax. Blanket	5.4	-69.3	-63.8	15.9	-72.3	-56.4	
All FUEL+Ax. blanket	85.9	-222.7	-136.9	248.4	-270.3	-21.8	
(Unit in pcm)				(Unit in pcm)			

One item to be noted is relatively negative SVRW measured in BFS-62-3A than that calculated in the BN-600 hybrid core, as shown in Table 2. The significant difference in SVRW is mainly due to temperature and CR axial position differences. It surely suggests both difficulty in applying the bias correction method and possible effectiveness of the nuclear constant adjustment method, in decreasing predicted uncertainty of SVRW of the BN-600 hybrid core by reflecting BFS-62-3A measurement data.

Table 2 Comparison of SVRW^{*1} between BFS-62-3A and BN-600 hybrid core
(Unit in cent)

Sodium-voided ^{*2} region	(a) BFS-62-3A	(b) BN-600 Hybrid core	Difference (a)-(b)
LEZ	-7.3	+7.1	-14.4
MEZ	-2.1	+0.7	-2.8
MOX	-5.4	-1.9	-3.5
HEZ	-10.3	-9.6	-0.7
All Fuel Regions	-22.1	-3.7	-18.4

^{*1} Exact perturbation theory based on diffusion calculation values using 3-D Hex model

^{*2} Sodium voided at 60-degree sector in all the fuel regions & those upper blanket regions

(Copied from “Reduction of Cross-Section-Induced Errors of the BN-600 Hybrid Core Nuclear Parameters by Using BFS-62 Critical Experiment Data” presented by A. SHONO at PHYSOR2004)

Appendix X

MORE INFORMATION ON THE DIFFERENCES OF SVRW BETWEEN BFS-62-3A AND BN-600 HYBRID CORE

T. Hazama

Japan Nuclear Cycle Development Institute, Japan

In the PHYSOR2004 paper by A.SHONO, it is described that temperature is a major reason of the differences in region-wise SVRW values between BFS-62-3A and BN-600 hybrid core.

The effect of temperature on the SVRW was evaluated by changing temperature in the BFS-62-3A benchmark model to those specified in the BN-600 hybrid core benchmark model.

Calculation were based on heterogeneous cell calculation in fuel zones, and SVRW in BN-600 hybrid core was calculated by voiding 60 degree sector as in BFS-62-3A.

There is a small difference in the way to calculate SVRW in the perturbation analysis. In BN-600 cases, regions located inside the voided region were not voided, and the core before perturbation was always before voiding. This causes little difference on the results as confirmed in the IAEA CRP 5th meeting. Results are summarized in Table 1, in a similar form presented in Action 5.12v1. Concerning the Na density correction, the ratios of the Na weights were used in the previous note. The true values shown in Table 2 is used in this note.

The non-leakage and scattering (or slowing down) components are compared in Figs 1-4 and Figs 5-8, for LEZ and MOX region, respectively. The Na density correction was applied to the BFS-62-3A results. Adjoint and forward neutron fluxes are compared in Figs 9-10 and Figs11-12, for the two regions.

TABLE 1. EFFECT OF TEMPERATURE AND NA DENSITY ON SVRW FOR EACH REGION

Void region	BFS-62-3A			BN-600 hybrid core			Ratio BFS-62-3A/BN-600		
	NL	L	Total	NL	L	Total	NL	L	Total
LEZ + Ax.B	41.7	-86.0	-44.3	141.3	-99.8	41.4	0.295	0.861	-1.069
MEZ + Ax.B	15.1	-28.0	-12.9	36.5	-32.2	4.2	0.413	0.867	-3.061
MOX + Ax.B	25.9	-59.2	-33.3	54.1	-65.2	-11.1	0.479	0.908	2.993
HEZ +Ax.B	5.7	-72.6	-66.9	15.9	-72.3	-56.4	0.358	1.004	1.186
All FUEL + Ax.B	85.8	-243.2	-157.4	248.4	-270.3	-21.8	0.345	0.900	7.215
Void region	BFS-62-3A(HT)			BN-600 hybrid core			Ratio BFS-62-3A/BN-600		
	NL	L	Total	NL	L	Total	NL	L	Total
LEZ + Ax.B	86.1	-91.0	-4.9	141.3	-99.8	41.4	0.610	0.911	-0.118
MEZ + Ax.B	27.6	-31.2	-3.6	36.5	-32.2	4.2	0.756	0.968	-0.863
MOX + Ax.B	42.6	-66.9	-24.3	54.1	-65.2	-11.1	0.787	1.025	2.178
HEZ +Ax.B	11.9	-84.5	-72.5	15.9	-72.3	-56.4	0.751	1.168	1.285
All FUEL + Ax.B	164.2	-269.5	-105.3	248.4	-270.3	-21.8	0.661	0.997	4.826
Void region	BFS-62-3A(HT+Density)			BN-600 hybrid core			Ratio BFS-62-3A/BN-600		
	NL	L	Total	NL	L	Total	NL	L	Total
LEZ + Ax.B	86.0	-90.9	-4.9	141.3	-99.8	41.4	0.609	0.911	-0.118
MEZ + Ax.B	31.4	-35.6	-4.1	36.5	-32.2	4.2	0.863	1.104	-0.984
MOX + Ax.B	54.5	-85.5	-31.0	54.1	-65.2	-11.1	1.007	1.310	2.785
HEZ +Ax.B	15.0	-106.3	-91.3	15.9	-72.3	-56.4	0.945	1.470	1.617
All FUEL + Ax.B	183.8	-301.6	-117.9	248.4	-270.3	-21.8	0.740	1.116	5.402

TABLE 2. EFFECT OF TEMPERATURE ON SVRW FOR EACH REGION

Void region	BFS-62-3A			BN-600			Ratio of Na density BFS-62-3A/BN-600
	Removed Na weight (g)	Region volume (cc)	Na density (g/cc)	Removed Na weight (g)	Region volume (cc)	Na density (g/cc)	
LEZ + Ax.B	85,758	354,310	0.242	95,540	395,034	0.242	1.001
MEZ + Ax.B	25,850	111,097	0.233	32,940	124,153	0.265	0.877
MOX + Ax.B	37,274	174,152	0.214	49,420	180,587	0.274	0.782
HEZ +Ax.B	29,568	138,121	0.214	39,530	146,727	0.269	0.795
All FUEL + Ax.B	178,450	777,680	0.229	217,430	846,500	0.257	0.893

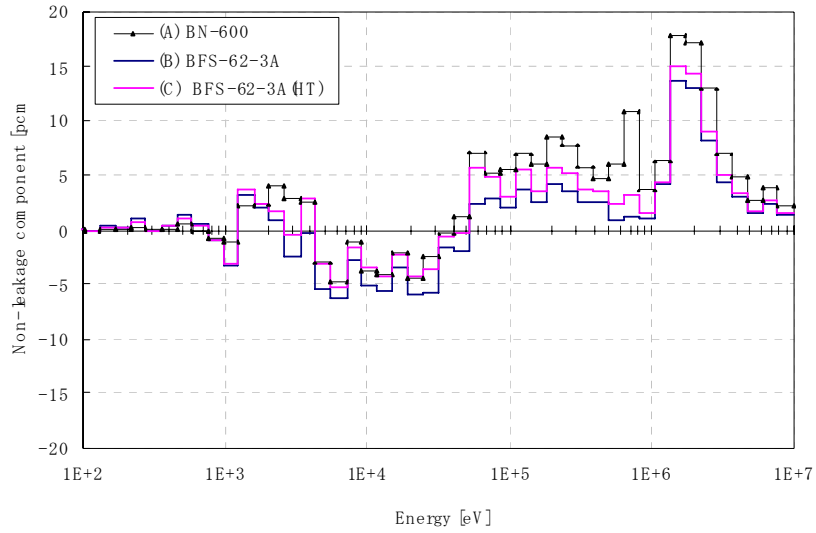


FIG. 1. Comparison of the non-leakage component (LEZ region void).

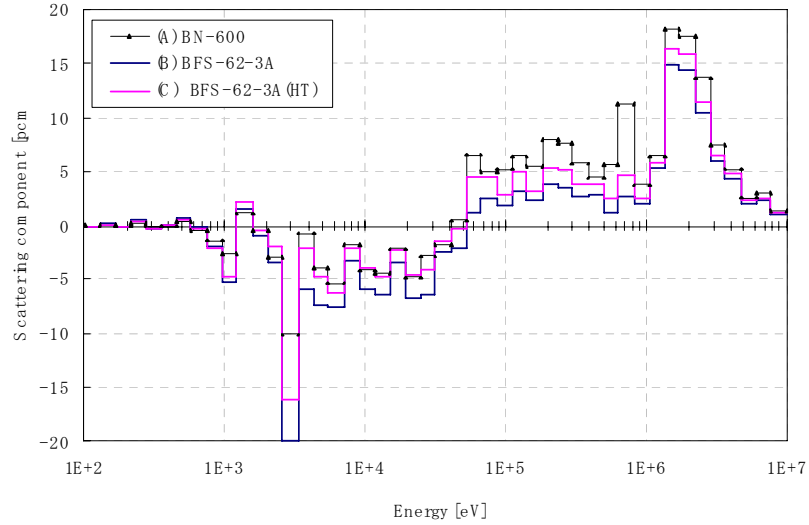


FIG. 2. Comparison of the scattering component (LEZ region void).

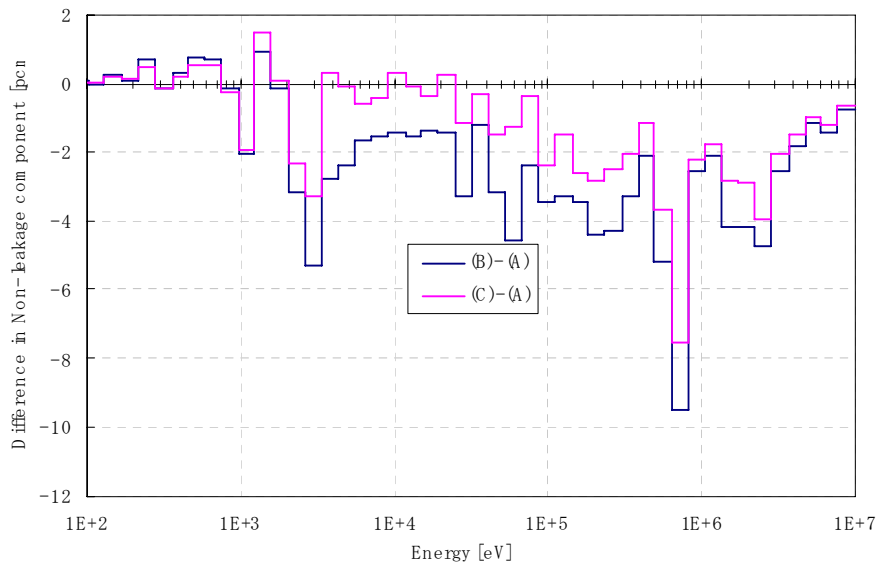


FIG. 3. Difference in the non-leakage component from BN-600's (LEZ region void).

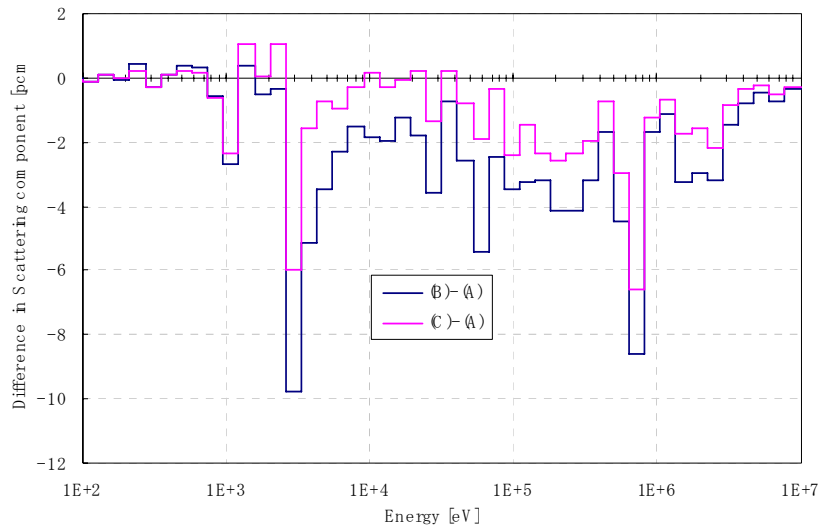


FIG. 4. Difference in the scattering component from BN-600's (LEZ region void).

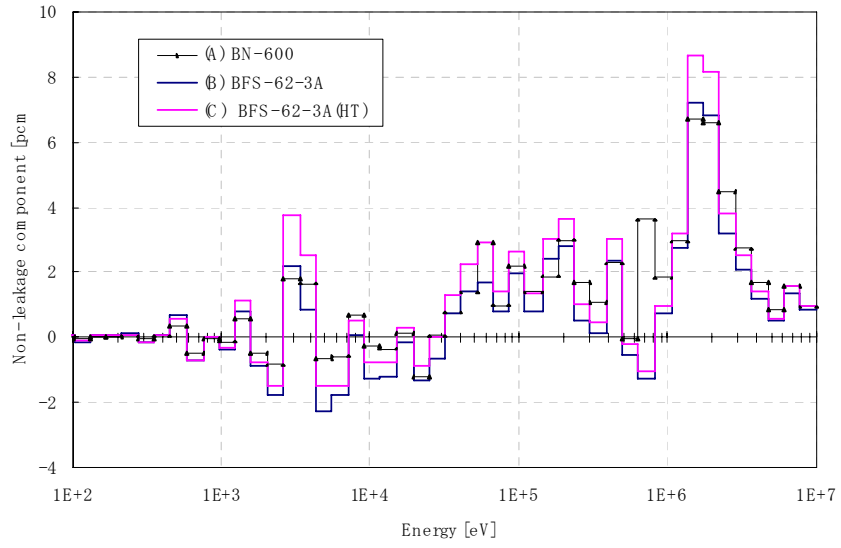


FIG. 5. Comparison of the non-leakage component (MOX region void).

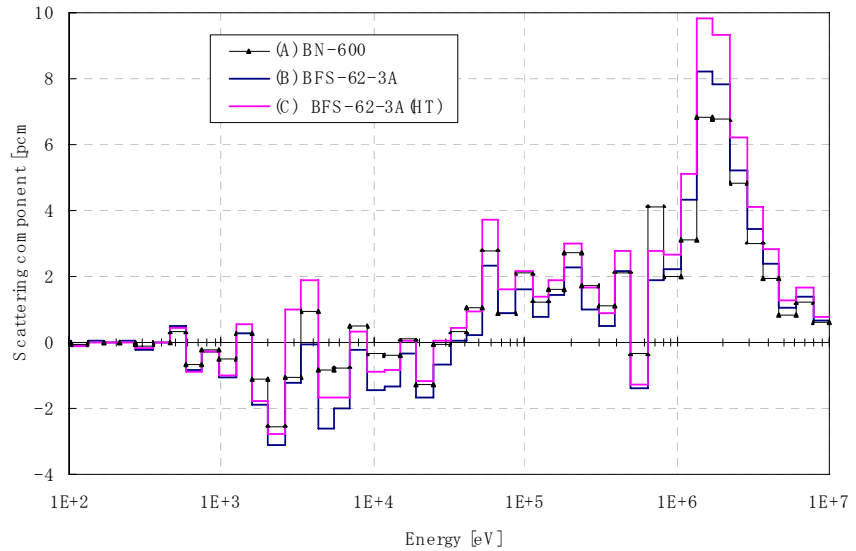


FIG. 6. Comparison of the scattering component (MOX region void).

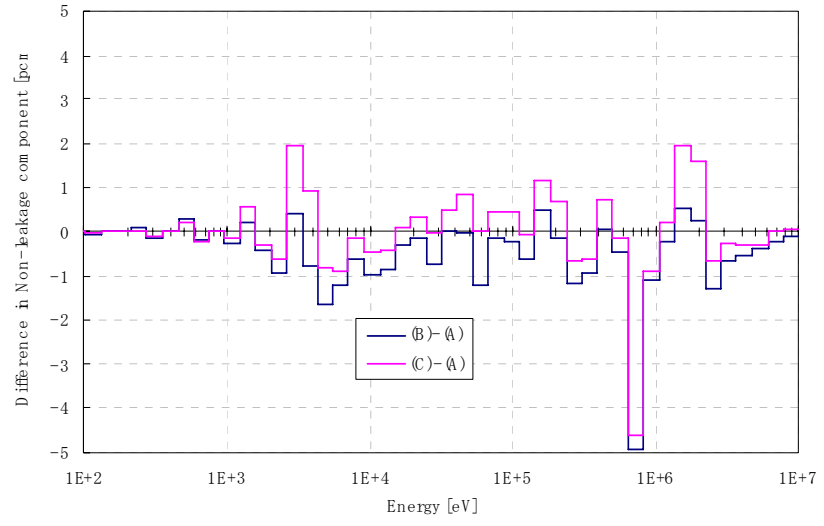


FIG. 7. Difference in the non-leakage component from BN-600's (MOX region void).

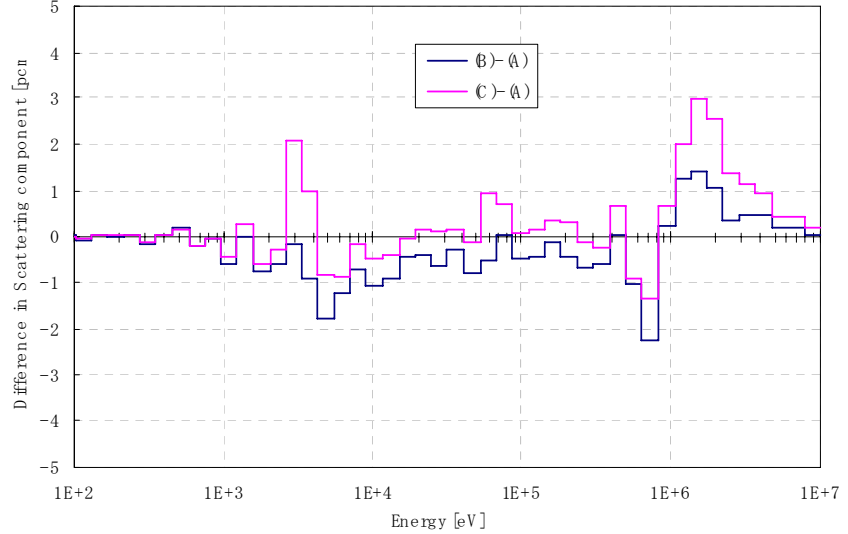


FIG. 8. Difference in the scattering component from BN-600's (MOX region void).

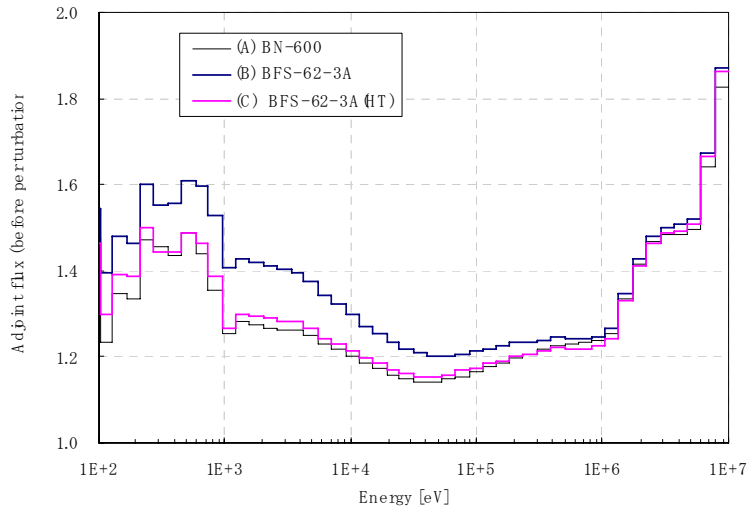


FIG. 9. Comparison of the adjoint flux near the core center (LEZ region)(normalized with core total importance of produced neutrons).

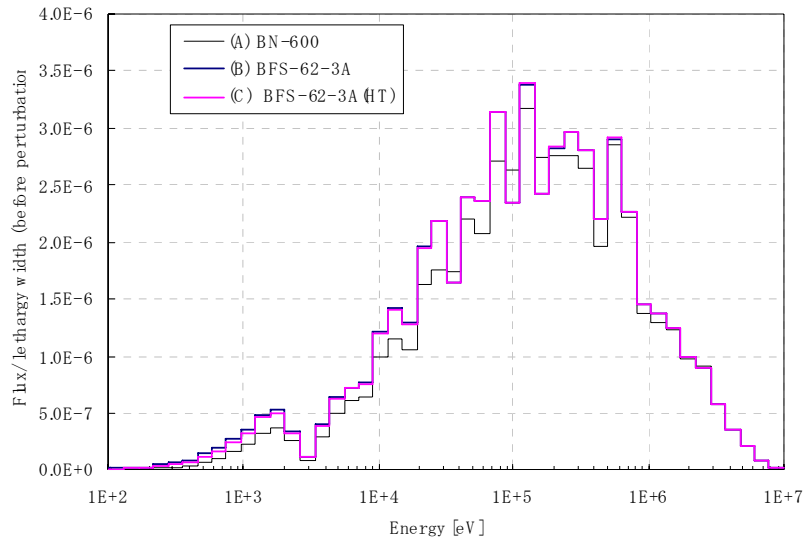


FIG. 10. Comparison of flux near the core center (LEZ region)(normalized with core total neutron production).

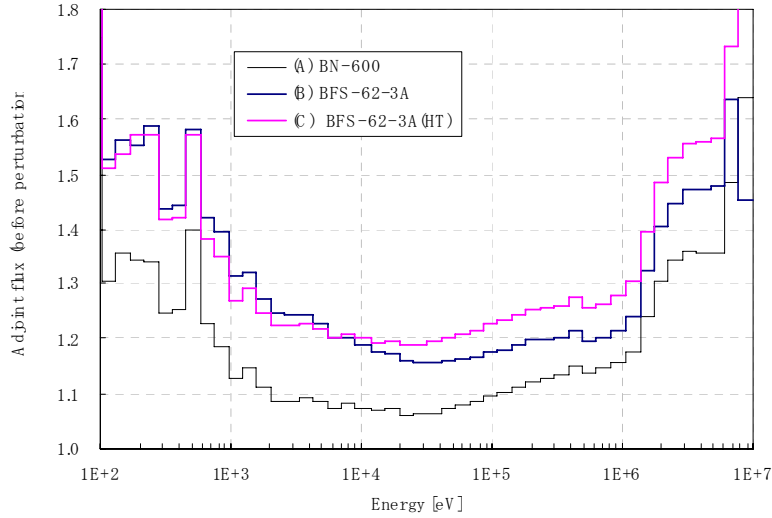


FIG. 11. Comparison of adjoint flux in MOX region (BN-600 at inner row, BFS-62-3A at middle row).

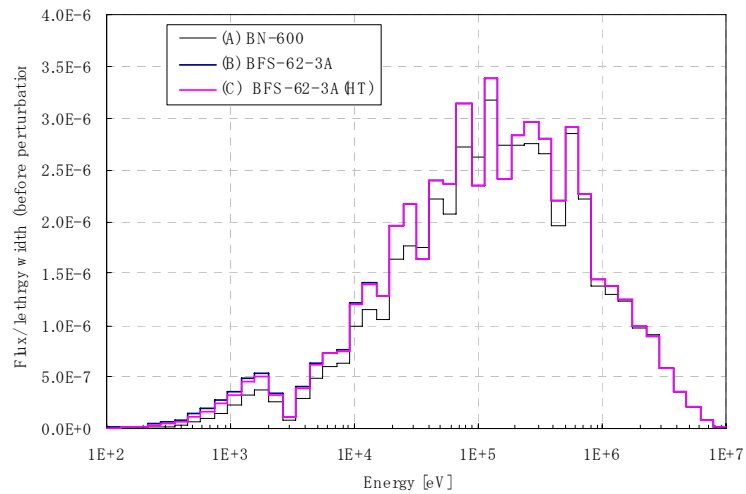


FIG. 12. Comparison of flux in MOX region.

Appendix XI

REPRESENTATIVITY FACTORS

G. Rimpault
Commissariat à l'énergie atomique, France

A standard methodology used in ERANOS enables the calculation of representativity factors r_{RE} (Aliberti, 2001), for integral parameters such as the multiplication factor k_{eff} and specific reaction rate ratios, on the basis of first-order perturbation theory. These factors quantifying the impact of nuclear data uncertainties on the prediction of I , the parameter of interest depending on cross sections P_1, \dots, P_N , are obtained as follows:

Sensitivity coefficients S_i for $I(P_1, \dots, P_N)$ are computed according to Equation (1):

$$S_i = \frac{\Delta I}{I} \left/ \frac{\Delta P_i}{P_i} \right. .(1)$$

The relative uncertainty σ of I (σ_I) is derived by using a covariance matrix D as shown in Equation (2):

$$\sigma_I^2 = S^T D S .(2)$$

It should be noticed that D is associated with a specific nuclear data library.

For the parameter I , the representativity factor r_{RE} between two systems, e.g. the specific BFS-62-3A experimental set-up and a given reactor BN-600, is determined from Equation (3), the covariance matrix being taken either from the adjusted data library ERALIB-1 or from any other data library:

$$r_{RE} = \frac{S_{BFS62}^T D S_{BN600}}{\sqrt{(S_{BFS62}^T D S_{BFS62})(S_{BN600}^T D S_{BN600})}} .(3)$$

The value of r_{RE} lies between 0.0 and 1.0. The closer r_{RE} is to 1.0, the more representative is BFS-62-3A of the BN-600.

Representativity factors can also be used to quantify the uncertainty reduction possible for the prediction of I on the basis of suitable integral measurements. This occurs via Equation (4):

$$\sigma_{I,BN600_reduced}^2 = \sigma_{I,BN600}^2 \left(1 - \frac{r_{RE}^2}{1 + \sigma_{I,exp}^2 / \sigma_{I,BFS62}^2} \right) , (4)$$

where $\sigma_{I,BN600}^2$ and $\sigma_{I,BFS62}^2$ are computed from Equation (2).

Thereby, the experimental uncertainty of the parameter I , i.e. as measured in BFS-62 ($\sigma_{I,exp}$), also plays a significant role. The smaller the experimental uncertainty, the stronger is the uncertainty reduction for the predicted value of I in the system of interest, the closeness of r_{RE} to 1.0 remaining an important aspect. In the most optimistic case (zero experimental uncertainty), Equation (4) becomes:

$$\sigma_{I,BFS62_reduced}^2 = \sigma_{I,BFS62}^2 (1 - r_{RE}^2) .(5)$$

The representativity strategy between BFS-62-3A SVRE experiments and the corresponding BN-600 SVRE should be evaluated component per component based on the following scheme:

1. Assessment of nuclide-specific 'integral sensitivities' on the basis of calculations of sensitivity coefficients S_i (see Equation (1)).
2. Determination of the uncertainty of I with the correct covariance matrix D from ERALIB-1 or from any other data library (see Equation (2)).

3. Calculation of the representativity factor rRE (see Equation (3)).
4. Determination of the reduced uncertainty (see Equations (4) and (5)).

An important additional reason for currently using the adjusted data library ERALIB-1 is to avoid the well known dominating effect of ^{239}Pu , which was observed in the analysis of MUSE3 in conjunction with the (unadjusted) JEF-2.2 library (Aliberti, 2001). The main goal here is thus to track the impact of larger remaining uncertainties, which may be more specific to the ADS situation.

BIBLIOGRAPHY TO APPENDIX XII

ALIBERTI, G., ‘Caractérisation neutronique des systèmes hybrides en régimes stationnaire et transitoire’, Thèse de l’Université Louis Pasteur de Strasbourg, 2001.

REFERENCES

- [1] DANILYTCHEV, A., et al., "Input data for BN-600 hybrid core benchmark calculations", paper presented in the First Research Co-ordination Meeting of the Research Co-ordination Project "Updated Codes and Methods to Reduce the Calculational Uncertainties of the LMFR Reactivity Effects", 24-26 November 1999, Vienna.
- [2] HENRYSON, H., TOPPEL, B.J., STENBERG, C.G., "MC2-2: A Code to Calculate Fast Neutron Spectra and Multigroup Cross Sections", ANL-8144, Argonne National Laboratory (1976).
- [3] ERSTINE, K.L., "DIF3D: A Code to Solve One-, Two-, and Three-Dimensional Finite Difference Diffusion Theory Problems", ANL-82-64, Argonne National Laboratory (April 1984).
- [4] ADAMS, C.H., "Specifications for VARI3D — A Multidimensional Reactor Design Sensitivity Code", FRA-TM-74, Argonne National Laboratory (April 1975).
- [5] ALCOUFFLE, R.E., BRINKLEY, F.W., MARR, D.R., O'DELL, R.D., "A User's Guide for TWODANT: A Code Package for Two-Dimensional, Diffusional, Diffusion-Accelerated, Neutral-Particle Transport", LA-10049-M (1990).
- [6] TOFFEL, B.J., "A User's Guide for the REBUS-3 Fuel Cycle Analysis Capability", Argonne National Laboratory Report ANL-83-2 (March 1983).
- [7] BRIEMEISTER, J. Editor, "MCNP—A General Monte Carlo Code N-Particle Transport Code Version 4A", LA-12625-M, Los Alamos National Laboratory Report (Nov 1993).
- [8] DORIATH, J.Y., MCCALLIEN, C.W., KIEFHABER, E., WEHMANN, U. and RIEUNIER, J.M., "ERANOS: The Advanced European System of Codes for Reactor Physics Calculations", paper presented in Intl Con on Mathematical Methods and Super Computing in Nuclear Computations, April 1993, Karlsruhe, Germany.
- [9] RIMPAULT, G., "Algorithmic Features of the ECCO Cell Code for Treating Heterogeneous Fast Reactor Sub-assemblies", paper presented in Intl Conf on Mathematics and Computations, Reactor Physics and Environmental Analysis, May 1995, Portland, Oregon.
- [10] HARDIE, W., LITTLE, Jr., W.W., "1DX, A One-Dimensional Diffusion Code for Generating Effective Nuclear Cross Section", BNWL-954 (1969).
- [11] KIDMAN, R.B., MacFARLANE, R.E., Lib-IV, A Library of Group Constants for Nuclear Reactor Calculations. LA-6260-MS, Los Alamos scientific laboratory (1976).
- [12] LITTLE, Jr., W.W., HARDIE, R.W., "2DB User's Manual," BNWL-831 (1968).
- [13] Hex-Nodal Diffusion Code (internal report) (1996).
- [14] HARDIE, R.W., LITTLE, Jr., W.W., "PERT-V, A Two-Dimensional Perturbation Code for Fast Reactor Analysis," BNWL-1162 (1969).
- [15] MCNP3B Monte Carlo Neutron and Photon Transport Code System, CCC-200 (May 1989).
- [16] O'DELL, R.D., "Standard Interface Files and Procedures for Reactor Physics Codes, Version IV" LA-6941-MS (1977).
- [17] KIEFHABER, E., "Updating of an 11-groups nuclear cross section set for transmutation applications", FZKA-6480 (August 2000).
- [18] KONDO, S., MORITA, K., TOBITA, Y., SHIRAKAWA, N., "SIMMER-III: An Advanced Computer Program for LMFBR Severe Accident Analysis", Proc. Int. Conference on Design and Safety of Advanced Nuclear Power Plants (ANP'92), Tokyo, Japan, Oct. 25-29, No. 40-5 (1992).
- [19] RINEISKI, A., SINITA, V., MASCHECK, W., " C^4P , a Multigroup Nuclear CCCC Data Processing System for Reactor Safety and Scenario Studies", Int: Proc. Jahrestagung Kerntechnik 2005, Nürnberg, Germany, May 10-12, 2005.
- [20] RINEISKI, A. et al., "Kinetics and cross-section developments for analyses of reactor transmutation concepts with SIMMER", paper presented in M&C 2005, Avignon, France.
- [21] ALCOUFFLE, R.E., BAKER, R.S., MARR, D.R., O'DELL, R.D., WALTERS, W.F., "DANTSYS: A Diffusion Accelerated Neutral Particle Transport Code System," LA-12969-M (June 1995).
- [22] LEWIS, E.E., CARRICO, C.B., PALMIOTTI, G., "Variational Nodal Formulation for the Spherical Harmonics Equations", Nucl. Sci. Eng. 122, p. 194 (1996).

- [23] REICHE, Chr., et al., "Reactor-Code-System RHEIN für ESER Computer", ZfK-668, Rossendorf (1989).
- [24] MOHANAKRISHNAN, P., "Guide to Input Preparation of Computer code TREDFR", RG/RPD/CPS/48 (1992).
- [25] RSICC COMPUTER CODE COLLECTION, "TWODANT-SYS. One- and Two-Dimensional, Multigroup, Discrete-Ordinates Transport Code System," ORNL.CCC-547 (1992).
- [26] MANTUROV, G.N., NIKOLAEV, M.N., TSIBOULIA, A.M., "ABBN-93 group constants system. Part 1: Nuclear Constants for Calculation of Neutron and Photon Radiation Fields", Issues of Nuclear Science and Technology, Series: Nuclear Constants, Vol. 1, p.59 (1996), (in Russian). Also: "BNAB-93 Group Data Library. Part 1: Nuclear Data for Calculation of Neutron and Photon Radiation Fields", INDC(CCP)-409/L, IAEA, p.65-110 (1997).
- [27] MANTUROV, G.N., NIKOLAEV, M.N., TSIBOULIA, A.M., "Code for Constants Preparation CONSYST", Preprint IPPE, 2828 (2000) (in Russian).
- [28] SERYOGIN, A.S., KISLITSYNA, T.S., "Abstract of TRIGEX-CONSYST-ABBN-90", Preprint IPPE, 2655 (1997) (in Russian).
- [29] BLYSKAYA, A.A., MANTUROV, G.N., NIKOLAEV, M.N., TSIBOULIA, A.M., "Complex code CONSYST/MMKKENO to calculate nuclear reactors by the Monte-Carlo method in multigroup approximation with scattering indicatrix in Pn – approximation", Preprint IPPE, 2887 (2001) (in Russian).
- [30] NAKAGAWA, T., et al., "Japanese Evaluated Nuclear Data Library Version 3 Revision-2: JENDL-3.2", Journal of Nuclear Science and Technology 32, p.1259 (Dec. 1995).
- [31] ISHIKAWA, M., "JNC's Response to Action 4.3 in the 4th CRP Meeting" (Oct. 2003).
- [32] KIM, J.D. and GIL, C.S., "KAFAK-F22: Development and Benchmark of Multi-group Library for Fast Reactor Using JEF-2.2", KAERI/TR-842/97, KAERI (1997).
- [33] MACFARLANE, R.E., "TRANSX 2: A Code for Interfacing MATXS Cross-Section Libraries to Nuclear Transport Codes", LA-12312-MS, LANL (Dec. 1993).
- [34] KIM, T.K., et al., "Development of A Multi-Group, Multi-Dimensional Simplified P2 Transport Code, SOLTRAN, in Hexagonal Geometry", KAERI/TR-1449/1999, KAERI (Jan. 2000).
- [35] KIM, T.K., et al., "Development of A Perturbation Code for Hexagonal Core", Proceedings of '98 KNS Autumn Conference, KNS (1998).
- [36] KIM, T.K., et al., "Development of An Effective Delayed Neutron Fraction Calculation Code for Hexagonal Core, BETA-K", Proceedings of '98 KNS '98 Autumn Conference, KNS (1998).
- [37] FARAKSHIN, M., VASILYEV, B., "The influence of an energy groups number and mesh size on results of reactivity coefficients calculations for BN-600 benchmark core", paper presented in the Third Research Co-ordination Meeting of the Research Coordination Project "Updated Codes and Methods to Reduce the Calculational Uncertainties of the LMFR Reactivity Effects", CE/Cadarache, France, 12-16 November 2001.
- [38] "Summary Report" prepared in the Second Research Co-ordination Meeting of the Research Coordination Project "Updated Codes and Methods to Reduce the Calculational Uncertainties of the LMFR Reactivity Effects", Vienna, 20-24 November 2000.
- [39] GRIMM, K.N., HILL, R.N., "BN-600 Phase III Benchmark Calculation," paper presented in the Third Research Co-ordination Meeting of the Research Coordination Project "Updated Codes and Methods to Reduce the Calculational Uncertainties of the LMFR Reactivity Effects", CE/Cadarache, France, 12-16 Nov. 2001.
- [40] MOHANAKRISHNAN, P., NARAYANAN, R., "BN-600 hybrid core benchmark Phase III results," ibid.
- [41] RIMPAULT, G., NEWTON, T.D., SMITH, P.J., "European contribution to Phase 3 of the benchmark analysis for the BN-600 hybrid core," ibid.
- [42] ISHIKAWA, M., "JNC results of BN-600 benchmark calculation (Phase 3)," ibid.
- [43] LI, Z.H., "Heterogeneous Calculation of BN-600 Benchmark Core," ibid.
- [44] SHONO, A., et al., "BFS-2 Critical Experiment and Analysis on MOX-Fuelled BN-600 Core", Proc. 2001 Annual Meeting of AESJ, March 27-29, 2001, Tokyo, Japan, Session 5: Weapon Plutonium Disposition, Atomic Energy Society of Japan (2001).

- [45] KOCHETKOV, A., MATVEENKO, I., MATVEEV, V., TSHBOULIA, A., SHONO, A., HAZAMA, T., ISHIKAWA, M., "BN-600 Hybrid Core Mock-Up at BFS-2 Critical Facility", paper presented in PHYSOR 2002, 7-10 October 2002, Seoul, Korea.
- [46] MANTUROV, G., et al., "Development of a Three Dimensional Homogeneous Calculation Model for the BFS-62 Critical Experiment. Preparation of Adjusted Equivalent Measure Values for Sodium Void Reactivity Values," paper presented in the Fifth Research Coordination Meeting of the Research Co-ordination Project "Updated Codes and Methods to Reduce the Calculational Uncertainties of the LMFR Reactivity Effects", 1-5 November 2004, Vienna, Austria,
- [47] ISHIKAWA, M., "JNC Results of BFS-62-3A Benchmark Calculation (CRP: Phase 5)," ibid.
- [48] HAZAMA, T., "Effect of void conditions before perturbation in BFS-62-3A SVR calculation", ibid.
- [49] ISHIKAWA, M., "Sensitivity analysis of the difference between JENDL and JEF libraries," paper presented in the Third Research Coordination Meeting of the Research Coordination Project "Updated Codes and Methods to Reduce the Calculational Uncertainties of the LMFR Reactivity Effects", 12-16 November 2001, CEA Cadarache, France.
- [50] ISHIKAWA, M., "Sensitivity Analysis of JEF and JENDL (Action 3.6)" (May 2002).
- [51] BELOV, S., FARAKSHIN, M., VORONOV, S., "Results of comparative dynamics calculations of BN-600 hybrid core benchmark on the basis of different input data on reactivity coefficients", paper presented in the Third Research Coordination Meeting of the Research Coordination Project "Updated Codes and Methods to Reduce the Calculational Uncertainties of the LMFR Reactivity Effects", 12-16 November 2001 CEA Cadarache, France.
- [52] DANILYTCHEV, A., ELISTRATOV, D., STOGOV, V., "Simplified approach to dynamic process modeling," ibid.
- [53] SHONO, A., et al., "Reduction of Cross Section Induced Errors of the BN600 Hybrid Core Nuclear Parameters by Using BFS62 Critical Experiment Data", paper presented in PHYSOR 2004, Chicago, USA.
- [54] HAZAMA, T., et al., "Verification of a Nuclear Analysis System for Fast Reactors Using BFS--62 Critical Experiment", NST journal.

ABBREVIATIONS

AR	Axial Reflector
HEZ	High Enrichment Zone
LB	Lower axial Blanket
LEZ	Low Enrichment Zone
MEZ	Medium Enrichment Zone
MOX	Mixed OXide (U, Pu)O ₂ fueled zone
RR	Radial Reflector
SHR	SHim Rod absorber
SCR	SCram Rod absorber
SSA	Steel shielding SubAssembly
SA	SubAssembly
UB	Upper axial Blanket

LIST OF PARTICIPANTS

Belov, S.	OKBM Mechanical Engineering Department of Thermohydraulics and Structural Mechanics Analisis 603074 Nizhny Novgorod Russian Federation
Cherny, V.	Institute of Physics and Power Engineering (IPPE) 1 Bondarenko square 249 020 Obninsk, Kaluga Region Russian Federation
Danyltchev*, A.	Institute of Physics and Power Engineering (IPPE) 1 Bondarenko square 249 020 Obninsk, Kaluga Region Russian Federation
Elistratov	Institute of Physics and Power Engineering (IPPE) 1 Bondarenko square 249 020 Obninsk, Kaluga Region Russian Federation
Farakshin*, M.	OKBM Mechanical Engineering Department of Thermohydraulics and Structural Mechanics Analisis 603074 Nizhny Nov gorod Russian Federation
Finck , P.	Argonne National Laboratory (ANL) Reactor Analysis and Engineering Divison 9700 South case Avenue Argonne, IL 60439-4814, USA
Gang, Z.	China Institute of Atomic Energy (CIAE) P.O. Box 275 95 102413 Beijing, China
Grimm*, K. N.	Argonne National Laboratory (ANL) Reactor Analysis and Engineering Divison 9700 South case Avenue Argonne, IL 60439-4814, USA
Hill, R. N.	Argonne National Laboratory (ANL) Reactir Analysis and Engineering Divison 9700 South case Avenue Argonne, IL 60439-4814, USA
Hazama, T.	Japan Nuclear Cycle Development Institute (JNC) Reactor Physics Analysis and Evaluation Group 4002 Narita-cho, Oarai-machi Ibaraki, Higashi-Ibaraki-gun 311-1393, Japan
Hosking, J. G.	SERCO Assurance (SA) Building A32, Room 303 Winfrith Technology Centre, Dorchester Dorset DT2 8 DH A32 Winfrith, Dorchester, United Kingdom
Ishikawa*, M.	Japan Nuclear Cycle Development Institute (JNC) Reactor Physics Analysis and Evaluation Group 4002 Narita-cho, Oarai-machi Ibaraki, Higashi-Ibaraki-gun 311-1393, Japan

John, T. M.	Indira Gandhi Centre for Atomic Research (IGCAR) Reactor Physics Division CDO Building Kalpakkam, Tamil Nadu 603 102, India
Kim*, Y. I ¹⁾	International Atomic Energy Agency Divison of Nuclear Power Wagramer Strasse 5 P.O. Box 100 A-1400 V Vienna, Austria
Korobeinikova,V.	Institute of Physics and Power Engineering (IPPE) 1 Bondarenko square 249 020 Obninsk, Kaluga Region Russian Federation
Lee*. K. B.	Korea Atomic Energy Research Institute (KAERI) P.O. Box 105, Yusong Daejon, 305-600, Republic of Korea
Li*, Z. H.	China Institute of Atomic Energy (CIAE) P.O. Box 275 95 102413 Beijing, P. R. China
Lykova, L.	Institute of Physics and Power Engineering (IPPE) 1 Bondarenko square 249 020 Obninsk, Kaluga Region Russian Federation
Manturov*, G.	Institute of Physics and Power Engineering (IPPE) 1 Bondarenko square 249 020 Obninsk, Kaluga Region Russian Federation
Mohanakrishnan*, P.	Indira Gandhi Centre for Atomic Research (IGCAR) Reactor Physics Division CDO Building Kalpakkam, Tamil Nadu 603 102, India
Narayanan, R.	Indira Gandhi Centre for Atomic Research (IGCAR) Reactor Physics Division CDO Building Kalpakkam, Tamil Nadu 603 102, India
Newton*, T. D.	SERCO Assurance (SA) Building A32, Room 303 Winfrith Technology Centre, Dorchester Dorset DT2 8 DH A32 Winfrith, Dorchester, United Kingdom
Rimpault*, G	DER/SPRC/LEDC Bat 230 (DER/SES Bat 212) F-13108 CE/Cadarache, St Paul Lez Durance, Cedex, France
Rineiski*, A.	Institut fuer Kern- und Energietechnik (IKET) Institute for Nuclear and Energy Technologies Forschungszentrum Karlsruhe Hermann-von-Helmholtz-Platz 1 D-76344 Eggenstein-Leopoldshaf, Germany

Semenov, M.	Institute of Physics and Power Engineering (IPPE) 1 Bondarenko square 249 020 Obninsk, Kaluga Region Russian Federation
Seregin, A.	Institute of Physics and Power Engineering (IPPE) 1 Bondarenko square 249 020 Obninsk, Kaluga Region Russian Federation
Shono, A.	Japan Nuclear Cycle Development Institute (JNC) Reactor Physics Analysis and Evaluation Group, 4002 Narita-cho, Oarai-machi Ibaraki, Higashi-Ibaraki-gun 311-1393, Japan
Song*, H.	Korea Atomic Energy Research Institute (KAERI) P.O. Box 105, Yusong Daejon, 305-600, Republic of Korea
Stanculescu, A. ²⁾	International Atomic Energy Agency Divison of Nuclear Power Wagramer Strasse 5 P.O. Box 100 A-1400 V Vienna, Austria
Stogov*, V.	Institute of Physics and Power Engineering (IPPE) 1 Bondarenko square 249 020 Obninsk, Kaluga Region Russian Federation
Tang, Z. L.	China Institute of Atomic Energy (CIAE) P.O. Box 275 95 102413 Beijing, China
Vasilyev, B.	OKBM Mechanical Engineering Department of Thermohydraulics and Structural Mechanics Analisis 603074 Nizhny Novgorod Russian Federation
Voronov, P. J. S.	OKBM Mechanical Engineering Department of Thermohydraulics and Structural Mechanics Analisis 603074 Nizhny Novgorod Russian Federation
Yu, H.	China Institute of Atomic Energy (CIAE) P.O. Box 275 95 102413 Beijing, China
Zhao, S. Z.	China Institute of Atomic Energy (CIAE) P.O. Box 275 95 102413 Beijing, China
Zhou, P. D.	China Institute of Atomic Energy (CIAE) P.O. Box 275 95 102413 Beijing, P.R. China

* participated in the drafting and review of the IAEA-TECDOC.

*1) participated in Phase 1 and 2 as a KAERI participant.

*2) participated in Phase 1 and 2.

CONTRIBUTORS TO DRAFTING AND REVIEW

Yuri KHOMYAKOV
Mi XU

IPPE, Russia
CIAE, China

Consultants Meeting
Vienna, Austria: 21-23 September 2005

Research Coordination Meetings (RCMs)

First RCM Vienna, Austria: 24-26 November 1999
Second RCMVienna, Austria: 20-24 November 2000
Third RCMCadarache, France, 12-16 November 2001
Fourth RCMObninsk, Russia, 19-23 May 2003
Fifth RCMVienna, Austria: 1-5 November 2004



IAEA

International Atomic Energy Agency

No. 21, July 2006

Where to order IAEA publications

In the following countries IAEA publications may be purchased from the sources listed below, or from major local booksellers. Payment may be made in local currency or with UNESCO coupons.

Australia

DA Information Services, 648 Whitehorse Road, Mitcham Victoria 3132
Telephone: +61 3 9210 7777 • Fax: +61 3 9210 7788
Email: service@dadirect.com.au • Web site: <http://www.dadirect.com.au>

Belgium

Jean de Lannoy, avenue du Roi 202, B-1190 Brussels
Telephone: +32 2 538 43 08 • Fax: +32 2 538 08 41
Email: jean.de.lannoy@infoboard.be • Web site: <http://www.jean-de-lannoy.be>

Canada

Bernan Associates, 4611-F Assembly Drive, Lanham, MD 20706-4391, USA
Telephone: 1-800-865-3457 • Fax: 1-800-865-3450
Email: order@bernan.com • Web site: <http://www.bernan.com>

Renouf Publishing Company Ltd., 1-5369 Canotek Rd., Ottawa, Ontario, K1J 9J3
Telephone: +613 745 2665 • Fax: +613 745 7660
Email: order.dept@renoufbooks.com • Web site: <http://www.renoufbooks.com>

China

IAEA Publications in Chinese: China Nuclear Energy Industry Corporation, Translation Section, P.O. Box 2103, Beijing

Czech Republic

Suweco CZ, S.R.O. Klecakova 347, 180 21 Praha 9
Telephone: +420 26603 5364 • Fax: +420 28482 1646
Email: nakup@suweco.cz • Web site: <http://www.suweco.cz>

Finland

Akateeminen Kirjakauppa, PL 128 (Keskuskatu 1), FIN-00101 Helsinki
Telephone: +358 9 121 41 • Fax: +358 9 121 4450
Email: akatilaus@akateeminen.com • Web site: <http://www.akateeminen.com>

France

Form-Edit, 5, rue Janssen, P.O. Box 25, F-75921 Paris Cedex 19
Telephone: +33 1 42 01 49 49 • Fax: +33 1 42 01 90 90 • Email: formedit@formedit.fr

Lavoisier SAS, 14 rue de Provigny, 94236 Cachan Cedex
Telephone: + 33 1 47 40 67 00 • Fax +33 1 47 40 67 02
Email: livres@lavoisier.fr • Web site: <http://www.lavoisier.fr>

Germany

UNO-Verlag, Vertriebs- und Verlags GmbH, August-Bebel-Allee 6, D-53175 Bonn
Telephone: +49 02 28 949 02-0 • Fax: +49 02 28 949 02-22
Email: info@uno-verlag.de • Web site: <http://www.uno-verlag.de>

Hungary

Librotrade Ltd., Book Import, P.O. Box 126, H-1656 Budapest
Telephone: +36 1 257 7777 • Fax: +36 1 257 7472 • Email: books@librotrade.hu

India

Allied Publishers Group, 1st Floor, Dubash House, 15, J. N. Heredia Marg, Ballard Estate, Mumbai 400 001,
Telephone: +91 22 22617926/27 • Fax: +91 22 22617928
Email: alliedpl@vsnl.com • Web site: <http://www.alliedpublishers.com>

Bookwell, 24/4800, Ansari Road, Darya Ganj, New Delhi 110002
Telephone: +91 11 23268786, +91 11 23257264 • Fax: +91 11 23281315
Email: bookwell@vsnl.net • Web site: <http://www.bookwellindia.com>

Italy

Libreria Scientifica Dott. Lucio di Biasio "AEIOU", Via Coronelli 6, I-20146 Milan
Telephone: +39 02 48 95 45 52 or 48 95 45 62 • Fax: +39 02 48 95 45 48

Japan

Maruzen Company, Ltd., 13-6 Nihonbashi, 3 chome, Chuo-ku, Tokyo 103-0027
Telephone: +81 3 3275 8582 • Fax: +81 3 3275 9072
Email: journal@maruzen.co.jp • Web site: <http://www.maruzen.co.jp>

Korea, Republic of

KINS Inc., Information Business Dept. Samho Bldg. 2nd Floor, 275-1 Yang Jae-dong SeoCho-G, Seoul 137-130
Telephone: +02 589 1740 • Fax: +02 589 1746
Email: sj8142@kins.co.kr • Web site: <http://www.kins.co.kr>

Netherlands

Martinus Nijhoff International, Koraalrood 50, P.O. Box 1853, 2700 CZ Zoetermeer
Telephone: +31 793 684 400 • Fax: +31 793 615 698 • Email: info@nijhoff.nl • Web site: <http://www.nijhoff.nl>

Swets and Zeitlinger b.v., P.O. Box 830, 2160 SZ Lisse
Telephone: +31 252 435 111 • Fax: +31 252 415 888 • Email: infoho@swets.nl • Web site: <http://www.swets.nl>

New Zealand

DA Information Services, 648 Whitehorse Road, MITCHAM 3132, Australia
Telephone: +61 3 9210 7777 • Fax: +61 3 9210 7788
Email: service@dadirect.com.au • Web site: <http://www.dadirect.com.au>

Slovenia

Cankarjeva Zalozba d.d., Kopitarjeva 2, SI-1512 Ljubljana
Telephone: +386 1 432 31 44 • Fax: +386 1 230 14 35
Email: import.books@cankarjeva-z.si • Web site: <http://www.cankarjeva-z.si/uvoz>

Spain

Díaz de Santos, S.A., c/ Juan Bravo, 3A, E-28006 Madrid
Telephone: +34 91 781 94 80 • Fax: +34 91 575 55 63 • Email: compras@diazdesantos.es
carmela@diazdesantos.es • barcelona@diazdesantos.es • julio@diazdesantos.es
Web site: <http://www.diazdesantos.es>

United Kingdom

The Stationery Office Ltd, International Sales Agency, PO Box 29, Norwich, NR3 1 GN
Telephone (orders): +44 870 600 5552 • (enquiries): +44 207 873 8372 • Fax: +44 207 873 8203
Email (orders): book.orders@tso.co.uk • (enquiries): book.enquiries@tso.co.uk • Web site: <http://www.tso.co.uk>

On-line orders:

DELTA Int. Book Wholesalers Ltd., 39 Alexandra Road, Addlestone, Surrey, KT15 2PQ
Email: info@profbooks.com • Web site: <http://www.profbooks.com>

Books on the Environment:

Earthprint Ltd., P.O. Box 119, Stevenage SG1 4TP
Telephone: +44 1438748111 • Fax: +44 1438748844
Email: orders@earthprint.com • Web site: <http://www.earthprint.com>

United Nations (UN)

Dept. I004, Room DC2-0853, First Avenue at 46th Street, New York, N.Y. 10017, USA
Telephone: +800 253-9646 or +212 963-8302 • Fax: +212 963-3489
Email: publications@un.org • Web site: <http://www.un.org>

United States of America

Bernan Associates, 4611-F Assembly Drive, Lanham, MD 20706-4391
Telephone: 1-800-865-3457 • Fax: 1-800-865-3450
Email: order@bernan.com • Web site: <http://www.bernan.com>

Renouf Publishing Company Ltd., 812 Proctor Ave., Ogdensburg, NY, 13669
Telephone: +888 551 7470 (toll-free) • Fax: +888 568 8546 (toll-free)
Email: order.dept@renoufbooks.com • Web site: <http://www.renoufbooks.com>

Orders and requests for information may also be addressed directly to:

Sales and Promotion Unit, International Atomic Energy Agency

Vienna International Centre, PO Box 100, 1400 Vienna, Austria
Telephone: +43 1 2600 22529 (or 22530) • Fax: +43 1 2600 29302
Email: sales.publications@iaea.org • Web site: <http://www.iaea.org/books>